

# Metal Chelation in Medicine

## RSC Metallobiology Series

### *Editor-in-Chief:*

Professor C. David Garner, *University of Nottingham, UK*

### *Series Editors:*

Professor Hongzhe Sun, *University of Hong Kong, China*

Professor Anthony Wedd, *University of Melbourne, Australia*

Professor Stefano L. Ciurli, *University of Bologna, Italy*

### *Editorial Advisor:*

Professor Alison Butler, *University of California Santa Barbara, USA*

### *Titles in the Series:*

- 1: Mechanisms and Metal Involvement in Neurodegenerative Diseases
- 2: Binding, Transport and Storage of Metal Ions in Biological Cells
- 3: 2-Oxoglutarate-Dependent Oxygenases
- 4: Heme Peroxidases
- 5: Molybdenum and Tungsten Enzymes: Biochemistry
- 6: Molybdenum and Tungsten Enzymes: Bioinorganic Chemistry
- 7: Molybdenum and Tungsten Enzymes: Spectroscopic and Theoretical Investigations
- 8: Metal Chelation in Medicine

### *How to obtain future titles on publication:*

A standing order plan is available for this series. A standing order will bring delivery of each new volume immediately on publication.

### *For further information please contact:*

Book Sales Department, Royal Society of Chemistry, Thomas Graham House,  
Science Park, Milton Road, Cambridge, CB4 0WF, UK

Telephone: +44 (0)1223 420066, Fax: +44 (0)1223 420247,

Email: [booksales@rsc.org](mailto:booksales@rsc.org)

Visit our website at [www.rsc.org/books](http://www.rsc.org/books)

# *Metal Chelation in Medicine*

Edited by

**Robert Crichton**

*Universite Catholique de Louvain, Louvain-la-Neuve, Belgium*

*Email: robert.crichton@uclouvain.be*

**Roberta J. Ward**

*Universite Catholique de Louvain, Louvain-la-Neuve, Belgium*

*Email: roberta.ward@uclouvain.be*

and

**Robert C. Hider**

*King's College London, London, UK*

*Email: robert.hider@kcl.ac.uk*



RSC Metallobiology Series No. 8

Print ISBN: 978-1-78262-064-8

PDF eISBN: 978-1-78262-389-2

EPUB eISBN: 978-1-78262-921-4

ISSN: 2045-547X

A catalogue record for this book is available from the British Library

© The Royal Society of Chemistry 2017

*All rights reserved*

*Apart from fair dealing for the purposes of research for non-commercial purposes or for private study, criticism or review, as permitted under the Copyright, Designs and Patents Act 1988 and the Copyright and Related Rights Regulations 2003, this publication may not be reproduced, stored or transmitted, in any form or by any means, without the prior permission in writing of The Royal Society of Chemistry or the copyright owner, or in the case of reproduction in accordance with the terms of licences issued by the Copyright Licensing Agency in the UK, or in accordance with the terms of the licences issued by the appropriate Reproduction Rights Organization outside the UK. Enquiries concerning reproduction outside the terms stated here should be sent to The Royal Society of Chemistry at the address printed on this page.*

The RSC is not responsible for individual opinions expressed in this work.

The authors have sought to locate owners of all reproduced material not in their own possession and trust that no copyrights have been inadvertently infringed.

Published by The Royal Society of Chemistry,  
Thomas Graham House, Science Park, Milton Road,  
Cambridge CB4 0WF, UK

Registered Charity Number 207890

For further information see our web site at [www.rsc.org](http://www.rsc.org)

Printed in the United Kingdom by CPI Group (UK) Ltd, Croydon, CR0 4YY, UK

# *Preface*

The importance of metals in biology and medicine has grown exponentially since the emergence, in the early 1980s, of the scientific discipline once known as Inorganic Biochemistry or Bioinorganic Chemistry, which is now designated as Biological Inorganic Chemistry (BIC). Since the first International BIC Conference (ICBIC) in Florence in 1983, the role of metals in medicine has never been far from the programme. However, metals, even when they are essential, can be toxic, as can a number of non-essential metals, often referred to as 'heavy metals'. As Paracelsus pointed out in the 1500 s, anything can be toxic, only dependent on the dose and, while in the case of essential metals toxicity is associated with excessive accumulation of the metal ion, often in specific organs, tissues or cell types, non-essential metal ions become toxic when a particular threshold concentration of the metal ion is exceeded.

As we point out in this latest contribution to the RSC Metallobiology series, in very many clinical situations, the only realistic and appropriate therapeutic option is to administer a specific metal chelator which can remove the metal excess. For essential metals, the aim is to restore the perturbed metal ion homeostasis, whereas for non-essential metal ions the objective is to remove the 'xenometal' (my apologies for this literary extravaganza).

We begin with an introductory chapter on metal toxicity, by both essential and non-essential metal ions, which is followed by a chapter reviewing the principles involved in the design of metal chelates. The removal of heavy metals by chelation therapy is then reviewed, followed by chapters on the use of iron chelators in the treatment of transfusional iron overload and their potential in the treatment of neurodegenerative diseases where iron loading in specific brain regions involved in the particular disease highlights the need to target iron chelation to specific locations. Then, the development of

---

RSC Metallobiology Series No. 8

Metal Chelation in Medicine

Edited by Robert Crichton, Roberta J. Ward and Robert C. Hider

© The Royal Society of Chemistry 2017

Published by the Royal Society of Chemistry, [www.rsc.org](http://www.rsc.org)

octadentate chelators for selective complexation of actinides, which would be absolutely essential in the unthinkable scenario of the terrorist use of a 'dirty bomb', is cogently reviewed (representing a totally different level of chelation therapy). The concluding chapters detail the non-invasive techniques which are being increasingly developed for the evaluation of iron overload and their use in diagnostic imaging.

We hope that this volume will help in the search for appropriate therapeutic measures to deal with the complex problems of metal toxicity.

Robert R. Crichton, Roberta J. Ward and Robert C. Hider

# Contents

<b>Chapter 1</b>	<b>Metal Toxicity – An Introduction</b>	<b>1</b>
	<i>Robert R. Crichton</i>	
1.1	Introduction	1
1.2	Essential Metals	2
1.2.1	Sodium and Potassium	2
1.2.2	Magnesium and Calcium	2
1.2.3	Zinc	3
1.2.4	Other Essential Metals	3
1.3	Toxicity Due to Essential Metals	4
1.3.1	Sodium and Potassium	4
1.3.2	Calcium and Magnesium	7
1.3.3	Zinc	8
1.3.4	Other Essential Metals	9
1.4	Non-Essential Metals	12
1.5	Toxicity Due to Non-Essential Metals	13
1.5.1	Lead	13
1.5.2	Cadmium	14
1.5.3	Mercury	15
1.5.4	Aluminium	15
1.6	Sources and Routes of Exposure with Particular Reference to Non-Essential Metals	18
1.7	Conclusions	19
	Abbreviations	20
	References	20

---

RSC Metallobiology Series No. 8

Metal Chelation in Medicine

Edited by Robert Crichton, Roberta J. Ward and Robert C. Hider

© The Royal Society of Chemistry 2017

Published by the Royal Society of Chemistry, [www.rsc.org](http://www.rsc.org)

**Chapter 2 Basic Principles of Metal Chelation and Chelator Design 24**  
*Robert C. Hider and Yongmin Ma*

2.1	Introduction	24
2.2	Ligand Chemistry	26
2.3	Ligand Selectivity	29
2.4	Comparison of Bidentate Ligands	31
2.4.1	Catechols	31
2.4.2	Hydroxamates	33
2.4.3	Hydroxypyridinones	33
2.4.4	Hydroxypyranones	35
2.4.5	Aliphatic Diamines	35
2.4.6	Heterocyclic Amines	35
2.4.7	Hydroxyquinolines	36
2.4.8	Aminocarboxylates (Including Oligodentate Ligands)	36
2.4.9	Hydroxycarboxylates (Including Tri- and Hexadentate Ligands)	37
2.5	Ligand Denticity – The Chelate Effect	37
2.6	Complex Lability	39
2.7	Redox Activity	41
2.8	Biological Properties	43
2.9	Lipophilicity and Molecular Weight	43
2.10	Ligand Metabolism	44
2.11	Ligand Binding to Serum Albumin	45
2.12	Chelator Pharmacokinetics	47
2.13	Toxicity of Chelators	49
2.13.1	Inhibition of Metal-Dependent Enzymes	49
2.13.2	Nephrotoxicity	51
2.13.3	Neurotoxicity	51
2.13.4	Immunotoxicity	51
2.13.5	Genotoxicity	52
2.14	Chelators and Nutrition	52
2.15	Conclusions	53
	Abbreviations	53
	References	53

**Chapter 3 Chelation Therapy For Heavy Metals 56**  
*Peter Nielsen*

3.1	Introduction	56
3.2	General Strategies Against Heavy Metal Intoxication	58
3.2.1	Toxicology of Heavy Metals	58
3.2.2	Treatment for Heavy Metal Intoxication	59
3.2.3	Drawbacks and Misuse of Chelators	62

3.3 Arsenic	63
3.3.1 Absorption and Metabolism of Arsenicals	63
3.3.2 Toxicity of Arsenicals	64
3.3.3 Diagnostic Measures and Interventional Levels	66
3.3.4 Chelation Therapy for Arsenic Intoxication	66
3.4 Mercury	68
3.4.1 Absorption and Metabolism of Mercurials	70
3.4.2 Toxicology of Mercury	73
3.4.3 Diagnostics and Intervention Levels	75
3.4.4 Chelation Treatment for Mercury Poisoning	76
3.5 Lead	78
3.5.1 Lead Absorption and Metabolism	78
3.5.2 Toxicity of Lead	80
3.5.3 Diagnostic Measures and Intervention Levels	82
3.5.4 Treatment of Lead Poisoning	82
3.6 Cadmium	85
3.6.1 Absorption and Metabolism of Cadmium	86
3.6.2 Toxicity of Cadmium	87
3.6.3 Diagnostic Markers and Intervention Level for Cd Intoxication	90
3.6.4 Chelation Treatment for Cadmium Poisoning	90
3.7 Noble Metals	92
3.7.1 Silver Poisoning	92
3.7.2 Gold Poisoning	93
3.8 Other Metals	94
3.8.1 Acute Iron Poisoning	94
3.8.2 Acute Copper Poisoning	95
3.8.3 Thallium Poisoning	95
3.9 Conclusion	96
Abbreviations	97
References	98

## **Chapter 4 Treatment of Systemic Iron Overload 106**

*John Porter*

4.1 Consequences of Transfusional Iron Overload	106
4.1.1 Iron Homeostasis in the Absence of Blood Transfusion	106
4.1.2 Effects of Inherited Anaemias and Blood Transfusion on Iron Homeostasis	107
4.2 Impact of Transfusion on Iron Distribution and its Consequences	109
4.3 Desirable Features of Clinically Useful Iron Chelators	113
4.3.1 High Iron Binding Constant and Selectivity for Iron	113

4.3.2	Chelation of Iron Pools for Balance Without Inhibition of Key Metabolic Pools	114
4.4	Monitoring Iron Overload and Its Treatment	117
4.4.1	Monitoring Trajectory of Iron Overload and Distribution	117
4.5	Properties and Clinical Beneficial Effects of Available Iron Chelators	124
4.5.1	Desferrioxamine (Desferal) DFO	124
4.5.2	Deferiprone (DFP)	127
4.5.3	Deferasirox (Exjade®) DFX	130
4.6	Unwanted Effects of Iron Chelators	132
4.6.1	Role of Iron Deprivation in Chelator Toxicity	132
4.6.2	Desferrioxamine Tolerability and Unwanted Effects	133
4.6.3	Deferiprone Tolerability and Unwanted Effects	134
4.6.4	Deferasirox Tolerability and Unwanted Effects	134
4.7	Practical Use of Chelators: A Personal Approach	135
4.7.1	Patients with Acceptable Levels of Body Iron but Continuing Transfusion	135
4.7.2	Patients with Unacceptably High Levels of Body Iron	136
4.7.3	Patients with Unacceptably High Levels of Myocardial Iron	136
4.7.4	Patients in Heart Failure	137
4.7.5	Patients with Rapidly Falling Serum Ferritin or Low Values $<1000 \mu\text{L}^{-1}$	138
4.7.6	Patients not Responding to Monotherapy Regimes: Combined Chelators	139
4.7.7	Combinations of DFP with DFO	139
4.7.8	Combinations of DFO Plus DFX	140
4.7.9	Combination of DFP Plus DFX	140
4.8	Conclusions	140
	Abbreviations	141
	References	141

## **Chapter 5 Treatment of Neurodegenerative Diseases by Chelators** 153

*Roberta J. Ward, David T. Dexter and Robert R. Crichton*

5.1	Introduction	153
5.2	The Aging Brain	154
5.2.1	Brain Iron Homeostasis and Aging	154
5.2.2	Brain Copper Homeostasis and Aging	156
5.2.3	Brain Zinc Homeostasis and Aging	156
5.3	Inflammation and Aging	157

<i>Contents</i>	xi
5.4 Neurodegenerative Diseases	157
5.5 Blood Brain Barrier	158
5.6 Metal Ions and Neurodegenerative Diseases	159
5.6.1 Parkinson's Disease (PD)	160
5.6.2 Alzheimer's Disease (AD)	163
5.6.3 Intracerebral Haemorrhage	166
5.6.4 Multiple Sclerosis	168
5.6.5 Friederich's Ataxia	168
5.7 Neurodegeneration with Brain Iron Accumulation (NBIA) Diseases	169
5.7.1 Mutation in Genes Associated with Iron Metabolism	169
5.8 Macular Degeneration	176
5.9 Conclusion and Perspectives	177
Abbreviations	177
References	177
<b>Chapter 6 Chelation of Actinides</b>	<b>183</b>
<i>Rebecca J. Abergel</i>	
6.1 The Medical and Public Health Relevance of Actinide Chelation	183
6.1.1 Actinide Metabolism and Clinical Course	184
6.1.2 Current Treatment Recommendations for Actinide Contamination	186
6.1.3 Limitations of Current Therapies	187
6.2 Designing Chemical Structures for Actinide Chelation	187
6.2.1 Coordination Chemistry Criteria	188
6.2.2 Synthetic Approaches to New Actinide-Selective Agents	188
6.3 Evaluating Actinide Chelation Efficacy	193
6.3.1 <i>In vitro</i> Evaluation Techniques	193
6.3.2 <i>In vivo</i> Efficacy Determination	196
6.4 Development of Viable Actinide Chelation Treatments	199
6.4.1 Formulation Development	199
6.4.2 Safety Determination and Regulatory Approval	202
Abbreviations	206
References	207
<b>Chapter 7 Evaluation of Iron Overload by Non-Invasive Measurement Techniques</b>	<b>213</b>
<i>Roland Fischer</i>	
7.1 Introduction	213

7.2 Principles of Iron Measurement Techniques	215
7.2.1 Reference Standards for Iron Quantification Methods	215
7.2.2 Biochemical Properties of Iron Storage Molecules	217
7.2.3 Magnetic Properties of Iron Storage Molecules	218
7.3 Iron Measurements: Technique, Analysis, and Calibration	224
7.3.1 Spin-Echo Relaxometry (R2/T2)	226
7.3.2 Spin-Lattice Relaxometry (T1/R1)	229
7.3.3 Gradient-Echo Relaxometry (T2*/R2*)	229
7.3.4 Biomagnetic Susceptometry	233
7.3.5 Other MRI Iron Measurement Techniques	235
7.3.6 Quantitative X-ray Iron Measurement Techniques	237
7.4 Applications of <i>In vivo</i> Iron Assessment	237
7.4.1 Liver	238
7.4.2 Spleen	239
7.4.3 Heart	240
7.4.4 Pancreas	240
7.4.5 Pituitary	241
7.4.6 Brain	242
7.4.7 Iron in Other Organs, Glands, and Tissue	244
7.5 Conclusion and Prospects	247
Abbreviations	248
Acknowledgement	248
References	248
<b>Chapter 8 Chelators for Diagnostic Molecular Imaging with Radioisotopes of Copper, Gallium and Zirconium</b>	<b>260</b>
<i>Michelle T. Ma and Philip J. Blower</i>	
8.1 Introduction	260
8.1.1 Positron Emission Tomography and Molecular Imaging with Peptides and Proteins	261
8.1.2 Reactive Functional Groups for Attachment to Biomolecules	262
8.1.3 Requirements for Chelators that Complex Positron-Emitting Metal Radioisotopes	263
8.2 Macrocyclic Chelators for Copper-64: Lessons in Kinetic Stability	265
8.2.1 Cu Complexes of Macrocycles: Radiolabelling and <i>In vivo</i> Stability	266
8.2.2 Kinetic Stability is Critical to <i>In vivo</i> Stability – You Can't Have One Without the Other	275

<i>Contents</i>	xiii
8.2.3 Targeting Based on Chelate Reactivity: Bio-reduction and Dissociation	281
8.2.4 Outlook for Clinical Applications of Copper-64	282
8.3 Acyclic and Macrocyclic Chelators for Gallium-68: A Short Half-Life Necessitates Efficient Radiolabelling	283
8.3.1 Gallium-68 in the Clinic: Its Current Utility and Future Potential	283
8.3.2 Macrocycles for Gallium-68	286
8.3.3 Halfway Between Macrocycles and Open-Chain Chelators: Data Derivatives	289
8.3.4 Acyclic Chelators for Gallium-68 Provide Rapid Radiolabelling at Room Temperature	290
8.3.5 Siderophores for Coordination of Gallium-68	294
8.3.6 Chelator Design and Clinical Impact	295
8.4 Development of Chelators for Zirconium-89: Work in Progress	295
8.4.1 Hexadentate Chelators for Zirconium-89: Sufficient, But Suboptimal	296
8.4.2 Octadentate Chelators for $^{89}\text{Zr}^{4+}$ : Will Saturation of the Coordination Sphere Provide Enhanced Stability <i>In vivo</i> ?	299
8.4.3 Metastable Lipophilic Zirconium Chelates	302
8.5 Conclusions	303
Abbreviations	304
Acknowledgements	305
References	305
<b>Subject Index</b>	<b>313</b>

## CHAPTER 1

# *Metal Toxicity – An Introduction*

ROBERT R. CRICHTON<sup>a</sup>

<sup>a</sup>Universite Catholique de Louvain, 1348 Louvain-la-Neuvre, Belgium

\*E-mail: [Robert.crichton@uclouvain.be](mailto:Robert.crichton@uclouvain.be)

## 1.1 Introduction

Metal toxicity<sup>1</sup> can be caused by both metal ions, which are considered to be essential for humans, like iron and copper, as well as by non-essential metals, like cadmium, lead and mercury, which are not at all necessary for life but which, when introduced into the human environment, can have toxic effects, often with disastrous consequences. So, we begin by asking what are the essential metal ions, why they are required, and under what circumstances certain of them can be toxic. We then discuss which are the non-essential metal ions which pose toxicity problems to the human population. For each of these two groups of metal ions, general chemical considerations and the basic principles involved in their toxicity are briefly considered, as well as how the metal ion is bound within cells or tissues, since this is a key element in devising strategies for its removal by chelation. Finally, we briefly review the sources and routes of exposure to metal toxicity, with particular reference to non-essential metals.

Whereas essential metal ion toxicity can be attributed to accumulation of excessive concentrations of the metal ion, often in specific tissues or organs, the toxicity of non-essential metal ions is a consequence of environmental

---

RSC Metallobiology Series No. 8

Metal Chelation in Medicine

Edited by Robert Crichton, Roberta J. Ward and Robert C. Hider

© The Royal Society of Chemistry 2017

Published by the Royal Society of Chemistry, [www.rsc.org](http://www.rsc.org)

exposure leading to their accumulation within the body. Both types of metal toxicity can, in principle, be treated by the use of appropriate metal ion chelators, and this constitutes the subject of this contribution to the RSC Metallobiology series.

## 1.2 Essential Metals

There are around twenty five elements that are required by most biological systems, including an important number of metal ions. However, for humans, there are ten essential metal ions. Of these, four: sodium, potassium, calcium and magnesium, can be considered as 'bulk elements', and together constitute approximately 99% of the metal ion content of the human body. The other five transition metals manganese, iron, cobalt, copper, zinc and molybdenum, are known as 'trace elements', with much lower dietary requirements than the bulk elements; they are nonetheless indispensable for human life.<sup>2</sup>

### 1.2.1 Sodium and Potassium

The two essential alkali metal ions  $\text{Na}^+$  and  $\text{K}^+$  (together with  $\text{H}^+$  and  $\text{Cl}^-$ ) are only weakly bound to organic ligands and are extremely mobile. This makes them ideally suited to generate ionic gradients across biological membranes and to ensure the maintenance of osmotic balance, and this is precisely what they do. The  $\text{Na}^+$  and  $\text{K}^+$  contents of the average 70 kg adult human are about 100 g and 140 g, respectively, but their distribution in most mammalian cells is quite different.  $\text{Na}^+$ , together with  $\text{Cl}^-$ , is the major electrolyte in the extracellular fluid, whereas  $\text{K}^+$  is retained within the cells. The concentration of  $\text{Na}^+$  in the extracellular fluid (*i.e.*, the plasma) is maintained within narrow limits at about  $145 \text{ mmol L}^{-1}$ , whereas the intracellular concentration is about  $12 \text{ mmol L}^{-1}$ . In contrast, the concentration of  $\text{K}^+$  is  $150 \text{ mmol L}^{-1}$  within the cells and typically  $4\text{--}5 \text{ mmol L}^{-1}$  in the extracellular fluids. This concentration differential, which is maintained by the  $(\text{Na}^+\text{--}\text{K}^+)\text{--ATPase}$  of the plasma membrane, ensures a number of major biological processes, such as cellular osmotic balance, signal transduction and neurotransmission.

### 1.2.2 Magnesium and Calcium

In contrast to  $\text{Na}^+$  and  $\text{K}^+$ , the alkaline earths  $\text{Mg}^{2+}$  and  $\text{Ca}^{2+}$  have intermediate binding strengths to organic ligands and are therefore less mobile. They play important structural and catalytic roles and, in the particular case of  $\text{Ca}^{2+}$ , serve as a charge carrier and a trigger for signal transmission within the cell.  $\text{Ca}^{2+}$  is the fifth most abundant element and most abundant metal ion in the human body, representing 14% of body mass (1 kg for a 70 kg human), whereas  $\text{Mg}^{2+}$  accounts for only 19 mg. Most (99%) of the body's  $\text{Ca}^{2+}$  is found within the biominerals that constitute bone and teeth, but the 1% found within cells and tissues has enormous importance in regulating a series of

important cellular responses, from initial fertilisation to being a harbinger of cell death, intervening between these limits of the life of the cell to include secretion, mobility, metabolic control, synaptic regulation and gene regulation. Although  $\text{Mg}^{2+}$  represents the least abundant of the 'bulk elements', it is the most abundant cation within cells, with roughly half of cytosolic  $\text{Mg}^{2+}$  bound to ATP and most of the rest bound, together with  $\text{K}^+$ , to ribosomes; the intracellular concentration of free  $\text{Mg}^{2+}$  is around 0.5 mM, and less than 0.5% of total body  $\text{Mg}^{2+}$  is in the plasma. Unlike the other three bulk cations,  $\text{Mg}^{2+}$  has a much slower water exchange rate, allowing it to play a structural role, for example, participating in ATP binding in many enzymes involved in phosphoryl transfer reactions—six of the ten reactions of glycolysis are phosphoryl transfers.

### 1.2.3 Zinc

Of the six trace metal ions, *in senso stricto*, zinc is not a transition metal ion. Zn has ligand binding constants intermediate between those of  $\text{Mg}^{2+}$  and  $\text{Ca}^{2+}$  and the other five transition metals, and, in marked contrast, does not have access to any other oxidation state other than  $\text{Zn}^{2+}$ , which may be one of the reasons why it is found in more than 300 enzymes, representing all of the six classes of enzymes represented by the International Union of Biochemistry, since it avoids generation of free radicals.  $\text{Zn}^{2+}$  not only plays a structural and catalytic role, often functioning, like  $\text{Mg}^{2+}$ , as a Lewis acid; it can also fulfil a very important function in the structural motifs known as 'zinc fingers' involved in the regulation of transcription and translation *via* its DNA- and RNA-binding.  $\text{Zn}^{2+}$  is the second most abundant of the trace metals (after iron), and is extensively involved in brain function. Bioinformatic analysis reveals that the zinc proteome represents about 10% of the entire proteome in humans, compared to 5–6% in prokaryotes.<sup>3</sup>

### 1.2.4 Other Essential Metals

The other five transition metal ions: Mn, Fe, Co, Cu and Mo, bind tightly to organic ligands, are therefore effectively immobile and participate in a wide range of redox reactions. Fe and Cu are constituents of a large number of proteins involved in electron transfer chains in humans, the respiratory chain in the inner membrane of the mitochondria, with Fe-S proteins, cytochromes and the terminal component, the Cu-Fe-dependent cytochrome c oxidase. Fe also plays an important role in the oxygen transport and storage proteins, haemoglobin and myoglobin, while both Fe and Cu are involved in oxygen activation (oxidases, hydroxylases) and detoxification (Cu-Zn superoxide dismutase). Co is required in the diet as vitamin B<sub>12</sub>, and is an essential cofactor for a number of B<sub>12</sub>-dependent isomerases and methyltransferases. Mn plays an important role in the detoxification of oxygen free radicals (mitochondrial Mn superoxide dismutase). Mo, while relatively rare in the earth's crust, is the most abundant transition metal in seawater, and is an important component

of nitrogenase, the key enzyme of nitrogen-fixing organisms. However, in humans there are a number of Mo-dependent enzymes, which all contain Mo in the form of a molybdenum pyranopterin-dithiolate cofactor. They include xanthine oxidase, involved in the catabolism of purine bases, sulphite oxidase involved in sulphur metabolism and aldehyde oxidase, involved in the metabolism of many drugs.

Ni<sup>2+</sup>, V and Cr appear to be beneficial and have been proposed to be essential for man but we will not discuss their roles further.

### 1.3 Toxicity Due to Essential Metals

*Alle Dinge sind Gift, und nichts ist ohne Gift; allein die dosis machts, daß ein Ding kein Gift sei.* Paracelsus (1493–1541)

This celebrated dictum of Paracelsus, the Swiss physician, alchemist, mystic and philosopher (born Phillip von Hohenheim, later called Philippus Theophrastus Aureolus Bombastus von Hohenheim, and ultimately Paracelsus), can be loosely translated as ‘Everything is poisonous and nothing is not poisonous; only the dose determines whether something is poisonous or not’.

Nowhere is this more true than in describing the toxicity of essential metal ions. The concentration of each of the essential metal ions needs to be maintained within strict limits in each cell and tissue of the body. This is what the celebrated French physiologist Claude Bernard defined as homeostasis—*‘the fixity of the internal environment is the condition for free life’*. He continued *“The living body, though it has need of the surrounding environment, is nevertheless relatively independent of it. This independence which the organism has of its external environment, derives from the fact that in the living being, the tissues are in fact withdrawn from direct external influences and are protected by a veritable internal environment which is constituted, in particular, by the fluids circulating in the body.”*. Thus, any factor, whether hereditary, environmental or other, which perturbs the homeostatic equilibrium of a metal ion can result in a shift from that equilibrium state to a condition of either deficiency or excess, and it is the latter that is the origin of the toxicity of essential metals.

It is clearly beyond the scope of this chapter to discuss the homeostasis of each of the essential metal ions and in what follows we will highlight some of the major causes of essential metal toxicity in humans with a particular focus on those that are accessible to therapeutic treatment by chelation therapy and to identifying areas involving essential metal overload that may become amenable to chelation therapy.

#### 1.3.1 Sodium and Potassium

Selectivity in the coordination of the alkali metals, Na<sup>+</sup> and K<sup>+</sup>, can be easily achieved since the difference in their ionic radii is large (0.35 Å) and hence the dimensions of the cavity surrounding the unhydrated monovalent cation effectively solves the problem of Na<sup>+</sup>–K<sup>+</sup> selectivity in both complexation and transport. This was established by early studies on synthetic model

compounds,<sup>4</sup> confirmed by the high resolution structures of membrane transporters of  $K^+$ <sup>5,6</sup> and, more recently, the structure of an  $Na^+$  transporter.<sup>7</sup>

The structure of the KcsA  $K^+$  channel<sup>5</sup> from *Streptomyces lividans*, an integral membrane protein with sequence similarity to all known  $K^+$  channels, reveals that it is constructed in the form of an inverted teepee, with the narrow 12 Å long selectivity filter in its outer end. Whereas the central cavity of the pore is wider and lined with hydrophobic amino acids, the selectivity filter is lined by main chain carbonyl oxygen atoms (Figure 1.1a) and is held open by structural constraints to coordinate unhydrated  $K^+$  ions but not the smaller  $Na^+$  ions. Thus, the architecture of the pore establishes the physical principles underlying selective  $K^+$  conduction.<sup>5</sup> In order to transport unhydrated  $K^+$  ions in the selectivity filter, the  $K^+$  ion's hydration shell must be removed. The structure of the KcsA  $K^+$  channel in complex with a

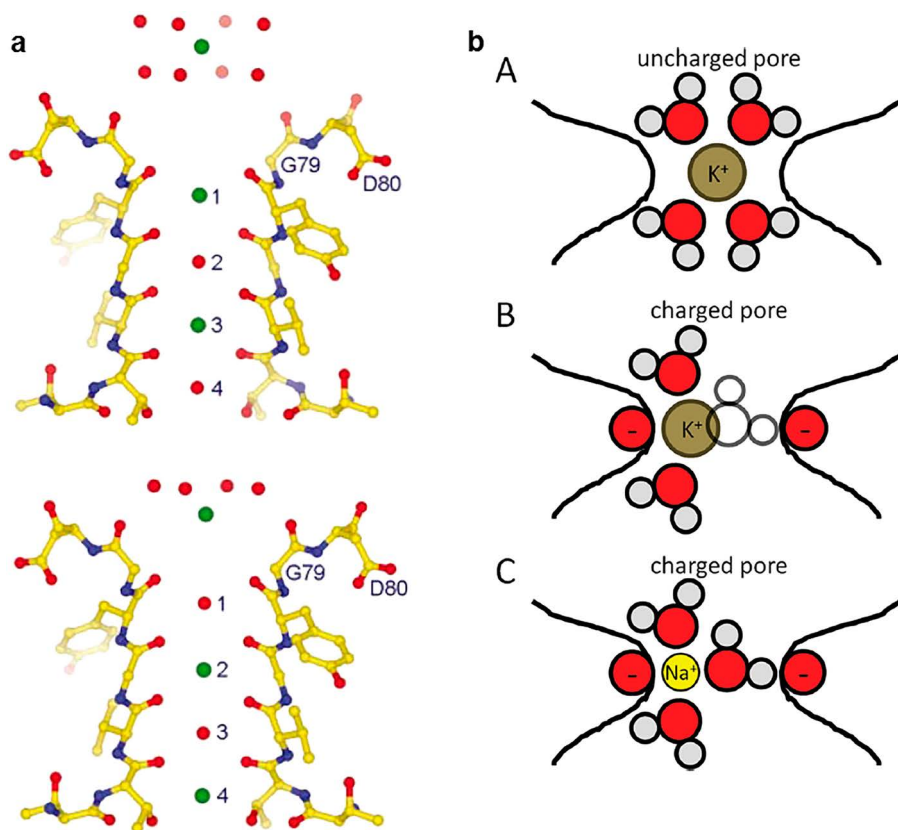


**Figure 1.1** (a) The KcsA  $K^+$  channel showing the selectivity pore and the  $K^+$  ion dehydration at the extracellular pore entryway. Reprinted by permission from Macmillan Publishers Ltd: Nature, Zhou *et al.*<sup>8</sup> Copyright 2001. (b) A schematic depiction of the proposed mechanism of ion selectivity in NavAb. Reprinted with permission from Corry and Thomas.<sup>9</sup> Copyright (2012) American Chemical Society.

monoclonal Fab antibody fragment at 2.0 Å resolution<sup>8</sup> shows how this is achieved. The transfer of a K<sup>+</sup> ion between the extracellular solution (where a K<sup>+</sup> ion is hydrated) and the selectivity filter (where the ion is unhydrated) is mediated by a specific arrangement of carbonyl oxygen atoms that protrude into solution. The selectivity filter contains two K<sup>+</sup> ions about 7.5 Å apart. When the configuration of ions (green spheres) and water (red spheres) inside the filter is K<sup>+</sup>-water-K<sup>+</sup>-water (top, 1,3 configuration), a K<sup>+</sup> ion at the entryway is surrounded by eight ordered water molecules ready to enter the selectivity filter. When the configuration is water-K<sup>+</sup>-water-K<sup>+</sup> (bottom, 2,4 configuration), the K<sup>+</sup> ion at the filter threshold senses the electrostatic field due to the ion distribution within the filter and is drawn closer to the channel from the fully hydrated position to a position where it is half hydrated.

Using the structure of the voltage gated sodium channel, NavAb from *Arco-bacter butzleri*,<sup>7</sup> the location and probable mechanism used to discriminate between Na<sup>+</sup> and K<sup>+</sup> has been pinpointed.<sup>9</sup> The overall topography of the NavAb channel is similar to that of the K<sup>+</sup> channel,<sup>8</sup> in the form of an inverted tepee, but differs significantly from the K<sup>+</sup> channel in the narrow 'selectivity filter', which is both wider and shorter as well as being lined by amino acid side chains. The proposed mechanism of ion selectivity in NavAb is presented in Figure 1.1b. The first surprise is that, whereas in the K<sup>+</sup> channel<sup>5</sup> (Figure 1.1b) *unhydrated* K<sup>+</sup> ions transit the selectivity filter, *hydrated* Na<sup>+</sup> ions pass through the NavAb channel. Although K<sup>+</sup> could fit through the narrow portion of the pore with a complete hydration shell as shown in Figure 1.1b (A), it cannot do so due to the presence of charged glutamate residues Figure 1.1b (B). Selectivity arises due to the inability of K<sup>+</sup> to fit between the plane of glutamate residues with the preferred solvation geometry, which involves water molecules bridging between the ion and carboxylate groups. In contrast, the smaller Na<sup>+</sup> ion can fit in the pore with its preferred solvation geometry Figure 1.1b.

Retention of Na<sup>+</sup> (hypernatraemia) is one of the most common electrolyte disorders in clinical medicine, occurring when Na<sup>+</sup> intake exceeds renal clearance. It can be caused by excessive ingestion of salt, too-rapid infusion of saline, congestive heart failure, renal failure, or when there is excessive production of aldosterone, resulting in hypervolaemia and hypertension.<sup>10</sup> Hypernatraemia and dehydration are commonly encountered among the elderly, and when they occur in nursing homes are considered indicators of neglect.<sup>11</sup> The treatment involves correcting the underlying cause and correcting the water deficit.

Hyperkalaemia,<sup>12,13</sup> defined as serum K<sup>+</sup> levels in excess of 5.5 mM, has become more common in cardiovascular practice due to the growing population of patients with chronic kidney disease and the broad application of drugs that modulate renal elimination of potassium by reducing production of angiotensin II (angiotensin-converting enzyme inhibitors, direct renin inhibitors, β-adrenergic receptor antagonists), blocking angiotensin II receptors (angiotensin receptor blockers), or antagonizing the action of aldosterone on mineral corticoid receptors (mineralocorticoid receptor antagonists).

Current therapies for hyperkalaemia either do not remove excess potassium or have poor efficacy and tolerability. Two new polymer-based, non-systemic oral agents, patiromer calcium (RLY5016) and zirconium silicate (ZS-9), currently in development,<sup>12–14</sup> are designed to induce potassium loss *via* the GI tract, particularly the colon, and reduce plasma  $K^+$  levels, and both have demonstrated efficacy and safety in recent trials. Patiromer sorbitex calcium is a polymer resin and sorbitol complex that binds potassium in exchange for calcium; ZS-9, a non-absorbed, highly selective inorganic cation exchanger, traps potassium in exchange for sodium and hydrogen.

### 1.3.2 Calcium and Magnesium

Differences in  $Ca^{2+}$  *versus*  $Mg^{2+}$  complexation are more difficult to achieve than between  $K^+$  and  $Na^+$ , although the recent structure determinations of  $Ca^{2+}$  and  $Mg^{2+}$  channels promises to improve our understanding of how selectivity is achieved.<sup>15,16</sup> The selectivity filter of a voltage-gated  $Ca^{2+}$  channel is presented in Figure 1.2.

Calcium and, to a lesser extent, magnesium balance is achieved through a complex interplay between the parathyroid gland, bone, the intestine and the kidney.<sup>17,18</sup> Hypercalcaemia is a common metabolic perturbation and the most common causes are malignancy and hyperparathyroidism, which account for around 80% of cases,<sup>17</sup> although the increase in over-the-counter purchase of  $Ca^{2+}$  and vitamin D supplements, notably to combat osteoporosis in the ageing population, is also a factor.<sup>19,20</sup> Management of hypercalcaemia

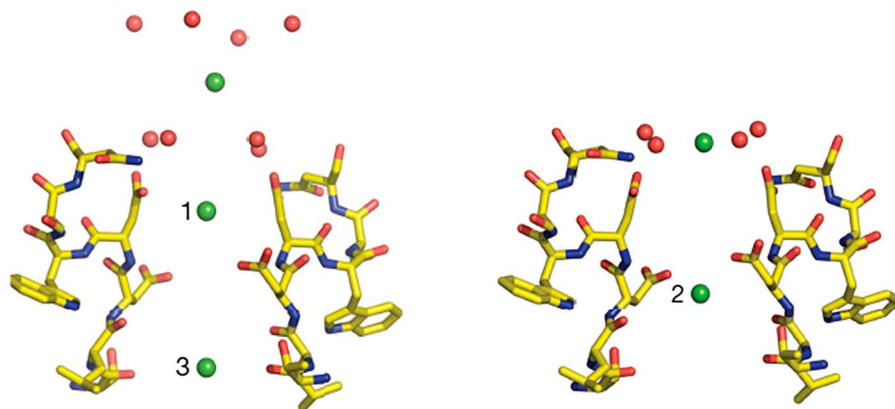


**Figure 1.2** Catalytic cycle for  $Ca^{2+}$  conductance by  $Ca_vAb$ . Coupling of extracellular  $Ca^{2+}$  binding sites and the three sites within the selectivity filter in the two proposed ionic occupancy states. When two  $Ca^{2+}$  ions bind to position 1 and 3 in the filter, the entryway  $Ca^{2+}$  ion is placed furthest from the pore (left). When one  $Ca^{2+}$  ion binds to position 2 within the filter, the ion outside the filter is pulled closer to the pore (right). Reproduced by permission from Macmillan Publishers Ltd: Nature, Tang *et al.*<sup>15</sup> Copyright 2013.

has been based on the use of bisphosphonates (*e.g.*, zoledronic acid) and calcimimetic agents, although recently the nuclear factor- $\kappa$  ligand monoclonal antibody Denosumab has also been introduced for the treatment of hypercalcaemia of malignancy.<sup>21,22</sup> Clinically significant hypermagnesaemia is uncommon, generally occurring only in the setting of renal insufficiency and excessive magnesium intake.

### 1.3.3 Zinc

The essential transition metal ions, manganese, iron, cobalt, copper and zinc present a very different picture concerning their complexation. It is difficult to selectively chelate the divalent state of these metal ions, which have very similar coordination preferences. However the selective complexation of  $\text{Fe}^{3+}$  and  $\text{Cu}^+$  is relatively easy.  $\text{Fe}^{3+}$  has no other biological counterpart in terms of its preference for hexacoordinate geometry with predominantly 'hard' ligands such as oxygen, although, as we will see later,  $\text{Al}^{3+}$  and  $\text{Ga}^{3+}$  can use the iron transport protein transferrin as  $\text{Fe}^{3+}$  surrogates. In marked contrast, the rather 'soft'  $\text{Cu}^+$  ion is ideally coordinated by sulphur ligands, and it comes as no great surprise that this is the coordination used by intracellular copper chaperones.

The human body contains about 2 g of Zn, mostly found in testes, muscle, liver, and brain. Zinc deficiency due, for example, to poor nutrition, ageing, and deregulation of zinc homeostasis, is much more frequently encountered in the human population than zinc excess.<sup>23</sup> Only exposure to high doses has toxic effects. However, long-term, high-dose zinc supplementation interferes with copper uptake, such that many of the toxic effects are a consequence of copper deficiency. Zinc-induced myeloneuropathy resulting from secondary copper deficiency has been recently rediscovered,<sup>24,25</sup> in reports published by Schlockow dating from the 1870s<sup>24</sup> this was a recognised problem among zinc smelter workers in Upper Silesia who developed symptoms identical to those reported in the modern descriptions of copper-deficiency myeloneuropathy.<sup>24,25</sup> The highest concentration of brain zinc is found in the hippocampus, amygdala, cerebral cortex, thalamus, and olfactory cortex.<sup>26</sup> Some 10% of brain zinc is histochemically detectable by chelating agents, mainly stored in the presynaptic vesicles of specific excitatory glutamatergic neurons, and is secreted from these vesicles into the synaptic clefts along with glutamate during neuronal excitation. Although the role of Zn in the brain remains elusive, recent studies suggest that secreted  $\text{Zn}^{2+}$  plays crucial roles in information processing, synaptic plasticity, learning, and memory.<sup>27,28</sup> There is considerable evidence that either deficiency or overload of Zn in the brain, resulting from perturbations in Zn homeostasis, are associated with the pathogenesis of several neurodegenerative diseases including senile dementia (Alzheimer's disease (AD) and vascular dementia),<sup>29–35</sup> prion diseases,<sup>36</sup> and amyotrophic lateral sclerosis (ALS).<sup>37</sup> It has been proposed that  $\text{Zn}^{2+}$  may play two roles<sup>35</sup> in the pathogenesis of AD. On the negative side, in common with other metals,  $\text{Zn}^{2+}$  enhances the oligomerization of

amyloid beta (A $\beta$ ) peptide, which is deposited in the neurotic plaques that characterise AD, yet it also appears to have a protective function by inhibiting A $\beta$  peptide-induced Ca<sup>2+</sup> entry into amyloid channels, which disrupts Ca homeostasis and provokes neuronal death.

### 1.3.4 Other Essential Metals

#### 1.3.4.1 Cobalt Toxicity

Cobalt is an essential micronutrient in the form of vitamin B<sub>12</sub> (hydroxocobalamin), present as a corrin cofactor in several enzymes, but inorganic cobalt is not required as such in human diets. Methionine aminopeptidase (MetAP), which removes the initiator methionine residue from the N-terminus of nascent polypeptide chains, and is conserved from yeast to humans, is a candidate to be a non-corrin Co<sup>2+</sup>-activated enzyme in humans.<sup>38</sup> The MetAPs, essential from bacteria to higher eukaryotes, are dinuclear metalloenzymes with evolutionary similarities to creatinase, prolidase (DPP) and aminopeptidase P (APP).<sup>39</sup> Metal requirement studies indicate that MetAPs can be activated by various divalent metal cations.<sup>40</sup>

Cobalt is acutely toxic in large doses<sup>41,42</sup> and the consequences were dramatically observed in the 1960s among heavy beer drinkers (15–30 pints per day), when Co<sup>2+</sup> salts were added to beer as foam stabilisers,<sup>43,44</sup> resulting in severe and often lethal cardiomyopathy. The effects were virtually absent in well nourished drinkers whereas an identical Co dose was severe and often resulted in death.<sup>45</sup> Evidence of Co toxicity was also found when Co was used therapeutically to treat anaemia.<sup>41</sup> However, since these practices have been discontinued, several subpopulations with elevated Co exposures have emerged, confirming that cumulative, long-term exposure, even at a low level, can give rise to adverse health effects related to various organs and tissues. These include occupational cobalt exposure, consuming Co-containing dietary supplements, the misuse of Co as a blood doping agent by athletes (Co stabilises hypoxia-inducible factor, mimicking hypoxia and stimulating erythropoiesis) and most recently, concerns about elevated blood Co levels in patients who have undergone orthopaedic joint replacements with cobalt–chromium hard metal alloys.<sup>41,42</sup> Corrosion and wear produce soluble metal ions and debris in the form of Co–Cr nanoparticles, from which Co ions are released, and so we progress from nanotechnology to nanotoxicology. It is suggested that implant patients should be monitored for signs of hypothyroidism and polycythaemia when levels of Co in the circulation exceed 100  $\mu\text{g L}^{-1}$ .<sup>42</sup>

#### 1.3.4.2 Manganese Toxicity

Overexposure to manganese leads to toxicity, particularly neurotoxicity.<sup>46–52</sup> Neurons are more susceptible than other cells to Mn-induced toxicity, and accumulation of Mn in the brain results in the condition known as manganism, first observed in miners during the 19th century, which presents with

Parkinson's disease-like symptoms. Mn neurotoxicity has been attributed to impaired dopaminergic, glutamatergic and GABAergic neurotransmission, disruption of mitochondrial function leading to oxidative stress and neuroinflammation. Preferential accumulation of Mn in dopaminergic cells of the basal ganglia, in particular the globus pallidus, results in the extrapyramidal motor dysfunction characteristic of manganism. Causes of Mn toxicity include occupational and environmental exposures as well as mutations in the SLC30A10 gene, recently identified as a Mn transporter in humans. Current treatment strategies combine chelation therapy and iron supplementation, the latter to reduce Mn binding to proteins that interact with both Mn and Fe.

### 1.3.4.3 Iron and Copper Toxicity

Both iron and copper are characterised by genetic disorders associated with accumulation of the metal in particular tissues, resulting in toxic consequences. There are two classic disorders of Cu metabolism, which are both caused by defective copper transporting ATPases.<sup>53–55</sup> Menkes disease is an X-chromosome linked fatal neurodegenerative disorder of childhood characterised by massive copper deficiency.<sup>56</sup> In contrast, Wilson's disease (WD) is a chronic disease of brain and liver, accompanied by progressive neurological dysfunction, due to a disturbance of copper metabolism, with progressive accumulation of copper in the brain, liver, kidneys, and the cornea of the eye.

WD is caused by mutations in the ATP-driven copper transporter ATP7B,<sup>57</sup> which is expressed in various tissues, including liver and the central nervous system.<sup>58</sup> In the hepatocyte, copper is taken up *via* CTR1 (Figure 1.3), and

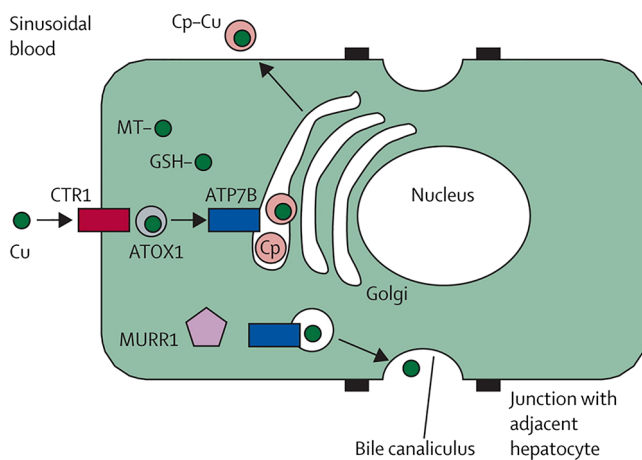


**Figure 1.3** Pathways of copper metabolism in the hepatocyte. Cu – copper. CTR1 – copper transporter 1. MT – metallothioneins. GSH – glutathione. Cp – ceruloplasmin. Reproduced from The Lancet, 369: 9559, Aftab Ala *et al.* Wilson's Disease, 397–408, Copyright 2007 with permission from Elsevier.

the  $\text{Cu}^+$  is delivered by the copper chaperone ATOX1 to ATP7B.<sup>59</sup> ATP7B then transports copper from the cytosol into the lumen of the *trans*-Golgi network (TGN) for incorporation into secreted copper-dependent enzymes, such as ceruloplasmin (Figure 1.4). In conditions of copper loading, it also transports copper into vesicles for export into bile.<sup>60</sup> This biliary excretion process involves another protein, COMMD1 (originally called MURR1), which interacts directly with ATP7B.<sup>61</sup>

In WD, ATP7B expression, function, and/or intracellular targeting are disrupted by mutations, resulting in impairment of both copper delivery to the trans Golgi network and copper excretion, causing copper to accumulate to very high levels in the liver. WD can be effectively treated, the aim of treatment is to reduce the amount of free copper. WD therapy has not really evolved over the last two decades and relies essentially on chelation therapy with copper chelators (penicillamine, trientine, and tetrathiomolybdate), zinc salts, or both.<sup>55</sup> Chelating agents bind copper directly in blood and tissues and facilitate its excretion, whereas zinc interferes with the intestinal uptake of copper. Early recognition of the disease by means of clinical, biochemical or genetic examination and initiation of therapy is essential for a favourable outcome. For WD patients who present with acute liver failure or end-stage cirrhosis, liver transplantation is the only effective treatment, see Chapter 4.

Iron overload is essentially due to genetic defects in iron absorption from the gastrointestinal tract.<sup>62,63</sup> Systemic iron homeostatic balance is regulated by hepcidin, a peptide released by the liver that binds to the iron exporter

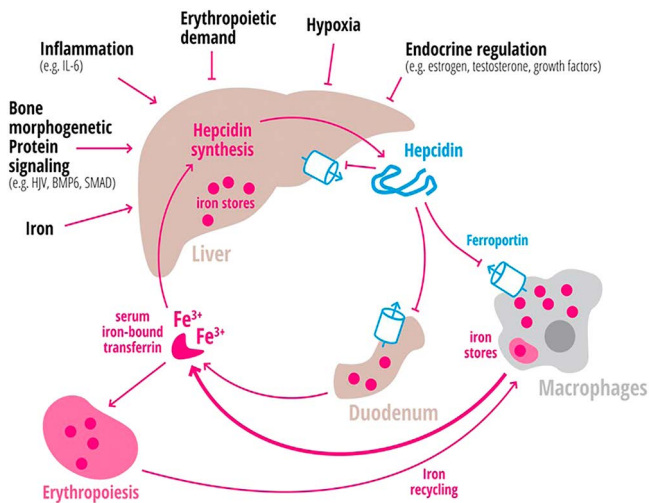


**Figure 1.4** Regulation of hepatic hepcidin production. Transferrin-iron is a critical indicator for systemic iron homeostasis and a regulator of hepcidin expression. Reproduced from Steinbicker and Muckenthaler, 2013.<sup>64</sup> This is an open access article distributed under the *Creative Commons Attribution License*.

ferroportin, blocking the export of iron from intestinal cells, hepatocytes and macrophages when iron is in excess, and permitting its export from these same cells when iron is in short supply. Hepatic hepcidin synthesis is regulated by iron, bone morphogenetic protein signaling, inflammation, erythropoiesis, hypoxia, or endocrine stimuli (Figure 1.4). FPN1, which is expressed predominantly in hepatocytes, macrophages and enterocytes is internalized and degraded following hepcidin binding.

Thus, there will be two major classes of disease resulting from disequilibrium of hepcidin synthesis: anaemia and iron loading. Elevated levels of hepcidin will decrease ferroportin expression, trap iron within enterocytes, hepatocytes and macrophages, and decrease gut iron absorption resulting in iron deficiency. In contrast, inappropriately low levels of hepcidin will result in uncontrolled expression of ferroportin, increasing iron absorption from the gut and its release from hepatocytes and macrophages, causing iron overload. This is what we see in hereditary haemochromatosis (HH), which will not be considered here since its therapy involves venesection, but also in secondary haemochromatosis resulting from genetic dysfunction of erythropoiesis, which clearly requires chelation therapy and is described in Chapter 4.

#### 1.3.4.4 *Molybdenum Toxicity*

The last of the essential transition metal ions, molybdenum, is present within the pterin-based molybdenum cofactor (Moco) in the active site of four mammalian enzymes and, while there is a large literature concerning the frequently fatal consequences of Mo deficiency, cases of Mo toxicity are much rarer.<sup>64</sup> Epidemiological studies suggest that living near mountaintop coal mining activities is one of the contributing factors for high lung cancer incidence. A recent study established the long-term carcinogenic potential of molybdenum, the main inorganic chemical constituent of MTM particulate matter.<sup>65</sup>

## 1.4 Non-Essential Metals

The toxicity of heavy metals is one of the oldest environmental problems and remains a serious health concern today. But what exactly are these heavy metals? Consulting any database for 'heavy metal' one might rapidly conclude that it concerns the development of a particular form of hard rock music characterised by a massive, highly amplified, distorted and very loud sound with aggressive male chauvinist lyrics. Alternatively, heavy metals used to be defined as dense metals or metalloids, which were potentially toxic, notably in an environmental context—typical heavy metals are cadmium (Cd), lead (Pb), mercury (Hg), and arsenic (As). We prefer to designate the 'heavy metals' as non-essential toxic metals, and we will devote most of our attention to Cd and Pb, Hg and As, although we will encounter a few others along the way. These will include chromium, thalium, and,

why not, aluminium, implicated in Alzheimer's disease—the curse of our ageing population. Then again, there is the silent menace posed by radio-nuclides, when something as disastrous as Chernobyl, Three Mile Island or Fukushima occurs, not forgetting polonium-210, hitting the headlines very publicly when it was used to poison the Russian dissident Alexander Litvinchenko in London in a very English cup of tea. Their selective chelation is dealt with in Chapter 6.

We will not consider here non-essential metal ions that are employed in therapy, such as Pt and Ru derivatives in cancer treatment, Li for manic depression or Au for rheumatoid arthritis, nor those such as Gd derivatives used as MRI contrast agents—their potential toxicity is the price we are prepared to pay for their therapeutic or diagnostic value.

## 1.5 Toxicity Due to Non-Essential Metals

### 1.5.1 Lead

Thirty years ago, Jerome Nriagu argued in a paper,<sup>66</sup> which was widely discussed in the press at the time, that Roman civilization collapsed as a result of chronic lead poisoning (saturnism). We are now acutely aware that saturnism is a major cause of environmental concern, although the Roman world was clearly unaware of these risks. However, whereas lead is no longer seen as the prime culprit of the Fall of Rome, a recent study<sup>67</sup> has shown that, nonetheless, “tap water” from ancient Rome had 100 times more Pb than local spring waters. Pb toxicity affects several organ systems including the nervous, haematopoietic, renal, endocrine and skeletal systems. It causes behavioural and cognitive deficits during brain development in infants and young children, and there is growing evidence that exposure to Pb in early life may predispose to neurodegeneration later in life. Despite numerous global initiatives to reduce the use of Pb, Pb exposure remains a widespread problem,<sup>68,69</sup> particularly in the developing world. Even in the last decade, blood lead levels (BLL) in children living in Pb polluted areas of China, India and Egypt have exceeded the  $10 \mu\text{g dL}^{-1}$  level set in 1991, and subsequently reduced to zero by the US Disease Control and Prevention Centre, in 10–44% of tested children.<sup>70</sup>

Pb appears to target proteins that naturally bind calcium and zinc.<sup>71</sup> Examples of proteins that are targeted by lead include synaptotagmin, which acts as a calcium sensor in neurotransmission, and  $\delta$ -aminolaevulinate synthase (ALAD), the second enzyme in the haem biosynthetic pathway (Figure 1.5). Despite its size, lead ( $1.19 \text{ \AA}$ ) can substitute for calcium ( $0.99 \text{ \AA}$ ) in synaptotagmin and zinc ( $0.74 \text{ \AA}$ ) in ALAD. Human ALAD is activated by  $\text{Zn}^{2+}$  with a  $K_m$  of  $1.6 \text{ pM}$  and inhibited by  $\text{Pb}^{2+}$  with a  $K_i$  of  $0.07 \text{ pM}$ .  $\text{Pb}^{2+}$  and  $\text{Zn}^{2+}$  appear to compete for a single metal binding site.<sup>72</sup> Like Mn, Pb causes presynaptic dysfunction but, in contrast to Mn, which affects the dopaminergic system,  $\text{Pb}^{2+}$  appears to interfere with hippocampal glutamatergic neurotransmission.<sup>73</sup>

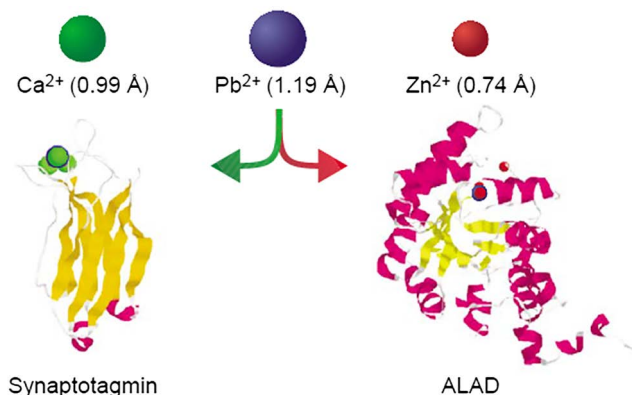


**Figure 1.5** Lead can substitute for calcium in synaptotagmin and zinc in  $\delta$ -amino-laevulinate synthase (ALAD). Reproduced from Current Opinion in Chemical Biology, 5, 2, Hilary Arnold Godwin, The biological chemistry of lead, 223–227, Copyright 2001 with permission from Elsevier.

### 1.5.2 Cadmium

$\text{Cd}^{2+}$ , a soft Lewis acid with a preference for easily oxidized soft ligands, particularly sulphur, can displace  $\text{Zn}^{2+}$  from proteins where the Zn coordination environment is sulphur dominated, while, on account of the similarity of its ionic radius with that of  $\text{Ca}^{2+}$ , it can exchange with  $\text{Ca}^{2+}$  in calcium-binding proteins.<sup>74</sup> Both  $\text{Zn}^{2+}$  and  $\text{Cd}^{2+}$  induce the iron export protein ferroportin (FPN1) transcription through the action of Metal Transcription Factor-1 (MTF-1)<sup>75</sup> and it has recently been shown that both  $\text{Zn}^{2+}$  and  $\text{Cd}^{2+}$  are transported by FPN1.<sup>76</sup>  $\text{Cd}^{2+}$  bioavailability and retention is favoured by poor iron status.

Cadmium occurs in the environment naturally and as a pollutant emanating from industrial and agricultural sources. Exposure to cadmium in the non-smoking population occurs primarily through food, and chronic exposure results in respiratory disease, emphysema, renal failure, bone disorders and immuno-suppression.<sup>77</sup> Recent data also suggest increased cancer risks and increased mortality in environmentally exposed populations.<sup>78</sup> At the cellular level,  $\text{Cd}^{2+}$  affects proliferation, differentiation and causes apoptosis. However, since  $\text{Cd}^{2+}$  is not redox active, the generation of reactive oxygen species (ROS) and DNA damage must be due to indirect effects. Recent studies indicate that Cd is able to induce various epigenetic changes,<sup>79,80</sup> such as DNA methylation, histone modification, and non-coding RNA expression. It also modulates gene expression and signal transduction, reduces the activities of proteins involved in antioxidant defences, and interferes with DNA repair, see Chapter 3.

The most commonly used therapeutic strategy for heavy metal poisoning is chelation therapy to promote metal excretion. Chelators such as  $\text{CaNa}_2\text{EDTA}$  and *meso*-2,3-dimercaptosuccinic acid (DMSA) have been reported to have protective effects against Cd toxicity.<sup>81,82</sup>

### 1.5.3 Mercury

The brutal reality of mercury toxicity was highlighted in 1956 by an environmental disaster that struck the population of Minamata, Japan and its surroundings; we now refer to mercury toxicity as Minamata disease.<sup>83</sup> Of the 2265 victims officially recognised by March 2001, 1784 died. This neurological syndrome is caused by severe mercury poisoning with symptoms including ataxia, numbness in the hands and feet, general muscle weakness, narrowing of the field of vision and damage to hearing and speech. As we point out later, it was only in 2004 that the chemical company responsible for the pollution was obliged to clean up its contamination.

Of the three biological forms of Hg: organic mercury (predominantly methyl mercury, MeHg), metallic mercury, and inorganic mercury compounds (principally mercuric chloride), MeHg was the one responsible for the Minamata hecatomb. MeHg is derived from the methylation of inorganic mercury in aquatic sediments and soils, is well absorbed from the diet and distributes within a few days to all tissues of the body. It is present as water-soluble complexes attached to thiol ligands, and crosses the blood–brain barrier as an MeHg–cysteine complex. The brain is the principal target tissue of MeHg and its major toxic effects are on the central nervous system, accumulating particularly in astrocytes. While it might be expected that the biochemical targets of Hg would be thiol groups of SH-dependent enzymes, it turns out that selenocysteine has a much higher affinity for Hg than cysteine. In reality, while Se can act as an effective blocker of Hg toxicity, the biological effects of Hg are much more direct.<sup>84</sup> Selenoenzymes, in particular glutathione peroxidase, thioredoxin reductase and thioredoxin glutathione reductase, are required to prevent and reverse oxidative damage in the brain and neuroendocrine system,<sup>85</sup> and these enzymes themselves are vulnerable to irreversible inhibition by methyl mercury (MeHg).<sup>86</sup> Selenoenzyme inhibition appears likely to cause most if not all of the pathological effects of mercury toxicity, as outlined in Figure 1.6. A simplified portrayal of the normal cycle of selenoprotein synthesis is depicted on the left. Disruption of this cycle by exposure to toxic quantities of Hg (MeHg) is depicted on the right. Selenide freed during selenoprotein breakdown becomes bound to Hg, forming HgSe that accumulates in cellular lysosomes. If Hg is present in stoichiometric excess, formation of insoluble Hg selenides abolishes the bioavailability of Se for protein synthesis and results in loss of normal physiological functions that require selenoenzyme activities, see Chapter 3.<sup>86</sup>

### 1.5.4 Aluminium

Al<sup>3+</sup>, although the most abundant metal in the Earth's crust, has been excluded from biological systems, essentially due to its lack of bioavailability. However, as we discuss later, several factors have increased the access of Al to the biosphere.<sup>87,88</sup> This enhanced bioavailability has

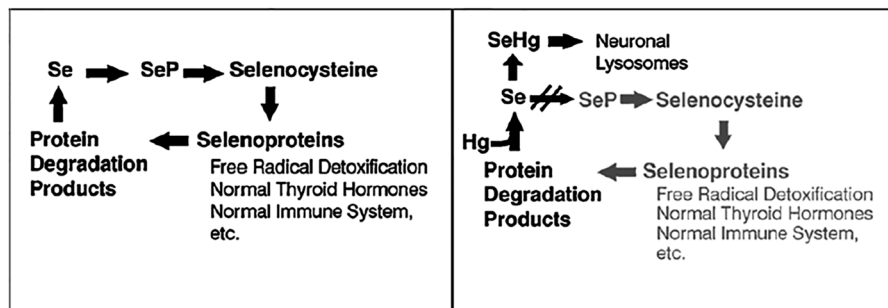


**Figure 1.6** Schematic of Se sequestration mechanism of Hg toxicity. A simplified portrayal of the normal cycle of selenoprotein synthesis is depicted on the left. Disruption of this cycle by exposure to toxic quantities of Hg (MeHg) is depicted on the right. Reproduced from Toxicology, 278, N. V. C. Ralston and L. J. Raymond, Dietary selenium's protective effects against methylmercury toxicity, 112–123, Copyright 2010 with permission from Elsevier.

resulted in the accumulation of the metal in living organisms including humans, particularly in the skeletal system, the liver, and the brain. The toxicity of  $\text{Al}^{3+}$  is associated with anaemia, osteomalacia, hepatic disorders, and certain neurological disorders, notably Alzheimer's disease.<sup>89</sup> These disorders can be the consequence of long term chronic exposure to the metal, for example, in dialysis patients where  $\text{Al}^{3+}$  has been used as a phosphate buffer.<sup>90</sup>

The molecular targets of Al toxicity involve disruption of the homeostasis of essential metal ions, notably Fe, Ca and Mg.<sup>91,92</sup> Al can replace Ca in the bone and interfere with Ca-based signalling events, while Mg binding to phosphate groups on cell membranes, ATP, and DNA can be replaced by Al. However, it is likely that the main targets of Al toxicity are Fe-dependent biological processes. As we pointed out earlier,  $\text{Al}^{3+}$  and  $\text{Ga}^{3+}$  both have coordination geometry similar to  $\text{Fe}^{3+}$ , which, in principle, should enable  $\text{Al}^{3+}$  to subvert the plasma iron transport pathway. Although  $\text{Al}^{3+}$  has a lower affinity for transferrin (Tf) than  $\text{Fe}^{3+}$ ,  $\text{Al}^{3+}$  can indeed bind to transferrin,<sup>93</sup> as illustrated in Figure 1.7 in the structure of  $\text{Al}^{3+}$ -transferrin.<sup>94</sup> However, no interaction between  $\text{TfAl}_2$  and TfR is detectable in *in vitro* binding studies.<sup>95</sup> In the cytosol,  $\text{Al}^{3+}$  is unlikely to be incorporated into ferritin, which requires redox cycling between  $\text{Fe}^{2+}$  and  $\text{Fe}^{3+}$ . It seems likely that most aluminium accumulates in mitochondria, where it can interfere with  $\text{Ca}^{2+}$  homeostasis.

Regardless of the pathway by which it gains access to cells,  $\text{Al}^{3+}$  exerts many of its toxic effects by interfering with iron homeostasis, generating oxidative stress (Figure 1.8). Free Fe within the cell produces ROS through Fenton chemistry, which then interfere with numerous cellular constituents including lipids, protein, and nucleic acids.

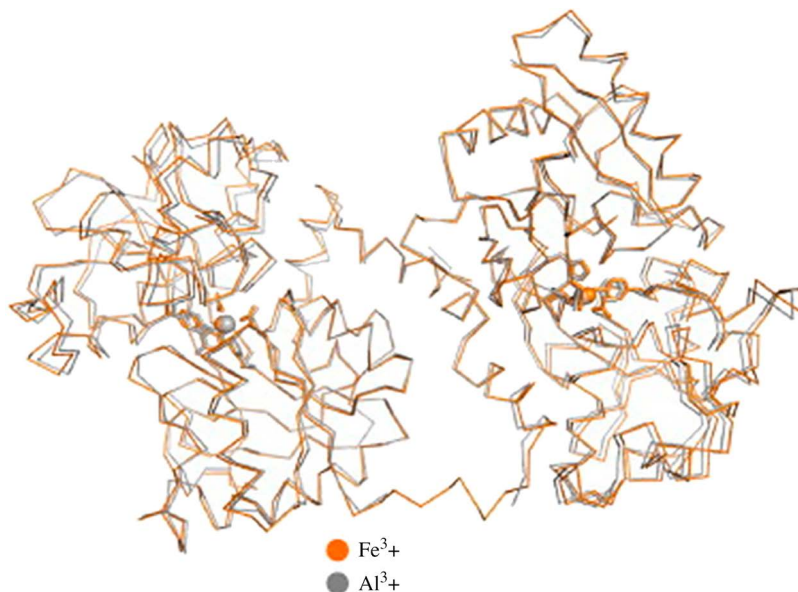


**Figure 1.7** Aluminum-bound ovotransferrin (PDB: 2D3I) and iron-bound ovotransferrin (PDB: 1OVT) are shown in gray and orange, respectively. Aluminium and iron are shown as gray and orange spheres, respectively. Metal binding sites and bound carbonate anion of both forms are shown as stick models. Reproduced from *Biochimica et Biophysica Acta (BBA) – General Subjects*, 1820, K. Mizutani *et al.*, X-ray structures of transferrins and related proteins, 203–211, Copyright 2012 with permission from Elsevier.

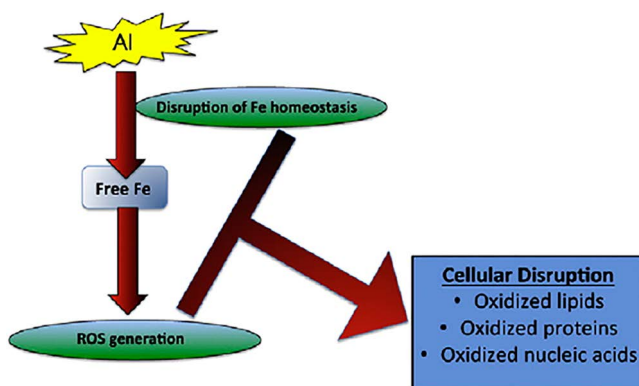


**Figure 1.8** Al toxicity leads to defective Fe homeostasis and oxidative stress. Reproduced from *Journal of Inorganic Biochemistry*, 105, J. Lemire and V. D. Appanna, Aluminium toxicity and astrocyte dysfunction: A metabolic link to neurological disorders, 1513–1517, Copyright 2011 with permission from Elsevier.

## 1.6 Sources and Routes of Exposure with Particular Reference to Non-Essential Metals

Sources of low-level environmental exposure to Pb, in addition to water from lead pipes, include lead-based paint and household dust from surfaces covered with such paints, and Pb in air and food. The main routes for Pb are inhalation and ingestion, with inhalation being the more efficient route of absorption. Since Pb can adsorb onto particulate matter and thus be inhaled, the removal of the Pb<sup>4+</sup>-derived anti-knock agent (tetraethyl lead), which was commonly added to petrol to improve automotive engine efficiency, has greatly reduced blood Pb levels in the urban population.

Minamata disease was caused by the release of methyl mercury in the industrial wastewater from a chemical factory, where it bioaccumulated in aquatic food chains reaching its highest concentrations in shellfish and fish which, when eaten by the local population, resulted in mercury poisoning. In 1956 symptoms such as sensory disturbance in the distal portions of all extremities, partial paralysis, cerebellar ataxia, bilateral concentric contraction of the visual field, disturbed ocular movement, impairment of hearing and equilibrium disturbance were exhibited in increasing numbers of persons, including newborns. The disease, later described as “Minamata disease”, affected mainly local fishermen and their families. Fish-eating animals in the area (cats and seagulls) had similar neurological signs and led to the identification of an obvious heavy metal intoxication. However, it took several years to show the connection to a chemical factory that, for 36 years until 1968, discarded about 30 t of methyl mercury-associated waste into the Minamata Bay. MeHg present in fish and shellfish from the Bay was consumed in the surrounding area led to the various symptoms. As of March 2001, 2665 victims had been officially recognised as having Minamata disease (1784 of whom have died).

The second severe epidemic of methyl mercury poisoning happened in Iraq in 1972 and arose from the consumption of mercury-contaminated bread. This was the result of baking bread from wheat seed that had been treated with a mercury-based fungicide and was not supposed to have been planted.<sup>86</sup> As a result, about 7000 people were affected and 460 died from mercury poisoning. Both the Japanese and Iraq methyl mercury poisoning incidents produced not only deaths, but also multiple and long-lasting symptoms, mainly in children and newborns, that included blindness, deafness, mental retardation, and cerebral palsy.

Asia is today the largest contributor of anthropogenic atmospheric mercury (Hg), accounting for over half of global emissions, with serious Hg pollutions to the local environment influenced principally by the chemical industry and by mining of gold and mercury. Studies have shown that in humans and selected Arctic marine mammals and birds of prey there has been an order of magnitude increase in Hg that began in the mid to late 19th century and accelerated in the 20th century. The man-made contribution to present day Hg concentrations is estimated at 92%.

There are several factors that account for the increased access of  $\text{Al}^{3+}$  to the biosphere. Firstly, an increase in anthropogenic acidification of soils, due to acid rain generated by emissions of sulphur dioxide and nitrogen oxides in the atmosphere, has resulted in elevated concentrations of  $\text{Al}^{3+}$  in ground waters. On account of its lightness and corrosion resistance, aluminium is widely used for industrial purposes, from the aerospace industry to construction, from food packaging to pharmaceuticals. Aluminium salts are extensively utilised as a flocculent in water treatment.

$\text{Cd}^{2+}$  is a widespread environmental contaminant, with exposure largely *via* the respiratory or gastrointestinal tracts. The most important non-industrial sources of exposure are cigarette smoke and contaminated food and beverages.  $\text{Cd}^{2+}$  has a high rate of transfer from soil to plants, and certain plant species, including tobacco, rice, wheat, peanuts and cocoa accumulate large amounts of  $\text{Cd}^{2+}$  even from soils with a low  $\text{Cd}^{2+}$  content. In Europe, the highest levels of  $\text{Cd}^{2+}$  were found in topsoil soon after the distribution of  $\text{P}_2\text{O}_5$ , suggesting that the soil contamination is derived from the use of rock phosphate fertiliser in intensive arable agriculture. The effects of chronic oral ingestion of  $\text{Cd}^{2+}$  first manifested themselves in the form of Itai–itai disease among the inhabitants of the Jinzu river basin in Toyama Prefecture, Japan. This was the first time that  $\text{Cd}^{2+}$  pollution was shown to have severe consequences for human health, particularly in women. The most important effects were softening of the bones and kidney failure, the name of the disease deriving from the painful screams caused by the excruciating pain in the joints and the spines of the victims. The cause of the disease was traced to environmental pollution originating in effluent from a zinc mine located in the upper reaches of the river (Figure 1.9). In the case of Itai–itai disease most of the  $\text{Cd}^{2+}$  ingested orally was derived from contaminated rice.

## 1.7 Conclusions

In this brief overview we have outlined the importance of metal toxicity involving both essential and non-essential metal ions. It is clear that excessive accumulation of either of these classes of metal ion can result in a variety of toxic effects. The objective of this volume in the RSC Metallobiology series is to provide a clear and up-to-date perspective on the therapeutic potential of chelating agents in the management of metal excess. Such chelating agents should, as far as possible, fulfil the following criteria: (i) display a degree of selectivity towards the metal ions that they are intended to remove (for example,  $\text{Fe}^{3+}$  can be chelated selectively relatively easily from other essential transition metal ions); (ii) access potential sites where chelation is desired; (iii) cause minimal, if possible zero, interference with essential biologically important metal ions and the metabolic processes in which they are involved; (iv) be excreted from the cellular site of chelation and subsequently eliminated from the body without causing toxic effects *en route* (e.g., nephrotoxicity).

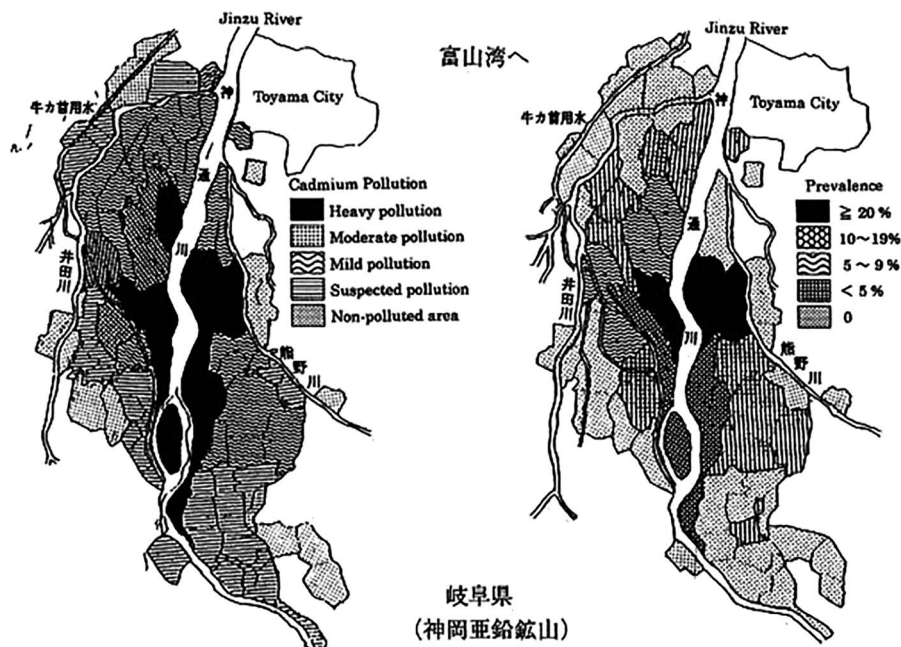


**Figure 1.9** Itai-itai disease. Left: the degree of Cd pollution in parts of the endemic area; right: prevalence of the disease in women over 50 years of age.

## Abbreviations

<b>AD</b>	Alzheimer's disease
<b>ALS</b>	Amyotrophic lateral sclerosis
<b>BLL</b>	Blood lead levels
<b>HH</b>	Hereditary haemochromatosis
<b>MR (MRI)</b>	Magnetic resonance (imaging)
<b>ROS</b>	Reactive oxygen species
<b>WD</b>	Wilson's disease

## References

1. G. F. Nordberg, B. A. Fowler, M. Nordberg and N. T. Friberg, *Handbook on the Toxicology of Metals*, Elsevier, 3rd edn, 2007.
2. R. R. Crichton, *Biological Inorganic Chemistry. A New Introduction to Molecular Structure and Function*, Elsevier, Amsterdam and Oxford, 2nd edn, 2012.
3. C. Andreini, I. Bertini and A. Rosato, *Bioinformatics*, 2009, **25**, 2088.
4. B. Dietrich, *J. Chem. Educ.*, 1985, **62**, 954.
5. E. Gouaux and R. Mackinnon, *Science*, 2005, **310**, 1461.
6. D. A. Doyle, J. Morais Cabral, R. A. Pfuetzner, A. Kuo, J. M. Gulbis, S. L. Cohen, B. T. Chait and R. MacKinnon, *Science*, 1998, **280**, 69.

7. J. Payandeh, T. Scheuer, N. Zheng and W. A. Catterall, *Nature*, 2011, **356**, 353.
8. Y. Zhou, J. H. Morais-Cabral, A. Kaufman and R. Mackinnon, *Nature*, 2001, **414**, 43.
9. B. Corry and M. Thomas, *J. Am. Chem. Soc.*, 2012, **134**, 1840.
10. M. M. Braun, C. H. Barstow and N. J. Pyzocha, *Am. Fam. Physician*, 2015, **91**, 299.
11. M. K. Shah, B. Workeneh and G. E. Taffet, *Clin. Interventions Aging*, 2014, **19**, 1987.
12. P. A. McCullough, M. R. Costanzo, M. Silver, B. Spinowitz, J. Zhang and N. E. Lepor, *Rev. Cardiovasc. Med.*, 2015, **16**, 140.
13. D. K. Packham and M. Kosiborod, *Am. J. Cardiovasc. Drugs*, 2015, **16**, 19.
14. C. P. Kovesdy, *Am. J. Med.*, 2015, DOI: 10.1016/s0002-s9343(15)00541-0.
15. L. Tang, T. M. Gamal El-Din, J. Payandeh, G. Q. Martinez, T. M. Heard, T. Scheuer, N. Zheng and W. A. Catterall, *Nature*, 2014, **505**, 56.
16. J. Payandeh, R. Pfoh and E. F. Pai, *Biochim. Biophys. Acta*, 2013, **1828**, 2778.
17. S. M. Moe, *Primary Care*, 2008, **35**, 215.
18. E. J. Hoorn and R. Zietse, *Pediatr. Nephrol.*, 2013, **28**, 1195.
19. M. C. Machado, A. Bruce-Mensah, M. Whitmire and A. A. Rizvi, *J. Clin. Med.*, 2015, **4**, 414.
20. A. M. Patel, G. A. Adeseun and S. Goldfarb, *Nutrients*, 2013, **5**, 4880.
21. A. Fountas, M. Andrikoula, Z. Giotaki, C. Limniati, E. Tsakiridou, S. Tigas and A. Tsatsoulis, *Endocr. Pract.*, 2015, **21**, 468.
22. A. Dietzek, K. Connelly, M. Cotugno, S. Bartel and A. M. McDonnell, *J. Oncol. Pharm. Pract.*, 2015, **21**, 143.
23. L. M. Plum, L. Rink and H. Haase, *Int. J. Environ. Res. Public Health*, 2010, **7**, 1342.
24. D. J. Lanska and B. Remler, *Neurology*, 2014, **82**, 1175.
25. B. P. Goodman, *Continuum*, 2015, **21**, 84.
26. C. J. Frederickson, S. W. Suh, D. Silva, C. J. Frederickson and R. B. Thompson, *J. Nutr.*, 2000, **130**, 1471S.
27. S. Ueno, M. Tsukamoto, T. Hirano, K. Kikuchi, M. K. Yamada, N. Nishiyama, T. Nagano, N. Matsuki and Y. Ikegaya, *J. Cell Biol.*, 2002, **158**, 215.
28. J. Ceccom, E. Bouhsira, H. Halley, S. Daumas and J. M. Lassalle, *Learn. Mem.*, 2013, **20**, 348.
29. X. Huang, M. P. Cuajungco, C. S. Atwood, R. D. Moir, R. E. Tanzi and A. I. Bush, *J. Nutr.*, 2000, **130**, 1488S.
30. A. I. Bush and R. E. Tanzi, *Neurotherapeutics*, 2008, **5**, 421.
31. S. L. Sensi, P. Paoletti, J. Y. Koh, E. Aizenman, A. I. Bush and M. Hershfinkel, *J. Neurosci.*, 2011, **31**, 16076.
32. C. W. Shuttleworth and J. H. Weiss, *Trends Pharmacol. Sci.*, 2011, **32**, 480.
33. B. R. Roberts, T. M. Ryan, A. I. Bush, C. L. Masters and J. A. Duce, *J. Neurochem.*, 2012, **120**, 149.
34. A. I. Bush, *J. Alzheimer's Dis.*, 2013, **33**, S277.
35. M. Kawahara, D. Mizuno, H. Koyama, K. Konoha, S. Ohkawara and Y. Sadakane, *Metallomics*, 2014, **6**, 209.

36. N. T. Watt and N. M. Hooper, *Trends Biochem. Sci.*, 2003, **28**, 406.
37. J. S. Valentine and P. J. Hart, *Proc. Natl. Acad. Sci. U. S. A.*, 2003, **100**, 3617.
38. X. V. Hu, X. Chen, K. C. Han, A. S. Mildvan and J. O. Liu, *Biochemistry*, 2007, **46**, 12833.
39. C. Giglione, A. Boularot and T. Meinel, *Cell. Mol. Life Sci.*, 2004, **61**, 1455.
40. W. T. Lowther and B. W. Matthews, *Chem. Rev.*, 2002, **102**, 4581.
41. L. O. Simonsen, H. Hrabak and P. Bennekou, *Sci. Total Environ.*, 2012, **432**, 210.
42. D. J. Pauschenbach, B. E. Tvermoes, K. M. Unice, B. L. Finley and B. D. Kerger, *Crit. Rev. Toxicol.*, 2013, **43**, 316.
43. S. M. Mohiuddin, P. K. Taskar, M. Rheault, P.-E. Roy, J. Chenard and Y. Morin, *Am. Heart J.*, 1970, **80**, 532.
44. P. Seghizzi, F. D'Adda, D. Borleri, F. Barbic and G. Mosconi, *Sci. Total Environ.*, 1994, **150**, 105.
45. H. Kesteloot, J. Roelandt, J. Willems, J. H. Claes and J. V. Joossens, *Circulation*, 1968, **37**, 854.
46. K. Tuschl, P. B. Mills and P. T. Clayton, *Int. Rev. Neurobiol.*, 2013, **110**, 277.
47. A. P. Neal and T. R. Guilarte, *Toxicol. Res. (Cambridge, U. K.)*, 2013, **1**, 99.
48. B. Michalke and K. Fernsebner, *J. Trace Elem. Med. Biol.*, 2014, **28**, 106.
49. K. Fernsebner, J. Zorn, B. Kanawati, A. Walker and B. Michalke, *Metallomics*, 2014, **6**, 921.
50. J. A. Roth, *Neurotoxicology*, 2014, **44**, 314.
51. P. Chen, S. Chakraborty, T. V. Peres, A. B. Bowman and M. Aschner, *Toxicol. Res. (Cambridge, U. K.)*, 2015, **4**, 191.
52. S. L. O'Neal and W. Zheng, *Curr. Environ. Health Rep.*, 2015, **2**, 315.
53. E. Madsen and J. D. Gitlin, *Annu. Rev. Neurosci.*, 2007, **30**, 317.
54. A. Ala, A. P. Walker, K. Ashkan, J. S. Dooley and M. L. Schilsky, *Lancet*, 2007, **369**, 397.
55. O. Bandmann, K. H. Weiss and S. G. Kaler, *Lancet Neurol.*, 2015, **14**, 103.
56. J. H. Menkes, M. Alter, G. K. Steigleder, D. R. Weakley and J. H. Sung, *Pediatrics*, 1962, **29**, 764.
57. S. K. Das and K. Ray, *Nat. Clin. Pract. Neurol.*, 2006, **2**, 482.
58. S. Lutsenko, N. L. Barnes, M. Y. Bartee and O. Y. Dmitriev, *Physiol. Rev.*, 2007, **87**, 1011.
59. M. Y. Bartee and S. Lutsenko, *Biometals*, 2007, **20**, 627.
60. E. M. van Dongen, L. W. Klomp and M. Merckx, *Biochem. Biophys. Res. Commun.*, 2004, **323**, 789.
61. T. Y. Tao, F. Liu, L. Klomp, C. Wijmenga and J. D. Gitlin, *J. Biol. Chem.*, 2003, **278**, 41593.
62. R. R. Crichton, *Iron Metabolism. From Molecular Mechanisms to clinical Consequences*, John Wiley & Sons, Chichester, 4th edn, 2016.
63. A. U. Steinbicker and M. U. Muckenthaler, *Nutrients*, 2013, **5**, 3034.
64. G. Schwarz and A. A. Belaidi, *Met. Ions Life Sci.*, 2013, **13**, 415.
65. S. Luanpitpong, M. Chen, T. Knuckles, S. Wen, J. Luo, E. Ellis, M. Hendryx and Y. Rojanasakul, *Environ. Sci. Technol.*, 2014, **48**, 12912.
66. J. O. Nriagu, *N. Engl. J. Med.*, 1983, **308**, 660.

67. H. Delile, J. Blichert-Toft, J. P. Goiran, S. Keay and F. Albarède, *Proc. Natl. Acad. Sci. U. S. A.*, 2014, **111**, 6594.
68. P. A. Meyer, M. J. Brown and H. Falk, *Mutat. Res.*, 2008, **659**, 166.
69. A. C. Callan and A. L. Hinwood, *Rev. Environ. Health*, 2011, **26**, 13.
70. Q. Zhai, A. Narbad and W. Chen, *Nutrients*, 2015, **7**, 552.
71. H. A. Godwin, *Curr. Opin. Chem. Biol.*, 2001, **5**, 223.
72. T. J. B. Simons, *Eur. J. Biochem.*, 1995, **234**, 178.
73. A. P. Neal, K. H. Stansfield, P. F. Worley, R. E. Thompson and T. R. Guilarte, *Toxicol. Sci.*, 2010, **116**, 249.
74. J.-M. Moulis, *Biometals*, 2010, **23**, 877.
75. M. B. Troadec, D. M. Ward, E. Lo, J. Kaplan and I. De Domenico, *Blood*, 2010, **116**, 4657.
76. C. J. Mitchell, A. Shawki, T. Ganz, E. Nemeth and B. Mackenzie, *Am. J. Physiol.: Cell Physiol.*, 2014, **306**, C450.
77. L. Järup and A. Akesson, *Toxicol. Appl. Pharmacol.*, 2009, **238**, 201.
78. A. R. Nair, O. Degheselle, K. Smeets, E. Van Kerckhove and A. Cuypers, *Int. J. Mol. Sci.*, 2013, **14**, 6116.
79. B. Wang, Y. Li, C. Shao, Y. Tan and L. Cai, *Curr. Med. Chem.*, 2012, **19**, 2611.
80. J. Luevano and C. Damodaran, *J. Environ. Pathol., Toxicol. Oncol.*, 2014, **33**, 183.
81. S. W. Smith, *J. Med. Toxicol.*, 2013, **9**, 355.
82. R. A. Bernhoft, *Sci. World J.*, 2013, 394652, DOI: 10.1155/2013/394652.
83. K. Eto, *Neuropathology*, 2000, **20**, S14.
84. N. V. C. Ralston and L. J. Raymond, *Toxicology*, 2010, **278**, 112.
85. H. Steinbrenner and H. Sies, *Arch. Biochem. Biophys.*, 2013, **536**, 152.
86. N. V. C. Ralston and L. J. Raymond, *Toxicology*, 2010, **278**, 112.
87. M. Kawahara, T. Nagata and Y. Sadakane, *Biomed. Res. Trace Elem.*, 2007, **18**, 211.
88. M. Gomez, J. L. Esparza, M. Cabre, T. Garcia and J. L. Domingo, *Toxicology*, 2008, **249**, 214.
89. R. J. Mailloux, J. Lemire and V. D. Appanna, *Exp. Cell Res.*, 2011, **16**, 2231.
90. S. V. Verstraeten, L. Aimo and P. I. Oteiza, *Arch. Toxicol.*, 2008, **82**, 789.
91. R. J. Mailloux, J. Lemire and V. D. Appanna, *Exp. Cell Res.*, 2011, **317**, 2231.
92. J. Lemire and V. D. Appanna, *J. Inorg. Biochem.*, 2011, **105**, 1013.
93. J. B. Vincent and S. Love, *Biochim. Biophys. Acta*, 2012, **1820**, 362.
94. K. Mizutani, M. Toyoda and B. Mikami, *Biochim. Biophys. Acta*, 2012, **1820**, 203.
95. J. M. El Hage Chahine, M. Hémadi and N. T. Ha-Duong, *Biochim. Biophys. Acta*, 2012, **1820**, 334.

## CHAPTER 2

# *Basic Principles of Metal Chelation and Chelator Design*

ROBERT C. HIDER\*<sup>a</sup> AND YONGMIN MA<sup>b</sup>

<sup>a</sup>Institute of Pharmaceutical Science, King's College London, UK;

<sup>b</sup>Zhejiang Chinese Medical University, Hangzhou, China

\*E-mail: [Robert.hider@kcl.ac.uk](mailto:Robert.hider@kcl.ac.uk)

## 2.1 Introduction

Metals that have an influence on biological systems fall into five general classes (Table 2.1). Group I and II metals, for instance sodium and calcium, are present in relatively large amounts, whereas many of the transition metals, for example cobalt and nickel, are only present in trace amounts. Toxic metals are typically “heavy metals” such as lead and mercury. Radioisotopes are another group and have important roles in medical imaging and radiotherapy. Metals can also form an essential component of many widely used pharmaceuticals. The Group I and II metals are highly solvated by water and are recognised by cells as positive charges of differing radius and charge density. For this reason they are mainly used to create membrane potentials (Na and K) and for signaling (Ca), although Mg is often utilised as a coenzyme, facilitating ternary complex formation with phosphate-containing substrates (see Chapter 1). Trace metals mainly function as coenzymes, for instance zinc behaves as a Lewis acid and iron and copper as redox active metals.<sup>1</sup> Toxic metals are typically those metals which bind to enzymes at coenzyme binding sites, failing to function as the normal metal occupant; for example, Al

---

RSC Metallobiology Series No. 8

Metal Chelation in Medicine

Edited by Robert Crichton, Roberta J. Ward and Robert C. Hider

© The Royal Society of Chemistry 2017

Published by the Royal Society of Chemistry, [www.rsc.org](http://www.rsc.org)

**Table 2.1** Metals that influence biological systems.

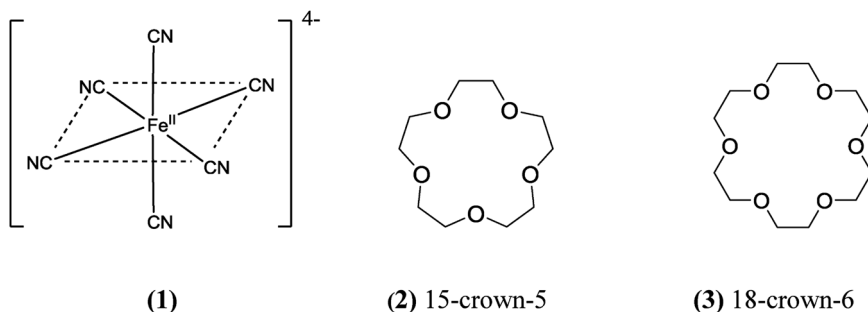
General classification	Metals	Function in cells	Applications
Bulk metals (Gp. I and Gp. II metals.)	Na, K, Mg, Ca	Control tonicity of solution Control membrane potentials Signaling	Calcium supplements and bone formation
Trace metals (transition metals)	Mn, Fe, Co, Ni, Cu, Zn, Mo	Enzyme cofactors (Mg) Signaling (Fe and Zn) Enzyme cofactors Redox centres in respiratory chains (Cu and Fe)	Regularly formulated for treatment of anaemia and zinc deficiency
Toxic metals (Gp. III and heavy metals)	Al, Cd, Sn, Pb, Hg, U, Pu	Bind to enzyme metal cofactor sites	
Metals used for imaging and radiotherapy	Gd, Ga, In, Tc, Re, Y		Complexes used in nuclear medicine
Metals used for chemotherapy	Pt, Au, Mn, Bi		Complexes used as prescribed pharmaceuticals

binds to Fe sites on transferrin and Cd binds to Zn sites on metallothionein.<sup>2</sup> Essential metals can be toxic if they are present at higher than normal levels for instance iron  $>10^{-5}$  M, zinc and copper  $>10^{-9}$  M and nickel and cobalt  $>10^{-10}$  M. Many non-essential metal ions are poisonous at almost any concentration *e.g.*  $\text{As}^{3+}$ ,  $\text{Hg}^{2+}$ ,  $\text{Pb}^{2+}$  and  $\text{Ag}^+$ .<sup>3</sup> A wide range of xenobiotic metals are used in medicine for imaging, radiotherapy and chemotherapy (Table 2.1).

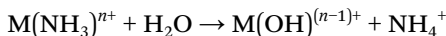
All metals form complexes with molecules which possess electron rich centres, such as  $\text{H}_2\text{O}$ ,  $-\text{NH}_2$  and  $-\text{CO}_2^-$ , which can donate electrons to positively charged species such as transition metal ions. Such molecules are called ligands. A classic example of a metal complex is potassium hexacyanoferrate(II),  $[\text{K}_4\text{Fe}(\text{CN})_6]$  **1**. This is prepared by mixing colourless KCN with colourless  $\text{Fe}^{\text{II}}(\text{CN})_2$ , whereupon the brown-yellow  $\text{K}_4\text{Fe}(\text{CN})_6$  is formed, which lacks the lethal properties of KCN. Werner originally explained such phenomena on the basis that metals possess two types of valency: primary which is ionic and secondary which is covalent.<sup>4</sup> Most metals possess a fixed number of secondary valencies, called the coordination number; for iron(II) this is 6 and for copper(II) this is typically 4. Secondary valencies are directional in nature; 6 pointing to the corners of an octahedron and 4 pointing either to the corners of a tetrahedron or a square. These shapes are directed by the d orbitals of the metal. The metal and all its secondary valency ligands are written inside square brackets *e.g.*  $[\text{Fe}(\text{CN})_6]^{4-}$ . This species ionizes as an intact anion **1** and shows none of the properties of its component ions (*i.e.* the tests for  $\text{Fe}^{2+}$  and  $\text{CN}^-$  are negative). The anion **1** has a net charge of  $4^-$  ( $\text{Fe}^{2+}$  and  $6\text{CN}^-$ ) and so is associated with 4 positive ions in Werner's complex,  $\text{K}_4\text{Fe}(\text{CN})_6$ .

## 2.2 Ligand Chemistry

Donor atoms such as O, N, P and S are the most commonly encountered non metals in ligands. In this section, we focus on O and N as donor atoms, as these are the most frequently found coordinating atoms in clinically useful chelators. The neutral oxygen donor atom is of little interest because crown ethers **2** and **3**, for instance, do not compete efficiently with water for metal complex formation and thus the affinity of such ligands for metal cations is generally weak. However many ligands contain negatively charged oxygen donors with widely differing basicities, such as carboxylate, phenolate, hydroxamate, phosphonate and alkoxide (Figure 2.1). The simple dependence of  $\log K_{ML}$  on ligand  $pK_a$  is demonstrated for iron(III) in Figure 2.2. This results in a competition between protons and iron(III) cations for the negatively charged ligands. Under strong acid conditions protons tend to dominate the competition and displace the coordinated metal. The affinities of metal ions for ligands containing negatively charged oxygen donor atoms are strongly related to their affinity for the hydroxide anion (Figure 2.3A). As the charge density of the cation increases ( $Z/r^2$ ), so does the affinity for the charged oxygen donor ligands.<sup>5</sup>

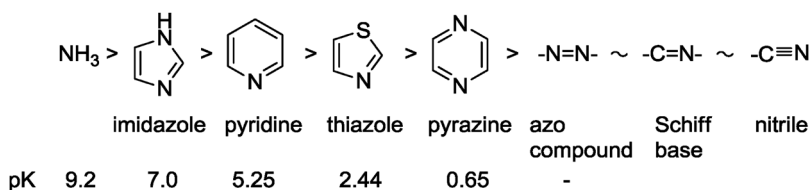


Nitrogen donors can also be separated into two groups, namely those containing either saturated or unsaturated nitrogen donors. Ammonia is a typical saturated nitrogen donor, as are the alkylamines ( $RNH_2$ ). A particular problem with ammonia is that most metal ions do not form stable ammonia complexes in aqueous solution as they favor the reaction:



Thus when ammonia is added to metal ions such as  $Fe^{3+}$  in aqueous solution, only the metal hydroxide is obtained.

The order of basicity of some nitrogen donors in water is given in the series:



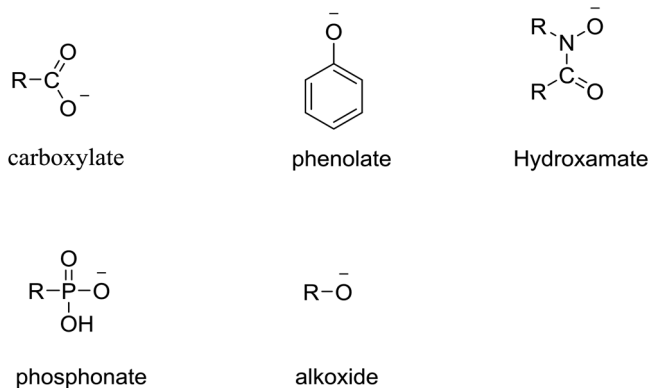


**Figure 2.1** Charged oxygen ligands.

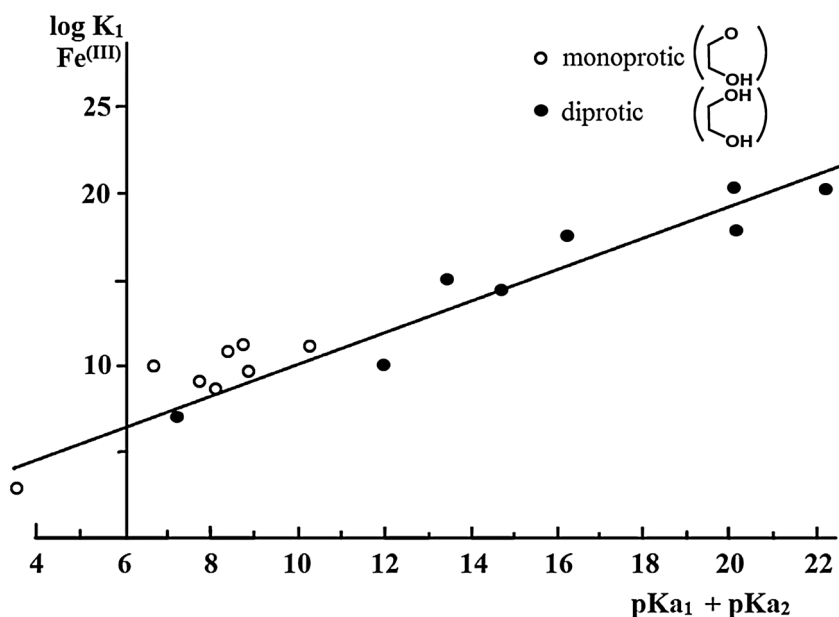


**Figure 2.2** Relationship between  $\log K_1$  values for iron(III) complexes with  $\Sigma pK_{a1}$  and  $pK_{a2}$  for a range of mono- and diprotic oxygen-containing bidentate ligands.

The nitrogen in unsaturated ligands is either  $sp^2$  or  $sp$  hybridized, which leads to a greater 's' contribution in the orbitals used for bonding to the metal ion, when compared to the  $sp^3$  hybridized nitrogen of ammonia or amines. These unsaturated ligands can exert high ligand field strengths, even though their proton basicity may be less than that of  $sp^3$  hybridized nitrogen. However, a common problem associated with heterocyclic aromatic bases such as pyridines, pyrazines and thiazoles is the steric hindrance to coordination

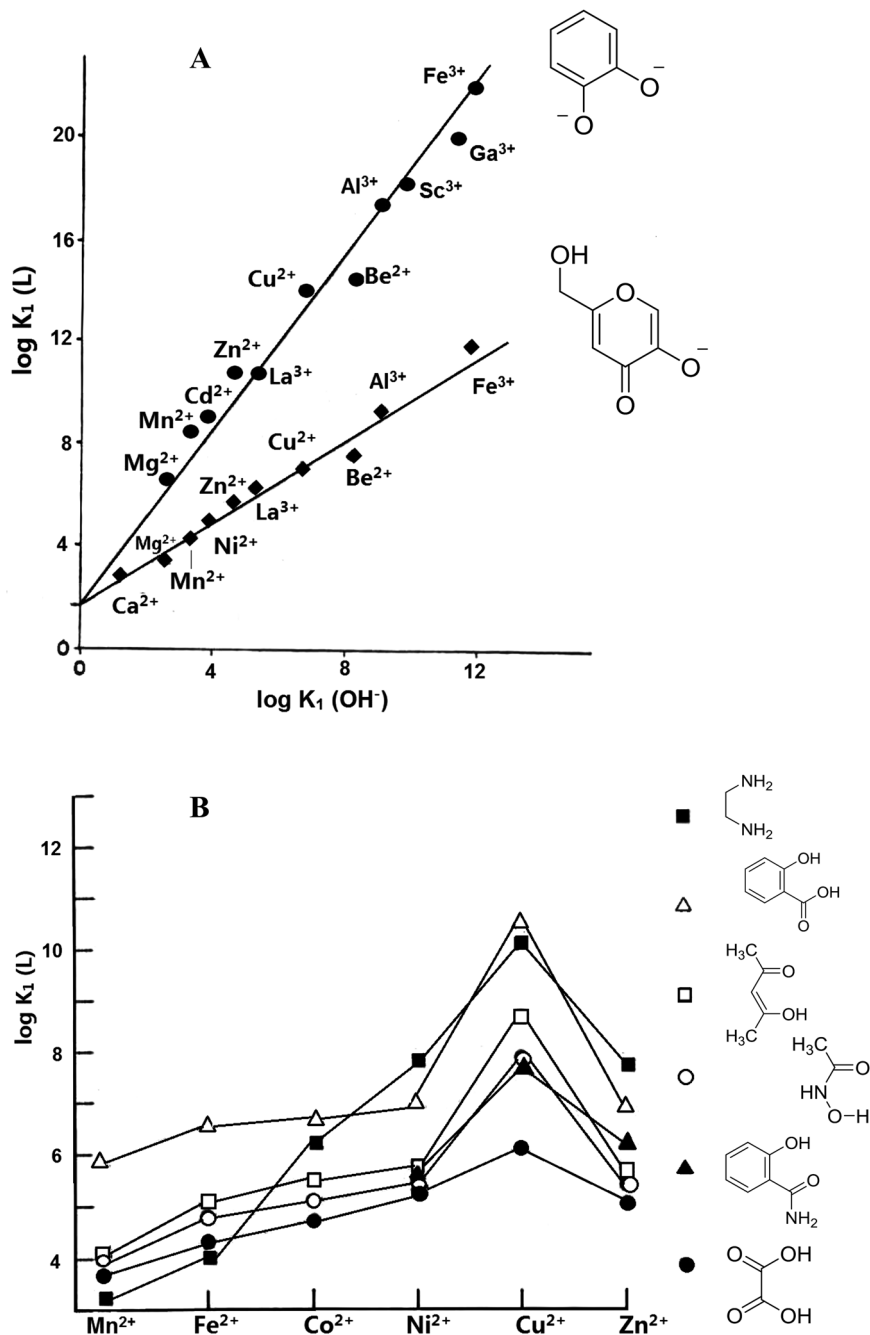
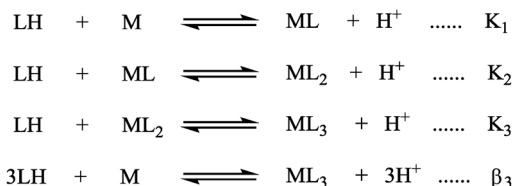


**Figure 2.3** (A) Relation between  $\log K_1$  for chelating ligands containing negative oxygen donors and  $\log K_1$  for the formation of the hydroxide complex, for a variety of metal ions. Adapted with permission from ref. 5. © Springer Science + Business Media New York 1996. (B) Affinity constants ( $K_1$ ) of the first row transition metals with a range of bidentate oxygen-containing ligands.

of metal ions caused by the hydrogens *ortho* to the nitrogen donors. These problems can be overcome by joining pyridyl and other groups to produce more sterically efficient bi- or multi-dentate ligands.<sup>5</sup>

The affinity of a metal for a ligand is measured by a series of equilibrium constants. For a bidentate ligand there are typically 3 different complexes ML, ML<sub>2</sub> and ML<sub>3</sub> and their respective affinity constants are related by the following equations:



Where  $\beta_3 = K_1 \times K_2 \times K_3$ .

### 2.3 Ligand Selectivity

In order to design metal chelators for clinical use, ligand selectivity and stability are two key parameters for consideration. The selection of an appropriate ligand for a given metal can be rationalized according to the theory of 'hard' and 'soft' acids and bases.<sup>6</sup> Soft metal ions prefer ligands with soft donor atoms, and hard metal ions prefer ligands with hard donor atoms. Basically, metal ions such as Ca(II), Mg(II), Al(III), Ga(III) and Fe(III) are considered as hard metal ions and, effectively, rigid spheres whereas Ag(I), Hg(II), Cu(I) ions are considered to be soft and deformable spheres of relatively low charge density. Some metal ions such as Mn(II), Fe(II), Co(II), Ni(II), Cu(II) and Zn(II) are on the borderline between the two classes. The most electronegative elements, such as F<sup>-</sup> or O<sup>-</sup>, form the hardest donor atoms and the less electronegative elements, such as P and N, are soft donors. Particular to iron, iron(II)-favored ligands usually contain "soft" donor atoms, exemplified by nitrogen-containing ligands such as 2,2'-bipyridyl and 1,10-phenanthroline (Figure 2.4). Although this type of ligand is selective for Fe(II) over Fe(III), they also have a high affinity for other biologically important bivalent metal ions such as Cu(II) and Zn(II) (Table 2.2). In contrast, high-spin Fe(III) is a tripositive cation of radius 0.65 Å and classified as a hard Lewis acid by virtue of its high charge density. Oxygen-containing ligands, such as catechols, hydroxamate and hydroxypyridinones (Figure 2.4), generally prefer tribasic metal cations over dibasic cations (Table 2.2). This type of ligand possesses a high affinity for Fe(III), Al(III) and Ga(III), but as Fe(III) is the only tribasic cation present in appreciable concentration in living cells, such ligands are effectively selective for Fe(III) over other biologically important metals. In addition, high-affinity Fe(III)-selective ligands will chelate Fe(II) under aerobic conditions and auto-oxidise the metal to Fe(III).<sup>8</sup> Thus, this type of ligand binds both Fe(III) and Fe(II) under most physiological conditions.

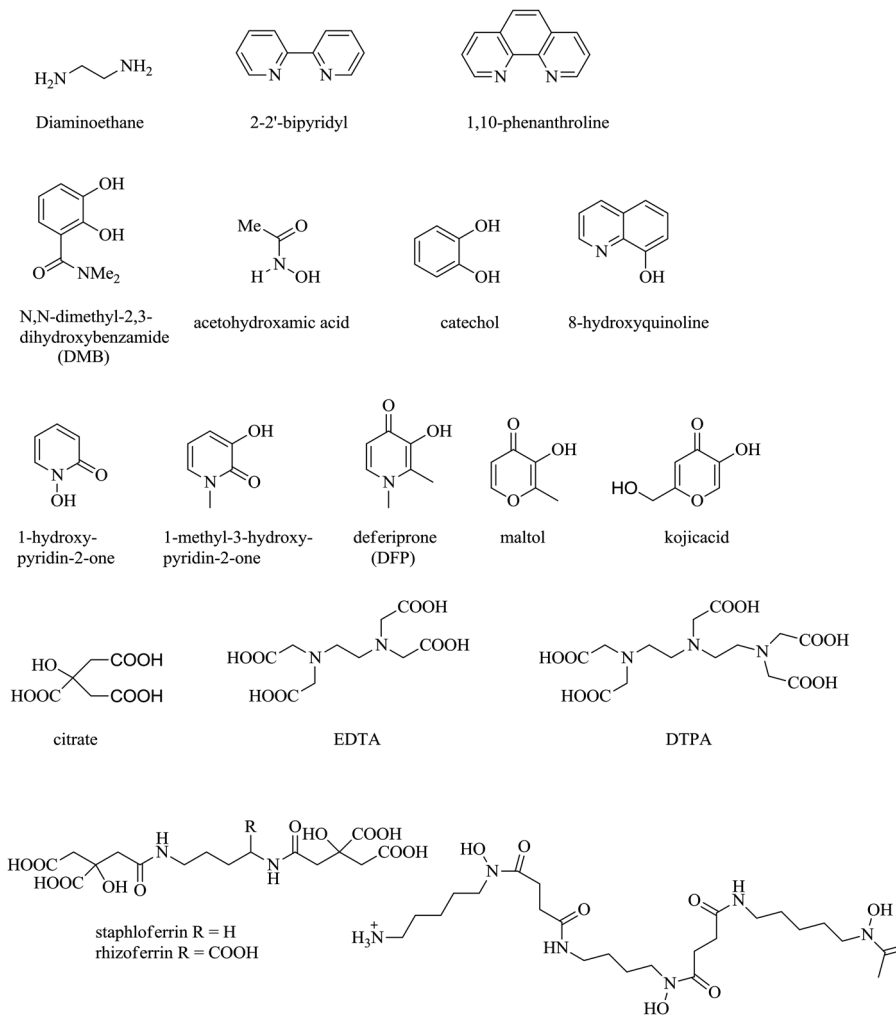


**Figure 2.4** The structures of clinically important chelators; staphloferrin, rhizoferrin and desferrioxamine are bacterial siderophores.

The fact that ligands with a selectivity favoring divalent transition metals also bind  $\text{Fe}^{\text{II}}$ ,  $\text{Cu}^{\text{II}}$ ,  $\text{Zn}^{\text{II}}$ ,  $\text{Co}^{\text{II}}$ ,  $\text{Mn}^{\text{II}}$  and  $\text{Ni}^{\text{II}}$  with similar affinities renders the design of chelators selective for just one of these cations problematic. This general trend and lack of selectivity is described by the Irvine–Williams series (Figure 2.3B) and can be explained by the various different d orbital populations.<sup>5</sup>

Ligands lacking a carboxylate function, for instance catechols, hydroxamates and hydroxypyridinones generally possess a low affinity for the alkaline earth cations  $\text{Mg}(\text{II})$  and  $\text{Ca}(\text{II})$ .<sup>9</sup> For heterocyclic N-containing ligands the affinity for  $\text{Cu}(\text{II})$  tends to be larger than that for  $\text{Fe}(\text{III})$  (Table 2.2), and that for  $\text{Fe}(\text{II})$  larger than for  $\text{Fe}(\text{III})$ . The reverse is true for the O-containing

**Table 2.2** Metal affinity constants for selected ligands.<sup>a</sup>

Ligand	log cumulative stability constant					
	Cu(II)	Zn(II)	Fe(II)	Fe(III)	Al(III)	Ga(III)
N-containing ligands						
Diaminoethane	19.6	13.2	9.7	—	—	—
2,2'-Bipyridyl	16.9	13.2	17.2	16.3	—	7.7
1,10-Phenanthroline	21.4	17.5	21.0	14.1	—	9.2
O-containing ligands						
DMB	24.9	13.5	17.5	40.2	—	—
Acetohydroxamic acid	7.9	9.6	8.5	28.3	21.5	—
Deferiprone	21.7	13.5	12.1	37.2	35.8	32.6
DFO	14.1	11.1	7.2	30.6	25.0	27.6
O- and N-containing ligands						
8-Hydroxyquinoline	23.0	15.8	15.0	36.9	33.4	32.9
EDTA	18.8	16.5	14.3	25.1	16.5	21.0
DTPA	21.6	18.4	16.5	28.0	18.6	25.5

<sup>a</sup>For ligand structures see Figure 2.4.

ligands. For EDTA and DTPA, which contain both aliphatic N atoms and charged O atoms, the position is intermediate.

## 2.4 Comparison of Bidentate Ligands

In order to compare the ability of different ligands to bind a given metal under biological conditions, for instance at pH 7.4, the parameter pM is used rather than the thermodynamic affinity constant presented in Table 2.2. In order to compare the behavior of metals under clinically relevant conditions, pM values which are equal to  $\log[M^{n+}]$  are typically determined under the conditions:  $[M^{n+}]_{\text{total}} = 10^{-6}$  M,  $[\text{Ligand}]_{\text{total}} = 10^{-5}$  M, at pH 7.4.<sup>10</sup> The pFe<sup>3+</sup> value for water falls in the range 17–18, thus chelators with a pFe<sup>3+</sup> value less than this range will not dissolve Fe[III] under neutral conditions, instead they will form Fe(III) hydroxide and precipitate from solution. In contrast, a ligand with a pFe<sup>3+</sup> value greater than 18 will be able to solubilise Fe(III) and prevent Fe(III) hydroxide formation.

In aqueous solution all vacant coordination positions of metal M are fully occupied by water molecules (Figure 2.5a). At neutral pH it is possible for protons to be liberated from some of these coordinated water molecules in order to produce hydroxyl complexes (Figure 2.5b and c). These hydroxyl complexes can undergo condensation, leading to  $\mu$ -oxo link formation (Figure 2.5d) and the elimination of water. As more hydroxyl complexes link up oligomers, and then polymers, form where the oxide ion acts in a bridging role.

### 2.4.1 Catechols

Catechols (Figure 2.4) possess an extremely high affinity for tripositive metal cations resulting from the high electron density of both chelating oxygen atoms. However, the high charge density of oxygen atoms is also

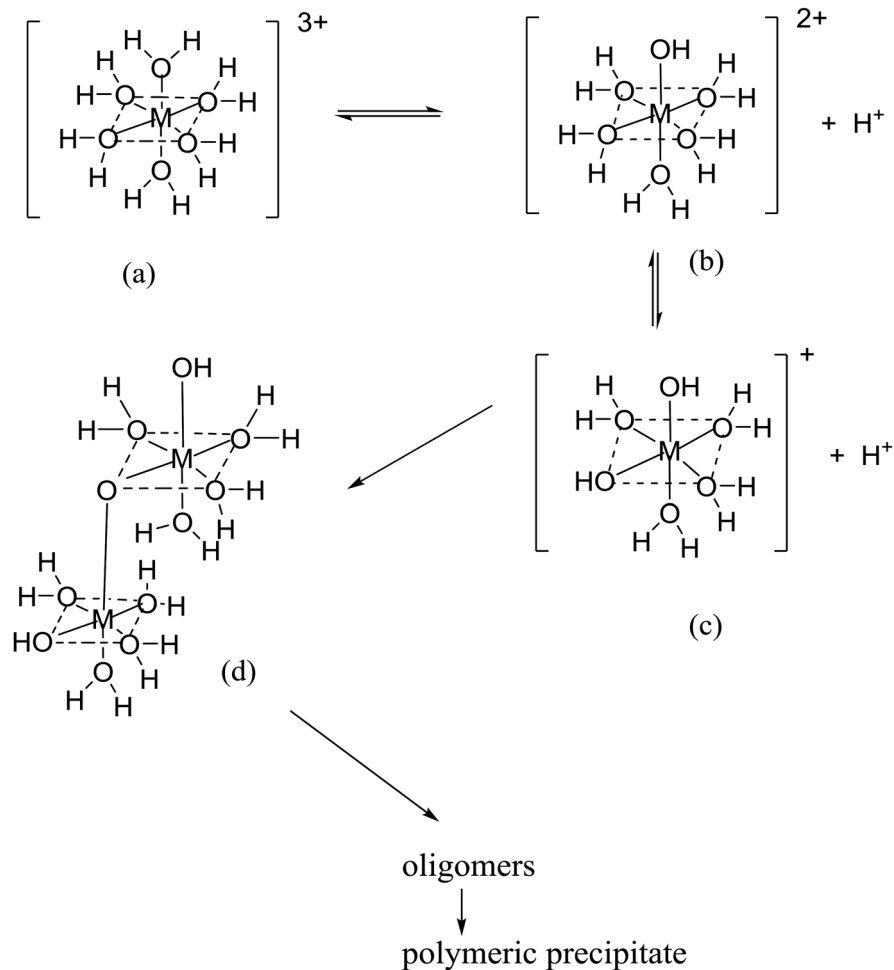


**Figure 2.5** Metal ion hydrolysis. Dissociation of protons from the hexaquo  $M^{3+}$  complex leads to the formation of hydroxyl species; (b),  $M(OH)^{2+}$ ; (c),  $M(OH)_2^+$  and condensation of these hydroxyl species leads to the formation of  $\mu$ -oxo links (d).

associated with a high affinity for protons. For instance, the  $pK_a$  values of *N,N*-dimethyl-2,3-dihydroxybenzamide (DMB) are 8.4 and 12.1 (Table 2.3). Thus the binding of catechol with iron(III) is strongly pH sensitive.<sup>9</sup> For simple bidentate catechols, the 2:1 complex dominates in the pH range 5.5–7.5 (Figure 2.6A) and the remaining sites are occupied by water. With such unsaturated complexes, the iron atom is not completely shielded by the catechol's hydroxyl groups. Bidentate catechols tend to have relatively low  $pFe^{3+}$  values (Table 2.3).

**Table 2.3**  $pK_a$  values and affinity constants of dioxo-bidentate ligands for iron(III).

Ligand	ClogP <sup>a</sup>	$pK_{a1}$	$pK_{a2}$	$\log\beta_3$	$pFe^{3+ b}$
DMB	0.05	8.4	12.1	40.2	15
Acetohydroxamic acid	-1.59	—	9.4	28.3	13
Maltol	0.10	—	8.7	28.5	15
1-Hydroxypyridin-2-one	-1.09	—	5.8	27	16
1-Methyl-3-hydroxypyridin-2-one	-0.22	0.2	8.6	32	16
Deferiprone	-0.90	3.6	9.9	37.2	20.5

<sup>a</sup>ClogP were calculated by using ChemBioOffice 2010 from Cambridgesoft (Cambridge, UK).

<sup>b</sup> $pFe^{3+} = -\log[Fe^{3+}]$  when  $[Fe^{3+}]_{total} = 10^{-6}$  M and  $[ligand]_{total} = 10^{-5}$  M at pH 7.4.

### 2.4.2 Hydroxamates

Hydroxamate moieties (*e.g.* acetohydroxamate, Figure 2.4) possess a lower affinity for metal ions than catechols, although the selectivity of hydroxamates, like catechols, favors tribasic cations over dibasic cations (Table 2.2). Unlike catechols, hydroxamates have only one deprotonation constant ( $pK_a \sim 9$ ). Due to this lower  $pK_a$  value, the oxygen atom at physiological pH is relatively more deprotonated than that of catechol ligands, consequently the 3 : 1 complex predominates at pH 7.4 (Figure 2.6B). However the affinity of a simple bidentate hydroxamate for iron(III) is insufficient to solubilise iron(III) at pH 7.0 at clinically achievable concentrations (Figure 2.6C), *i.e.* it has a low  $pFe^{3+}$  value (Table 2.3). Note the molar ratio of L : Fe in Figure 2.6B is 100 whereas in Figure 2.6C it is 10. In the latter plot the hydroxyl complexes make a major contribution to the speciation of iron and precipitation of iron hydroxide will occur at pH 7.4.

### 2.4.3 Hydroxypyridinones

Hydroxypyridinones combine the characteristics of both hydroxamate and catechol groups, forming 5-membered chelate rings in which the metal is coordinated by two vicinal oxygen atoms. The hydroxypyridinones are monoprotic acids at pH 7.4 and thus like hydroxamates, form neutral tris-trivalent metal complexes. There are three classes of hydroxypyridinone chelator, namely 1-hydroxypyridin-2-one, 3-hydroxypyridin-2-one and 3-hydroxypyridin-4-one (Figure 2.4). The affinity of such compounds for metal ions is associated with the  $pK_a$  values of the chelating oxygen atoms; as an example, the higher the  $pK_a$  value, the higher the affinity for iron(III) (Table 2.3). Of the three classes, 3-hydroxypyridin-4-ones possess highest affinity and are selective for tribasic metal cations over dibasic cations (Table 2.2). The surprisingly high  $pK_a$  value of the carbonyl function of 3-hydroxypyridin-4-one ( $\sim 3.5$ ) results from extensive delocalisation of the lone pair of electrons associated with the ring nitrogen atom (Figure 2.7). 3-Hydroxypyridin-4-ones form neutral 3 : 1 complexes with metal ions which are stable over

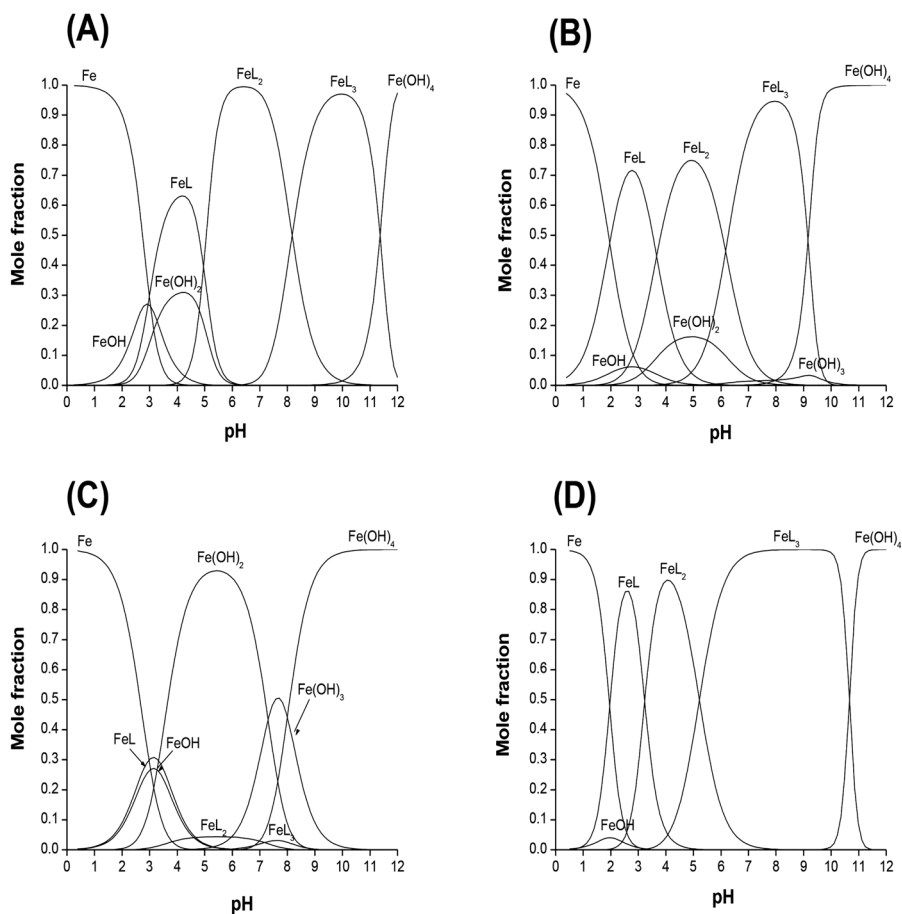


**Figure 2.6** Speciation plot of iron(III) in the presence of (A) *N,N*-dimethyl-2,3-dihydroxybenzamide,  $[\text{Fe}^{3+}]_{\text{total}} = 1 \times 10^{-6} \text{ M}$ ;  $[\text{Ligand}] = 1 \times 10^{-5} \text{ M}$ ; (B) acetohydroxamic acid,  $[\text{Fe}^{3+}]_{\text{total}} = 1 \times 10^{-6} \text{ M}$ ;  $[\text{Ligand}] = 1 \times 10^{-4} \text{ M}$ ; (C) acetohydroxamic acid,  $[\text{Fe}^{3+}]_{\text{total}} = 1 \times 10^{-6} \text{ M}$ ;  $[\text{Ligand}] = 1 \times 10^{-5} \text{ M}$ ; (D) 1,2-dimethyl-3-hydroxypyridin-4-one,  $[\text{Fe}^{3+}]_{\text{total}} = 1 \times 10^{-6} \text{ M}$ ;  $[\text{Ligand}] = 1 \times 10^{-5} \text{ M}$ . Speciation is the description of an element in different identifiable forms; it defines the oxidation state, concentration and composition of each chemical species under given conditions. The above plots display the mole fraction of different chemical species as a function of pH.  $\text{FeL}_1$ ,  $\text{FeL}_2$  and  $\text{FeL}_3$  are the three iron(III) complexes that form with bidentate ligands.  $\text{Fe}(\text{OH})$ ,  $\text{Fe}(\text{OH})_2$ ,  $\text{Fe}(\text{OH})_3$  and  $\text{Fe}(\text{OH})_4$  are the iron(III) hydroxyl complexes.

a wide range of pH values (Figure 2.6D). Although bidentate hydroxypyridinones possess lower  $\beta_3$  values for iron(III) than that of catechol derivatives, the corresponding  $\text{pFe}^{3+}$  values are higher (Table 2.3). This difference is due to the relatively higher affinity of catechol for protons. Thus of all bidentate dioxygen ligand classes, 3-hydroxypyridin-4-ones possess the greatest affinity

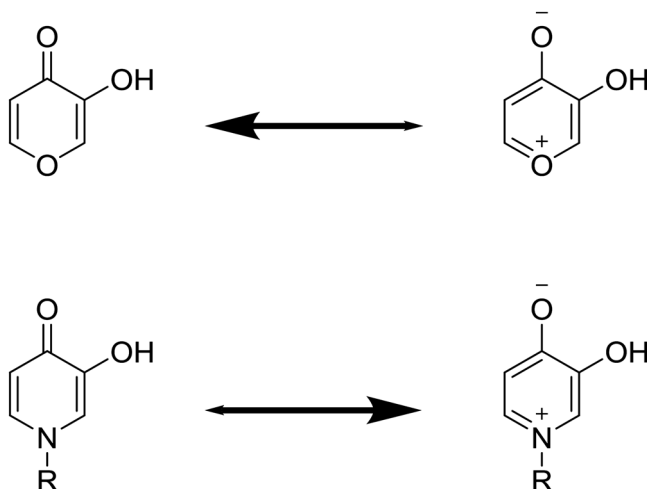


**Figure 2.7** Mesomers of pyridine-4-ones and pyran-4-ones.

for iron(III) over the physiological pH range, as indicated by their respective  $pFe^{3+}$  values (Table 2.3).<sup>11</sup>

#### 2.4.4 Hydroxypyranones

The 3-hydroxypyran-4-ones (*e.g.* maltol and kojic acid, Figure 2.4) possess lower metal affinities than the corresponding 3-hydroxypyridin-4-ones (Table 2.3). This is because there is a much reduced delocalisation of electrons from the ring oxygen when compared with the corresponding delocalisation of electrons from the ring nitrogen of the 3-hydroxypyridin-4-ones (Figure 2.7).

#### 2.4.5 Aliphatic Diamines

Diaminoethane (Figure 2.4) binds divalent transition metal cations quite tightly, particularly Cu(II) (Table 2.2). In contrast it binds tribasic cations weakly in the presence of water at pH 7.4.

#### 2.4.6 Heterocyclic Amines

Heterocyclic amines are typified by 2,2'-bipyridyl and 1,10-phenanthroline (Figure 2.4). Since its discovery at the end of the nineteenth century, 2,2'-bipyridyl has been used very widely as a metal chelator. It forms stable complexes with a wide range of metal ions. Heterocyclic amine chelators are neutral ligands and therefore form charged metal complexes favoring low valent metal ions over high valent ions, *i.e.*  $Fe^{II} > Fe^{III}$  and  $Cu^I > Cu^{II}$ .

### 2.4.7 Hydroxyquinolines

8-Hydroxyquinoline (Figure 2.4) possesses one pyridine donor and one phenolate donor that are situated in *peri* positions with respect to each other. The deprotonated form is monoanionic and forms neutral bis-divalent metal complexes and tris-trivalent metal complexes. The ligand can be considered to be a hybrid of 1,10-phenanthroline and catechol and as such to possess affinity constants for a range of metals which fall between those of 1,10-phenanthroline and catechol. Indeed this is termed the “Rule of average environment of chelating ligands” and an example of such a relationship is presented Figure 2.8.<sup>5</sup> 8-Hydroxyquinoline has a high affinity constant for Fe(III), Cu(II) and Zn(II). It binds divalent metal ions more tightly than 3-hydroxypyridin-4-one (Table 2.2).

### 2.4.8 Aminocarboxylates (Including Oligodentate Ligands)

Simple amino acids are weak chelating agents but polyaminocarboxylate ligands form excellent chelators. There are two donor groups: the amino nitrogen and the carboxyl oxygen. The amino nitrogen favors copper

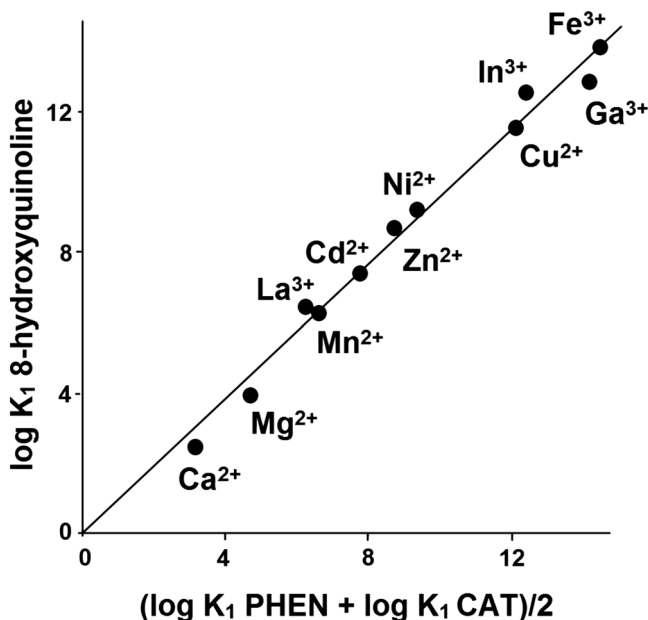


**Figure 2.8** The rule of average environment in complex stability, as illustrated by the relationship between  $\log K_1$  for 8-hydroxyquinoline complexes, and the mean of  $\log K_1$  (PHEN) (PHEN = 1,10-phenanthroline) and  $\log K_1$  (CAT) (CAT = catecholate, 1,2-dihydroxybenzene) for the complex of each metal ion. Data from ref. 5 and 7. Adapted with permission from ref. 5. © Springer Science + Business Media New York 1996.

and zinc, and the carboxylate function can chelate almost all metal ions. Ethylenediaminetetraacetic acid (EDTA) and diethylenetriaminepentaacetic acid (DTPA) are classic polyaminocarboxylate chelators (Figure 2.4) and have been extensively used as chelating agents. However, the selectivity of these compounds is relatively poor (Table 2.2). They tend to bind most metal cations.

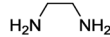
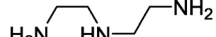
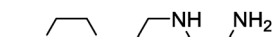
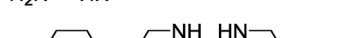
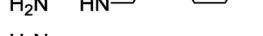
### 2.4.9 Hydroxycarboxylates (Including Tri- and Hexadentate Ligands)

Hydroxycarboxylate ligands are powerful trivalent metal chelating agents and are more selective for iron(III) than the corresponding aminocarboxylates. All the chelating units are composed of oxygen atoms. The interaction between iron(III) and citrate (Figure 2.4) has been well characterized<sup>12</sup> but, by virtue of its multi-chelating arm nature, a large number of complexes have been identified<sup>13</sup> including iron/citrate polymers. In contrast, hexadentate hydroxycarboxylate ligands such as staphloferrin and rhizoferrin (Figure 2.4) have simple iron(III) complex chemistries dominated by the formation of 1:1 complexes.<sup>14</sup>

## 2.5 Ligand Denticity – The Chelate Effect

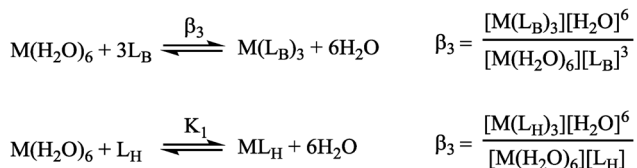
The chelate effect leads to an increased thermodynamic stability of metal complexes, where polydentate ligands possess higher affinity constants than unidentate ligands. This is demonstrated by the gradual increase in  $K_1$  values of interaction of a series of amines with Ni(II) (Table 2.4). Ligands can be structurally classified as bidentate, tridentate, tetradentate, hexadentate or generally multidentate according to the number of donor atoms

**Table 2.4**  $\log K_1$  values for the interaction of polyamines with nickel(II).

Amine	Denticity	$\log K_1$
	2	7.47
	3	10.7
	4	14.4
	5	17.4
	6	19.1

that each ligand possesses. A factor of great importance relating to the stability of a metal complex is the number and size of chelate rings formed in the resultant ligand–metal complex. The most favorable chelate ring sizes consist of five or six atoms. The number of chelate rings can be enhanced by increasing the number of donor atoms attached to a single chelator; for example, a metal ion with coordination number six may form three rings with a bidentate ligand or five rings with a hexadentate ligand (Figure 2.9). The metal affinity for the ligand generally decreases in the sequence: hexadentate > tridentate > bidentate. For example, although the overall stability constant for bidentate may be not much different compared to that of a hexadentate congener (for example, acetohydroxamic acid *vs.* DFO at 28.3 *vs.* 30.6, respectively), the  $\text{pFe}^{3+}$  value of DFO (25.0) is 12 log units different when compared to that of its bidentate congener (13 for acetohydroxamic acid).  $\text{pM}$  values, unlike the stability constants, take into account the effects of ligand protonation and metal hydrolysis as well as differences in metal–ligand stoichiometries.

The formation of a complex will also be dependent on both free metal and free ligand concentrations and as such will be sensitive to concentration changes. The degree of dissociation for a tris-bidentate ligand–metal complex is dependent on the cube of [ligand] whilst the hexadentate ligand–metal complex dissociation is only dependent on [ligand] as indicated in the following equations:



$\text{L}_\text{B}$ , bidentate;  $\text{L}_\text{H}$ , hexadentate ligand

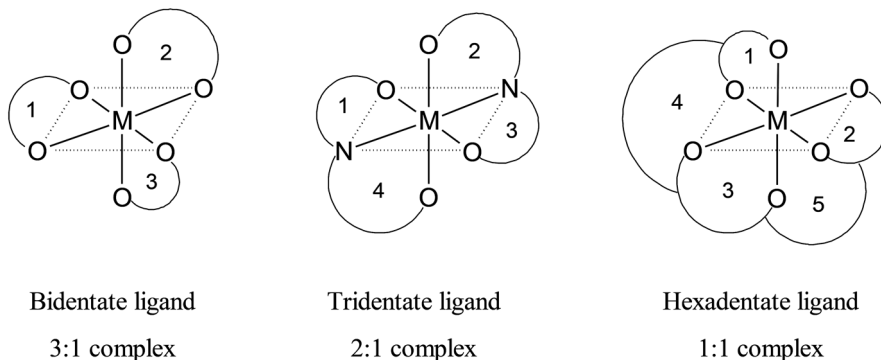


**Figure 2.9** Schematic representation of chelate ring formation in metal–ligand complexes.

Hence the dilution sensitivity to complex dissociation for ligands follows the order hexadentate < tridentate < bidentate. It is for this reason that the majority of natural siderophores are hexadentate compounds and can therefore scavenge iron(III) efficiently at low metal and low ligand concentrations.<sup>14</sup>

The origin of the chelate effect has been explained by Schwarzenbach. When the first 'unident' has attached itself to the metal ion, the second and subsequent 'unident's' can only move in a restricted volume around the metal ion. Thus, the entropy of these subsequent donor atoms is markedly reduced as compared to an equal number of unidentate ligands.<sup>15</sup> Schwarzenbach's model predicted that the chelate effect would indicate itself by a more favorable entropy for the forming complex than the analogous unidentate ligand complex. It also predicted that an increase of chelate ring size leads to a decrease in complex stability as this permits the second donor atom to translate in a larger volume after the first donor atom has been attached. This is an important factor in chelating agent design.

## 2.6 Complex Lability

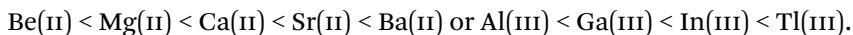
The rates at which ligands substitute for water molecules or other ligands coordinated to a metal ion fall into a typical range for each metal ion. There is an extensive range of rates at which water in the inner coordination sphere of the metal ion exchanges with water in the bulk solvent as indicated in the following equation for  $D_2O$ :



Water exchange rates are typical of the rates at which a metal ion forms complexes with other ligands, and may thus be taken as representative of reaction rates for that metal ion, as summarized in Figure 2.10. There is an enormous range of exchange rates from  $10^{11} \text{ s}^{-1}$  for the large alkali metals to  $10^{-8} \text{ s}^{-1}$  for Rh(III), *i.e.* from  $10^{11}$  exchanges per second to 1 exchange every 3 years! When one ligand competes with another already attached to the metal ion, in general, there are two possible mechanisms. In both mechanisms the incoming ligand would first form an outer-sphere complex in order to be correctly positioned into the inner sphere. In the  $S_N1$  mechanism, the metal ion first loses a ligand from its coordination sphere to create a space which is then filled by the incoming ligand; in the  $S_N2$  mechanism the incoming ligand moves into the coordination sphere and at the same time as the departing ligand is lost. In general, the mechanism is determined by how tightly ligands chelate with the metal ion. The small Be(II) ion, with its strong covalent M-L bonds, strongly favors tetrahedral four coordination, being reluctant to form either three- or five-coordinate complexes, and so typically reacts very slowly with all ligands. In contrast a large metal ion such as Sr(II) has predominately ionic M-L bonds, and displays a variable coordination number. It thus changes coordination number with ease and so ligand substitution reactions are rapid. There are three general rules which give an indication of whether a metal ion will undergo rapid or slow ligand substitution

reactions; these rules relate to factors that cause stronger M–L bonds and strongly defined coordination geometries:

- (1) For metal ions with the same ionic charge, substitution rates with the same ligand will increase with increasing metal ion size. Typical reaction rates are in the sequence (see Figure 2.10):<sup>16</sup>



- (2) For metal ions with similar size, rates of reaction will increase with decreasing cation charge, for example,  $\text{In(III)} < \text{Mg(II)} < \text{Li(I)}$ .
- (3) Electrons in d-orbitals in arrangements that lead to ligand field stabilization energy (LFSE) cause slower rates of ligand substitution in direct relation to the extent of the LFSE, *e.g.*  $\text{Cr(III)} < \text{Ga(III)}$ .

In general, rule 3 overrides rules 1 and 2. For example, rule 1 would suggest that the M–L bond lengths for the trivalent ions of Group VIII tend to increase:  $\text{Co(III)} < \text{Rh(III)} < \text{Ir(III)}$ . However, LFSE converts the reaction rate sequence to:  $\text{Co(III)} > \text{Rh(III)} > \text{Ir(III)}$ . Rule 3 also overcomes rule 2, as  $\text{Ru(II)}$  reacts more slowly than most trivalent non-transition metal ions. An important point for rule 3 is that when a metal ion changes spin state, a large change in lability may happen. Thus, high-spin complexes of iron(II) are labile and low-spin complexes are inert.

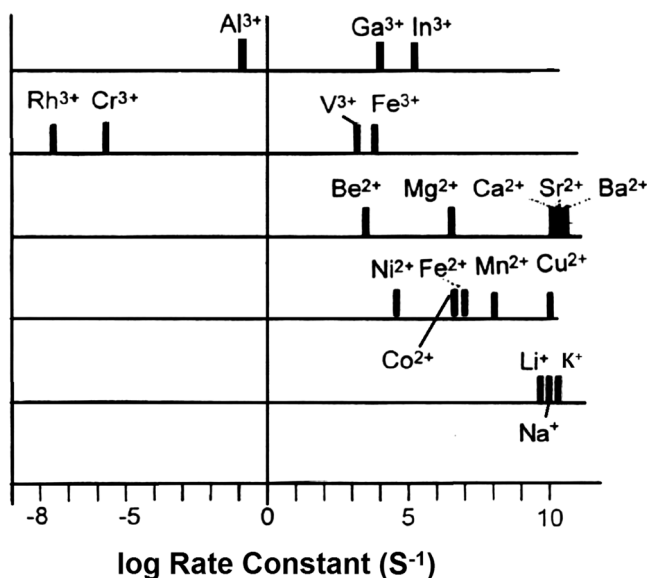


**Figure 2.10** Logarithms of characteristic rate constants ( $s^{-1}$ ) for substitution of inner-sphere water molecules on various metal ions (see Chapter 4). Adapted with permission from ref. 5. © Springer Science + Business Media New York 1996.

As mentioned above, the metal affinity sequence is hexadentate > tridentate > bidentate. Hexadentate metal complexes tend to be inert, the rate of dissociation of the complex being vanishingly small at neutral pH.<sup>14</sup> This renders such molecules ideal metal scavengers. In contrast to the kinetically inert hexadentate metal complexes, bidentate and tridentate metal complexes are kinetically more labile and they tend to dissociate at low ligand concentrations, thereby possibly facilitating metal redistribution. Partial dissociation of bi- and tridentate ligand–metal complexes renders the metal cation surface accessible to other ligands or water. Such a property is undesirable for most therapeutic applications, where efficient metal excretion is required. In order to avoid appreciable metal redistribution in mammalian body tissues, chelators possessing a high metal affinity are essential.

## 2.7 Redox Activity

Chelators that are capable of binding both iron(II) and iron(III) at neutral pH exhibit redox cycling, a property that has been utilised by a wide range of enzymes.<sup>17</sup> However, this is an undesirable property for iron-scavenging molecules, as redox cycling can also lead to the production of reactive oxygen radicals (Figure 2.11). Significantly, the high selectivity of siderophores for iron(III) over iron(II) minimises redox cycling under biological conditions. Most hexadentate ligands with oxygen-containing ligands such as DFO are kinetically inert and reduce hydroxyl radical production to a minimum by failing to redox cycle. The redox potentials of the iron complexes of enterobactin and desferrioxamine are extremely low, namely  $-750$  and  $-468$  mV (*vs.* NHE),<sup>14</sup> thus they bind Fe(III) much more tightly than Fe(II) (see Table 2.2). In principle, iron complexes with redox potentials above  $-200$  mV (*vs.* NHE) are likely to redox cycle under aerobic conditions. Due to their high iron(III) affinity

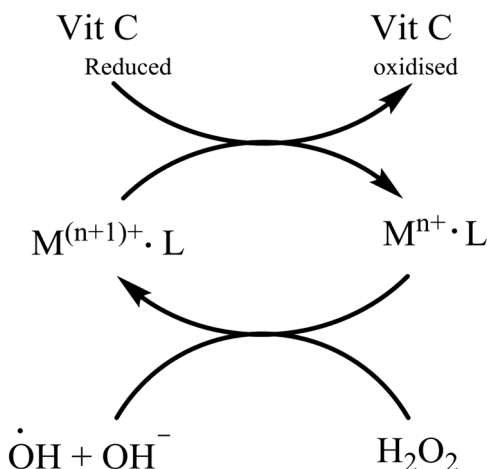


**Figure 2.11** Redox cycling of a metal complex.

constants, bidentate 3-hydroxypyridin-4-ones cause minimal hydroxyl radical production;<sup>18</sup> iron–deferiprone has a low redox potential ( $-620$  mV vs. NHE).<sup>19</sup> Ligands with a nitrogen-coordinating atom tend to possess higher redox potentials, and the coordinated iron can be reduced enzymatically under biological conditions. Such complexes may redox cycle under aerobic conditions.

In order to minimise free-radical production, iron should be coordinated in such a manner as to avoid direct access to oxygen and hydrogen peroxide. Most hexadentate ligands such as DFO are kinetically inert and reduce hydroxyl radical production to a minimum by entirely masking the surface of the iron. However, not all hexadentate ligands are of sufficient dimensions to entirely mask the surface of the bound iron, in which case the resulting complex may enhance the ability of iron to generate free radicals. This phenomenon is particularly marked at neutral or alkaline pH values when the solubility of non-complexed iron(III) is limited. The classic example of this type of behavior is demonstrated by EDTA, where a seventh coordination site is occupied by a water molecule. This water molecule is kinetically labile and is capable of rapidly exchanging with oxygen, hydrogen peroxide and many other ligands present in biological media. As a result iron(III) EDTA is toxic, readily generating hydroxyl radicals under *in vivo* conditions.<sup>20</sup> In contrast to the kinetically stable ferrioxamine complex, bidentate and tridentate ligands are kinetically more labile and the iron(III) complexes tend to dissociate at low ligand concentrations. Partial dissociation of bi- and tridentate ligand iron complexes renders the iron(III) cation surface-accessible to other ligands. However, the concentration dependence of 3-hydroxypyridin-4-one iron complex speciation is minimal at pH 7.4 when the ligand concentration is above  $1 \mu\text{M}$ , due to the relatively high affinity of the ligand for iron(III). Thus, bidentate 3-hydroxypyridin-4-ones behave more like hexadentate ligands as the 3 : 1 complex is the dominant species at pH 7.4 (Figure 2.6D) and the iron atom is completely coordinated. Even at low hydroxypyridinone concentrations there is minimal hydroxyl radical production.<sup>18</sup>

In principle, complexes of copper, chromium, vanadium, titanium and cobalt can also cycle between two oxidation states, but in practice only copper and iron are found to readily redox cycle under biological conditions. Copper exists in two oxidation states: Cu(I) and Cu(II). Cu(I) prefers relatively soft polarizable ligands such as thioethers, nitriles, cyanides, iodide and thiolates to form complexes with flexibility in geometric arrangement, while the oxidized state, Cu(II), favors amines, imines and oxygen donors to form square-planar, trigonal-pyramidal and square-pyramidal geometric conformations.<sup>21</sup> The geometry of the ligand field influences the redox state of copper and therefore leads to the possibility of redox cycling. For example, Cu(I) complexes with 2,2'-bipyridyl and 1,10-phenanthroline adopt a tetrahedral geometry and may be readily oxidized to a more stable square-planar Cu(II) species in the absence of restricting steric effects, rendering Cu(I) complexes susceptible towards oxidation. However, 2,9-dimethyl-substituted phenanthroline disfavors octahedral tris-chelate or square-planar bis-chelate coordination due to the steric interference of the methyl substituents *ortho* to

the imine nitrogen. The molecule preferentially binds Cu(I) in a tetrahedral geometry rendering it less likely to participate in redox cycling.<sup>22</sup>

## 2.8 Biological Properties

Having established the features of chelator design which control the affinity and metal selectivity in the absence of living systems, we now must consider the influence of living cells on both the free ligand and the metal complex and the influence of such ligands and complexes on cellular biochemistry. Ligand behavior *in vivo* is largely governed by distribution and disposition, which in turn is influenced by the ability of the ligand to permeate membranes, the rate of ligand metabolism and the extent of protein binding by the ligand (particularly to serum albumin).

## 2.9 Lipophilicity and Molecular Weight

Ideally, a chelating agent should be orally active as this greatly facilitates drug formulation (it need not be sterile) and drug administration (patients prefer pills to injections). In order to exert its pharmacological effect, a chelating drug must be capable of reaching the sites of excess metal deposition. Typical target organs are the liver, heart, endocrine tissue and brain. Thus a key property for an orally-active chelator is its ability to be efficiently absorbed from the gastrointestinal tract and to cross biological membranes thereby gaining access to intracellular sites. Two major factors influence the non-facilitated penetration of biological membranes, including the absorption of a drug from the lumen of the gastrointestinal tract: the oil/water distribution coefficient ( $\log D_{7.4}$ ) and the molecular weight. Whereas there is considerable quantitative information concerning distribution coefficients,<sup>23</sup> there are few studies devoted to the influence of molecular size on membrane penetration.

With respect to the oil/water distribution coefficient, *n*-octanol is widely adopted as a suitable model for the membrane lipid phase. The aqueous phase should be buffered to pH 7.4 with MOPS (25 mM), as the presence of charges on the ligand will severely limit the rate of non-facilitated diffusion. The charged state of many ligands is strongly pH dependant. MOPS is a useful buffer when working with metals and ligands as it possesses weak chelating properties. In general terms, a  $\log D_{7.4}$  value falling in the range 5–0.1 will ensure that most ligands (subject to molecular weight restrictions, see below) will penetrate membranes.<sup>9</sup> However values at the higher end of this range are likely to be toxic, particularly for copper- and iron-selective ligands,<sup>9,24</sup> and so a suitable range for chelators (ligands) with clinical potential is for the  $\log D_{7.4}$  to fall in the range 2–0.1.

Regarding the influence of molecular weight on the absorption of small molecules from the lumen of the small intestine, the cut-off molecular weight value for the transcellular route of absorption, as judged by polyethylene glycol permeability, is 500.<sup>25</sup> This value agrees with the value presented

by Lipinski and coworkers<sup>26</sup> based on the analysis of 2245 compounds, where they state that a compound with a molecular weight in excess of 500 is likely to be associated with poor absorption from the intestine and poor permeation of biological membranes. Thus as a general guide, clinically useful chelators should possess a molecular weight less than 500 and a  $\log D_{7.4}$  falling between 2 and 0.1.

## 2.10 Ligand Metabolism

Xenobiotics tend to be metabolised by enzymes which are present in the intestine walls and the liver. The major objective of metabolism is to render xenobiotics, which in the context of this review are ligands, more hydrophilic and water soluble. This facilitates excretion *via* the urine and the bile. The efficacy of deferiprone (Figure 2.4) is to some extent limited by the rapid glucuronidation of the iron-coordinating site of the ligand

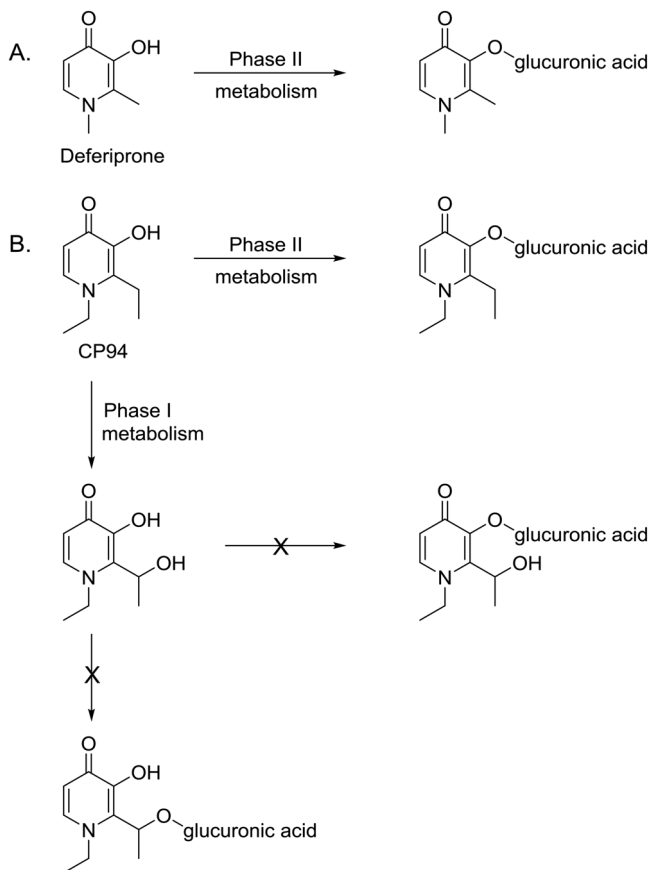
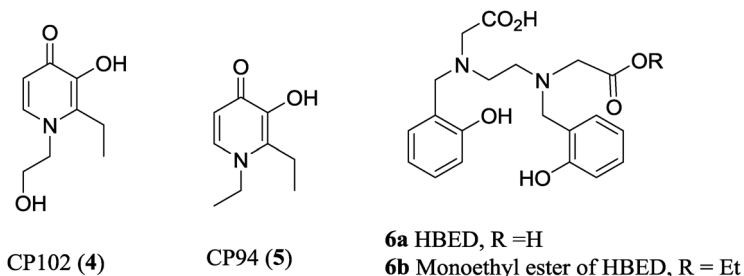


**Figure 2.12** Metabolism of (A) deferiprone and (B) CP94.

(Figure 2.12A).<sup>27,28</sup> More hydrophilic analogues are less rapidly glucuronidated, for instance CP102 (**4**), whereas more hydrophobic analogues, for instance CP94 (**5**), are more rapidly glucuronidated.<sup>29</sup> Interestingly, metabolism can vary between species, for instance CP94 (**5**) is glucuronidated extremely rapidly in guinea pig and man, but is predominately hydroxylated in rat,<sup>29</sup> yielding an iron-coordinating metabolite (Figure 2.12B). Consequently CP94 is extremely active at iron removal in the rat, but not in man.<sup>30</sup> The choice of an animal model for the study of chelators can be critical, see for instance the plasma stability of desferrioxamine (DFO) in different species (Figure 2.13).<sup>31</sup> Clearly rodents and the rabbit are not suitable for desferrioxamine-based investigations, whereas the guinea pig, dog, monkey and human are suitable. Interestingly man does not metabolise desferrioxamine rapidly (Figure 2.13) but some metabolism does occur and significantly all the major metabolites coordinate iron(III) (Figure 2.14).<sup>32</sup> Metabolite B is formed in appreciable amounts and this may influence the distribution of scavenging chelators, as the net charge of both metabolite B and its iron complex is  $1^-$ , whereas the net charge of both desferrioxamine and ferrioxamine is  $1^+$ .



Chelator metabolism has been investigated for potential enhancement of oral activity. HBED (**6a**) is an extremely powerful scavenger of iron(III) but it possesses poor oral bioavailability. In an attempt to enhance oral absorption, the mono-ethyl ester of HBED (**6b**) was investigated and found to possess a marked enhanced oral absorption in marmosets.<sup>33</sup> On absorption, the monoesters were hydrolysed, so generating HBED. Unfortunately the monoesters proved to be toxic and were not developed further as 'prochelators'. Hydroxypyridinone-based prochelators have also been investigated where hydrophobic esters are converted to hydrophilic chelators,<sup>34</sup> however, the enhancement of iron excretion was only found to be marginal.

## 2.11 Ligand Binding to Serum Albumin

With hydrophilic chelating agents, albumin binding does not have a major influence on chelator distribution, as a large portion of the chelator remains non-protein-bound (typically greater than 50%). This unattached chelator

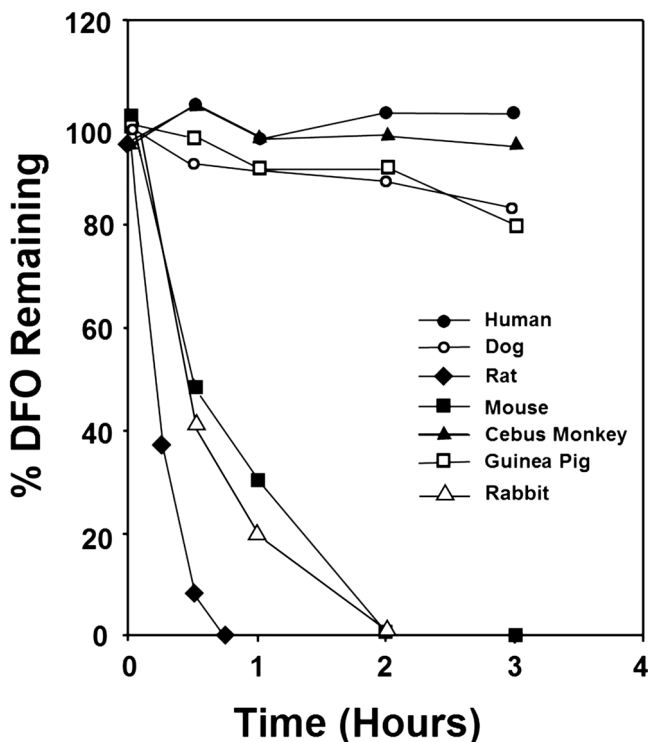


**Figure 2.13** The stability of DFO in Human, Dog, Rat, Mouse, Cebus Monkey, Guinea Pig and Rabbit plasma over 3 hours. Adapted with permission from ref. 31, 1996 Blackwell Science Ltd.

will be available to penetrate the different tissues perfused by the blood. Furthermore, chelator binding to albumin is generally readily reversible and so as the concentration of free chelator is reduced, it is rapidly replenished by dissociation from albumin. This situation holds for a wide range of chelators, for instance, penicillamine (7), EDTA, deferiprone and desferrioxamine (Figure 2.4). However, for more hydrophobic chelators, for instance deferasirox (8), albumin binding has a major influence on chelator distribution. 99% of serum deferasirox is bound to albumin and 99.5% of the iron–deferasirox complex is albumin bound.<sup>35</sup> This phenomenon has a major influence on the distribution of the chelator as the resulting concentration of the unbound ligand is extremely low and therefore has less opportunity to enter peripheral tissue. Indeed as the  $\log P$  (octanol/water) value for deferasirox is high (3.6), albumin binding probably protects tissues from exposure to this hydrophobic chelator. Deferasirox is currently in worldwide use for the removal of iron from iron-overloaded patients.

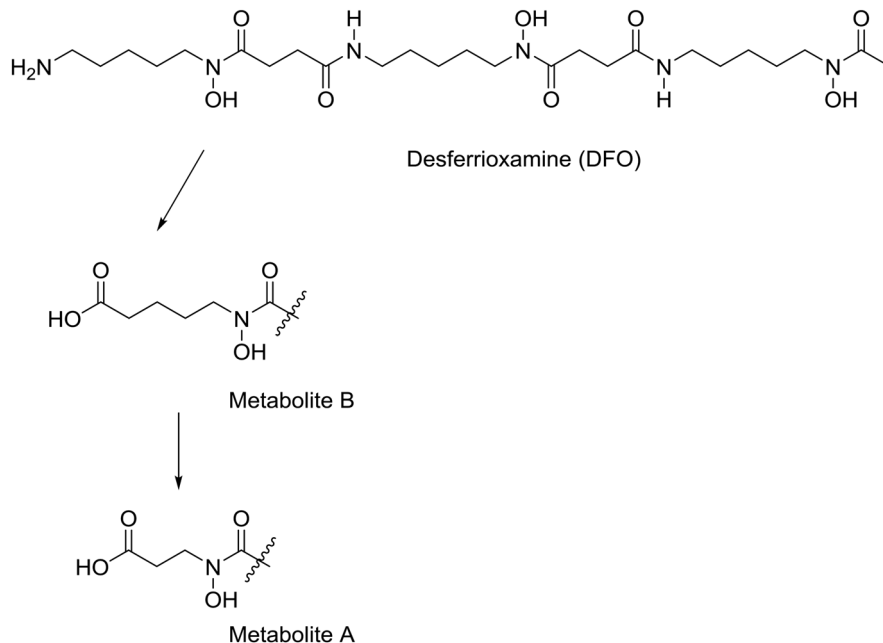
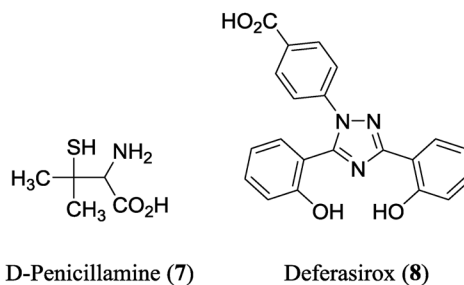


**Figure 2.14** Metabolism of desferrioxamine in man.



## 2.12 Chelator Pharmacokinetics

The pharmacokinetic properties of chelators vary over a wide range, some are orally active, for instance deferiprone, and others are almost completely non-absorbed when presented *via* the oral route, for instance desferrioxamine. This difference is predicted by Lipinski's guidelines, namely, poor oral absorption is associated with molecular weights >500;  $\log P > 5$ ; number of H-bond donors >5 and number of H-bond acceptors >10.<sup>26</sup> For desferrioxamine the molecular weight is 547, number of H-bond donors is 7 and the number of H-bond acceptors is 9; for deferiprone the corresponding numbers are

139, 1 and 2. Desferrioxamine (Figure 2.4) is also cleared by the kidney very rapidly ( $T^{1/2} \approx 20$  min) and so is presented to patients as an intramuscular infusion over a period of 5–8 h. In contrast, deferiprone is rapidly absorbed from the gastrointestinal tract (Figure 2.15A).<sup>37</sup> The peak serum value is typically attained between 40 and 80 minutes and the concentration resulting from a  $50 \text{ mg kg}^{-1}$  dose decreases from  $300 \text{ }\mu\text{M}$  to  $30 \text{ }\mu\text{M}$  over a 6 h period. Due to the extensive glucuronidation of deferiprone, the concentration of the non-chelating metabolite (Figure 2.12) is higher than that of the free ligand 60 min after the oral dose (Figure 2.15A). As deferiprone is cleared from the blood quite rapidly it is usually administered in three equal doses every 24 h.

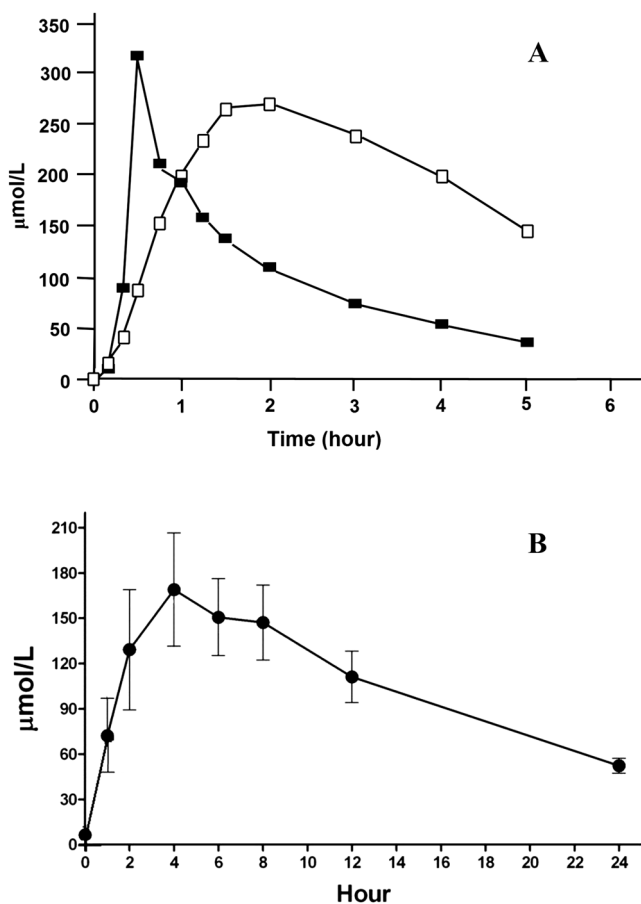


**Figure 2.15** (A) Pharmacokinetics of deferiprone in man ( $\blacksquare$ , deferiprone;  $\square$ , deferiprone glucuronide) following an oral dose of  $50 \text{ mg kg}^{-1}$ . (B) Pharmacokinetics of deferasirox in man following an oral dose of  $35 \text{ mg kg}^{-1}$ .

Deferasirox (**8**), another iron-selective chelator in clinical use, is also orally active, again as predicted by Lipinski's guidelines: molecular weight, 353;  $\log P$ , 3.6; number of H-donors, 3; number of H-acceptors, 5. However, in contrast to deferiprone, the maximum serum concentration of deferasirox is reached after 4 h and the drug remains in the blood stream for much longer periods of time experiencing a slow renal clearance (Figure 2.15B);<sup>36</sup> this is a direct result of its tight binding to albumin. Indeed, in many patients there are appreciable levels of the chelator present after 24 h.<sup>38</sup> Consequently deferasirox is usually administered once every 24 h (see Chapter 4).

## 2.13 Toxicity of Chelators

A prime cause of toxicity of a metal chelator is its lack of selectivity for the particular metal that needs to be removed from an overloaded individual. Thus the use of EDTA or DTPA (Figure 2.4) is likely to lead to toxic side effects by virtue of their ability to coordinate a wide range of metals with relatively high affinity (Table 2.2). Even the clinically proven iron chelators desferrioxamine and deferiprone are known to cause increased excretion of zinc when administered to patients in high dose. This occurs even though there is an enormous difference in the affinity constants for iron(III) and zinc(II); for desferrioxamine the  $\log K_1$  values are 30.6 and 11.1, respectively, and for deferiprone the log cumulative stability constants are 37.2 and 13.5, respectively (Table 2.2).

In addition to metal selectivity, other potential causes of toxicity are associated with kinetic lability (Section 2.6) and redox activity (Section 2.7). These three biochemical parameters can lead to different forms of chelator toxicity, in particular inhibition of enzymes, nephrotoxicity, neurotoxicity, immunotoxicity and genotoxicity.

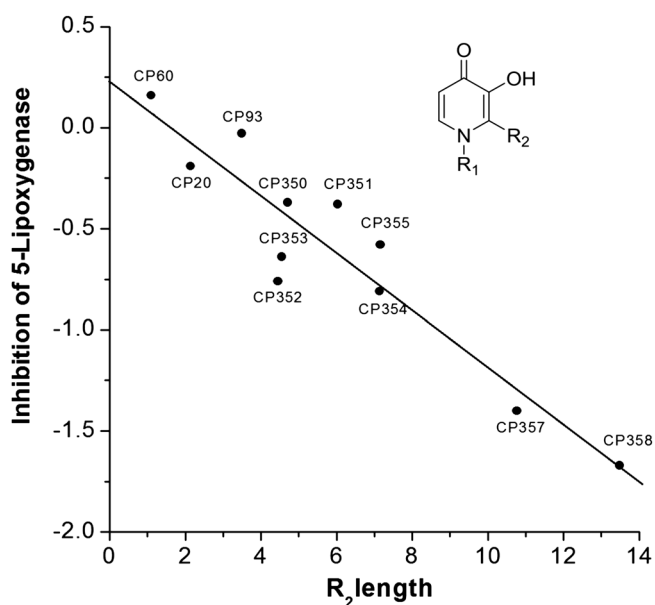
### 2.13.1 Inhibition of Metal-Dependent Enzymes

In addition to insufficient metal selectivity, another cause of chelator toxicity is enzyme inhibition. In principle chelating agents can inhibit metallo-enzymes by reducing the concentration of labile metal pool in the cytosol or mitochondrial matrix *via* three different mechanisms: removal of the essential cofactor, formation of a stable ternary complex at the active site or deprivation of the normal source of metal ion for the apo enzyme. Haem- or iron-sulfur cluster-containing enzymes, *e.g.* cytochrome P450-dependent enzymes and succinate dehydrogenase, are generally not susceptible to inhibition by chelating agents, but enzymes that contain single metals directly coordinated to protein side chains for instance  $\text{Fe}^{\text{II}}$ ,  $\text{Cu}^{\text{II}}$  and  $\text{Zn}^{\text{II}}$  are susceptible towards the presence of chelators (Table 2.5).

Lipoxygenases are generally inhibited by hydrophobic chelators, particularly those containing a long alkyl substituent (Figure 2.16), however

**Table 2.5** Metalloenzymes that are inhibited by chelators.

Enzyme	Metal at active site
Lipoxygenase family (5-, 12- and 15-)	Fe
Aromatic hydroxylase family (Phe, Tyr and Trp hydroxylase)	Fe and Cu
Ribonucleotide reductase	Fe
Ferrochelatase	Fe
Iron(II) 2-oxoglutarate dioxygenases (prolyl-4-hydroxylase, lysine-4-hydroxylase, HIF, histone demethylases)	Fe
Carboxypeptidase	Zn
Carbonic anhydrase	Zn
Superoxide dismutase	Zn and Cu

**Figure 2.16** Relationship between the chemical nature of the ligand and the inhibition of 5-lipoxygenase; HPOs with different  $R_2$  substituents.

the introduction of a hydrophilic group into the chelator reduces the ability to inhibit this enzyme family.<sup>39</sup> The aromatic amino acid hydroxylases are particularly susceptible towards inhibition induced by hydroxypyridinones due to the similarity of the molecular characteristics of some chelators to those of the normal substrates. However, the introduction of an alkyl function at position 2 of the pyridinones markedly increases the  $K_i$  value into the mM range.<sup>40</sup> The iron(II)-2-oxoglutarate dioxygenases form an extremely large enzyme family; there are more than 400 present in the cytosol of hepatocytes, many can be inhibited by decreasing the level of

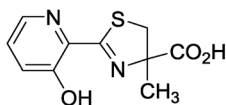
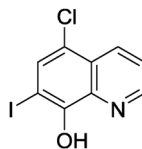
the labile iron pool as their iron(II) affinity constants fall in the range  $10^{-8}$ – $10^{-6}$  M.<sup>41</sup> These relatively low affinity constants render this large group of enzymes susceptible to chelator-induced inhibition. Ferrochelatase is the enzyme which inserts iron(II) into heme, the protoporphyrin IX binding site is hydrophobic and hydrophobic iron chelators tend to inhibit this important enzyme. Ribonucleotide reductase has a rapid turnover; consequently; full activity is dependent on normal levels of the labile iron pool. Scavenging this pool leads to inhibition of the enzyme which, in turn, causes depletion of deoxynucleotide pools, thereby inhibiting DNA synthesis, interfering with the G1 → S transition and blocking the cell cycle.<sup>42</sup> This activity is probably associated with the well-documented antiproliferative property of some chelators.

### 2.13.2 Nephrotoxicity

The kidney has many essential transport functions having a high energy requirement and so this organ is sensitive to loss of ATP. The levels of creatinine in the urine are generally used as a reliable marker for renal function. EDTA and deferasirox (**8**) have both been reported to elevate urine creatinine levels. Desferrithiocin (**9**) and some of its analogues cause structural changes in the proximal tubules which give rise to nephrotoxicity.<sup>43</sup>

### 2.13.3 Neurotoxicity

Neurotoxicity is associated with various changes in morphology, physiology and biochemistry in the central and peripheral nervous systems. These changes may lead to either behavioral or motor defects. Halogen-containing 8-hydroxyquinolines, for instance clioquinol (**10**), are neurotoxic, as demonstrated by the induction of myelo-optic neuropathy.<sup>44</sup> At high doses, desferrioxamine is neurotoxic and has been directly associated with both auditory and ocular defects.

Desferrithiocin (**9**)Clioquinol (**10**)

### 2.13.4 Immunotoxicity

Immunotoxicity is mainly expressed as hypersensitivity in the presence of chelating agents and results in an exaggerated immune response. Many chelator-induced hypersensitivity reactions are idiosyncratic and difficult

to predict. Penicillamine (7) can cause anaphylactic reactions in patients that are allergic to penicillin. Desferrioxamine, deferiprone and deferasirox can all give rise to rashes in a small proportion of patients receiving these compounds for the treatment of iron overload.

The most serious side effect of deferiprone is agranulocytosis and related neutropenia. The precise mechanism of the induction of these conditions is unknown, but is likely to have immunological cause.<sup>45</sup> In a careful 4-year clinical study, Cohen *et al.* demonstrated an incidence of 0.5% for agranulocytosis and 8.5% for mild neutropenia in a cohort of 187 thalassaemia patients.<sup>46</sup> Both conditions are induced apparently irrespective of dose, but are fully reversible on the cessation of deferiprone treatment.

### 2.13.5 Genotoxicity

Genotoxicity occurs when there are changes induced in the genetic material. Chelators may possess both mutagenic (changes in the chemistry of the DNA molecule) and clastogenic (changes to chromosomal structure) properties. Mutagenicity can be investigated by the Ames test and the mouse lymphoma assay. Clastogenicity can be investigated by the mouse micronucleus test. Many chelators possess mutagenic properties at high concentration for instance HBED (6a) and deferiprone, but lack mutagenicity at concentrations less than 100  $\mu\text{M}$ .<sup>47</sup> Surprisingly, desferrioxamine and 1,10-phenanthroline are mutagenic at concentrations as low as 1  $\mu\text{M}$ . In contrast, EDTA is not mutagenic at any dose tested.<sup>47</sup>

Many chelators possess some clastogenic activity and in particular all iron chelators have been demonstrated to possess this property, however those in clinical use possess a low level of activity. In a careful study comparing chromosomal aberration frequencies in patients with thalassaemia, deferiprone and desferrioxamine were demonstrated to possess low clastogenic activities which were not significantly different from each other.<sup>48</sup>

## 2.14 Chelators and Nutrition

Normally humans receive trace metals through the diet, however under conditions of famine, food preferences, ageing and disease, the diet sometimes fails to meet the body's requirements. Mineral supplementation in humans typically uses the oral route, the supplement being given as a capsule, tablet, solution, or as fortified food. Iron, zinc and copper are the most prevalent metals in supplementation treatments. Typically, simple salts or preferably weak complexes are used in such therapy. Weak complexes permit the donation of the coordinated metal to the endogenous transport systems. Typical complexes are iron(II) gluconate, iron(II)-EDTA, iron(III) polymaltose,<sup>49</sup> copper-methionine, zinc acetate and zinc picolinate.<sup>50</sup>

## 2.15 Conclusions

This chapter presents an overview of the chemistry and biology underlying the design of selective metal chelators. Although many high affinity iron chelators are based on siderophore structures, some relatively new chelating moieties have been demonstrated to possess clinical potential.

The design of highly selective chelators for different divalent metals, for instance  $\text{Zn}^{2+}$ ,  $\text{Cu}^{2+}$ ,  $\text{Cd}^{2+}$ ,  $\text{Co}^{2+}$ ,  $\text{Ni}^{2+}$ ,  $\text{Ca}^{2+}$  is difficult and indeed may not be possible. The successful design of relatively selective  $\text{Fe}^{3+}$  chelators is dependent on the fact that  $\text{Fe}^{3+}$  is the only kinetically labile trivalent cation present in biological tissue. Indeed most so-called  $\text{Fe}^{3+}$ -selective chelators will also bind  $\text{Al}^{3+}$ ,  $\text{Ga}^{3+}$  and  $\text{In}^{3+}$ , a property which extends their application to medical imaging.

## Abbreviations

LFSE Ligand field stabilisation energy

NHE Normal hydrogen electrode

## References

1. J. J. R. Frausto da Silva and R. J. P. Williams, *The Biological Chemistry of the Elements*, Clarendon Press, Oxford, UK, 1991.
2. W. Maret and A. Wedd, *Binding, Transport and Storage of Metal Ions in Biological Cells*, Royal Society of Chemistry, Cambridge, UK, 2014.
3. R. J. P. Williams and J. J. R. Frausto da Silva, *Coord. Chem. Rev.*, 2000, **200–202**, 247.
4. G. B. Kauffman, *Coord. Chem. Rev.*, 1972–73, **9**, 339.
5. A. E. Martell and R. D. Hancock, *Metal complexes in Aqueous Solutions*, Plenum Press, New York, 1996, ch. 2.
6. R. G. Pearson, *Chem. Br.*, 1967, **3**, 103.
7. A. E. Martell and R. M. Smith, *Critical Stability Constants*, Plenum Press, New York, 1972–89, vol. 1–6.
8. D. C. Harris and P. Aisen, *Biochim. Biophys. Acta*, 1973, **329**, 156.
9. Z. D. Liu and R. C. Hider, *Med. Res. Rev.*, 2002, **22**, 26.
10. K. N. Raymand and C. J. Carrano, *Acc. Chem. Res.*, 1979, **12**, 183.
11. T. Zhou, Y. M. Ma, X. Kong and R. C. Hider, *Dalton Trans.*, 2012, **41**, 6371.
12. A. M. Silva, X. Kong, M. C. Parkin, R. Cammack and R. C. Hider, *Dalton Trans.*, 2009, 8616.
13. J. L. Pierre and I. Gautier-Luneau, *Biometals*, 2000, **13**, 91.
14. R. C. Hider and X. Kong, *Nat. Prod. Rep.*, 2010, **27**, 637.
15. G. Schwarzenbach, *Helv. Chim. Acta*, 1952, **35**, 2344.
16. L. Helm and A. E. Merbach, *Chem. Rev.*, 2005, **105**, 1923.
17. S. J. Lippard and J. M. Berg, *Principles of Bioinorganic Chemistry*, University Science Books, California, 1994.

18. L. D. Devanur, H. Neubert and R. C. Hider, *J. Pharm. Sci.*, 2008, **97**, 1454.
19. M. Merkofer, R. Kissner, R. C. Hider and W. H. Koppenol, *Helv. Chim. Acta*, 2004, **87**, 3021.
20. G. S. H. Tilbrook and R. C. Hider, in *Metal Ions in Biological Systems, Volume 35, Iron Transport and Storage in Microorganisms, Plants, and Animals*, ed. A. Sigel and H. Sigel, Marcel Dekker, New York, 1988, ch 18.
21. K. L. Haas and K. J. Franz, *Chem. Rev.*, 2009, **109**, 4921.
22. X. Ding, H. Xie and J. Kang, *J. Nutr. Biochem.*, 2011, **22**, 301.
23. Z. Liu and R. C. Hider, *Coord. Chem. Rev.*, 2002, **232**, 151.
24. S. Bertrand, J. J. Helesbeux, G. Larcher and O. Duval, *Mini-Rev. Med. Chem.*, 2013, **13**, 1311.
25. D. G. Maxton, I. Bjarnason, A. P. Reynolds, S. D. Caff, T. J. Peters and I. S. Menzies, *Clin. Sci.*, 1986, **71**, 71.
26. C. A. Lipinski, F. Lombardo, B. W. Dominy and P. J. Feeney, *Adv. Drug Delivery Rev.*, 1997, **23**, 3.
27. G. J. Kontoghiorghes, A. N. Bartlett, A. V. Hoffbrand, J. G. Goddard, L. Sheppard, J. Barr and P. Nortey, *Br. J. Haematol.*, 1990, **76**, 301.
28. S. Singh, R. O. Epemolu, P. S. Dobbin, G. S. Tilbrook, B. L. Ellis, L. A. Damani and R. C. Hider, *Drug Metab. Dispos.*, 1992, **20**, 256.
29. J. B. Porter, R. D. Abeysinghe, K. P. Hoyes, C. Barra, E. R. Huehns, P. N. Brooks, M. P. Blackwell, M. Araneta, G. Brittenham, S. Singh, P. Dobbin and R. C. Hider, *Br. J. Haematol.*, 1993, **85**, 159.
30. J. B. Porter, S. Singh, K. P. Hoyes, O. Epemolu, R. D. Abeysinghe and R. C. Hider, *Adv. Exp. Med. Biol.*, 1994, **356**, 361.
31. A. Steward, I. Williamson, T. Madigan, A. Bretnall and I. F. Hassan, *Br. J. Haematol.*, 1996, **95**, 654.
32. S. Singh, R. C. Hider and J. B. Porter, *Anal. Biochem.*, 1990, **187**, 212.
33. B. Faller, C. Spanka, T. Sergejew and V. Tschinke, *J. Med. Chem.*, 2000, **43**, 1467.
34. R. Choudhury, R. O. Epemolu, B. L. Rai, R. C. Hider and S. Singh, *Drug Metab. Dispos.*, 1997, **25**, 332.
35. H. M. Weiss, M. Fresneau, G. P. Camenisch, O. Kretz and G. Gross, *Drug Metab. Dispos.*, 2006, **34**, 971.
36. R. Galanello, A. Piga, D. Alberti, M. C. Rouan, H. Bigler and R. Sechaud, *J. Clin. Pharmacol.*, 2003, **43**, 565.
37. F. N. Al-Refaie, L. N. Sheppard, P. Nortey, B. Wonke and A. V. Hoffbrand, *Br. J. Haematol.*, 1995, **89**, 403.
38. D. Chirnomas, A. L. Smith, J. Braunstein, Y. Finkelstein, L. Pereira, A. K. Bergmann, F. D. Grant, C. Paley, M. Shannon and E. J. Neufeld, *Blood*, 2009, **114**, 4009.
39. R. D. Abeysinghe, P. J. Roberts, C. Cooper, K. H. MacLean, R. C. Hider and J. B. Porter, *J. Biol. Chem.*, 1996, **271**, 7965.
40. R. C. Hider and K. Lerch, *Biochem. J.*, 1989, **257**, 289.
41. A. Ozer and R. K. Bruick, *Nat. Chem. Biol.*, 2007, **3**, 144.
42. K. P. Hoyes, H. M. Jones, R. D. Abeysinghe, R. C. Hider and J. B. Porter, *Exp. Haematol.*, 1993, **21**, 86.

43. R. J. Bergeron, J. Wiegand, J. S. McManis, N. Bharti and S. Singh, *J. Med. Chem.*, 2008, **51**, 5993.
44. G. P. Oakley, *JAMA, J. Am. Med. Assoc.*, 1973, **225**, 395.
45. C. Pontikoglou and H. A. Papadaki, *Hemoglobin*, 2010, **34**, 291.
46. A. R. Cohen, R. Galanello, A. Piga, V. De Sanctis and F. Tricta, *Blood*, 2003, **102**, 1583.
47. P. Whittaker, H. E. Seifried, R. H. C. San, J. J. Clarke and V. C. Dunkel, *Environ. Mol. Mutagen.*, 2001, **38**, 347.
48. R. Marshall, F. Tricta, R. Galanello, G. Leoni, D. Kirkland, S. Minto and M. Spino, *Mutagenesis*, 2003, **18**, 457.
49. British Nutrition Foundation, *Iron, Nutritional and Physiological Significance*, Chapman and Hall, London, 1995.
50. F. H. Kratzer and P. Vohra, *Chelates in Nutrition*, CRC press, Florida, 1986.

## CHAPTER 3

# *Chelation Therapy For Heavy Metals*

PETER NIELSEN<sup>a</sup>

<sup>a</sup>Institute of Biochemistry and Molecular Cell Biology, Centre of Experimental medicine, University medical Centre Hamburg-Eppendorf, 20246 Hamburg, Germany

\*E-mail: nielsen@uke.de

## 3.1 Introduction

Out of 118 elements known today, about 80 of them are metals. So-called heavy metals comprise a group of naturally occurring elements that form positive ions in solution and have a density five times greater than that of water. Some heavy metals are essential trace elements (*e.g.*, iron, zinc, copper, manganese) and are toxic only in cases of overload, as outlined in Chapter 1, whereas others have no physiological function and may be toxic even at low levels of exposure. The term *toxic heavy metals* describes a subgroup of metals, notably lead, mercury, arsenic, and cadmium, all of which appear in the World Health Organisation's list of 10 chemicals of major concern to health.<sup>1</sup> Exposure to heavy metals can occur from geogenic or anthropogenic sedimentation and emission. Metals may be inhaled as dust or fumes, or may be ingested involuntarily through food and drink. Once a heavy metal is absorbed, it distributes among tissues and organs and can disturb metabolic pathways and damage cells.

---

RSC Metallobiology Series No. 8

Metal Chelation in Medicine

Edited by Robert Crichton, Roberta J. Ward and Robert C. Hider

© The Royal Society of Chemistry 2017

Published by the Royal Society of Chemistry, [www.rsc.org](http://www.rsc.org)

Following industrial development, since the middle of the 19th century the production of heavy metals has increased steeply for more than 100 years, with concomitant emissions into the environment. From the end of the 20th century, however, there has been an increasing global public health concern associated with heavy metal contamination and between 1990 and 2001<sup>2</sup> the emissions have fallen in developed countries (USA, Europe) by over 50%.

Nevertheless, in developing or industrialised transition countries, where mining, smelting, and other metals-based industrial operations are important economic factors but where environmental protection and controls are poorly developed, nationwide or local exposure to heavy metals continues.

The term “heavy metals” is poorly defined and describes a rather heterogeneous group of metals ion with different properties.

According to the Pearson concept of “hard/soft” (Lewis) acids and bases (HSAB), and the class A/B classification of heavy metals, “soft” (or class B) metal ions such as  $\text{Hg}^{2+}$ ,  $\text{Pb}^{2+}$ ,  $\text{Cu}^+$ ,  $\text{Au}^+$ ,  $\text{Ag}^+$ ,  $\text{Cu}^+$ ,  $\text{Pd}^{2+}$  and  $\text{Pt}^{2+}$  preferentially bind to “soft” bases such as sulphur- or selenium-containing groups to form stable complexes (Figure 3.1).<sup>3,4</sup>

Class A metals ions ( $\text{Na}^+$ ,  $\text{Ca}^{2+}$ ,  $\text{Mg}^{2+}$ ,  $\text{Al}^{3+}$ ) bind more to hard bases such as  $\text{F}^-$ ,  $\text{Cl}^-$  and  $\text{O}$ . A borderline group of metals:  $\text{As}^{3+}$ ,  $\text{Fe}^{2+/3+}$ ,  $\text{Mn}^{2+}$ ,  $\text{Cd}^{2+}$  and  $\text{Cu}^{2+}$ , show features intermediate between the A and B classes.

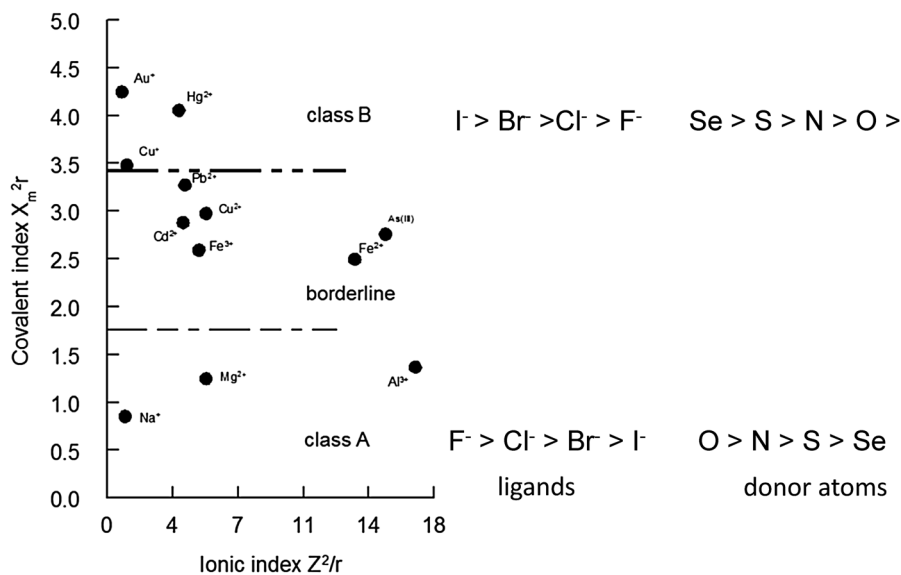


**Figure 3.1** Classification of heavy metal ions (class A, class B, borderline). Modified from E. Nieboer and D.H.Richardson.<sup>4</sup> Class B or borderline metal ions such as  $\text{As}^{3+}$  and  $\text{Hg}^{2+}$  bind *in vivo* preferentially to donor groups containing S or Se. Adapted from ref. 4.

## 3.2 General Strategies Against Heavy Metal Intoxication

### 3.2.1 Toxicology of Heavy Metals

While the toxic effects of heavy metals have been acknowledged for a considerable time, the underlying molecular mechanisms are complex and still not entirely understood.

At the cellular level, heavy metals and metalloids:<sup>5-7</sup>

- bind to enzymes and proteins and perturb their function and activity
- generate reactive oxygen species and elicit oxidative stress
- cause DNA damage and/or impair DNA repair mechanisms;
- interfere with nutrient assimilation

A modern mechanistic view reflects two general mechanisms which are responsible, at the molecular level, for all metal toxicity:

- primary displacement of essential metals (“ionic mimicry”)<sup>8</sup>
- a secondary effect of oxidative stress that interferes with enzymes that maintain reducing state in cells (Figure 3.2).<sup>9</sup>

In addition, some heavy metals may also induce carcinogenesis. The International Agency for Research on Cancer (IARC) classifies cadmium as an established carcinogen, inorganic lead as a probable carcinogen, and methylmercury as a possible carcinogen.<sup>10</sup>

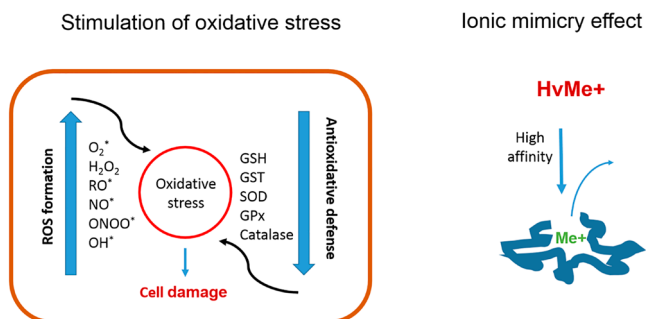


**Figure 3.2** Mechanism of heavy metal toxicity. Heavy metal toxicity often includes the onset of oxidative stress by various mechanisms (down regulation of antioxidative defense or increased ROS formation). Heavy metals can also mimic physiological metals in their natural surroundings in the active centres of peptides or proteins. Due to partly much higher affinities for the target structure, even picomolar concentrations of a given heavy metal such as  $\text{Pb}^{2+}$  can replace a physiological element such as  $\text{Ca}^{2+}$ .

During unpreventable low exposition to heavy metals, cells and organisms always try to maintain metal homeostasis within physiological or sub-toxic levels, both by use of physiological regulation mechanisms and by metal detoxification. However, their capacity to handle toxic metals is limited and in cases of extended contamination, only a fast and efficient medical intervention can limit the damage to cells and organs.

### 3.2.2 Treatment for Heavy Metal Intoxication

Heavy metal poisoning and the need to have an effective antidote in cases of acute or chronic intoxication has a very long history in the medical profession. A rational approach started with “British anti-Lewisite” (BAL), an antidote against the arsenic warfare agent Lewisite.<sup>11</sup> This and more modern chelators are rather unspecific but can be used for different toxic heavy metals. In the following sections, I will review their benefits, limitations and side-effects in detail.

For professional handling of acute or chronic intoxications with a heavy metal a number of strategies are available which are based on prevention, supportive care procedures, and treatment with a metal chelator (Figure 3.3).

The most efficient strategy is to reduce the global use of highly toxic heavy metals, replace them in products wherever possible, identify contamination and emission sites, educate adults and especially children about the risk of

*Prevention* → Identify sources, eliminate or control sources, monitor environmental exposures and hazards

#### *Acute poisoning*

##### Supportive Care:

- forced diuresis
- natural antidotes
- antioxidatives

##### Chelators

###### - classical chelators:

- EDTA
- BAL
- DMSA
- DMPS

###### - new chelators:

- DMSA monoester
- DMSA diesters

##### - Combination Therapy

- with antioxidants
- with second chelator

#### *Chronic poisoning*

↓  
Remove from source.  
Chelators?

**Figure 3.3** Strategies used and discussed in the treatment of intoxication by heavy metals such as arsenic, mercury or lead. On a global view, prevention strategies are most relevant to diminish low-dose exposure which could lead to chronic intoxication in the most vulnerable groups, such as small children. Supportive care combined with chelator treatment is the method of choice in case of acute intoxication. Modified from Kalia and Flora, 2005.<sup>12</sup>

heavy metal intoxication and remove workers and the normal population from sources of acute or chronic heavy metal exposure.<sup>12</sup>

When heavy metal intoxication has occurred or is suspected, a healthcare professional should be consulted as quickly as possible. Detailed information is important: which metal, at which dosage and by which route has it been received. Supportive healthcare measures are saving life in the first phase, before rational diagnosis and a treatment strategy is established, and the appropriate antidote is ready for use. For example, forced diuresis can prevent death in acute arsenic poisoning but is not as useful in other heavy metal intoxications.<sup>13</sup> Not every medical unit can provide expert knowledge and will not have experienced many heavy metal poisonings, so the assistance from specialized physicians or toxicologists is mandatory for optimal results.

Some food ingredients have been suggested to reduce absorption or reabsorption of toxic heavy metals and to support natural detoxification pathways. Micronutrients such as vitamins, sulphur-containing amino acids, antioxidants, and essential minerals (selenium, calcium, zinc) can reduce adverse effects of toxic elements.<sup>14</sup>

Nutritional status also affects uptake since toxic cations are transported by the same proteins as essential nutrients, for example magnesium, zinc, and iron. Therefore children, particularly those with chronic deficiencies of these essential elements, have a greater risk of chronic toxicity of heavy metals such as lead or cadmium. Calcium supplementation reduces lead mobilization from bones and iron supplementation blunts lead accumulation.<sup>15</sup>

The principles of chelation selectivity are discussed in Chapter 2.

Crucial properties of a successful chelator for medical use include a high affinity towards the toxic metal combined with a low toxicity, and appropriate pharmacokinetics of excretion of the metal chelate (see Chapter 2).

Depending on the heavy metal, a number of chelating agents have been developed and used as antidotes against a variety of heavy metal poisons (Table 3.1).

**Table 3.1** List of FDA approved chelators for treatment of heavy metal poisoning or removal of radioisotopes.

Compound	Metal
Dimercaprol (BAL) (1)	arsenic, gold, and mercury poisoning; acute lead: concomitantly with EDTA.
Edetate calcium disodium (calcium EDTA)	acute and chronic lead poisoning
Succimer (DMSA) (4)	lead, mercury and arsenic.
Penicillamine (5)	Copper
Trientine hydrochloride	Copper
Deferoxamine mesylate	iron
Deferiprone	iron
Deferasirox	iron
Pentetate calcium trisodium (Ca-DTPA) (6)	Plutonium and americium
Pentetate zinc trisodium (Ca-DTPA) (6)	Plutonium and americium
Prussian blue (Radiogardase)	Radiocaesium ( <sup>137</sup> Cs), thallium

### 3.2.2.1 Conventional Chelators

The chemical structures of well known chelators for toxic heavy metal poisoning in humans are outlined in Figure 3.4. All these compounds have shown their effectiveness against serious poisoning with a toxic metal or radionuclide. As far as heavy metal intoxication is concerned, chelators form non-toxic metal complexes, remove metals from soft tissues and are normally very effective against acute poisoning.

There is a trend to use *combined treatment* with different chelating agents in order to improve the efficiency in mobilising the body's burden of toxic metals. The rationale is that different chelators are likely to mobilize metals from different tissue compartments and can also act synergistically in a shuttle mechanism. Therefore combined treatments tend to be superior to monotherapy. Interesting results in this direction were obtained when two isoforms of DMSA (either *meso*- and *racemic*-) were given simultaneously with  $\text{CaNa}_2\text{EDTA}$  to reduce tissue lead concentrations in rats.<sup>16</sup>

### 3.2.2.2 New Chelators

Most of the currently used chelating agents have limitations in their effectiveness, mainly against subacute or chronic metal poisoning but also on account of their serious side effects.<sup>17</sup> Thus, it is of immediate concern to develop new drugs that are more effective, especially in cases of low, long-term exposure to toxic metals.

One attractive starting point for new drugs is *meso*-2,3-dimercaptosuccinic acid (DMSA) which, is effective by itself against lead poisoning in children. It has a large therapeutic window and is the least toxic among the dithiol compounds. However, its hydrophilic properties are thought to prevent it crossing cell membrane, which limits its capacity to chelate metals from inside cells. In

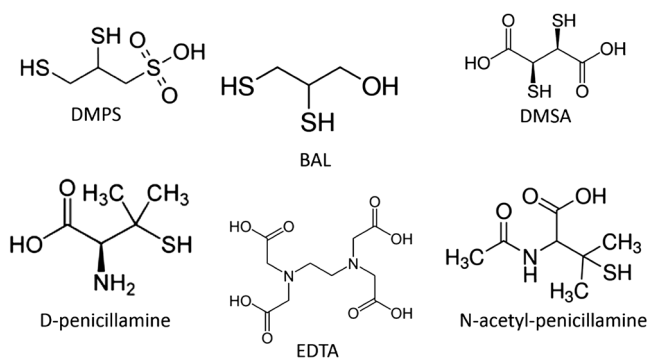


**Figure 3.4** Chelators that have been used therapeutically in man as an antidotes for acute or chronic heavy metal poisoning. BAL: British anti-Lewisite, DMPS: 2,3-Dimercapto-1-propanesulfonic acid, DMSA: dimercaptosuccinic acid, EDTA: ethylenediaminetetraacetic acid and its Na or Ca salt.

the last decades a variety of mono- and di-esters of DMSA have been synthesized to achieve optimal chelation and transport effects.<sup>18,19</sup> In order to render the compounds more lipophilic, the carbon chain length of the parent DMSA was increased by controlled esterification with the corresponding alcohol (methyl, ethyl, propyl, isopropyl, butyl, isobutyl, pentyl, isopentyl and hexyl). It has been reported that these analogues of DMSA are capable of crossing cell membranes and were more effective in reducing, for example, the arsenic burden in acute and sub-chronic intoxication.<sup>20</sup> Monoesters such as monoisoamyl DMSA (MiADMSA) or monomethyl DMSA (MmDMSA) are regarded as attractive new chelator candidates to reduce intracellular heavy metal burdens including cadmium, which is one of the most challenging tasks.<sup>21</sup>

Important future research topics should address the interaction between intracellular and extracellular chelation for the mobilization of metal deposits accumulated over long periods of time and to limit the redistribution of mobilized metals from regions where they are relatively innocuous into more sensitive organs, especially the brain.

A global technical aspect also involves removing and clearing heavy metals from *contaminated soils*.<sup>22,23</sup> In this expanding scientific field, chelators can be used to solubilize heavy metals which can then be removed by a phyto-extraction technique, in which specialized plants function as metal hyper-accumulators.<sup>24</sup> However, this more specialised application of chelators will not be discussed in this Chapter.

### 3.2.3 Drawbacks and Misuse of Chelators

The increasing environmental contamination with heavy metals in some countries can result in slow, low-dose, chronic metal poisoning (especially with lead and arsenic).

To date, prevention, education, and removal of toxic metals from sources are successful whereas the use of chelators is mostly equivocal. Dietrich *et al.* enrolled 780 lead-exposed children with referral blood lead levels between 20 and 44  $\mu\text{g dL}^{-1}$  ( $0.96\text{--}2.12 \mu\text{mol L}^{-1}$ ) at 12 to 33 months of age into a randomized placebo-controlled double-blind trial with DMSA. At age 7 years, the follow-up found no improvement in the scores on behaviour or neuropsychological functions in the chelator-treated group.<sup>25</sup> Since all chelating medicaments do have side effects, this study clearly showed that the use of chelators should be limited to manifest metal poisonings or metal overload diseases diagnosed by appropriate clinical and laboratory evaluation. Low-level exposure to lead, mercury or arsenic also may not justify the use of chelators.

However, experience shows a different handling of metal chelating drugs worldwide. In 2007, the National Centre for Health Statistics in the USA reported that 111 000 adults and 72 000 children under the age of 18 used chelation therapy.<sup>26</sup> Unfortunately, unconventional testing for metal overload and non-indicated chelation therapy has become an interesting field for complementary and alternative medicine in many countries.<sup>26</sup> Unnecessary

chelation therapy can be associated with fatalities.<sup>27</sup> For example, a 53-year-old woman without evident heavy metal poisoning died during chelation therapy by a naturopath; a 2-year-old girl with mild lead poisoning died after the wrong chelation drug caused her blood calcium to drop too low,<sup>28</sup> while a 5-year-old boy with autism died after being inappropriately treated in a doctor's office with a chelating drug.<sup>29</sup>

### 3.3 Arsenic

The word arsenic has its origin in the Syrian language meaning “gold-coloured, yellow”. This metalloid represents only a trace amount (1.7 ppm, 0.00017%) of the Earth's crust, but can become concentrated in some parts of the world because of natural mineralization.<sup>30</sup> Despite its long-known toxicity, arsenic compounds are today widely used in the microelectronics industry (gallium arsenide), in wood preservatives, pesticides, herbicides, and insecticides. Arsenic has been used as a pharmaceutical since ancient times and is still part of non-western traditional medicine products in China. The German scientist Paul Ehrlich developed Salvarsan (a mixture of triaminotrihydroxy-arsenobenzol and pentaaminopentahydroxy-arsenobenzol) as the first successful antibiotic to treat syphilis from 1910 onwards.<sup>31</sup> A remarkable new application of arsenic trioxide (in combination with all-trans retinoic acid) is the treatment of acute promyelocytic leukaemia (APL), which transformed this highly fatal form of blood cancer to a highly curable form.<sup>32</sup> Arsenic-based drugs are still used in treating certain tropical diseases such as African sleeping sickness and amoebic dysentery.

#### 3.3.1 Absorption and Metabolism of Arsenicals

Arsenic exposure mostly occurs by ingestion of contaminated water, which is a serious global health problem.<sup>1,33</sup> The high concentrations in drinking water derive either from contact of water sources with arsenic-rich geological formations or from industrial mining or processing of arsenic compounds. According to the US Environmental Protection Agency (EPA) the maximum permissible limit (MPL) for arsenic consumption through drinking water is  $10 \mu\text{g L}^{-1}$ ,<sup>34</sup> but millions of individuals not only from Bangladesh, parts of China, Japan, Taiwan, Argentina, but also the USA have access to drinking water with much higher arsenic concentrations ( $>50\text{--}3200 \mu\text{g L}^{-1}$ ).<sup>35</sup> A major source of arsenic exposure is also food, of which the main contaminated forms are seafood, rice, mushrooms and poultry. However, arsenicals in fish represent primarily non-toxic organic compounds, such as arsenobetaine and arsenocholine, which are efficiently absorbed but also rapidly excreted in the urine in unchanged form. Arsenic trioxide is the most prevalent form found in air. A minor absorption of arsenic takes place from inhalation and skin contact (Figure 3.5).

Arsenic compounds resemble those of phosphorus. The most common oxidation states for arsenic are:  $-3$  in the arsenides,  $+3$  in the arsenites, and

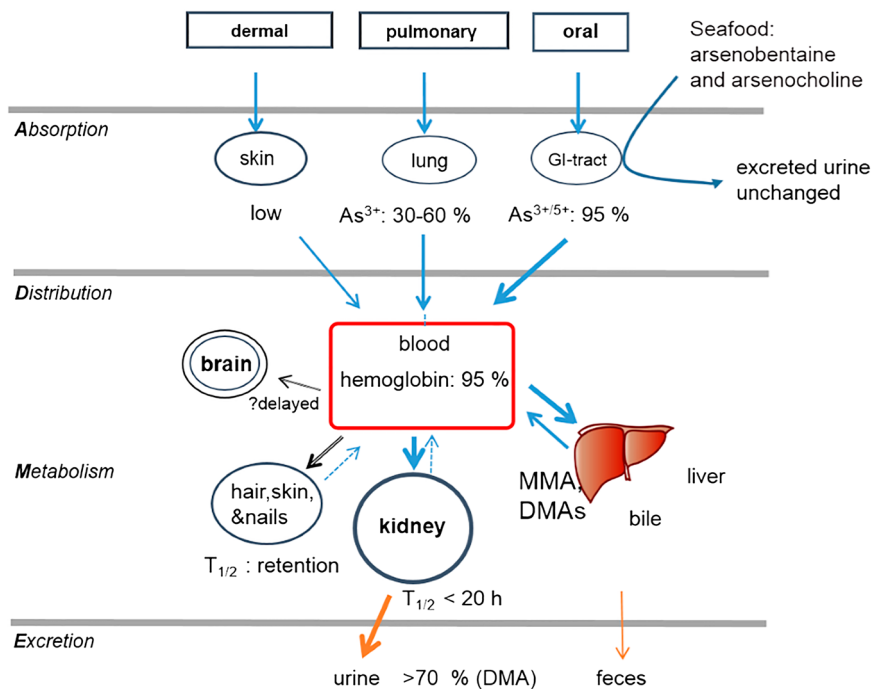


**Figure 3.5** Absorption, distribution, and excretion of arsenic compounds. Arsenicals are absorbed from the gut and the lung quite efficiently. Methylation to mono- or dimethyl arsenic (MMA, DMA) take place in the liver and a large fraction of absorbed As is then excreted in the urine mainly in form of DMA.

+5 in the arsenates and most organoarsenic compounds.<sup>36</sup> A large variety of organoarsenic compounds are known, which are in general less toxic than inorganic arsenic. When exposed in water, food, or chemicals, at least 90% of ingested arsenic is absorbed mostly in form of As(III). Only a small fraction of As(V) can be transported through membranes and is reduced to As(III) *in vivo*. Arsenic is mainly metabolized in the liver by conversion to monomethylarsinic acid (MMA<sup>V</sup>) or dimethylarsinic acid (DMA<sup>V</sup>) by arsenic methyltransferase (AS3MT).<sup>37</sup> Both inorganic and organic forms of arsenic are excreted by the kidneys.<sup>38</sup> The biological half-life of inorganic arsenic compounds ranges from several days up to months, whereas organic compounds are cleared more rapidly.<sup>39</sup>

### 3.3.2 Toxicity of Arsenicals

#### 3.3.2.1 Mechanism of Arsenic Toxicity

Many mechanistic studies of arsenic toxicity have shown that the generation of reactive oxygen (ROS) and nitrogen species (RNS) plays an important role during inorganic arsenic metabolism in living cells.<sup>40</sup> In addition, trivalent

arsenic inhibits the production of glutathione, which protects cells against oxidative damage. The consequence of overwhelming the antioxidative defences within cells can be carcinogenic. Exposure to arsenicals can lead to cancers mainly of the skin, but also lung, bladder, liver and kidney cancers.<sup>41</sup>

Inorganic As(III) binds the thiol and sulfhydryl groups of tissue proteins in the liver, lungs, kidney, gastrointestinal mucosa and keratin-rich tissues and nails and hair. As-GSH complexes are formed which *mimic* substrates for a transport system using “multiple drug resistance proteins” (MRPs).<sup>42</sup> As(V) forms less stable structures which, however, inhibit a great number of enzymes involved in cellular energy production and DNA replication and repair, such as pyruvate dehydrogenase. Arsenic disrupts cellular energy production through several mechanisms. At the level of the citric acid cycle, arsenic inhibits pyruvate dehydrogenase and, by competing with phosphate, it uncouples oxidative phosphorylation, thus inhibiting energy-linked reduction of NAD<sup>+</sup>, mitochondrial respiration, and ATP synthesis. Hydrogen peroxide production is also increased, which might initiate the formation of reactive oxygen species and oxidative stress. These metabolic interferences can lead to death from multi-system organ failure.<sup>43–45</sup>

### 3.3.2.2 Clinical Toxicity of Arsenicals

Given the toxic nature of this element and that most of its compounds are colourless and tasteless, the name *arsenic* was, in public life, synonymous for poison to bring about homicide. Napoleon Bonaparte might have been a victim of arsenic poisoning. One hundred years ago “Good Mary” of Leiden, Netherlands, was convicted as a notorious poisoner, who offered arsenic trioxide in hot milk to at least 102 friends and relatives (45 became seriously ill, 27 died) in order to profit from their life insurance policies.<sup>45</sup>

A precise lethal dose of ingestion is not available in acute arsenic poisonings. An estimate from older clinical reports resulted in the minimum lethal dose to be about 130 mg (about 2 mg kg<sup>-1</sup>).<sup>46</sup> However, single cases have survived even higher doses of 13 mg kg<sup>-1</sup> (ingestion of arsenic trioxide).<sup>13</sup> After ingestion, symptoms such as vomiting, diarrhoea, weakness, and abdominal pain are frequently present. If the first 24 h are survived, death can still occur over the next days from irreversible circulatory insufficiency, or from hepatic or renal failure. Cardiac manifestations include acute cardiomyopathy, sub-endocardial haemorrhages, and electrocardiographic changes. A fatal case of arsenic trioxide inhalation manifested widespread tracheobronchial mucosal and submucosal haemorrhages with mucosal sloughing, alveolar haemorrhages, and pulmonary edema.<sup>47</sup>

Intake of inorganic arsenic over a long period can lead to chronic arsenic poisoning (arsenicosis) which is observed in a mild form in millions of people worldwide who have access to contaminated drinking water. According to WHO, consumption of arsenic-contaminated drinking water in Bangladesh resulted in about 9100 deaths and 125000 disability-adjusted life years (DALYs\*) in 2001.<sup>48</sup> Variable effects, which can take years to develop

depending on the exposure level, include skin lesions, peripheral neuropathy, gastrointestinal symptoms, diabetes, renal system effects, and cardiovascular diseases. There is also good evidence that the most striking long-term effect of chronic exposure to arsenicals is cancer development in humans, but not in animals, if exposed orally (skin cancer) or by inhalation (lung cancer).<sup>49</sup> Animal studies suggest that ingested arsenic may induce a high rate of p53 mutations in skin cancer cells, but the data so far are too limited to show the exact molecular basis of arsenic-induced carcinogenesis.

Acute arsenic intoxication is much less frequent today than 50–100 years ago. Nevertheless, arsenic poisoning is still an important issue in toxicology.

### 3.3.3 Diagnostic Measures and Interventional Levels

Arsenic (or metabolites) concentrations in blood, hair, nails and urine have been used as biomarkers of exposure.<sup>38,39</sup> Arsenic in hair and nails can be useful indicators of past arsenic exposure. Urinary arsenic is generally considered as the most reliable indicator of recent exposure to inorganic arsenic. Increased urinary As in excess of  $50 \mu\text{g L}^{-1}$  urine sample or  $100 \mu\text{g}$  in 24 h of urine. Levels between  $0.1$  and  $0.5 \text{ mg kg}^{-1}$  in a hair sample indicate chronic poisoning.

### 3.3.4 Chelation Therapy for Arsenic Intoxication

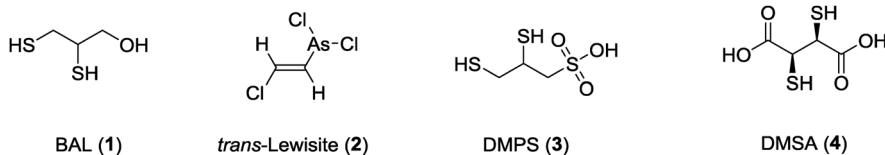
Medication with arsenic chelators offers clear therapeutic benefit in *acute intoxication* if administered promptly, within minutes to hours after an exposure.<sup>50</sup> The first chelating agent, “British anti-Lewisite” (BAL, dimercaprol or 2,3-dimercaptopropanol) **1** was developed during the Second World War as an antidote against the highly toxic gas, lewisite (2-chlorovinyl-dichloroarsine)<sup>13</sup> **2**.

It was recognized that the inhibition of important enzymes, such as pyruvate dehydrogenase, was the main problem in arsenic intoxication and that binding to sulfhydryl groups was the mechanism. Lipoic acid, a component of active PDH has vicinal SH groups and therefore various dithiol compounds were tested, and BAL turned out to be most active as an antidote. The results were published after the Second World War. It was subsequently shown that BAL was helpful against other acute heavy metal intoxications and was the first therapeutic agent for the treatment of Wilson’s disease to remove excess copper.<sup>51</sup>

The most stable complexes between BAL **1** and metal ions are formed with Class B metals (arsenic, mercury, and gold). BAL is the drug of choice for treatment of acute arsenic, inorganic or elemental mercury, gold, and inorganic lead poisoning,<sup>50</sup> as well as antimony, bismuth, chromium, copper, nickel, tungsten, or zinc poisoning. One of the major advantages of chelation with BAL is its ability to remove heavy metals from intracellular sites because of its lipophilic nature. One of the few controlled studies was performed 1948 in pediatric patients with inorganic arsenic intoxication at Charity Hospital

in New Orleans, USA.<sup>52</sup> In 111 controls with supportive care treatment only, 46.2% were symptomatic on admission and 29.3% after 12 h. The average length of stay in the hospital was 4.2 days and three children died. By comparison, in 42 patients treated with BAL, 47.6% were symptomatic on admission, but 0% after 12 h. The average length of stay was 1.6 days, and there were no deaths. It should be noted, however, that these children presented only mild symptoms at hospital admission and that the full efficacy of BAL and its modern derivatives is more pronounced in cases with severe arsenic exposure. The administration of BAL is typically 3–5 mg kg<sup>-1</sup> intramuscularly every 4 hours for 2 days, two times on the third day, and once daily thereafter for ten more days.<sup>51</sup> BAL is suspended in peanut oil and therefore special caution is needed in allergic patients. The injection is painful and may need a local anaesthetic at the injection site. The half-life of dimercaprol (in BAL) is very short, with complete excretion within 4 hours. Free BAL may be rapidly metabolized to inactive products, some of which are glucuronide-conjugated.<sup>50</sup> BAL has a low therapeutic index and the major adverse effects include a possible redistribution of arsenic to brain and testes.<sup>53</sup> Common adverse symptoms include fever, conjunctivitis, crying, constricted feeling, headache, paresthesias (tingling sensation), tremor, and nausea. More serious complications include infections (abscesses) at the injection site, liver damage, elevated blood pressure and heart rate, and hemolysis in patients with glucose-6-phosphate deficiency.<sup>54</sup>

During the period of the Cold War, the antidote capability of compounds with vicinal SH groups was independently investigated both in Russia and China. This resulted in the development of two water-soluble chelators, namely 2,3-dimercaptopropane sulfonic acid **3** also known as unithiol or DMPS, and dimercaptosuccinic acid **4** known as *succimer* or DMSA.<sup>55,56</sup>



Animal experiments have established that early treatment with BAL **1**, DMPS **3**, and DMSA **4** can prevent the lethal effects of inorganic arsenic poisoning. Aposhian has shown in a series of publications that DMPS and DMSA have lower toxicity and clearly a higher therapeutic index than BAL in the treatment of acute arsenic poisoning<sup>57,58</sup> (Table 3.2).

DMPS and DMSA reversed, *in vivo*, the inhibitory effect of arsenite on pyruvate dehydrogenase. In addition, DMPS does not redistribute arsenic, lead, or inorganic mercury to the brain and DMSA chelation decreases the deposition of lead and methylmercury in the brain.<sup>53</sup> Following all these positive results, the two water-soluble compounds have replaced BAL in Europe for the treatment of arsenic intoxication. However, with severe intoxication by organic arsenicals, when a point-of-no-return is a limiting factor, BAL may still have a place as an arsenic antidote.<sup>54,59</sup>

**Table 3.2** Therapeutic index of dimercaprol and the disulfides: DMPS and DMSA in mice which were given an  $Ld_{99}$  of  $NaAsO_2$  subcutaneously (data from Aposhian *et al.* 1984.)<sup>57</sup>

Compound	Therapeutic index <sup>a</sup>	$LD_{50}$ (mmol $kg^{-1}$ )	$ED_{50}$ <sup>b</sup> (mmol $kg^{-1}$ )
<i>dl</i> -BAL (1)	8.76	1.48 (1.11, 1.97)	0.169 (0.088, 0.325)
<i>dl</i> -DMPS (3)	119	6.53 (5.49, 7.71)	0.055 (0.026, 0.082)
<i>meso</i> -DMSA (4)	369	13.7 (11.4, 15.2)	0.037 (0.026, 0.047)

<sup>a</sup>Therapeutic index,  $TI = LD_{50}/ED_{50}$ <sup>b</sup>Given 10 min after 0.15 mmol  $kg^{-1}$   $NaAsO_2$ .

### 3.3.4.1 Chronic Arsenic Poisoning

An important health problem which still remains is the lack of an efficient treatment regime in cases of chronic arsenic intoxications, which is a serious worldwide problem involving millions of people with contaminated drinking water.<sup>60</sup> Guha Mazumder and colleagues conducted one of the few randomized, placebo-controlled trials of DMPS in 21 adults with chronic arsenic ingestion (average duration of exposure 20 years). All subjects had dermal manifestations of chronic arsenicism and had been removed from exposure for less than 3 months.<sup>61</sup> However, no significant difference was found between patients treated with 2,3-dimercaptosuccinic acid and those treated with a placebo. It should be recalled that the hydrophilic DMSA can only act extracellularly and cannot mobilize intracellular arsenic stores directly. Also other clinical trials using different chelators failed to show a clear beneficial effect in cases of chronic arsenic intoxication.<sup>62</sup> Further studies with new lipophilic chelators or combination strategies are awaited which can remove arsenic stores and improve symptoms of chronic arsenicosis.

## 3.4 Mercury

Mercury (Hg, hydrargyrium, “silver water”) occurs in the Earth’s crust in low amounts (40 ppb).<sup>30</sup> It is produced by melting of  $HgS$  (cinnabar ore) as a by-product of gold or aluminium mining. In its elemental form, Hg is liquid at room temperature. Mercury has numerous technical applications worldwide as chemical catalyst, in paints, preservatives or pigments, in dental fillings, electric switches, batteries and control equipment, lamps, and in fungicides. This heavy metal exists in three oxidation states  $Hg^0$  (metallic),  $Hg^+$  (mercurous) and  $Hg^{2+}$  (mercuric) mercury. All these forms play a distinct role in the environment as the result of natural processes (emission: 1500 tonnes annually) and human activities (2320 tonnes per year).<sup>63–65</sup> Due to its well-known toxicity, the industrial demand for mercury has declined substantially in recent years.

A most important property of elemental Hg is the relatively low vapor pressure of 0.0013 mm Hg (0.17 Pa) at 20° forming at room temperature already a saturated atmosphere of 14 mg  $Hg\ m^{-3}$ , which is 140 times higher than the

maximum allowable concentration (MAC) of  $0.1 \text{ mg Hg m}^{-3}$ .<sup>66</sup>  $\text{Hg}^0$  is highly volatile in the vapor phase, can remain suspended in the atmosphere for up to 1 year, and is transported and deposited globally (Figure 3.6).  $\text{Hg}^0$  can be oxidized in air to its inorganic forms ( $\text{Hg}^+$ ,  $\text{Hg}^{2+}$ ) and is then released rather quickly in heavy rain and deposited in soil, or into the waters of oceans, lakes, and rivers. Inorganic mercury, derived from industrial release and from contaminated water, becomes methylated or can be transformed into other organomercurials. The methylation is believed to involve a methylcobalamine compound that is produced by bacteria.<sup>67</sup> This reaction takes place primarily in aquatic systems by bacteria and phytoplankton.<sup>68</sup> The intestinal bacterial flora of various animal species, including fish, are also able to convert ionic mercury into methyl mercuric compounds ( $\text{CH}_3\text{Hg}^+$ ), although to a much lower degree.<sup>69</sup>

In addition, methanogenic and sulfate-dependent bacteria are thought to be involved in the conversion of  $\text{Hg}^{2+}$  to  $\text{MeHg}^+$  under anaerobic conditions in river sediments, wetlands, as well as in certain soils. So far, the detailed mechanisms by which mercury enters the food chain from microorganisms, to small fish, then to fish-eating species including man, are still incompletely understood. Mercury-cycling pathways in aquatic environments are

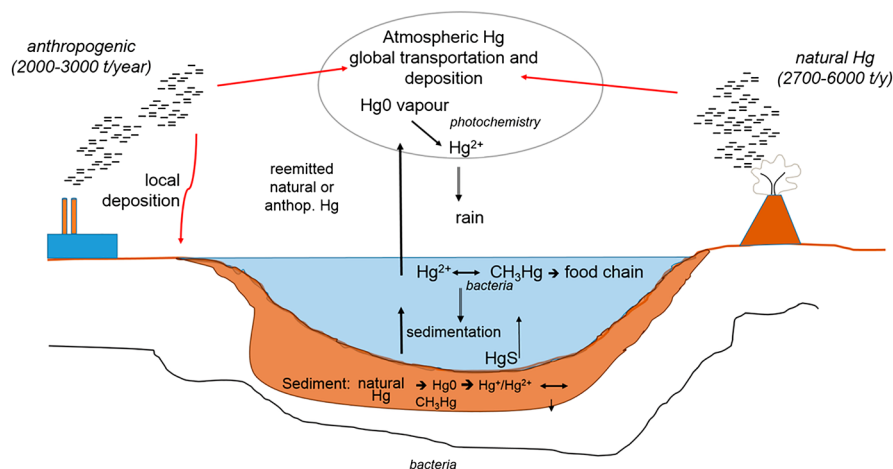


**Figure 3.6** Global cycling pathways of mercury between the atmosphere, water, sediment and soil. Mercury is emitted to the atmosphere from volcanoes and industrial sources of pollution. Different forms of Hg can be transformed into one another. Most important is the methylation of inorganic mercury by bacteria forming highly toxic organic mercurials which can accumulate in the food chain. There are two main types of reaction in the mercury cycle that convert mercury through its various forms: oxidation–reduction and methylation–demethylation. In oxidation–reduction reactions, mercury is either oxidized to a higher valence state (e.g. from relatively inert  $\text{Hg}^0$  to the more reactive  $\text{Hg}^{2+}$ ) through the loss of electrons, or mercury is reduced to a lower valence state.

complex.<sup>67</sup> The various forms of mercury can be interconverted; the most important is the conversion to methylmercury, which is the most toxic form. Mercury can accumulate in the food chain (biomagnification), and terminates in sediments, fish and wildlife, or escapes back to the atmosphere by volatilization.

### 3.4.1 Absorption and Metabolism of Mercurials

The different chemical forms of ingested mercury have different biodistributions, toxicity profiles and implications for health.<sup>70</sup> In general, exposure to metallic ( $\text{Hg}^0$ ) and organic ( $\text{CH}_3\text{Hg}$ ) mercury leads to accumulation mainly in the brain, whereas mono- and divalent salts of mercury affect mainly the kidneys (Figure 3.7, Table 3.3).

#### 3.4.1.1 $\text{Hg}^0$

Due to its uncharged, monoatomic and highly volatile behaviour,  $\text{Hg}^0$  is highly diffusible within in the lipid bilayer of cell membranes and cell organelles, such as mitochondria. It enters the body after inhalation, where 80–100% is absorbed by alveoli in the lungs.

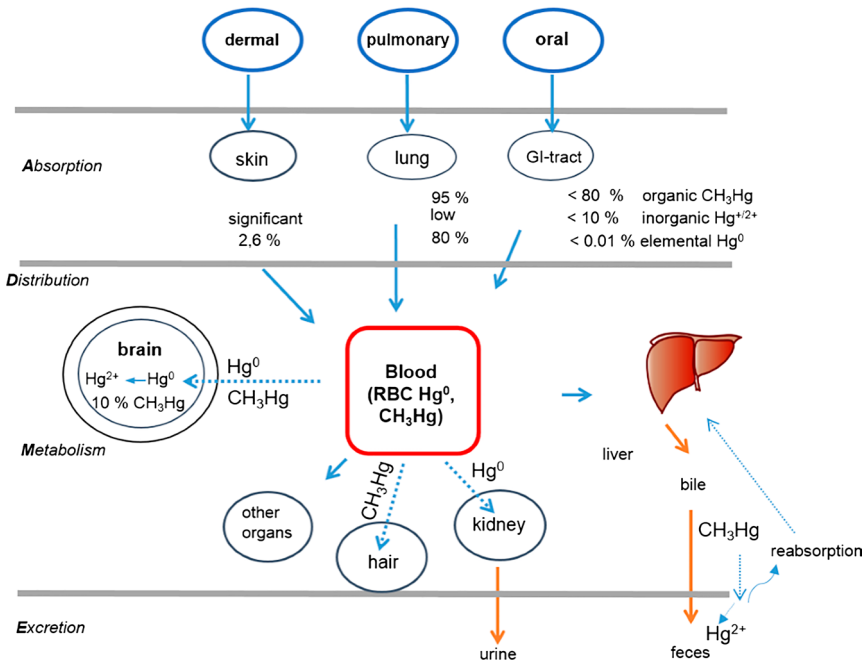


**Figure 3.7** Absorption and distribution of elemental, inorganic or organic mercury in humans. The absorption, distribution, storage or excretion of mercury strictly depends on its chemical form (elemental, inorganic, organic).

**Table 3.3** Estimated intake of mercury from various sources in adults. Data taken from ref. 70 and 75.

	Daily Intake (retention) $\mu\text{g}$ per day		
	elemental	inorganic	organic
atmosphere	0.04–0.2	0	0
Food: Fish	0	0.6	2.4
Non-fish	0	3.6	?
Drinking water	0	0.05	0
Dental fillings	1.2–27	0	0
Total	1.2–27	4.3	2.4

$\text{Hg}^0$  enters the blood stream, is transported to cells and can cross the blood–brain barrier and the placenta.<sup>71</sup> The principal organs for inhaled mercury deposition are the brain and kidney dependent upon the concentration and the duration of mercury exposure. Within cells, elemental mercury can be oxidized by the action of catalase to form  $\text{Hg}^{2+}$ , which can then only be exported from these cells with difficulty. Experimental studies in human volunteers have shown a median retention of elemental mercury after 30 days of 69% of the inhaled dose.<sup>72</sup> This would correspond to the estimated half-life of approximately 60 days for elemental mercury. However, this relatively low value does not exclude relevant bioaccumulation in particular tissues, such as the brain, with a rather longer half-life in the range of years. The most typical exposure to elemental mercury today results from inappropriate clean-up of spilled mercury from broken thermometers.<sup>72</sup> However, this does not lead to demonstrable harm if the exposure period is short and the mercury is adequately cleaned up. Another frequent exposure comes from the use of dental amalgam fillings, which today should contain no more than 3% of metallic Hg (Figure 8). This material has been used for over 100 years, is relatively cheap and has an increased durability compared to modern alternative dental materials. The problem is that amalgam surfaces release mercury vapor into the mouth. The Hg vapor levels are greatly increased by mildly abrasive action, such as chewing gum and brushing, and the ingestion of hot beverages (Figure 3.8).<sup>73</sup>

The estimated average daily pulmonary absorption of mercury vapor from dental fillings varies between 3 and 27  $\mu\text{g}$  Hg (Table 3.3). Amalgam bearers have therefore about 2- to 12-fold more mercury in their tissues, including the brain, than individuals without amalgams.<sup>74</sup> The ongoing question is controversial as to how relevant these findings are, as all measured values are clearly below any threshold risk concentration.<sup>75</sup>

### 3.4.1.2 Inorganic Mercury

The absorption of  $\text{Hg}^{2+}$  in the digestive tract is relatively low (Figure 3.7), however, a large intake of  $\text{Hg}^{2+}$ , such as in accidental or suicidal ingestion, causes digestive tract and kidney disorders often resulting in death.<sup>76</sup>

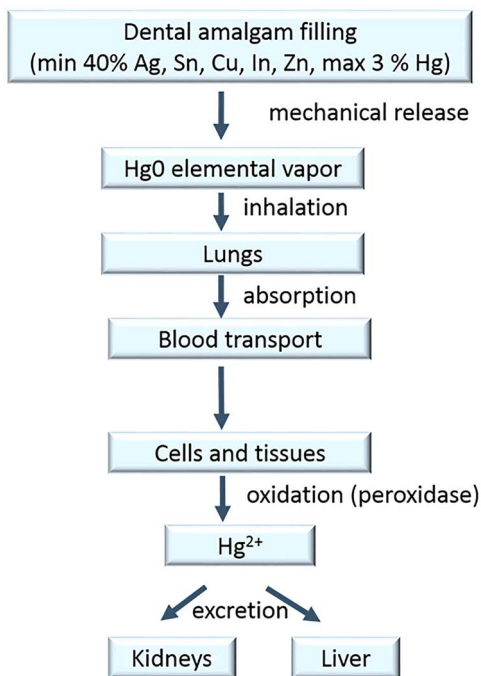


**Figure 3.8** Fate of inhaled elemental mercury vapor in the body from atmospheric contaminations and also from dental amalgams. The latter continuously release small amounts of  $\text{Hg}^0$  in mildly abrasive actions, such as chewing gum and brushing, and through the ingestion of hot beverages. Mercury absorbed from amalgams ranges from 9 to 17  $\mu\text{g}$  per day. Teeth grinding and intensive chewing of gum increases the release of mercury.

Inorganic mercury itself cannot access the brain directly. However, as elemental mercury, ethylmercury and methylmercury, are all metabolised to inorganic mercury within the brain, the biochemistry of inorganic mercury within the cell is relevant to mercury neurotoxicity.<sup>77</sup> The half-life of inorganic mercury in the human brain is regarded as an important factor. A recent re-evaluation using model calculations excludes a short half-life and suggests a value of at least several years and even up to decades.<sup>78</sup> As is briefly described in Chapter 1, inhibition of selenium enzymes, due to the higher affinity of mercury for selenium rather than sulphur, is the principal cause of mercury toxicity, leading to increased neurodegeneration.

### 3.4.1.3 Organic Mercury

While the gastrointestinal (GI) tract is the primary route of absorption, the lipophilic organic mercurials, mainly methylmercury, can also be absorbed through the skin and the lungs. Once absorbed into the circulation, methylmercury

enters erythrocytes where more than 90% is bound to haemoglobin. Lesser amounts will be bound to plasma proteins. About 10% of the burden of methylmercury is found in the brain where it slowly undergoes demethylation to an inorganic mercuric form. Methylmercury readily crosses the placenta to the fetus, where deposition can occur within the developing fetal brain.

The rate of excretion of mercury in both laboratory animals and humans is directly proportional to the simultaneous body burden and can be described by a single-compartment model with a biological half-time, for instance in fish-eating humans, of 39–70 days.<sup>76</sup>

### 3.4.2 Toxicology of Mercury

Mercury intoxication has long been a major focus of clinical toxicology. Mercury has no known physiological role in humans and is among the most toxic of metals.<sup>76–78</sup>

#### 3.4.2.1 Mechanism of Mercury Toxicity

Mercuric ions have a high affinity for biomolecules containing thiol (SH) or seleno groups (SeH), such as glutathione (GSH), cysteine (Cys), homocysteine (Hcy), *N*-acetylcysteine (NAC), metallothionein (MT) and albumin. Thus, in biological systems, mercuric ions are always bound to one or more of these compounds or proteins. Lund *et al.* demonstrated that inorganic or organic mercury-induced *oxidative stress* in rats by GSH depletion, increased lipid peroxidation as well as the formation of H<sub>2</sub>O<sub>2</sub> in the kidneys.<sup>79</sup> For a more detailed account of the biochemistry of mercury toxicity, in particular its effects on selenium-containing enzymes, see Chapter 1, in particular Figure 1.6.

Mercuric-thiol conjugates formed under these conditions appear to be stable in an aqueous environment from pH 1 to 14. The kidney is the primary target organ that takes up and accumulates Hg<sup>2+</sup> from the blood.<sup>80</sup> Within the kidney, the segments of the proximal tubule are the principal portions of the nephron that take up and accumulate Hg<sup>2+</sup> in the form of Cys–S–Hg–S–Cys that can serve as a *mimic* of cystine at the active site of its amino acid transporter. A similar effect is assumed for the transport of HgCH<sub>3</sub> into the brain. CH<sub>3</sub>Hg–S–Cys is easily formed which can act a substrate for the L neutral amino acid carrier. Within all these cells, mercury compounds will cause serious, deleterious effects on intracellular processes which are not known in detail.<sup>8</sup>

Mercury and methylmercury induce mitochondrial dysfunction, which reduces ATP synthesis and increases lipid, protein and DNA peroxidation. The levels of metallothioneins, GSH, selenium and omega-3 fatty acids appear to be strongly related to the degree of inorganic and organic mercury toxicity, and with the protective detoxifying mechanisms in humans.

### 3.4.2.2 Clinical Toxicity of Mercury

The clinical presentation depends upon the dose, the duration, and form of exposure. Acute toxicity is more commonly associated with the inhalation of elemental mercury or ingestion of inorganic mercury. Chronic toxicity is usually as a result of exposure to organic mercury. For all mercurials, the kidney and the brain are the main target organs of toxicity (Table 3.4).

Acute intoxications following the inhalation of mercury vapor, oral intake of inorganic or organic mercury or intoxication with chemicals were frequently described in the past, but are less common today, although there have been some recent case reports. Children are more sensitive to mercury and are at greater risk than adults after certain mercury exposures.<sup>81</sup>

Organic mercury, particularly methylmercury, is the most prevalent and most toxic form of mercury exposure outside occupational settings. Organic mercury compounds can be found in processed woods, plastics, and paper. They are also used in antiseptics, pesticides, fungicides, insecticides, and diuretics. Methylmercury, in the form of *thimerosal*, has been used as an additive to vaccines since the 1930s because of its efficacy in preventing bacterial contamination. The FDA Modernization Act of 1997 revealed that some of the vaccines currently in use in the United States contain thimerosal and that infants who receive such vaccines at several visits may be exposed to more mercury than recommended by federal guidelines for total mercury exposure.

The action of organic mercury is characterized by a latent period between exposure and onset of symptoms which can be several months. The most dramatic example of a fatal poisoning was a case of a chemistry professor who was exposed to some drops of dimethyl mercury on her gloves.<sup>82</sup> It took 6 months before symptoms appeared, which then increased quickly, and

**Table 3.4** Clinical symptoms of acute or chronic mercury poisoning.

Target system	Acute exposure	Chronic exposure
Digestive tract	Inflammation, gingivitis, nausea, severe pain, diarrhea	Constipation, diarrhea
Pulmonary tract	Inflammation, pneumonitis, dyspnoea, edema, cough, fibrosis, respiratory distress syndrome	
Central nervous system	Tremor, convulsion, decreased reflexes, lethargy, confusion	Tremor, erethismus, memory loss, depression, ataxia,
Peripheral nervous system		Polyneuropathy, paraesthesia
Kidney	Oliguria, anuria, hematuria, proteinuria, organ failure	Polyuria, polydipsia, albuminuria

could not be cured despite all the treatment procedures known today, including chelators.

Historically, the most widespread and harmful exposure to inorganic mercury was caused by the use of calomel (mercurous chloride) in teething powder. These exposures caused thousands of cases of acrodynia in children from the 1920s into the 1950s.<sup>76–78</sup>

There are two epidemics that have occurred from MeHg poisoning events that dramatically illustrated the risk of environmental mercury contamination. Firstly, in the Japanese villages of Minamata Bay where 10 000 Japanese lived<sup>83,84</sup> there were 2665 victims of which 1784 have died.<sup>85</sup> Secondly, where bread was contaminated with methylmercury and eaten by local residents in Iraq<sup>86</sup> (see Chapter 1.)

### 3.4.3 Diagnostics and Intervention Levels

Diagnosis of mercury overload is difficult. Reliable laboratory tests for a given mercury intoxication must pay attention to the different chemical natures of mercury exposure and the timepoint of intoxication. It is also important to recall that blood, hair, and urine mercury levels mostly reflect recent exposure and do not correlate well with the total body burden.<sup>87</sup>

Among the poor determinants of body burden of mercury from long-term exposure to elemental or inorganic (but not organic Hg), urine samples are considered to be the best, and the US Federal Biological Exposure Index (BEI) is currently set at 50  $\mu\text{g Hg L}^{-1}$  urine.<sup>87</sup> In acute intoxication, concentration of methyl mercury in red blood cells is high, but it varies in chronic toxicity. A mean value of 2  $\mu\text{g L}^{-1}$  is regarded as the background blood level of mercury in persons who do not eat fish. Concentrations greater than 100  $\mu\text{g L}^{-1}$  produce clear neurological signs while levels greater than 800  $\mu\text{g L}^{-1}$  are often associated with death.<sup>89</sup>

Hair has a high sulfhydryl content and mercury compounds have strong tendencies to bind sulfur. In general, mercury concentrations in the hair do not exceed 10  $\text{mg kg}^{-1}$ .<sup>87</sup> After exposure to methylmercury, total mercury levels in hair and blood can be used as biomarkers to evaluate the extent of poisoning (moderate-to-severe: 200–2400  $\text{mg kg}^{-1}$ ).<sup>88</sup> However, as summarized by Kazantzis, it has so far not been possible to set a level for mercury in blood or urine below which mercury-related symptoms will not occur.<sup>89</sup>

Because of these difficulties, chelation challenge with DMPS 3, 2,3-dimercaptopropane sulfonic acid, has been proposed as a more reliable estimate of body burden, safer than BAL 1 and more potent than DMSA, dimercaptosuccinic acid 4.<sup>90</sup> However, controversies in the discussion of chelation therapies also include criticism against inappropriate comparisons of results from such chelation challenge tests. Some go so far as to say that any testing for heavy metals, when the exposure has not been identified, is inappropriate because of the possibility that false positives may lead to inappropriate, ineffective therapies and their attendant risks.<sup>91</sup>

An increased urinary excretion of high molecular mass proteins (albumin, transferrin, IgG) is indicative of an early glomerular dysfunction; the proximal tubular cells are also affected as shown by an increased urinary excretion of lysosomal  $\beta$ -galactosidase activity. These biomarkers of tubular and glomerular effects correlate significantly with urinary Hg. A threshold of 50  $\mu\text{g Hg g}^{-1}$  creatinine demonstrates a reversible effect of glomerular and/or tubular proteinuria.<sup>92</sup>

### 3.4.4 Chelation Treatment for Mercury Poisoning

Experience with chelators to treat *acute mercury intoxication* dates back to the late 1940s, when BAL was first used in the treatment of patients acutely poisoned by suicidal ingestion of mercuric chloride. From 86 patients who presented after consuming  $\geq 1$  g of mercuric chloride and treated by conventional supportive methods within 4 h, there were 27 deaths (mortality rate of 31.4%), whereas from 41 patients treated with BAL within 4 h, there were no deaths.<sup>93</sup>

Animal experiments in rats supported the efficacy of different dithiol chelators when used promptly in the treatment of acute intoxication by inorganic mercury salts, such as mercuric chloride (Table 3.5). Intervention with DMPS 3 after a delay of 24 h showed no protective effect.<sup>94</sup>

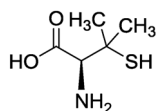
The standard dosage regime of BAL 1 for inorganic mercury poisoning is 3  $\text{mg kg}^{-1}$  i.m. every 4 hours for 2 days, and every 12 hours thereafter for 7 to 10 days or until 24-hour urinary excretion levels are less than 50  $\mu\text{g L}^{-1}$ . Contraindications to BAL include concurrent use of medicinal iron (which can form a toxic complex with BAL), organic mercury poisoning, pre-existing renal impairment, and pregnancy (except in life-threatening circumstances). Adverse effects are dose related and may include: pain; a self-limited increase in heart rate and blood pressure; nausea; vomiting; headache; burning sensation of the lips, mouth, throat, and eyes; lacrimation; rhinorrhea; salivation; muscle aches; burning and tingling in the extremities; tooth pain, diaphoresis; chest pain; anxiety; and agitation. BAL, however, has been found to increase brain mercury in mice exposed to short-chain organic mercury; such an increase could lead to increased neurotoxicity.

**Table 3.5** Effectiveness of BAL, DMPS, and DMSA against acute mercury intoxication using oral  $\text{HgCl}_2$  in rats.<sup>a</sup>

Chelator	Dose	Mortality	Death (%)
Control	—	9/10	90
BAL i.p. 1	400 $\mu\text{M}$ (50 $\text{mg kg}^{-1}$ )	5/10	50
DMSA oral 4	1600 $\mu\text{M}$ (291 $\text{mg kg}^{-1}$ )	4/10	40
DMPS 2	1600 $\mu\text{M}$ (336 $\text{mg kg}^{-1}$ )	0/10	0

<sup>a</sup> $\text{HgCl}_2$  (109  $\text{mg kg}^{-1}$  p.o.) was given to rats. A single dose of chelator was given 15 min later. Mortality was assessed within 14 days. Data is from ref. 94.

D-Penicillamine **5** can also mobilize mercury and can be combined with BAL treatment. However, it is inferior to DMSA **4** and DMPS **3** in removal of mercury from animals, with no effect on levels in the brain and is not useful for organic mercury toxicity.



D-penicillamine (**5**)

Succimer, DMSA **4**, is a water-soluble analogue of BAL, approved by the FDA in 1991. DMSA prevents mercury-induced symptoms and is used in addition to BAL for treatment of inorganic mercury poisoning in adults in the USA. In children where the urine mercury levels are equal to or greater than 50  $\mu\text{g mL}^{-1}$  creatinine, even if they are asymptomatic, WHO recommends that DMSA should be started.<sup>95</sup>

Unithiol, DMPS **3**, is also a water-soluble analogue of BAL. It has been approved for use in Russia since 1958 and in Germany since 1976. Together with DMSA it has replaced BAL for heavy metal poisoning in Europe almost completely. In the body, DMPS is oxidized to the disulfide form within the first 30 minutes. Approximately 84% of total DMPS is excreted by the renal system. DMPS penetrates the kidney cells and removes mercury from renal tissues by excretion into the urine. Based on clinical and experimental evidence, it has been shown that DMPS removes mercuric mercury deposits in all human tissues except brain. DMPS is given either orally or by i.v. injection. The adult dose is 250 mg intravenously every 4 hours for the first 48 hours then 250 mg i.v. every 6 hours for the second 48 hours and subsequently 250 mg i.v. every 8 hours. After i.v. administration, oral therapy may be started with 300 mg, 3 times per day, for 7 weeks. The duration of treatment depends on the concentration of mercury in blood and urine. Side effects are rare but, rash, nausea, and leucopenia are possible. Although not currently FDA-approved, DMPS **3**, showed statistically significant increases in urinary mercury output in mercury exposed workers. In a large study in the Philippines, gold miners who sustained ongoing exposure to elemental mercury were compared to another group of people eating fish contaminated with methylmercury, and to a final control group without significant known mercury exposure. Probands from the two exposed areas were chosen with elevated blood, urine and hair mercury levels, and appropriate symptoms (tremor, sleeplessness, memory loss, *etc.*). Controls had normal levels and were asymptomatic. One hundred and six probands completed the fourteen day trial with oral DMPS at 400 mg per day. Whereas blood mercury remained unchanged during the trial, urine mercury increased up to 85-fold. Despite the short (fourteen day) duration of the trial, significant improvements were observed in objective measures such as hypomimia, Romberg test, and tremor and ataxia.<sup>96</sup> In a study involving two subjects with occupational exposures to mercury vapor in the USA, DMPS (100 mg per day) was given orally for 8 weeks. Reduction of

symptoms, such as muscle twitching, arthralgias, paresthesias, night sweats and weight loss, closely paralleled urine mercury output which tapered over time.<sup>97</sup>

Due to the low toxicity and high efficacy of DMSA and DMPS, both compounds are chosen today as the antidotes of choice in various forms of mercury poisoning.<sup>98</sup> The animal experimental data and the limited human data indicate that DMPS is a highly effective chelation antidote in acute and possibly chronic intoxication with inorganic Hg compounds, including elementary Hg vapor, while DMSA is more effective for detoxification of organic mercury compounds.<sup>99</sup>

### 3.5 Lead

Lead is a heavy post-transition metal that is found at low concentrations (18 ppm) in the earth's crust predominantly as lead sulphide.<sup>30</sup> Lead is a soft metal with attractive properties, such as high malleability, high ductility, low melting point and resistance to corrosion. It was therefore discovered very early in human history and has been utilized in numerous applications such as construction, paint, ceramics, pipes, batteries and leaded gasoline. The production of lead, now 2.5 million tons per year, has accompanied population and economic growth.<sup>100</sup> Lead poisoning, known as saturnism or plumbism, has been a companion to humans for thousands of years. For example, it has been suggested that lead intoxication from drinking vessels may have contributed to the fall of the Roman Empire.<sup>101</sup> High concentrations of lead in paints may also have caused illnesses, such as deafness, in famous painters like van Gogh, Goya, and Rembrandt. The widespread use of lead in the past has resulted in extensive present-day environmental contamination, human exposure and significant public health problems in many countries of the world.<sup>102</sup>

In Europe, USA and many other countries the use of lead has been banned from industry during recent decades. Especially, the replacement of leaded gasoline in many countries has resulted in a substantial decrease in blood lead levels (BLL).<sup>103</sup> However, lead never disappears completely from our environment and the current focus of attention is on the subclinical effects of exposure which may be especially harmful in small and growing children.<sup>104</sup>

#### 3.5.1 Lead Absorption and Metabolism

Lead incorporation comes from environmental and anthropogenic sources mainly by inhalation or ingestion of lead compounds and less through cutaneous absorption (typically far less than 1%, organic more than inorganic lead). Fine lead particles in vapor or fumes generated during burning, smelting and recycling, or from leaded gasoline, are absorbed directly through the lungs, whereas larger particles are carried more by mucus to the throat, then swallowed and absorbed *via* the gastrointestinal (GI) system.<sup>105</sup>

The percentage of lead absorption through the GI tract is variable. Children are at greater risk for lead absorption than adults. In general, approximately 30–50% of lead ingested by children is absorbed, compared with approximately 10% of that ingested by adults (Figure 3.9). Lead absorption is dependent on several factors, including the physical form of lead, the particle size ingested, the GI transit time, and the nutritional status of the person ingesting. Lead absorption is augmented in the presence of iron, zinc, and calcium deficiency which use the same absorption mechanism.<sup>106</sup> Iron deficiency leads to increased absorption of divalent cations in the duodenum and may thus increase blood concentration of neurotoxic lead or cadmium metals in children.<sup>107</sup>

After absorption, lead enters the blood compartment and is distributed between plasma and red blood cells (RBCs). Although the blood generally carries only a small fraction of the total lead body burden, it serves as the initial pool and distributes lead throughout the body, making it available to other tissues or for excretion. Lead moves quickly in and out of soft tissues.<sup>105</sup> Animal studies indicate that the liver, lungs, and kidneys have the greatest soft tissue lead concentrations immediately after acute exposure. The brain is also a site of lead retention, selective brain accumulation may occur in the hippocampus. Lead in soft tissues has an approximate half-life of 30–40 days. Children retain more lead in soft tissue than adults do. Most retained lead in the human body is ultimately deposited in bones.<sup>107</sup> The bones and teeth of adults contain more than 90% of their total lead body burden, and those of children contain approximately 75%. Lead in mineralizing tissues is not uniformly distributed, with a labile compartment (trabecular bone), where the elimination half-life is 90 days, and a deep inert compartment (cortical bone) where the elimination half-life may be 10–30 years. The labile component readily exchanges bone lead with blood, whereas lead in the inert component

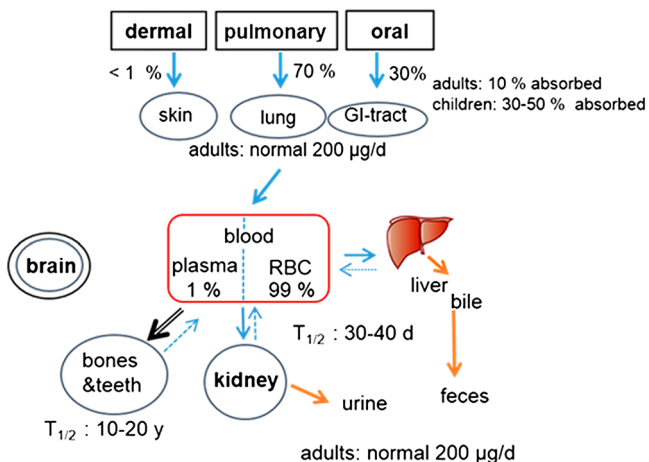


**Figure 3.9** Uptake, distribution, and excretion of lead.

may be stored for decades. In times of physiologic stress, the body can mobilize lead from bone, thereby increasing the level of lead in the blood.<sup>108</sup>

There is no active elimination of lead. Elimination occurs mainly by glomerular filtration (90%) and biliary secretion (10%). Minor amounts are lost through skin desquamation, and by nail growth. Under normal conditions, the daily uptake of lead from inhalation (70%) and from food is approximately 200  $\mu\text{g}$  in adults, which is similar to the excreted amount of lead per day. Any increase of lead intake leads to an accumulation of lead in the body, mainly in the form of lead phosphate in bones and teeth (90%).

Other toxic forms of lead include organic forms such as tetraethyl lead (TEL), a former lead fuel additive, which is well absorbed through the skin and lung. TEL is rapidly metabolized to triethyl lead and is slowly processed to inorganic lead.<sup>109</sup>

“Modern forms” of lead intoxication are caused through gunshot wounds and exist among consumers of Ayurvedic medicine, which can in part be directly enriched with lead and other heavy metals.<sup>110,111</sup> In 2007, around the Saxon city of Leipzig in Germany, a series of 35 subjects with signs of undiagnosed lead intoxication were hospitalized. A hitherto unknown common source of exposure was revealed as marijuana that had been adulterated with lead chloride. Symptoms were colic, nausea, chronic fatigue, and hypochromic anemia.<sup>112</sup>

### 3.5.2 Toxicity of Lead

Lead is known to induce a broad range of physiological, biochemical, and behavioural dysfunctions *in vivo*, including the haemopoietic system, kidneys, liver, central and peripheral nervous systems, cardiovascular system, and male and female reproductive systems.

#### 3.5.2.1 Mechanism of Lead Toxicity

*Oxidative stress* is induced by lead. Lead has a high affinity for sulfhydryl groups with obvious essential target proteins such as superoxide dismutase (SOD), catalase (CAT) and glutathione peroxidase (GPx). This clearly represses the antioxidative defence system leading to increased lipid peroxidation of red blood cells.<sup>113</sup>

The *ionic mimicry effect of lead* has long been recognised for replacing divalent cations such as  $\text{Ca}^{2+}$ ,  $\text{Zn}^{2+}$ ,  $\text{Mg}^{2+}$ ,  $\text{Fe}^{2+}$  in various enzymes and transporters (see Chapter 1, Figure 1.5, illustrating the replacement of lead for zinc and calcium in  $\delta$ -aminolevulinic acid dehydratase and synaptotagmin, respectively). One of the oldest known targets of lead toxicity is the haem synthesis pathway by inhibiting  $\delta$ -aminolevulinic acid dehydratase (ALAD) where  $\text{Pb}^{2+}$  replaces  $\text{Zn}^{2+}$ . This leads to a cascade of ALA-accumulation which can then stimulate the production of reactive oxidative species (ROS).<sup>114</sup> In the same pathway, ferrochelatase is also inhibited which can affect erythrocyte fragility and shape.<sup>115</sup>

Lead can interact with stereospecific  $\text{Ca}^{2+}$  sites reflecting its much higher affinity compared to the physiological  $\text{Ca}^{2+}$ .<sup>116</sup> As  $\text{Ca}^{2+}$  is a key player in second messenger systems, this replacement dramatically affects different biologically significant calcium-dependent processes,  $\text{Ca}^{2+}$  channels and the  $\text{Ca}^{2+}$  pump transport systems especially in mitochondria, energy metabolism, apoptosis, ionic conduction, cell adhesion, enzymatic processes, protein maturation, and genetic regulation.<sup>115</sup>

Ionic mimicry for calcium contributes to neurological deficits, as some forms of lead are able to cross the blood–brain barrier (BBB) and accumulate in astroglial cells.<sup>117</sup> In addition, lead, even at picomolar concentrations, can replace calcium, thereby affecting key transmitters such as protein kinase C, which regulates long-term neural excitation and memory storage. Lead can also interfere with sodium ion concentration, which is responsible for numerous vital biological activities like the generation of action potentials in the excitatory tissues for the purposes of cell to cell communication (see Chapter 1), the uptake of neurotransmitters (acetylcholine, dopamine and GABA) and the regulation of uptake and retention of calcium by synaptosomes.

The *clinical toxicity of lead* may include symptoms from various organs. Renal toxicity may be reversible with lower exposure, as early pathological changes affect only the proximal tubules. Higher exposure leads to interstitial fibrosis and progressive nephropathy. Lead also affects the renin–angiotensin system, causing hypertension.<sup>118</sup> Compared to other organ systems, the nervous system appears to be the most sensitive and the main organ for lead-induced toxicity.<sup>119</sup> The effects on the peripheral nervous system are more pronounced in adults while the central nervous system is more prominently affected in children. Encephalopathy with a progressive degeneration of certain parts of the brain is a direct consequence of lead exposure and the major symptoms in children include irritability, agitation, poor attention span, headache, confusion, ataxia, drowsiness, convulsions and coma.<sup>120</sup> Before 1925, toxic neuropathy caused by lead was a frequent phenomenon. Today it is a distinct rarity.

However, humans are in positive lead balance from birth. In the United States the average blood lead concentration has been reported at  $0.03 \text{ mg L}^{-1}$  ( $3 \text{ } \mu\text{g dL}^{-1}$ ) in children aged 1 year and  $11 \text{ } \mu\text{g dL}^{-1}$  in children aged 5 years. Recent research demonstrates that there is no safe threshold for lead and, in small children, even in the BLL range  $<10 \text{ mg dL}^{-1}$  there is a significant inverse relationship between BLL and mental and psychomotor development.<sup>121,122</sup>

The adverse health effects of lead exposure range, both in adults and children, from impaired cognitive and behavioral development to death (Figure 3.10).

Fatal lead poisoning in developed countries has rarely been reported in recent decades. However, in resource-poor countries, local intoxications are being reported with increasing frequency. An outbreak in Senegal in 2007 associated with unprofessional lead–acid battery recycling resulted in the poisoning of children with a mean blood lead level (BLL) of  $130 \text{ mg dL}^{-1}$  in 50 children of which 18 died.<sup>124</sup>

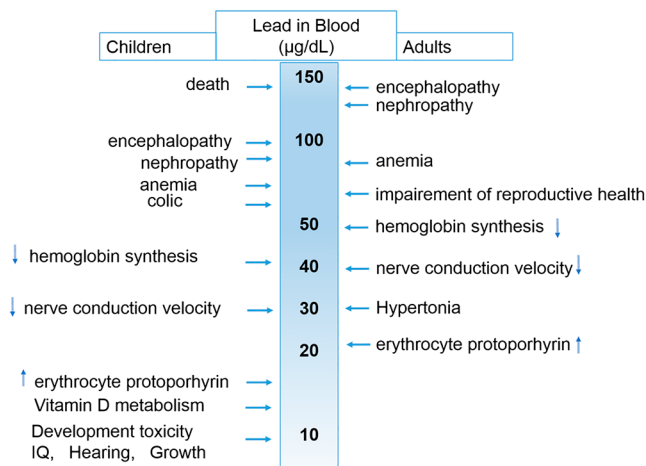


**Figure 3.10** Lead blood levels in children and adults associated with adverse health effects (modified from Meyer *et al.* 2008).<sup>121</sup>

### 3.5.3 Diagnostic Measures and Intervention Levels

Blood Lead Level (BLL) testing is the most useful screening and diagnostic test for recent or ongoing lead exposure. The intervention level for children has been lowered several times during the past decades (from 60  $\mu\text{g dL}^{-1}$  in 1960 to 5  $\mu\text{g dL}^{-1}$  in 2012) as it became clear that even minute amounts of lead have detrimental health effects on brain development in small children (Table 3.6).<sup>121</sup>

From May 2012 the Centre for Disease Control and Prevention lowered the BLL threshold to 5  $\mu\text{g dL}^{-1}$  which would affect about 450 000 children in the United States between the ages of 1 and 5 who have blood lead levels in this range.<sup>115</sup> It is hoped that lowering the threshold will impact efforts to address this public health problem, improving detection so that action can be taken sooner.<sup>122,123</sup>

To date, no safe blood lead threshold for the adverse effects of lead on infant or child neurodevelopment has been identified.<sup>122</sup> Comorbidities such as iron deficiency can enhance lead absorption.<sup>107</sup> Several management protocols are available for children and adults based on the blood lead level. At low concentration, confirmation with a blood test, general education on lead sources in the home and in food, and a follow-up strategy are most important. When the BLL is greater than 45  $\mu\text{g dL}^{-1}$  in children, chelator treatment should be considered. In adults, a BLL of <20  $\mu\text{g dL}^{-1}$  in all workers seems feasible and should be permitted. Removal from work should be initiated at 60  $\mu\text{g L}^{-1}$ , and chelator treatment is advised at BLL < 100  $\mu\text{g L}^{-1}$ .

### 3.5.4 Treatment of Lead Poisoning

Due to the high affinity for lead, sodium calcium ethylenediaminetetraacetic acid ( $\text{CaNa}_2\text{EDTA}$ ) alone or in combination with BAL has been the main therapeutic agent for lead poisoning over the last 50 years.<sup>125</sup> Both have

**Table 3.6** Intervention levels for lead intoxication derived from blood lead levels and supposed handling procedures.

BLL	Handling procedures
<b>Children</b>	
5–19 $\mu\text{g dL}^{-1}$	Confirm BLL within 3 months, test on iron deficiency, educate on general nutrition ( <i>e.g.</i> , calcium and vitamin C levels)
20–24 $\mu\text{g dL}^{-1}$	Confirm BLL within 1 month, erythrocyte protoporphyrin (EP) potential sources?, physical exam, iron treatment if deficient
25–44 $\mu\text{g dL}^{-1}$	Confirm BLL within 1 week, EP, complete diagnostic evaluation, neurodevelopment monitoring, potential sources?, test other children in house, education on lead; DMSA only if persists at this level
45–69 $\mu\text{g dL}^{-1}$	Confirm BLL within 1 week, EP, complete diagnostic evaluation, neurodevelopment monitoring, test other children in house, education on lead; hospitalize for 5 days: DMSA chelation, follow up program
>70 $\mu\text{g dL}^{-1}$	Chelation treatment: 1. DMSA, 2. CaNa <sub>2</sub> -EDTA if DMSA is not tolerated; follow-up program, home chelation with DMSA
<b>Adults</b>	
< 5 $\mu\text{g dL}^{-1}$	Normal
< 20 $\mu\text{g dL}^{-1}$	Workers blood lead levels: prudent and feasible
10–40 $\mu\text{g dL}^{-1}$	Remove from source (??), repeat level 3–6 months
40–50 $\mu\text{g dL}^{-1}$	Remove from source (?), repeat level 1–2 months
50–60 $\mu\text{g dL}^{-1}$	Remove from work, chelation possibly considered
80–99 $\mu\text{g dL}^{-1}$	Chelation treatment strongly considered, DMSA chelation, EDTA if neurological features
< 100 $\mu\text{g dL}^{-1}$	Chelation treatment recommended

to be administered intravenously (*i.v.*) because they are poorly absorbed from the gastrointestinal tract. CaNa<sub>2</sub>EDTA is the safer variant of EDTA, which had previously shown a fatal danger of inducing severe hypocalcaemia. CaNa<sub>2</sub>EDTA is appreciably metabolized, and is almost entirely excreted in the urine, with an elimination half-life of between 1.4 and 3 hours.<sup>126</sup> A typical dose is 50–75 mg kg<sup>-1</sup> day<sup>-1</sup> for adults, and 1000–1500 mg m<sup>-2</sup> day<sup>-1</sup> for children for 5 days, followed by a two-day interruption, with repeated course(s) when necessary.<sup>127</sup> Contraindications for medication with CaNa<sub>2</sub>EDTA are anuria or active renal disease, hepatitis, and hypersensitivity to Edetate products.<sup>127</sup> For the use of CaNa<sub>2</sub>EDTA in patients with severe lead poisoning, numerous case histories have documented the rapid improvement in the severe features of lead poisoning,<sup>128,129</sup> including severe encephalopathies.<sup>130,131</sup>

Clinical improvement is usually evident within 24–48 h of commencing treatment. Byers *et al.* (1959) treated 45 children with severe lead poisoning, of whom 17 (38%) had acute lead encephalopathy. Treatment was with intravenous or intramuscular CaNa<sub>2</sub>EDTA at 65 mg kg<sup>-1</sup> day<sup>-1</sup> in two divided doses for 3–4 days. Each patient received at least two courses separated by a 4-day rest period. Of the encephalopathic children, four died, five remained

severely brain damaged, and six returned to normal or near-normal. From 45 cases, 21 made a full recovery, 15 made a partial recovery, and 4 died.<sup>132</sup> However, following findings in animal studies where  $\text{CaNa}_2\text{EDTA}$  causes internal redistribution of lead during therapy with no net loss of lead from liver and brain, it is generally advised today to treat cases with high blood lead levels with a combined i.v. medication of  $\text{CaNa}_2\text{EDTA}$  and BAL.<sup>126,133</sup> As an alternative treatment, DMSA can be used together with EDTA.<sup>134</sup>

Less severely poisoned patients were also found to improve symptomatically following administration of  $\text{CaNa}_2\text{EDTA}$ . It was shown that  $\text{CaNa}_2\text{EDTA}$  chelation therapy can effectively delay the progression of chronic kidney disease in patients with measurable body lead burdens as far as estimated glomerular filtration rate (eGFR) and creatinine clearance rate (Ccr) are concerned. However, proteinuria could not be decreased.<sup>135</sup>

In recent years, DMSA 4 has gained wide acceptance as an effective drug which can be much more easily applied, also under suboptimal conditions in developing countries. In a review, Bradberry and Vale (2009) compared  $\text{CaNa}_2\text{EDTA}$  and DMSA 4 in the treatment of inorganic lead poisoning.<sup>136</sup> Both antidotes are distributed predominantly extracellularly, have short half-lives of less than 60 min and do not cross the blood–brain barrier.

Using equimolar chelator doses.

- DMSA is generally more effective than  $\text{CaNa}_2\text{EDTA}$  in reducing the kidney lead concentrations (“soft lead”)
- $\text{CaNa}_2\text{EDTA}$  is generally more effective than DMSA in reducing bone lead concentrations (“hard lead”).
- There are inconsistent observations concerning brain lead reduction, however, several studies demonstrated that sodium calcium EDTA could increase brain lead concentrations.

Although there is less extensive experience with DMSA, a rapid, life-saving treatment was also reported with this oral chelator. For example, nine lead-intoxicated smelters with a mean blood lead concentration of  $97 \mu\text{g dL}^{-1}$  experienced headache, insomnia, abdominal pain, and constipation. All symptoms were completely alleviated within a few days of starting a 5-day course of oral DMSA at  $8.4\text{--}42.2 \text{ mg kg}^{-1} \text{ day}^{-1}$ .<sup>137</sup>

Fatal lead poisonings from local intoxication are being reported with increasing frequency from undeveloped countries. In a large retrospective analysis of clinical data from a cohort of more than 1000 lead-poisoned children <5 years of age from rural Zamfara, Nigeria, Thurtle *et al.* evaluated the changes in BLL after oral chelation treatment with DMSA and the occurrence of adverse drug effects associated with the medication.<sup>138</sup> It was concluded that DMSA is suitable for use as a single agent in children with severe lead poisoning, particularly in resource-limited settings. The establishment of chelation treatment in parallel with an environmental remediation programme to reduce ongoing exposure was associated with a large and rapid decrease in the number of deaths due to lead poisoning. Only six deaths were considered

to be solely due to lead poisoning, and occurred during the 13 month period analysed, compared with over 400 fatalities in the three preceding months.

There are academic centres that use D-penicillamine (DPA) 5 also for lead poisoning. Its safety and efficacy, however, have not been established. The American Academy for Pediatrics considers DPA to be a third-line drug for lead poisoning.<sup>139</sup>

### 3.6 Cadmium

Cadmium is a soft, malleable and ductile, silver-white metal which has a relatively high vapor pressure. It occurs in the earth's crust in ores together with zinc, copper and lead at low amounts of about 0.1 part per million.<sup>30</sup> Like zinc, cadmium prefers oxidation state +2 in most of its compounds and shows a chemical behaviour similar to that of Zn. Cadmium is widely used in industrial processes, in Ni–Cd batteries, as a colour pigment, as a stabilizer in PVC products, in electroplating, as an anticorrosive agent, in television screens, as a neutron absorber in nuclear power plants, and in fluorescent nanoparticles and quantum dots. The actual production of cadmium is in the range of 20 000 tons per year but has declined in recent years because of its well known environmental accumulation and toxicity.<sup>140</sup> Discharge of cadmium into natural waters is mainly from the electroplating industry, but also from the nickel–cadmium battery industry and from smelter operations.<sup>141</sup>

Volcanic activities are a natural source of Cd exposure that increases environmental cadmium deposits by 140–1500 metric tons per year. The global cadmium emission from anthropogenic sources (mainly non-ferrous metal production) is twice as high, but declined from 7600 tons in 1983 to 3000 tons in 1991. Although some cadmium-containing products can be recycled, a large proportion of the general cadmium pollution is caused by dumping and incinerating cadmium-polluted waste.<sup>142</sup> In Scandinavia, for example, the cadmium concentration in agricultural soil increases by 0.2% per year.

Inhalation due to industrial exposure can be significant in occupational settings, for example, welding and soldering. People who live near hazardous waste sites or factories that release cadmium into the air experience a risk of exposure to cadmium in both the air and from eating locally-produced food. Such local contaminations of cadmium were frequent in the past and are still occurring in developing countries. In many Western countries strict regulations now limit the amount of cadmium that can be released into the atmosphere.<sup>143</sup>

The most common form of cadmium exposure for the general population is through food and cigarette smoke; the contribution from other pathways to total uptake is small.<sup>144</sup> Daily intake of cadmium through food varies by geographic region. Intake is reported to be approximately 8 to 30  $\mu\text{g}$  in Europe and the United States *versus* 59 to 113  $\mu\text{g}$  in various areas of Japan.<sup>145</sup>

Shellfish, liver and kidney meats, leafy vegetables and raw potatoes are relatively rich in Cd, whereas fruits and beverages contain low amounts of cadmium.

Tobacco is a plant, which accumulates Cd from a contaminated soil. A single cigarette typically contains 1–2  $\mu\text{g}$  of cadmium. When burned, cadmium is present at a level of 1000–3000 ppb in the smoke. Approximately 40–60% of the cadmium inhaled from cigarette smoke is able to pass through the lungs and into the body. Smokers thus absorb additional amounts of Cd comparable to those from food; therefore organ concentration of Cd in smokers is twice as high as in non-smokers.<sup>141,143</sup>

### 3.6.1 Absorption and Metabolism of Cadmium

Cadmium is more efficiently absorbed from the lungs (25–60% absorbed) than the gastrointestinal tract (5–10% absorbed) (Figure 3.11). It is estimated that adults absorb 1.4–8  $\mu\text{g}$  of cadmium per day by oral exposure. Gastrointestinal absorption is largely dependent on the solubility of the cadmium

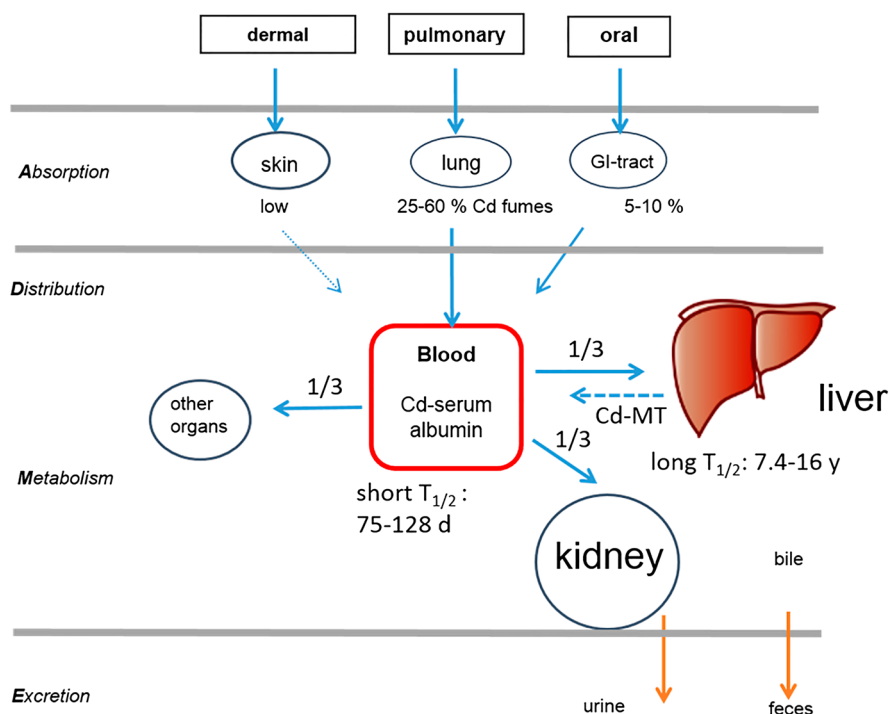


**Figure 3.11** Absorption and metabolism of cadmium. Inhaled Cd fumes are efficiently absorbed from the lung. Gastrointestinal absorption is somewhat limited but higher in subjects with iron deficiency because the commonly used absorption mechanism *via* DMT1 is upregulated when the essential trace element iron is deficient in the body. Absorbed Cd is bound to serum albumin and distributed mainly to the liver from where it returns in part bound to metallothionein (Cd-MT). Cd accumulates in the body because the half-life is in the range of years.<sup>146</sup>

compound but physiological and nutritional factors may also modify the amount absorbed. Cadmium absorption is decreased in the presence of divalent and trivalent cations ( $\text{Zn}^{2+}$ ,  $\text{Mg}^{2+}$ ,  $\text{Cr}^{3+}$ ) and stimulated in subjects with iron and calcium deficiencies indicating that absorption of non-physiological Cd follows the regulation of absorption mechanism of essential metals.<sup>147,148</sup> The divalent metal transporter 1 (DMT1), which has been identified as the main non-heme food iron transporter, also plays a role in cadmium absorption.<sup>148</sup>

Absorption of cadmium *via* inhalation is dependent on solubility and the particle size and hence the site of deposition in the respiratory tract. Small particles in cadmium fumes for example are taken up efficiently by the lung alveoli. Absorption of cadmium through the skin is extremely low (0.5%) and would be of concern only in situations where concentrated solutions would be in contact with the skin for several hours or longer.<sup>141</sup>

After uptake from the lung or the gastrointestinal tract, cadmium is transported in blood plasma initially bound to albumin or high molecular weight proteins, as demonstrated in experimental animals.<sup>145</sup> Protein-bound cadmium is then preferentially taken up by the liver. In the liver, cadmium induces the synthesis of metallothionein and, a few days after exposure, metallothionein-bound cadmium appears in the blood plasma. Metallothionein (MT) is a low molecular weight protein (6500 Da) with high cysteine content and high metal affinity which plays a major role in the kinetics of absorption and the metabolism of cadmium. The balance between Cd–MT and non-bound Cd in renal tissue has been shown to be of crucial importance for expression of toxicity. The extensively studied metallothioneins MT1 and MT2 are expressed in almost all mammalian tissues.<sup>149</sup> Since the blood–brain barrier keeps Cd outside the CNS, reported neurotoxic effects of Cd during development are likely to be secondary, due to interference of Cd with Zn metabolism and not a direct effect of Cd on brain cells.

Because of its low molecular weight, cadmium–metallothionein (Cd–MT) is efficiently filtered through the glomeruli and thereafter taken up by the tubules. Cadmium accumulates in the human kidney over the entire lifetime. For individuals who are chronically exposed to environmental levels of cadmium either through diet or by smoking, the highest concentrations of cadmium are measured in the renal cortex.<sup>150</sup> Following gastrointestinal absorption, most of the oral dose is excreted in the faeces. Following inhalation, excretion *via* the urine and faeces are approximately equal. In individuals continuously exposed to cadmium, the amount excreted in urine will progressively increase in proportion with body burden. However, the amount excreted is only a small fraction of the total body burden, unless kidney toxicity occurs in which case urinary cadmium increases substantially.

### 3.6.2 Toxicity of Cadmium

Cadmium is extremely toxic and has biological effects at lower concentration than most other metals.<sup>141,151</sup>

### 3.6.2.1 Mechanism of Cadmium Toxicity

Cadmium has high affinity for thiol groups and the major thiol antioxidant, glutathione (GSH) is a primary target for free Cd ions.<sup>151</sup> Cadmium also binds to O- and N-containing ligands. Cd is non redox-active and it cannot induce ROS production directly. However, there is clear evidence that *oxidative stress* is the principal molecular basis underlying cytotoxicity because Cd indirectly provokes oxidative damage to the DNA, leading to the induction of cellular proliferation, inhibition of the apoptotic mechanisms and blocking of DNA repair mechanisms.<sup>152</sup>

Cadmium can also influence the absorption and distribution of essential elements and can replace them in enzymes (Fe and Zn). The formation of a Cd–Se–cysteine complex in the livers and kidneys of mice can lead to a selenium (Se) depletion affecting the function of GSH.<sup>151,153</sup> In the liver, the toxicity of cadmium is reduced because sufficient amounts of metallothionein (MT1 and MT2) can be synthesized to bind all accumulated Cd. MT-bound cadmium is released from the liver into the blood where it is cleared by glomerular filtration in the kidney and taken up by the renal tubules, where the MT is cleaved and cadmium is released. The synthesis of MT in the kidney is insufficient to bind all the free cadmium, resulting in tubular damage or cell membrane destruction *via* activation of oxygen species.<sup>151</sup>

### 3.6.2.2 Clinical Toxicity of Cd

The most dangerous characteristic of cadmium is the long biological half-life, from 17–30 years in man, and its accumulation in the liver and kidneys, leading to severe kidney damage.<sup>154</sup> For acute oral ingestion of cadmium, lethal doses of cadmium of 350–8900 mg have been reported.<sup>155</sup> Nausea and vomiting occur, normally without delay. Death is caused by massive fluid loss, edema, and widespread organ destruction (Table 3.7). Acute exposure by inhalation can result from brief inhalation exposure to high concentrations of cadmium compounds. These exposure types can occur in occupational settings such as in cadmium alloy production, welding involving cadmium-coated steel, and cadmium smelting and refining. The lethal concentration of cadmium oxide fumes for humans has been estimated to be about 5 mg cadmium m<sup>-3</sup> for an 8-hour exposure.<sup>156</sup>

Onset of symptoms from inhalation is usually delayed for 4–10 hours. Initial symptoms resemble the onset of a flu-like illness, fever and myalgias. Later symptoms include chest pain, cough, and dyspnea. Bronchospasm and hemoptysis may also occur.<sup>158</sup> An informative case was reported of a healthy 34 year-old welder who worked for 30 minutes with an oxyacetylene torch and a silver solder. His workbench was in a large airy building with a high ceiling and large, open doors. He died 5 days later with both lungs showing changes typical of acute pneumonitis.<sup>159</sup> The source of cadmium was the rod of solder which, unsuspectedly, contained 20% cadmium!

**Table 3.7** Dose levels and symptoms of acute cadmium intoxication from inhalation or oral ingestion (modified from ref. 157).

Dose	Signs and symptoms
Inhalation ( $\text{mg m}^{-3}$ )	
0.01–0.15	Cough, irritation of the throat, gastroenteritis symptoms: vomiting, abdominal cramps, diarrhea
0.5	Threshold for respiratory effects after 8 hour exposure
1–5	Immediately dangerous to health – facial edema, hypotension, dysrhythmias, confusion, oliguria, metabolic acidosis, acute centrilobular necrosis of the liver, pulmonary edema, tracheobronchitis, pneumonitis
5	Lethal after 8 hours
39	Lethal after 20 min
Oral ingestion ( $\text{mg kg}^{-1}$ )	
0.07	Emetic dose
>15	Gastrointestinal symptoms: vomiting, abdominal cramps, diarrhea
20–30	Extensive fluid loss, shock, pulmonary edema, hypotension, oliguria, multiorgan failure, death

Chronic oral exposure leads to renal failure, characterised by proteinuria. Chronic inhalation causes loss of renal tubular function, leading to proteinuria and impairs lung function by causing bronchitis, obstructive lung disease and, in some cases, interstitial fibrosis.

The dangerous exposure to chronic environmental cadmium was first recognized in the Toyama Prefecture Japan around 1950 in elderly women who suffered from symptoms such as strong pains, kidney disease and osteomalacia and/or osteoporosis, representing a new disease which was named “itai-itai” (“it hurts – it hurts”) disease.<sup>160</sup> The cause was linked to the presence of cadmium in the drinking water from the Jinzugawa River basin derived from a mining and smelting company. The effect on the bone is not caused by substantial uptake of Cd into the bone but by a strong effect on vitamin D metabolism in the kidney leading to impairment of gut absorption of calcium and derangement of collagen metabolism.<sup>161</sup>

Cadmium has also been shown to induce chromosome damage and DNA strand breaks. Cadmium has been classified as a category 1 carcinogen, *i.e.*, is carcinogenic to humans following inhalation only, not oral exposure.<sup>152,162</sup>

As a summary, high-level Cd exposure can clearly give rise to nephropathy and osteopathy and, after inhalation, may lead also to cancer. In addition, recent epidemiological studies suggest that levels of Cd body burden occurring commonly in the general population can significantly increase risk of renal tubular damage and osteoporosis, as well as vascular diseases, cancer, diabetes, and total mortality.<sup>155–157</sup> Cd may thus be one of the most toxic environmental contaminants.<sup>157</sup>

### 3.6.3 Diagnostic Markers and Intervention Level for Cd Intoxication

Cadmium levels in blood, urine, faeces, liver, kidney, hair, and other tissues have been used as biological indicators of exposure to cadmium. For recent exposure to Cd, blood concentration is the best measure of exposure, but is not a good measure for whole-body Cd accumulation.<sup>141</sup> In the United States, the 50<sup>th</sup> percentile of blood cadmium concentrations in adults was 0.330  $\mu\text{g L}^{-1}$  (Table 3.8). Environmental or occupational exposure can elevate blood cadmium concentration substantially.

For long-term, low-level exposure, urine cadmium concentration best reflects the total body burden, provided renal tubular function is normal.<sup>163</sup> Impaired kidney function has been followed by measuring proteins in the urine which are normally not excreted, such as  $\beta_2$ -microglobulin,  $\alpha_1$ -microglobulin, or retinol-binding protein. However, all these sensitive markers are not specific for cadmium-induced damage in the kidney. Roels *et al.* correlated a number of cadmium markers in blood and urine in workers occupationally exposed to cadmium. It was concluded that a recommendation of 5  $\mu\text{g Cd g}^{-1}$  creatinine in urine as the biological exposure limit for occupational exposure seems justified to prevent the earliest damage to the kidney.<sup>165</sup>

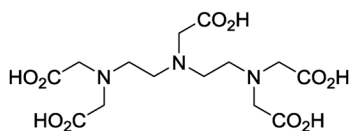
### 3.6.4 Chelation Treatment for Cadmium Poisoning

The treatment of acute and chronic cadmium poisoning has been a topic of clinical interest for decades. As far as chelation therapy is concerned the summary of the scientific discussion in reviews and toxicology report over the last 40 years is disappointing—there is still no effective, safe and approved drug.<sup>141,166</sup> Nevertheless, a number of animal studies and a few anecdotal human studies have investigated chelators to prevent acute cadmium poisoning. The most promising candidates are so far polyaminocarboxylic acids ( $\text{CaNa}_2\text{EDTA}$  or  $\text{CaNa}_3\text{DTPA}$ ) **6**.<sup>166</sup> In animals, the body burden of cadmium is reduced and the urinary excretion of cadmium increased.<sup>166</sup> EDTA seems to be superior to other chelators such as DMSA in mobilizing intracellular Cd. On the other hand, EDTA has also been demonstrated to increase the

**Table 3.8** Biomarkers used to identify or quantify exposure to cadmium. Data from ref. 141 and 164

Parameter	Environmental		
	General population	exposed	Exposed workers
Blood Cd ( $\mu\text{g L}^{-1}$ )	0.330		50
Urine Cd ( $\mu\text{g g}^{-1}$ creatinine)	0.247	50	50
Kidney cortex ( $\mu\text{g g}^{-1}$ w/w)	25–40		300

nephrotoxicity of cadmium after repeated exposure in rabbits.<sup>167</sup> However, the efficacy of EDTA can apparently be improved with concomitant use of glutathione which also protects against nephrotoxicity.<sup>168</sup> Efficacy may also be improved with concomitant use of antioxidants.<sup>150</sup>



DTPA (6)

Dreisbach (1983) proposed in cases of acute cadmium poisoning 15–25 mg EDTA kg<sup>-1</sup> (0.08–0.125 ml of 20% solution per kg body weight) in 250–500 ml of 5% dextrose intravenously over a 1–2-hour period twice daily. The maximum dose should not exceed 50 mg kg<sup>-1</sup> day<sup>-1</sup>. The drug should be given in 5-day courses with an interval of at least 2 days between courses.<sup>169</sup>

Cotter (1958) reported the case of three men exposed to cadmium fumes who were subsequently treated with calcium disodium EDTA at a dose of 0.5 g every 2 hours for 1–2 weeks.<sup>170</sup> At the end of the treatment period the patients were either asymptomatic or had made a significant recovery, as indicated by a reduction in blood urea nitrogen, blood cadmium and urinary cadmium.

Dimercaprol (BAL) should not be used in cases of acute cadmium poisoning because it increases the uptake of cadmium in the kidneys.<sup>171</sup>

The use of various chelators has been found to reduce gastrointestinal absorption following acute oral exposure to cadmium in various animal studies.<sup>172–174</sup> CaDTPA, ZnDTPA and DMSA appeared to be the most effective antidotes, but DMSA increased the Cd–kidney concentration.<sup>172</sup>

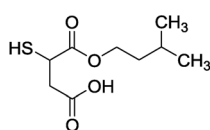
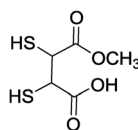
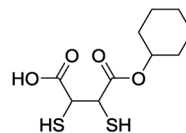
Concerning chronic cadmium poisoning, the current consensus appears to be that there is so far no recommended chelation treatment.<sup>170,175</sup>

In a retrospective analysis of blood samples from a trial in children with lead poisoning who were treated with DMSA (4), Cao *et al.* found that the blood cadmium levels from the background exposure did not decrease during treatment.<sup>176</sup> One reason could be that most of the Cd is stored tightly bound to MT intracellularly and cannot be mobilized by chelators.

On the other hand, Fatemi *et al.* studied the efficacy of desferrioxamine (DFO) and deferasirox (DFX) in removing cadmium from whole-body stores in rats over 7 days, following cadmium accumulation from drinking water of 60 days. Individually, and in combination, DFO and DFX removed cadmium from the body leaving the iron stores unchanged.<sup>177,178</sup> (See Chapter 2, Figure 2.14 for structures.)

However, so far no controlled studies are available to show the reduction of cadmium burden or an improvement of kidney damage in humans affected with a chronic cadmium intoxication. This may reflect the fact that chelators have poor access to the interior of cells where most Cd is stored in the form of Cd–MT.<sup>166</sup>

Among the new chelators, DMSA monoesters **7** are reported to be capable of mobilizing intracellularly bound cadmium as well as promoting antioxidant effects by removing cadmium from the site of deleterious oxidation reactions. Jones *et al.* exposed mice to cadmium for seven days, observed that administration of MmDMSA **8** and MchDMSA **9** produced significant reductions in whole body cadmium levels. Furthermore, no redistribution of cadmium in the brain was observed.<sup>179</sup>

MiADMSA (**7**)MinDMSA (**8**)MchDMSA (**9**)

The successful treatment of chronic cadmium intoxication is yet to be clarified. Unfortunately, both cross-sectional and prospective epidemiological studies have linked high-normal Cd body levels with increased risk for osteoporosis, nephropathy, vascular disease, cancer, diabetes, and total mortality.<sup>2,175</sup>

Many individuals in Europe already exceed these exposure levels. Therefore, measures should be taken to reduce cadmium exposure in the general population in order to minimize the risk of adverse health effects. Avoiding cigarette smoke is the most obvious way to limit Cd exposure. Excessive intake of shellfish or organ meats may also be inadvisable in this regard.

## 3.7 Noble Metals

Besides the most relevant toxic heavy metals, As, Hg, Pb and Cd, others can also result in acute or chronic poisoning. This is less common but can be serious—sometimes deadly. Some of these intoxications can also be treated with chelation therapy.

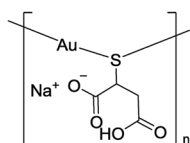
### 3.7.1 Silver Poisoning

Silver has a long and intriguing history as an antibiotic in human health-care.<sup>180</sup> The antimicrobial action of silver or silver compounds is proportional to the bioactive silver ion ( $\text{Ag}^+$ ) released and its availability to interact with bacterial or fungal cell membranes. Silver nanoparticles in deodorants or in textiles act in the same way and are important new developments. Nanocrystalline silver dressings may become an important part of local MRSA (*Methicillin-resistant Staphylococcus aureus*) management. Silver exhibits low toxicity in the human body and minimal risk is expected due to clinical exposure by inhalation, ingestion, or dermal application. However, the inappropriate swallowing or inhalation of silver compounds, mainly in the

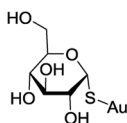
form of alternative medicines, can lead to local or generalized argyria.<sup>181</sup> The most dramatic symptom of argyria or argyrosis is that the skin turns blue (“blue-man”).<sup>182</sup> Generalized argyria affects large areas of the visible surface of the body. Local argyria shows in limited regions of the body, such as patches of skin, parts of the mucous membrane or the conjunctiva. Argyria is usually believed to be benign and limited to skin discolouration, but there are isolated reports of more serious neurological, renal, or hepatic complications. A silver dose of 50–500 mg per kg body weight is described as the lethal toxic dose in humans.<sup>183</sup> The formation of silver selenides as stable, rather non-toxic compounds may explain the permanence and irreversibility of the metallic tinge in the skin and the unsuccessful attempts of chelation with BAL and DMSA to remove silver from the body.<sup>183</sup>

### 3.7.2 Gold Poisoning

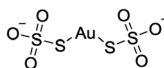
The use of gold compounds in medicine is called “chrysotherapy”. Since 1929, when a French doctor discovered its anti-inflammatory properties, gold compounds in drugs have been used to treat rheumatoid arthritis.<sup>184</sup> Four gold(I) complexes are widely used throughout the World (10–13). Auranofin 13 has the advantage of being orally active, the others having to be administered by injection. Gold(I) is a soft metal cation and consequently favours sulphur and phosphorous as ligands. Chrysotherapy is an effective treatment for approximately 70% of rheumatoid arthritis patients. Gold drugs have a well known anti-inflammatory action, with some patients achieving long-term remission of the disease. It is still not known exactly how these drugs work, but they clearly modify the immune response in these patients. The complexes undergo rapid metabolism *via* thiol exchange, generating substantial levels of Au(1)–glutathione. It is possible that this gold complex is responsible for the immunomodulatory properties of clinically used gold-based drugs. Due to frequent side effects and the availability of better drugs (low dose methotrexate) the use of gold in rheumatoid arthritis treatment has declined since 1990. However, in recent years these gold compounds have been shown to be promising agents for HIV and cancer treatments.



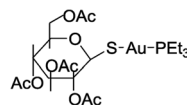
Myochryesine (10)



Solganol (11)



Sanochryesine (12)



Auranofin (13)

The toxic complications of gold therapy include frequent initial hypersensitivity reactions or rare cumulative toxic manifestations.<sup>185</sup> A typical course of medication using either sodium aurothiomalate (Myochryesine) or aurothioglucose (Solganol-B) is to give increasing doses of gold until a rather high total dose of 1800–2000 mg is reached which can cause unpredictable toxicity, such as dermatitis, urticaria, purpura, secondary anemia, exfoliative

dermatitis, stomatitis, thrombopenic purpura, or agranulocytosis.<sup>184</sup> It has been found in those rare cases that treatment with BAL can mobilize gold into the urine and can have considerable merit in the treatment of the toxic complications of gold salts.<sup>185</sup> Experiments with acute gold intoxication in rats have shown that DMPS can also remove gold from the body.<sup>186</sup>

## 3.8 Other Metals

### 3.8.1 Acute Iron Poisoning

Acute iron poisoning is a frequent problem in developed countries where iron preparations are easily available at pharmacies. Unintentional ingestion of iron preparations by children younger than 6 years accounts for 16 000 intoxication per year in the USA; suicide attempts are rare but more typical of adults.<sup>187</sup>

Iron has two distinct toxic effects. First, it is directly caustic to the gastrointestinal mucosa, leading to vomiting, diarrhea, and abdominal pain. In severe cases, it can result in hemorrhagic necrosis with bleeding, perforation, and peritonitis. Second, it impairs intracellular metabolism, primarily through lipid peroxidation and free radical formation. One of its most important consequences is the impairment of mitochondrial adenosine triphosphate synthesis. Results from examination of the poisoned subjects may show overlapping phases of clinical manifestation:<sup>189</sup>

- Gastrointestinal phase: (30 minutes to 6 hours) Abdominal pain, vomiting, diarrhea, hematemesis, melena, lethargy, shock (from capillary leak and third spacing), metabolic acidosis
- Latent phase: (6 to 24 hours) Improvement in gastrointestinal symptoms; may have poor perfusion, tachypnea, tachycardia
- Shock and metabolic acidosis: (4 hours to 4 days) Hypovolemic, distributive, or cardiogenic shock with profound metabolic acidosis, coagulopathy, renal insufficiency/failure, pulmonary dysfunction/failure, central nervous system dysfunction
- Hepatotoxicity: (within 2 days) Coma, coagulopathy, jaundice. Severity is dose dependent.
- Bowel obstruction: (2 to 4 weeks) Vomiting, dehydration, abdominal pain, usually gastric outlet obstruction

If the patient has ingested more than 20 mg kg<sup>-1</sup> of elemental iron or shows signs of mild toxicity, whole bowel irrigation with polyethylene glycol electrolyte lavage solution is recommended, 1.5–2 L h<sup>-1</sup> in adults, 20–40 mL kg<sup>-1</sup> h<sup>-1</sup> for children until the rectal effluent is clear. The serum iron peak should be monitored, which typically occurs 3–5 hours after ingestion, but may also be delayed (Table 3.9). If peak serum iron levels are greater than 500 µg dL<sup>-1</sup>, intravenous deferoxamine (DFO) therapy should be commenced at a starting dose of 15 mg kg<sup>-1</sup> h<sup>-1</sup>.

**Table 3.9** Symptoms and intervention levels in acute iron intoxication. Data taken from ref. 187 and 188

Peak serum iron ( $\mu\text{g dL}^{-1}$ )	Toxicity	Desferrioxamine
50–150	none	—
150–300	Mild	—
300–500	Moderate (rarely develop serious complications)	—
>500	Severe (serious systemic toxicity)	Should be initiated $15 \text{ mg kg}^{-1} \text{ h}^{-1}$
>1000	Significant morbidity and mortality	Strongly recommended ( $15\text{--}35 \text{ mg kg}^{-1} \text{ h}^{-1}$ )

The utility of other oral iron chelators (deferiprone, deferasirox) for acute iron poisoning in humans has hitherto not been described.

### 3.8.2 Acute Copper Poisoning

Copper sulphate ingestion is a rare form of poisoning usually found especially in the Indian subcontinent, where this chemical is sold over the counter. It is commonly used as a pesticide, in the leather industry and also in the preparation of homemade glue. Ingestion of more than 1 g of copper sulphate results in symptoms of toxicity such as intravascular haemolysis, methaemoglobinaemia, acute kidney injury and rhabdomyolysis. The lethal dose for ingested copper sulphate is 10–20 g, but can also be lower.<sup>190</sup>

Several chelators have been used in different single cases such as D-penicillamine 5,<sup>190</sup> or EDTA.<sup>191</sup> For severe cases of cupric poisoning, Takeda *et al.* recommended BAL 1 ( $4 \text{ mg kg}^{-1}$  every 5–6 hours over 5–7 days), and 250–500 mg D-penicillamine (5) every 8–12 hours.<sup>192</sup>

### 3.8.3 Thallium Poisoning

Thallium (Tl) is one of the most toxic metals. Until the early years of the 20th century, thallium salts were used extensively to treat syphilis, to reduce night sweats in tuberculosis patients and also to kill rodents. As thallium salts are odourless, tasteless and extremely toxic, these aspects made thallium compounds the choice for homicidal poisoning during the early part of the 20th century. Thallium salts are rapidly absorbed by virtually all routes, with gastrointestinal exposure being the most common route to produce toxicity. Thallium enters cells by a unique process governed by its similarity in charge and ionic radius to potassium. Although the exact mechanism of toxicity has not been established, thallium interferes with energy production at essential steps in glycolysis, the Krebs cycle, and oxidative phosphorylation. Additional effects include inhibition of sodium potassium adenosine triphosphatase and binding to sulfhydryl groups. The major manifestations

of toxicity consist of a rapidly progressive, ascending, extremely painful sensory neuropathy and alopecia. The continued use of thallium as a rodenticide in many developing countries and its increasing use in an expanding number of new technologies raise concerns about exposure risk to animals and humans.<sup>193</sup>

A report published in 1934 reviewed 778 cases of human thallium poisoning of which 46 were fatal. Today, thallium is no longer readily available, thus accidental poisonings or suicides have become rare.

There are no controlled trials of treatments in thallium-poisoned patients. Strong evidence speaks against the use of traditional metal chelators such as dimercaprol (British anti-Lewisite) (1) and penicillamine (5); the latter may cause redistribution of thallium into the central nervous system.<sup>196</sup> Likewise, forced potassium diuresis appears harmful. The use of single- or multiple-dose activated charcoal is supported by *in vitro* binding experiments and some animal data, and charcoal haemoperfusion may be a useful adjunct.

A rather specific possibility to remove thallium comes from the chemical similarity to potassium which has the same charge and a similar ionic radius. Thallium salts thus follow potassium distribution pathways and alter a number of K-dependent processes. The same is true for caesium ions, which represent a serious contamination problem in the form of <sup>137</sup>Cs in any nuclear catastrophes. Cs and Tl ions have a high affinity for crystal lattice sites of potassium in Prussian blue (soluble and insoluble Prussian blue).<sup>194</sup> Prussian blue when orally applied, is almost not absorbed, but can interrupt the enterohepatic cycling of Tl, thus enhancing fecal elimination of the metal.<sup>195</sup>

Multiple animal studies give evidence for enhanced elimination and improved survival with Prussian blue. Unfortunately, despite the fact that many humans have been treated with Prussian blue, the data presented are insufficient to comment definitively on its efficacy. However, Prussian blue's safety profile is superior to that of other proposed therapies and it should be considered the drug of choice in acute thallium poisoning. Public health efforts should focus on greater restrictions on access to, and use of, thallium salts.<sup>195,196</sup>

### 3.9 Conclusion

Heavy metal poisoning, especially with the most relevant: arsenic, mercury, lead and cadmium, has followed the technical development and accompanied medical history for many centuries (Table 3.10). Heavy metals can be very reactive within biological systems. The toxicity generally is provided by (i) a mimicry effect in which ions of essential, non-heavy metals are replaced due to higher affinities for the respective binding sites in the various proteins and (ii) a strong increase of oxidative stress caused by inhibiting the antioxidative defence systems or by stimulation of ROS or RNS formation.

Cases of acute poisoning with heavy metals still occur today due to various causes, however, at a much lower frequency than 100 years ago. Symptoms may begin after a few hours, can be non-specific and are not easy to interpret at a

**Table 3.10** Medical impact, symptoms and treatment of acute and chronic heavy metals poisoning.

	As	Hg	Pb	Cd
Acute poisoning				
Importance	today rare, suicide, homicide	today rare, suicide, homicide	today rare, suicide, homicide	Very rare
Symptoms				
Treatment	DMSA, DMPS, BAL	DMSA, DMPS, BAL	CaNa <sub>2</sub> EDTA, DMPS, DMSA	CaNa <sub>2</sub> EDTA
Chronic poisoning				
Importance	Global impact with chronic exposure in contaminated drinking water	Local organic Hg contaminations; unclear dental amalgam Hg	Local lead contaminations possible; very toxic to developing brain in children, no safe levels <i>in vivo</i>	Exposure levels also in Europe critical
Symptoms	Neuropathy, diabetes, renal system, cardiovascular diseases, cancer	Central + peripheral neuropathy	impaired cognitive and behavioral development	Osteoporosis, nephropathy, vascular disease, cancer,
Treatment	No	Hg <sup>0</sup> , inorganic: DMPS?; organic Hg: DMSA?	DMPS?	CaNa <sub>2</sub> EDTA, DMSA

first glance. However, every minute counts and detailed information on the respective heavy metal exposure is critical to the individual outcome. If the correct chelator is available during the first hours, many symptoms can be reversed within a short time and the patient can survive even after deadly doses.

However, subacute and even more chronic poisoning with heavy metals is still an unsolved problem, especially with arsenic or cadmium exposure. Therefore, on a global perspective, prevention strategies are important and more successful than the widespread intake of chelators without medical indications.

## Abbreviations

<b>BBB</b>	Blood-brain barrier
<b>BEI</b>	US Federal biological exposure index
<b>BLL</b>	Blood lead levels
<b>DALYs</b>	Disability-adjusted life years
<b>EPA</b>	US Environmental Protection Agency
<b>FDA</b>	(US) Food and Drug Administration

<b>GI</b>	Gastrointestinal
<b>MAC</b>	Maximum allowable concentration
<b>MPL</b>	Maximum permissible limit
<b>MRP</b>	Multiple drug resistance protein
<b>MRSA</b>	Methicillin-resistant staphylococcus aureus
<b>RBC</b>	Red blood cell
<b>RNS</b>	Reactive nitrogen species
<b>ROS</b>	Reactive oxygen species

## References

1. *Ten Chemicals of Major Public Health Concern*, World Health Organisation, 2015.
2. L. Järup, *Br. Med. Bull.*, 2003, **68**, 167.
3. R. G. Pearson, *Coord. Chem. Rev.*, 1990, **100**, 403.
4. E. Nieboer and D. H. Richardson, *Environ. Pollut., Ser. B*, 1980, **1**, 3.
5. J. Aasetha, M. A. Skaugb, Y. Caoc and O. Andersend, *J. Trace Elem. Med. Biol.*, 2015, 31260.
6. P. B. Tchounwou, C. G. Yedjou, A. K. Patlolla and D. J. Sutton, *EXS*, 2012, **101**, 133.
7. B. Sharma, S. Singh and N. J. Siddiqi, *BioMed. Res. Int.*, 2014, **2014**, Article ID 640754.
8. C. C. Bridges and R. K. Zalups, *Toxicol. Appl. Pharmacol.*, 2005, **204**(3), 274.
9. S. J. S. Flora, M. Mitta and A. Mehta, *Indian J. Med. Res.*, 2008, **28**, 501.
10. International Agency for Research on Cancer (IARC), Agents Classified by the IARC Monographs, *Sci. World J.*, 2012, **10**, 1–106.
11. J. Vilensky and K. Redman, *Ann. Emerg. Med.*, 2003, **41**(3), 378.
12. K. Kalia and S. J. F. Flora, *J. Occup. Health*, 2005, **47**, 1.
13. Y. Kamijo, K. Soma, Y. Asari and T. Ohwada, *J. Toxicol. Clin. Toxicol.*, 1998, **36**(1–2), 27.
14. M. E. Sears, *Sci. World J.*, 2013 Article ID 219840.
15. A. S. Ettinger, H. Lamadrid-Figueroa, M. M. Tellez-Rojo, A. Mercado-García, K. E. Peterson, J. Schwartz, H. Hu and M. Hernández-Avila, *Environ. Health Perspect.*, 2009, **117**, 26.
16. S. J. S. Flora, R. Bhattacharya and R. Vijayaraghavan, *Fundam. Appl. Toxicol.*, 1995, **25**, 233.
17. S. J. S. Flora and V. Pachauri, Chelation in Metal Intoxication, *Int. J. Environ. Res. Public Health*, 2010, **7**, 2745.
18. M. M. Jones, P. K. Singh, G. R. Gale, L. M. Atkins and A. B. Smith, *Toxicol. Appl. Pharmacol.*, 1988, **95**, 507.
19. M. Rivera, D. J. Levine, V. Aposhian and Q. Fernando, *Chem. Res. Toxicol.*, 1991, **4**, 107.
20. E. M. Walker, A. Stone, L. B. Milligan, G. R. Gale, L. M. Atkins, A. B. Smith, M. M. Jones, P. K. Singh and M. A. Basinger, *Toxicology*, 1992, **76**, 79.

21. M. M. Jones, P. K. Singh, G. R. Gale, A. B. Smith and L. M. Atkins, *Pharmacol. Toxicol.*, 1992, **70**, 336.
22. G. I. Chauhan, K. K. Pant and K. D. Nigam, *Environ. Sci.: Processes Impacts*, 2015, **17**(1), 12.
23. L. Di Palma and R. Mecozzi, *J. Hazard. Mater.*, 2007, **147**, 768.
24. M. Misbahuddin and A. Fariduddin, *Arch. Environ. Health*, 2002, **57**(6), 516.
25. K. Dietrich, J. Ware, M. Salganik, J. Radcliffe, W. Rogan, G. Rhoads, M. E. Fay, C. T. Davoli, M. B. Denckla, R. L. Bornschein, D. Schwarz, D. W. Dockery, S. Adubato and R. L. Jones, *Pediatrics*, 2004, **114**(1), 19.
26. P. M. Barnes, B. Bloom, and R. L. Nahin *National Health Statistics Report*, December 10, 2008.
27. D. J. Felton, N. S. N. Kales and R. H. Goldman, *Toxics*, 2014, **2**, 403.
28. Centers for Disease Control and Prevention, *MMWR*, 2006, **55**, 204.
29. A. J. Baxter and E. P. Krenzelok, *Clin. Toxicol.*, 2008, **46**, 1083.
30. K. H. Wedepohl, *Geochim. Cosmochim. Acta*, 1995, **59**, 1217.
31. C. L. Nicholas, H. W. Morgan, B. K. Nicholson and R. S. Ronimus, *Angew. Chem., Int. Ed. Engl.*, 2005, **44**, 941.
32. C. C. Coombs, M. Tavakkoli and M. S. Tallman, *Blood Cancer J.*, 2015, **5**, e304.
33. J. C. Ng, J. Wang and A. Shraim, *Chemosphere*, 2003, **52**, 1353.
34. United States Environmental Protection Agency, *Arsenic and Clarifications to Compliance and New Source Monitoring Rule 66 FR 6976*, 2001.
35. L. Huanga, H. Wua and T. J. van der Kuijp, *Int. J. Environ. Health Res.*, 2014, **3**, 1.
36. T. Watanabe and S. Hirano, *Arch. Toxicol.*, 2013, **87**, 969.
37. S. Lin, Q. Shi, F. B. Nix, M. Styblo, M. A. Beck, K. M. Herbin-Davis, L. L. Hall, J. B. Simeonsson and D. J. Thomas, *J. Biol. Chem.*, 2002, **277**, 10795.
38. A. Shraim, X. Cui, S. Li, J. C. Ng, J. Wang, Y. Jin, Y. Liu, L. Guo, D. Li, S. Wang, R. Zhang and S. Hirano, *Toxicol. Lett.*, 2003, **137**, 35.
39. H. V. Aposhian, E. S. Gurzau, X. C. Le, A. Gurzau, S. M. Healy, X. Lu, M. Ma, L. Yip, R. A. Zakharyan, R. M. Maiorino, R. C. Dart, M. G. Tircus, D. Gonzalez-Ramirez, D. L. Morgan, D. Avram and M. M. Aposhian, *Chem. Res. Toxicol.*, 2000, **13**(8), 693.
40. H. Shi, X. Shi and K. J. Liu, *Mol. Cell. Biochem.*, 2004, **255**, 67.
41. S. X. Liu, M. Athar, I. Lippai, C. Waldren and T. K. Hei, *Proc. Natl. Acad. Sci. U. S. A.*, 2001, **98**, 1643.
42. S. V. Kala, G. Kala, C. I. PraterI, A. C. Sartorelli and M. W. Lieberman, *Chem. Res. Toxicol.*, 2004, **17**, 243.
43. R. N. Ratnaike, *Postgrad. Med. J.*, 2003, **79**, 391.
44. A. Vahidnia, G. B. van der Voet and F. A. de Wolff, *Hum. Exp. Toxicol.*, 2007, **26**(10), 823.
45. F. A. De Wolff and P. M. Edelbroek, in *Handbook of clinical neurology*, ed. P. Vinken and G. Bruyn, Elsevier Science BV, 1994, p. 283.
46. D. M. Opresko, *Risk Assessment Information System database, Oak Ridge Reservation Environmental Restoration Program*, 1992.

47. L. Gerhardsson, E. Dahlgren, A. Eriksson, B. E. A. Lagerkvist, J. Lundstrom and G. P. Nordberg, *Scand. J. Work, Environ. Health*, 1988, **14**, 130.
48. K. M. Lokuge, W. Smith, B. Caldwell, K. Dear and A. H. Milton, *Environ. Health Perspect.*, 2004, **112**, 1172.
49. K. M. Hunt, R. K. Srivastava, C. A. Elmets and M. Athar, *Cancer Lett.*, 2014, **354**, 211.
50. M. J. Kosnett, The Role of Chelation in the Treatment of Arsenic and Mercury Poisoning, *J. Med. Toxicol.*, 2013, **9**, 347.
51. A. Catsch and A. E. Harmuth-Hoehne, *Pharmacol. Ther.*, 1976, **A1**, 1.
52. N. C. Woody and J. T. Kometani, BAL in the treatment of arsenic ingestion of children, *Pediatrics*, 1948, **1**, 372.
53. T. D. Hoover and H. V. Aposhian, *Toxicol. Appl. Pharmacol.*, 1983, **70**, 160.
54. O. Andersen, *Chem. Rev.*, 1999, **99**, 2683.
55. V. E. Petrunkin, *Ukr. Khem. Z.*, 1956, **22**, 603.
56. Y. Liang, C. Chu, Y. Tsen and K. Ting, *Acta Physiol. Sin.*, 1957, **21**, 24.
57. H. V. Aposhian, D. E. Carter, T. D. Hoover, C. A. Hsu, R. M. Maiorino and E. Stine, *Fundam. Appl. Toxicol.*, 1984, **4**, S58.
58. H. V. Aposhian and M. M. Aposhian, *Ann. Rev. Pharmacol. Toxicol.*, 1990, **30**, 279.
59. H. Mückter, B. Liebl, F. X. Reichl, G. Hunder, U. Walther and B. Fichtl, *Hum. Exp. Toxicol.*, 1997, **16**, 460.
60. M. M. Rahman, U. K. Chowdhury, S. C. Mukherjee, B. K. Mondal, K. Paul, D. Lodh, B. K. Biswas, C. R. Chanda, G. K. Basu, K. C. Saha, S. Roy, R. Das, S. K. Palit, Q. Quamruzzaman and D. Chakraborti, *J. Toxicol. Clin. Toxicol.*, 2001, **39**, 683.
61. D. N. Guha Mazumder, U. C. Ghoshal, J. Saha, A. Santra, A. Chatterjee, S. Dutta, C. R. Angel and J. A. Centeno, *Clin. Toxicol.*, 1998, **36**, 683.
62. E. Stenehjem, M. Vahter, B. Nermell, J. Aasen, S. Lierhagen, J. Morland and D. Jacobsen, *Clin. Toxicol.*, 2007, **45**, 424.
63. WHO air quality guidelines for Europe, 2nd edn, 2000, [www.euro.who.int/data/assets/pdf\\_file/0005/74732/E71922.pdf](http://www.euro.who.int/data/assets/pdf_file/0005/74732/E71922.pdf).
64. S. Lindberg, P. M. Stokes, E. Goldberg and C. Wren, Group report: mercury, in *Lead, mercury, cadmium and arsenic in the environment*, ed. T. W. Hutchinson and K. M. Meena, New York, Wiley, 1987, p. 17.
65. Environmental Health Criteria, No. 118, *Inorganic mercury*, World Health Organization, Geneva, 1991.
66. Occupational Health Guidelines for Chemical Hazards DHHS (NIOSH) Publication No. 81-123, in *Inorganic Mercury*, 1981, <http://www.cdc.gov/niosh/docs/81-123/pdfs/0383.pdf>.
67. S. Jensen and A. Jernevlöv, *Nature*, 1969, **223**, 753.
68. AMAP, *AMAP assessment 2011: mercury in the Arctic. Oslo, Norway: Arctic Monitoring and Assessment Programme (AMAP)*, 2011, <http://www.amap.no/documents/doc/amap-assessment-2011-mercury-in-the-arctic/90>.
69. X. Zhou, X. L. Wang, X. Sun, X. Yang, C. Chen, Q. Wang and X. Yang, *J. Ethnopharmacol.*, 2011, **135**(1), 110.

70. *Elemental mercury and inorganic mercury compounds*, [www.who.int/ipcs/publications/cicad/.../cicad50.pdf](http://www.who.int/ipcs/publications/cicad/.../cicad50.pdf).
71. L. G. Dales, *Am. J. Med.*, 1972, **53**, 219.
72. (a) J. P. K. Rooney, *Toxicol. Appl. Pharmacol.*, 2013, **274**, 425; (b) T. W. Clarkson, *Environ. Health Perspect.*, 2002, **110**(suppl.1), 11.
73. M. Mare, *J. Dent. Res.*, 1990, **69**, 1167.
74. S. Halbac, *J. Dent. Res.*, 1995, **74**, 1103.
75. A. Berglund, *J. Dent. Res.*, 1990, **69**, 1646.
76. L. A. Broussard, C. A. Hammett-Stabler, R. E. Winecker and J. D. Roper-Miller, *Lab. Med.*, 2002, **8**, 614.
77. A. Carocci, N. Rovito, M. S. Sinicropi and G. Genchi, in *Reviews of Environmental Contamination and Toxicology*, ed. D. M. Whitacre, Springer International Publishing, Switzerland, 2014, p. 229.
78. R. A. Bernhoft, *J. Environ. Public Health*, 2012, 460508.
79. B. O. Lund, D. M. Miller and J. S. Wods, *Biochem. Pharmacol.*, 1993, **45**, 2017.
80. R. K. Zalups, *Pharmacol. Rev.*, 2000, **52**, 113.
81. S. Bose-O'Reilly, K. M. McCarty, N. Steckling and B. Lettmeier, *Curr. Prob. Pediatr. Adolesc. Health Care*, 2010, **40**, 186.
82. D. W. Nierenberg, R. E. Nordgren, M. B. Chang, W. Siegler, M. G. Blayney, F. Hochberg, T. Y. Toribara, E. Cernichiari and T. Clarkson, *N. Engl. J. Med.*, 1998, **338**, 1672.
83. M. Harada, *Crit. Rev. Toxicol.*, 1995, **25**, 1.
84. T. Takeuchi, K. Eto, H. Tokunaga and Y. Takizawa, *Shokei Gakuen Coll. Bull.*, 1991, **23**, 9.
85. Ministry of Environment, Japan, *Minamata Disease The History and Measures*, <http://www.env.go.jp/en/chemi/hs/minamata2002/ch1.html>.
86. F. Bakir, S. F. Damluji and I. A. Zaki, *Science*, 1973, **181**, 230.
87. G. Drasch, E. Wanghofer and G. Roeder, *Trace Elem. Med.*, 1997, **14**, 116.
88. R. C. Baselt, *Disposition of Toxic Drugs and Chemicals in Man*, Chemical Toxicology Institute, 5th edn, Foster City, CA, 1999, p. 61.
89. G. Kazantzis, *Med. Lav.*, 2002, **93**, 139.
90. H. V. Aposhian, A. Arroyo, M. E. Cebrian, L. M. de Razom, K. M. Hurlbut, R. C. Dart, D. Gonzalez-Ramirez, H. Kreppel, H. Speisky, A. Smith, M. E. Gonsebatt, P. Ostrosky-Wegman and M. M. Aposhian, *J. Pharmacol. Exp. Therapeut.*, 1997, **282**, 192.
91. H. E. Hoffman, I. Buka and S. Phillips, *Pediatr. Clin. North Am.*, 2007, **54**, 399.
92. H. Roels, J. P. Gennart, R. Lauwerys, J. P. Buchet, J. Malchaire and A. Bernard, *Am. J. Ind. Med.*, 1985, **7**, 45.
93. W. T. Longcope and J. A. Luetscher, *Ann. Intern. Med.*, 1949, **31**, 545.
94. J. B. Nielse and O. Andersen, *Hum. Exp. Toxicol.*, 1991, **10**, 423.
95. J. Forman, J. Moline, E. Cernichiari, S. Sayegh, C. Torres, M. M. Landrigan, J. Hudson, H. N. Adel and P. J. Landrigan, *Environ. Health Perspect.*, 2000, **108**, 575.

96. S. Bose-O'Reilly, G. Drasch, C. Beinhoff, S. Maydl, M. R. Vosko, G. Roider and D. Dzaja, *Sci. Total Environ.*, 2003, **307**(1–3), 71.
97. J. R. Campbell, T. W. Clarkson and M. D. Omar, *J. Am. Med. Assoc.*, 1986, **256**, 3127.
98. D. Gonzalez-Ramirez, M. Zuniga-Charles, M. A. Narro-Juarez, Y. Molina-Recio, K. M. Hurlbut, R. C. Dart and H. V. Aposhian, *J. Pharmacol. Exp. Ther.*, 1998, **287**, 8.
99. S. J. S. Flora and V. Pachauri, *Int. J. Environ. Res. Public Health*, 2010, **7**(7), 2745.
100. C. I. Davidson, and M. Rabinowitz, in *Human lead exposure*, ed. H. Needleman, CRC Press, Boca Raton, FL, 1992.
101. J. O. Nriagu, *N. Engl. J. Med.*, 1983, **308**, 660.
102. L. Fewtrell, R. Kaufmann and A. Prüss-Üstün, *WHO Environmental Burden of Disease Series, No. 2*, World Health Organization, Geneva, 2003.
103. P. A. Meyer, M. J. Brown and H. Fal, *Mutat. Res.*, 2008, **659**, 166.
104. T. L. Guidotti and L. Ragain, *Pediatr. Clin. North Am.*, 2007, **54**(2), 227.
105. D. E. B. Fleming, D. R. Chettle, C. E. Webber and E. J. O'Flaherty, *Toxicol. Appl. Pharmacol.*, 1999, **161**, 100.
106. I. P. L. Coleman, J. A. Blair and M. E. Hilburn, *Biochem. Educ.*, 1983, **11**, 16.
107. Y. Kim and S. Park, *Korean J. Pediatr.*, 2014, **57**(8), 345.
108. E. J. O'Flaherty, *Toxicol. Appl. Pharmacol.*, 1993, **118**, 16.
109. B. K. Wills, J. Christensen, J. Mazzoncini and M. Miller, *J. Med. Toxicol.*, 2010, **6**, 31.
110. P. R. de Madureira, E. M. De Capitani and R. J. Vieira, *Sao Paulo Med. J.*, 2000, **118**(3), 78.
111. L. Breeher, M. A. Mikulski, T. Czczok, K. Leinenkugel and L. J. Fuorte, *Int. J. Occup. Environ. Health*, 2015, **21**, 303.
112. F. Busse, L. Omidi and A. Leichtle, *N. Engl. J. Med.*, 2008, **358**, 1641.
113. S. J. S. Flora, *J. Nutr. Environ. Med.*, 2002, **12**, 53.
114. A. Bernard and R. Lauwerys, *Ann. N. Y. Acad. Sci.*, 1978, **514**, 41.
115. T. I. Lidsky and J. S. Schneider, *Brain*, 2003, **126**, 5.
116. M. A. Quintanar-Escorza, M. T. González-Martínez, L. Navarro, M. Maldonado, B. Arévalo and J. V. Calderón-Salinas, *Toxicol. Appl. Pharmacol.*, 2007, **220**(1), 1.
117. A. Garza, R. Vega and E. Soto, *Med. Sci. Monit.*, 2006, **12**(3), RA57.
118. N. D. Vaziri, *Am. J. Physiol.*, 2008, **295**, 454.
119. G. Flora, D. Gupta and A. Tiwaria, *Interdiscip Toxicol.*, 2012, **5**(2), 47.
120. International Programme on Chemical Safety (IPCS), *Evaluation – Monograph on Lead, Inorganic*, 2007.
121. National Center for Environmental Health, *New Blood Lead Level Information*, 2012, <http://www.cdc.gov/nceh/lead/ACCLPP/bloodleadlevels.htm>.
122. P. A. Meyer, M. A. McGeehin and H. Falk, *Int. J. Hyg. Environ. Health*, 2003, **206**, 363.
123. P. A. Meyer, M. J. Brown and H. Falk, *Mutat. Res.*, 2008, **659**, 166.

124. P. Haefliger, M. Mathieu-Nolf, S. Lociciro, C. Ndiaye, M. Coly, A. Diouf, A. L. Faye, A. Sow, J. Tempowski, J. Pronczuk, A. P. Filipe Junior, R. Bertollini and M. Neira, *Environ. Health Perspect.*, 2009, **117**, 1535.
125. M. J. Kosnett, in *Poisoning and Drug Overdose*, ed. K. R. Olson, Lange Medical Publishing/McGraw Hill, New York, 2004, pp. 238–242.
126. M. Blanus, V. M. Varnai, M. Piasek and K. Kostial, *Curr. Med. Chem.*, 2005, **12**(23), 2771.
127. DRUGDEX Drug Evaluations, *Thomson MICROMEDEX Healthcare Series (monograph on CD-ROM)*, 2004, vol. 122.
128. H. Shrand, *Lancet*, 1961, **1**, 310.
129. A. C. Markus and A. G. Spencer, *Br. Med. J.*, 1955, **2**, 883.
130. S. P. Bessman, M. Rubin and S. Leikin, *Pediatrics*, 1954, **14**, 201.
131. C. L. Whitfield, L. T. Chien and J. D. Whitehead, *Am. J. Med.*, 1972, **52**, 289.
132. R. K. Byers, *Pediatrics*, 1959, **23**, 585.
133. American Academy of Pediatrics, Committee on Drugs, *Pediatrics*, 1995, **96**, 155.
134. W. J. Crinnion, *Altern. Med. Rev.*, 2011, **16**(2), 109.
135. S.-K. Yang, L. Xiao, P. A. Song, X.-X. Xu, F. Y. Liu and L. Sun, *Nephology*, 2014, **19**, 56.
136. S. Bradberry and A. Vale, *Clin. Toxicol.*, 2009, **47**, 841.
137. E. Friedheim, J. Graziano, D. Popovac, D. Dragovic and B. Kaul, *Lancet*, 1978, **2**, 1234.
138. N. Thurtle, J. Greig, L. Cooney, Y. Amitai, C. Ariti, M. J. Brown, M. J. Kosnett, K. Moussally, N. Sani-Gwarzo, H. Akpan, L. Shanks and P. I. Dargan, *PLoS Med.*, 2014, **11**(10), e1001739.
139. American Academy of Pediatrics, Committee on Drugs, Treatment guidelines for lead exposure in children, *Pediatrics*, 1995, **96**, 155.
140. J. M. Pacyna and E. G. Pacyna, *Environ. Rev.*, 2001, **9**, 269.
141. O. Faroon, A. Ashizawa, S. Wright, P. Tucker, K. Jenkins, L. Ingerman and C. Rudisill, *Toxicological Profile for Cadmium*, Agency for Toxic Substances and Disease Registry, US, 2012, [www.atsdr.cdc.gov/toxprofiles/tp5](http://www.atsdr.cdc.gov/toxprofiles/tp5).
142. International Programme on Chemical Safety (IPCS), Cadmium, *Environmental Health Criteria 134*, World Health Organisation, Geneva, 1992, <http://www.inchem.org/documents/ehc/ehc/ehc134.htm>.
143. L. Jarup, M. Berglund, C. G. Elinder, G. Nordberg and M. Vahter, *Scand. J. Work, Environ. Health*, 1998, **24**(Suppl 1), 1.
144. EFSA, Scientific Opinion of the Panel on Contaminants in the Food Chain. Cadmium in food, *EFSA J.*, 2009, **980**, 1.
145. M. Nordberg, *Environ. Health Perspect.*, 1984, **54**, 13.
146. L. Jarup, A. Rogenfelt and C. G. Elinder, *Scand. J. Work, Environ. Health*, 1983, **9**, 327.
147. F. Thevenod, *Biometals*, 2010, **23**, 857.
148. J. P. Bressler, L. Olivi, J. H. Cheong, Y. Kim and D. Bannona, *Ann. N. Y. Acad. Sci.*, 2004, **1012**, 142.

149. M. Vašák and D. W. Hasler, *Curr. Opin. Chem. Biol.*, 2000, **4**, 177.
150. R. A. Bernhoft, *Sci. World J.*, 2013Article ID 394652.
151. A. Cuypers, M. Plusquin, T. Remans, M. Jozefczak, E. Keunen, H. Gielen, K. Opdenakker, A. R. Nai, E. Munters, T. J. Artois, T. Nawrot, J. van Gronsveld and K. Smeets, *Biometals*, 2010, **23**, 927.
152. A. Zarros, N. Skandali, H. Al-Humadi and C. Liapi, *Pneumon*, 2008, **21**, 172.
153. A. A. Newairy, A. S. Ei-Sharaky, M. M. Badreldeen, S. M. Eweda and S. A. Sheweita, *Toxicology*, 2007, **242**(1–3), 23.
154. A. Rania, A. Kumar, A. Lala and M. Panta, *Int. J. Environ. Health Res.*, 2014, **24**, 378.
155. A. Bernard and R. Lauwerys, in *Handbook of experimental pharmacology*, ed. E. C. Foulkes, 1986, vol. 80, p. 135.
156. L. Friberg, M. Piscator, G. F. Nordberg and T. Kjellstrom, *Cadmium in the environment*, CRC Press, 2nd edn, Cleveland, 1974.
157. Cadmium Toxicological overview – Gov.UK, <https://www.gov.uk/government/.../hpa>.
158. A. Newman-Taylor, Cadmium, in *Environmental and Occupational Medicine*, ed. W. N. Rom, Lippincott-Raven, Philadelphia, 1998, pp. 1005–1010.
159. P. A. Lucas, A. G. Jariwalla, J. H. Jones, L. Gough and P. T. Vale, *Lancet*, 1980, **2**, 205.
160. K. Tsuchiya, *Keio J. Med.*, 1969, **18**(4), 195.
161. T. Kjellström, *IARC Sci. Publ.*, 1992, **118**, 301.
162. L. Järup, T. Bellander, C. Hogstedt and G. Spång, *Occup. Environ. Med.*, 1998, **55**(11), 755.
163. H. A. Roels, P. Hoet and D. Lison, *Renal Failure*, 1999, **21**, 251.
164. CDC, *Fourth national report on human exposure to environmental chemicals, updated tables*, February 2011, [http://www.cdc.gov/exposurereport/pdf/Updated\\_Tables.pdf](http://www.cdc.gov/exposurereport/pdf/Updated_Tables.pdf), accessed January 11, 2012.
165. H. Roels, A. M. Bernard, A. Cárdenas, J. P. Buchet, R. R. Lauwerys, G. Hotter, I. Ramis, A. Mutti, I. Franchini and I. Bundschuh, *Br. J. Ind. Med.*, 1993, **50**, 37.
166. M. Blanusa, V. M. Varnai, M. Piasek and K. Kostial, *Curr. Med. Chem.*, 2005, **12**(23), 2771.
167. O. Andersen and J. B. Nielsen, *Pharmacol. Toxicol.*, 1988, **63**, 386.
168. H. W. Gil, E. J. Kang, K. H. Lee, J. O. Yang, E. Y. Lee and S. Y. Hong, *Hum. Exp. Toxicol.*, 2011, **30**, 79.
169. R. H. Dreisbach, *Handbook of poisoning: prevention, diagnosis and treatment*, Los Altos, California, Lange Medical Publications, 1983, p. 247.
170. L. H. Cotter, *J. Am. Med. Assoc.*, 1958, **166**, 735.
171. L. Friberg and C. G. Elinder, in *Encyclopedia of occupational health and safety*, ed. L. Parmeggiani, International Labour Organization Publications, Geneva, 1983, pp. 356–357.
172. V. Eybl, J. Sýkora, J. Koutenský, D. Caisová, A. Schwartz and F. Mertl, *Environ. Health Perspect.*, 1984, **54**, 267.

173. L. R. Cantilena and C. D. Klaassen, *Toxicol. Appl. Pharmacol.*, 1981, **58**, 452.
174. L. R. Cantilena and C. D. Klaassen, *Toxicol. Appl. Pharmacol.*, 1982, **63**, 173.
175. M. M. Jones and M. G. Cherian, *Toxicology*, 1990, **62**, 1.
176. Y. Cao, A. Chen, M. Bottai, K. L. Caldwell and W. J. Rogan, *J. Pediatr.*, 2013, **163**(2), 598.
177. S. J. Fatemi, A. S. Saljooghi, F. D. Balooch, M. Iranmanesh and M. R. Golbafan, *Toxicol. Ind. Health*, 2012, **28**(1), 35.
178. A. S. Saljooghi and S. J. Fatemi, *Biometals*, 2010, **23**, 707.
179. M. M. Jones, P. K. Singh, G. R. Gale, A. B. Smith and L. M. Atkins, *Pharmacol. Toxicol.*, 1992, **70**, 336.
180. A. B. G. Lansdown, *Curr. Prob. Dermatol.*, 2006, **33**, 17.
181. M. J. Rosenblatt and T. C. Cymet, *J. Am. Osteopath. Assoc.*, 1987, 509.
182. F. S. Gerbasi and A. R. Robinson, *Am. J. Clin. Pathol.*, 1949, **19**(7), 668.
183. J. Aaseth, J. Halse and J. Falch, *Acta Pharmacol. Toxicol.*, 1986, 471.
184. W. C. Kuzell, *Calif. Med.*, 1949, **71**(2), 140.
185. C. Ragan and R. H. Boots, *JAMA*, 1947, **15**, 752.
186. B. Gabard, *Br. J. Pharmacol.*, 1980, **68**(4), 607.
187. A. C. Bronstein, D. A. Spyker, L. R. Cantilena, J. L. Green, B. H. Rumack and R. C. Dart, 2010 Annual Report of the American Association of Poison Control Centers' National Poison Data System (NPDS): 28th Annual Report, *Clin. Toxicol.*, 2011, **49**(10), 910.
188. L. L. Liebelt and R. Kronfol, *Acute iron intoxication*, UpToDate.com.[http://www.uptodate.com/contents/image?imageKey=EM%2F61711&topicKey=EM%2F6498&source=see\\_link&utmPopup=true](http://www.uptodate.com/contents/image?imageKey=EM%2F61711&topicKey=EM%2F6498&source=see_link&utmPopup=true), 2015, [http://www.uptodate.com/contents/image?imageKey=EM%2F61711&topicKey=EM%2F6498&source=see\\_link&utmPopup=true](http://www.uptodate.com/contents/image?imageKey=EM%2F61711&topicKey=EM%2F6498&source=see_link&utmPopup=true).
189. L. L. Velez and K. A. Delaney, in *Rosen's Emergency Medicine Concepts and Clinical Practice*, ed. J. A. Marx, R. S. Hockberger, R. M. Wallas et al., Mosby, 6th edn, Philadelphia, Pennsylvania, 2006, p. 2418.
190. A. Faure, L. Mathon, J. C. Poupelin, B. Allaouchiche and D. Chassard, *Ann. Fr. Anesth. Reanim.*, 2003, **22**, 557.
191. N. Franchitto, P. Gandia-Mailly, B. Georges, A. Galiniere, N. Telmon, J. L. Ducassé and D. Rougé, *Resuscitation*, 2008, **78**, 92.
192. T. Takeda, T. Ukioka and S. Shimazaki, *Intern. Med.*, 2000, **39**, 253.
193. J. C. Munch, *J. Am. Med. Assoc.*, 1934, **102**, 1929.
194. D. F. Thompson and E. D. Callen, *Ann. Pharmacother.*, 2004, **38**(9), 1509.
195. R. S. Hoffman, *Toxicol. Rev.*, 2003, **22**(1), 29.
196. D. E. Rusyniak, L. W. Kao, K. A. Nanagas, M. A. Kirk, R. B. Furbee, E. J. Brizendine and P. E. Wilmot, *J. Toxicol. Clin. Toxicol.*, 2003, **41**(2), 137.

## CHAPTER 4

# *Treatment of Systemic Iron Overload*

JOHN PORTER<sup>a</sup>

<sup>a</sup>Joint Red Cell Disorders Unit, UCL and Whittington Hospitals, UK

\*E-mail: J.porter@ucl.ac.uk

## 4.1 Consequences of Transfusional Iron Overload

### 4.1.1 Iron Homeostasis in the Absence of Blood Transfusion

Iron metabolism in humans is essentially conservative, so that once excess iron has accumulated in the body, it can only be removed by phlebotomy or with iron chelators. In health, total body iron is typically about 40–50 mg kg<sup>-1</sup>, of which 30 mg kg<sup>-1</sup> is contained within red blood cell haemoglobin.<sup>1</sup> Storage iron, ferritin and haemosiderin, is the largest remaining component of body iron—about 20 mg kg<sup>-1</sup> (or 1–2 g in a healthy adult). This iron storage is found mainly within macrophages of the liver, spleen and bone marrow and in hepatocytes. The quantity of other iron pools is relatively small but is metabolically critical, consisting of about 4 mg kg<sup>-1</sup> as muscle myoglobin and about 2 mg kg<sup>-1</sup> as cellular iron-containing enzymes. Transferrin-bound iron is only about 4 mg at any moment but is a pool, through which about 20–30 mg of iron is delivered daily to tissues expressing transferrin receptors. Most storage iron is found in the liver and body iron stores and can be predicted accurately from the liver iron concentration (LIC) (total body iron stores in

---

RSC Metallobiology Series No. 8

Metal Chelation in Medicine

Edited by Robert Crichton, Roberta J. Ward and Robert C. Hider

© The Royal Society of Chemistry 2017

Published by the Royal Society of Chemistry, [www.rsc.org](http://www.rsc.org)

$\text{mg kg}^{-1} = 10.6 \times \text{the LIC (in mg g}^{-1} \text{ dry weight)}$ ).<sup>2</sup> In health, LIC rarely exceeds  $1.8 \text{ mg g}^{-1}$  dry weight (dw).

Body iron homeostasis is achieved by modulating dietary iron absorption to balance iron losses from the skin, gut, through menstruation or during pregnancy. By contrast, iron excretion cannot be modulated physiologically. About 1–2 mg of iron or 10% of dietary iron is absorbed daily from food in health but this increases with anaemia or ineffective erythropoiesis through modulation of ferroportin channels in gut enterocytes. This mechanism of iron absorption is modulated by plasma hepcidin which, after synthesis in liver hepatocytes, binds to ferroportin in enterocytes, resulting in its degradation and hence decreased iron absorption. When hepcidin levels are low, such as with anaemia, hypoxia, ineffective erythropoiesis (IE), or the presence of variant HFE genes, iron absorption is increased. Inherited disorders that result in increased iron absorption in the absence of anaemia are not addressed directly in this chapter. These are typically associated with dysregulation of hepcidin synthesis with inappropriately low hepcidin levels and are referred to as hereditary haemochromatosis. Readers are referred elsewhere to recent reviews of genetic haemochromatosis.<sup>3</sup> However, it is important to point out here that the treatment of these conditions differs fundamentally from that of transfusional iron overload. The first line treatment for most forms of haemochromatosis is phlebotomy, where typically one unit of blood (about 470 mL) removes about 200 mg of iron. This can be repeated weekly in a patient with normal erythropoiesis capability. However when an individual is anaemic, it is not possible to remove blood therapeutically so iron chelation therapy is then necessary.

#### 4.1.2 Effects of Inherited Anaemias and Blood Transfusion on Iron Homeostasis

Inherited anaemias are usually associated with increased iron absorption. Haemoglobin disorders such as thalassaemia and sickle cell disorders are the most common worldwide. Thalassaemia disorders result from imbalanced globin chain synthesis and, depending on the extent of imbalance, result in varying levels of anaemia. In non-transfusion-dependent thalassaemias (NTDT) often referred to as ‘thalassaemia intermedia’, as well as in other conditions associated with ineffective erythropoiesis, increased erythropoiesis, and possibly other bone marrow derived factors, inhibit hepcidin synthesis and lead to increased dietary iron absorption.<sup>4</sup> The variable degree of ineffective erythropoiesis (IE), the extent of erythroid expansion and the severity of the anemia will impact on this mechanism. Iron absorption is about  $0.1 \text{ mg kg}^{-1}$  per day<sup>5,6</sup> but varies considerably<sup>7</sup> from 5–10 times normal. NTDT patients absorbed 60% (range: 17–90%) of a 5 mg dose of ferrous sulfate while healthy controls absorbed 10% (range: 5–15%).<sup>8</sup> In HbE/ $\beta$ -thalassaemia, similar iron absorption was found which correlated with plasma iron turnover, transferrin saturation and liver iron concentration in unchelated patients.<sup>9</sup> In other anaemias, the extent of excess iron absorption is

anticipated to be related to the degree of bone marrow expansion from ineffective erythropoiesis and hence the degree of erythroferrone production. In sickle cell disease, the degree of marrow expansion is less than in NTDT, consequent to less ineffective erythropoiesis (IE)<sup>10</sup>-so that iron absorption and iron overload is less than in NTDT even at similar levels of anaemias; furthermore urinary iron excretion can be substantial in sickle cell disease as high levels of intravascular haemolysis may be present.<sup>11</sup>

In transfusion-dependent thalassaemia (TDT), the rate of iron accumulation from blood transfusion is about 10 times greater than dietary absorption in NTDT, most commonly between 0.3 and 0.5 mg kg<sup>-1</sup> day<sup>-1</sup> or 20–35 mg day<sup>-1</sup> in a 70 kg adult.<sup>12</sup> The average rates of body iron accumulation from transfusion in TDT and from iron absorption in NTDT have been reported<sup>12,13</sup> together with recent data about the average iron loading rates in NTDT.<sup>6</sup> In TDT, the objective of transfusion is not only to treat anaemia but also to suppress the IE, which was historically responsible for the bony deformities and facial changes characteristic of under-transfused patients. Blood transfusion also suppresses excessive iron absorption to some extent by suppressing erythroid expansion in the bone marrow. The current recommended transfusion strategy in TDT aims to suppress IE while not transfusing unnecessarily. IE suppression can be monitored by measuring soluble transferrin receptors, although this is not necessary in routine clinical management. IE shows more suppression when pre-transfusion hemoglobin is maintained greater than 9.5–10.5 g dL<sup>-1</sup>.<sup>14,15</sup> With less aggressive transfusion regimes, iron absorption rises to 3–5 mg day<sup>-1</sup> with consequently 1–2 grams of additional iron loading yearly.<sup>15</sup> In practice, pre-transfusion Hb values are between 9.5 and 10.5 g dL<sup>-1</sup> in most patients, and maintained between 12 and 14 g dL<sup>-1</sup> post-transfusion. Exceptions to this are that some patients experience low back pain when Hb values fall below 10–11 g dL<sup>-1</sup>, presumably due to cyclical bone marrow expansion from erythropoietic stress as Hb values fall. In these circumstances pre-transfusion Hb about 1 g higher can be effective; this approach is often successful in preventing back pain from this cause. A higher transfusion rate may also be required if the spleen size is expanding. Transfusion requirement is on average 30% higher in un-splenectomised patients,<sup>12</sup> but is not in itself a justification for splenectomy because modern chelation therapy should keep pace with blood transfusion other than in exceptional cases. Hyper-transfusion, with complete suppression of endogenous erythropoiesis is often successful over a period of 6 months to two years, shrinking the spleen size and ultimately reducing the transfusion requirement. Splenectomy is best avoided whenever possible because of the high thrombosis risk in TDT and particularly in NTDT.<sup>16</sup>

The impact of blood transfusion on iron balance in any individual can be calculated from the volume transfused and the haematocrit of the blood given. Transfused iron (in mg mL<sup>-1</sup> of blood) can be estimated from 1.16 × the haematocrit of the transfused blood product. In some centres the haematocrit and volume of each blood unit is, or can be, provided by the blood transfusion centre and this is important when assessing novel chelation

regimes in a trial situation. However it is generally acceptable to know the mean haematocrit of the blood product provided by the transfusion centre and the mean volume given. For a very approximate, quick assessment of iron loading rate it is useful to assume that a unit of blood contains about 200 mg of iron. Without chelation therapy, LIC reaches  $15 \text{ mg g}^{-1} \text{ dw}$  after less than 5 years of blood transfusion. This level is associated with a high rate of liver dysfunction<sup>17</sup> and progression of fibrosis,<sup>18</sup> and prolonged high LIC levels can be associated with an increased risk of cardiomyopathy.<sup>19,20</sup> The rates of iron accumulation vary considerably between different patients however.<sup>12</sup> While most patients have transfusion rates between  $0.3$  and  $0.5 \text{ mg kg}^{-1} \text{ day}^{-1}$ , about one third of patients have requirements below or above this range. This impacts on the time taken to reach defined levels of iron overload and on the most appropriate chelation regime. It is therefore particularly important to calculate the rate of iron accumulation periodically, particularly in growing children.

Transition from NTDT to TDT can occur in some patients who thus become dependent on regular transfusion, and this can happen as early as the first decade and as late as the 6th decade. Much has been written about the criteria for transitioning from NTDT to TDT. Some guidelines give absolute cut-off values for initiating transfusion, for example  $<7 \text{ g dL}^{-1}$ . However this is too rigid as, for example, generally patients with E $\beta$ Thal tend to tolerate lower Hb values between  $6 \text{ g dL}^{-1}$  and  $7 \text{ g dL}^{-1}$  better than classic  $\beta$ thal intermedia because of the right and left shifts of the oxygen dissociation curves, respectively. Transitioning to transfusion should be based on factors such as failure to thrive, or growth in childhood and the development of worsening exercise tolerance, pulmonary hypertension or thrombotic complications later in life. This transitioning will inevitably require chelation and will also increase the risk of myocardial iron accumulation (see below).

## 4.2 Impact of Transfusion on Iron Distribution and its Consequences

In order to manage patients appropriately with chelation, it is necessary to understand the risks and consequences of under-chelation as well as the extent of reversibility of iron overload and/or its consequences. Transfusion-dependent thalassaemia (TDT) is the condition in which both the consequences of transfusional iron overload and the benefits of chelation therapy are best described. The transfused red cell is the predominant route of iron entry into the body where iron accumulates initially in the erythrophagocytic macrophage system (EMS) after phagocytosis of effete red cells. After haemoglobin catabolism in the EMS, iron can be rapidly released from macrophages for extracellular binding to transferrin, or can be retained within macrophages as storage iron (ferritin or haemosiderin). Egress of iron(II) from the EMS is through membrane ferroportin, which is modulated (decreased) by the binding of hepcidin to membrane ferroportin. The capacity of the macrophage system to store

iron is thought to be about 10 g of iron (or about 50 units of transfused blood). Once the macrophage system is replete, increasing proportions of storage iron are delivered to hepatocytes through diferric transferrin and/or through iron species that are found in plasma when transferrin saturation exceeds about 75%. This is a paradigm shift in tissue iron delivery whereby plasma iron species are present that are unbound to transferrin (plasma non-transferrin-bound iron, NTBI). These iron species are cleared rapidly by hepatocytes but also by the endocrine system and myocardium, probably through LVDCC in the myocardium<sup>21</sup> and possibly also through ZIP14 in the endocrine system.<sup>22,23</sup> NTBI is thought to account for both the distribution and pathology of transfusional iron overload. Evidence is based on cellular and animal models as the clinical evidence for the association between NTBI and iron distribution is not strong. Nevertheless, NTBI is considered to be the key mechanism for myocardial iron loading. Several factors other than iron overload determine NTBI levels, however.<sup>10</sup> While NTBI is raised by iron overload, it is also lowered when erythropoiesis is active but raised when erythropoiesis is relatively inactive, such as following blood transfusion. Iron chelation has only transient effects on NTBI levels.<sup>24,25</sup> Another issue is that NTBI is heterogeneous,<sup>26,27</sup> so NTBI, as currently measured, may not be representative of the key NTBI species responsible for extrahepatic iron distribution. It is possible that the redox active component of NTBI, as measured by the LPI assay,<sup>28,29</sup> is more representative of the species responsible for extrahepatic iron distribution but this remains to be shown convincingly.

The concept of a 'threshold' of body iron load that increases the risk of extrahepatic iron distribution is controversial as many factors are involved in addition to absolute body iron load. These include iron chelation and levels of erythropoiesis. However there is convincing evidence of a link between the volume of blood transfused and the risk of myocardial iron accumulation. The first data of this kind comes from post-mortem analysis of myocardial iron in transfused patients with a range of anaemias in the 'pre-chelation era'.<sup>30</sup> It was found that 100% of patients with over 200 transfusions had increased myocardial iron at post-mortem. This fell to 60% after 100 units and 10% after 25–50 units of blood.<sup>30</sup> In an early MRI study, a link between myocardial iron and units of blood transfused was found in unchelated or lightly chelated patients with myelodysplasia.<sup>31</sup> Others have failed to find a link between liver iron and myocardial iron by MRI,<sup>32</sup> (see Chapter 7). However, such analysis failed to take into account the rapid reduction of LIC by recent chelation compared with a slower reduction in myocardial iron. Therefore any cross-sectional attempt at linking liver and heart iron in chelated patients is likely to miss the underlying relationship between heart and liver iron. The importance of examining trajectories of heart and liver iron in chelated patients rather than 'one off' cross-sectional measures has been recently demonstrated.<sup>20</sup> However, it is not just iron chelation that confounds the relationship between liver and heart iron. For example, it is clear that in NTDT, very high levels of LIC are frequently found without extrahepatic iron spread.<sup>33</sup> This is likely to be due to high levels of erythropoiesis in

NTDT acting as a 'sink' for iron turnover and directing iron released from macrophages to erythropoiesis *via* transferrin.<sup>10</sup> Furthermore, when patients transition from NTDT to TDT, iron overload subsequently develops in the heart. Clearly then, the rate of iron accumulation from transfusion impacts on iron distribution, partly due to its effects on suppressing endogenous erythropoiesis. Indeed, patients lacking endogenous erythropoiesis (such as those with Diamond-Blackfan anaemia) are more susceptible to extrahepatic iron overload than patients with a more active bone marrow.<sup>10</sup>

The pathological consequences of NTBI uptake into extrahepatic tissues are best understood from data obtained in the pre-chelation era, as body iron distribution is fundamentally altered by chelation therapy.<sup>34</sup> In patients dying from transfusional iron overload, high iron concentrations were found in the liver, endocrine tissues and heart, and very low concentrations in striated muscle and the CNS.<sup>35</sup> While nearly all these patients died of heart failure, the myocardial iron concentrations were only a fraction of hepatic iron concentrations. Today, MRI can be used to examine the distribution of storage iron, usually by T2\* or more recently T1.<sup>36</sup> The myocardial iron content has been calibrated with post-mortem material and it has been shown that average myocardial iron concentrations in patients dying from iron-mediated heart failure was only about 6 mg g<sup>-1</sup> dw<sup>37</sup> which is only a fraction of that which can be accommodated by the liver, where levels <7 mg g<sup>-1</sup> dw are regarded as acceptable for iron control. Thus, the myocardium is less capable of withstanding increased tissue iron concentrations than the liver. Whereas heart failure can develop as early as in the second and third decades of life, cirrhosis and hepatocellular carcinoma typically take longer being rare before 40 years of age.

The pathophysiological mechanisms by which tissue damage occurs have recently been reviewed by this author.<sup>1</sup> In this chapter, the focus will be on how this impacts on chelation strategy. There is no doubt that chelation therapy has radically impacted on complications of iron overload, including mortality in TDT. In the pre-chelation era, iron-mediated cardiomyopathy was the major cause of death and endocrine damage, including hypogonadotrophic hypogonadism, hypothyroidism, hypoparathyroidism and diabetes mellitus were common. For example, in birth cohorts Italy from 1970–74, 65% of patients had hypogonadism, 16% diabetes, and 18% hypothyroidism. Regular subcutaneous desferrioxamine was introduced in the late 1970s and early 1980s and complications fell to 14%, 0.8% and 5%, retrospectively, in the birth cohort from 10 years later.<sup>38,39</sup>

Hypogonadism is often the earliest presenting feature of transfusional iron overload and is still common (typically hypogonadotrophic hypogonadism) as the anterior pituitary seems particularly sensitive to the effects of iron overload. In TM, this typically presents with primary or secondary amenorrhoea in females or poor growth and delayed puberty.<sup>38</sup> It is noteworthy that most guidelines still suggest waiting to begin chelation until the ferritin reaches 1000 µg L<sup>-1</sup> or until 2 years of age, although this is later than ideal if it were not for the fear of over-chelation.<sup>40,41</sup> These recommendations

were based on experience with desferrioxamine, where starting treatment before 2 years of age or when ferritin was  $<1000 \mu\text{g L}^{-1}$  was associated with audiometric and bone toxicity.<sup>42–45</sup> It is likely that lower thresholds for starting chelation could be used with newer chelation regimes. While this is in principle highly desirable, and could decrease the risk of HH still further, the safety of such an approach needs to be carefully demonstrated before it can be adopted into official guidelines.

The commonest cause of mortality in TDT until recently has been iron-induced cardiomyopathy.<sup>46,47</sup> This typically presents as left- or right-sided ventricular failure. Importantly, heart failure can be reversible using desferrioxamine, if recognized early. Clinically evident heart failure is often preceded by a more subtle decline in LVEF which allowed early intensification of chelation therapy.<sup>48</sup> Many patients are alive today, decades after presenting with heart failure and receiving emergency desferrioxamine infusions.<sup>48,49</sup> While heart failure can be reversed within days or weeks of intensive continuous intravenous desferrioxamine infusions<sup>48,50</sup> it takes longer to remove iron from the heart as evidenced by MRI monitoring of cardiac iron using the T2\* techniques<sup>50</sup> (see Chapter 7). This technique has been validated by *ex vivo* calibration<sup>37</sup> and has shown a link between cardiac T2\* and the risk of developing heart failure in the next 12 months. Myocardial T2\* values  $<20$  ms indicate increased myocardial iron, whereas T2\* values  $<10$  ms indicate increased risk of developing heart failure and values  $<6$  ms indicate a very high risk.<sup>37</sup> In recent years the incidence of heart failure in TDT patients under regular monitoring has declined.<sup>51,52</sup> This is most likely due to increased recognition of high-risk patients using T2\* of the myocardium as well as the availability and application of an increasing range of chelation regimes (see below).

The relationship between levels of iron overload and risk of extra-hepatic spread has also been hotly debated but has been unnecessarily confused by using only cross-sectional analysis and including patients who have received varying degrees of chelation therapy. This is not simply a theoretical issue as it has practical implications for managing patients with chelation (see below). It is important to know the duration of blood transfusion necessary for this extra-hepatic spread to occur, particularly to the myocardium, for practical clinical reasons. Without chelation, increased myocardial iron is seen in 100% of patients post-mortem after 200 units of blood transfusion; myocardial iron correlated with liver iron and the number of units transfused.<sup>30</sup> Generally thalassaemia patients died in their second and third decades from blood transfusions without chelation.<sup>53</sup> Early work suggested a close relationship between the control of LIC with desferrioxamine and long-term outcome from cardiomyopathy.<sup>19</sup> Similarly, long-term control of serum ferritin (SF) was associated with better outcome than when SF remained above  $2500 \mu\text{g L}^{-1}$  on more than two thirds of occasions.<sup>46</sup> This was consistent with post-mortem data in other diseases where a relationship between transfusional iron load rate (ILR), LIC and MI was found in patients who had not received chelation therapy.<sup>30,54</sup> However, when CMR cardiac T2\* became available, only weak correlations between LIC and myocardial iron (mT2\*)

were seen. It was then argued that control of LIC was therefore not important to control of MIC in TM.<sup>32</sup> However this lack of correlation was mainly due to the high proportion of patients in this study having been on intensive chelation therapy with DFO, which removes iron rapidly from the liver and slowly from cardiomyocytes, thus obscuring a link between liver and heart iron.<sup>32,50</sup> An interesting recent study among a large population of Chinese 'poorly chelated' TDT patients (based on inadequate dose or persistently high SF) observed increased myocardial iron as early as 6 years of age by T2\*.<sup>55</sup> Noetzli and colleagues<sup>20</sup> have provided insight into this issue by examining longitudinal trajectories of LIC and myocardial T2\*. They showed that changes in LIC in both directions typically preceded changes in myocardial T2\*. It can be concluded that LIC control (and thus ferritin control) is important both for limiting liver damage and for controlling myocardial iron, thus markedly reducing the risk of iron-mediated cardiomyopathy with heart failure.

Cirrhosis and hepatocellular carcinoma are becoming increasingly common as thalassaemia populations live longer.<sup>56,57</sup> Cirrhosis is present in about 50% of patients at post-mortem, particularly in those with chronic hepatitis. Similarly, hepatocellular carcinoma<sup>56</sup> is also becoming more common particularly in NTDT patients. This may reflect the early accumulation of iron in hepatocytes through iron entry *via* the portal system and the relatively late use of iron chelation in this population.

The importance of bacterial infection to morbidity and mortality in iron overload is often overlooked. In fact it has been the second commonest cause of death in TDT over many decades.<sup>53</sup> Some organisms are particularly virulent in the presence of free iron. A particularly important example is *Klebsiella*<sup>58,59</sup> but other organisms such as *Pseudomonas* can cause serious complications such as meningitis.<sup>60</sup> Another organism that has been associated with increased virulence during iron overload is *Klebsiella enterocolitica*, whose virulence is further enhanced by desferrioxamine as its iron bound form, ferrioxamine can be used as a growth enhancing siderophore by this organism.<sup>61</sup>

## 4.3 Desirable Features of Clinically Useful Iron Chelators

### 4.3.1 High Iron Binding Constant and Selectivity for Iron

Iron chelators need to have access to chelateable iron pools and to selectively bind iron(III). The iron complex needs to be sufficiently stable for excretion in urine or bile and to prevent redox cycling of chelated iron. For example, EDTA does not diminish the reactivity of iron salts in the Fenton reaction and may actually catalyze such reactions.<sup>62</sup> Another example of the relevance of stability of iron-chelate complexes is that of bidentate hydroxypyridinones, which, being less stable than the hexadentate DFO, can generate free radicals and damage cell membranes with increased lipid peroxidation, particularly if the chelators have high lipid solubility.<sup>63</sup> Coordination of all six sites of iron(III) can be achieved by one chelator molecule possessing six coordination sites

(hexadentate chelation), two molecules possessing three coordination sites (tridentate chelation) or three chelator molecules binding two sites each (bidentate chelation). Hexadentate chelators tend to be more stable in their iron-complexed form but are typically larger molecules than bidentate or tridentate chelators and are therefore not readily absorbed through the oral route. The strength and stability of iron(III) binding can be expressed by the binding (stability) constant,<sup>64,65</sup> but a modification of this measure which has been termed the pM is a more clinically relevant expression of iron binding and is defined as  $-\log$  of the uncoordinated metal (iron) concentration calculated at pH 7.4, 10  $\mu\text{M}$  ligand concentration and 1  $\mu\text{M}$  iron(III) (Table 4.1). This measure takes into account the tendency of bidentate chelators to dissociate at low concentrations and is therefore a more useful indicator of the ability of a chelator to scavenge iron at low chelator concentrations (Section 2.3 and 2.4).

Chelators also need to have a degree of selectivity for iron(III) over other metals such as zinc and copper. For example, a chelator that was clinically evaluated in early trials, DTPA, lacked this selectivity and led to zinc deficiency. In practice, all chelators exhibit some affinity for other metals such as zinc, copper and aluminum but clinically available chelators do not appear to be limited in their use by such metal binding.

### 4.3.2 Chelation of Iron Pools for Balance Without Inhibition of Key Metabolic Pools

The bio-distribution, and hence the access of chelators to iron pools intracellularly and extracellularly, is determined by the size, charge and lipid solubility of the chelators.<sup>66,67</sup> Smaller molecules can be absorbed from the gut more effectively so that orally active chelators tend to be bidentate or tridentate. It is difficult to design hexadentate molecules with molecular weights less than 400 and thus desferrioxamine has very little oral absorption. In addition to being absorbed more rapidly from the GI tract, small neutral-ly-charged bidentate molecules such as the hydroxypyridinone DFP are able to access intracellular iron pools more rapidly than DFO.<sup>66,67</sup>

Chelatable iron is quantitatively derived mainly from two major iron pools and is excreted in urine and/or the faeces depending on the chelator used but the major chelateable pools are essentially the same with all chelators. This accounts for about half of all chelateable iron. Iron derived from red cell catabolism is released to plasma transferrin or, if this is saturated, is present as plasma NTBI. Iron chelators can potentially intercept this source of iron released from macrophages before it binds to transferrin or to plasma albumin and citrate to form NTBI. Evidence from both studies in animals<sup>68</sup> and in humans<sup>69</sup> show that iron derived from the breakdown of red cells in macrophages is chelated directly by DFO and excreted in urine. With deferiprone, macrophage-derived iron is also excreted in urine<sup>70</sup> but with deferasirox (Exjade®), iron derived from red cell catabolism is excreted in bile and hence faeces.<sup>71</sup>

The ability of chelators to bind these pools will be relatively independent of factors that affect access to intracellular iron and will be significantly

**Table 4.1** Pharmacokinetics and metabolism of chelators.

Compound	Desferrioxamine (DFO)	Deferasirox (DFX)	Deferiprone (DFP)
Route of absorption	Subcutaneous, intravenous, intramuscular	Oral	Oral
Route of iron excretion	Urinary and faecal	Faecal	Urinary
Max. plasma levels ( $\mu\text{M}$ ) of iron-free drug	7–10 <sup>138</sup>	80 <sup>91</sup>	90–450 <sup>167</sup>
Concentration of iron complex	Complex remains similar (about 7 $\mu\text{M}$ ) with ascending doses but iron-free drug and metabolites increase <sup>138</sup>	Complex accounts for about 10% of plasma drug in steady state <sup>219</sup>	Complex correlates with urine iron excretion and predicts response to therapy <sup>86</sup>
Min. plasma level ( $\mu\text{M}$ ) with daily dosing	0	20	0
Elimination of iron complex	Urine and faeces Iron complex removed more slowly than free drug	Faeces	Urine
Metabolism	Intrahepatic to metabolite B which binds iron <sup>140</sup>	>90% eliminated in faeces, 60% unmetabolised. Metabolism mainly in liver to glucuronides. Oxidative metabolism by cytochrome P450 accounts for <10%. Most metabolites bind iron <sup>218</sup>	Glucuronide formed in liver does not bind iron <sup>167</sup>
Recommended dose $\text{mg kg}^{-1} \text{day}^{-1}$	30–60 5–7 times per week	20–40 once daily	75–100 in 3 divided doses
Chelation efficiency (% of drug excreted iron-bound)	13	27	7
Main adverse effects (for more information see text)	Ocular, auditory, bone growth retardation, local reactions, allergy	Gastrointestinal increased creatinine, Hepatitis	Gastrointestinal, arthralgia, agranulocytosis/neutropenia
Potential drug interactions	Vitamin C (in doses >200 mg) Prochlorperazine	- Inducers of uridine diphosphate glucuronosyl transferase - Bile acid sequestrants  - Cytochrome P450 (CYP) 3A4/5, CYP2C8, or CYP1A2 substrates <sup>185</sup>	Drugs inducing neutropaenia Aluminium-based antacids Vitamin C ?

determined by duration of plasma residency (long plasma half-life) and by slow rates of inactivation by metabolism. Once a chelator is cleared from the plasma compartment, NTBI and labile plasma iron rebound rapidly<sup>25</sup> because NTBI and LPI are highly labile.<sup>26</sup>

By contrast, the mobilization of intracellular iron (and hence hepatocyte iron) by chelators is favoured by properties such as lipid solubility, low molecular weight and neutral charge<sup>66,72-74</sup> (see Chapter 2, Section 2.9). Thus hydroxypyridinones, such as deferiprone, access labile iron pools more rapidly than DFO,<sup>66,67,75,76</sup> the latter taking about 4 hours whereas hydroxypyridinones may take only a few minutes. Deferasirox (DFX, Exjade®) appears to access labile intracellular iron rapidly as well as having access to iron pools within organelles.<sup>67,74</sup>

The second major chelateable pool, accounting for about half of all chelated iron, is intracellular iron derived from ferritin catabolism in hepatocytes, which is excreted in faeces with all of the above chelators. Iron stored as ferritin and haemosiderin (and MRI visible) does not directly damage cells and is not directly chelateable at clinically relevant rates. However its catabolism within cells every few days contributes to the labile iron pool. The magnitude of this labile iron pool is proportional to the amount of storage iron within cells and the rate of turnover within cells. Turnover and catabolism of storage iron is faster in hepatocytes than cardiomyocytes, making chelation more efficient in the former. Interaction of chelators with isolated ferritin *in vitro*, in cell culture, in experimental animals<sup>68,77</sup> or in the clinic<sup>69</sup> is not direct at any moment in time. Only the potentially toxic transient chelateable iron pool fraction, derived from ferritin or haemosiderin catabolism, accounting for up to 20% of cellular iron, is available for rapid chelation.<sup>78</sup> This means that simply increasing a chelation dose may not be beneficial if all the labile iron pools have already been chelated. Indeed if the dose is increased beyond this point, this increases the risk of chelating metabolically critical iron pools, with inhibition of metalloenzymes such as ribonucleotide reductase.<sup>76</sup> Unfortunately, the same properties that favour rapid absorption also favour inactivation and inhibition of essential metalloenzymes, such as ribonucleotide reductase, within cells.<sup>79</sup> Thus larger and less lipophilic molecules tend to interact with intracellular metalloenzymes more slowly than small lipid-soluble molecules.<sup>76,79,80</sup>

Because both major chelateable iron pools are being constantly generated, either by red cell catabolism within the macrophage system or by ferritin catabolism mainly in hepatocytes,<sup>81</sup> continuous exposure to moderate doses of iron chelation are preferable therapeutically to intermittent high doses. In addition to maximizing iron excretion, continuous exposure to chelation will remove NTBI and labile plasma iron (LPI) while present in plasma. Thus success of iron chelators is also affected by their pharmacokinetic and pharmacodynamic interactions. Depending on the rate of absorption, elimination and metabolism, plasma and cellular concentrations of chelators and their iron complexes differ considerably. The metabolism of chelators has been shown to have a key bearing on their efficacy and toxicity both in laboratory

animals<sup>82–84</sup> and in humans.<sup>85</sup> It is often forgotten that the iron–chelate complex can be considerably slower to be eliminated than the free ligand. Thus, for example, the iron complexes of DFP can be detected in the plasma of patients a week after the last dose of the drug, and levels can be used to predict chelation response.<sup>86</sup>

As these two chelateable iron pools are finite at any moment, increasing the dose of a chelator may not have a proportionately increased effect on iron excretion, while increasing the risk of toxicity disproportionately due to an excess of free chelator. This limits the efficiency of chelation therapy (the proportion of the drug that ends up being excreted in the iron-bound form). Thus the efficiency of DFO is about 13% in iron-overloaded patients, whereas that of DFP is about 4%, and DFX about 27%.<sup>87,88</sup> The variable efficiency of these different chelators can be understood from the principles that have just been discussed. Thus the relatively low efficiency of DFP relates not only to its rapid metabolism to forms that do not bind iron but also to its short plasma half-life.<sup>89</sup> Conversely, the long plasma half-life of DFX together with its slower metabolic inactivation<sup>90</sup> contributes to the higher efficiency of this drug.<sup>91</sup> Also, consistent with these principles is the observation that iron excretion with DFX,<sup>92</sup> as with DFO,<sup>93,94</sup> is directly proportional to the AUC (area under the curve). A further advantage of slow elimination of chelators is that 24 h protection from labile iron species in plasma or within cells can be achieved.<sup>24,95</sup>

At this time there are 3 chelators that are licensed for the treatment of transfusional iron overload: desferrioxamine (DFO), deferiprone (DFP) and deferasirox (DFX) (Table 4.1). It can be seen from Table 4.2 how the molecular size and pharmacokinetics of the three chelators differ.

## 4.4 Monitoring Iron Overload and Its Treatment

Monitoring iron overload and the effects of chelation is critical to the success of chelation treatment. The monitoring of iron overload in patients receiving blood transfusion and chelation therapy falls into three categories:

- monitoring trajectory of iron overload and distribution
- monitoring for end-organ damage from iron overload
- monitoring for unwanted effects of iron chelators

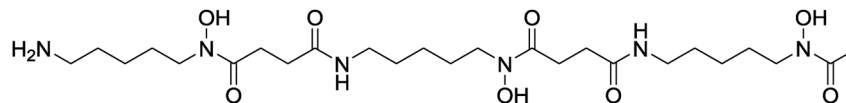
### 4.4.1 Monitoring Trajectory of Iron Overload and Distribution

#### 4.4.1.1 Serum Ferritin (SF)

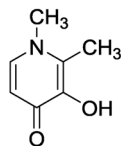
Serum ferritin is the most convenient marker of iron overload as it is inexpensive and simple to repeat, for example, at the time of cross-matching and the taking of other blood samples. SF is measured immunologically which takes no account of the iron content of SF which is typically very low as SF

**Table 4.2** Physicochemical properties of chelators.

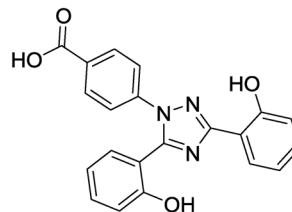
Chelator	Molecular weight	Chelator:Iron binding ratio	Stability constant $\log\beta_n$	pM	Charge of free complex	Charge of iron complex	Lipid solubility of free ligand ( $\log K_{part}$ )	Lipid solubility of iron complex ( $\log K_{part}$ )
DFO	561	1:1	33	26.6	1+	1+	-2.0	-1.5
DFP	139	3:1	37.2	20.5	0	0	-0.8	-1.1
DFX	373	2:1	26.5	22.5	1-	3-	+6.3	Not known



DFO



DFP



DFX

is secreted from macrophages in its iron-free glycosylated form.<sup>96</sup> Iron-rich, unglycosylated ferritin may be found in serum when hepatocellular damage occurs<sup>96,97</sup> but the contribution of this form of SF under different clinical scenarios has not been fully characterized. SF mainly reflects iron in the erythrophagocytic macrophage system (EMS) (formerly called the reticuloendothelial system, RES) and in the hepatocyte once the macrophage system is 'full'. SF measures do not always predict body iron or trends in body iron accurately and variation in body iron stores account for only 57% of the variability in plasma ferritin<sup>40</sup> in thalassaemia major. This variability is partly because inflammation increases serum ferritin and partly because the distribution of liver iron between macrophages and hepatocytes in the liver has a major impact on plasma ferritin. A sudden increase in serum ferritin should prompt a search for hepatitis, other infections, or inflammatory conditions. As most SF assays were developed for detecting iron deficiency, the linear range of the assay at high SF values has not always been validated. SF must therefore be performed in a laboratory that has established the linear range of the assay at high SF concentrations.

It is important to appreciate that while SF does not measure iron in the endocrine system or myocardium, there is an important relationship between the control of ferritin and the risk of extrahepatic iron, which has sometimes been underplayed by those who measure myocardial iron more than treating patients. Early work showed the long-term control of ferritin or indeed liver iron over many years is key to treatment success and long-term survival.<sup>38,44,46,48</sup> Specifically there was a significantly lower risk of cardiac disease and death in at least two-thirds of cases where serum ferritin levels had been maintained below 2500  $\mu\text{g L}^{-1}$  (with DFO) over a period of a decade or more.<sup>46</sup> Observations with larger patient numbers show that maintenance of an even lower serum ferritin of 1000  $\mu\text{g L}^{-1}$  confers additional advantages.<sup>38</sup>

SF is most useful in the management of iron-overloaded patients on chelation therapy in identifying trends. This may reflect the efficacy of treatment or patient compliance with treatment. A decreasing trend is good evidence of decreasing body iron burden, as there is rarely any other explanation (other than vitamin C deficiency). On the other hand, the absence of a decreasing trend does not exclude a decreasing iron burden. While an increasing SF trend implies an increasing iron burden, other factors such as inflammation or tissue damage may increase SF sometimes making interpretation difficult.

Particularly, at higher levels of SF, the relationship between body iron and SF is not always linear and body iron can fall considerably from a high starting point (e.g. LIC > 30  $\text{mg g}^{-1}$  dw) before a change in ferritin is clear. Below 3000  $\mu\text{g L}^{-1}$ , SF values are influenced mainly by iron stores in the macrophage system whereas above 3000  $\mu\text{g L}^{-1}$  they are determined increasingly by ferritin leakage from hepatocytes.<sup>48,98</sup> Day-to-day variations are particularly marked at these levels. The relationship between serum ferritin and body iron stores may also vary with the chelator being used<sup>99</sup> and with the

duration of chelation therapy.<sup>100</sup> A lack of decrease in SF in response to chelation may not be a true indication of lack of response: thus while among 374 patients who showed no SF response to 1 year of deferasirox, 52% actually decreased their LIC, indicating that a lack of SF response should be interpreted with caution; half the patients may be responding with respect to iron balance.<sup>101</sup> Conversely, since a decrease in SF predicts a decrease in LIC in 80% of patients, MRI measurement (where available) can be prioritized for patients with SF increase or no change (see below).

#### 4.4.1.2 Liver Iron Concentration (LIC) Monitoring

Liver iron concentration (LIC) is the most reliable indicator of body iron stores. Total body iron stores in  $\text{mg kg}^{-1} = 10.6 \times$  the LIC (in  $\text{mg g}^{-1}$  dry weight).<sup>2</sup> Adequate control of LIC is linked to the risk of hepatic damage, as well as the risk of the extrahepatic spread of iron. Normal LIC values are up to  $1.8 \text{ mg g}^{-1}$  dw, with levels of up to  $7 \text{ mg g}^{-1}$  dw seen in some non-thalassaemic populations without apparent adverse effects. Sustained high liver iron content (LIC) (above  $15\text{--}20 \text{ mg g}^{-1}$  dw) have been linked to worsening prognosis,<sup>19,102</sup> liver fibrosis progression<sup>18</sup> or liver function abnormalities.<sup>17</sup> In the absence of prior iron chelation therapy, the risk of myocardial iron loading increases with the number of blood units transfused and hence with iron overload.<sup>30,31</sup> However, the relationship between LIC and extra-hepatic iron is complicated by chelation therapy. This is because iron tends to accumulate initially in the liver and only later in the heart, but also because it is removed more rapidly from the liver than the heart by chelation therapy.<sup>20,50</sup> Thus in patients receiving chelation therapy, whilst high LIC increases the risk of cardiac iron overload, a single measurement of LIC will not reliably predict myocardial iron and hence cardiac risk. The trend or trajectory of LIC, and SF, are more important indicators of the trajectory of myocardial iron.<sup>20</sup>

Because of the issues with SF measurement described above, sequential measurement of LIC is the best way to determine whether body iron is increasing or decreasing with time (iron balance). Sequential LIC determination is the gold standard in assessing new chelation therapies in clinical trials. In routine clinical practice, LIC determination should be considered for those patients whose SF levels deviate from expected trends. LIC determination should also be considered more frequently for those patients with suspected co-existing hepatitis or patients on chelation regimens with variable or uncertain responses. Patients with SF values  $<1000 \mu\text{g L}^{-1}$  may also benefit from LIC determination as, in all these cases, LIC determination may reduce the risk of giving either inadequate or excessive doses of chelation therapy. LIC may be particularly useful when new chelating regimes are being used where the relationship between iron balance and SF may not have been established. When a patient fails to show a fall in SF over several months, the change in LIC can identify whether the current regime is adequate or needs to be modified (increased frequency or adherence, increased dose, or change in regime).

#### 4.4.1.3 Methods for Measuring LIC

**Biopsy:** Chemical determination on a liver biopsy sample (fresh, fixed or from dewaxing of paraffin-embedded material) was the so-called gold standard for many years. This has a number of disadvantages however. Biopsy is an invasive procedure which, in experienced hands, has a low complication rate<sup>103</sup> but this is not zero and patients find the procedure uncomfortable and occasionally frightening. Misleading results can also be obtained due to inadequate sample size ( $<1 \text{ mg g}^{-1}$  dry wt,  $4 \text{ mg g}^{-1}$  wet wt or about a 2.5 cm core length) or uneven distribution of iron, particularly in the presence of cirrhosis.<sup>104</sup> An advantage of biopsy is that it also allows the evaluation of liver histology, which cannot yet be reliably estimated by non-invasive means. The use of fibro-scanning,<sup>105</sup> with or without serological markers of liver damage, as a tool for determining cirrhosis in iron overload has yet to be fully validated so biopsy is still required, when histology is essential, particularly in the presence of concomitant hepatitis.

**MRI:** MRI techniques are now becoming the most widely used methods for quantitation of liver iron concentration (LIC). However there are a variety of methods, which may not be equivalent (see Chapter 7). It is critical that any measurements are validated and calibrated and that a consistent technique is used for any given patient in order to interpret trends. The principle shared by all currently used MRI techniques is the application of a radio frequency (RF) magnetic field pulse to the tissue (*e.g.*, liver or myocardium), whereupon the protons take up energy, altering their spin orientation before they later relax returning to their original state.

Spin echo and gradient echo techniques have been used. With spin echo, after the pulse, the time the nuclei take to relax gives the relaxation times: T1 in the longitudinal plane and T2 in the transverse plane. High tissue iron increases the rate (R) of decline in this signal. Gradient echo techniques are achieved by applying a strong and graded magnetic field to the RF pulse. An important point is that tissue iron concentration is not linearly related to either T2\* or T2 but is linearly related to their reciprocals  $1/\text{T2}^*$  and  $1/\text{T2}$  (also referred to as R2\* and R2, respectively). Both gradient and spin echo techniques can be achieved with a single held breath while T2 or R2 take a little longer to acquire data. The strength of the magnetic field applied is measured in tesla (T) units; 1.5 T machines are more suitable for iron measurement because 3 T machines give worse susceptibility artefacts and the maximum detectable iron level is also halved (which is too low for many patients).<sup>106,107</sup> Liver biopsy was used to calibrate the first widely used T2\* technique<sup>32</sup> but it now appears that LIC was significantly underestimated by a factor of two.<sup>108</sup> While this has now been recalibrated<sup>108</sup> the technique is still not equivalent to a widely used and externally validated technique (FerriScan®) which measures  $1/\text{T2}$  (or R2)<sup>109</sup>. This technique shows acceptable linearity and reproducibility up to LIC values of about  $30 \text{ mg g}^{-1}$  dry wt<sup>109</sup> and can be introduced into hospitals with little training, as data acquired is sent electronically for central analysis by dedicated FerriScan® software (payment is per scan analyzed).

#### 4.4.1.4 Myocardial Iron Estimation ( $T2^*$ or Other Measures)

The principles of iron measurement for the heart are the same as for the liver but there is the extra challenge of measuring a moving object, the myocardium. The shorter acquisition time for  $T2^*$  allowed data collection over a single breath hold.<sup>110</sup> A  $T2^*$  of  $<20$  ms (and especially  $<10$  ms) was associated with a decreased left ventricular ejection fraction.<sup>32</sup> Subsequently the  $T2^*$  method has been correlated with biochemical iron measurement in post-mortem samples.<sup>111</sup> Myocardial iron concentrations associated with heart failure were only  $5.98 \text{ mg g}^{-1}$  dry wt; levels that would not be harmful in the liver. Myocardial iron concentration ( $\text{mg g}^{-1}$  dry wt) can now be derived from  $T2^* = 45 \times (T2^* \text{ ms})$ .<sup>112</sup> The proportion of patients developing heart failure in the next year increases progressively to 18%, 31% and 52% with  $T2^*$  values of 8–10 ms, 6–8 ms and  $<6$  ms, respectively.<sup>112</sup> These risks may be considerably less in patients taking regular chelation. Indeed, prospective studies of patients with  $T2^* < 10$  ms receiving DFX, failed to develop heart failure over a 2–3 year period. EPIC<sup>113</sup>  $mT2^*$  has been validated internationally<sup>114</sup> and is now recommended for yearly monitoring. The method in a given treatment centre must be independently validated and calibrated. More recently,  $T1$  has been used to assess myocardial iron and may be more sensitive to mild levels of myocardial iron overload.<sup>36</sup>

*Heart function:* Prior to the development of  $mT2^*$ , sequential monitoring of LVEF was adopted.<sup>48,115</sup> When LVEF fell below the reference value there was a 35-fold increased risk of clinical cardiac failure and death with a median interval to progression of 3.5 years, allowing time for intensification of chelation therapy. This approach requires a reproducible method for determination of LVEF. MUGA was originally used here but assessment of LVEF is now more convenient by MRI. Echocardiography is generally too operator-dependent for sequential monitoring, although much useful information can be obtained in the hands of an experienced cardiologist. As only a subset of patients with  $T2^*$  values less than 20 ms have abnormal heart function, sequential measurement of LVEF can identify the patients who develop decompensation of LV function and are at exceptionally high risk, thus requiring very intensive chelation therapy. This should ideally be with a regime containing 24 h desferrioxamine, which can reverse LV dysfunction and heart failure if started in a timely way.<sup>50,116,117</sup>

#### 4.4.1.5 Monitoring of Other Organ Functions and Iron-Mediated Damage

Endocrine function has to be monitored in order to detect and correct deficiencies but usually by the time diabetes, hypothyroidism, hypoparathyroidism or hypogonadotropic hypogonadism (HH) have been identified, irreversible damage has occurred. The focus is then on replacing the missing hormones. Endocrine failures of this nature are late effects and the primary aim of chelation therapy is to prevent such damage. There is some data that

glucose tolerance can be improved when iron levels are brought very low<sup>118</sup> but generally endocrine damage is irreversible.

Iron overloaded patients should be monitored for evidence of damage to the most susceptible tissues. Hypogonadotrophic hypogonadism (HH) occurs early in the evolution of endocrine dysfunction and affects growth and sexual development as well as biochemical markers of HH. Diabetes mellitus needs to be screened by yearly oral glucose tolerance testing and random urine screening. Hypothyroidism and hypoparathyroidism can be screened by simple blood testing. There has been recent interest in using MRI as a way of identifying the risks of iron-mediated damage to the endocrine system. Early work in this area showed good correlation between MRI findings (loss of pituitary volume) and biochemical markers of pituitary damage.<sup>119</sup> With improved MRI imaging, other endocrine organs have also been evaluated.<sup>120</sup> The close correlation between iron deposition in the heart and deposition in endocrine tissues such as pituitary and pancreas is of interest.<sup>121,122</sup> This is consistent with the notion of shared uptake mechanisms for NTBI in heart and endocrine tissue.

#### 4.4.1.6 Urinary 24 h Iron Estimation

This is used less frequently than in the past for a variety of reasons. Firstly, day-to-day fluctuation of urine iron is considerable, sometimes varying by 100% within an individual patient. Secondly, DFX excretes virtually no iron in the urine. Thirdly, the proportion of urinary iron seen with DFO is also variable, varying considerably with transfusion cycle but consisting of approximately half of the total iron excretion.<sup>123</sup> Thus the urine iron measurement is mainly used for assessing excretion with DFP.<sup>86,124</sup> However the inherent variability of urine iron values and the inconvenience of 24 h collections mean that this is not widely used in routine monitoring.

#### 4.4.1.7 Plasma Non-Transferrin Iron (NTBI) and Labile Plasma Iron (LPI)

Plasma NTBI and LPI are a heterogeneous collection of plasma species unbound to transferrin, some of which are bound to citrate and plasma proteins.<sup>50</sup> Various assays provide variable reference ranges but generally correlate with each other.<sup>125</sup> NTBI can be estimated using a chelation capture method followed by HPLC<sup>126</sup> or by colorimetric analysis.<sup>127</sup> Alternatively NTBI species can be estimated by their ability to oxidize a fluorochrome, such as in the LPI assay.<sup>25,95</sup> This may be better suited to measurements when iron chelators are present in plasma.<sup>25,26</sup> More recently, a bead assay that measures NTBI directly using a hexadentate ligand has been compared to established methods.<sup>128</sup> Because NTBI is considered the main route through which iron is distributed to liver and extrahepatic tissues in thalassaemia major, NTBI levels might be expected to correlate with the risk of damage

to these tissues. NTBI broadly correlates with transferrin saturation,<sup>24</sup> as does LPI.<sup>129</sup> Weak correlations with serum ferritin and LIC have also been noted.<sup>130</sup> More recently, clear correlations of LPI with the transfusional iron loading rate have been observed as well as an inverse relationship with circulating transferrin receptors and hence transferrin iron clearance by the erythron.<sup>131</sup> LPI values also decline immediately after a single dose of chelator,<sup>132</sup> and progressively with chelation treatments.<sup>130</sup> However whilst some loose associations of NTBI,<sup>133</sup> or LPI<sup>134</sup> with some markers of cardiac iron or response to chelation have been reported,<sup>133</sup> so far measurements have not been sufficiently strongly predictive of cardiac risk to be recommended for routine clinical practice. This is partly because NTBI and LIP are highly labile, rapidly returning or even rebounding<sup>24</sup> after an iron chelator has been cleared.<sup>25</sup> NTBI is also affected by other factors such as ineffective erythropoiesis, phase of the transfusion cycle and rate of blood transfusion,<sup>135</sup> adding to the complexity of interpreting levels.<sup>136</sup> In addition, it is not clear whether the various methods identify the species most stringently linked to myocardial iron uptake. Therefore, although the measurement of NTBI (or LPI) has proved a useful tool for evaluating how chelators interact with plasma iron pools, its value as a guide to routine treatment or prognosis has yet to be clearly demonstrated.

## 4.5 Properties and Clinical Beneficial Effects of Available Iron Chelators

### 4.5.1 Desferrioxamine (Desferal) DFO

#### 4.5.1.1 Physicochemical Properties and Iron Binding

Desferrioxamine (DFO) is a naturally occurring, hexadentate siderophore derived from *Streptomyces pilosus*. DFO has a hexadentate structure where one molecule completely coordinates the 6 potential iron binding sites of one iron(III) atom. For one molecule of a chelator to achieve this, a relatively high molecular weight of 560 results, which severely limits gastrointestinal absorption, so that parenteral administration is necessary. Due to its hexadentate structure  $\text{Fe}^{3+}$ , is efficiently scavenged even at low concentrations of iron, as evidenced by the high pM (Table 4.2). The resulting DFO–iron complex, ferrioxamine (FO), is very stable (stability constant =  $10^{31}$ ). Other metals are bound with a much lower affinity; only the chelation of aluminum has clinical significance (stability constant =  $10^{22}$ – $10^{26}$ ) and DFO has been successfully used to treat aluminum overload in renal dialysis patients at doses of 5–10 mg  $\text{kg}^{-1}$  once weekly.<sup>137</sup> The affinity of DFO for other metal ions is much lower, namely,  $\text{Cu}^{2+}$  ( $10^{14}$ ),  $\text{Co}^{2+}$  ( $10^{11}$ ),  $\text{Zn}^{2+}$  ( $10^{11}$ ),  $\text{Fe}^{2+}$  ( $10^{10}$ ),  $\text{Ni}^{2+}$  ( $10^{10}$ ), and  $\text{Ca}^{2+}$  ( $10^2$ ).<sup>49</sup>

The distribution of DFO and its iron complex ferrioxamine (FO) are determined by molecular size, charge and lipid solubility of both species. The positive charge of DFO, together with the negative resting potential of vertebrate

cells, favours cellular uptake of DFO, but this is counteracted by the low lipophilicity and the high molecular weight of DFO.<sup>94</sup> Thus uptake of DFO is slow in cells, as has been demonstrated in K562 cells *in vitro*, where concentrations approaching those outside cells are not seen for about 4 hours.<sup>66,79</sup> Hepatocytes however appear to have a facilitated uptake mechanism for DFO. The iron complex FO also has a uni-positive charge that tends to retard the egress of the iron complex from cells such as cardiomyocytes.<sup>94</sup> In hepatocytes however active excretion mechanisms exist for excretion in the bile. Furthermore metabolism of DFO to metabolite B, which has a negative charge, favours egress of this metabolite from hepatocytes.<sup>94</sup> DFO enters most cells much more slowly than deferiprone (DFP) because of its low lipid solubility, high molecular weight and charge.<sup>94</sup>

#### 4.5.1.2 Pharmacokinetics of Free Ligand and Iron Complexes

The plasma half-life is short with an initial half-life of 0.3 hours and a terminal half-life of 3 hours.<sup>138</sup> Mean steady state concentrations of 7.4  $\mu\text{M}$  are achieved with an intravenous infusion of 50 mg  $\text{kg}^{-1}$   $\text{day}^{-1}$  24 138. The major iron-binding metabolite and levels of metabolite B are generally lower than those of DFO.<sup>138</sup> DFO is cleared by the liver and by the kidney, but once iron is bound to form ferrioxamine in the plasma, clearance is almost exclusively renal as ferrioxamine is not cleared by the liver. This means that in renal disease the iron complex ferrioxamine rather than the free ligand DFO accumulates in plasma. Fortunately, as ferrioxamine is highly stable it does not redistribute iron significantly within the body. Metabolism of the iron-free drug, but not the iron complex, occurs within hepatocytes, a decrease in the availability of chelateable iron increases the proportion of metabolites.<sup>94,139</sup> Faecal iron excretion as ferrioxamine is almost entirely due to intra-hepatic iron chelation after uptake of DFO into hepatocytes. This results in chelation of cytosolic and possible lysosomal iron to form ferrioxamine that is then excreted in the bile.<sup>77</sup> About a third of chelated iron is excreted through bile into the faeces, and this increases proportionately relative to urinary excretion with higher DFO doses.<sup>140</sup> By contrast, urinary iron is mainly derived from iron released into the plasma compartment after red cell catabolism in macrophages.<sup>141</sup>

#### 4.5.1.3 Effects on Iron Balance and Ferritin

The ability of DFO to induce negative iron balance has been known for three decades and is usually effective at excreting enough iron in urine plus faeces to keep pace with iron accumulated by transfusion.<sup>123</sup> This requires treatment as an infusion 5–7 nights per week over 12 hours. Most information obtained about the doses and frequency required for iron balance were not randomised studies and will not be reviewed here. However, formal evaluation of DFO as a comparator has occurred in more recent randomised studies that compare its effects with DFX. These studies have clarified the relationships

between dose, iron loading rates and iron balance, and hence response to treatment. At typical transfusional iron loading rates ( $0.3\text{--}0.5\text{ mg kg}^{-1}\text{ day}^{-1}$ ) negative balance was achieved in 75% of patients prescribed  $35\text{--}49\text{ mg kg}^{-1}\text{ day}^{-1}$  given subcutaneously 5 days per week, whereas at doses of  $50\text{ mg kg}^{-1}\text{ day}^{-1}$  or greater, response rates increased to 86%. At higher iron loading rates ( $0.5\text{ mg kg}^{-1}\text{ day}^{-1}$ ) a response was seen in only half (50%) of the patients prescribed  $35\text{--}49\text{ mg kg}^{-1}\text{ day}^{-1}$  given subcutaneously 5 days per week, but this increased to 89% at doses of  $50\text{ mg kg}^{-1}$  or greater.<sup>12</sup> As described above, SF is a convenient marker of trends in iron overload and dose-dependent reductions with DFO have been recognized for several decades. In general, the trend in serum ferritin often reveals more about compliance and trends in iron balance than do body iron levels. The impact of dose on ferritin decrements has been shown in a large-scale trial.<sup>142</sup> At a daily dose of  $40\text{ mg kg}^{-1}$   $5\times$  per week in thalassaemia major, the mean serum ferritin fell by approximately  $360\text{ }\mu\text{g L}^{-1}$  at 1 year, and by  $1000\text{ }\mu\text{g L}^{-1}$  at  $50\text{ mg kg}^{-1}$ . The planned dose should be increased if the transfusional iron intake is higher than average.

#### 4.5.1.4 Long-Term Effects on Survival

After the introduction of infused subcutaneous DFO in the late 1970s, the impact of this regime on overall survival began to emerge in the 1980s<sup>143</sup> but the full impact was clearly documented only subsequently.<sup>19,38,44,46,53</sup> A study of nearly 1000 Italian patients in 2004 showed that cohorts born in 1970–74 showed 5% mortality by the age of 20 whereas this fell to 1% in cohorts born from 1980–84 after subcutaneous DFO infusions were in widespread use from about 1980.<sup>38</sup> The age of starting treatment is also a key factor in several studies<sup>19,38,48</sup> although the optimal age has not been formally assessed. Adherence to therapy is key to long-term survival. Life table analysis shows that patients who comply well with treatment can have 100% survival at age 25 whereas survival for patients who comply poorly is only 32%.<sup>19</sup> When subcutaneous infusions of DFO are more than 250 times a year (equivalent to about 5 times per week) survival is 95% at 30 years of age but below this frequency, survival is only 12%.<sup>44</sup> The setting in which patients are treated impacts on adherence and hence on survival; in patients treated by DFO at a single expert institution, survival at 40 years was 83% and in compliant patients born after 1975 survival at 25 years was 100%,<sup>144</sup> contrasting with survival in the UK as a whole.<sup>145</sup>

#### 4.5.1.5 Effects on the Heart

Cardiac mortality has decreased markedly since DFO infusions were first introduced in the late 1970s though this remained the leading cause of death, mainly due to inadequate adherence with the demanding subcutaneous infusion therapy 5–7 nights per week. This, together with the reversal of cardiac failure with continuous intravenous DFO, provides strong evidence of its cardio-protective effects. DFO can thus prevent,<sup>19,46,53</sup> and can also reverse,

cardiac toxicity from iron overload.<sup>146–149</sup> MRI evidence shows that that DFO also removes myocardial iron, even in very severe cases of myocardial iron loading (T2\* values of 5 ms), a 58% improvement in mT2\* was seen over 1 year of intravenous therapy.<sup>150</sup> Improvement in LVEF preceded changes in T2\*, suggesting that beneficial chelation of labile iron pools functions independently of changes in storage iron (visible as mT2\*). However, unless storage iron has been cleared from the heart, with mT2\* > 20 ms interruption of intensive treatment carries high risk. Furthermore, normalisation of mT2\*, even with continuous intravenous DFO, may take up to 5 years in the most severely loaded patients.<sup>144</sup> Intravenous therapy is not necessarily required provided heart function is good and myocardial iron loading is moderate (10–20 ms). Thus, subcutaneous DFO, 5 days per week also improved myocardial iron in such patients in the context of randomized clinical trials over 1 year.<sup>151</sup> Reported response to such regimes is variable for reasons that are not entirely clear but may relate to baseline liver iron concentration. Thus change in T2\* over 1 year differed considerably in patients in different centres but given similar regimes (1.1% change<sup>150</sup> vs. 2.2% change in mT2\*<sup>151</sup>).

#### 4.5.1.6 Other Long-Term Effects on Morbidity

The other documented improvements with DFO therapy include: improvement in liver fibrosis,<sup>152</sup> decreased severity of hypogonadism,<sup>153</sup> improved glucose tolerance<sup>154</sup> and decreased incidence of diabetes,<sup>19</sup> hypothyroidism and hyperparathyroidism in successive birth cohorts of patients.<sup>38</sup> Unlike heart failure, once evidence of advanced endocrine dysfunction has developed, reversal has not been documented. Evidence of prevention of iron-mediated organ damage is also persuasive. Very early studies showed that intramuscular DFO at relatively modest doses stabilized hepatic fibrosis. In patients receiving subcutaneous infusions of DFO, in the absence of histological evidence of active hepatitis, hepatic fibrosis was stabilized over an 8 year period.<sup>155</sup> Introduction of subcutaneous infusions of DFO before the age of 10 years significantly reduces gonadal dysfunction from iron overload, with improvement in pubertal status and growth.<sup>153</sup> Concomitant improvement in fertility has also been seen, although secondary amenorrhea is still common.<sup>156</sup> The onset of glucose intolerance is delayed and may be improved<sup>154</sup> by the timely use of DFO. Hypothyroidism can be prevented and may also be reversed.<sup>157</sup>

## 4.5.2 Deferiprone (DFP)

### 4.5.2.1 Physicochemical Properties and Iron Binding

1,2-Dimethyl-3-hydroxypyrid-4-one, deferiprone (DFP, L1, CP20, kelfer, ferriprox) is a bidentate iron chelator and a member of the family of 3-hydroxypyrid-4-one chelators.<sup>158</sup> DFP is less hydrophilic than DFO, with about one third the molecular weight ( $M_r = 139$ ), but is still not truly lipophilic, being about 5

times more soluble in water than lipid.<sup>159</sup> The simple stability constant for iron(III) is about six orders of magnitude higher than for DFO. However, more clinically relevant is the pM ( $-\log$  of the uncoordinated metal) [ $M = \text{iron}$ ] concentration, calculated when: pH = 7.4 with 10  $\mu\text{M}$  ligand and 1  $\mu\text{M}$  iron(III), which is 20, and lower than that of DFO at 26.6 (see Chapter 2, Section 2.4.3).<sup>160</sup> Thus, while iron(III) binding is efficient at high concentrations of DFP, at lower chelator concentrations, such as 10  $\mu\text{M}$ , and at clinically relevant iron concentrations of 1  $\mu\text{M}$ , DFO will scavenge iron more efficiently than DFP. The lower pM also increases the potential to redistribute iron within the body<sup>161</sup> with the potential formation of incomplete 1:1 and 1:2 iron–chelate complexes which, theoretically, could participate in the generation of hydroxyl radicals.<sup>63</sup> This may explain the arthropathy occasionally seen in heavily iron-loaded patients possibly due to free radical generation by iron complexes in the joint space.<sup>162</sup> There is a potential advantage to the low pM, however, because as chelateable iron concentrations fall in tissues, the risk of over chelation, such as occurs with DFO, may be less. DFP and its 3:1 iron complex are both neutrally charged which, together with the less hydrophilic nature of the iron chelator and its complex than DFO, encourages a rapid diffusion of the free chelator into cells, and its iron complex out of cells. This is unlike DFO, which slowly accumulates within cells reaching concentrations exceeding those in the plasma; DFP egresses relatively quickly,<sup>66,79,94</sup> although the iron complexes of DFP are still detectable in plasma a week after ceasing regular clinical dosing of this drug and levels can be used to predict chelation response.<sup>86</sup>

#### 4.5.2.2 Pharmacokinetics

Absorption is rapid following oral administration and DFP is detectable in plasma within 5 to 10 minutes (see Chapter 2, Figure 2.15A). In contrast to DFO, iron excretion with DFP in humans is almost exclusively in the urine.<sup>163–165</sup> High DFP concentrations are achieved at commonly prescribed doses, with plasma levels exceeding 300  $\mu\text{M}$  after a 50 mg  $\text{kg}^{-1}$  dose orally.<sup>89,166</sup> Such levels are 5 to 10 times higher than infused DFO.<sup>139,164</sup> Cell culture studies in myocytes show that these high concentrations, together with rapid access to intracellular iron, may favour the scavenging of chelateable iron.<sup>74</sup> However, these high levels are short-lived with an elimination half-life of 1.52 hours.<sup>89</sup> This means that at currently prescribed dosing, three times daily, low plasma and tissue levels are likely between doses, particularly overnight. DFP is metabolized in hepatocytes to the inactive glucuronide, which is the predominant form recovered in the urine.<sup>166,167</sup> A constant ratio of AUC of the DFP–glucuronide to DFP at increasing doses indicates that increasing the dosage does not influence deferiprone biotransformation.<sup>168</sup> Rapid hepatocellular glucuronidation<sup>82</sup> may limit effective iron chelation in the liver.<sup>88</sup> By contrast, in other cells, such as myocytes, glucuronidation is predicted to be less than in liver, which may explain why DFP appears to be more effective in the heart than the liver. A more recent study<sup>169</sup> found the  $C_{\text{max}}$  and the AUC as

well as the urine iron excretion, were significantly higher in splenectomised patients than in non-splenectomised patients possibly due to higher levels of iron overload in this group as ferritin and NTBI also correlated with AUC and UIE. Further analyses using multiple linear regressions indicated that the iron profiles (non-transferrin-bound iron and ferritin) were significant predictors of the pharmacokinetic parameters of non-conjugated deferiprone, deferiprone-chelated iron and UIE.

#### 4.5.2.3 Effects on Iron Balance

At 50 mg kg<sup>-1</sup> daily of either DFO (12 infusion) or DFP, mean daily urinary iron excretion was lower during DFP.<sup>164</sup> In sickle cell disease, total daily excretion of 0.53 mg kg<sup>-1</sup> day<sup>-1</sup> was observed with excretion mainly in the urine.<sup>165</sup> Long-term LIC trends from meta-analysis of several studies show considerable inter-study variation, reflecting the heterogeneity of dosing schedules, transfusion rates, baseline LIC values, and follow-up periods.<sup>170</sup> The response rate (percentage of patients showing an LIC decrease) was variable but is higher at high baseline LIC values. 76% of patients with TM showed an LIC response (decrease in LIC) at a mean of 3 years,<sup>171</sup> but this decreased to 56% after further follow-up.<sup>172</sup> In another 2 year prospective study, only 24% of patients overall showed negative iron balance within 2 years but this was higher (50%) in patients where LIC exceeded 9 mg g<sup>-1</sup> dry wt.<sup>100</sup>

Considerably more data are available with SF used as a surrogate marker of iron balance in studies comparing DFP with DFO.<sup>151,173–175</sup> The relative effects of the two drugs differ considerably among the studies, most likely reflecting different study population characteristics. Pooled analysis<sup>170</sup> shows a statistically significant decrease in serum ferritin at 6 months, in favour of DFO. Ferritin response rates (percentage of patients showing decrements in serum ferritin) are lower at baseline SF < 2500 mg L<sup>-1</sup>. The response rate for ferritin tends to be greater (e.g., 58%) than for LIC (24%) and ferritin response is lower when baseline values are less than 2500 mg L<sup>-1</sup>.

#### 4.5.2.4 Effects on the Heart

A beneficial effect on cardiac deaths has been reported although outcomes vary considerably between studies. An early study showed continued cardiac mortality in thalassaemic patients treated with DFP: in 51 patients previously poorly chelated with DFO, four died of cardiac causes while receiving DFP.<sup>176</sup> In a large retrospective analysis of 532 Italian thalassaemia major patients over 3 years of treatment, 9 died of heart failure while being treated with DFP.<sup>177</sup> However, another retrospective analysis of survival in seven Italian hospitals over 4.3 years reported significantly better survival in DFP- than DFO-treated patients.<sup>178</sup> In a retrospective analysis of patients treated in Cyprus, improving mortality over time was attributed to the introduction of DFP.<sup>179</sup> In a prospective randomized MRI study, high DFP doses (92 mg kg<sup>-1</sup> day<sup>-1</sup>)

were compared with subcutaneous DFO at 53 mg kg<sup>-1</sup> given 5 days per week at standard doses (mean daily dose 43 mg kg<sup>-1</sup> day<sup>-1</sup>).<sup>150</sup> After 1 year there was significant improvement in T2\* and increase in left ventricular ejection fraction (LVEF) with DFP treatment, which was greater than that seen at the standard DFO doses. In an earlier randomized study, where lower doses of DFO were used (75 mg kg<sup>-1</sup> day<sup>-1</sup>), a similar and significant improvement in cardiac MR signal was seen with DFO- and DFP-treated patients.<sup>173</sup> The dosing and patient selection is likely to be important to the relative outcomes when two chelators are compared.

### 4.5.3 Deferasirox (Exjade®) DFX

4-[3,5-bis(2-Hydroxyphenyl)-1,2,4-triazol-1-yl]benzoic acid (DFX, deferasirox) has a molecular weight of 373. The tridentate structure results in the chelator binding iron(III) in a 2:1 ratio. This results in an iron complex coordinated by 4 oxygen and two nitrogen atoms. The stability of this complex, as estimated by the pM values, is intermediate between DFO and DFP. DFX is lipophilic but highly protein-bound in plasma. Despite the protein binding, good tissue penetration is seen with faster mobilization of tissue iron than DFO.<sup>180,181</sup> Mobilization of myocyte iron appears to be efficient;<sup>71,74</sup> this has been confirmed in studies with iron-overloaded gerbils.<sup>182</sup>

#### 4.5.3.1 Pharmacokinetics and Metabolism

The drug has low water solubility and is given as an oral suspension once daily. More recently a tablet preparation has been developed by Novartis that is clinically available in the USA, but not yet in Europe. Pharmacokinetics (PK) by the oral route were examined in the first Phase I randomized double-blind study using single doses, in 24 patients with thalassemia major who received single oral doses of dispersible tablets ranging from 2.5–80 mg kg.<sup>91</sup> Absorption was rapid with plasma half-life of 11–19 hours, supporting once-daily oral administration (see Chapter 2, Figure 2.15B). The AUC 0–24 h and C<sub>max</sub> of the iron-free ligand increased proportionally with the dose. At doses of 10–40 mg kg<sup>-1</sup> day<sup>-1</sup> the AUC of the iron complex was approximately 20–30% of the iron-free drug. Once-daily repeat dosing at 20 mg kg<sup>-1</sup> resulted in peak plasma levels of 80 μM with trough values of 20 μM<sup>183</sup>. Administration of single doses of <sup>14</sup>C DFS showed that metabolism occurred at several sites, but predominantly by glucuronidation in the liver at a position not involved in iron coordination.<sup>90</sup> Elimination of this and other metabolites was predominantly *via* the faeces. The urinary excretion of DFX and its iron complex is less than 0.1% of the dose. The final elimination of DFX, the iron complex, and metabolites appears to be by hepatobiliary anion transport and dose adjustment is required for patients with hepatic impairment.

Drug interactions may in principle affect either levels of co-administered drugs or of DFX itself. A recent review suggested that co-administration of DFX with strong uridine diphosphate glucuronosyl transferase inducers

or bile acid sequestrants should be avoided where possible, and patients should be monitored if there is co-administration with cytochrome P450 (CYP) 3A4/5, CYP2C8, or CYP1A2 substrates.<sup>184</sup> Using *in vitro* assays, some displacement of both diazepam and warfarin from albumin was observed but only at very high DFX concentrations (268  $\mu\text{mol L}^{-1}$ ). There is broad agreement however that the clinical relevance of this protein displacement is minimal with no requirement for dose adjustment.<sup>54-56</sup> Interactions between DFX and midazolam suggest modest induction of CYP3A4/5 by DFX:<sup>185</sup> the label recommends close patient monitoring for reduced efficacy with co-administration of any drug metabolized by CYP3A4/5.<sup>186</sup> Interactions between DFX and repaglinide, a substrate for Cytochrome P<sub>450</sub>2C8 (CYP2C8), indicate moderate inhibition of (CYP2C8) by DFX.<sup>185</sup> Interactions between DFX and theophylline (a substrate for CYP1A2) suggest weak inhibition of CYP1A2 by DFX. Patients should therefore be closely monitored for signs of drug toxicity when the chelator is co-administered with CYP2C8 or CYP1A2 substrates, particularly with substrates possessing a narrow therapeutic range.<sup>186</sup> Specifically, possible theophylline dose reduction should be considered with DFX co-administration. With respect to drug interactions leading to changes in DFX levels, co-administration of rifampicin led to induction of the glucuronidation pathway (through UGT1A), resulting in a 44% reduction in DFX AUC.<sup>185</sup> Dose increase may be therefore required when DFX is administered with strong UGT inducers.<sup>186</sup> Use of DFX with bile acid sequestrants is not advised, although a higher DFX dose may be considered if treatment is essential.<sup>186</sup>

#### 4.5.3.2 Iron Excretion and Iron Balance

Iron excretion in metabolic iron balance studies is dose dependent and almost entirely faecal,<sup>91,92</sup> averaging 0.13, 0.34, and 0.56  $\text{mg kg}^{-1} \text{day}^{-1}$  at doses of 10, 20, and 40  $\text{mg kg}^{-1} \text{day}^{-1}$ , respectively. This predicts iron balance at daily doses of about 20 mg depending on the blood transfusion rate.<sup>92</sup> Over 1 year in a study with conservative dosing, dose-dependent reduction in LIC was seen.<sup>142</sup> The importance of blood transfusion rate to iron balance was demonstrated so that at low transfusion rates  $<0.3 \text{ mg kg}^{-1} \text{day}^{-1}$ , 96% of patients had a negative iron balance at 30  $\text{mg kg}^{-1} \text{day}^{-1}$  whereas at higher transfusion rates only 82% of patients had a negative iron balance at the same dose.<sup>12</sup> The broad ferritin trends also reflect iron balance, as shown by the significant correlation between the SF trend and LIC trend across a wide range of diagnoses.<sup>187</sup> However, a lag in ferritin response may occur, possibly reflecting preferential iron removal from hepatocytes compared with macrophages<sup>188</sup> which are the main source of serum ferritin at levels below 4000  $\text{mg L}^{-1}$ . The finding of a lack of SF response in 52% of patients showing a reduction in LIC is consistent with preferential early removal of hepatocellular, rather than macrophage, iron.<sup>101</sup> This is also consistent with the proportion of patients with downward ferritin trends increasing with duration.<sup>189</sup> In the 1 year EPIC of 1700 patients, dosing was adjusted successfully at a median of

24 weeks, based on baseline ferritin, trends in ferritin, and transfusional iron loading rates.<sup>190</sup> Based on these findings, and the theoretical considerations discussed earlier, dose escalation based on ferritin trends should typically be considered only after at least 3 months of treatment and ideally confirmed by serial LIC determination.

#### 4.5.3.3 *Effects on the Heart*

Early pilot observations of improved cardiac T2\*,<sup>191</sup> showed significant improvement in mT2\* using variable dosing from 10 to 30 mg kg<sup>-1</sup> day<sup>-1</sup> with 73% of patients showing improved T2\* at 12 months. Larger prospective studies with defined dosing regimens then followed.<sup>192</sup> Patients with beta-thalassemia with T2\* from 5 to 20 ms, left ventricular ejection fraction (LVEF) of 56% or more, serum ferritin of more than 2500 µg L<sup>-1</sup>, and liver iron concentration of more than 10 mg Fe g<sup>-1</sup> dry wt<sup>192</sup> were followed up to 3 years; a significant improvement in mT2\* from 14.6 to 17.4 ms was seen at 1 year at mean doses of 33 mg kg<sup>-1</sup> day<sup>-1</sup>.<sup>192</sup> In patients with baseline T2\* values less than 10 ms, the T2\* also increased significantly from 7.4 to 8.2 ms over 1 year. The response rate for improvement of mT2\* at 1 year was 70% in this study. 71 patients elected to continue into the third year. 68.1% of patients with baseline T2\* of 10 to <20 ms normalized mT2\* and 50.0% of patients with baseline T2\* >5 to <10 ms improved to 10 to <20 ms. There was no significant variation in left ventricular ejection fraction over the three years and no deaths occurred.<sup>113</sup> In a randomized controlled trial of deferasirox (target dose 40 mg kg<sup>-1</sup>) versus deferoxamine for myocardial iron removal in beta-thalassemia major (CORDELIA),<sup>193</sup> the geometric mean  $G_{\text{mean}}$  myocardial T2\* improved with deferasirox from 11.2 ms at baseline to 12.6 ms at 1 year.<sup>193</sup> At 2 years,<sup>194</sup> sustained improvement was seen with mT2\* increased from a baseline of 11.6 to 15.9 ms with improvement across all subgroups of baseline T2\* with LVEF remaining stable. These studies have included only patients with normal LVEF's and no significant changes have been seen.<sup>195</sup>

## 4.6 Unwanted Effects of Iron Chelators

### 4.6.1 Role of Iron Deprivation in Chelator Toxicity

A detailed discussion of the unwanted effects of over-chelation, as well as unwanted effects of chelators that are not related to over-chelation, has been undertaken elsewhere. Readers are referred to a recent review by this author for more detailed discussion.<sup>81</sup> Most of the unwanted effects have an increased probability at higher doses of the chelator and/or when iron overload is less apparent. The increased risk of neurotoxicity with DFO at higher doses and at lower levels of iron overload has been known for decades and led to the development of a therapeutic index which combined these two variables into a risk score.<sup>196</sup> Such work has not been undertaken with oral chelators. There are no studies on deferiprone where an attempt has been made to investigate

the relationship of the key unwanted effects of this drug (agranulocytosis) to dose or level of iron overload. However it is the authors view that should such a relationship be sought, it may be found. This is based on observations in non-iron-overloaded patients who have received deferiprone for neurological disorders and where incidence of agranulocytosis appears to be above 1% (personal communication), although the small series so far published does not report on either neutropaenia or agranulocytosis.<sup>197,198</sup> On a theoretical basis, inhibition of RR by DFP, a key enzyme in cell cycle progression, in a dose-dependent manner combined with dose-dependent marrow hypoplasia in animal models<sup>199</sup> makes this a plausible mechanism. However, it must be noted that predicting patients most likely to develop agranulocytosis on the basis of dose and iron load is not straightforward. Thus while a clear link between dose, iron overload and agranulocytosis has not been systematically investigated, reasonable precaution about reducing the dose in patients without iron overload or with low levels of iron overload would seem sensible.

In the case of deferasirox, the majority of unwanted effects have been linked to the dose given. Mild to moderate gastrointestinal disturbances are the most common unwanted effects and can be improved by dose reduction or by dividing the dose. However the most important and dose-limiting toxicity is renal dysfunction. A 30% increase in serum creatinine is seen in about one third of patients but this is usually manageable without dose interruption. In patients who start with high baseline creatinine levels, such as older patients with myelodysplasia, such an increase is more likely.

#### 4.6.2 Desferrioxamine Tolerability and Unwanted Effects

Most of the toxic effects of DFO are dose-related; thus effects on growth, skeletal changes, and audiometric and retinopathic effects are more likely at higher doses. These effects are unlikely with subcutaneous infusions in adults if the dose does not exceed 50 mg kg<sup>-1</sup> and care is taken to reduce the dose as ferritin levels fall. Retinal effects can present with a loss of visual acuity, field defects, and defects in night or color vision, particularly with continuous 25 h infusions. Doses of 100 mg kg<sup>-1</sup> day<sup>-1</sup>, at which these effects were originally described,<sup>200</sup> are rarely given today. Drug-related ototoxicity is typically symmetrical, high-frequency sensorineural.<sup>196</sup> Some adverse effects are more likely when iron stores are low particularly neurotoxic complications, where standard doses can be associated with coma in patients without iron overload. Audiometric and retinopathic effects are more likely at lower serum ferritin levels,<sup>196</sup> particularly less than 1000 mg L<sup>-1</sup>.<sup>201</sup> In patients who develop complications whilst receiving DFO, treatment should be temporarily stopped and reintroduced at lower doses when symptoms or signs have improved. In children, doses greater than 40 mg kg<sup>-1</sup> have been associated with an increased risk of impaired growth and skeletal changes. Thus growth retardation was seen when DFO was started early (<3 years) or at higher doses.<sup>42,45</sup> Rickets-like bony lesions and genu valgum may occur. Metaphyseal changes, in the vertebrae may give a disproportionately short trunk, with

vertebral demineralization and flatness of vertebral bodies.<sup>43</sup> Local skin reactions, allergic reactions, and *Yersinia enterocolitica* infections are less obviously dose-related.

### 4.6.3 Deferiprone Tolerability and Unwanted Effects

An International Study Group on Oral Chelators found the most frequent complications were nausea and other gastrointestinal symptoms, arthralgia, zinc deficiency, and fluctuating liver function tests, especially in patients positive for anti-hepatitis C virus antibodies.<sup>202</sup> The effect of dose on tolerability has not been studied systematically. Agranulocytosis is the most serious effect, occurring in about 1% of patients<sup>203</sup> but the effect of dosing on agranulocytosis in humans has not been reported. In animal studies, bone marrow hypoplasia with leucopaenia is dose-related however.<sup>199</sup> In view of the risk of agranulocytosis, weekly blood counts are recommended for all patients on DFP therapy. Agranulocytosis may require GMFSF to aid recovery. Progression of liver fibrosis has been reported<sup>172</sup> but not confirmed in other studies.<sup>204</sup> Arthropathy, most commonly affecting the knees, may be more common with high levels of iron overload<sup>162</sup> suggesting a possible effect of the iron complex. The duration of observation may also influence the frequency of arthropathy, increasing from 6% at 1 year to 13% at 4 years.<sup>205</sup>

### 4.6.4 Deferasirox Tolerability and Unwanted Effects

More than 3000 patients have been studied in prospective trials of DFX, where the frequency of unwanted effects has been reported. Most studies lasted 1 year, several have been extended up to 5 years. Discontinuation rates were generally lower than those seen with long-term DFP administration. The most common adverse effects are generally mild to moderate gastrointestinal events, including abdominal pain, nausea and vomiting, diarrhea, and constipation, occurring in approximately 15% of patients with thalassemia,<sup>142</sup> and somewhat higher numbers of older patients with myelodysplasia. Skin rashes occur early in approximately 10% of patients and are usually transient.<sup>142</sup> Mild dose-dependent increases in serum creatinine in approximately one-third of patients were seen, occurring within a few weeks of starting or increasing therapy. These increases were usually not progressive and reversed or stabilized when doses were adjusted. Occasional cases of renal failure have been reported. It is important to monitor serum creatinine and to decrease or interrupt the dose if creatinine increments exceed 30% or if the creatinine increases above the normal range. Failure to do this can result in renal failure. Proteinuria, with or without a Fanconi type renal tubular acidosis,<sup>206</sup> has been reported and regular monitoring of urinary protein is recommended. In the presence of severe sepsis or hypotension, it is wise to interrupt dosing. Increased liver enzymes, judged to be related to DFX, occurred in fewer than 1% of patients. In a large prospective study 0.6% of patients showed increased liver enzymes 10× above the upper limit of

normal attributable to DFX.<sup>190</sup> Improvement or stabilization in liver pathology of patients with beta-thalassemia treated with DFX for at least 3 years has been reported in a prospective trial.<sup>207</sup> Audiometric effects and lens opacities did not differ significantly from the control arm treated with DFO,<sup>142</sup> and no clearly drug-related agranulocytosis has been observed in clinical trials. In pediatric patients, growth and development proceeded normally.<sup>208</sup> Follow-up data from the five core phase II/III studies, now at a median of 3.5 years, show no inhibitory effects on growth.<sup>209</sup>

## 4.7 Practical Use of Chelators: A Personal Approach

The correct choice regimen and dose titration combined with attention to adherence are key to successful chelation therapy which requires the background knowledge described above. When iron overload is already at unacceptably high levels, iron excretion needs to exceed iron input from transfusion and/or dietary iron absorption. If iron has distributed to the heart as evidenced by an mT2\* < 20 ms, then further consideration to dose and regime may be necessary. This requires an understanding of iron loading rates, factors affecting iron distribution and its consequences, as well as an understanding of how and where iron chelators act and at what dose.

### 4.7.1 Patients with Acceptable Levels of Body Iron but Continuing Transfusion

If a patient starts chelation when ferritin reaches 1000  $\mu\text{g L}^{-1}$  and it is taken regularly at recommended doses and transfusion requirements are not above average, then standard doses of chelation will usually be effective at maintaining body iron to acceptable levels (keeping ferritin <1000  $\mu\text{g L}^{-1}$ , LIC <7  $\text{mg g}^{-1}$  dry wt, myocardial T2\* > 20 ms).

Table 4.3 shows how the daily dose of DFX or DFO infusions, 8–10 h for 5 days per week, can be adjusted depending on the transfusional iron loading

**Table 4.3** Percentage of responders (percentage in negative iron balance) by dose and transfusion rate.<sup>a</sup>

Chelator	Transfusion rate	Transfusion rate	Transfusion rate
Dose ( $\text{mg kg}^{-1}$ )	Low <0.3 $\text{mg kg}^{-1}$ day <sup>-1</sup>	Intermediate 0.3–0.5 $\text{mg kg}^{-1}$ day <sup>-1</sup>	High >0.5 $\text{mg kg}^{-1}$ day <sup>-1</sup>
Desferrioxamine			
35–<50	76	75	52
≥50	100	86	89
Deferasirox			
10	29	14	0
20	76	55	47
30	96	83	82

<sup>a</sup>Adapted from ref. 41, Chapter 3, Porter and Viprakasit.

rate. This is typically 25–30 mg kg<sup>-1</sup> of DFX and 40–50 mg kg<sup>-1</sup> of DFO 5 days per week. Studies relating variable DFP doses to iron excretion have not been undertaken systematically but presumably the highest licensed dose of 100 mg kg<sup>-1</sup> in 3 divided doses will excrete more iron than 75 mg g<sup>-1</sup>. Only about one third of patients treated with DFP at this standard dose will be in iron balance and, for this reason, DFO has often been added to DFP (see below) when control is inadequate with monotherapy. For these reasons and for reasons of convenience, DFX at 25–30 mg kg<sup>-1</sup> day<sup>-1</sup> is usually the first-line treatment in this situation.

### 4.7.2 Patients with Unacceptably High Levels of Body Iron

If iron has been allowed to accumulate in the liver and hence ferritin values are high, then treatment will need intensification. Poor adherence to treatment is the commonest cause of poor control (see below) but if this has been excluded or worked upon and cannot be improved further, then dose escalation is likely to be needed. The dose of chelator can be adjusted according to the transfusion iron loading rate (Table 4.3). If the ferritin trend still fails to improve, work with the patient on adherence issues (including a clinical psychologist) is advisable. It is helpful to check sequential LIC values by MRI as about half of patients failing to show a clear downward trend after 1 year at a given dose of DFX are actually in negative iron balance which is not reflected by serum ferritin.<sup>101</sup> Occasionally a failure to show a downward trend in ferritin or LIC at maximum tolerated doses will require switching regimen either to another form of monotherapy or to a combined therapy regime. Here the individual preference of the patient and the willingness of the doctor to explain that treatment works if it is taken regularly can be the key to success. A willingness of the clinical team to listen carefully to issues a patient may have with the current regime will often provide insights into why this may be failing to show a clear improvement.

### 4.7.3 Patients with Unacceptably High Levels of Myocardial Iron

The risks of developing heart failure in the next year have been linked to myocardial T2\* values.<sup>112</sup> This risk is low if myocardial T2\* is abnormal (<20 ms) while remaining >10 ms. Under these circumstances I usually work carefully on adherence issues and escalate the dosing of the currently prescribed chelator. This is because it is now clear that all 3 licensed chelators are effective at removing myocardial iron effectively if they are taken by the patient. Personally I would not prescribe 5 days per week of DFO at 40 mg kg<sup>-1</sup> to patients with increased myocardial iron loading; this dose was used in several trials and I regard this dose as inadequate when there is increased myocardial iron. If the ferritin is not <1000 µg L<sup>-1</sup>, increasing the DFO exposure is an option, either by increasing the dose to 50–60 mg kg<sup>-1</sup> and/or encouraging therapy >5 times per week. This can be a simple and effective strategy. Another approach

under these circumstances, particularly if increased dosing cannot be tolerated or low levels of body iron increase the risk of chelator toxicity, is to switch patients from monotherapy to some form of combined therapy. The most extensively evaluated is DFP given at standard doses with DFO at standard dose and infusion times (8–10 h) added 2–5 times per week. The frequency of the DFO may be determined by levels of body iron (reducing the frequency when ferritin is  $<1000 \mu\text{g L}^{-1}$ ) or if the patients will not take DFO as often as may be therapeutically indicated.

It is difficult to compare the relative efficacy of different chelators under these circumstances unless they were examined head-to-head in a randomized trial. Even then the doses chosen for one arm of the trial may not have been optimal; such results need to be interpreted with caution. It must be remembered that improvement in myocardial  $T2^*$  is slow so that, provided the trajectory of  $mT2^*$  shows improvement, patience and persistence with treatment are important.

Provided the ferritin and/or LIC are improving, treatment is being taken regularly and the last  $T2^*$  was  $>10$  ms, the current therapy can be continued. If the ferritin trend is worsening this is usually an indication of continued poor compliance or inadequate dosing. It may be necessary then to consider changing to another monotherapy or a combined regime to aid adherence and patient acceptability. When the  $T2^*$  is 7–10 ms, the risk of heart failure is increased but, with the caveat for patients described above, my approach to the regime is similar to that described immediately above. When the  $T2^*$  is  $\leq 6$  ms there is a high risk of developing heart failure, particularly if treatment is not being taken often enough. Under these circumstances switching the regimen to a combined therapy may be unavoidable. When myocardial iron is increased, there is a risk of decreased left ventricular function and of heart failure. The nature of this risk has been defined by studies using  $T2^*$  to estimate myocardial iron.

#### 4.7.4 Patients in Heart Failure

In patients with decreased left ventricular function or in frank heart failure, continuous DFO infusion is more beneficial than intermittent infusions because it reduces the exposure to toxic free iron (NTBI), which rebounds to pre-treatment levels within minutes of stopping infusions.<sup>24</sup> 24 hour intravenous DFO administration *via* an implanted intravenous delivery system<sup>116</sup> or subcutaneously<sup>48</sup> has been shown to normalise heart function, reverse heart failure, improve myocardial  $T2^*$ <sup>50,117</sup> with long-term survival, provided treatment is maintained. A dose of at least  $50 \text{ mg kg}^{-1} \text{ day}^{-1}$  and not exceeding  $60 \text{ mg kg}^{-1} \text{ day}^{-1}$  is recommended.<sup>116</sup> The question of whether to add DFP to this regimen needs to be considered as combined DFP–DFO has been found to improve  $T2^*$  more rapidly than conventional doses of DFO.<sup>152</sup> However, patients in this study were not in heart failure. Furthermore these studies compared conventional intermittent non-intensified DFO with the DFP-containing regimes; such low DFO doses should not be recommended

for patients with heart failure. The only randomized study to examine the effect of additional DFP to intensified DFO found no difference between the two study arms with or without DFP.<sup>117</sup> No major extra toxicities in the study arm containing DFP were seen, so that the addition of DFP to intensified DFO would seem a reasonable course of action. DFX has not been formally evaluated for patients in heart failure.

#### 4.7.5 Patients with Rapidly Falling Serum Ferritin or Low Values $<1000 \mu\text{L}^{-1}$

It is as important to decrease dosing as iron overload falls as it is to escalate when levels are too high. Having dealt with the challenges of achieving adequate chelation, it is to some extent gratifying that we are now in an era when we have to consider what to do when chelation is effective and ferritin is falling fast or has reached low levels. Here the drug licensing and guidelines have fallen behind what clinicians working in iron chelation every day would recommend. It is bad clinical practice to operate a 'stop-start' approach with chelation therapy. This is because both plasma NTBI and intracellular iron pools rebound rapidly after chelation has stopped, leading to potential iron toxicity and resurgent uptake into endocrine and myocardial tissues. Furthermore in TDT, iron loading continues apace so there is no logic in stopping chelation (unlike NTDT). Instead a policy of a 'soft landing' is preferable.<sup>210</sup> This means that as the ferritin trend shows that a value of  $1000 \mu\text{g L}^{-1}$  is approaching, the dose is modified downwards (not interrupted) so that the dose is changed in relation to the degree of iron overload and the loading rate is not excessive. Here personal experience is helpful because drug labelling is inadequate and clinical trials about what to do are almost completely lacking with some chelation regimes.

Current guidelines recommend downwardly adjusting mean daily DFO in line with the SF so that the ratio of the dose to the SF is not excessive. A therapeutic index was developed based on retrospective analysis of audiometric toxicity in relation to these parameters (mean daily dose in  $\text{mg kg}^{-1} \text{day}^{-1}$  divided by SF (in  $\mu\text{g L}^{-1}$ ) to be  $<0.025$ )<sup>196</sup>. Further fine-tuning of this principle has been suggested using the LIC rather than the SF,<sup>211</sup> although the LIC is rarely performed often enough for this to be practical. However, it is worth noting that SF can give a misleading indication of iron overload (see below).

Current guidelines recommend interruption of deferasirox when SF reaches  $500 \mu\text{g L}^{-1}$ . It is preferable to reduce the deferasirox dose before this value is reached. Provided the dose is downwardly titrated the risk of over-chelation can be minimised and patients can be maintained around, or slightly below,  $500 \mu\text{g L}^{-1}$  at lower doses. However there are cases where a sudden rise in creatinine occurs when SF is  $>1000 \mu\text{g L}^{-1}$  (while falling rapidly) only to find that LIC was undetectable by MRI. I suspect that a careful analysis of the relationship between absolute levels or relative changes in LIC and serum creatinine for example would lead to clearer guidelines on achieving soft landings.

While it is clear that over-chelation relative to iron overload is the principle cause of DFO and deferasirox toxicity, there is virtually no data relating the

dose of DFP to either its bone marrow or liver toxicities. Although this drug is licensed up to 100 mg kg<sup>-1</sup>, the number of patients studied in prospective trials is very small and there is no study comparing toxicity at 50, 75 and 100 mg kg<sup>-1</sup>.

#### 4.7.6 Patients not Responding to Monotherapy Regimes: Combined Chelators

The use of DFO with DFP in the context of low myocardial T2\* of <10 ms has been discussed (in Section 4.7.3) but there are other circumstances under which some combination of chelators may be useful. Combined use of iron chelators has attracted much debate. This is partly because the term 'combination therapy' has been used as a 'catch-all' phrase to cover a wide variety of ways in which chelators can be combined, and partly because the quality of data available has not always been of a quality that allows clear interpretation. Nevertheless the use of more than one chelator can be valuable to: (a) improve the efficacy of a given drug that is not keeping pace with iron loading rates; (b) to improve adherence with, and exposure to, iron chelation overall; (c) to improve tolerability or patient acceptance relative to monotherapy. Combinations of chelators may improve outcome because there is increased overall exposure to chelators, or because there may be genuine synergistic interaction of the chelators. Although there are *in vitro* data for true synergism in plasma<sup>212</sup> or in cells,<sup>181</sup> the clinical evidence for true synergism is rather sparse, particularly when using DFP during the day and DFO at night when the opportunity for drug interaction is limited.

#### 4.7.7 Combinations of DFP with DFO

Deferiprone when used as monotherapy at standard recommended doses fails to keep up with rates of transfusional iron loading in about two-thirds of cases. For this reason and others (see below) the addition of subcutaneous DFO to DFP, as often as a patient is prepared to take DFO, is practically valuable as it leads to increased overall exposure to chelation and leads to improved SF and LIC trends<sup>213,214</sup> compared with DFP monotherapy.

Adding DFP to a patient already on DFO results in the two drugs being used as above but has a different genesis. While this concept may superficially seem the same, it differs because the starting point differs. Many patients still begin their treatment with DFO or have been on this as monotherapy for many years. DFP has been added to DFO monotherapy to improve adherence and overall exposure to chelation when patients tire of taking DFO 5–7 nights per week. The ferritin trend was found to be largely unaltered in one randomised study.<sup>213</sup> However, outside formal trial conditions, improved removal of storage iron may be achieved with a combination regime due to improved compliance and this overall exposure to chelation.

A third reason that these drugs have been used together is when patients have developed myocardial iron overload. In a randomized study the combination of DFP with DFO (subcutaneously 5 nights per week) was more effective at removing heart iron than DFO at low-to-standard doses 5 days per week.<sup>151</sup>

Whether this difference would have been shown if higher doses of DFO were used is debatable. Indeed, I have achieved myocardial iron removal in patients who can take their DFO by simply increasing the dose to 50 or 60 mg kg<sup>-1</sup> day<sup>-1</sup> at the same frequency. In practice, however, it can be difficult to persuade patients to take DFO subcutaneously more than 5 nights per week, although this is certainly possible and effective in the right patient. Practically speaking, this combination is often a useful option when monotherapy with DFO is not acceptable to the patient or deferasirox cannot be tolerated. The necessity to adopt this combination will depend on the degree of myocardial iron load. My practice is to work on adherence and dosing with patients when myocardial iron overload is mild to moderate (*i.e.*, >10 ms and heart function is normal) and to consider combination of DFP with DFO when myocardial iron overload is more severe and when monotherapies have failed.

#### 4.7.8 Combinations of DFO Plus DFX

Rather than adding DFP to DFO when body iron or myocardial iron is not controlled, another option is to add DFX. Early studies suggested this might be a well tolerated combination for increasing iron removal from heart or liver.<sup>215</sup> This has recently been evaluated in a prospective 24 month Phase II study (HYPERION) in 60 patients with severe transfusional myocardial siderosis (mT2\* < 10 ms and LVEF ≥ 56%). Mean dose was 30 mg kg<sup>-1</sup> day<sup>-1</sup> DFX and 36 mg kg<sup>-1</sup> day<sup>-1</sup> DFO on a 5 day regimen. This led to a significant improvement in mT2\* over 24 months with a stable LVEF and an impressive 52% reduction in LIC.<sup>216</sup> I have used this combination when monotherapy with either drug has been slow, or simply to improve LIC at a greater rate than with monotherapy, or when myocardial T2\* is <10 ms. The regime appears to be well tolerated and consistent with the known side effects of the monotherapies.

#### 4.7.9 Combination of DFP Plus DFX

A further possible combination is that of the two oral drugs. *In vitro*, this combination performed particularly well with evidence of synergism.<sup>181</sup> One randomised study has been reported in 96 young thalassaemia major patients<sup>217</sup> using a combination of DFP with DFO as a comparator. The combination of DFX with DFP appeared more effective at improving compliance, quality of life and mT2\* than DFO with DFP. I have used this combination occasionally when other options were not possible.

### 4.8 Conclusions

Iron overload causes progressive damage to tissues where it is present in excess, although levels that cause toxicity vary from tissue to tissue. Iron chelation therapy is a highly effective treatment modality. Morbidities to the endocrine system and mortality from cardiomyopathy have decreased progressively since the introduction of chelation, initially with

desferrioxamine, in the late 1970s. Recent additions of oral chelators together with improved monitoring of iron overload, using MRI techniques for heart and liver, have improved outcomes further. The full benefits of chelation in patients with transfusional iron overload are yet to accrue. Challenges remain however in achieving optimal outcomes. These challenges relate to adherence by patients to daily chelation therapies or to increasing chelator toxicities as body iron levels approach normal levels. The latter limits the ability to achieve normal body iron levels with chelation therapies. Future strategies should aim to identify chelation regimes that allow greater adherence by the patients and to identifying better how chelators can be combined to improve adherence and to decrease chelator toxicities.

## Abbreviations

<b>AUC</b>	Area under the curve
<b>CMR</b>	Cardiac magnetic resonance
<b>CNS</b>	Central nervous system
<b>EMS</b>	Erythrophagocytic macrophage system
<b>gdw•</b>	gram dry weight
<b>gww•</b>	gram wet weight
<b>HH</b>	Hereditary haemochromatosis
<b>HPLC</b>	High pressure liquid chromatography
<b>IE</b>	Ineffective erythropoiesis
<b>ILR</b>	Iron load rate
<b>LIC</b>	Liver iron concentration
<b>LPI</b>	Labile plasma iron
<b>LV</b>	Left ventricular
<b>LVDC</b>	L-type voltage dependent channels
<b>LVEF</b>	Left ventricular ejection fraction
<b>MI(C)</b>	Myocardial iron (content)
<b>MR (MRI)</b>	Magnetic resonance (imaging)
<b>MUGA</b>	Multiple-gated acquisition
<b>NTBI</b>	Non-transferrin bound iron
<b>NTDT</b>	Non-transfusion-dependent thalassaemia
<b>RF</b>	Radio frequency
<b>SF</b>	Serum ferritin
<b>TDT</b>	Transfusion-dependent thalassaemia
<b>TM</b>	Thalassaemia major

## References

1. J. B. Porter and M. Garbowski, *Hematol. Oncol. Clin. North Am.*, 2014, **28**, 683.
2. E. Angelucci, G. M. Brittenham, C. E. McLaren, M. Ripalti, D. Baronciani, C. Gardini, M. Galimberti, P. Polchi and G. Lucarelli, *N. Engl. J. Med.*, 2000, **343**, 327.

3. P. Brissot, *Expert Rev. Gastroenterol.Hepatol.*, 2016, **10**, 359.
4. L. Kautz, G. Jung, E. V. Valore, S. Rivella, E. Nemeth and T. Ganz, *Nat. Genet.*, 2014, **46**, 678.
5. V. R. Gordeuk, B. R. Bacon and G. M. Brittenham, *Annu. Rev. Nutr.*, 1987, **7**, 485.
6. A. T. Taher, J. Porter, V. Viprakasit, A. Kattamis, S. Chuncharunee, P. Sutcharithchan, N. Siritanaratkul, R. Galanello, Z. Karakas, T. Lawniczek, J. Ros, Y. Zhang, D. Habr and M. D. Cappellini, *Blood*, 2012, **120**, 970.
7. N. F. Olivieri and G. M. Brittenham, *Blood*, 1997, **89**, 739.
8. M. J. Pippard, S. T. Callender, G. T. Warner and D. J. Weatherall, *Lancet*, 1979, **2**, 819.
9. P. Pootrakul, K. Kitcharoen, P. Yansukon, P. Wasi, S. Fucharoen, P. Charoenlarp, G. Brittenham, M. J. Pippard and C. A. Finch, *Blood*, 1988, **71**, 1124.
10. J. B. Porter, P. B. Walter, L. D. Neumayr, P. Evans, S. Bansal, M. Garbowski, M. G. Weyhmler, P. R. Harmatz, J. C. Wood, J. L. Miller, C. Byrnes, G. Weiss, M. Seifert, R. Grosse, D. Grabowski, A. Schmidt, R. Fischer, P. Nielsen, C. Niemeyer and E. Vichinsky, *Br. J. Haematol.*, 2014, **167**, 692.
11. J. Porter and M. Garbowski, *Hematology Am. Soc. Hematol. Educ. Program*, 2013, 447.
12. A. R. Cohen, E. Glimm and J. B. Porter, *Blood*, 2008, **111**, 583.
13. N. F. Olivieri, Erratum, *N. Engl. J. Med.*, 1999, **341**, 99.
14. M. Cazzola, P. De Stefano, L. Ponchio, F. Locatelli, Y. Beguin, C. Dessi, S. Barella, A. Cao and R. Galanello, *Br. J. Haematol.*, 1995, **89**, 473.
15. M. Cazzola, C. Borgna-Pignatti, F. Locatelli, L. Ponchio, Y. Beguin and P. De Stefano, *Transfusion*, 1997, **37**, 135.
16. A. Taher, H. Isma'eel, G. Mehio, D. Bignamini, A. Kattamis, E. A. Rachmilewitz and M. D. Cappellini, *Thromb. Haemostasis*, 2006, **96**, 488.
17. P. D. Jensen, F. T. Jensen, T. Christensen, J. L. Nielsen and J. Ellegaard, *Blood*, 2003, **101**, 91.
18. E. Angelucci, P. Muretto, A. Nicolucci, D. Baronciani, B. Erer, J. Gaziev, M. Ripalti, P. Sodani, S. Tomassoni, G. Visani and G. Lucarelli, *Blood*, 2002, **100**, 17.
19. G. M. Brittenham, P. M. Griffith, A. W. Nienhuis, C. E. McLaren, N. S. Young, E. E. Tucker, C. J. Allen, D. E. Farrell and J. W. Harris, *N. Engl. J. Med.*, 1994, **331**, 567.
20. L. J. Noetzli, S. M. Carson, A. S. Nord, T. D. Coates and J. C. Wood, *Blood*, 2008, **112**, 2973–2978.
21. G. Y. Oudit, H. Sun, M. G. Trivieri, S. E. Koch, F. Dawood, C. Ackerley, M. Yazdanpanah, G. J. Wilson, A. Schwartz, P. P. Liu and P. H. Backx, *Nat. Med.*, 2003, **9**, 1187.
22. J. P. Liuzzi, F. Aydemir, H. Nam, M. D. Knutson and R. J. Cousins, *Proc. Natl. Acad. Sci. U. S. A.*, 2006, **103**, 13612.

23. J. L. Pinilla-Tenas, B. K. Sparkman, A. Shawki, A. C. Illing, C. J. Mitchell, N. Zhao, J. P. Liuzzi, R. J. Cousins, M. D. Knutson and B. Mackenzie, *Am. J. Physiol.: Cell Physiol.*, 2011, **301**, C862.
24. J. B. Porter, R. D. Abeysinghe, L. Marshall, R. C. Hider and S. Singh, *Blood*, 1996, **88**, 705.
25. G. Zanninelli, W. Breuer and Z. I. Cabantchik, *Br. J. Haematol.*, 2009, **147**, 744.
26. R. W. Evans, R. Rafique, A. Zarea, C. Rapisarda, R. Cammack, P. J. Evans, J. B. Porter and R. C. Hider, *J. Biol. Inorg. Chem.*, 2008, **13**, 57.
27. A. M. Silva and R. C. Hider, *Biochim. Biophys. Acta*, 2009, **1794**, 1449.
28. B. P. Esposito, W. Breuer, P. Sirankapracha, P. Pootrakul, C. Hershko and Z. I. Cabantchik, *Blood*, 2003, **102**, 2670.
29. W. Breuer, H. Ghoti, A. Shattat, A. Goldfarb, A. Koren, C. Levin, E. Rachmilewitz and Z. I. Cabantchik, *Am. J. Hematol.*, 2012, **87**, 55.
30. L. M. Buja and W. C. Roberts, *Am. J. Med.*, 1971, **51**, 209.
31. P. D. Jensen, F. T. Jensen, T. Christensen, H. Eiskjaer, U. Baandrup and J. L. Nielsen, *Blood*, 2003, **101**, 4632.
32. L. J. Anderson, S. Holden, B. Davis, E. Prescott, C. C. Charrier, N. H. Bunce, D. N. Firmin, B. Wonke, B. J. Porter, J. M. Walker and D. J. Pennell, *Eur. Heart J.*, 2001, **22**, 2171.
33. A. T. Taher, K. M. Musallam, J. C. Wood and M. D. Cappellini, *Am. J. Hematol.*, 2010, **85**, 288.
34. B. Modell, *Br. Med. Bull.*, 1976, **32**, 270.
35. B. Modell and R. Matthews, *Birth Defects, Orig. Artic. Ser.*, 1976, **12**, 13.
36. D. M. Sado, V. Maestrini, S. K. Piechnik, S. M. Banypersad, S. K. White, A. S. Flett, M. D. Robson, S. Neubauer, C. Ariti, A. Arai, P. Kellman, J. Yamamura, B. P. Schoennagel, F. Shah, B. Davis, S. Trompeter, M. Walker, J. Porter and J. C. Moon, *J. Magn. Reson. Imaging.*, 2015, **41**, 1505.
37. J. P. Carpenter, T. He, P. Kirk, M. Roughton, L. J. Anderson, S. V. de Noronha, A. J. Baksi, M. N. Sheppard, J. B. Porter, J. M. Walker, J. C. Wood, G. Forni, G. Catani, G. Matta, S. Fucharoen, A. Fleming, M. House, G. Black, D. N. Firmin, T. G. St Pierre and D. J. Pennell, *Circulation*, 2011, **123**, 1519.
38. C. Borgna-Pignatti, S. Rugolotto, P. De Stefano, H. Zhao, M. D. Cappellini, G. C. Del Vecchio, M. A. Romeo, G. L. Forni, M. R. Gamberini, R. Ghilardi, A. Piga and A. Cnaan, *Haematologica*, 2004, **89**, 1187.
39. C. Borgna-Pignatti, M. D. Cappellini, P. De Stefano, G. C. Del Vecchio, G. L. Forni, M. R. Gamberini, R. Ghilardi, R. Origa, A. Piga, M. A. Romeo, H. Zhao and A. Cnaan, *Ann. N. Y. Acad. Sci.*, 2005, **1054**, 40.
40. M. D. Cappellini, A. Cohen, A. Eleftheriou, A. Piga, J. Porter and A. Taher, *Guidelines for the Clinical Management of Thalassaemia*, Nicosia, CY, 2nd edn, 2008.
41. M. D. Cappellini, A. Cohen, J. Porter, A. Taher and V. Viprakasit, *Guidelines for the Management of Transfusion Dependent Thalassaemia (TDT)*, Thalassaemia International Federation, Nicosia, CY, 3rd edn, 2014.

42. S. De Virgillis, M. Congia, F. Frau, F. Argioli, G. Diana, F. Cucca, A. Varsi, G. Sanna, G. Podda and M. Fodde, *et al.*, *J. Pediatr.*, 1988, **113**, 661.
43. N. F. Olivieri, G. Koren, J. Harris, S. Khattak, M. H. Freedman and D. M. Templeton, *Am. J. Pediatr. Hematol./Oncol.*, 1992, **14**, 48.
44. V. Gabutti and A. Piga, *Acta Haematol.*, 1996, **95**, 26.
45. A. Piga, L. Luzzatto, P. Capalbo, S. Gambotto, F. Tricta and V. Gabutti, *Eur. J. Haematol.*, 1988, **40**, 380.
46. N. F. Olivieri, D. G. Nathan, J. H. MacMillan, A. S. Wayne, P. P. Liu, A. McGee, M. Martin, G. Koren and A. R. Cohen, *N. Engl. J. Med.*, 1994, **331**, 574.
47. C. Borgna-Pignatti, S. Rugolotto, P. De Stefano, A. Piga, F. Di Gregorio, M. R. Gamberini, R. Ghilardi, R. Origa, A. Piga, M. A. Romeo, H. Zhao and A. Cnaan, *Ann. N. Y. Acad. Sci.*, 2005, **1054**, 40.
48. B. A. Davis, C. O'Sullivan, P. H. Jarritt and J. B. Porter, *Blood*, 2004, **104**, 263.
49. B. A. Davis and J. B. Porter, *Adv. Exp. Med. Biol.*, 2002, **509**, 91.
50. L. J. Anderson, M. A. Westwood, S. Holden, B. Davis, E. Prescott, B. Wonke, J. B. Porter, J. M. Walker and D. J. Pennell, *Br. J. Haematol.*, 2004, **127**, 348.
51. B. Modell, M. Khan, M. Darlison, M. A. Westwood, D. Ingram and D. J. Pennell, *J. Cardiovasc. Magn. Reson.*, 2008, **10**, 42.
52. A. Thomas, M. Garbowski, A. L. Ang, F. Shah, M. Walker and J. Moon, *et al.*, A Decade Follow-up of a Thalassemia Major (TM) Cohort Monitored by Cardiac Magnetic Resonance Imaging (CMR): Significant Reduction In Patients with Cardiac Iron and In Total Mortality, *ASH*, 2011, **116**(21), Abstract 1011.
53. M. G. Zurlo, P. De Stefano, C. Borgna-Pignatti, A. Di Palma, A. Piga, C. Melevendi, F. Di Gregorio, M. G. Burattini and S. Terzoli, *Lancet*, 1989, **2**, 27.
54. T. G. St Pierre, K. C. Tran, J. Webb, D. J. Macey, B. R. Heywood, N. H. Sparks, V. J. Wade, S. Mann and P. Pootrakul, *Biol. Met.*, 1991, **4**, 162.
55. J. Arpa, I. Sanz-Gallego, F. J. Rodriguez-de-Rivera, F. J. Dominguez-Melcon, D. Prefasi, J. Oliva-Navarro and M. Moreno-Yangüela, *Acta Neurol. Scand.*, 2014, **129**, 32.
56. C. Borgna-Pignatti, G. Vergine, T. Lombardo, M. D. Cappellini, P. Cianciulli, A. Maggio, D. Renda, M. E. Lai, A. Mandas, G. Forni, A. Piga and M. G. Bisconte, *Haematol.*, 2004, **124**, 114.
57. C. Borgna-Pignatti, M. C. Garani, G. L. Forni, M. D. Cappellini, E. Cassinerio, C. Fidone, V. Spadola, A. Maggio, G. Restivo Pantalone, A. Piga, F. Longo, M. R. Gamberini, P. Ricchi, S. Costantini, D. D'Ascola, P. Cianciulli, M. E. Lai, M. P. Carta, A. Ciancio, P. Cavalli, M. C. Putti, S. Barella, G. Amendola, S. Campisi, M. Capra, V. Caruso, G. Colletta and S. Volpato, *Br. J. Haematol.*, 2014, **167**, 121.
58. C. F. Hwang, C. Y. Lee, P. I. Lee, J. M. Chen, K. H. Lli, D. T. Lin and M. H. Chang, *Zhonghua Minguo Xiaoeke Yixuehui Zazhi*, 1994, **35**, 466.

59. C. K. Li, M. M. Shing, K. W. Chik, V. Lee and P. M. Yuen, *Pediatr. Hematol. Oncol.*, 2001, **18**, 229.
60. K. Ghosh, S. Daar, D. Hiwase and N. Nursat, *Haematologia*, 2000, **30**, 69.
61. R. Robins-Browne and J. Prpic, *Infect. Immun.*, 1985, **47**, 774.
62. J. Gutteridge and B. Halliwell, *Bailliere's Clin. Haematol.*, 1989, **2**, 195.
63. P. S. Dobbin, R. C. Hider, A. D. Hall, P. D. Taylor, P. Sarpong, J. B. Porter, G. Xiao and D. van der Helm, *J. Med. Chem.*, 1993, **36**, 2448.
64. J. Porter, M. Gyparaki, L. Burke, E. Huehns, P. Sarpong, V. Saez and R. C. Hider, *Blood*, 1988, **72**, 1497.
65. R. C. Hider, O. Epemolu, S. Singh and J. P. Porter, *Adv. Exp. Med. Biol.*, 1994, **356**, 343.
66. K. P. Hoyes and J. B. Porter, *Br. J. Haematol.*, 1993, **85**, 393.
67. H. Glickstein, R. B. El, M. Shvartsman and Z. I. Cabantchik, *Blood*, 2005, **106**, 3242.
68. C. Hershko, R. Grady and A. Cerami, *J. Lab. Clin. Med.*, 1978, **92**, 144.
69. C. Hershko and E. Rachmilewitz, *Br. J. Haematol.*, 1979, **42**, 125.
70. G. Link, A. M. Konijn, W. Breuer, Z. I. Cabantchik and C. Hershko, *J. Lab. Clin. Med.*, 2001, **138**, 130.
71. C. Hershko, A. M. Konijn, H. P. Nick, W. Breuer, Z. I. Cabantchik and G. Link, *Blood*, 2001, **97**, 1115.
72. J. B. Porter, E. R. Huehns and R. C. Hider, *Bailliere's Clin. Haematol.*, 1989, **2**, 257.
73. G. Zanninelli, H. Glickstein, W. Breuer, P. Milgram, P. Brissot, R. C. Hider, A. M. Konijn, J. Libman, A. Shanzer and Z. I. Cabantchik, *Mol. Pharmacol.*, 1997, **51**, 842.
74. H. Glickstein, R. B. El, G. Link, W. Breuer, A. M. Konijn, C. Hershko, H. Nick and Z. I. Cabantchik, *Blood*, 2006, **108**, 3195.
75. C. E. Cooper and J. B. Porter, *Biochem. Soc. Trans.*, 1997, **25**, 75.
76. R. Kayyali, J. B. Porter, Z. D. Liu, N. A. Davies, J. Nugent, C. E. Cooper and R. C. Hider, *J. Biol. Chem.*, 2001, **276**, 48814.
77. C. Hershko, *Blood*, 1978, **51**, 415.
78. R. Bailey-Wood, G. White and A. Jacobs, *Br. J. Exp. Pathol.*, 1975, **56**, 358.
79. C. E. Cooper, G. R. Lynagh, K. P. Hoyes, R. C. Hider, R. Cammack and J. B. Porter, *J. Biol. Chem.*, 1996, **271**, 20291.
80. Z. D. Liu, R. Kayyali, R. C. Hider, J. B. Porter and A. E. Theobald, *J. Med. Chem.*, 2002, **45**, 631.
81. J. Porter, A. Cohen and J. Kwiatkowski, in *Disorders of Hemoglobin Genetics, Pathophysiology, and Clinical Management*. M.H. Steinberg, B.G. Forget, D.R. Higgs and D.J. Weatherall, Cambridge University Press, 2nd edn, 2009, ch 29.
82. J. B. Porter, R. D. Abeyasinghe, K. P. Hoyes, C. Barra, E. R. Huehns, P. N. Brooks, M. P. Blackwell, M. Araneta, G. Brittenham, S. Singh, P. Dobbin and R. C. Hider, *Br. J. Haematol.*, 1993, **85**, 159.

83. S. L. Lu, I. Gosriwatana, D. Y. Liu, Z. D. Liu, A. I. Mallet and R. C. Hider, *Drug Metab. Dispos.*, 2000, **28**, 873.
84. D. Y. Liu, Z. D. Liu, S. L. Lu and R. C. Hider, *Pharmacol. Toxicol.*, 2000, **86**, 228.
85. J. B. Porter, S. Singh, K. P. Hoyes, O. Epemolu, R. D. Abeysinghe and R. C. Hider, *Adv. Exp. Med. Biol.*, 1994, **356**, 361.
86. Y. Aydinok, P. Evans, C. Y. Manz and J. B. Porter, *Haematologica*, 2012, **97**, 835.
87. J. Porter, C. Borgna-Pignatti, M. Baccarani, A. Saviano, S. Abish and R. Malizia, *et al.*, *Blood*, 2005, **106**, Abstract 2690.
88. A. V. Hoffbrand, A. Cohen and C. Hershko, *Blood*, 2003, 10217.
89. F. N. al-Refaie, L. N. Sheppard, P. Nortey, B. Wonke and A. V. Hoffbrand, *Br. J. Haematol.*, 1995, **89**, 403.
90. J. Porter, F. Waldmeier, G. Bruin, K. Hazell, S. Warrington and K. Delage, *et al.*, *Blood*, 2003, 1025bAbstract 3720.
91. R. Galanello, A. Piga, D. Alberti, M. C. Rouan, H. Bigler and R. Sechaud, *J. Clin. Pharmacol.*, 2003, **43**, 565.
92. E. Nisbet-Brown, N. F. Olivieri, P. J. Giardina, R. W. Grady, E. J. Neufeld, R. Sechaud, A. J. Krebs-Brown, J. R. Anderson, D. Alberti, K. C. Sizer and D. G. Nathan, *Lancet*, 2003, **361**, 1597.
93. J. Porter, B. Davis, T. Weir, D. Alberti, V. Voi and A. Piga, *et al.*, in *Iron Chelators, New Development Strategies*, ed. D. G. Badman, R. J. Bergeron and G. M. Brittenham, The Saratoga Group, Florida, USA, 2000, pp. 343–352.
94. J. B. Porter, R. Rafique, S. Srichairatanakool, B. A. Davis, F. T. Shah, T. Hair and P. Evans, *Ann. N. Y. Acad. Sci.*, 2005, **1054**, 155–168.
95. Z. I. Cabantchik, W. Breuer, G. Zanninelli and P. Cianciulli, *Best Pract. Res., Clin. Haematol.*, 2005, **18**, 277.
96. M. Worwood, S. J. Cragg, M. Wagstaff and A. Jacobs, *Clin. Sci.*, 1979, **56**, 83.
97. M. Worwood, *Crit. Rev. Clin. Lab. Sci.*, 1979, **10**, 171.
98. M. Worwood, S. J. Cragg, A. Jacobs, C. McLaren, C. Ricketts and J. Economidou, *Br. J. Haematol.*, 1980, **46**, 409.
99. A. L. Ang, F. Shah, B. Davis, A. Thomas, G. Murugachandran and J. Kumuradevan, *et al.*, *ASH*, 2010, **116**, Abstract 4246.
100. R. Fischer, F. Longo, P. Nielsen, R. Engelhardt, R. C. Hider and A. Piga, *Br. J. Haematol.*, 2003, **121**, 938.
101. J. B. Porter, M. Elalfy, A. T. Taher, L. L. Chan, S.-H. Lee, P. Sutcharitchan, D. Habr, N. Martin and A. El-Beshlawy, *Blood*, 2014, **124**, 52.
102. P. T. Telfer, E. Prestcott, S. Holden, M. Walker, A. V. Hoffbrand and B. Wonke, *Br. J. Haematol.*, 2000, **110**, 971.
103. E. Angelucci, A. Giovagnoni, G. Valeri, E. Paci, M. Ripalti, P. Muretto, C. McLaren, G. M. Brittenham and G. Lucarelli, *Blood*, 1997, **90**, 4736.
104. J. P. Villeneuve, M. Bilodeau, R. Lepage, J. Cote and M. Lefebvre, *J. Hepatol.*, 1996, **25**, 172.
105. M. S. Elalfy, G. Esmat, R. M. Matter, E. Abdel Aziz and W. A. Massoud, *Ann. Hepatol.*, 2013, **12**, 54.
106. J. C. Wood and N. Ghugre, *Hemoglobin*, 2008, **32**, 85.

107. P. Storey, A. A. Thompson, C. L. Carqueville, J. C. Wood, R. A. de Freitas and C. K. Rigsby, *J. Magn. Reson. Imaging*, 2007, **25**, 540.
108. M. Garbowski, J. P. Carpenter, G. Smith, D. Pennell and J. Porter, *J. ASH*, 2009, **114**, Abstract 2004..
109. T. G. St Pierre, P. R. Clark, W. Chua-anusorn, A. J. Fleming, G. P. Jeffrey, J. K. Olynyk, P. Pootrakul, E. Robins and R. Lindeman, *Blood*, 2005, **105**, 855.
110. P. Kirk, T. He, L. J. Anderson, M. Roughton, M. A. Tanner, W. W. Lam, W. Y. Au, W. C. Chu, G. Chan, R. Galanello, G. Matta, M. Fogel, A. R. Cohen, R. S. Tan, K. Chen, I. Ng, A. Lai, S. Fucharoen, J. Laothamata, S. Chuncharunee, S. Jongjirasiri, D. N. Firmin, G. C. Smith and D. J. Pennell, *J. Magn. Reson. Imaging*, 2010, **32**, 315.
111. J. P. Carpenter, T. He, P. Kirk, M. Roughton, L. J. Anderson, S. V. de Noronha, A. J. Bakshi, M. N. Sheppard, J. B. Porter, J. M. Walker, J. C. Wood, G. Forni, G. Catani, G. Matta, S. Fucharoen, A. Fleming, M. House, G. Black, D. N. Firmin, T. G. St Pierre and D. J. Pennell, *J. Cardiovasc. Magn. Reson*, 2014, **16**, 62.
112. P. Kirk, M. Roughton, J. B. Porter, J. M. Walker, M. A. Tanner, J. Patel, D. Wu, J. Taylor, M. A. Westwood, L. J. Anderson and D. J. Pennell, *Circulation*, 2009, **120**, 1961.
113. D. J. Pennell, J. B. Porter, M. D. Cappellini, L. L. Chan, A. El-Beshlawy, Y. Aydinok, H. Ibrahim, C. K. Li, V. Viprakasit, M. S. Elalfy, A. Kattamis, G. Smith, D. Habr, G. Domokos, B. Roubert and A. Taher, *Haematologica*, 2012, **97**, 842.
114. P. Kirk, T. He, L. J. Anderson, M. Roughton, M. A. Tanner, W. W. Lam, W. Y. Au, W. C. Chu, G. Chan, R. Galanello, G. Matta, M. Fogel, A. R. Cohen, R. S. Tan, K. Chen, I. Ng, A. Lai, S. Fucharoen, J. Laothamata, S. Chuncharunee, S. Jongjirasiri, D. N. Firmin, G. C. Smith and D. J. Pennell, *J. Magn. Reson. Imaging*, 2010, **32**, 315.
115. B. Davis, C. O'Sullivan and J. Porter, *8th International Conference on Thalassemia and the hemoglobinopathies*, Athens, 2001, p. 147, Abstract 056.
116. B. A. Davis and J. B. Porter, *Blood*, 2000, **95**, 1229.
117. J. B. Porter, J. Wood, N. Olivieri, E. P. Vichinsky, A. Taher, E. Neufeld, P. Giardina, A. Thompson, B. Moore, P. Evans, H. Y. Kim, E. A. Macklin and F. Trachtenberg, *J. Cardiovasc. Magn. Reson.*, 2013, **15**, 38.
118. V. Berdoukas, K. Farmaki, S. Carson, J. Wood and T. Coates, *J. Blood Med.*, 2012, **3**, 119.
119. R. Chatterjee, M. Katz, A. Oatridge, G. M. Bydder and J. B. Porter, *Ann. N. Y. Acad. Sci.*, 1998, **850**, 479.
120. J. C. Wood, *Am. J. Hematol.*, 2007, **82**, 1132.
121. W. Y. Au, W. W. Lam, W. W. Chu, H. L. Yuen, A. S. Ling, R. C. Li, H. M. Chan, H. K. Lee, M. F. Law, H. S. Liu, R. Liang and S. Y. Ha, *Haematologica*, 2008, **93**, 784.
122. L. J. Noetzli, J. Papudesi, T. D. Coates and J. C. Wood, *Blood*, 2009, **114**, 4021.
123. M. J. Pippard, S. T. Callender and C. A. Finch, *Blood*, 1982, **60**, 288.

124. F. H. Mourad, A. V. Hoffbrand, M. Sheikh-Taha, S. Koussa, A. I. Khoriaty and A. Taher, *Br. J. Haematol.*, 2003, **121**, 187.
125. L. de Swart, J. C. Hendriks, L. N. van der Vorm, Z. I. Cabantchik, P. J. Evans, E. A. Hod, G. M. Brittenham, Y. Furman, B. Wojczyk, M. C. Janssen, J. B. Porter, V. E. Mattijssen, B. J. Biemond, M. A. MacKenzie, R. Origa, R. Galanello, R. C. Hider and D. W. Swinkels, *Haematologica*, 2015, **101**, 38.
126. S. Singh, R. C. Hider and J. B. Porter, *Anal. Biochem.*, 1990, **186**, 320.
127. I. Gosriwatana, O. Loreal, S. Lu, P. Brissot, J. Porter and R. C. Hider, *Anal. Biochem.*, 1999, **273**, 212.
128. Y. Ma, M. Podinovskaia, P. J. Evans, G. Emma, U. E. Schaible, J. Porter and R. C. Hider, *Biochem. J.*, 2014, **463**, 351.
129. E. M. Jacobs, J. C. Hendriks, B. L. van Tits, P. J. Evans, W. Breuer, D. Y. Liu, E. H. Jansen, K. Jauhainen, B. Sturm, J. B. Porter, B. Scheiber-Mojdehkar, L. von Bonsdorff, Z. I. Cabantchik, R. C. Hider and D. W. Swinkels, *Anal. Biochem.*, 2005, **341**, 241.
130. S. Daar, A. Pathare, H. Nick, U. Kriemler-Krahn, A. Hmissi, D. Habr and A. Taher, *Eur. J. Haematol.*, 2009, **82**, 454.
131. M. W. Garbowski, P. Evans and J. B. Porter, *Blood*, 2015, **126**, 539.
132. P. Pootrakul, W. Breuer, M. Sametband, P. Sirankapracha, C. Hershko and Z. I. Cabantchik, *Blood*, 2004, **104**, 1504.
133. A. Piga, F. Longo, L. Duca, S. Roggero, T. Vinciguerra, R. Calabrese, C. Hershko and M. D. Cappellini, *Am. J. Hematol.*, 2009, **84**, 29.
134. J. C. Wood, T. Glynos, A. Thompson, P. Giardina, P. Harmatz, B. P. Kang, C. Paley and T. D. Coates, *Haematologica*, 2011, **96**, 1055.
135. J. B. Porter, K. H. Lin, P. Beris, G. L. Forni, A. Taher, D. Habr, G. Domokos, B. Roubert and S. L. Thein, *Eur. J. Haematol.*, 2011, **87**, 338.
136. E. A. Hod, N. Zhang, S. A. Sokol, B. S. Wojczyk, R. O. Francis, D. Ansaldi, K. P. Francis, P. Della-Latta, S. Whittier, S. Sheth, J. E. Hendrickson, J. C. Zimring, G. M. Brittenham and S. L. Spitalnik, *Blood*, 2010, **115**, 4284.
137. M. Andriani, N. Nordio and E. Saporiti, *Nephron*, 1996, **72**, 218.
138. P. Lee, N. Mohammed, R. D. Abeysinghe, R. C. Hider, J. B. Porter and S. Singh, *Drug Metab. Dispos.*, 1993, **21**(4), 640–644.
139. J. B. Porter, A. Faherty, L. Stallibrass, L. Brookman, I. Hassan and C. Howes, *Ann. N. Y. Acad. Sci.*, 1998, **850**, 483–487.
140. M. J. Pippard, *Bailliere's Clin. Haematol.*, 1989, **2**, 323.
141. C. Hershko, J. Cook and C. Finch, *J. Lab. Clin. Med.*, 1973, **81**, 876.
142. M. D. Cappellini, A. Cohen, A. Piga, M. Bejaoui, S. Perrotta, L. Agaoglu, L. Y. Aydinok, A. Kattamis, Y. Kilinc, J. Porter, M. Capra, R. Galanello, S. Fattoum, G. Drelichman, C. Magnano, M. Verissimo, M. Athanassiou-Metaxa, P. Giardina, A. Kourakli-Symeonidis, G. Janka-Schaub, T. Coates, C. Vermynen, N. Olivieri, I. Thuret, H. Opitz, C. Ressayre-Djaffer, P. Marks and D. Alberti, *Blood*, 2006, **107**, 3455.
143. B. Modell, E. Letsky, D. Flynn, R. Peto and D. Weatherall, *Br. Med. J.*, 1982, **284**, 1081.
144. J. B. Porter and B. A. Davis, *Best Pract. Res., Clin. Haematol.*, 2002, **15**, 329.

145. B. Modell, M. Khan and M. Darlison, *Lancet*, 2000, **355**, 2051.
146. R. E. Marcus, S. C. Davies, H. M. Bantock, S. R. Underwood, S. Walton and E. R. Huehns, *Lancet*, 1984, **1**, 392.
147. P. S. Rahko, R. Salerni and B. F. Uretsky, *J. Am. Coll. Cardiol.*, 1986, **8**, 436.
148. A. P. Freeman, R. W. Giles, V. A. Berdoukas, P. A. Talley and I. P. Murray, *Clin. Lab. Haematol.*, 1989, **11**, 299.
149. M. A. Aldouri, A. V. Hoffbrand, D. M. Flynn, S. E. Ward, J. E. Agnew and A. J. W. Hilson, *Acta Haematol.*, 1990, **84**, 113.
150. D. J. Pennell, V. Berdoukas, M. Karagiorga, V. Ladis, A. Piga, A. Aessopos, E. D. Gotsis, M. A. Tanner, G. C. Smith, M. A. Westwood, B. Wonke and R. Galanello, *Blood*, 2006, **107**, 3738.
151. M. A. Tanner, R. Galanello, C. Dessi, G. C. Smith, M. A. Westwood, A. Agus, R. Assomull, S. V. Nair, J. M. Walker and D. J. Pennell, *Circulation*, 2007, **115**, 1876.
152. M. Barry, D. Flynn, E. Letsky and R. Risdon, *Br. Med. J.*, 1974, **2**, 16.
153. N. Bronsiegel-Weintrob, N. F. Olivieri, B. Tyler, D. F. Andrews, M. H. Freedman and F. J. Holland, *N. Eng. J. Med.*, 1990, **323**, 713.
154. M. Fosburg and D. G. Nathan, *Blood*, 1990, **76**, 435.
155. M. A. Aldouri, B. Wonke, A. V. Hoffbrand, D. M. Flynn, M. Laulicht, L. A. Fenton, P. J. Scheuer, C. C. Kibbler, C. A. Allwood, D. Brown and H. C. Thomas, *J. Clin. Pathol.*, 1987, **40**, 1353.
156. R. Chatterjee, M. Katz, T. F. Cox and J. B. Porter, *Clin. Endocrinol.*, 1993, **39**, 287.
157. D. M. Flynn, A. V. Hoffbrand and D. Politis, *Birth Defects, Orig. Artic. Ser.*, 1982, **18**, 347.
158. R. Hider, G. Kontoghiorghes and J. Silver, UK Patent Gb2118176A, 1982.
159. J. B. Porter, J. Morgan, K. P. Hoyes, L. C. Burke, E. R. Huehns and R. C. Hider, *Blood*, 1990, **76**, 2389.
160. R. C. Hider, R. Choudhury, B. L. Rai, L. S. Dehkordi and S. Singh, *Acta Haematol.*, 1996, **95**, 6.
161. M. J. Pippard, K. Pattanapanyssat, J. Tiperkae and R. C. Hider, *Proceedings of the European Iron Club, 1989*, Budapest, Hungary, 1989. p. 55.
162. C. J. Kellenberger, M. Schmutge, T. Saurenmann, L. Di Gennaro, S. W. Eber, U. V. Willi and P. S. Babyn, *Am. J. Roentgenol.*, 2004, **183**, 989.
163. G. Kontoghiorghes, L. Sheppard and J. Barr, *et al*, *Br. J. Haematol.*, 1988, **69**, 129.
164. N. F. Olivieri, G. Koren, C. Hermann, Y. Bentur, D. Chung, J. Klein, P. St Louis, M. H. Freedman, R. A. McClelland and D. M. Templeton, *Lancet*, 1990, 3361275.
165. A. F. Collins, F. F. Fassos, S. Stobie, N. Lewis, D. Shaw, M. Fry, D. M. Templeton, R. A. McClelland, G. Koren and N. F. Olivieri, *Blood*, 1994, **83**, 2329.
166. G. J. Kontoghiorghes, J. G. Goddard, A. N. Bartlett and L. Sheppard, *Clin. Pharmacol.*, 1990, **48**, 255.

167. R. Lange, W. Lameijer, K. L. Roozendaal and M. Kersten, *Proceedings of 4th International Conference on Oral Chelation*, Limasol, Cyprus, 1993.
168. S. Rodrat, P. Yamanont, P. J. Tankanitlert, U. Chantrarakasri, S. Fucharoen and N. P. Morales, *Pharmacology*, 2012, **90**, 88.
169. L. M. Limenta, T. Jirasomprasert, P. Jittangprasert, P. Wilairat, P. Yamanont, U. Chantharakasri, S. Fucharoen and N. P. Morales, *Clin. Pharmacokinet.*, 2011, **50**, 41.
170. D. Roberts, S. Brunskill, C. Doree, S. Williams, J. Howard and C. Hyde, *Cochrane Database Syst. Rev.*, 2007, CD004839.
171. N. F. Olivieri, G. M. Brittenham, D. Matsui, M. Berkovitch, L. M. Blendis, R. G. Cameron, R. A. McClelland, P. P. Liu, D. M. Templeton and G. Koren, *N. Engl. J. Med.*, 1995, **332**, 918.
172. N. F. Olivieri, G. M. Brittenham, C. E. McLaren, D. M. Templeton, R. G. Cameron, R. A. McClelland, A. D. Burt and K. A. Fleming, *N. Engl. J. Med.*, 1998, **339**, 417.
173. A. Maggio, G. D'Amico, A. Morabito, M. Capra, C. Ciaccio, P. Cianciulli, F. Di Gregorio, G. Garozzo, R. Malizia, C. Magnano, A. Mangiagli, G. Quarta, M. Rizzo, D. G. D'Ascola, A. Rizzo and M. Midiri, *Blood Cells, Mol., Dis.*, 2002, **28**(2), 196–208.
174. S. Gomber, R. Saxena and N. Madan, *Indian Pediatr.*, 2004, **41**, 21.
175. S. K. Ha, K. W. Chik, S. C. Ling, A. C. Lee, C. W. Luk, C. W. Lam, I. O. Ng and G. C. Chan, *Hemoglobin*, 2006, **30**, 263.
176. V. A. Hoffbrand and B. Wonke, *Adv. Exp. Med. Biol.*, 2002, **509**, 127.
177. A. Ceci, P. Baiardi, M. Felisi, M. D. Cappellini, V. Carnelli, V. De Sanctis, R. Galanello, A. Maggio, G. Masera, A. Piga, F. Schettini, I. Stefàno and F. Trieta, *Br. J. Haematol.*, 2002, **118**, 330.
178. C. Borgna-Pignatti, M. D. Cappellini, P. De Stefano, G. C. Del Vecchio, G. L. Forni, M. R. Gamberini, R. Ghilardi, A. Piga, M. A. Romeo, H. Zhao and A. Cnaan, *Blood*, 2006, **107**, 3733.
179. P. Telfer, P. G. Coen, S. Christou, M. Hadjigavriel, A. Kolnakou, E. Pangalou, N. Pavlides, M. Psiloinis, K. Simamonian, G. Skordos, M. Sitarou and M. Angastiniotis, *Haematologica*, 2006, **91**, 1187.
180. H. Nick, P. Acklin, R. Lattmann, P. Buehlmayer, S. Hauffe, J. Schupp and D. Alberti, *Curr. Med. Chem.*, 2003, **10**, 1065.
181. E. Vlachodimitropoulou Koumoutsea, M. Garbowski and J. Porter, *Br. J. Haematol.*, 2015, **170**, 874.
182. J. C. Wood, M. Otto-Duessel, M. Aguilar, H. Nick, M. D. Nelson, T. D. Coates, H. Pollack and R. Moats, *Circulation*, 2005, **112**, 535.
183. A. Piga, R. Galanello, G. L. Forni, M. D. Cappellini, R. Origa, A. Zappu, G. Donato, E. Bordone, A. Lavagetto, L. Zanaboni, R. Sechaud, N. Hewson, J. M. Ford, H. Opitz and D. Alberti, *Haematologica*, 2006, **91**, 873.
184. C. Tanaka, *Clin. Pharmacokinet.*, 2014, **53**, 679.
185. A. Skerjanec, J. Wang, K. Maren and L. Rojkjaer, *J. Clin. Pharmacol.*, 2010, **50**, 205.
186. Information, NPEDup, 2013, <http://www.pharma.us.novartis.com/product/pi/pdf/exjade.pdf>, accessed 6 Jun 2014.

187. J. Porter, R. Galanello, G. Saglio, E. J. Neufeld, E. Vichinsky, M. D. Cappellini, N. Olivieri, A. Piga, M. J. Cunningham, D. Soulières, N. Gattermann, G. Tchernia, J. Maertens, P. Giardina, J. Kwiatkowski, G. Quarta, M. Jeng, G. L. Forni, M. Stadler, H. Cario, L. Debusscher, M. Della Porta, M. Cazzola, P. Greenberg, G. Alimena, B. Rabault, I. Gathmann, J. M. Ford, D. Alberti and C. Rose, *Eur. J. Haematol.*, 2008, **80**, 168.
188. Y. Deugnier, B. Turlin, M. Ropert, M. Bejaoui, M. Athanassiou-Metaxa and H. Cario, *et al.*, *Blood*, 2005, **106**, Abstract 2708.
189. J. B. Porter, A. Piga, A. Cohen, J. M. Ford, J. Bodner and L. Rojksjaer, *et al.*, *ASH*, 2008, 112 Abstract 5423.
190. M. D. Cappellini, J. Porter, A. El-Beshlawy, C. K. Li, J. F. Seymour, M. Elalfy, N. Gattermann, S. Giraudier, J. W. Lee, L. L. Chan, L. H. Lin, C. Rose, A. Taher, S. L. Thein, V. Viprakasit, D. Habr, G. Domokos, B. Roubert and A. Kattamis, *Haematologica*, 2010, **95**, 557.
191. J. B. Porter, *Blood*, 2005, **106**, 11Abstract 3600.
192. D. J. Pennell, J. B. Porter, M. D. Cappellini, A. El-Beshlawy, L. L. Chan, Y. Aydinok, M. S. Elalfy, P. Sutcharitchan, C. K. Li, H. Ibrahim, V. Viprakasit, A. Kattamis, G. Smith, D. Habr, G. Domokos, B. Roubert and A. Taher, *Blood*, 2010, **25**, 2364.
193. D. J. Pennell, J. B. Porter, A. Piga, Y. Lai, A. El-Beshlawy and K. M. Belhoul, *et al.*, *Blood*, 2014, **123**, 1447.
194. D. J. Pennell, J. B. Porter, A. Piga, Y. R. Lai, A. El-Beshlawy, M. Elalfy, A. Yesilipek, Y. Kiliñç, D. Habr, K. M. Musallam, J. Shen and Y. Aydinok, *Am. J. Hematol.*, 2015, **90**, 91.
195. D. J. Pennell, J. B. Porter, M. D. Cappellini, L. L. Chan, A. El-Beshlawy, Y. Aydinok, H. Ibrahim, C. K. Li, V. Viprakasit, M. S. Elalfy, A. Kattamis, G. Smith, D. Habr, G. Domokos, B. Roubert and A. Taher, *Haematologica*, 2011, **96**, 48.
196. J. B. Porter, M. S. Jaswon, E. R. Huehns, C. A. East and J. W. Hazell, *Br. J. Haematol.*, 1989, **73**, 403.
197. G. Cossu, G. Abbruzzese, G. Matta, D. Murgia, M. Melis, V. Ricchi, R. Galanello, S. Barella, R. Origa, M. Balocco, E. Pelosin, R. Marchese, U. Ruffinengo and G. L. Forni, *Parkinsonism Relat. Disord.*, 2014, **20**, 651.
198. D. Devos, C. Moreau, J. C. Devedjian, J. Kluza, M. Petrault, C. Laloux, A. Jonneaux, G. Ryckewaert, G. Garçon, N. Rouaix, A. Duhamel, P. Jis-sendi, K. Dujardin, F. Auger, L. Ravasi, L. Hopes, G. Grolez, W. Firdaus, B. Sablonnière, I. Strubi-Vuillaume, N. Zahr, A. Destée, J. C. Corvol, D. Pörtl, M. Leist, C. Rose, L. Defebvre, P. Marchetti, Z. I. Cabantchik and R. Bordet, *Antioxid. Redox. Signal.*, 2014, **21**, 195.
199. K. P. Hoyes, H. M. Jones, R. D. Abeyasinghe, R. C. Hider and J. B. Porter, *Exp. Hematol.*, 1993, **21**, 86.
200. S. C. Davies, R. E. Marcus, J. L. Hungerford, H. M. Miller, G. B. Arden and E. R. Huehns, *Lancet*, 1983, **2**, 181.
201. N. L. Olivieri, J. R. Buncic, E. Chew, T. Gallant, R. V. Harrison and N. Keenan, *et al.*, *N. Eng. J. Med.*, 1986, **314**, 869.

202. F. N. al-Refaie, C. Hershko, A. V. Hoffbrand, M. Kosaryan, N. F. Olivieri, P. Tondury and B. Wonke, *Br. J. Haematol.*, 1995, **91**, 224.
203. A. R. Cohen, R. Galanello, A. Piga, A. Dipalma, C. Vullo and F. Tricta, *Br. J. Haematol.*, 2000, **108**, 305.
204. I. R. Wanless, G. Sweeney, A. P. Dhillon, M. Guido, A. Piga, R. Galanello, M. R. Gamberini, E. Schwartz and A. R. Cohen, *Blood*, 2002, **100**, 1566.
205. A. R. Cohen, R. Galanello, A. Piga, V. De Sanctis and F. Tricta, *Blood*, 2003, **102**, 1583.
206. S. Grange, D. M. Bertrand, D. Guerrot, F. Eas and M. Godin, *Nephrol., Dial., Transplant.*, 2010, **25**, 2376.
207. Y. Deugnier, B. Turlin, M. Ropert, M. D. Cappellini, J. B. Porter, V. Giannone, Y. Zhang, L. Griffel and P. Brissot, *Gastroenterology*, 2011, **141**, 1202.
208. Y. Aydinok, S. Unal, Y. Oymak, C. Vergin, Z. D. Turker, D. Yildiz and A. Yesilipek, *Eur. J. Haematol.*, 2012, **88**, 431.
209. M. D. Cappellini, M. Bejaoui, L. Agaoglu, D. Canatan, M. Capra, A. Cohen, G. Drelichman, M. Economou, S. Fattoum, A. Kattamis, Y. Kilinc, S. Perrotta, A. Piga, J. B. Porter, L. Griffel, V. Dong, J. Clark and Y. Aydinok, *Blood*, 2011, **118**, 884.
210. J. B. Porter and F. T. Shah, *Hematol. Oncol. Clin. North Am.*, 2010, **24**, 1109.
211. R. Fischer, A. Piga, P. Harmatz and P. Nielsen, *Ann. N. Y. Acad. Sci.*, 2005, **1054**, 350.
212. P. Evans, R. Kayyali, R. C. Hider, J. Eccleston and J. B. Porter, *Transl. Res.*, 2010, **156**, 55.
213. Y. Aydinok, Z. Ulger, D. Nart, A. Terzi, N. Cetiner, G. Ellis, A. Zimmermann and C. Manz, *Haematologica*, 2007, **92**, 1599.
214. A. Maggio, A. Vitrano, M. Capra, L. Cuccia, F. Gagliardotto and A. Filosa, *et al.*, *Br. J. Haematol.*, 2009, **145**(2), 245–254.
215. A. Lal, J. Porter, N. Sweeters, V. Ng, P. Evans, L. Neumayr, L. G. Kurio, P. Harmatz and E. Vichinsky, *Blood Cells, Mol., Dis.*, 2013, **50**, 99.
216. Y. Aydinok, A. Kattamis, M. D. Cappellini, A. El-Beshlawy, R. Origa, M. Elalfy, Y. Kiliç, S. Perrotta, Z. Karakas, V. Viprakasit, D. Habr, N. Constantinovici, J. Shen and J. B. Porter, *Blood*, 2015, **125**, 3868.
217. M. S. Elalfy, A. M. Adly, Y. Wali, S. Tony, A. Samir and Y. I. Elhenawy, *Eur. J. Haematol.*, 2015, **95**, 411.
218. F. Waldmeier, G. J. Bruin, U. Glaenzel, K. Hazell, R. Sechaud, S. Warrington and J. B. Porter, *Drug Metab. Dispos.*, 2010, **38**, 808.

## CHAPTER 5

# *Treatment of Neurodegenerative Diseases by Chelators*

ROBERTA J. WARD<sup>\*a,b</sup>, DAVID T. DEXTER<sup>a</sup> AND  
ROBERT R. CRICHTON<sup>b</sup>

<sup>a</sup>Imperial College, London, UK; <sup>b</sup>Universite Catholique de Louvain,  
Louvain-la-Neuve, Belgium

\*E-mail: [Roberta.Ward@ic.ac.uk](mailto:Roberta.Ward@ic.ac.uk)

## 5.1 Introduction

Brain iron plays a crucial role in neuronal function. Although brain iron represents less than 2% of total body iron, homeostasis of iron is mandatory for normal physiological brain function. Iron plays an important role in various proteins and enzymes which are involved in neurotransmitter synthesis and the myelination of the axons of motor neurones; such iron-containing enzymes include tryptophan hydroxylase (serotonin synthesis) and tyrosine hydroxylase (dopamine synthesis) as well as the being the precursors of adrenaline and noradrenaline.

---

RSC Metallobiology Series No. 8

Metal Chelation in Medicine

Edited by Robert Crichton, Roberta J. Ward and Robert C. Hider

© The Royal Society of Chemistry 2017

Published by the Royal Society of Chemistry, [www.rsc.org](http://www.rsc.org)

## 5.2 The Aging Brain

### 5.2.1 Brain Iron Homeostasis and Aging

Although systemic iron homeostasis has been elucidated over the past decade,<sup>1</sup> its regulation within the brain is still unclear. Figure 5.1 summarizes our current understanding of iron homeostasis in the brain.<sup>2</sup>

Iron bound to transferrin, Tf, enters the endothelial cells of the blood brain barrier (BBB) by the transferrin/transferrin receptor system, Tf/TfR, TFR1 being highly expressed on the luminal side of endothelial cells.<sup>3</sup> Iron traverses the endothelial cell, to be released at the abluminal membrane by an unknown pathway, which might involve ferroportin, Fpn, and/or other transporters, in an unknown form, possibly as low molecular weight complexes (*e.g.*, citrate, ATP, ascorbate). The iron released in the extracellular compartment would then be taken up by glial cells and neurons. Transferrin is synthesized in the brain by the choroid plexus and oligodendrocytes, but only that in the choroid plexus is secreted.<sup>4</sup> It is thought that neurons acquire most of their iron using the Tf/TfR system, and it is likely that they can export iron *via* Fpn, since many neurons co-express TfR and Fpn.<sup>5</sup> Because their perivascular end-foot processes ensheath the abluminal membrane of the BBB<sup>6</sup> and also form direct connections to neurons, astrocytes are thought to

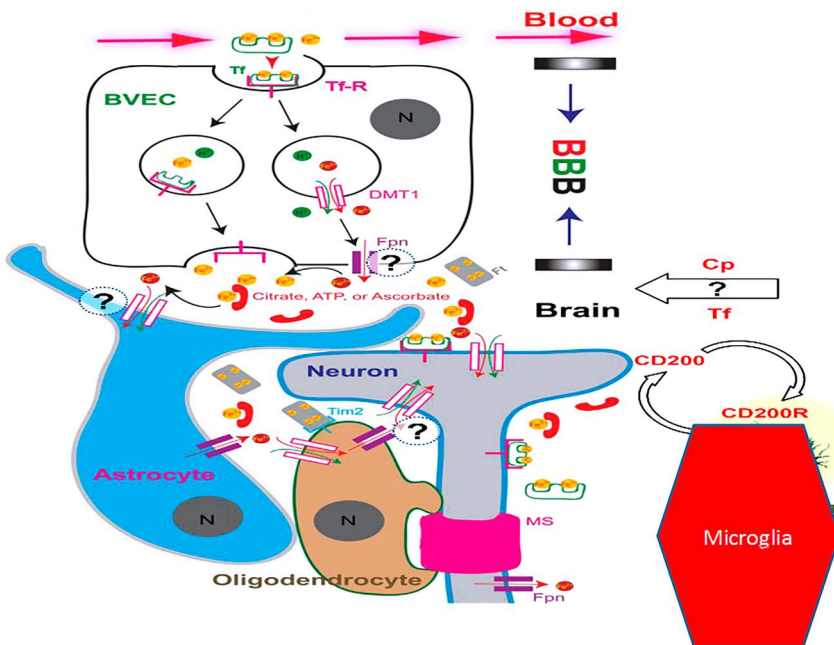


**Figure 5.1** Iron homeostasis in the brain – a hypothesis. Adapted from *The Lancet Neurobiology*, 13, Roberta J. Ward, Fabio A. Zucca, Jeff H. Duyn, Robert R. Crichton and Luigi Zecca, *The role of iron in brain aging and neurodegenerative disorders*, Copyright 2014 with permission from Elsevier.

play a key role in regulating brain iron absorption.<sup>7</sup> Astrocytes may take up iron *via* DMT1, which is expressed at the end-foot processes associated with the BBB.<sup>8</sup> Ferroportin, together with glycoposphatidylinositol-anchored ceruloplasmin constitutes the major efflux pathway by astrocytes.<sup>9,10</sup> There is continuous signalling between neurons, microglia and astrocytes, thereby reflecting any changing environment within the brain such that appropriate action can be taken when required. Iron must also be transported down the axons of neurons to synapses, by unidentified mechanisms. Brain iron is unevenly distributed throughout the brain, with the highest concentrations found in the basal ganglia<sup>11</sup> with notable amounts also in the globus pallidus, caudate nucleus, putamen, and substantia nigra,<sup>12</sup> (Figure 5.2). The explanation as to why such a differential in iron content occurs between different regions is unclear.

There is little doubt that iron concentration increases in different brain regions with age, maximal values being attained in approximately the sixth decade, specifically in the putamen,<sup>13–16</sup> the globus pallidus,<sup>14,15</sup> caudate nucleus,<sup>14,15</sup> basal ganglia,<sup>17,18</sup> as well as the cerebral cortex, cerebral white matter, brain stem and cerebellar cortex,<sup>18</sup> pallidus,<sup>16</sup> red nucleus<sup>16</sup> and substantia nigra (SN).<sup>15,16</sup> Characterisation of such iron forms in the ageing brain awaits elucidation. In one study it was shown that the concentrations of neuromelanin and H- and L- ferritins were higher in the substantia nigra than locus coeruleus, and this increased with age, the concentration of H- ferritin being higher than L- ferritin.<sup>19</sup> Both isoforms of ferritin were present in glial cells. The iron content of neuromelanin is variable.<sup>20</sup> Whether such marginal increases of iron will attenuate neuronal function or disrupt connectivity remains unclear, as there does not appear to be any drastic adverse effect on brain cellular function.

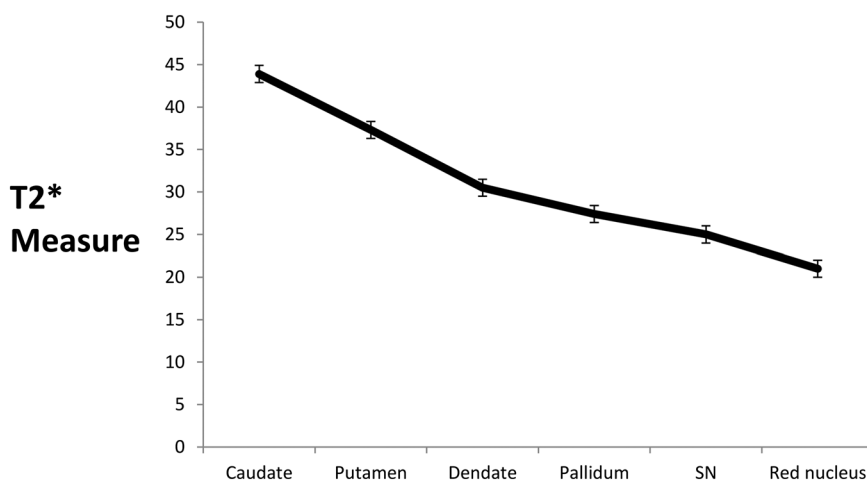


**Figure 5.2** Graph showing variation of iron in different brain regions as assessed by MRI.

## 5.2.2 Brain Copper Homeostasis and Aging

Copper is required as a cofactor for numerous critical enzymes that are involved in CNS processes, such as respiration, neurotransmitter synthesis, activation of neuropeptides and myelination. The redox cycling of  $\text{Cu}^{2+}$  to  $\text{Cu}^+$  is utilised by enzymes involved in these processes for catalytic reactions. It is important that there is precise regulation of copper levels in the brain for the maintenance of such brain functions. The exchange of copper between the periphery and the brain is highly regulated, copper primarily entering *via* the blood brain barrier. Copper fluxes into the brain parenchyma and the cerebrospinal fluid, CSF, are regulated by copper transporters CTR1, ATP7A and ATP7B (reviewed in ref. 21). Astrocytes may play an important role in copper transport from the blood and CSF toward neurons (reviewed in ref. 21); the transporter ATP7A is postulated to play the key role in such copper distribution.

In a recent study of young and aged rats, Fu *et al.*<sup>22</sup> showed that the subventricular zone (SVZ) along the wall of brain ventricles (which is in direct contact with cerebrospinal fluid) contained the highest Cu level compared with other brain regions analysed and the SVZ Cu level of old animals was 7.5- and 5.8-fold higher than those of young and adult rats, respectively. In addition, significant positive correlations were identified between age and copper levels in this region and choroid plexus. Quantitation by qPCR of the transcriptional expressions of Cu regulatory proteins showed that the subventricular zone expressed the highest level of the Cu storage protein metallothioneins while the choroid plexus expressed the highest level of Cu transporter protein, Ctr1. Another study of aging mice identified increases in global cerebral content<sup>23</sup> while lower concentrations were noted in the striatum and ventral cortex.<sup>24</sup> In human studies, the copper content decreased with age in the locus coeruleus while there were no significant changes in the substantia nigra.<sup>19</sup> In a study of aged human brains, (range 50–101 years), the highest levels of Cu were assayed in the putamen ( $36 \pm 13 \mu\text{g g}^{-1}$ ) and the lowest in the medulla ( $11 \pm 6 \mu\text{g g}^{-1}$ ),<sup>25</sup> the copper levels being negatively correlated with age.

## 5.2.3 Brain Zinc Homeostasis and Aging

Zinc is a structural or functional component of many proteins, being involved in numerous physiological functions. Within the CNS, zinc can be either tightly bound to proteins, free within the cytoplasm or extracellularly bound within presynaptic vesicles. This latter zinc is released from a subclass of glutamatergic neurons (zincergic neurons) and serves as a signal factor ( $\text{Zn}^{2+}$ ) both within the intracellular and extracellular compartments. Such signalling is dynamically linked to glutamate signalling and may be involved in synaptic plasticity, *e.g.*, long-term potentiation and cognitive activity.<sup>26</sup> Metallothioneins also play an important role in zinc homeostasis. In the human brain the highest levels of Zn are found in the hippocampus ( $70 \pm 10 \mu\text{g g}^{-1}$ ) and superior temporal gyrus ( $68 \pm 10 \mu\text{g g}^{-1}$ ) and the lowest in the pons

( $33 \pm 8 \mu\text{g g}^{-1}$ ),<sup>25</sup> which increases with aging. Under normal CNS conditions, homeostatic controls prevent excesses or deficiencies of zinc, by controlling uptake, excretion and intracellular storage/trafficking of zinc. These proteins include membranous transporters ZnT and Zip, and metallothioneins.

Metallothioneins (MTs) are low molecular weight, zinc-binding, anti-inflammatory, and antioxidant proteins that play an important role in the aging brain *via* zinc-mediated transcriptional regulation of genes involved in cell growth, proliferation, and differentiation. Although, there is a tendency for an age-related increase in Zn in most brain regions, treatment with metal chaperones, such as PBT2 to increase the zinc content of specific brain regions, *e.g.*, the hippocampus, could prevent age-related cognitive decline.<sup>27</sup> Preliminary studies in aged C57Bl/6 mice showed improvements in cognitive function such as memory, as well as increases in dendritic spine density, hippocampal neuron number and markers of neurogenesis.

### 5.3 Inflammation and Aging

With aging there are increased inflammatory responses, although the cause for this is unclear. Immune dysfunction occurs, with the concentration of various pro-inflammatory cytokines increasing—inflamm-aging—with the regulatory mechanisms responsible for dampening such responses becoming ineffective.<sup>28</sup> With aging, microglia become less efficient in function and tend to be over activated in response to stimulation, thereby instigating a too potent reaction. Activated microglia will assume an M1 phenotype, alter the expression of various iron efflux and influx proteins, *e.g.*, down regulation of ferroportin expression, caused by increased levels of hepcidin (as a result of the inflammation) interacting with ferroportin to form a complex which is then internalised. Therefore iron will accumulate within these cells. Whether such iron is available to the chelators is an important question. Blocking hepcidin expression or function represents a novel approach to control inflammation. Ferroportin expression would be increased such that iron bioavailability would be enhanced.

### 5.4 Neurodegenerative Diseases

Aging is a major risk factor for the development of neurodegenerative disease. Although some genetic defects have been identified in the rarer neurodegenerative diseases, such as neuroferritinopathy, aceruloplasminaemia and Friederich's ataxia (which help to explain the increase in iron content in specific brain regions and organelles), the exact mechanisms which are triggered in the more common neurodegenerative diseases, such as Parkinson's and Alzheimer's diseases, remain unknown. What has become apparent over the last decade has been the identification of alterations in brain metal ion homeostasis, particularly iron, copper and zinc, in many of these diseases. However, it remains unknown whether such metal dysregulation is a primary or secondary event. In each case, such perturbation of the metal ions may

drive the progression of the neurodegenerative disease, such that it has been suggested that: (a) its removal by metal ion chelators may slow the progression of the neurodegeneration, thereby improving cognition and brain function and hence the quality of life, or (b) supplementation with metal ions may correct the dysfunctional metal ion homeostasis.

## 5.5 Blood Brain Barrier

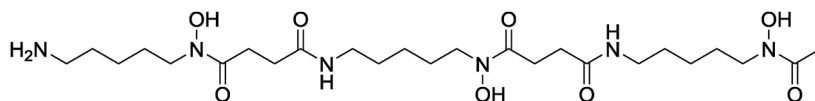
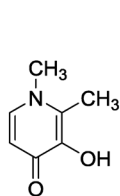
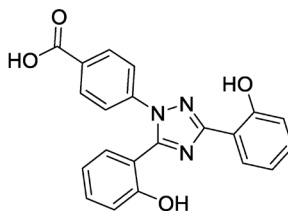
The blood brain barrier, BBB, is composed of capillary endothelial cells, basal lamina and astrocytes, and acts as a two-way diffusion barrier. Pericytes are also present (mesenchymal-like cells surrounding the endothelial cells) which play an important role in contracting brain capillaries, thereby altering blood flow (reviewed in ref. 29). The specific phenotype of the endothelial cells with their tight junctions will limit the paracellular flow of water, ions and larger molecules into the brain. Gases, such as O<sub>2</sub> and CO<sub>2</sub>, are exchanged through the lipid membranes as a result of gradient diffusion, while the influx of amino acids and glucose is regulated through specific transporters. Larger molecules are transported by receptor-mediated transcytosis, while other molecules with a molecular weight higher than 500 Da, as well as all other hydrophilic compounds including drugs, will be highly restricted under normal conditions. Therefore, for the chelators to cross the blood brain barrier, transporters may facilitate their movement across membranes, either by transcytosis or by association with transmembrane receptors, in addition to simple diffusion.

Astrocytes may play an important role in regulating the BBB and its permeability by controlling protein expression and distribution in endothelia *via* astrocyte-derived signals such as vascular endothelial growth factor (VEGF), basic fibroblast growth factor (bFGF), and the glial cell line-derived neurotrophic factor (GDNF).

For many years it has been suggested that changes in the permeability of the BBB occur with age, thereby allowing the passage of toxins and other molecules to access the brain and lead to an increase both in inflammation (inflammaging) and metal ion fluxes, such as iron, into the brain. For example, leakage of the BBB may induce microglial activation by allowing abnormal molecules (such as toxins from the gut) to pass into the brain parenchyma and in turn evoke the release of pro-inflammatory cytokines and free radicals from the microglia, thereby further altering the BBB, in a vicious cycle. In a recent review,<sup>30</sup> Farrall and Wardlaw assessed 31 permeability studies (1953 individuals) and showed that aging in healthy humans was associated with increased BBB permeability. It was also demonstrated that gut microbiota in older adults correlates with diet, location of residence and a basal level of inflammation which could ultimately enhance susceptibility to diseases.<sup>31</sup> Gut microbiota may aggravate inflammation during diet-induced obesity<sup>32</sup> which has been confirmed by brain imaging studies.<sup>29</sup> Manipulation of the microbiota and microbiome of older adults holds promise as an innovative strategy to influence the development of comorbidities associated with aging.

## 5.6 Metal Ions and Neurodegenerative Diseases

The etiology of the enhanced metal ion content in various neurodegenerative diseases may be attributable to a variety of factors which include changes in metal ion transport mechanisms across the BBB and local dysregulation of metal ion homeostatic control, possibly induced by neuroinflammation. Whether this is a primary event in each of these diseases, or is as a result of an initial insult remains unclear. However, in each case, the perturbation of the metal ions may drive the progression of the neurodegenerative disease, such that it has been suggested that its removal by metal ion chelators may slow the progression of the neurodegeneration, thereby improving cognition and brain function and hence the quality of life. In the majority of neurodegenerative diseases it is either iron, copper, or both, where there may be some dysregulation of their brain homeostatic control. Parkinson's and Alzheimer's diseases, as well as multiple sclerosis, are associated with iron dysregulation in regions of the brain where the specific pathology is most highly expressed. However the diversity of the pathological processes involved in these pathologies would indicate that this is not a primary abnormality of brain iron metabolism. Therefore, even if such disturbances in iron metabolism are secondary phenomena, the control of iron levels is a worthwhile therapeutic target. Disease-modifying therapies aimed at removing excess iron, without affecting iron-containing enzymes involved in neurotransmitter function, could be part of the therapeutic approaches utilised to prevent the progression of Parkinson's disease (PD). However, such iron is not in a free form but bound to various iron storage proteins such as ferritin and neuromelanin. Several commercially available iron chelators, *e.g.*, desferrioxamine (also known as deferoxamine, deferrioxamine, desferoxamine, DFO – hexadentate) **1**, deferiprone (bidentate) **2**, and deferasirox (tridentate) **3**, could potentially be utilised to treat PD. Although early studies reported that the BBB was relatively impermeable to DFO,<sup>33</sup> or showed restricted uptake,<sup>34</sup> our later studies of these three iron-chelating compounds showed that each was able to cross the BBB.<sup>35,36</sup>

Desferrioxamine B (**1**)Deferiprone (**2**)Deferasirox (**3**)

### 5.6.1 Parkinson's Disease (PD)

In early studies we demonstrated that the neurodegenerative process in PD was associated with elevated iron levels in the substantia nigra (SN),<sup>37–39</sup> and that individual dopaminergic neurons in this brain region showed raised iron levels. There were changes in the ratio of H- and L- ferritin in the SN of PD patients, the SN concentration of L- ferritin in PD ( $52.5 \pm 26.0$ ) was lower than in the control ( $97.9 \pm 54.9$ ) while the H- ferritin in PD ( $534.2 \pm 223.1$ ) was higher than in the control ( $374.8 \pm 169.3$ ). It was suggested that the decrease in L- ferritin may limit the amount of iron which could be safely sequestered into this iron storage molecule, such that there would be a higher availability of free iron.<sup>40</sup> Neuromelanin granules containing iron were observed both intra- and extra-neuronally in the SN of Parkinsonian patients.<sup>39</sup> As the iron content increases excessively in the SN of PD patients, there was a direct correlation with adverse changes in clinical scores, *i.e.*, UPDRS III and PDQ-39 mobility scores.<sup>41</sup> Glial iron will be mainly ferritin while neuronal iron is predominantly bound to neuromelanin. Copper levels are reportedly decreased in the SN of PD patients<sup>42</sup> which has implicated a possible role for ceruloplasmin in the iron accumulation. In a rat model of PD, the 6-hydroxydopamine model, 6-OHDA, (where ferroportin and ceruloplasmin co-localised in the SN), the number of dopaminergic neurons was reduced by 50% after 1 day, iron levels increased, and the mRNA and protein expressions of ceruloplasmin decreased compared with the control.<sup>43</sup> Such results possibly indicate that the lack of ceruloplasmin may play some role in the iron accumulation in the SN of PD patients.

Although alterations in iron homeostasis in the brain of PD patients have been suggested, various studies where the expression of a number of iron genes have been quantitated in the SN of PD brains, have not confirmed such alterations. Crichton *et al.*,<sup>44</sup> identified gene expression patterns that were typical of iron deficiency and inflammation, with no evidence of down-regulation of genes associated with iron overload, and the activity of IRP1<sup>45</sup> and IRP2 did not change in the iron-loaded SN.<sup>44</sup>

Chelation of the iron in the SN of PD brains has been proposed as a possible therapy. In our initial animal studies<sup>35,46</sup> we showed that chelators in current clinical use for the treatment of systemic iron overload, desferrioxamine 1, deferiprone 2, and deferasirox 3, were able to cross the BBB, reduce the iron content in various brain regions, as well as induce neuroprotection after their systemic administration in an animal model of PD. This was exemplified by the preservation of SN dopaminergic cell counts and the normalisation of dopamine metabolism in the striatum. Importantly, our microdialysis studies also indicated for the first time that focal administration of these chelators reduced hydroxyl radical formation induced by 6-OHDA. Such results have enabled us to embark on a clinical trial of deferiprone in PD patients to ascertain: (a) its tolerability and (b) whether there are decreases in SN iron content after chelation for 6 months measured by T2\* MRI techniques.

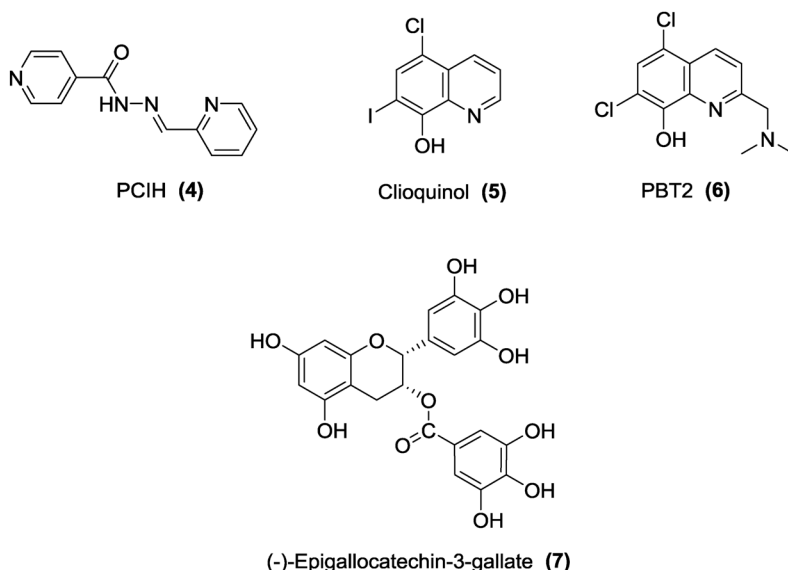
One earlier study, in 2010, reported the effects of deferiprone in one PD patient. The PD patient presented with a variety of symptoms including

dysarthria and orofacial dystonia, with iron accumulation in many brain regions including the dentate nuclei, substantia nigra and red nuclei (as assessed by T2\* MRI), and was administered deferiprone 30 mg kg<sup>-1</sup> day<sup>-1</sup> for 32 months. After 6 months there was an improvement in many of the symptoms, at 1 year an improvement in the UPDRS score, while the T2\* MRI showed a rapid onset decrease in iron accumulation in the bilateral dentate nuclei, with a milder but later decline in the substantia nigra. No significant change in the iron content of the red nuclei was reported.<sup>47</sup> More recently two further clinical trials have investigated the efficacy and safety of deferiprone in double-blind placebo studies for the treatment of Parkinson's disease. Either R2\* or T2\* MRI sequences were utilised to assess iron content, UPDRS motor scores were acquired at various intervals and serum ferritin, a marker of iron stores and inflammation, was also measured. Both studies indicated that deferiprone, 30 mg kg<sup>-1</sup> day<sup>-1</sup>, slightly improved motor signs after 6 months of treatment, decreased motor handicap progression (mean change in UPDRS motor score = -2) while the iron content in the substantia nigra was significantly decreased in the first study after one year,<sup>48</sup> while the second study showed decreases in the SN after 6 months in some PD patients administered 30 mg kg<sup>-1</sup> day<sup>-1</sup>.<sup>49</sup> In both studies, neutropenia or agranulocytosis occurred in approximately 8% of the subjects which resolved rapidly with cessation of the oral therapy.<sup>48,49</sup> In the latter study the iron content of other brain regions were assayed after administration of the iron chelator and showed that there were progressive decreases of the iron content in different brain regions—after only 3 months in the caudate nuclei and in the dentate nuclei at 6 months. In other brain regions investigated, the putamen, red nuclei, and pallidum, no change in their iron content was evident over the period of the clinical trial (6 months). Clearly the positive results from these 2 clinical trials indicate that chelation therapy may be of benefit in the treatment of PD. Furthermore, the efficacy of iron chelation in the PD patients was improved if the subject showed a low inflammatory index, *i.e.*, low ferritin and low IL-6 serum concentrations.<sup>49</sup> In a recent clinical study of deferiprone in PD patients, those subjects with the lower CP activity in the serum and cerebrospinal fluid responded better to iron chelation,<sup>50</sup> thereby confirming that low systemic inflammatory profile was associated with chelator efficacy.

The relationship between activated microglia and iron accumulation in the SN is worthy of further investigation. Activation of microglia in the SN to an M1 phenotype will enhance iron uptake and reduce iron efflux. From our recent study it would suggest that the ability of the chelators to remove this iron will be reduced.<sup>49</sup>

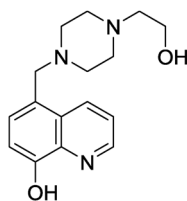
A range of other iron chelators have been tested for their ability to chelate iron *in vitro* or in animal models of PD as well as to prevent neurotoxicity and restore nigral degeneration. These include 2-pyridylcarboxaldehyde isonicotinoyl hydrazine (PCIH, 4),<sup>51</sup> as well as the antibiotic metal chelator, 5-chloro-7-iodo-8-hydroxyquinoline (clioquinol, 5)<sup>52</sup> and its various derivatives, PBT2 6, and derivative PBT434 (8-hydroxyquinazolin-4-(3*H*)-one).

Clioquinol (CQ, 5), may be of use in PD as it increased nigral tyrosine hydroxylase activity after a 5 month treatment of symptomatic tau KO mice; cognitive deficits were improved and there were raised BDNF levels in the hippocampus, attenuation of brain atrophy, and reduced iron content in the brain.<sup>55</sup> Selective natural plant-derived polyphenol flavonoids are claimed to have metal-chelating capacity, *e.g.*, green tea catechins and (-)-epigallocatechin-3-gallate (EGCG, 7), and possess neuroprotective actions.<sup>53</sup> In various animal models of neurodegeneration, EGCG reduces lipid peroxidation, apoptosis and attenuation of pro-inflammatory cytokines production. Such neuroprotection may not be related to its iron chelating ability but to its ability to down-regulate the RhoA protein.<sup>54</sup> Rho-associated kinase activates p38-MAPK, which is involved in the regulation of the pro-inflammatory cytokines, cyclooxygenase-2 and inducible nitric oxide synthase. Other intracellular pathways are also modulated by EGCG, such as NFkappaB, ERK1/2, Akt, JAK/STAT and JNK, thereby indicating the possibility of the development of EGCG derivatives with a higher potency than EGCG.

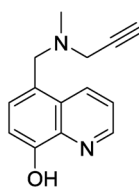


The development of multifunctional anti-PD drugs has also been advocated, with two compounds being linked, namely the iron-chelating pharmacophore of VK-28 **8** and the propargylamine MAO inhibitory activity of rasagiline to form M30 **9** and M30a **9a**. This compound is a potent iron chelator, radical scavenger and brain-selective irreversible MAO-A and -B inhibitor, with little inhibition of peripheral MAO.<sup>56</sup> Such compounds have been reported to have neuroprotective activity in both *in vitro* and *in vivo* models of PD, increasing brain dopamine, serotonin and noradrenaline. However, what must be emphasised here is that to bring such molecules to the clinic would require enormous sums of money (>£500 million UK). Their further development

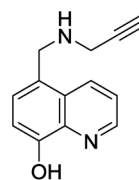
must be questioned, particularly now that it has been shown that clinically available chelators can cross the BBB and induce neuroprotection.



VK28 (8)



M30 (9)



M30A (9a)

### 5.6.2 Alzheimer's Disease (AD)

Alzheimer's disease (AD) is the most common cause of dementia. AD is characterized by discrete and predictable neuronal loss in the temporal lobe, parietal lobe, and parts of the frontal cortex and hippocampus, while areas such as the visual cortex and cerebellum are spared. Two hallmark deposits are associated with the disease: amyloid beta peptide, A $\beta$ , and neurofibrillary tangles of hyper-phosphorylated microtubule-associated tau. There is extensive literature on the effects of metal ions such as copper, zinc and iron, on A $\beta$  aggregation and AD symptoms; such metal ions alter the structure of amyloid aggregates and inhibit fibril formation. Furthermore, the presence of metal ions may alter the kinetic pathway of A $\beta$ , directing its aggregation away from a more stable fibrillar structure and towards a pathway resulting in more neurotoxic structures. Such enrichment of the amyloid plaques with these essential metals may induce deficiency of these essential metals in brain cells.

Previous studies have shown that in brain specimens of AD patients, amyloid deposition and neurofibrillary tangles co-localise with neuronal iron accumulation.<sup>57,58</sup> Iron is enriched approximately 3-fold in the affected regions (reviewed in ref. 59). Studies of the distribution of iron, and the iron-binding storage proteins, ferritin and haemosiderin, in sections of AD hippocampus<sup>60</sup> showed that ferritin was present in the coronal region associated with a non-beta-amyloid component and in the periphery of plaques, together with haemosiderin, in sulphur-rich dense bodies of dystrophic neurites. Haemosiderin was also found in lysosomes and siderosomes of glial cells. Ferritin was present in the cytoplasm and nucleus of oligodendrocytes and abundant in myelinated axons in association with oligodendrocyte processes. Whether this represents a dysfunction of ferritin in AD,<sup>61</sup> or merely evidence of inflammation with the incumbent changes in iron distribution, awaits identification. In a study of 191 AD patients the presence of both the C2 variant of transferrin (TF) gene and the C282Y allele of the haemochromatosis (HFE) gene was identified as a risk factor for developing AD<sup>62</sup> which could induce an excess of redox-active iron in some brain regions and the induction of oxidative stress in neurons. In animal models of AD L-ferritin accumulated in the cores of the

plaques in the frontal cortex as well as throughout the brain co-localising with A $\beta$ -42 particularly in the vicinity of blood vessels.<sup>63</sup> H-ferritin was limited to hippocampal neurons and did not co-localise with A $\beta$ -42.<sup>63</sup>

Variable results have been reported for the levels of zinc in AD brains. Although early studies reported no difference in zinc levels between AD and controls, later studies identified a decrease in zinc levels in the neocortex, superior frontal and parietal gyri, the medial temporal gyrus and thalamus, while there was an elevation of zinc in Alzheimer's-affected amygdala, cerebellum, olfactory areas and superior temporal gyrus (reviewed in ref. 59). In the hippocampus, variable results are reported, some indicating an increase while others show a decrease of divalent zinc (reviewed in ref. 59). Later studies also showed enriched zinc levels in amyloid plaque (reviewed by ref. 59), A $\beta$ -42 binding to zinc at residues 6–28 with up to three zinc ions bound to histidines 6, 13 and 14. Zinc binding will rapidly induce the aggregation of A $\beta$  into insoluble precipitates, typical of AD pathology. Such zinc sequestration into amyloid deposits induces loss of functional zinc in the synapse (reviewed in ref. 59). Overall it is suggested that there is mis-compartmentalization of zinc in the AD brain, with plaques containing three to four times the amount of zinc compared to the adjacent neuropil. The cause of this zinc dysregulation in AD remains unknown, but probably involves the failure of one or more of the proteins involved in zinc homeostasis, such as metallothionein I, II and III, and the zinc transporters, ZnT1, ZnT3, ZnT4 and ZnT6 (reviewed in ref. 59).

The concentration of copper is also decreased in the areas affected by AD, with the plaques and tangles containing high amounts of copper, (A $\beta$  interacts with copper), modifying A $\beta$ -42 and accelerating its aggregation. Such copper complexes are cytotoxic. There is a loss of copper in the synaptic clefts which in normal circumstances would be released into the glutamatergic synaptic cleft, facilitated by ATP7A, to cause *S*-nitrosylation of NMDA receptors and inhibit their activation.

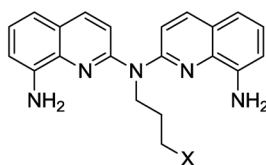
Reducing A $\beta$ -42 levels within the brain by inhibiting its production or removing it with immunotherapy, have been the approaches most extensively investigated but as yet with no conclusive results. This could reduce the metal ion content of these aggregated proteins. Another strategy would be to inhibit the interaction between A $\beta$  and transition metals by the use of agents which could facilitate redistribution of these metals into their appropriate physiological compartments. Whether iron chelators could be of use in AD is debatable since it remains unknown whether the affinity of the metal ions is higher for the amyloid protein than the iron chelator. Only one study where AD patients received an iron chelator has been reported,<sup>64</sup> where 48 AD patients received DFO 1, 125 mg intramuscularly twice daily, 5 days per week, for 24 months. A significant reduction in the rate of decline of their daily living skills was observed, such that it was concluded that sustained administration of the drug may slow the clinical progression of the dementia.

Various studies of animal models of AD have further explored the benefits of chelation for this disease. The iron chelators (–)-epigallocatechin-3-gallate 7 and M-30 9 reduced APP expression in cultured cells,<sup>65,66</sup> which could reduce A $\beta$  production since APP contains an iron-responsive element that will

induce translation of the protein in a high-iron environment.<sup>67</sup> Desferrioxamine (**1**) inhibited amyloidogenic APP processing in cultured cells and in APP/PS1 mice, which attenuated the A $\beta$  burden within the brain and reversed spatial memory impairment.

Animal studies have shown that when deferasirox was conjugated to lactoferrin molecules by a carbodiimide-mediated coupling reaction, this novel drug delivery system was shown to have higher brain permeability through receptor-mediated transcytosis. Intraperitoneal injection of such a lactoferrin conjugate was able to significantly attenuate learning deficits induced by beta amyloid injection in a rat model of Alzheimer's disease.<sup>68</sup>

It is thought that restoring normal copper homeostasis in the brain of AD patients by removing the excess copper from the amyloid plaques may be of therapeutic benefit.<sup>69</sup> The metal-binding attenuating compound, clioquinol **5**, was rediscovered to be a candidate drug for Alzheimer's disease when it was shown that it rapidly reduced plaque formation in Tg2576 transgenic mice.<sup>70</sup> A Phase 2 clinical trial in AD patients showed that the compound was well tolerated and cognitive function was improved.<sup>71</sup> This neuroprotection was possibly attributed to chaperoning of the various biometals<sup>72,73</sup> involved in disease pathogenesis<sup>59</sup> *i.e.*, as chelators for copper, zinc,<sup>73</sup> and iron.<sup>52</sup> Despite such promise, the phase II clinical trial of clioquinol concluded that there was no significant loss in plaque levels as compared to controls, no improvement in neural function or hippocampal atrophy and no change in cognitive function. It has recently been proposed that 8-HQs possess an additional mechanism of action that neutralizes neurotoxic A $\beta$  oligomer formation through stabilization of small (dimeric) nontoxic A $\beta$  conformers. New tetradentate ligands based on bis(8-aminoquinoline) are now being developed, **10a** and **10b**, while specific copper chelators maybe able to extract copper(II) from the amyloid plaque.<sup>74</sup> Interestingly, one of these copper ligands, PA1637, is able to efficiently delay the loss of episodic memory and is currently under preclinical development.<sup>69</sup>



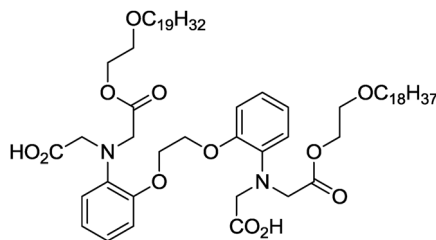
bis(8-aminoquinoline)s (**10**)

X = OH (**10a**)

X = N(CH<sub>3</sub>)<sub>2</sub> (**10b**)

Another lipophilic zinc/copper/iron chelator, DP-109 **11**, reduces the burden of amyloid plaques in brains from aged hAbPP-transgenic Tg2576 mice.<sup>75</sup> Despite these positive results significant controversy remains as to whether copper excess is involved in AD pathology. Some data suggests that increasing copper in the brain *via* amplification of the copper transporter ATPase7b, will reduce  $\beta$ -amyloid accumulation<sup>76</sup> – indeed, copper supplementation in APP23 transgenic mice lowered  $\beta$ -amyloid production. Therefore the

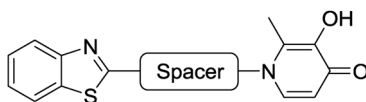
controversy remains as to whether too much, too little or abnormal redistribution of these metals is involved in AD pathogenesis.



DP-109 (11)

Recent studies have shown that zinc supplementation in the pre-symptomatic stages of the disease in AD transgenic mice could be beneficial by delaying the hippocampal-dependent memory deficits and strongly reducing both A $\beta$  and tau pathology in the hippocampus. In addition, the age-dependent respiratory deficits were prevented and increased levels of brain-derived neurotrophic factor (BDNF) were assayed.<sup>77</sup>

Recent drug development has attempted to design and develop new AD drugs which are multifunctional. In one study a compound was developed which showed metal attenuation, anti-A $\beta$  aggregation and anti-acetylcholinesterase activity. 3-Hydroxy-4-pyridinone (3,4-HP **12**) and benzothiazole molecular moieties, were selected as starting frameworks due to their well known affinity for iron and A $\beta$  peptides, respectively.<sup>78</sup> The linkers between these two main functional groups were selected on the basis of virtual screening, so that the final molecule could further inhibit the acetylcholinesterase responsible for cholinergic losses. Other multifunctional drugs have been reported, for example, benzylideneindanone derivatives have been synthesised and one was shown to inhibit both A $\beta$ -42 aggregation and MAO-B *in vitro*, as well as being an excellent antioxidant and metal chelator. In addition, it was capable of inhibiting Cu(II)-induced A $\beta$ -42 aggregation and disassembling the well-structured A $\beta$  fibrils.<sup>79</sup>



BTA-HP (12)

### 5.6.3 Intracerebral Haemorrhage

Intracerebral haemorrhage, ICH, is associated with approximately 15% of all strokes and shows high morbidity and mortality rates. Erythrocyte rupture into the brain induces a 3-fold increase in non-haem iron levels which can remain high for at least one month.

Iron has been shown to play an important role in ICH-induced brain injury in experimental animals and patients. Brain injury after ICH shows two phases: 1. An early phase involving the clotting cascade activations and thrombin production. 2. A phase involving erythrocyte lysis and iron toxicity, after which the iron content in the surrounding area increases dramatically (Figure 5.3). High serum ferritin levels are associated with severe brain oedema and poor outcome in ICH patients.

Various individual reports have shown the beneficial effects of iron chelation. A 65 year-old man presented with headaches and seizures in 2006 and was found by angiography to have subarachnoid hemorrhage associated with a transverse sinus thrombosis. Administration of deferiprone at  $30 \text{ mg kg}^{-1} \text{ day}^{-1}$  was commenced, gradually decreasing to  $15 \text{ mg kg}^{-1}$  for 1 year. MRI showed a reduction in hemosiderin deposition in the cortex and cerebellum after the treatment which correlated with the improvement in his symptoms, specifically in the brain stem.<sup>80</sup> Iron chelation therapy studies using deferiprone (2) to remove the excess iron showed decreased levels of hemosiderin, as detected by lessening of the T2 hypointensity, in four of nine subjects following a 90 day course of deferiprone ( $15 \text{ mg kg}^{-1}$ , twice daily), while three subjects had no change and two patients had slightly more hemosiderin.<sup>81</sup> Patient reporting of symptoms indicate that four patients had an improvement in symptoms, four were unchanged, and two were worse.<sup>81</sup> Longer term administration of deferiprone, *e.g.*, for 38 months in one patient, revealed resolution of ataxia and hearing loss, which were present prior to the initiation of treatment.<sup>82</sup>

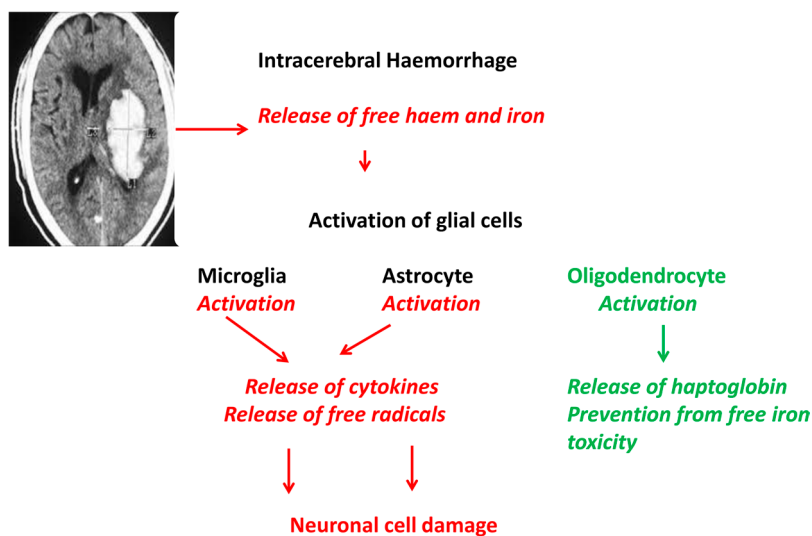


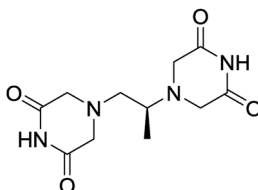
**Figure 5.3** Involvement of iron in intracerebral haemorrhage by inducing neuronal cell loss *via* glial cell activation.

### 5.6.4 Multiple Sclerosis

Multiple sclerosis (MS) is an autoimmune disorder of the CNS characterized by inflammatory destruction of the myelin sheaths of axons in the CNS. Myelin is wrapped around the axon, electrically isolating it from the surrounding media. Myelin is produced by the oligodendrocytes in the CNS. The oligodendrocyte is a principal target of attack in MS. Initially inflammation is transient and remyelination occurs but it is not durable. Elevated iron levels occur in certain brain regions in MS, in deep grey structures often with bilateral representation whereas in the white matter pathological iron deposits are usually located at the sites of inflammation. Such excess iron may amplify the activation of the microglia, promote mitochondrial dysfunction and catalyse ROS production.

MRI scans have revealed iron deposition in the cortical and deep GM areas (e.g., the red nucleus, thalamus, dentate nucleus, lentiform nucleus, caudate and rolandic cortex) in comparison with age-matched normal controls. Such changes were associated with brain atrophy, disability progression, and cognitive impairment in patients with MS.<sup>83</sup>

In initial studies the ability of desferrioxamine to improve symptoms was tested in two animal models of MS, experimental autoimmune encephalomyelitis (EAE), where a positive response was observed, as well as in the myelin basic protein-induced EAE model, when no response was evident when desferrioxamine was administered in a preclinical phase. However, if administered later, during a time of clinical symptoms, it effectively attenuated the disease. Dexrazoxane **13** also attenuated the course of EAE, but was less effective than DFO (reviewed in ref. 83). In one clinical trial of secondary progressive MS patients,<sup>84</sup> nine patients received up to 8 courses of desferrioxamine **1**. The drug was well tolerated but had little effect on their disability. One patient improved, 3 patients were unchanged, and 5 patients worsened. The oral iron chelators, deferasirox and deferiprone, may be more desirable for possible use in MS, although close patient monitoring and a carefully considered administration regimen will be needed.



Dexrazoxane (**13**)

### 5.6.5 Friederich's Ataxia

Friederich's ataxia is caused by a reduction in the expression of a small mitochondrial protein, frataxin, due to an anomalous expansion of unstable nucleotide repeats in a non-coding region of the frataxin gene. The major consequences

of its deficiency include impairment of biosynthesis of iron–sulphur clusters, alterations in cellular iron metabolism, and mitochondrial dysfunction, which is accompanied by iron overload and increased oxidative stress.<sup>85</sup>

In a clinical trial, deferiprone (10–15 mg kg<sup>-1</sup>, twice daily) was administered to Friedreich's ataxia patients in a small clinical trial over a 6 month period. A reduction of iron in the dentate nuclei was evident after this period, as well as improved scores on the ICARS (International Cooperative Ataxia Rating Scale) and a lessening of some clinical signs, *e.g.*, gait, balance.<sup>86</sup> In addition, there was restoration of impaired mitochondrial membrane and redox potential, increased ATP production and attenuation of mitochondrial DNA damage.<sup>87</sup> In a second clinical study, combined therapy of deferiprone (10 mg kg<sup>-1</sup>, twice daily) with idebenone (an analogue of coenzyme Q<sub>10</sub>, with antioxidant properties, that protects the heart and possibly the CNS in Friedreich's ataxia patients) at 20 mg kg<sup>-1</sup> per day was evaluated in 20 Friedreich's ataxia patients.<sup>88</sup> After 11 months of treatment iron content in the dentate nucleus was reduced, as assessed by MRI (T2\*), steady ICARS scores resulting from improved kinetic function were observed, but there was worsening of posture and gait compared to baseline in Friedreich's ataxia patients.<sup>88</sup>

## 5.7 Neurodegeneration with Brain Iron Accumulation (NBIA) Diseases

Neurodegeneration with brain iron accumulation is a group of progressive extrapyramidal and cognitive disorders, which include aceruloplasminemia, neuroferritinopathy and the most common NBIA disorder, pantothenate kinase-2-associated neurodegeneration, PKAN. NBIA are characterised by iron accumulation, predominantly in the globus pallidus, as well as extensive axonal spheroids in various regions of the brain. Recent studies indicate multiple genetic causes, although the illness can occur without an obvious genetic background.

### 5.7.1 Mutation in Genes Associated with Iron Metabolism

Two forms of brain iron loading have been linked to mutations in genes directly involved in iron metabolism: first, neuroferritinopathy associated with mutations in the *FTL* gene and secondly, aceruloplasminemia, where the ceruloplasmin gene is defective. Table 5.1 shows neurodegenerative diseases that are associated with brain iron accumulation caused by an enzyme deficiency and/or mutation.

#### 5.7.1.1 Aceruloplasminemia

Aceruloplasminemia is an autosomal recessive disorder where there is an absence of active ceruloplasmin (Cp). It is often diagnosed in adulthood although it may present at a younger age, *e.g.*, 16 years. Iron overload has

**Table 5.1** Neurodegenerative diseases where there is brain iron accumulation associated with an enzyme deficiency and/or mutation (adapted from ref. 97 under the terms of the Creative Commons Attribution License (CC BY): <http://creativecommons.org/licenses/by/3.0/>).<sup>a</sup>

Human disorder	Gene defect	Location of brain iron deposition
Acaeruloplasminemia	Caeruloplasmin absence	Dentate nucleus, globus pallidus, putamen, caudate nucleus
Neuroferritinopathy	<i>FTL</i>	Dense ferritin spheroid inclusions in dentate nuclei, globus pallidus, putamen, caudate, thalamus, red nuclei
Pantothenate kinase-associated (Hallervorden-Spatz syndrome)	PKAN, NBIA type 1	Globus pallidus
Phospholipase-2 group VI-associated (Karak syndrome)	PLAN, NBIA type II, INAD1	Globus pallidus, substantia nigra (50% patients)
Mitochondrial membrane protein	MPAN	Globus pallidus, substantia nigra
Fatty acid hydrolase	FAHN	Globus pallidus, substantia nigra in some patients
COASY protein (CoPAN)	COASY	Globus pallidus, substantia nigra
Beta propeller protein	BPAN	Globus pallidus, substantia nigra
Kufor-Rakeb syndrome		Globus pallidus, substantia nigra in few cases
Woodhouse-Sakati syndrome		Globus pallidus, substantia nigra in few cases

<sup>a</sup>Adapted from Levi and Finazzi, 2014.

been identified by MRI T2\* in the basal ganglia, the red nuclei and deep cerebellar nuclei as well as in the cortex as the disease progresses (Figure 5.4). In normal circumstances ceruloplasmin is synthesised as a glycoposphatidylinositol-anchored protein associated with astrocytes, this possibly being its major form in the CNS.

Over 50 mutations of the *Cp* gene have been reported. For example, Cys-881 is essential for the trafficking and secretion of the truncated mutant *Cp* in aceruloplasminemia,<sup>89</sup> therefore a mutant protein without Cys-881 accumulates in the ER, inducing ER stress and eventually cell death. Since *Cp* plays an important role in iron metabolism (promoting the oxidation of Fe<sup>2+</sup> to Fe<sup>3+</sup> after efflux of iron from the cell *via* ferroportin), an inability for such an occurrence will result in the accumulation of iron within cells. It is thought that iron will initially accumulate in a non-toxic form within ferritin, which gradually becomes filled to capacity because of the reduced ability of the cell to efflux iron. Iron accumulates in neurons and astrocytes of the brain, as well as in the retinas, the liver, and RE cells in the spleen and pancreatic cells. The cascade of events leading to neuronal death is not fully elucidated but oxidative stress, exacerbated by heavy metal accumulation, is the primary cellular toxic event.

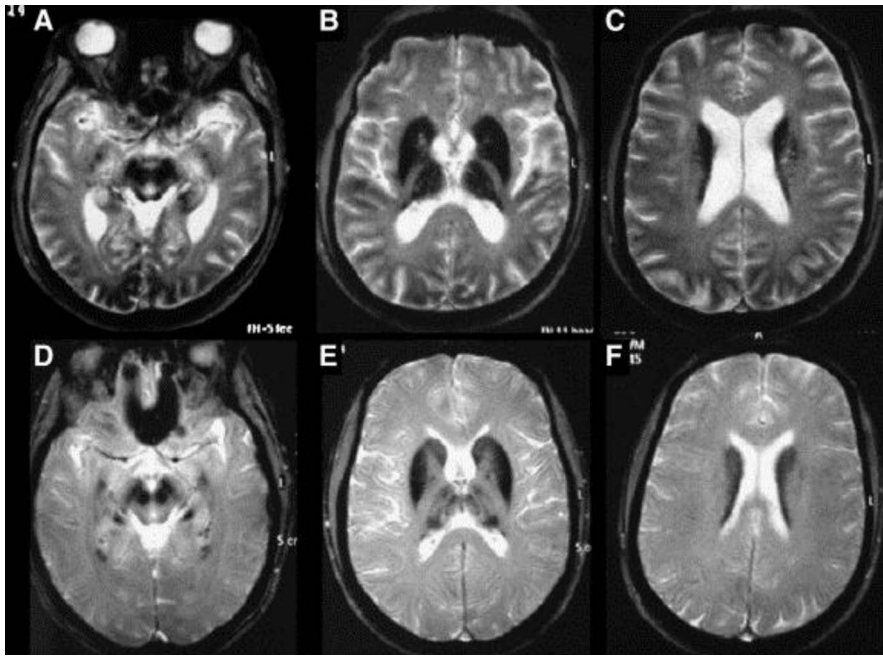


**Figure 5.4** Aceruloplasminemia. (A–C) Gradient echo (GE) T2\*-weighted images reveal profound hypointensities (iron deposition) in the caudate nucleus, putamen, globus pallidus, thalamus and midbrain with ventriculomegaly in a 56 year-old male proband. (D–F) Similar, but less florid, lesions of the basal ganglia and thalamus are demonstrable on neuroimaging of the proband's sister. Reproduced from *Biochimica et Biophysica Acta (BBA) – Molecular Basis of Disease*, 1822, Hyman M. Schipper, Neurodegeneration with brain iron accumulation – Clinical syndromes and neuroimaging, 350–360, Copyright 2012 with permission from Elsevier.

There have been several attempts to treat aceruloplasminaemic patients with the iron chelator, desferrioxamine, to remove the excess iron from both the liver and the brain. Variable results have been obtained, some reporting an improvement in clinical symptoms<sup>90–92</sup> while others have not.<sup>93</sup> However there was no evidence for a decrease in brain iron accumulation.<sup>90</sup> In another study, three aceruloplasminemia patients were administered the oral chelator, deferasirox ( $17\text{--}20\text{ mg kg}^{-1}\text{ day}^{-1}$ ), for periods of between 1 week and 5 months. Again decreases in liver iron were apparent but there was no change in brain iron content.<sup>94</sup> A case study that examined the combination of plasma (as a source of ceruloplasmin) together with desferrioxamine reported an improvement in clinical signs, *i.e.*, less ataxia and reduced choreoathetosis,<sup>95</sup> but it was unclear which compound was potentially responsible for the observed effect.

Lastly, there is a report of one aceruloplasminaemia patient who was administered desferrioxamine. This 52 year-old female patient, homozygous for the cG848C mutation in exon 5 of the Cp gene, presented with diabetes

mellitus, mild anaemia, retinal degeneration, and a range of neurological symptoms. A MRI scan showed pronounced hypointensity signals in the bilateral dentate nucleus, red nucleus, substantia nigra and basal ganglia. Administration of desferrioxamine, 500 mg in 5% glucose by intravenous infusion once per week for 4 years, although not improving her anaemia or other clinical parameters, showed interesting changes in the iron concentration in different brain regions before, and 4 years after, desferrioxamine treatment, with decreases in the iron content of substantia nigra and caudate nucleus of 25–30% with smaller changes in other regions. Such results clearly demonstrated that desferrioxamine is able to cross the blood brain barrier and induce changes in specific brain regions.<sup>96</sup> Such results would indicate that high doses of the chelators need to be administered for a considerable time to remove such iron in the brain of aceruloplasminaemic patients.

### 5.7.1.2 Neuroferritinopathy

A rare monogenic autosomal dominant disorder, where there is a nucleotide insertion in the ferritin light chain (*FTL*) polypeptide gene, causes mutations in the gene encoding the L chain ferritin, *FtL*. An insertion of adenine in the *FTL* gene was initially identified which has now been extended to a further 6 other alterations.<sup>97</sup> Changes in exon 4 of the *FTL* gene result in alterations of helix E of the *FtL* which determines a change in the C-terminal part of the protein. In addition, a mis-sense mutation causing A96T substitution on helix C may also be a causative agent of the disease.<sup>97</sup> Such changes induce substantial protein conformational changes localized at the 4-fold pore of ferritin, and reduce physical stability of the protein such that there is a greater propensity of ferritin to precipitation induced by iron. Aggregates of ferritin are present in the cerebral cortex, putamen, globus pallidus and thalamus (Figure 5.5), as well as in glial cells (reviewed in ref. 97). Structural evaluation of the mutations has shown that the mutated L chain overlaps exactly with wild type as far as glycine 157 while the downstream portion of the amino acid sequence has not been resolved, indicating that it is the final part of the chain that is unstructured.<sup>98</sup> There is no disease-modifying treatment for neuroferritinopathy but benzodiazepines and botulinum toxin may alleviate dystonia while tetrabenazine may relieve chorea and facial tics. It would appear that there is no role for iron chelation in this disease.<sup>99</sup>

### 5.7.1.3 Pantothenate Kinase-Associated Neurodegeneration

Pantothenate kinase-associated neurodegeneration, PKAN, occurs in childhood or in atypical cases during adolescence. Iron overload in PKAN is thought to be secondary to cysteine accumulation, cysteine binding iron to form a complex, which is as a result of the underlying genetic enzymatic defect in the PKAN isoform, present particularly within the basal ganglia (PANK2). In normal circumstances PANK2 generates phosphopantothenate and then condenses with cysteine in the coenzyme A synthesis pathway. This was the first neurodegenerative disease shown to be associated with a

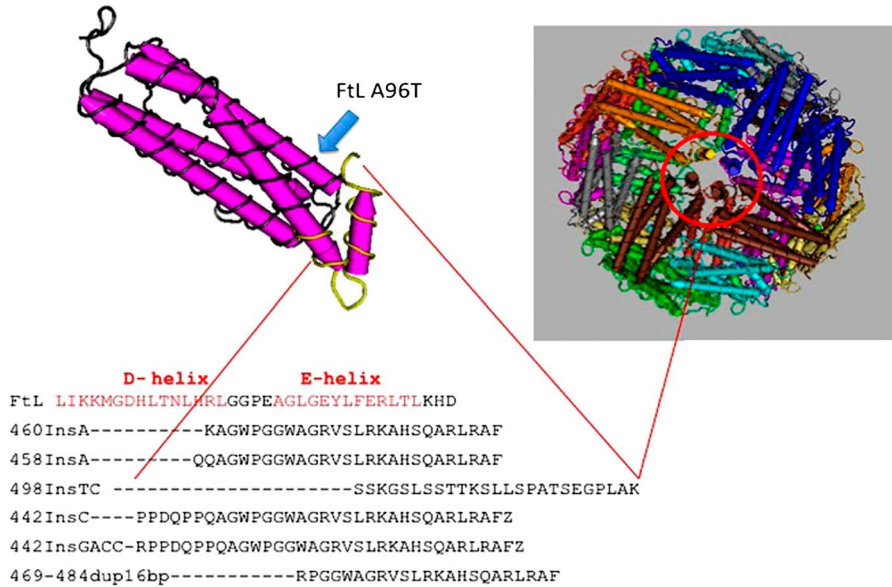


**Figure 5.5** Pile-up of the C-terminus amino acid sequences of L-ferritin and the mutants causing neuroferritinopathy. All mutations, localized in the exon 4 of *FTL*, are nucleotide insertions that cause large alterations of the C-terminal region of the subunit. This peptide portion forms the E-helix region, which is involved in the formation of the hydrophobic channel of the ferritin shell. Position of the A96T mutation is indicated by a blue arrow along the C-helix. Reproduced from ref. 97 under the terms of the *Creative Commons Attribution License (CC BY)*: <http://creativecommons.org/licenses/by/3.0/>.

mutation in a specific gene—pantothenate kinase 2 (PanK2). MRI analysis of the brains of such patients shows a specific pattern—‘the eye of the tiger’—at T<sub>2</sub>\* weighted MR images which corresponds to bilateral areas of hypointensity in the medial globus pallidus with central spots of hyperintensity<sup>100</sup> (Figure 5.6). The ‘eye of the tiger’ is characterized by a T<sub>2</sub> hyperintense core surrounded by T<sub>2</sub> hypointensity indicating pallidal iron deposition. A marked astrogliosis, microglial activation and overall parenchymal rarefaction were observed within the medial globus pallidus. The specific mechanism(s) by which defective pantothenate kinase 2 leads to neuronal degeneration, with the formation of neuroaxonal spheroids and iron deposition is(are) still unclear. Iron accumulation is present in the globus pallidus.

Variable results have been reported for chelation therapy in such patients. In one small study of PKAN patients, desferrioxamine (250 mg day<sup>-1</sup>) was administered by intramuscular injection for 6 months,<sup>101</sup> but no improvement in clinical symptoms was noted. However, in another study where deferiprone was administered (15 mg kg<sup>-1</sup>, twice daily) a modest clinical improvement was seen in two out of three patients with PKAN.<sup>102</sup> Lastly, some modest improvement was evident when oral deferiprone was combined with intrathecal baclofen in one PKAN patient.<sup>103</sup> The results of the

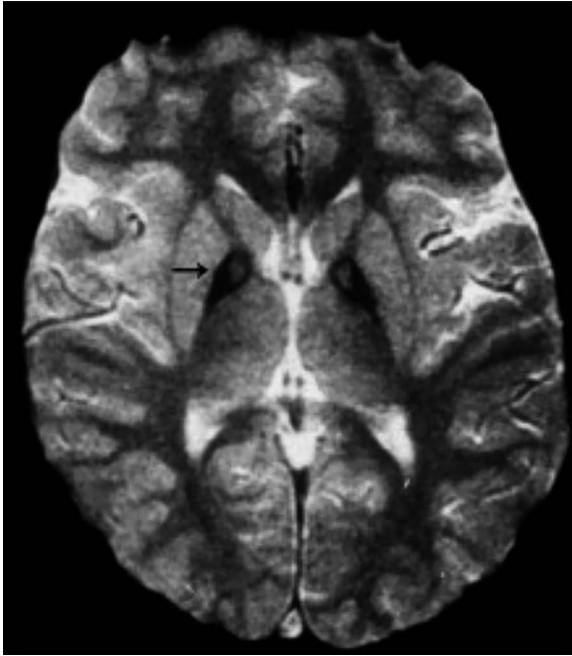


**Figure 5.6** Brain MRI of subject with pantothenate kinase 2-associated neurodegeneration (PKAN). T2\*-weighted echo-planar sequence demonstrates characteristic “eye-of-the-tiger” sign in the globus pallidus (arrow).<sup>111</sup> Reproduced from *Biochimica et Biophysica Acta (BBA) – Molecular Basis of Disease*, 1822, Hyman M. Schipper, Neurodegeneration with brain iron accumulation — Clinical syndromes and neuroimaging, 350–360, Copyright 2012 with permission from Elsevier.

first phase 2 pilot open trial of deferiprone in PKAN patients assessed the clinical and radiological effects of the oral iron chelator deferiprone at a dose of  $25 \text{ mg kg}^{-1} \text{ day}^{-1}$  over a 6 month period.<sup>104</sup> Of nine patients who completed the study, six had classic and three had atypical disease. Median disease duration was 11 years. No serious adverse effects were noted from the use of deferiprone. A significant (median 30%) reduction in globus pallidus iron content was observed, from 15–61%, although no clinical benefit, as rated on the Burke–Fahn–Marsden Rating Scale and SF-36 scale was reported. This may be due to the relatively short treatment duration, the dose and mode of deferiprone administration, or perhaps due to the fact that the long disease duration of neuronal damage was too advanced to allow a rescue of function.

#### 5.7.1.4 Huntington's Disease

Huntington's disease (HD) is a genetic disorder caused by a defect on chromosome 4 in which a CAG repeat in exon 1 of the gene for huntingtin (Htt) is present many more times than in unaffected individuals, *i.e.*, 36–120 repeats *vs.*

10–28 repeats, respectively. Mutant Htt induces a selective loss of neurons in the basal ganglia. Mitochondrial dysfunction is often associated with the pathogenesis of HD, *i.e.*, impaired mitochondrial ATP synthesis and deficits in the activity of complexes I, II and III, particularly in advanced disease. The exact nature and causes of mitochondrial dysfunction in HD remain unknown. Several studies have determined that mutant Htt physically associates with mitochondria. Post-mortem brain tissue from HD patients shows an increase in the expression of mitochondrial fission proteins, Drp1 and Fis1, and decreased expression of fusion proteins, mitofusin and OPA1. In addition, wild type Htt interacts with Drp1 increasing its enzymatic activity. Mutant Htt can impair mitochondrial function *via* several mechanisms. It will bind to Drp1 more tightly than wild type Htt, such that the balance of mitochondrial fission–fusion dynamics will be in favour of fission. There may be decreased axonal transport of mitochondria, and by binding to peroxisome proliferator-activated receptor coactivator-1 $\alpha$  (PGC-1 $\alpha$ ) protein, its transcription factor activity will be reduced, resulting in the reduced expression of PGC-1 $\alpha$  target genes. Such genes are involved in mitochondrial biogenesis and antioxidant defences. Overall ATP production will be reduced resulting in neuronal dysfunction followed by neuron death.

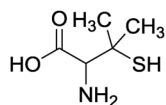
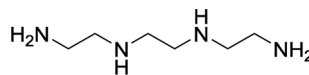
Iron accumulation does not seem to be an initial event in HD but may be an early indicator of a pathological cascade. Iron accumulates in the basal ganglia of both HD patients and murine models of HD, particularly in myelinating oligodendrocytes and in microglia. The release of inflammatory cytokines from activated microglia will result in premature myelin breakdown and subsequent remyelination as well as increasing iron levels which may contribute to HD pathogenesis.

Htt appears to be required for transferrin receptor 1 (TfR1)-mediated iron uptake. Because erythroid cells acquire iron *via* transferrin endocytosis, this might indicate a role for Htt in supporting iron uptake by transferrin-mediated endocytosis. Therefore, perturbation of the normal role of Htt in iron uptake by polyglutamine tract expansion may contribute to the iron accumulation that is observed in HD pathology.<sup>105</sup> Accumulation of copper in HD brain could result in interaction with low affinity binding sites on diverse biomolecules.

### 5.7.1.5 Wilson's Disease

Wilson's disease is a chronic disease affecting both brain and liver with progressive neurological dysfunction due to a disturbance of copper metabolism. It is characterised by progressive degeneration of the basal ganglia of the brain. Wilson disease is inherited as an autosomal recessive disorder with the affected gene located on Chromosome 13. The gene locus encodes a copper-transporting P-type ATPase which permits the efficient excretion of copper in the bile. The hepatocyte plays a key role in copper homeostasis both as a storage site (mostly in metallothioneins) and as the determinate which regulates biliary excretion, the only physiological route for copper excretion. In normal circumstances ATP7B regulates cytosol copper levels by transporting copper from the cytosol into the lumen of the *trans*-Golgi network where

it is incorporated into secreted copper-dependent enzymes such as ceruloplasmin. The mutation in the ATP7B gene induces an impaired functioning of a Cu-ATPase, causing impaired Cu detoxification in the liver, resulting in copper overload in the body. Such copper in excess will promote cytotoxic reactions leading to oxidative stress. D-Penicillamine **14** is currently the most widely used treatment worldwide<sup>106</sup> while triethylenetetramine **15**, and the powerful copper complexing agent tetrathiomolybdate (TTM, **16**) is available only in the USA. All show therapeutic efficacy.<sup>28</sup> TTM forms a stable complex with copper that is unavailable for cellular uptake, and when administered with food, binds copper preventing its absorption and leading to increased faecal excretion.<sup>28</sup> Supplementation with zinc salts, such as zinc acetate, has also shown efficacy, the zinc salts stimulating metallothionein synthesis in the enterocytes which have a higher capacity to chelate dietary Cu and therefore limit Cu-transfer into the portal circulation (reviewed in ref. 106). This medication is mainly used to treat pre-symptomatic patients, such as siblings known to have the genetic disease prior to manifesting any visible symptoms. Chelation is necessary for life and is not necessarily efficient in many cases. The development of a new generation of copper chelators is urgently needed.

Penicillamine (**14**)Triethylenetetramine (**15**)Tetrathiomolybdate (**16**)

## 5.8 Macular Degeneration

Age-related macular degeneration is the most common cause of irreversible vision loss in the elderly population throughout the world. There is evidence to show that iron may contribute to the pathology of this degeneration of the retina. Iron levels are higher in the retina of such subjects by comparison to age-matched controls, which could indicate that iron-mediated oxidative stress is contributing to retinal degeneration.<sup>107</sup> Retinal iron accumulation is present in aceruloplasminaemic patients (due to the lack of ferroxidase activity),<sup>108</sup> as well as in ceruloplasmin and hephaestin double knockout mice.<sup>109</sup> Cultured retinal pigment epithelial (ARPE-19) cells and ceruloplasmin/hephaestin double knockout mice were administered deferiprone at doses of 60  $\mu\text{M}$ , or 1  $\text{mg mL}^{-1}$  in their drinking water, respectively, which induced decreases in retinal iron levels as well as oxidative stress.<sup>110</sup> Such results indicate that deferiprone could provide protection against retinal and retinal pigment epithelial degeneration and is worthy of investigation in further clinical studies.

## 5.9 Conclusion and Perspectives

It is only during the last decade that the use of chelators to treat a range of neurological diseases (where there is an increase of metal ions in specific brain regions) has been accepted. Indeed, clinical trials which have investigated their safety, tolerance and efficacy have shown positive results in the main. However, such drugs have the disadvantage that they will be distributed throughout the body and show poor specificity towards the pathological site and may induce unwanted side-effects. Therefore, an ability to target the chelator to the actual site in the brain where the excess metal ion has accumulated presents a challenge for the design of future chelators. Combination therapy where anti-inflammatory agents, monoamine oxidase inhibitors as well as chelators are administered to the patient maybe the way forward for the treatment of neurodegenerative diseases.

### Abbreviations

<b>AD</b>	Alzheimer's disease
<b>BBB</b>	Blood-brain barrier
<b>BDNF</b>	Brain-derived neurotrophic factor
<b>bFGF</b>	Basic fibroblast growth factor
<b>CNS</b>	Central nervous system
<b>EAE</b>	Experimental autoimmune encephalomyelitis
<b>ER</b>	Endoplasmic reticulum
<b>GDNF</b>	Glial cell line-derived neurotrophic factor
<b>HD</b>	Huntington's disease
<b>ICH</b>	Intracerebral haemorrhage
<b>MR(MRI)</b>	Magnetic resonance (imaging)
<b>MS</b>	Multiple sclerosis
<b>NBIA</b>	Neurodegeneration with brain iron accumulation
<b>PD</b>	Parkinson's disease
<b>PKAN</b>	Pantothenate kinase-2-associated neurodegeneration
<b>RE</b>	Reticular endothelial cells
<b>SN</b>	Substantia nigra
<b>Svz</b>	Sub-ventricular zone
<b>VEGF</b>	Vascular endothelial growth factor

### References

1. R. R. Crichton, *Iron Metabolism. From molecular Mechanisms to Clinical Consequences*, J. Wiley and Sons Ltd, Chichester UK, 3rd edn, 2015, pp. 1–461.
2. R. J. Ward, F. A. Zucca, J. H. Duyn, R. R. Crichton and L. Zecca, *Lancet Neurol.*, 2014, **13**, 1045.
3. W. A. Jefferies, M. R. Brandon, S. V. Hunt, A. F. Williams, K. C. Gatter and D. Y. Masom, *Nature*, 1984, **312**, 162.
4. D. F. Leitner and J. R. Connor, *Biochim. Biophys. Acta*, 2012, **1820**, 393.

5. M. W. Boserup, J. Lichota, D. Haile and T. Moos, *Biometals*, 2011, **24**, 357.
6. N. J. Abbott, L. Ronnback and E. Hansson, *Nat. Rev. Neurosci.*, 2006, **7**, 41.
7. R. Dringen, G. M. Bishop, M. Koeppe, T. N. Dang and S. R. Robinson, *Neurochem. Res.*, 2007, **32**, 1884.
8. J. Xu and E. A. Ling, *J. Anat.*, 1994, **184**, 227.
9. S. Y. Jeong and S. David, *J. Biol. Chem.*, 2003, **278**, 27144.
10. L. J. Wu, A. G. Leenders, S. Cooperman, E. Meyron-Holtz, S. Smith, W. Land, R. Y. Tsai, U. V. Berger, Z. H. Sheng and T. A. Rouault, *Brain Res.*, 2004, **1001**, 108.
11. E. M. Haacke, N. Y. Cheng, M. J. House, Q. Liu, R. J. Ogg, A. Khan, M. Ayaz, W. Kirsch and A. Obenaus, *Magn. Reson. Imaging*, 2005, **23**, 1.
12. S. Aoki, Y. Okada, K. Nishimura, A. J. Barkovich, B. O. Kios, R. C. Brasch and D. Norman, *Radiology*, 1989, **172**, 381.
13. X. Xu, Q. Wang and M. Zhang, *Neuroimage*, 2008, **40**, 35.
14. V. Adisetiyo, J. H. Jensen, A. Ramani, A. Tabesh, A. Di Martino, E. Fieremans, F. X. Castellanos and J. A. Helpm, *J. Magn. Reson. Imaging*, 2012, **36**, 322.
15. L. Zecca, F. A. Zucca, M. Toscani, F. Adorni, G. Giaveri and E. Rizzio, *et al.*, *J. Radioanal. Nucl. Chem.*, 2005, **263**, 733.
16. B. Bilgic, A. Pfefferbaum, T. Rohlfing, E. V. Sullivan and E. Adalsteinsson, *Neuroimage*, 2012, **59**, 2625.
17. D. Aquino, A. Bizzi, M. Grisoli, B. Garavaglia, M. G. Bruzzone, N. Nardocci, M. Savoiaro and L. Chiapparini, *Radiology*, 2009, **252**, 165.
18. G. Hebbrecht, W. Maenhaut and J. D. Reuck, *Nucl. Instrum. Methods Phys. Res., Sect. B*, 1999, **150**, 208.
19. L. Zecca, A. Stroppolo, A. Gatti, D. Tampellini, M. Toscani, M. Gallorni, P. Arosio, P. Santambrogio, R. G. Fariello, E. Karatekin, M. H. Kleinman, N. Turro, O. Homykievicz and F. A. Zucca, *Proc. Natl. Acad. Sci. U. S. A.*, 2004, **101**, 9843.
20. F. A. Zucca, C. Bellei, S. Giannelli, M. R. Terreni, M. Gallorini, G. Rizzio, G. Pezzoli, A. Albertini and L. Zecca, *J. Neural Transm.*, 2012, **113**, 757.
21. J. Telianidis, Y. H. Hung, S. Materia and S. L. Fontaine, *Front. Aging. Neurosci.*, 2013, **5**, 44.
22. S. Fu, W. Jiang and W. Zheng, *Front. Mol. Neurosci.*, 2015, **8**, 22.
23. K. M. Massie, V. R. Aiewllo and A. A. Iodice, *Mech. Ageing Dev.*, 1979, **10**, 93.
24. L. M. Wang, J. S. Becker, Q. Wu, M. F. Oliveira, F. A. Bozza, A. L. Schwager, J. M. Hoffman and K. A. Morton, *Metallomics*, 2010, **2**, 348.
25. P. Ramos, A. Santos, N. R. Pinto, R. Mendes, T. Magalhaes and A. Almeida, *Biol. Trace Elem. Res.*, 2014, **161**, 190.
26. A. Takeda, H. Fujii, T. Minamino and H. Tamano, *J. Neurosci. Res.*, 2014, **92**, 819.
27. P. A. Adlard, A. Sedjahtera, L. Gunawan, L. Bray, D. Hare, J. Lear, P. Doble, A. I. Bush, D. I. Finkelstein and R. A. Cherny, *Aging Cell*, 2014, **13**, 351.
28. R. R. Crichton and R. J. Ward, *Metal-based Neurodegeneration*, J. Wiley and Sons Ltd, Chichester, UK, 2nd edn, 2013.

29. B. O. Popescu, E. C. Toescu, L. M. Popescu, O. Bajenaru, D. F. Muresanu, M. Schultzberg and N. Bogdanovic, *J. Neurol. Sci.*, 2009, **283**, 99.
30. A. J. Farrall and J. M. Wardlaw, *Neurobiol. Aging*, 2009, **30**, 337.
31. H. J. Zapata and V. J. Quagliarello, *J. Am. Geriatr. Soc.*, 2015, **63**, 776.
32. R. Caesar, V. Tremaroli, P. Kpvtcheva-Datchary, P. D. Cani and F. Backhed, *Cell Metab.*, 2015, **22**, 658.
33. M. Shachar, N. Kahana, V. Kampel, A. Warshawsky and M. B. Youdim, *Neuropharmacol.*, 2004, **46**, 254.
34. L. R. Hanson, A. Roeytenberg, P. M. Martinez, V. G. Coppes, D. C. Sweet, R. J. Rao, D. L. Marti, J. D. Hoekman, R. B. Matthews, W. H. Frey and S. S. Panter, *J. Pharmacol. Exp. Ther.*, 2009, **330**, 679.
35. D. T. Dexter, R. J. Ward, A. Florence, P. Jenner and R. R. Crichton, *Biochem. Pharmacol.*, 1999, **58**, 151.
36. R. J. Ward, D. Dexter, A. Florence, F. Aouad, R. Hider, P. Jenner and R. R. Crichton, *Biochem. Pharmacol.*, 1995, **49**, 1821.
37. D. T. Dexter, F. R. Wells, F. Agid, Y. Agid, A. J. Lees, P. Jenner and C. D. Marsden, *Lancet*, 1987, **2**, 1219.
38. D. T. Dexter, F. R. Wells, F. Agid, Y. Agid, A. J. Lees, P. Jenner and C. D. Marsden, *J. Neurochem.*, 1989, **52**, 1830.
39. K. Jellinger, E. Kienzl, G. Rumpelmair, P. Riederer, H. Stachelberger, D. Ben-Shachar and M. B. H. Youdim, *J. Neurochem.*, 1992, **59**, 1168.
40. D. Kozirowski, A. Friedman, P. Arosio, P. Santambrogio and D. Dziejulska, *Parkinsonism Relat. Disord.*, 2007, **13**, 214.
41. M. Wieler, M. Gee and W. R. Martin, *Parkinsonism Relat. Disord.*, 2015, **211**, 79.
42. D. T. Dexter, A. Cavayon, F. Javoy-Agid, Y. Agid, S. E. Daniel, A. J. Lees, P. Jenner and C. D. Marsden, *Brain*, 1991, **114**, 1953.
43. J. Wang, M. Bi and J. Xie, *Cell. Mol. Neurobiol.*, 2015, **35**, 661.
44. R. R. Crichton, D. T. Dexter and R. J. Ward, *J. Neural Transm.*, 2011, **118**, 301.
45. B. A. Fancheux, M. E. Martin, C. Beaumont, S. Hunot, J. J. Hauw, Y. Agid and E. C. Hirsch, *J. Neurochem.*, 2002, **83**, 320.
46. D. T. Dexter, S. A. Statton, C. Whitmore, W. Freinbichler, P. Weinberger, K. F. Tipton, L. Della Corte, R. J. Ward and R. R. Crichton, *J. Neural Transm.*, 2011, **118**, 223.
47. A. Kwiatkowski, G. Ryckewaert, P. Jissendi Tchofo, C. Moreau, I. Vuillauma, P. F. Chinnery, A. Destée, L. Defebvre and D. Devos, *Parkinsonism Relat. Disord.*, 2010, **18**, 110.
48. D. Devos, C. Moreau, J. C. Devedjian, J. Kluza, C. Laloux, A. Jonneaux, G. Ryckewaert, G. Garçon, N. Rouaix, A. Duhamel, P. Jissendi, K. Dujardin, F. Auger, L. Ravasi, L. Hopes, G. Grolez, W. Firdaus, B. Sablonnière, I. Strubi-Vuillaume, N. Zahr, A. Destée, J. C. Corvol, D. E. Pörtl, M. Leist, C. Rose, L. Defebvre, P. Marchetti, Z. I. Cabantchik and R. Bordet, *Antioxid. Redox Signaling*, 2013, **21**, 195.
49. A. Martin-Bastida, R. J. Ward, R. Newbould, P. Piccini, D. Sharp, C. Kabba, M. C. Patel, M. Spino, J. Connelly, T. Fernando, R. R. Crichton and D. T. Dexter, *Nat Commun*, 2016, in press.

50. G. Grolez, C. Moreau, B. Sablonnière, G. Garçon, J. C. Devedjian, S. Meguig, P. Gelé, C. Delmaire, R. Bordet, L. Defebvre, Z. I. Cabantchik and D. Devos, *BMC Neurol.*, 2015, **15**, 74.
51. C. A. Perez, Y. Tong and M. Gu, *Curr. Bioact. Compd.*, 2008, **4**, 150.
52. D. Kaur, F. Yantiri, S. Rajagopalan, J. Kumar, J. Q. Mo, R. Boonplueang, V. Viswanath, R. Jacobs, L. Yang, M. F. Beal, D. DiMonte, I. Volitaskis, L. Ellerby, R. A. Cherny, A. I. Bush and J. K. Andersen, *Neuron*, 2003, **37**, 899.
53. S. R. Bareggi and U. Cornelli, *CNS Neurosci.*, 2012, **18**, 41.
54. Y. Levites, O. Weinreb, G. Maor, M. B. H. Youdim and S. Mandel, *J. Neurochem.*, 2001, **78**, 1073.
55. B. Álvarez-Pérez, J. Homs, M. Bosch-Mola, T. Puig, F. Reina, E. Verdú and P. Boadas-Vaello, *Eur. J. Pain*, 2016, **20**, 341.
56. D. Mechlovich, T. Amit, S. A. Mandel, O. Bar-Am, K. Bloch, P. Vardi and M. B. Youdim, *J. Pharmacol. Exp. Ther.*, 2010, **333**, 874.
57. J. A. Duce and A. I. Bush, *Prog. Neurobiol.*, 2010, **92**, 1.
58. C. Exley, E. House, A. Polwart and M. M. Esiri, *J. Alzheimers Dis.*, 2012, **31**, 725.
59. S. Ayton, P. Lei and A. I. Bush, *Free Radical Biol. Med.*, 2012, **62**, 76.
60. C. Quintana, S. Bellefgh, J. Y. Laval, J. L. Guerguin-Kern, T. D. Wu, J. Avila, I. Ferrer, R. Arranz and C. Patino, *J. Struct. Biol.*, 2006, **153**, 42.
61. G. Bartzokis, *Neurobiol. Aging.*, 2004, **25**, 5.
62. K. J. Robson, D. H. Lehmann, V. L. Wimhurst, K. J. Livesey, M. Combrinck, A. T. Merryweather-Clarke, D. R. Warden and A. D. Smith, *J. Med. Genet.*, 2004, **41**, 261.
63. A. A. Raha, R. A. Vaisnav, R. P. RA Friedland, A. Bomford and R. Raha-Chowdhury, *Acta Neuropathol. Commun.*, 2013, **1**, 55.
64. D. R. McLachlan, W. L. Smith and T. P. Kruck, *Ther. Drug Monit.*, 1993, **15**, 602.
65. L. Reznichenko, T. Amit, H. Zheng, Y. Avramovich-Tirosh, M. B. Youdim, O. Weinreb and S. Mandel, *J. Neurochem.*, 2006, **97**, 527.
66. Y. Avramovich-Tirosh, T. Amit, O. Bar-Am, H. Zheng, M. Fridkin and M. B. Youdim, *J. Neurochem.*, 2007, **100**, 490.
67. J. T. Rogers, J. D. Randall, C. M. Cahill, P. S. Eder, X. Huang, H. Gunshin, L. Leiter, J. McPhee, S. S. Sarang, T. Utsuki, N. H. Greig, D. K. Lahiri, R. E. Tanzi, A. I. Bush, T. Giordano and S. R. Gullans, *J. Biol. Chem.*, 2002, **277**, 45518.
68. G. Kamalinia, F. Khodaghali, F. Atyabi, M. Amini, F. Shaerzadeh, M. Sharifzadeh and R. Dinarvand, *Mol. Pharmaceutics*, 2013, **10**, 4418.
69. A. Robert, Y. Liu, M. Nguyen and B. Meurnier, *Acc. Chem. Res.*, 2015, **48**, 1332.
70. R. A. Cherny, C. S. Atwood, M. E. Xilinas, D. N. Gray, W. D. Jones, C. A. McLean, K. J. Barnham, I. Volitakis, F. W. Fraser, Y. Kim, X. Huang, L. E. Goldstein, R. D. Moir, J. T. Lim, K. Beyreuther, H. Zheng, R. E. Tanzi, C. L. Masters and A. I. Bush, *Neuron*, 2001, **30**, 665.
71. C. W. Ritchie, A. I. Bush, A. Mackinnon, S. Macfarlane, M. Mastwyk, L. MacGregor, L. Kiers, R. Cherny, Q. X. Li, A. Tammer, D. Carrington,

- C. Mavros, I. Volitakis, M. Xilinas, D. Ames, S. Davis, K. Beyreuther, R. E. Tanzi and C. L. Masters, *Arch. Neurol.*, 2003, **60**, 1685.
72. C. Li, J. Wang and B. Zhou, *J. Alzheimers Dis.*, 2010, **21**, 1249.
73. P. A. Adlard, R. A. Cherny, D. I. Finkelstein, E. Gautier, E. Robb, M. Cortes, I. Volitakis, X. Liu, J. P. Smith, K. Perez, K. Loughton, Q. X. Li, S. A. Charman, J. A. Nicolazzo, S. Wilkins, K. deleva, T. Lynch, G. Kok, C. W. Richie, R. E. Tanzi, R. Cappai, C. L. Masters, K. J. Barnham and A. I. Bush, *Neuron*, 2008, **59**, 43.
74. T. M. Ryan, B. R. Roberts, G. McColl, D. [J. Hare, P. A. Doble, Q. X. Li, M. Lind, A. M. Roberts, H. D. Mertens, N. Kirby, C. L. Pham, M. G. Hunds, P. A. Adlard, K. J. Barnham, C. C. Curtain and C. L. Masters, *J. Neurosci.*, 2015, **35**, 2871.
75. M. Nguyen, A. Robert, A. Sournia-Saquet, L. Vendier and B. Meurnier, *Chem.*, 2014, **20**, 6771.
76. J. Y. Lee, J. E. Friedman, I. Angel, A. Kozak and J. Y. Koh, *Neurobiol. Aging.*, 2004, **25**, 1315.
77. A. L. Phinney, B. Drisaldi, S. D. Schmidt, S. Lugowski, V. Coronado, Y. Liang, P. Horne, J. Yang, J. Sekoulidis, J. Coomaraswamy, M. A. Chishti, D. W. Cox, P. M. Mathews, R. A. Nixon, G. A. Carlson, P. St George-Hyslop and D. Westaway, *Proc. Natl. Acad. Sci. U. S. A.*, 2003, **100**, 14193.
78. C. Corona, F. Masciopinto, E. Silvestri, A. D. Viscovo, R. Lattanzio, R. L. Sorda, D. Ciavardelli, F. Goglia, M. Piantelli, L. M. Canzoniero and S. L. Sensi, *Cell Death Dis.*, 2010, **1**, e91.
79. A. Nunes, S. M. Marques, C. Quintanova, D. F. Silva, S. M. Cardoso, S. Chaves and M. A. Santos, *Dalton Trans.*, 2013, **42**, 6058.
80. L. Huang, C. Lu, Y. Sun, F. Mao, Z. Luo, T. Su, H. Jiang, W. Shan and X. Li, *J. Med. Chem.*, 2012, **55**, 8483.
81. M. Levy and R. H. Llinas, *AJNR Am. J. Neuroradiol.*, 2011, **32**, E1–E2.
82. M. Levy and R. Llinas, *Stroke*, 2012, **43**, 120.
83. M. Levy and R. Llinas, *AJNR Am. J. Neuroradiol.*, 2012, **33**, E99.
84. J. M. Stankiewicz, M. Neema and A. Ceccarelli, *Neurobiol. Aging*, 2014, **35**, S51eS58.
85. S. G. Lynch, T. Fonseca and S. M. Levine, *Cell. Mol. Biol.*, 2000, **46**, 865e869.
86. M. Pandolfo, *J. Child. Neurol.*, 2012, **27**, 1204.
87. N. Boddaert, K. H. L. Quan Sang, A. Rotig, A. Leroy-Willig, S. Gallet, F. Brunelle, D. Sidi, J. C. Thalabard, A. Munnich and Z. I. Cabantchik, *Blood*, 2007, **110**, 401.
88. O. Kakhlon, H. Manning, W. Breuer, N. Melamed-Book, C. Lu, G. Cortopassi, A. Munnich and Z. I. Cabantchik, *Blood*, 2008, **112**, 5219.
89. D. Velasco-Sánchez, A. Aracil, R. Montero, A. Mas, L. Jiménez, M. O'Callaghan, M. Tondo, A. Capdevila, J. Blanch, R. Artuch and M. Pineda, *Cerebellum*, 2011, **10**, 1.
90. S. Kono, H. Suzuki, T. Oda, K. Shirakawa, Y. Shirakawa, Y. Takahashi, M. Kitagawa and H. Miyajima, *J. Hepatol.*, 2007, **47**, 844.

91. O. Loreal, B. Turlin, C. Pigeon, C. Moisan, A. Ropert, P. Morice, Y. Gandon, A. M. Louanolle, M. Verin, R. C. Hider, K. Yoshida and P. Brissot, *J. Hepatol.*, 2002, **36**, 851.
92. M. McNeill, J. Pandolfo, H. Kuhn, H. Shang and H. Miyajima, *Eur. Neurol.*, 2008, **60**, 200.
93. J. Kuhn, H. Bewermeyer, H. Miyajima, Y. Takahashi, K. F. Kuhn and T. U. Hoogenraad, *Brain Dev.*, 2007, **29**, 450.
94. M. Grisoli, A. Piperno, L. Chiapparini, R. Mariani and M. Savoiaro, *AJNR Am. J. Neuroradiol.*, 2005, **26**, 657.
95. E. Finkenstedt, E. Wolf, B. I. Hofner, S. Gasser, R. Bosch, M. Bakry, C. Creus, M. Kremser, M. Schoecke, P. Theurl, M. Moser, G. Schranz, W. Bonn, W. Poewe, W. Vogel, A. R. Janecke and H. Zoller, *J. Hepatol.*, 2010, **53**, 1101.
96. H. Miyajima, Y. Takahashi, T. Kamata, H. Shimizu, N. Sakai and J. D. Gitlin, *Ann. Neurol.*, 1997, **41**, 404.
97. P.-L. Pan, H.-H. Tang, Q. Chen, W. Song and H.-F. Shang, *Mov. Disord.*, 2011, **26**, 2142.
98. S. Levi and D. Finazzi, *Front. Pharmacol.*, 2014, **5**, 99.
99. M. A. Baraibar, B. B. Muhoberac, H. J. Garringer, T. D. Hurley and R. Vidal, *J. Biol. Chem.*, 2010, **285**, 1950.
100. A. McNeill and P. F. Chinnery, *Curr. Drug Targets.*, 2012, **13**, 1200.
101. S. J. Hayflick, *Curr. Opin. Pediatr.*, 2003, **15**, 572.
102. F. Gallyas and S. Környey, *Arch. Psychiatr. Nervenkrankh.*, 1968, **212**, 33.
103. G. Abbruzzese, G. Cossu, M. Balocco, R. Marchese, D. Murgia, M. Melis, R. Galanello, S. Barella, G. Matta, U. Ruffinengo, U. Bonuccelli and G. I. Forni, *Haematologica*, 2011, **96**, 1708.
104. N. R. Pratini, N. Sweeters, E. Vichinsky and J. A. Neufeld, *Am. J. Phys. Med. Rehabil.*, 2013, **92**, 728.
105. G. Zorzi, F. Zibordi, L. Chiapparini, E. Bertini, L. Russo, A. Piga, F. Longo, B. Garavaglia, D. Aquino, M. Savoiaro, A. Solari and N. Nardocci, *Mov. Disord.*, 2011, **26**, 1756.
106. N. P. Mena, O. García-Beltrán, F. Lourido, P. J. Urrutia, R. Mena, V. Castro-Castillo, B. K. Cassals and M. T. Núñez, *Biochem. Biophys. Res. Commun.*, 2015, **463**, 78.
107. P. Delangle and E. Mintz, *Dalton Trans.*, 2012, **41**, 6359.
108. R. W. Wong, D. C. Richa, P. Hahn, W. R. Green and J. L. Dunaief, *Retina.*, 2007, **27**, 997.
109. J. L. Dunaief, C. Richa, E. P. Franks, R. L. Schaltze, T. S. Aleman, J. F. Schenck, E. A. Zimmerman and D. G. Brooks, *Ophthalmol.*, 2005, **112**, 1062.
110. P. Hahn, Y. Qian, T. Dentchev, L. Chen, J. Beard, Z. L. Harris and J. L. Dunaief, *Proc. Natl. Acad. Sci. U. S. A.*, 2004, **101**, 13850.
111. M. Hadziahmetovic, Y. Song, N. Wolkow, J. Iacovelli, S. Grieco, J. Lee, A. Lyubarsky, D. Pratico, J. Connelly, M. Spino, Z. L. Harris and J. L. Dunaief, *Invest. Ophthalmol. Visual Sci.*, 2011, **52**, 959.

## CHAPTER 6

# *Chelation of Actinides*

REBECCA J. ABERGEL<sup>a</sup>

<sup>a</sup>Chemical Sciences Division, Lawrence Berkeley National Laboratory,  
One Cyclotron Road, Berkeley, CA 94720, USA

\*E-mail: [rjabergel@lbl.gov](mailto:rjabergel@lbl.gov)

## 6.1 The Medical and Public Health Relevance of Actinide Chelation

The use of actinides in the civilian industry and defense sectors over the past 60 years has resulted in persistent environmental and health issues, since a large inventory of radionuclides, including actinides such as thorium (Th), uranium (U), neptunium (Np), plutonium (Pu), americium (Am) and curium (Cm), are generated and released during these activities.<sup>1</sup> Controlled processing and disposal of wastes from the nuclear fuel cycle are the main source of actinide dissemination. However, significant quantities of these radionuclides have also been dispersed as a consequence of nuclear weapons testing, nuclear power plant accidents, and compromised storage of nuclear materials.<sup>1</sup> In addition, events of the last fifteen years have heightened public concern that actinides may be released as the result of the potential terrorist use of radiological dispersal devices or after a natural disaster affecting nuclear power plants or nuclear material storage sites.<sup>2,3</sup> All isotopes of the 15 elements of the actinide series (atomic numbers 89 through 103, Figure 6.1) are radioactive and have the potential to be harmful; the heaviest members, however, are too unstable to be isolated in quantities larger than a few atoms at a time,<sup>4</sup> and those elements cited above (U, Np, Pu, Am, Cm) are the most

---

RSC Metallobiology Series No. 8

Metal Chelation in Medicine

Edited by Robert Crichton, Roberta J. Ward and Robert C. Hider

© The Royal Society of Chemistry 2017

Published by the Royal Society of Chemistry, [www.rsc.org](http://www.rsc.org)

89 Ac	90 Th	91 Pa	92 U	93 Np	94 Pu	95 Am	96 Cm	97 Bk	98 Cf	99 Es	100 Fm	101 Md	102 No	103 Lr
----------	----------	----------	---------	----------	----------	----------	----------	----------	----------	----------	-----------	-----------	-----------	-----------

**Figure 6.1** The actinide series encompasses the 15 chemical elements with atomic numbers from 89 to 103, actinium to lawrencium.

likely to be encountered. Because of the impending growth of nuclear power and threats of nuclear weapon use, the amount of produced and released radioisotopes is increasing daily,<sup>5</sup> as is the risk of environmental contamination and larger human exposure to actinides. Internalized actinides have, in turn, the potential to induce both radiological and chemical toxicities, leading to serious health effects. In the past few years the challenge of limiting such exposure, contamination, and subsequent deleterious effects has given rise to unprecedented interest in developing therapeutic actinide decorporation agents, as well as cost-effective bioremediation approaches for environmental decontamination.<sup>6,7</sup>

### 6.1.1 Actinide Metabolism and Clinical Course

Contrary to some heavy metals, actinides have no known essential role in the normal biochemical reactions occurring in living organisms, and are a particular hazard due to their ionizing radiation properties.<sup>8–10</sup> Independent of the contamination route (inhalation, ingestion or wound), actinides are absorbed, then transported by the blood prior to deposition in the target organs (bone, liver and kidney), in which they are stored, then slowly and partially excreted through urine and feces. The biokinetics and bioinorganic chemistry of actinides following inhalation, ingestion and injection have been well studied in the past 50 years: models were reviewed and adopted in publications from the International Commission on Radiological Protection (ICRP) and from the U.S.-based National Council on Radiation Protection & Measurements (NCRP).<sup>11–13</sup> Such biokinetic models have been extremely useful in providing guidance for treatment, although they cannot be relied upon to clearly determine whether a chelating agent is conferring benefit at post-exposure time points in humans following internal contamination with actinides.

The actinides are all radioactive, and most of their isotopes decay by alpha particle emission.<sup>4</sup> Once internalized, the actinides are distributed to various tissues with patterns that depend on the chemical and physical form of the contaminant in question. The densely ionizing alpha particles emitted by actinides retained in bone and liver, and in the lungs if inhaled, damage and induce cancer in those tissues, in a dose-dependent manner.<sup>10</sup> Therefore, the tissue distribution of an actinide will determine the pattern of injury observed. Sufficiently high doses will also cause manifestations of acute radiation syndrome in absorption (as in the gastrointestinal tract) or inhalation (as in the pulmonary system) areas.<sup>13,14</sup> Although they belong to the same denomination in the periodic table, elements of the actinide series exhibit very different coordination chemistries affecting their biological behavior and distribution, as described briefly below for selected examples.

Among the four oxidation states of uranium (III, IV, V, VI), the uranyl ion ( $\text{UO}_2^{2+}$ , U(VI)) is the most stable form in aqueous solutions and *in vivo*, and uranyl compounds have therefore been the focus of most pharmacology studies.<sup>8,9</sup> In humans, biokinetic models predict the following distribution of uranium 24 hours after an intake: skeleton 15%, kidneys 17%, other tissues 5% and urine 63%.<sup>12</sup> Renal injury is the primary chemical damage caused by uranium poisoning, and is related to heavy metal toxicity. Nearly all of the long-retained uranium in the body remains in the bones.<sup>9</sup>

In comparison to uranium, much less is known about the coordination chemistry of the transuranic elements, neptunium, plutonium, americium, and curium. The scarcity and high specific activity  $\alpha$ -emission of the common isotopes  $^{237}\text{Np}$ ,  $^{238}\text{Pu}$ ,  $^{241}\text{Am}$ , and  $^{244}\text{Cm}$  have limited the study of their chemical and structural properties. Biological evidence indicates Pu(IV), Am(III), and Cm(III) are the main oxidation states present under physiological conditions, while all three of Np(IV), Np(V) and Np(VI) have been observed in living systems, with Np(V) as the neptunyl dioxocation ( $\text{NpO}_2^+$ ) being the most common.<sup>11,12,15</sup> Both Pu(IV) and Am(III) are linked to Fe(III) transport and storage systems in mammals, which may explain their retention patterns in soft tissue.<sup>9</sup> Although the deposition pattern of Np(IV) is similar to that of Pu(IV) in the liver, the rapid plasma clearance and urinary excretion of Np(V) resemble those of U(VI) and account for the chemical toxicity of Np, as even small fractional kidney deposition may result in renal tubular injury.<sup>9</sup> In contrast to U, one primary target tissue of all three actinides (Np, Pu and Am) is the skeleton. The endosteal bone surfaces are the preferential sites of Pu bone deposition, whereas Am and Np deposit nearly uniformly on all anatomical bone surfaces.<sup>9</sup> The carcinogenicity of Np, Pu and Am results mainly from the radiation damage caused by their retention in the skeleton. The substantial differences in actinide transport and retention in the body are depicted in Figure 6.2, which displays the 24 h excretion and tissue distribution of intravenously injected U(VI), Np(V), Pu(IV) and Am(III) in mice.

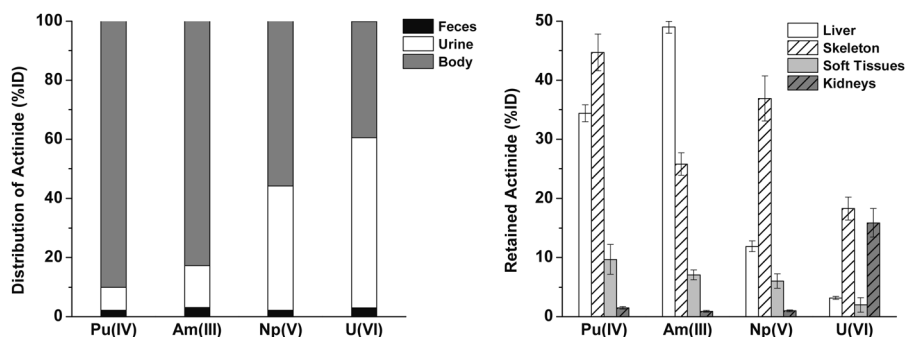


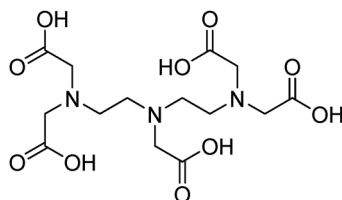
**Figure 6.2** Actinide transport and retention in mice. Excretion (left) and tissue distribution (right) of soluble actinides, as % of injected dose (%ID) in young adult female Swiss Webster mice, 24 hours after intravenous injection (1 ng of  $^{238}\text{Pu}$ , 7 ng of  $^{241}\text{Am}$ , 1.7  $\mu\text{g}$  of  $^{233}\text{U}$ , 4.1  $\mu\text{g}$  of  $^{237}\text{Np}$ ).

## 6.1.2 Current Treatment Recommendations for Actinide Contamination

The currently available treatments mainly vary as a function of the intake pathway, the level of contamination (mass and activity), the chemical and biological speciation of the radioisotope, as well as the intervention time after the incident.<sup>16,17</sup> For contamination by inhalation, which mainly results from internalization of aerosols that display different chemical solubilities, treatments include lung washing and chelation therapy. Such treatments aim at increasing the solubility of the actinides deposited in the human respiratory tract, removing the actinide mechanically, and allowing chelation of the absorbed blood fraction. For contamination by ingestion, treatments include gastric dressing, precipitation, purge and chelation therapy. For wound contamination, several treatments have been used including washing, surgical excision and dressings with additional specific chelating gels, as well as chelation therapy. Over the past fifty years, a great amount of work has been dedicated to developing methods for increasing the natural slow rate of elimination of actinides from the human body by the administration of chelating agents.<sup>16–18</sup> The rationale for chelation therapy is that the agent will chelate the targeted metal and form a stable complex that can easily be excreted, thus reducing both the radiation dose delivered to sensitive cells and the risk of late radiation effects such as cancer. Current chelation treatment recommendations have been reviewed extensively and are only briefly summarized below.<sup>14,16,17,19,20</sup>

The only currently approved chelation drugs designated for the decorporation of the transuranic actinides Pu, Am and Cm are the diethylenetriamine-pentaacetic acid trisodium calcium and trisodium zinc salts,  $\text{CaNa}_3\text{-DTPA}$  and  $\text{ZnNa}_3\text{-DTPA}$  (marketed as Ca-DTPA and Zn-DTPA, respectively) 1.<sup>21</sup> Although both drug products have been used investigationally for over 40 years,<sup>14</sup> the U.S. Food and Drug Administration (FDA) approved the corresponding New Drug Applications from the German manufacturer Hameln Pharmaceuticals GmbH. only recently, in 2004.<sup>21</sup> Ca-DTPA and Zn-DTPA can be administered by nebulizer or intravenously. If the route of internal contamination is through inhalation alone, then nebulized chelation therapy may suffice. If the routes of contamination are multiple (*e.g.*, inhalation and through wounds), then intravenous chelation therapy is preferred. The level of internal contamination and the individual's response to therapy dictate the duration of treatment: levels of internal contamination should be ascertained weekly during chelation therapy to determine when to terminate treatment. Treatment recommendations are based on decorporation efficacy and safety data collected in animals and humans.<sup>14</sup> For the Ca-DTPA product, the label recommended initial human dosage is a single administration of 1 g for adults and adolescents, and 14 mg  $\text{kg}^{-1}$  (not to exceed 1 g) for pediatrics. If prolonged therapy is needed, then Zn-DTPA is recommended at the same dosage.<sup>21</sup> The well-documented Hanford Americium accident<sup>22</sup> is the only human evidence to support the hypothesis that decorporation therapy and resulting acceleration of the natural rate of elimination of the contaminant will reduce the amount of radioactivity in the body, thus reducing the radiation dose received by sensitive tissues and

producing an at least proportional reduction in the risks of induction of serious radiation effects. In the Hanford treatment case, 583 g of DTPA, primarily as Zn-DTPA were administered to the patient over a 4 year period without any observed toxicological effects. It is believed that the aggressive treatment with Ca- and/or Zn-DTPA reduced the liver burden of  $^{241}\text{Am}$  enough to prevent the victim's early death from radiation-induced liver failure.<sup>22</sup>



DTPA 1

### 6.1.3 Limitations of Current Therapies

In contrast to the transuranic elements Pu, Am and Cm, little progress has been made on the decorporation of Np and U. While the results of several studies in laboratory animals have shown that Ca-DTPA was ineffective at promoting Np elimination, independent of the isotope used, the ligand dosage or the mode of administration, Ca-DTPA and Zn-DTPA are still the only recommended substances for Np decorporation, despite some added risk of nephrotoxicity.<sup>23</sup> The substance recommended by the NCRP for U decorporation is sodium bicarbonate, although there may be undesirable side effects such as hypokalaemia and alkalosis.<sup>24</sup> The use of DTPA salts is contraindicated for treatment of U contamination because of the added risk of renal damage.<sup>23,24</sup> Finally, the approved chelation treatments, Ca-DTPA and Zn-DTPA, can only be administered intravenously or through a nebulizer, which would make chelation therapy in mass casualty situations cumbersome and challenging and is a considerable limitation for the treatment of actinide contamination of a very large population of contaminated individuals in a crisis setting.<sup>2,25</sup> Therefore, the development of new orally active and effective broad-spectrum chelating agents for the treatment of actinide contamination remains critical for emergency human use.

## 6.2 Designing Chemical Structures for Actinide Chelation

The potential health hazards of the actinides were recognized early, especially for those synthetic heavy elements that were created by nuclear fission and that garnered great attention during the Manhattan Project.<sup>26,27</sup> The first efforts to identify effective ways to promote the removal of internally deposited radionuclides from the body therefore date back to the late 1940's.<sup>28,29</sup> Nevertheless, owing to the limited understanding of actinide biological chemistry and to the challenging task of specifically targeting toxicants over endogenous metal

ions without inducing toxicity, only a limited number of chelating molecular structures have stood out with the promise of therapeutic application.<sup>19</sup> The pace of research and development for new actinide chelation methods has also been greatly hampered by the non-existent profit prospects for such drugs and a resulting lack of interest from the pharmaceutical industry.

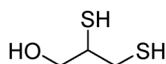
### 6.2.1 Coordination Chemistry Criteria

Although they belong to the same chemical series and display large similarities, the actinides exhibit different coordination properties determined mainly by their outermost electron shells. The lighter members of the series (Th through Pu) are known to exhibit multiple stable oxidation states, whereas the heavier elements (*i.e.*, Am and Cm) predominantly display the trivalent oxidation state.<sup>4,30</sup> However, complexation and hydrolysis under the conditions encountered in biological fluids favor specific oxidation states such as Th(IV), U(VI), Np(IV, V), Pu(IV), Am(III), and Cm(III), where the (VI) and (V) states of U and Np are the linear dioxocations uranyl and neptunyl, respectively.<sup>8,31</sup> Actinides are hard cations (where “hard” applies to species that have high charge states and are weakly polarizable according to the Pearson acid base concept) that preferentially bind organic ligands containing hard electron donors such as oxygen atoms. Bonding with such ligands is then mostly ionic. Partially covalent bonding is observed with softer nitrogen and sulfur donors as well as with halides other than fluoride.<sup>31,32</sup> Coordination numbers for actinide ions vary from 5 to 12, depending on the oxidation state of the metal center, but most common coordination numbers are 5 for uranyl and neptunyl, 8 to 9 for trivalent Am and Cm, and 8 for tetravalent Pu and Np species. These relatively large coordination numbers, necessary to fully satisfy the electronic requirements of the metal ions, will favor multidentate ligands that can form multiple bonds with actinides. Common classes of chelating ligands are those bearing several donor atoms that will form a five- or six-membered heterocyclic ring upon binding to the metal ion. Following those rules, the most stable actinide (III) and (IV) complexes are formed with ligands such as octadentate structures containing four chelating units, each incorporating two donor atoms, resulting in a complex with a 1 : 1 metal : ligand stoichiometry.<sup>32–34</sup> Relatively less stable complexes will be formed with tetradentate ligands containing only two chelating units (four electron donors) and resulting in a 1 : 2 metal : ligand stoichiometry. The geometry of the complex and its stability under physiological conditions also depend on the type of chelating units and scaffold incorporated in the ligand.<sup>32</sup>

### 6.2.2 Synthetic Approaches to New Actinide-Selective Agents

Early investigations to enhance actinide excretion rates targeted metabolic pathways of essential divalent metals through manipulation of dietary calcium, magnesium, and phosphorous and supplementation with vitamin D, parathyroid hormone, and ammonium chloride to increase Ca absorption, bone

resorption, and Ca excretion, respectively.<sup>28,35–37</sup> None of these attempts affected the biodistribution of actinides. Other unsuccessful attempts used the British anti-Lewisite (BAL, also known as dimercaprol 2) treatment, which is known for its effectiveness against arsenic poisoning but only incorporates sulfur chelating groups (see also Chapter 1 and Chapter 3) that do not complex actinides strongly.<sup>38</sup> One method that ameliorated acute U poisoning was treatment with sodium bicarbonate, NaHCO<sub>3</sub>,<sup>39</sup> which produces a uranyl bicarbonate complex in tubular urine that is less toxic than the unchelated uranyl, but it also promotes migration to extracellular fluids and deposition in the bone. Oral doses or infusions of sodium bicarbonate must be accompanied by diuretics and carefully monitored in order to keep the urine alkaline. Although not a chelator *per se*, sodium bicarbonate is currently the only treatment against contamination with U recommended by organizations such as NCRP.<sup>14</sup>

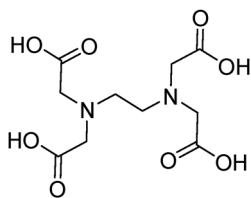


BAL 2

### 6.2.2.1 Polyamino-Carboxylic Acid Derivatives

The hexadentate polyaminocarboxylic acid ethylenediaminetetraacetic acid (EDTA, 3) had become widely distributed for a variety of industrial chemical applications by the early 1950's. Known for the high stabilities of its metal chelates,<sup>40</sup> as compared to other polycarboxylic acids, EDTA 3 was therefore among the first chelators to be tested for actinide chelation.<sup>41</sup> The calcium disodium salt of EDTA (CaNa<sub>2</sub>-EDTA), which does not deplete calcium and is therefore not as toxic as the protonated version of EDTA, was shown to enhance the excretion of Pu(IV) and Am(III) in rats. However, *in vivo* actinide chelation was only achieved after high doses and repeated injections, reaching toxic levels.<sup>42</sup> The octadentate analog of EDTA, DTPA 1 was purposely designed to overcome these limitations.<sup>43</sup> Because of the higher denticity of this ligand, the stabilities of the actinide complexes formed with DTPA are higher than those of the corresponding EDTA compounds, with a better selectivity over divalent metal ions such as Ca<sup>2+</sup>.<sup>44</sup> The CaNa<sub>3</sub>-DTPA salt was quickly recognized for its better ability to decorporate Pu(IV) from rats and has been studied extensively *in vitro* and *in vivo*, and used in humans since then.<sup>14,45</sup> However, frequent CaNa<sub>3</sub>-DTPA injections are still nephrotoxic and may result in manganese and zinc (Zn) depletion as DTPA forms stable chelates with those metals.<sup>44</sup> Although it is less effective than CaNa<sub>3</sub>-DTPA at removing exogenous metals, the ZnNa<sub>3</sub>-DTPA salt is less toxic and allows frequent injections or continuous infusion over extended time.<sup>14,46</sup> The EDTA and DTPA molecules have been the subject of many structural alterations, including elongation or replacement of the central aminoalkane skeleton, addition of aminocarboxylate moieties, and incorporation of ethyl alcohol

or hydroxamic acid units, but none resulted in increased affinity towards actinide ions.<sup>19,45,47</sup> Further modifications were predominantly aimed at increasing the low absorption of DTPA salts in the gastro-intestinal tract, leading to the formation of lipophilic pro-drug derivatives,<sup>19,20</sup> as detailed in a later section on formulation development approaches.

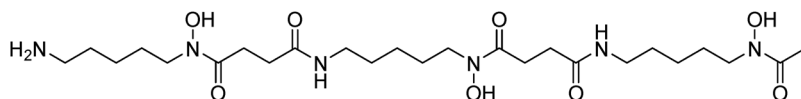
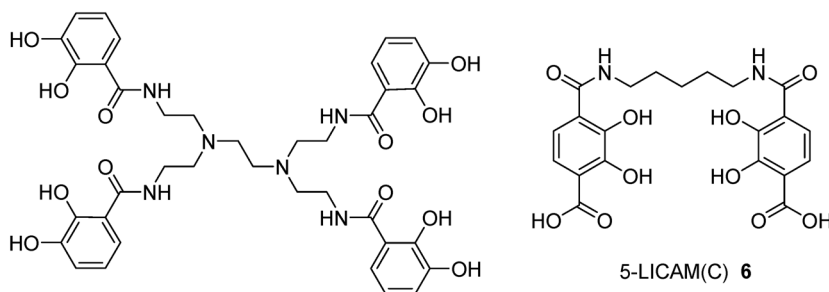
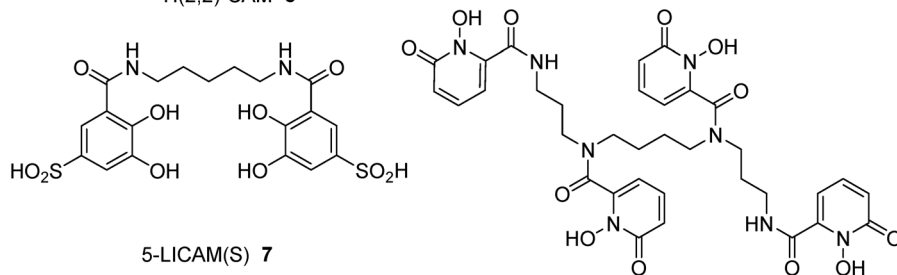
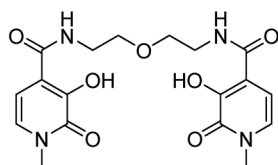


EDTA 3

### 6.2.2.2 Siderophore Mimics

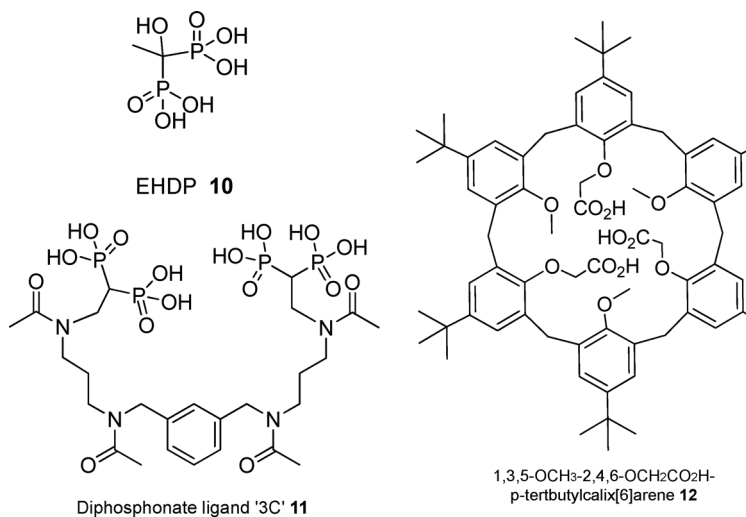
Siderophores, the microbial low molecular weight molecules used by bacterial organisms to scavenge iron, constitute another class of natural molecules that prompted early investigation for their actinide removal properties. The hundreds of known siderophores can be of different denticities, but all form thermodynamically stable hexacoordinate octahedral Fe(III) complexes and typically employ oxygen-containing iron-binding moieties.<sup>48</sup> The hexadentate ligand desferrioxamine B (DFO, Desferal, 4), a siderophore from *Streptomyces pilosus*, has been used for several decades as a therapeutic iron chelator for the treatment of iron-overload diseases.<sup>49</sup> However, DFO displayed lower efficacy than DTPA at removing Pu(IV) *in vivo*, presumably due to its lower denticity, and the weaker acidity of its hydroxamate iron-binding units.<sup>50</sup> Among biologically relevant metal ions, the ferric ion stands out as having a high charge/radius ratio, similar to that of Pu<sup>4+</sup>.<sup>8</sup> In the late 1970's, Raymond and coworkers at the University of California, Berkeley, hypothesized that synthetic ligands adapted from siderophores but with increased denticity would form extremely stable actinide complexes and structures suitable for *in vivo* metal scavenging.<sup>19,51</sup> In collaboration with Durbin from the Lawrence Berkeley National Laboratory, Berkeley, over 60 multidentate synthetic ligands were produced and evaluated for their *in vivo* Pu(IV) decorporation properties and potential toxicity, as described in detail in the literature.<sup>19,32</sup> These chelating structures used siderophore-inspired bidentate chelating units such as functionalized catechol-amides CAM, CAM(C), and CAM(S), for the unsubstituted, carboxylated, and sulfonated versions, respectively, attached to a variety of molecular polyamine backbones, enabling the development of new and improved chelating agents to evolve by providing an understanding of some of the relationships underlying the efficacy of a ligand for the decorporation of actinides (*e.g.*, denticity, binding group acidity, backbone flexibility, and solubility).<sup>32</sup> Examples of these ligands include the octadentate H(2,2)-CAM 5 as well as the tetradentate 5-LICAM(C) 6 and 5-LICAM(S) 7. The isomeric hydroxypyridinone metal-binding groups, 1,2-HOPO and Me-3,2-HOPO, are ionized at lower pH than catecholamide moieties, making them better ligands for the actinides, which are

more acidic than iron. Ligands incorporating these groups were among those most selective and efficacious at removing actinides *in vivo*, with little to no observed toxicity in animals.<sup>19,32,52</sup> After extensive toxicity and efficacy studies in mice and a limited number of tests in dogs and baboons, two particular molecules, 3,4,3-LI(1,2-HOPO) **8** and 5-LIO(Me-3,2-HOPO) **9**, were selected as promising orally available candidate actinide decorporation agents.<sup>53–66</sup> Both compounds were found to be 30 times more potent than DTPA for the decorporation of Pu(IV), and to sequester a wider spectrum of radionuclides, including U and Np, as well as particulate contaminants from mixed oxide fuel.<sup>52,67</sup> In addition, unlike DTPA, both molecules have the advantage of being efficacious in the oral delivery format.<sup>52</sup> Over the last 10 years remarkable progress has been made in the preclinical development of both agents. With 5-LIO(Me-3,2-HOPO) **9** remaining in the pipeline, the most efficacious octadentate structure, 3,4,3-LI(1,2-HOPO) **8**, was taken forward through a series of non-clinical efficacy, safety, pharmacology, and toxicology assessments, all necessary to demonstrate its viability as a therapeutic product.<sup>68–74</sup>

Desferrioxamine B **4**H(2,2)-CAM **5**5-LICAM(C) **6**5-LICAM(S) **7**3,4,3-LI(1,2-HOPO) **8**5-LIO(Me-3,2-HOPO) **9**

### 6.2.2.3 Poly-Phosphonic Acid Chelators and Macrocyclic Structures

Knowing that actinide ions tightly bind phosphate groups on the bone mineral surface,<sup>75</sup> a series of cyclic and linear polyphosphates and polyphosphonic or phosphinic acids were tested in rats, revealing enhanced urinary excretion of U but little reduction of U-induced nephrotoxicity.<sup>19,76</sup> Ethane-1-hydroxy-1,1-bisphosphonate **10** (EHBP), also known as etidronic acid, stood out as it inhibits bone resorption and had been used to treat bone remodeling disorders. Studies in rats contaminated with 50% lethal amounts of uranyl nitrate demonstrated the efficacy of EHBP, which prevented mortality with a 100% rate and significantly increased urinary U excretion and reduced U content in kidneys when injected intramuscularly at a wound site or intraperitoneally promptly after contamination.<sup>77</sup> More recent work identified a series of uranyl-binding diphosphonate ligands through novel high-throughput screening methods.<sup>78,79</sup> Several compounds showed promise in significant reduction of the uranium burden in the kidney (up to 50% for the structure named “3 C” **11**) liver, and skeletons of rats contaminated with uranyl. However, no further data has been reported since with these compounds. Finally, another more recent approach to actinide chelation has been the use of macrocyclic calixarene structures, previously developed as selective actinide extractants for analysis purposes.<sup>80</sup> Injection of the 1-hydroxy-4-sulfonatobenzene hexamer or octamer in rats did not alter uranyl retention.<sup>81</sup> However, these cage-like molecules provide conformational flexibility and can be functionalized with chelating groups. Substitution of the hexamer *p*-*tert*-butylcalix[6]arene structure with 3 carboxylic groups arranged in C3 symmetry provided much higher affinity for uranyl and led to the discovery of 1,3,5-OCH<sub>3</sub>-2,4,6-OCH<sub>2</sub>COOH-*p*-*tert*-butylcalix[6]arene **12** as a very promising compound for U decontamination.<sup>82,83</sup>



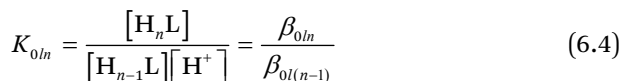
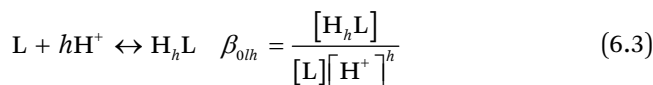
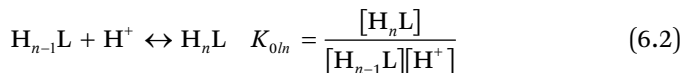
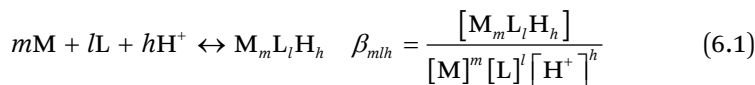
## 6.3 Evaluating Actinide Chelation Efficacy

### 6.3.1 *In vitro* Evaluation Techniques

The presumed mechanism of action of new actinide-binding ligands is expected to be a chelation mechanism, in which the compound binds the targeted actinide and forms a stable complex that can be eliminated through excretion pathways. Chelation is likely to be clinically efficacious if the affinity of the chelating agent for the targeted actinide metal ion is higher than those of potential biological ligands (such as proteins and bone matrices), and if its affinity for the targeted actinide metal ion is more specific than for essential divalent metal ions. Several tools are available to determine the affinity of new molecules for metal ions *in vitro* and are used to predict their *in vivo* actinide decorporation efficacy.

#### 6.3.1.1 Solution Thermodynamics

Solution thermodynamic equilibrium constants define the quantitative limits of designed ligands to compete for a particular metal. The strength of metal binding will not only dictate the actinide sequestration ability, it may also determine the mechanisms of actinide release (ligand exchange, redox reactions, or complex degradation), which make solution thermodynamic stability and metal exchange kinetics crucial parameters to assess. Complex formation constants are dependent on both the acidity of the ligand and the stoichiometry of the metal–ligand complex. By standard convention, overall equilibria are expressed as  $\beta_{mlh}$  values, as defined in eqn (6.1). However, very large differences in the acidity of various ligands at physiological pH do not account for the fact that ligands may still be protonated, as determined by their respective stepwise protonation association constants  $K_{0ln}$  (eqn (6.2)–(6.4)).



Hence, protons and metal cations compete with each other for binding to the ligand. In addition, different formation constants must be taken into account to compare ligands of varying denticities. To compare the true relative ability of different ligands to bind a metal, independent of proton concentration or

denticity, a parameter that is proportional to the free energy  $\Delta G$  released by metal–ligand binding must be used. To that extent, the pM value, defined as the negative logarithm of the free metal ion concentration, is calculated from the different conditional constants for a given metal–ligand system under defined conditions, such as pH and metal and ligand concentrations. Standard reference conditions for the purpose of comparing actinide chelating agents and biological ligands are physiological pH 7.4 and total concentrations of 10  $\mu\text{M}$  ligand and 1  $\mu\text{M}$  metal. For such comparisons, a higher pM value is indicative of a more competitive, therefore better, chelator. Examples of proton-independent stability constants as well as corresponding pM values are provided in Table 6.1 for the common chelator DTPA and the ligand under development, 3,4,3-LI(1,2-HOPO) **8**. (These properties are also discussed in Chapter 2.)

### 6.3.1.2 High-Throughput Screening Methods

While the determination of thermodynamic constants is a rigorous tool providing a quantitative measurement of the affinity of a particular ligand for specific metal ions, it is often tedious and may not be adequate for the evaluation of libraries of new molecules in the era of high-throughput synthesis. Recent methodologies for the evaluation of actinide ligands have included high-throughput *in vitro* screenings based on the competitive displacement of reference chelating agents.<sup>78</sup> A particular microtiter colorimetric assay following the disappearance of a chromogenic uranyl complex preformed with sulfochlorophenol S was applied to screen over 40 known ligands including polycarboxylate, hydroxamate, catecholate, hydroxypyridonate and hydroxyquinoline derivatives as well as 50 new bisphosphonate ligands for their U-binding properties.<sup>79</sup> More recently, an immunoassay based on surface plasmon resonance analysis was developed to measure uranyl affinity for proteins and small molecules and was described as fast, sensitive, and cost-effective.<sup>84</sup> This technique involves the immobilization of a specific monoclonal antibody raised against uranyl and uses 1,10-phenanthroline-2,9-dicarboxylic acid as the probe of uranyl capture by the antibody. While limited to specific conditions (pH, concentration, *etc.*) such screening methods offer a rapid and

**Table 6.1** Examples of solution thermodynamic parameters determined for selected actinide complexes of 3,4,3-LI(1,2-HOPO) and comparison with corresponding DTPA complexes.

Ligand	Cation	$\log\beta_{110}$	pM	Reference
3,4,3-LI(1,2-HOPO)	Th <sup>4+</sup>	<b>40.1</b>	<b>41.0</b>	33
	UO <sub>2</sub> <sup>2+</sup>	<b>18.0</b>	<b>18.8</b>	119
	Pu <sup>4+</sup>	<b>43.5</b>	<b>44.5</b>	120
	Cm <sup>3+</sup>	<b>21.8</b>	<b>22.7</b>	34
DTPA	Th <sup>4+</sup>	<b>28.7</b>	<b>26.8</b>	44
	UO <sub>2</sub> <sup>2+</sup>	<b>11.8</b>	<b>9.9</b>	121
	Pu <sup>4+</sup>	<b>33.7</b>	<b>31.7</b>	44
	Cm <sup>3+</sup>	<b>21.7</b>	<b>21.1</b>	122

robust readout and allow focusing on further *in vivo* evaluations. Combined with combinatorial synthetic methodologies, a high number of molecules may now be discovered and evaluated for their actinide affinity properties.

### 6.3.1.3 *In vitro and Ex vivo Binding*

The most important tissue biological ligands are the mineral phase of bone, for all actinides,<sup>85,86</sup> liver ferritin for trivalent and tetravalent actinides,<sup>85,87</sup> and the renal tubular epithelium for  $\text{UO}_2^{2+}$ . Few experimental examples have investigated the *ex vivo* or *in vitro* actinide removal efficacy of the most studied ligands from these biological pools. *Ex vivo* preparations of contaminated skeleton have been described in the literature: ashed bone samples were obtained from mice injected intravenously with uranyl chloride ( $^{233}\text{UO}_2\text{Cl}_2$ ) and sacrificed four hours later when uptake of bone U appears to be complete.<sup>88</sup> Bone ash in buffer was incubated without stirring or with occasional mixing for one or two hours at 20 or 37 °C with ligands such as Ca-DTPA and 3,4,3-LI(1,2-HOPO) **8** at ligand:U molar ratios of 75 and 250, respectively. Net removal of U from bone ash was about 2% for Ca-DTPA and 4% for 3,4,3-LI(1,2-HOPO). Removal of Pu and Am sorbed to well-characterized hydroxyapatite powder was also evaluated for 3,4,3-LI(1,2-HOPO) and Ca-DTPA.<sup>86,89</sup> Ca-DTPA was ineffective for Pu removal (100  $\mu\text{M}$ , 24–48 hours contact) while 3,4,3-LI(1,2-HOPO) showed removal of 3.8%. The most effective ligand for Am (100  $\mu\text{M}$ , 24–48 hours contact) was 3,4,3-LI(1,2-HOPO) showing 14.5% removal while Ca-DTPA removal was about 1.4%. The compound 3,4,3-LI(1,2-HOPO) also removed useful amounts of both Pu and Am from bone mineral.<sup>89</sup> These were the first successful demonstrations of removal of Pu or U from bone mineral with chelating agents in *ex vivo* or *in vitro* systems. Finally, *in vitro* studies have also investigated actinide removal from liver cytosol, to address mainly the binding of soluble liver proteins such as ferritin.<sup>85</sup> Using the highest concentrations of Ca-DTPA, less than 5% of the protein-bound Pu was rendered ultrafilterable.<sup>87</sup> A ferritin-rich liver cytosol was prepared from Pu-injected mice and ultrafiltered (100 kDa), with over 95% of the Pu retained on the filter. Incubation of the Pu-containing mouse liver cytosol with 3,4,3-LI(1,2-HOPO) ( $10^{-4}$  M, 1 hour, 37 °C) removed 50% of the Pu associated with the ferritin peak and 72% of the Pu associated with the very heavy protein fraction. These results were a dramatic improvement over the 5% Pu removed from dog liver cytosol with  $10^{-2}$  M Ca-DTPA.<sup>87</sup> Finally, more recent *ex vivo* studies have evaluated the decontamination efficacy of calixarene nanoemulsions using transdermal Franz diffusion cells for 24 hours on intact, wounded, and excoriated skins from pig ear contaminated with uranyl nitrate.<sup>90</sup> Of particular interest in these studies is the development of new superficial skin wound models, reproducing superficial cuts and stings, and mimicking contamination scenarios because of the mechanical injuries commonly encountered in the nuclear industry. Combined with the absence of toxicology findings, decontamination efficacies of up to 94% of the U applied to wounded skin were observed.

## 6.3.2 *In vivo* Efficacy Determination

### 6.3.2.1 *Animal Model Selection*

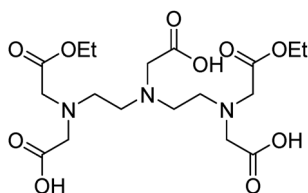
Although *in vitro* and *ex vivo* screens are certainly a first approach to delineate the potential of new actinide chelating molecules and products, *in vivo* studies are ultimately necessary to demonstrate the viability of these agents and to establish their therapeutic index based on efficacy results as well as toxicology findings. Live animals must be used in these studies, because the phenomena investigated (efficacy, function, and toxicity) depend on kinetic transfers of ligands and metals between and among the several fluid and cellular compartments of the intact animal in the presence of its homeostatically controlled fluid medium. Efficacy should be assessed in more than one animal species, especially considering the high reliance on biokinetic models in humans and different mammalian species. A large majority of the decorporation efficacy studies performed over the past three decades with new chelating agents such as 3,4,3-LI(1,2-HOPO) **8** were conducted on laboratory mice.<sup>19,32,52</sup> Mice are commonly used for metabolic and toxicity studies, because they are appropriate small-scale acute models for larger mammals. Mice were used in those studies in part because Pu metabolism and chelate action had already been studied in that animal,<sup>9,18</sup> but there were other factors to consider as well. The animal chosen for the primary investigations was the young adult female Swiss Webster mouse, an outbred strain of stable size and docile behavior. The mice were used at 11–15 weeks of age and  $30 \pm 3$  g body weight. At that age, the female mouse skeleton is nearly mature, and the long bones have attained 98% of their maximum length.<sup>9,91</sup> An animal model with a mature skeleton more closely resembles a human adult with respect to the degree and extent of bone remodeling. These are important considerations in interpreting the results of chelation therapy, as they will significantly affect the retention of actinides deposited in the skeleton. The last important advantage, unique to the study of actinide chelators, is the generation of much smaller amounts of radioactively contaminated wastes.

Unlike the mouse model system, adult rats have slowly but continuously growing skeletons. This means that the direct comparison of rats to larger mammals in terms of the efficacy of a chelating agent may be masked by a decrease in the amount of actinide retained in rat bone, making a chelator tested in rats appear better for the removal of actinides from bone than it would be when applied to other mammals.<sup>9</sup> However, because rats are commonly used in standardized safety pharmacology and toxicology tests, decorporation efficacy studies may be useful in providing correspondences to assess therapeutic indices. Work with larger mammals, such as dogs and baboons, allows a closer approach to human physiology. However, one of the difficulties in utilizing the non-human primate data as stand-in for humans is that non-human primates possess an efficient biliary outlet for actinides. There is no evidence for an efficient biliary outlet for actinides in humans or dogs. In view of the available literature observations,<sup>9,18,92,93</sup> mice, rats, and dogs have appeared to be the species of choice to pursue decorporation

efficacy studies with the most advanced programs developing new formulations of DTPA and the new chelating agent 3,4,3-LI(1,2-HOPO).

### 6.3.2.2 In vivo Decorporation Studies

Decorporation experiments in animals mostly consist in contaminating animals with radionuclides of interest and subsequently administering the chelating drug under different treatment regimens. Metabolic balances of the radionuclides and biodistribution profiles are then established. Decorporation efficacy is then based on direct measurement of the elimination of the radioactive contaminant through feces and/or urine (or exhalation, as appropriate) at various time points after administration of the decorporation agent. Residual body burden and specific organ content may also provide information on the potential internal relocation of the radionuclide and subsequent toxicity due to concentration. These measurements are in turn used to calculate changes in whole-body committed radiation dose following product administration. While the endpoints for such experiments are therefore mostly limited to reduction in whole body burden and committed radiation, a large number of parameters can be varied, in addition to the treatment regimen, including the route of contamination, the isotopic ratio, and chemical form of the contaminant, or the amount of contaminant and the associated radiation dose administered. Various routes of contamination have been investigated, comprising intravenous injection, inhalation, and wound simulation through subcutaneous or intramuscular injections.<sup>16,19,92–94</sup> An important difference in these contamination modes is the unit mass of contaminant deposited in specific tissues such as the lungs and respiratory tract for inhalation studies. The particular actinide isotopes chosen for decorporation experiments will depend on the desired indication, and the chemical form used for the contaminant will also largely affect its solubility properties and biokinetic distribution. A large number of actinide decorporation efficacy studies have been performed and reported over the years.<sup>16,19,92–94</sup> We have chosen to summarize here the results of only two recently published series of studies conducted with the new chelating agent 3,4,3-LI(1,2-HOPO)<sup>69</sup> **8** and with the DTPA diethyl ester pro-drug C2E2,<sup>95</sup> **13**, respectively, which are most representative of ongoing efforts to develop new treatment solutions for actinide contamination and follow well-defined animal contamination models.



C2E2 **13**

In an effort to establish a dosing regimen for 3,4,3-LI(1,2-HOPO), a series of dose-dependent Pu and Am decorporation efficacy studies, spanning a range of parenteral and oral treatment doses, were carried out in young adult female Swiss Webster mice intravenously administered (through a warmed lateral tail vein, 0.43 to 0.74 kBq or 10 to 20 nCi per mouse) soluble  $^{238}\text{Pu}$ -citrate or  $^{241}\text{Am}$ -citrate. Both parenteral and oral treatment with 3,4,3-LI(1,2-HOPO) resulted in dose-dependent elimination rates and total body burden and distinct tissue content reductions, compared to saline- and DTPA-treated groups (Figure 6.3). The results of these studies allowed the determination of an optimal dose level of 3,4,3-LI(1,2-HOPO) for a specific route of treatment administration. The minimum dose levels that produced maximum decorporation efficacy of soluble  $^{238}\text{Pu}$  and  $^{241}\text{Am}$  in mice were  $1\ \mu\text{mol kg}^{-1}$  ip and  $100\ \mu\text{mol kg}^{-1}$  po, and  $1\ \mu\text{mol kg}^{-1}$  ip and  $200\ \mu\text{mol kg}^{-1}$  po, respectively. These studies also demonstrated that extremely high oral doses of Ca-DTPA would be needed to reach efficacious decorporation levels observed at the presumed efficacious level of  $200\ \mu\text{mol kg}^{-1}$ . Finally, following the body

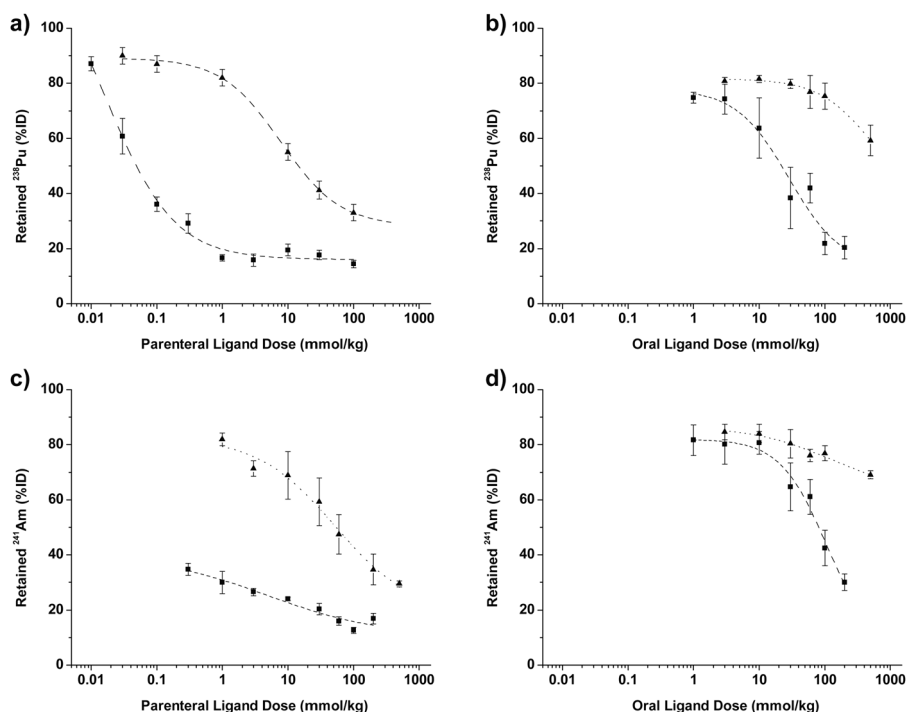


**Figure 6.3** Dose-dependent total body retention of  $^{238}\text{Pu}$  and  $^{241}\text{Am}$  after parenteral or oral treatment with 3,4,3-LI(1,2-HOPO) (squares) and Ca-DTPA (triangles). Ligands were given to groups of five mice by intraperitoneal injection (panels a and c) or oral gavage (panels b and d) 1 h after intravenous injection of  $^{238}\text{Pu}$ -citrate (panels a and b) or  $^{241}\text{Am}$ -citrate (panels c and d). Mice were euthanized 24 h after contamination. Adapted graphical presentation based on data from ref. 69.

surface area conversion model, an accepted conversion system of animal doses into human equivalent doses (HED), a 200  $\mu\text{mol kg}^{-1}$  dose level in mice corresponds to a 16  $\mu\text{mol kg}^{-1}$  human dose, which is well within the safety range defined through parallel pharmacology and toxicology studies.

The  $^{241}\text{Am}$  decorporation efficacy of C2E2 **13** was assessed in Beagle dogs (~13 months of age) exposed to an  $^{241}\text{Am}$  aerosol atmosphere for 8 min, with each dog receiving an average of 111 kBq (3  $\mu\text{Ci}$ ). Single doses of C2E2 (three dose levels from 100 to 500  $\text{mg kg}^{-1}$ ) were administered by oral gavage 24 h after contamination to mimic a realistic treatment delay, resulting in statistically significant increases in  $^{241}\text{Am}$  elimination over control and reductions in liver, kidney and lung  $^{241}\text{Am}$  burden in all treatment groups. Urinary excretion of  $^{241}\text{Am}$  increased in a dose-dependent manner and fecal elimination showed modest enhancement for three days after treatment before returning to control levels. While no direct comparison with intravenous DTPA was provided, these efficacy results combined with findings from safety studies constitute supporting evidence for the promise of this bio-available ester **13**.

## 6.4 Development of Viable Actinide Chelation Treatments

As detailed above, one of the main requirements for an effective actinide sequestering agent is its high affinity and selectivity towards metal binding. While chelation efficacy remains the first parameter to evaluate, effective actinide chelators need to respond to a series of other criteria including low toxicity under administration conditions, and preferably high bioavailability as well as ease of administration, which may be through the oral, transdermal or inhalation routes. Finally, feasibility of further development requires that prospective therapeutics be prepared at low cost on a large and rapid scale and exhibit long shelf-lives to facilitate the logistics associated with stockpile maintenance and emergency response. This section summarizes most current efforts in pursuing the pharmaceutical development of drug products incorporating chelating agents selected for their respective high actinide decorporation potential.

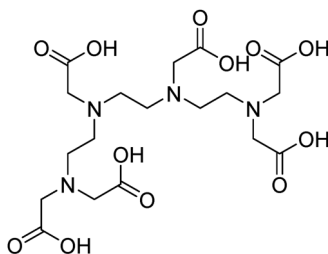
### 6.4.1 Formulation Development

In the context of developing actinide chelating drugs as medical countermeasures against radiological and nuclear threats for use in emergency situations, emphasis was laid on routes of administration that allow rapid distribution to the population, essentially excluding the intravenous route currently recommended for the sole approved DTPA-based products. Unfortunately, molecules presenting the highest affinity for actinides are commonly large molecules, as they must accommodate the larger denticity requirements to fully coordinate the metal ions. The quest for optimized thermodynamics therefore conflicts with properties needed for a chelator

to exert pharmacological effects, such as low molecular weight, appreciable lipid solubility, and the ability to cross biological membranes (see Chapter 2). Such criteria were taken into account in the design of new chelating compounds such as the hydroxypyridinone ligands, bisphosphonates, and calixarene structures. More targeted approaches have been the structural modification of DTPA or the formulated use of excipients and delivery agents with existing ligands for enhanced bioavailability.

#### 6.4.1.1 Structural Modifications of DTPA

Charge and hydrophilicity are the main factors of DTPA's permeability-limited absorption and resulting poor oral bioavailability (approximately 3%).<sup>96</sup> Following methods well established in drug delivery and small molecule modification, several attempts have been made to increase the lipophilicity of DTPA through esterification of carboxylic acid moieties of DTPA.<sup>19,20</sup> An early lipophilic derivative of DTPA, named "Puchel", incorporated two undecanoic acid chains with the specific goal of enhancing intracellular penetration; no actinide-removal efficacy enhancement or toxicity reduction was observed *in vivo*, however, in comparison to Ca-DTPA.<sup>97</sup> Long alkane chains were then added to triethylenetetramine hexaacetic acid (TTHA) **14**, a nonadentate analog of DTPA, in studies focusing on oral bioavailability enhancements.<sup>98</sup> Among that series of  $C_n$ TT compounds ( $n$  varying from 8 to 22 carbons), the  $C_{16}$ TT and  $C_{22}$ TT chelators were found most effective at reducing  $^{241}\text{Am}$  and  $^{239}\text{Pu}$  content in the tissues of contaminated rats, but were not more effective or less toxic than Ca-DTPA.<sup>99</sup>



TTHA **14**

More recently, while focusing on bioavailability enhancement, Jay and coworkers prepared and evaluated a series of DTPA esters for their physico-chemical properties and permeability characteristics.<sup>95,100-104</sup> The penta-ethyl and di-ethyl esters of DTPA, referred to as C2E5 and C2E2 **13**, respectively, initially emerged as candidates for further development. However, although C2E5 was shown efficacious in a  $^{241}\text{Am}$  wound-contamination animal model,<sup>103,104</sup> concerns were raised over its hepatotoxicity and potential to form up to 10 metabolites. On the other hand, C2E2 is still under investigation as a promising oral chelator for transuranic elements. Recent studies reported its decorporation efficacy in Beagle dogs, using the  $^{241}\text{Am}$

nitrate inhalation contamination model (*vide supra*), and suggested that it is well tolerated at therapeutic levels.<sup>95,101</sup> Finally, a comprehensive assessment of the genotoxic potential (including the *in vitro* bacterial reverse mutation Ames test, mammalian cell chromosome aberration cytogenetic assay and an *in vivo* micronucleus test), indicated that C2E2 is not mutagenic or clastogenic. Further efficacy and toxicity studies for C2E2 are ongoing at this time, making this compound a promising orally available candidate for transuranic actinide chelation.

#### 6.4.1.2 Pharmaceutical Approaches

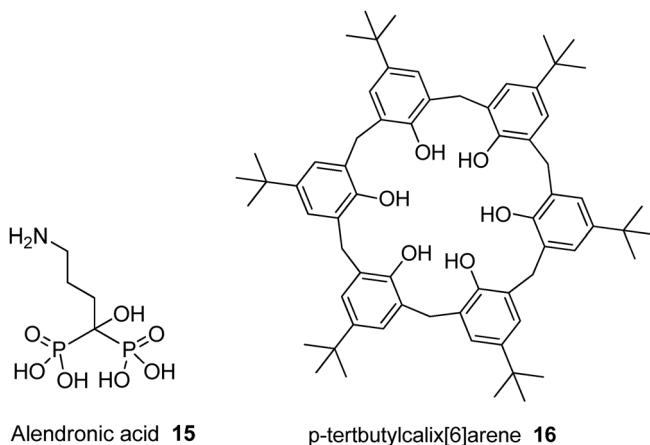
In an effort to improve the pharmacokinetic properties and bioavailability of DTPA, a number of classical and novel formulation approaches have been explored. To target the major actinide deposition sites more efficiently and improve its ability to cross biological membranes, liposome delivery systems were applied to DTPA.<sup>20,105</sup> After intravenous delivery, conventional liposomes and stealth® multilamellar liposomes were found to lengthen the circulation time of DTPA and to increase its distribution specifically in the liver and in the bones. Dramatic improvements in <sup>238</sup>Pu removal from rats were also noted by Phan and coworkers: a dose of 0.3  $\mu\text{mol kg}^{-1}$  of polyethylene glycol-coated stealth® liposomes with a mean diameter of 100 nm induced the same skeletal <sup>238</sup>Pu reduction as four injections of DTPA (30  $\mu\text{mol kg}^{-1}$ ).<sup>106</sup>

To enhance oral delivery, Shankar and coworkers developed Zn-DTPA tablets, an oral solid dosage form containing permeation enhancers.<sup>107,108</sup> Limited efficacy and safety studies are available for these tablets, however recent publications reported that daily oral administration at a 1325  $\text{mg}^{-1} \text{kg}^{-1} \text{day}^{-1}$  level for 7 days was well tolerated in Beagle dogs. In addition, decorporation efficacy in rats injected with <sup>241</sup>Am and treated once with oral tablets (575  $\mu\text{mol kg}^{-1}$ ) or intravenous DTPA (30  $\mu\text{mol kg}^{-1}$ ) was comparable.<sup>107,108</sup> In a different process developed by the company Nanotherapeutics Inc., nano-particulate aggregates of DTPA and zinc acetate were encapsulated within entero-coated capsules providing the most advanced oral delivery product for DTPA, NanoDTPA®.<sup>109,110</sup> Under this form, DTPA displayed significantly improved bioavailability in dogs and promoted as much <sup>241</sup>Am removal as intravenous DTPA.<sup>109</sup>

Because inhalation is considered the most likely route of contamination, targeting the actinide particles deposited in the lungs has also been an active area of research. Efforts to aerosolize Ca-DTPA either as a powder or as a nebulized solution provided thorough characterizations of the resulting particles and droplets.<sup>111</sup> In parallel, the French military complex produced a micronized dry powder of DTPA, of which only 3% deposited in the alveolar region of the lungs when inhaled through a dry powder inhaler (Spinhaler®).<sup>112</sup> In spite of such low aerosolization performance, this product is currently available in France for emergency administration to nuclear workers exposed to Pu. In more recent studies, porous particles were prepared by spray-drying DTPA in a mixture of ethanol and water together with

excipient dipalmitoylphosphatidylcholine and ammonium bicarbonate. Optimization of the spray-drying conditions resulted in about 56% of the powder deposited in the lungs and 27% in the alveoli upon inhalation.<sup>113</sup> Administration of this powder to rats contaminated with inhaled, poorly soluble Pu oxide aerosols promoted as much plutonium removal as intravenous DTPA,<sup>114</sup> warranting further safety and efficacy studies that would confirm the viability of this new formulation as an emergency treatment.

It is interesting to note that other molecules have been the subjects of pharmaceutical development work. The sodium salt of alendronic acid **15**, a diphosphonate chelator that acts as a specific inhibitor of osteoclast-mediated bone resorption, has been formulated into nanoparticles to be spray-dried and mixed with lactose for lung delivery.<sup>115</sup> Although not yet tested for efficacy, the pharmacokinetic profile of the resulting product is promising, as the molecule crosses the pulmonary barrier rapidly and 34% of the inhaled powder was found in the lungs of healthy human volunteers. Other chelating structures based on the calixarene architecture have been the focus of formulation development efforts for skin decontamination: most notably, Fattal and coworkers, in collaboration with the French Institute for Radiological Protection and Nuclear Safety, recently produced an oil-in-water nanoemulsion containing *p*-tert-butylcalix[6]arene **16** together with nonionic surfactants.<sup>83</sup> This particular emulsion was shown to induce a 98% decrease in U transcutaneous diffusion on pig ear skin contaminated with uranyl nitrate.<sup>83</sup> A more viscous mixture of this nanoemulsion containing a hydrogel subsequently displayed similar U binding properties and was deemed more suitable for skin applications.<sup>116</sup>



#### 6.4.2 Safety Determination and Regulatory Approval

Clearly, as summarized above, the past few decades have seen a resurgence in scientific interest for the development of new molecules and formulated products of existing compounds as actinide chelation therapeutics. However,

the path from research discovery to commercialization and availability to the patient is long and arduous, especially for such new drug products; due to the inherently rare nature of the contamination threat, radionuclide decorporation agents are predominantly produced for Government stockpiles, they have limited marketability and will not benefit from the expertise and machinery of large pharmaceutical corporations. Fortunately, international organizations such as the International Council for Harmonisation of Technical Requirements for Pharmaceuticals for Human Use (ICH) and regulatory authorities such as the FDA in the United States provide a number of guidelines and documents discussing the scientific and technical aspects of drug registration and providing well-defined development criteria and milestones.

#### 6.4.2.1 *The Animal Rule*

Actinide chelating agents are categorized as medical countermeasures, which are the drugs, vaccines, and medical devices that are needed to respond to a public health emergency, including products to prevent and respond to anthrax, smallpox, radiological/nuclear agents, pandemic influenza and other emerging diseases.<sup>25</sup> For such products, well-controlled efficacy studies in humans cannot be ethically conducted because the studies would involve administering a potentially lethal or permanently disabling toxic substance or organism to healthy human volunteers. It is for example not feasible or ethical to perform controlled clinical trials in which humans are purposely exposed to radionuclides such as isotopes of Pu, Am, Cm, Np and U. To address this issue, in May 2002 the FDA promulgated a rule allowing for approval of new drug products based on animal data.<sup>117</sup> The intent of this “Animal Efficacy Rule” was to facilitate the development of medical countermeasures against chemical, biological, nuclear, or radiological threats, including new actinide decorporation treatment strategies. It indicates that the FDA will rely on the evidence from the studies in animals to provide substantial evidence of the effectiveness of the proposed new agent when: (i) there is a reasonably well-understood pathophysiological mechanism of the toxicity of the substance and its prevention or substantial reduction by the product; (ii) the effect is demonstrated in more than one animal species expected to react with a response predictive for humans, unless the effect is demonstrated in a single animal species that represents a sufficiently well-characterized animal model for predicting the response in humans; (iii) the animal study endpoint is clearly related to the desired benefit in humans, generally the enhancement of survival or prevention of major morbidity; and (iv) the data or information on the pharmacokinetics and pharmacodynamics of the product or other relevant data or information, in animals and humans, allows selection of an effective dose in humans. Additional guidelines specific to the development of new decorporation agents under the Animal Rule are found in other FDA guidance documents and must also be taken into consideration throughout the development of new chelating

products.<sup>118</sup> Finally, in addition to meeting the criteria under the Animal Efficacy Rule, general essential elements required for the animal models to be used in studies to support efficacy are presented in Table 6.2.

Although specific to drug development and regulatory approval in the U.S., these guidelines have been adapted and are valid in other countries, especially in the European Union, under a harmonization effort. Below is a brief summary of a typical sequence of requisite nonclinical and clinical studies that will support regulatory approval of a new radionuclide decorporation countermeasure.

- Tests of effectiveness *in vitro*, including solution thermodynamics and kinetics of complexation of the targeted element by the proposed substance.
- Assay development and validation, standard for most new chemical entities, including manufacturing, purification, and characterization methods.
- Preliminary or exploratory animal efficacy studies, typically in rodents or other suitable small animal model, following methods such as those described above.
- Animal safety pharmacology studies to investigate potential undesirable pharmacodynamics effects on physiological functions and to

**Table 6.2** Essential characterization elements for the selection and justification of animal models under the Animal Efficacy Rule.

---

<p><i>A. Characteristics of the etiologic agent:</i></p> <ol style="list-style-type: none"> <li>1. The challenge agent</li> <li>2. Pathogenic determinants</li> <li>3. Route of exposure</li> <li>4. Quantification of exposure</li> </ol> <p><i>B. Host susceptibility and response to the etiologic agent</i></p> <p><i>C. Natural history of the disease:</i></p> <ol style="list-style-type: none"> <li>1. Time to onset of disease</li> <li>2. Time course of progression of disease</li> <li>3. Manifestations (signs and symptoms)</li> </ol> <p><i>D. Trigger for intervention</i></p> <p><i>E. Characterization of the medical intervention:</i></p> <ol style="list-style-type: none"> <li>1. Product class</li> <li>2. Mechanism of action</li> <li>3. <i>In vitro</i> activity</li> <li>4. Activity in disease of similar pathophysiology</li> <li>5. PK in unaffected animals/humans</li> <li>6. PK in affected animals/humans</li> <li>7. PK interactions with medical products likely to be used concomitantly</li> <li>8. Synergy or antagonism of medical products likely to be used in combination</li> </ol> <p><i>F. Design considerations for the efficacy studies:</i></p> <ol style="list-style-type: none"> <li>1. Endpoints</li> <li>2. Timing of intervention</li> <li>3. Route of administration</li> <li>4. Dosing regimen</li> </ol>
---

---

assess effects on the cardiovascular, central nervous, pulmonary, and renal systems before first administration in humans.

- Animal toxicology studies should include at a minimum (i) expanded single- and repeat-dose toxicity studies in two mammalian species (one non-rodent), with the duration of the repeat-dose toxicity studies equal to or exceeding the duration of the intended treatment in humans; (ii) genotoxicity studies *in vitro* and *in vivo*.
- Single-dose, dose escalation, safety, and tolerability studies in humans (initial first inhuman studies), using doses supported by animal data.
- Pivotal efficacy studies supporting approval conducted in the most appropriate animal species; the animal species selected should be similar to humans with respect to the pharmacokinetic profile of the decorporation agent and the distribution of the radioactive contaminant.
- Definitive safety studies in humans; these studies should be conducted at the highest dose anticipated to be marketed and be performed in parallel with the animal efficacy study or studies intended to support approval, assuming the product is reasonably likely to produce clinical benefits in humans.

Along this sequence are specific milestones such as (i) the Investigational New Drug (IND) stage that indicates an initial review of nonclinical data by the FDA and a permission to proceed with first-in-human clinical studies; (ii) the Orphan Drug (OD) designation that grants special status to a drug to treat a rare disease or condition upon request of a sponsor; and the final New Drug Application (NDA) submission, which is the vehicle through which drug sponsors formally propose that the FDA approve a new pharmaceutical for sale and marketing in the U.S.

#### 6.4.2.2 *Current Status of Existing Actinide Chelation Products*

As stated earlier, Ca-DTPA and Zn-DTPA solutions have officially been approved for intravenous and inhalation use in the U.S. since 2004.<sup>21</sup> However, they had already been stockpiled for different governmental agencies such as the U.S. Departments of Energy and Defense and used in contaminated workers. DTPA-based products, including the micronized dry-powder inhalation product have also been available and used for years in European and Asian countries, especially in France, where there is a significant at-risk population due to the heavy reliance on nuclear power. The regulatory approval of DTPA by the FDA was therefore mostly grandfathered in based on a large database of human use assembled by the Radiation Emergency Assistance Center/Training Site (REAC/TS) and reviewed by the FDA itself.<sup>14</sup> There is currently no new approved product for an actinide decorporation agent that was approved through the newly implemented Animal Rule development path. With the help and great interest from the Department of Health and Human Services in the U.S. as well as from other public institutions such as the Atomic Energy and Alternative Energies Commission and Institute for

Radiological Protection and Nuclear Safety in France, Public Health England in the United Kingdom, or Atomic Energy Of Canada Limited in Canada, new products have now embarked on the regulatory approval route.

Among the different drugs and products listed in the different sections of this chapter are some remarkably advanced projects aiming to provide new chelating options:

In 2011, Nanotherapeutics Inc. obtained the FDA orphan-drug status for NanoDTPA™ capsules to treat radiation exposure. Most recent published reports from this company provide encouraging americium decorporation efficacy data and indicate that nonclinical studies are still ongoing. The C2E2 DTPA 13 pro-drug developed by Jay and coworkers at the University of North Carolina and the DTPA oral tablet developed by Shankar and colleagues at SRI International have both undergone substantial safety and efficacy testing, with projected submissions of IND applications in the mid-2010's. The most advanced program is that of an oral product of the new decorporation agent 3,4,3-LI(1,2-HOPO) **8** led by the Lawrence Berkeley National Laboratory. Based on extensive nonclinical safety and efficacy data in three animal species, mice, rats, and dogs, the IND status was formally provided by the FDA in the summer of 2014, with first-in-human safety studies currently under preparation.

Although undeniable progress has been made in the development of sequestering agents for actinide decorporation since the identification of potential health hazards from those radionuclides in the 1950's, only one molecule, DTPA, has been used internationally and officially approved for distribution, with significant limitations such as potential nephrotoxicity, reduced decorporation efficacy, and cumbersome recommended use of intravenous injections. Several formulations for oral and inhalation use of DTPA have been pursued with promising prospects. In parallel, only one other ligand, 3,4,3-LI(1,2-HOPO), has been developed far enough to warrant hopes for availability in the next decade. There is therefore still a pressing need for new chelating molecules as well as advanced studies that will complete the existing research and development efforts. Beyond mere approval of new drug products, one needs to be able to define a reasonable treatment regimen, a challenging task when relying solely on animal data, in an accident scenario where a large population would be exposed to different isotopes, at different contamination levels, through different routes, and at different times.

## Abbreviations

<b>BAL</b>	British anti-Lewisite (dimercaprol)
<b>CAM</b>	functionalized catecholamides
<b>DTPA</b>	Diethylenetriaminepentaacetic acid
<b>EDTA</b>	Ethylenediaminetetraacetic acid
<b>EHBP</b>	Ethane-1-hydroxy-1,1-bisphosphonate
<b>FDA</b>	(US) Federal Drug administration
<b>HED</b>	Human Equivalent Dose

<b>HOPO</b>	hydroxypyridone
<b>ICRP</b>	International Commission on Radiological Protection
<b>NRCP</b>	(US) National Council on Radiation Protection and Measurements
<b>REAC/TS</b>	Radiation Emergency Assistance Center/Training Site
<b>TTHA</b>	Triethylenetetramine hexaacetic acid

## References

1. D. Albright, F. Berkhout and W. Walker, *Plutonium and Highly Enriched Uranium 1996: World Inventories, Capabilities, and Policies*, Stockholm International Peace Research Institute, New York, 1997.
2. D. R. Cassatt, J. M. Kaminski, R. J. Hatchett, A. L. DiCarlo, J. M. Benjamin and B. W. Maidment, *Radiat. Res.*, 2008, **170**, 540–548.
3. T. C. Pellmar and S. Rockwell, *Radiat. Res.*, 2005, **163**, 115–123.
4. J. J. Katz, G. T. Seaborg and L. R. Morss, *The Chemistry of the Actinide Elements*, Chapman and Hall, London, U.K., 2nd edn, 1986.
5. D. L. Clark, D. E. Hobart and M. P. Neu, *Chem. Rev.*, 1995, **95**, 25–48.
6. D. R. Cassatt, J. M. Kaminski, R. J. Hatchett, A. L. DiCarlo, J. M. Benjamin and B. W. Maidment, *Radiat. Res.*, 2008, **170**, 540–548.
7. F. W. Whicker, T. G. Hinton, M. M. MacDonell, J. E. Pinder III and L. J. Habegger, *Science*, 2004, **303**, 1615–1616.
8. E. Ansoborlo, O. Prat, P. Moisy, C. Den Auwer, P. Guilbaud, M. Carriere, B. Gouget, J. Duffield, D. Doizi, T. Vercouter, C. Moulin and V. Moulin, *Biochimie*, 2006, **88**, 1605–1618.
9. P. W. Durbin, in *The Chemistry of the Actinide and Transactinide Elements*, ed. L. R. Morss, N. M. Edelstein and J. Fuger, Springer, Netherlands, 2006, vol. V, ch. 31, pp. 3339–3440.
10. F. Paquet, S. Frelon, G. Cote and C. Madic, *Radiat. Prot. Dosim.*, 2003, **105**, 179–185.
11. ICRP, *Age-Dependent Doses to Members of the Public from Intake of Radionuclides: Part 2*, Elsevier, Oxford, 1993.
12. ICRP, *Age-Dependent Doses to Members of the Public from Intake of Radionuclides: Part 3*, Elsevier, Oxford, 1995.
13. NCRP, *Development of a Biokinetic Model for Radionuclide-Contaminated Wounds and Procedures for their Assessment, Dosimetry and Treatment*, Bethesda, 2007.
14. NCRP, *Management of Persons Contaminated with Radionuclides*, Bethesda, 2008.
15. D. M. Taylor, *J. Alloys Compd.*, 1998, **271**, 6–10.
16. E. Ansoborlo, B. Amekraz, C. Moulin, V. Moulin, F. Taran, T. Bailly, R. Burgada, M. H. Henge-Napoli, A. Jeanson, C. Den Auwer, L. Bonin and P. Moisy, *C. R. Chim.*, 2007, **10**, 1010–1019.
17. R. Wood, C. Sharp, P. Gourmelon, B. Le Guen, G. N. Stradling, D. M. Taylor and M. H. Henge-Napoli, *Radiat. Prot. Dosim.*, 2000, **87**, 51–57.

18. P. W. Durbin, *Health Phys.*, 2008, **95**, 465–492.
19. P. W. Durbin, *Health Phys.*, 2008, **95**, 465–492.
20. E. Fattal, N. Tsapis and G. Phan, *Adv. Drug Delivery Rev.*, 2015, **90**, 40–54.
21. *Guidance for industry calcium DTPA and zinc DTPA drug products—submitting a new drug application*, US Food and Drug Administration, Silver Spring, MD, 2004.
22. B. D. Breitenstein and H. E. Palmer, *Radiat. Prot. Dosim.*, 1989, **26**, 317–322.
23. Update on chelation therapy: Chelators should not be used for uranium or neptunium, *REAC/TS Newsletter*, Radiation Emergency Assistance Center/Training Site, Oak Ridge, TN, 1981.
24. NCRP, *Management of Persons Accidentally Contaminated with Radionuclides*, Bethesda, 1980.
25. C. Maher, J. Hu-Primmer, T. MacGill, B. Courtney and L. Borio, *Microb. Biotechnol.*, 2012, **5**, 588–593.
26. E. Painter, E. Russell, C. L. Prosser, M. N. Swift, W. Kisielski and G. Sacher, *Clinical physiology of dogs injected with plutonium. Effect of oral and intravenous sodium citrate and intravenous hypertonic saline on plutonium excretion.*, U.S. Atomic Energy Commission, Oak Ridge, TN, 1946.
27. R. S. Stone, *Industrial medicine on the plutonium project*, McGraw-Hill Book Co., New York, 1951.
28. J. E. Wirth, *Industrial medicine in the plutonium project*, McGraw-Hill Book Co., New York, 1951, pp. 264–275.
29. H. C. Hodge, E. A. Maynard and W. E. Downs, *J. Pharmacol. Exptl. Therap.*, 1951, **101**, 17–18.
30. *The chemistry of the actinide and transactinide elements*, ed. L. R. Morss, N. M. Edelstein and J. Fuger, Springer, Dordrecht, 2006.
31. G. R. Choppin and M. P. Jensen, in *The chemistry of the actinide and transactinide elements*, ed. L. R. Morss, N. M. Edelstein and J. Fuger, Springer, Dordrecht, 2006.
32. A. E. V. Gorden, J. Xu, K. N. Raymond and P. W. Durbin, *Chem. Rev.*, 2003, **103**, 4207–4282.
33. J. P. Deblonde, M. Sturzbecher-Hoehne and R. J. Abergel, *Inorg. Chem.*, 2013, **52**, 8805–8811.
34. M. Sturzbecher-Hoehne, B. Kullgren, E. E. Jarvis, D. D. An and R. J. Abergel, *Chem.–Eur. J.*, 2014, **20**, 9962–9968.
35. D. H. Copp, D. M. Greenberg, J. G. Hamilton, M. J. Chace, L. Van Middleworth, E. M. Cuthbertson and D. M. Axelrod, *The deposition of plutonium and certain fission products in bone as a decontamination problem*, Metallurgical Laboratory, Chicago, IL, 1946.
36. D. H. Copp, D. M. Axelrod and J. G. Hamilton, *Am. J. Roentgenol. Radium Ther.*, 1947, **58**, 10–16.
37. B. Kawin, D. H. Copp and J. G. Hamilton, *Studies of the metabolism of certain fission products and plutonium*, University of California Radiation Laboratory, Berkeley, CA, 1950.

38. R. A. Allen and W. F. Neuman, in *The pharmacology and toxicology of uranium compounds*, ed. C. Voegtlin and H. C. Hodge, McGraw-Hill Book Co., New York, 1953, pp. 2092–2100.
39. H. C. Hodge, in *Pharmacology and toxicology of uranium compounds*, ed. C. Voegtlin and H. C. Hodge, McGraw-Hill Book Co., New York, 1949, pp. 1–13.
40. G. Schwarzenbach and H. Ackermann, *Helv. Chim. Acta*, 1947, **30**, 1798–1804.
41. J. G. Hamilton and K. G. Scott, *Proc. Soc. Exp. Biol. Med.*, 1953, **83**, 301–305.
42. J. Schubert, *Annu. Rev. Nucl. Sci.*, 1955, **5**, 369–412.
43. H. Kroll, *Development of chelating agents potentially more effective than EDTA in radioelement removal*, Argonne National Laboratory, Lemont, IL, 1956.
44. A. E. Martell, R. M. Smith and R. J. Motekaitis, *NIST Critically Selected Stability Constants of Metal Complexes*, Version 8.0.
45. V. Volf, *Treatment of incorporated transuranium elements*, IAEA, Vienna, 1978.
46. R. A. Guilmette and M. A. Muggenburg, *Int. J. Radiat. Biol.*, 1988, **53**, 261–271.
47. P. N. Turowski, S. J. Rodgers, R. C. Scarrow and K. N. Raymond, *Inorg. Chem.*, 1988, **27**, 474–481.
48. K. N. Raymond, B. E. Allred and A. K. Sia, *Acc. Chem. Res.*, 2015, **48**, 2496–2505.
49. J. Porter, *Br. J. Haematol.*, 2001, **115**, 239–252.
50. P. W. Durbin, N. Jeung, S. J. Rodgers, P. N. Turowski, F. L. Weigl, D. L. White and K. N. Raymond, *Radiat. Prot. Dosim.*, 1989, **26**, 351–358.
51. K. N. Raymond and W. L. Smith, *Struct. Bonding*, 1981, **43**, 159–185.
52. R. J. Abergel, P. W. Durbin, B. Kullgren, S. N. Ebbe, J. Xu, P. Y. Chang, D. I. Bunin, E. A. Blakely, K. A. Bjornstad, C. J. Rosen, D. K. Shuh and K. N. Raymond, *Health Phys.*, 2010, **99**, 401–407.
53. P. W. Durbin, N. Jeung, S. J. Rodgers, P. N. Turowski, F. L. Weigl, D. L. White and K. N. Raymond, *Radiat. Prot. Dosim.*, 1989, **26**, 351–358.
54. P. W. Durbin, B. Kullgren, J. Xu and K. N. Raymond, *Int. J. Radiat. Biol.*, 2000, **76**, 199–214.
55. S. A. Gray, G. N. Stradling, M. Pearce, I. Wilson, J. C. Moody, R. Burgada, P. W. Durbin and K. N. Raymond, *Radiat. Prot. Dosim.*, 1994, **53**, 319–322.
56. F. Paquet, J.-L. Poncey, H. Metivier, G. Grillon, P. Fritsch, R. Burgada, T. Bailly, K. N. Raymond and P. W. Durbin, *Int. J. Radiat. Biol.*, 1995, **68**, 663–668.
57. F. Paquet, J.-L. Poncey, G. Rateau, R. Burgada, T. Bailly, Y. G. P. Leroux, K. N. Raymond, P. W. Durbin and R. Masse, *Radiat. Prot. Dosim.*, 1994, **53**, 323–326.
58. J.-L. Poncey, G. Rateau, R. Burgada, T. Bailly, Y. G. P. Leroux, K. N. Raymond, P. W. Durbin and R. Masse, *Int. J. Radiat. Biol.*, 1993, **64**, 431–436.
59. G. N. Stradling, *Radiat. Prot. Dosim.*, 1994, **53**, 297–304.

60. G. N. Stradling, S. A. Gray, M. Ellender, J. C. Moody, A. Hodgson, M. Pearce, I. Wilson, R. Burgada, T. Bailly, Y. G. P. Leroux, D. E. Manouni, K. N. Raymond and P. W. Durbin, *Int. J. Radiat. Biol.*, 1992, **62**, 487–497.
61. G. N. Stradling, S. A. Gray, J. C. Moody, M. Pearce, I. Wilson, R. Burgada, T. Bailly, Y. G. P. Leroux, K. N. Raymond and P. W. Durbin, *Int. J. Radiat. Biol.*, 1993, **64**, 133–140.
62. G. N. Stradling, S. A. Gray, M. Pearce, I. Wilson, J. C. Moody, R. Burgada, P. W. Durbin and K. N. Raymond, *Hum. Exp. Toxicol.*, 1995, **14**, 165–169.
63. V. Volf, R. Burgada, K. N. Raymond and P. W. Durbin, *Int. J. Radiat. Biol.*, 1993, **63**, 785–794.
64. V. Volf, R. Burgada, K. N. Raymond and P. W. Durbin, *Int. J. Radiat. Biol.*, 1996, **70**, 109–114.
65. V. Volf, R. Burgada, K. N. Raymond and P. W. Durbin, *Int. J. Radiat. Biol.*, 1996, **70**, 765–772.
66. D. L. White, P. W. Durbin, N. Jeung and K. N. Raymond, *J. Med. Chem.*, 1988, **31**, 11–18.
67. F. Paquet, V. Chazel, P. Houpert, R. A. Guilmette and M. A. Muggenburg, *Radiat. Prot. Dosim.*, 2003, **105**, 521–525.
68. D. D. An, J. A. Villalobos, J. A. Morales-Rivera, C. J. Rosen, K. A. Bjornstad, S. S. Gauny, T. A. Choi, M. Sturzbecher-Hoehne and R. J. Abergel, *Int. J. Radiat. Biol.*, 2014, **90**, 1055–1061.
69. D. I. Bunin, P. Y. Chang, R. S. Doppalapudi, E. S. Riccio, D. An, E. E. Jarvis, B. Kullgren and R. J. Abergel, *Radiat. Res.*, 2013, **179**, 171–182.
70. P. Y. Chang, D. I. Bunin, J. Gow, R. Swezey, W. Shinn, D. K. Shuh and R. J. Abergel, *J. Chromatogr. Sep. Tech.*, 2011, 2013.
71. T. A. Choi, A. N. Endsley, D. I. Bunin, C. Colas, D. D. An, J. A. Morales-Rivera, J. A. Villalobos, W. M. Shinn, J. E. Dabbs, P. Y. Chang and R. J. Abergel, *Drug Dev. Res.*, 2015, **76**, 107–122.
72. T. A. Choi, A. M. Furimsky, R. Swezey, D. I. Bunin, P. Byrge, L. V. Iyer, P. Y. Chang and R. J. Abergel, *J. Pharm. Sci.*, 2015, **104**, 1832–1838.
73. E. E. Jarvis, D. D. An, B. Kullgren and R. J. Abergel, *Drug Dev. Res.*, 2012, **73**, 281–289.
74. B. Kullgren, E. E. Jarvis, D. D. An and R. J. Abergel, *Toxicol. Mech. Methods*, 2013, **23**, 18–26.
75. C. Vidaud, D. Bourgeois and D. Meyer, *Chem. Res. Toxicol.*, 2012, **25**, 1161–1175.
76. M. H. Henge-Napoli, E. Ansoborlo, P. Houpert, H. Mirto, F. Paquet, R. Burgada, S. Hodgson and G. N. Stradling, *Radiat. Prot. Dosim.*, 1998, **79**, 449–452.
77. M. H. Henge-Napoli, E. Ansoborlo, V. Chazel, P. Houpert, H. Mirto, F. Paquet and P. Gourmelon, *Int. J. Radiat. Biol.*, 1999, **75**, 1473–1477.
78. M. Sawicki, D. Lecercle, G. Grillon, B. Le Gall, A.-L. Serandour, J.-L. Poncy, T. Bailly, R. Burgada, M. Lecouvey, V. Challeix, A. Leydier, S. Pellet-Rostaing, E. Ansoborlo and F. Taran, *Eur. J. Med. Chem.*, 2008, **43**, 2768–2777.
79. M. Sawicki, J.-M. Siauge, C. Jacopin, C. Moulin, T. Bailly, R. Burgada, S. Meunier, P. Baret, J.-L. Pierre and F. Taran, *Chem.-Eur. J.*, 2005, **11**, 3689–3697.

80. C. Dinse, N. Baglan, C. Cossonnet and C. Bouvier, *Appl. Radiat. Isot.*, 2000, **53**, 381–386.
81. M. Archimbaud, M.-H. Henge-Napoli, D. Lilianbaum, M. Deslorges and C. Montagne, *Radiat. Prot. Dosim.*, 1994, **53**, 327–330.
82. K. Araki, N. Hashimoto, H. Otsuka, T. Nagasaki and S. Shinkai, *Chem. Lett.*, 1993, **22**, 829–832.
83. A. Spagnul, C. Bouvier-Capely, G. Phan, F. Rebiere and E. Fattal, *Health Phys.*, 2010, **99**, 430–434.
84. O. Averseng, A. Hagege, F. Taran and C. Vidaud, *Anal. Chem.*, 2010, **82**, 9797–9802.
85. J. Duffield and D. M. Taylor, *The Biochemistry of the Actinides, Handbook on the Physics and Chemistry of the Actinides*, Elsevier Science, Amsterdam, 1991.
86. R. A. Guilmette, P. S. Lindhorst and L. L. Hanlon, *Radiat. Prot. Dosim.*, 1998, **79**, 453–458.
87. F. W. Bruenger, B. J. Stover and W. Stevens, *Health Phys.*, 1971, **21**, 679–687.
88. P. W. Durbin, B. Kullgren, J. Xu and K. N. Raymond, *Health Phys.*, 1997, **72**, 865–879.
89. R. A. Guilmette, R. Hakimi, P. W. Durbin, J. Xu and K. N. Raymond, *Radiat. Prot. Dosim.*, 2003, **105**, 527–534.
90. S. Grives, G. Phan, G. Morat, D. Suhard, F. Rebiere and E. Fattal, *J. Pharm. Sci.*, 2015, **104**, 2008–2017.
91. P. W. Durbin, N. Jeung, B. Kullgren and G. K. Clemons, *Health Phys.*, 1992, **63**, 427–442.
92. G. N. Stradling, M. H. Henge-Napoli, F. Paquet, J.-L. Poncey, P. Fritsch and D. M. Taylor, *Radiat. Prot. Dosim.*, 2000, **87**, 29–40.
93. G. N. Stradling, M. H. Henge-Napoli, F. Paquet, J.-L. Poncey, P. Fritsch and D. M. Taylor, *Radiat. Prot. Dosim.*, 2000, **87**, 19–27.
94. D. M. Taylor, G. N. Stradling and M.-H. Henge-Napoli, *Radiat. Prot. Dosim.*, 2000, **87**, 11–17.
95. J. E. Huckle, M. P. Sadgrove, E. Pacyniak, M. G. Leed, W. M. Weber, M. Doyle-Eisele, R. A. Guilmette, B. J. Agha, R. L. Susick, R. J. Mumper and M. Jay, *Int. J. Radiat. Biol.*, 2015, **91**, 568–575.
96. V. Volf, *Radiat. Environ. Biophys.*, 1984, **23**, 141–143.
97. E. Peter and V. Volf, *Health Phys.*, 1981, **40**, 753–755.
98. F. W. Bruenger, G. Kuswik-Rubiega and S. C. Miller, *J. Med. Chem.*, 1992, **35**, 112–118.
99. S. C. Miller, G. Liu, F. W. Bruenger and R. D. Lloyd, *Radiat. Prot. Dosim.*, 2006, **118**, 412–420.
100. J. Fitzsimmons and M. Jay, *J. Radioanal. Nucl. Chem.*, 2015, **305**, 329–336.
101. J. E. Huckle, M. P. Sadgrove, R. J. Mumper and M. Jay, *Health Phys.*, 2015, **108**, 443–450.
102. M. P. Sadgrove, M. G. D. Leed, S. Shapariya, D. B. Madhura and M. Jay, *Drug Dev. Res.*, 2012, **73**, 243–251.
103. K. Sueda, M. P. Sadgrove, J. M. Fitzsimmons and M. Jay, *J. Pharm. Sci.*, 2012, **101**, 2844–2853.

104. K. Sueda, M. P. Sadgrove, J. E. Huckle, M. G. D. Leed, W. M. Weber, M. Doyle-Eisele, R. A. Guilmette and M. Jay, *J. Pharm. Sci.*, 2014, **103**, 1563–1571.
105. G. Phan, B. Ramounet-Le Gall, J. Manceau, M. Fanet, P. Benech, P. Fritsch, E. Fattal and J. R. Deverre, *Int. J. Radiat. Biol.*, 2004, **80**, 413–422.
106. G. Phan, B. Le Gall, G. Grillon, E. Rouit, M. Fouillit, H. Benech, E. Fattal and J. R. Deverre, *Biochimie*, 2006, **88**, 1843–1849.
107. G. N. Shankar, S. Potharaju and C. E. Green, *Drug Dev. Res.*, 2014, **75**, 37–46.
108. G. N. Shankar, W. Weber, M. Doyle-Eisele and R. A. Guilmette, *Drug Dev. Res.*, 2012, **73**, 290–298.
109. J. P. Wilson, R. R. Cobb, N. W. Dungan, L. L. Matthews, B. Eppler, K. V. Aiello, S. Curtis, T. Boger, R. A. Guilmette, W. M. Weber, M. Doyle-Eisele and J. D. Talton, *Health Phys.*, 2015, **108**, 308–318.
110. J. D. Reddy, N. W. Cobb, N. W. Dungan, L. L. Matthews, K. V. Aiello, G. Ritter, B. Eppler, J. F. Kirk, J. A. Abernethy, D. M. Tomisaka and J. D. Talton, *Drug Dev. Res.*, 2012, **73**, 232–242.
111. Y. Yamada, A. Koizumi and S. Fukuda, *Jpn. J. Health Phys.*, 1997, **32**, 167–172.
112. H. Tymen, D. Schoulz, A.-M. Caire-Maurisier, F. Chervrier and P. M. Curet, *Radioprotection*, 2000, **35**, 473–485.
113. C. Gervelas, A.-L. Serandour, S. Geiger, G. Grillon, P. Fritsch, C. Taulelle, B. Le Gall, H. Benech, J. R. Deverre, E. Fattal and N. Tsapis, *J. Controlled Release*, 2007, **118**, 78–86.
114. O. Gremy, N. Tsapis, S. Bruel, D. Renault and A. Van der Meeren, *Radiat. Res.*, 2012, **178**, 217–223.
115. S. Sultana, A. Bhatnagar, H. Rawat, D. K. Nishad, S. Talegaonkar, F. J. Ahmad and G. Mittal, *Pharm. Dev. Technol.*, 2014, **19**, 623–633.
116. C. Belhomme-Henry, G. Phan, N. Huang, C. Bouvier, F. Rebiere, M. Agarande and E. Fattal, *Pharm. Dev. Technol.*, 2014, **19**, 692–701.
117. US Food and Drug Administration. *Approval of new drugs when human efficacy studies are not ethical or feasible*, Washington, DC: US FDA. CIT0028, 2010.
118. US Food and Drug Administration, *Guidance for industry internal radioactive contamination—Development of decorporation agents*. Silver Spring, MD: US Food and Drug Administration, 2006.
119. M. Sturzbecher-Hoehne, J. P. Deblonde and R. J. Abergel, *Radiochim. Acta*, 2013, **101**, 359–366.
120. M. Sturzbecher-Hoehne, T. A. Choi and R. J. Abergel, *Inorg. Chem.*, 2015, **54**, 3462–3468.
121. C. Stefano, A. De Gianguzza, D. Milea, A. Pettignano and S. Sammartano, *J. Alloys Compd.*, 2006, **424**, 93–104.
122. G. Tian, Z. Zhang, L. R. Martin and L. Rao, *Inorg. Chem.*, 2015, **54**, 1232–1239.

## CHAPTER 7

# *Evaluation of Iron Overload by Non-Invasive Measurement Techniques*

ROLAND FISCHER<sup>a,b</sup>

<sup>a</sup>University Medical Centre Hamburg-Eppendorf, Department of Pediatric Hematology/Oncology, D-20246 Hamburg, Germany; <sup>b</sup>UCSF Benioff Children's Hospital and Research Center Oakland, Department of Hematology/Oncology, Oakland, CA 94609, USA

\*E-mail: [fischer@uke.uni-hamburg.de](mailto:fischer@uke.uni-hamburg.de)

## 7.1 Introduction

The concentration and total amount of iron in different tissues are critical parameters that determine clinical outcome in all forms of systemic iron overload, independent of whether the iron overload is caused by blood transfusion (*i.e.*, transfusion-dependent thalassaemia, sickle cell disease, aplastic or sideroblastic anaemia, or myelodysplastic syndrome) or by up-regulated intestinal iron absorption (*i.e.*, hereditary haemochromatosis, non-transfusion dependent thalassaemia, iron loading anaemia). The precise assessment of the size of the iron storage pool, which may also include organ volume,<sup>1</sup> is essential for the treatment of chronically transfused patients with

---

RSC Metallobiology Series No. 8

Metal Chelation in Medicine

Edited by Robert Crichton, Roberta J. Ward and Robert C. Hider

© The Royal Society of Chemistry 2017

Published by the Royal Society of Chemistry, [www.rsc.org](http://www.rsc.org)

iron chelators to avoid both toxicity from increased organ iron concentration and side-effects from an excessive chelator dose.<sup>2</sup>

Iron stores can be assessed by *direct* and *indirect* methods. Since the introduction of the serum ferritin test<sup>3</sup> additional indirect iron quantification parameters (histological total iron score,<sup>4</sup> non-transferrin bound iron NTBI,<sup>5</sup> labile plasma iron LPI,<sup>6</sup> hepcidin<sup>7</sup>) were developed for the estimation of iron stores and/or to resolve our understanding of iron pathways. Many of the indirect parameters are well suited for the quantitative determination of normal iron stores or to diagnose iron deficiency, but fail in the measurement of iron overload. For example, the relationship of 8 mg storage iron per 1  $\mu\text{g L}^{-1}$  serum ferritin as found in normal subjects by exhaustive quantitative phlebotomy cannot be transferred to iron-overloaded patients.<sup>8,9</sup>

In recent years there has been increased interest in non-invasive quantitative iron measurements. These developments were especially influenced by the progress in molecular biology, which led to the discovery of different genes and mutations of hereditary haemochromatosis.<sup>10</sup> Interest was further fuelled by the development of novel oral iron chelators such as deferiprone and deferasirox for the treatment of transfusional iron overload.<sup>11-13</sup> The recognition that cardiomyopathy and arrhythmia are the most frequent causes of death in thalassaemia has provided a further stimulus for the further development of non-invasive measurements of cardiac iron.<sup>14,15</sup>

Progress in measurement technology added another stimulus to the development of non-invasive iron assessments. Biomagnetic liver susceptometry (BLS) based on low temperature (4 K, SQUID) and high (77 K) or room temperature systems is available, or under development, as a routine method at a few centers.<sup>16-18</sup> Quantitative magnetic resonance imaging (MRI-R2) now allows the measurement of iron distribution and its averaged concentration in an entire slice of the liver.<sup>19</sup> The application of fast MRI-GRE methods (GRE = Gradient Recalled Echo, MRI-R2\*/T2\*) to the heart and liver has offered new strategies in the treatment of transfusional siderosis.<sup>15,20</sup> MRI-R2 and -R2\* methods have now also been used to assess iron in the spleen, pancreas, bone marrow, pituitary, and brain.<sup>21-23</sup>

Other methods, such as computer tomography (CT), even dual energy CT, iron-specific X-ray fluorescence (XRF) and nuclear resonance scattering (NRS), have not gained clinical significance. Since most *in vivo* measurement techniques are non-specific for iron (except XRF and NRS), they need tissue samples with physico-chemical measurement of iron (MRI-T2/R2, -T2\*/R2\*) for calibration, or at least for validation (biosusceptometry).

The following review articles give an overview of non-invasive iron measurements in different application areas: Brittenham, 1988 (biopsy, X-ray techniques, SQUID Biosusceptometry);<sup>24</sup> Jensen, 2004 (liver, heart, pituitary);<sup>25</sup> Haacke *et al.*, 2005 (brain regions: MRI methods, autopsy iron);<sup>26</sup> Fischer and Harmatz, 2009 (SQUID Biosusceptometry, MRI-R2, -R2\*);<sup>27</sup>

Wood, 2015 (cardiac, endocrine MRI).<sup>28</sup> This work concentrates on non-invasive iron overload measurement techniques mainly developed after 2000.

## 7.2 Principles of Iron Measurement Techniques

### 7.2.1 Reference Standards for Iron Quantification Methods

The reference method for direct measurement of non-heme iron is a biopsy with iron-specific quantification methods such as atomic absorption spectroscopy (AAS) or inductively coupled plasma mass spectrometry (ICP-MS) and XRF. For many organs, tissue samples are not, or only rarely, available (heart, glands, or brain). In these cases iron measurements in tissue samples from autopsy can serve as reference standards. However, *in vitro* calibration of iron-proportional MRI parameters by biopsy or autopsy samples is problematic due to the temperature dependence.

#### 7.2.1.1 Liver Biopsy

In patients with iron overload, 70–90% of the total body storage iron is stored in the liver, which made the liver biopsy the favoured reference target for non-invasive iron measurement methods.<sup>1,29</sup>

Since the execution of the first liver biopsy by Paul Ehrlich (1883), and its expanding use during and after World War II in connection with hepatitis infections, different liver biopsy techniques have been introduced into the clinical routine.<sup>30</sup> The most frequent complications are hypotension caused by haemorrhage and pain in about 30% of the patients.<sup>31</sup> Using the liver iron concentration from a small biopsy sample as the reference method, which is representative of total or regional liver iron (“gold standard”), is a continuously discussed question. A minimum wet weight of 4 mg or 1 mg dry weight ( $\text{mg}_{\text{d.w.}}$ ) is still recommended.<sup>32</sup> Moreover, a homogeneous iron distribution in the liver is assumed, which may not always be true for iron overload diseases.<sup>33</sup> In iron-overloaded patients without liver disease, an agreement of 7.1% (CV) was reported between two liver biopsies (mean: 10  $\text{mg}_{\text{d.w.}}$ ) from distant liver regions.<sup>34</sup> Intraorgan variability between large, biopsy-sized, local and remote samples was also studied and resulted in large variabilities with CVs from 4 to 73%.<sup>35</sup> With modern spring-loaded cutting needles, a similar agreement (mean: 7.6%) between 2 local percutaneous biopsy specimens (1  $\text{mg}_{\text{d.w.}}$ ) was achieved in patients with transfusion-dependent thalassaemia (TDT) and sickle cell disease (SCD) but with differences of up to 30%.<sup>36</sup> Intraorgan variability is also affected by the disease state (high iron concentration, fibrosis, cirrhosis, hepatitis).<sup>35,37</sup>

Further effects with potential impact on iron concentration measurements by non-invasive techniques are the diurnal variation of liver volume, the cellular iron distribution, the size of the iron deposits,<sup>38–40</sup> and also the wet-to-dry weight ratio in different tissue with respect to total organ iron and *in vivo* biosusceptometry (see Section 7.3.4).<sup>16,29</sup>

### 7.2.1.2 Quantitative Heart Biopsy and Autopsy

In contrast to the liver, the direct physico-chemical determination of heart iron (CIC = cardiac iron concentration) by a catheter-directed right ventricular endocardial biopsy is rarely performed. In addition, the endocardial biopsy is not representative for the entire heart iron because of the small sample size and the inhomogeneity of the iron distribution in the myocardial tissue.<sup>41,42</sup>

In autopsy hearts with significant histological iron staining, CIC values between 160 and 1470  $\mu\text{g g}_{\text{wet weight}}^{-1}$  were found by Buja and Roberts with an iron concentration gradient from the endocardium to the iron-richer epicardium, and with a relatively high wet-to-dry weight ratio of  $6.5 \pm 0.6$ .<sup>43</sup> All patients with  $\text{CIC} > 600 \mu\text{g-Fe g}_{\text{w.w.}}^{-1}$  and more than 23 g of transfused iron had developed heart insufficiency. In autopsy hearts of patients with hereditary haemochromatosis, CIC values of  $> 500 \mu\text{g g}_{\text{w.w.}}^{-1}$  (normal: 20–125  $\mu\text{g g}_{\text{w.w.}}^{-1}$ ) were found in the entire left ventricular free wall, in the septum, and also in the atrial myocardium, especially in the AV node.<sup>44</sup>

Similar CIC values of 860 and 17  $\mu\text{g g}_{\text{w.w.}}^{-1}$  were observed before and after heart transplantation, respectively, in a juvenile hereditary haemochromatosis patient.<sup>45</sup> Autopsy CIC data from a 24-year-old transfusion-dependent thalassaemia (TDT) patient were also reported by Ghugre *et al.* in a range of 770–1500  $\mu\text{g g}_{\text{w.w.}}^{-1}$  with higher iron concentrations in the epicardium and a wet-to-dry weight ratio of  $7.0 \pm 0.4$ .<sup>46</sup> In largest autopsy study thus far, with 12 hearts from TDT patients, no significant difference between whole heart and septum was found in a CIC range of 500–4000  $\mu\text{g g}_{\text{w.w.}}^{-1}$ . RV wall and LV atrial CIC was found to be lower by 22% and 28%, respectively.<sup>47</sup>

### 7.2.1.3 Bone Marrow Iron

In the bone marrow, macrophages predominantly store iron in the siderosomes of the cytosol in the form of aggregated haemosiderin and/or ferritin. In iron overload, also other (plasma) cells contribute to the iron store.<sup>48</sup> Bone marrow iron is usually estimated by histological grading and only a few quantitative studies were performed in the past. Non-heme iron concentrations between 20 and 8647  $\mu\text{g g}_{\text{w.w.}}^{-1}$  were measured in autopsy samples from White and Bantu males/females with a good correlation between histological grading and marrow iron concentrations. The ratio of ferritin/haemosiderin iron was about 1 : 5 in iron-overloaded samples with less than 5% of heme iron.<sup>49</sup> In post-mortem bone marrow transplants from transfusion-dependent leukaemia patients, iron was determined in a range from 932–3942  $\mu\text{g g}_{\text{d.w.}}^{-1}$  and was correlated ( $p = 0.006$ ) with the morphometrically-estimated percentage of macrophage iron-(haemosiderin)-containing area.<sup>50</sup>

### 7.2.1.4 Post-Mortem Brain Iron

Iron is an essential trace element in many metabolic processes in the brain (*e.g.*, protein synthesis, enzyme cofactors, myelin formation). Iron deficiency in the brain may alter these processes leading to cognitive deficits or

to disturbed motor function (*e.g.*, restless leg syndrome).<sup>51</sup> In contrast, iron accumulation in the brain leads to various neurodegenerative diseases (*e.g.*, NBIA, Parkinson's, Alzheimer's). For calibration, *in vivo* MR relaxation measurement techniques rely on autopsy brain tissue samples, often on historically measured iron concentrations.<sup>52–54</sup> A reliable judgement on significant iron loading needs age adjustment, especially in paediatric and adolescent patients.<sup>26,52</sup> High iron concentrations were found in the globus pallidus of normal controls by Hallgren and Sourander, which exponentially increased from 182 to 215  $\mu\text{g-Fe g}_{\text{w.w.}}^{-1}$  at age 20 to 50 years, respectively.<sup>52</sup> However, there is a significant disagreement with the data of Loeffler *et al.*, who found, for example, in the globus pallidus of young (27–63 year-old) and elderly (67–88 year-old) control subjects iron concentrations of 56 and 29  $\mu\text{g-Fe g}_{\text{w.w.}}^{-1}$ , respectively.<sup>53</sup> These values could not be confirmed in later reports (see Section 7.4.6).

## 7.2.2 Biochemical Properties of Iron Storage Molecules

Both magnetic resonance imaging (MRI) and biomagnetic susceptometry (BS) are mainly based on the antiferromagnetic and paramagnetic properties of ferritin and haemosiderin iron. Their distribution can be different in the liver, spleen, heart, brain and other organs, with different impacts on relaxation time shortening or specific magnetic volume susceptibility. Ferritin iron shortens both T1 and T2, while the cluster-sized haemosiderin iron lacks significant T1 shortening and has a stronger T2 impact.<sup>54,55</sup> Ferritin and its degradation product, haemosiderin, were preferentially studied by Moessbauer spectroscopy, electron microscopy, elemental analysis by ICP, and AC magnetic susceptometry in tissue samples from thalassaemic heart and spleen, in human, from rat liver, and from horse spleen.<sup>40,56–60</sup> Differences between these two main iron storage compounds with potential implications in MR relaxation and biosusceptometrical measurements were observed with respect to blocking temperatures,<sup>56,60</sup> superparamagnetism,<sup>60</sup> chemical composition,<sup>58</sup> and core diameter.<sup>40,56,57,61</sup> Especially, core diameters of 6.4–7.5 nm and 5.7 nm were found for ferritin and haemosiderin cores, respectively, and even smaller (3.3 nm) for brain ferritin cores.<sup>57,61</sup> Considering the cluster size of aggregated haemosiderin cores, with a diameter of about 500 nm, a  $10^5$ -fold volume difference would be calculated.<sup>40,57</sup>

In heavily iron-overloaded patients with hereditary haemochromatosis (HH) and iron-loading anaemias, equal amounts of ferritin and haemosiderin (non-ferritin) iron were found by Zuyderhoudt *et al.* in liver needle biopsies, while ferritin iron increased relatively in low grade iron overload.<sup>62</sup> Using a modified fractionating micro-method in liver samples from dietary iron-loaded rats, Nielsen *et al.* determined a ferritin : haemosiderin iron ratio of 1.8, which slowly decreased by 0.14 per 10 mg  $\text{g}_{\text{w.w.}}^{-1}$  of accumulated non-heme liver iron.<sup>63,64</sup> This modified micro-method was also applied to liver biopsies from patients with HH and TDT in the framework of the validation of SQUID biosusceptometry (see Figure 7.1).<sup>65</sup> The haemosiderin : ferritin ratio increased from 1:1 at 400 (upper normal threshold) to 3:1 at

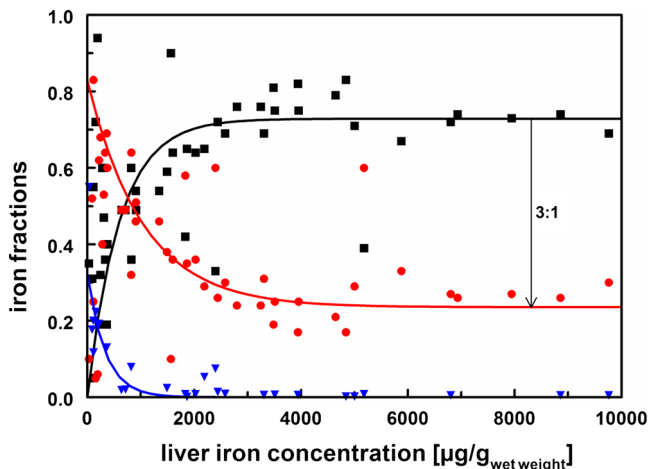


**Figure 7.1** Haemosiderin (black), ferritin (red), and haem (blue) iron fractions were determined according to Zuyderhoudt *et al.* (1978)<sup>63</sup> in liver biopsies (mean wet weight:  $15 \pm 11$  mg, recovery:  $95 \pm 8\%$ ) from patients with hereditary haemochromatosis and transfusion-dependent thalassaemia. The data can be described by one-term exponential functions ( $r^2 = 0.91\text{--}0.99$ ) with a haemosiderin: ferritin ratio of 3:1 beyond LIC  $>5000 \mu\text{g g}_{\text{wet weight}}^{-1}$ .

$8000 \mu\text{g g}_{\text{w.w.}}^{-1}$  of total LIC. Assuming a smaller specific magnetic susceptibility for haemosiderin than for ferritin iron could explain the curvilinear relationship of biosusceptometrically-assessed LIC beyond 4–5000  $\mu\text{g g}_{\text{w.w.}}^{-1}$  similarly to MRI-R2.<sup>19</sup>

### 7.2.3 Magnetic Properties of Iron Storage Molecules

Both magnet resonance imaging (MRI) and biomagnetic liver susceptometry (BLS) exploit the paramagnetic property of ferritin and haemosiderin iron, and, in principle, also that of deoxyhaemoglobin. The magnetic dipole moments, both of the proton (MRI) and of the iron electrons (BLS) become aligned with the magnetic field direction, but disturbed by thermal movement. Thus, only a small fraction of dipole moments will finally generate the diagnostically usable signal. The sum of all magnetic dipole moments  $\Sigma m_i$  in a volume element  $dV$  accounts for the magnetization  $\mathbf{M}$ , which is proportional to the external magnetic field  $B_f$  multiplied by the magnetic susceptibility  $\chi$  (a material constant) of diamagnetic and paramagnetic biological tissue. The change of the magnetic flux  $\Delta\Phi$ , is picked up by protons or an electronic detector coil, which itself generates a virtual magnetic field  $B_d$  (eqn (7.1)). The magnetic flux change (as function of time  $t$ ) will *directly* induce a voltage change in the magnetometer coil (BLS) or will *indirectly* generate a radio wave signal emitted by the protons and received by the MR imager body coil (see Figure 7.2).<sup>66</sup>

## From Signal to Liver Iron Concentration (LIC)

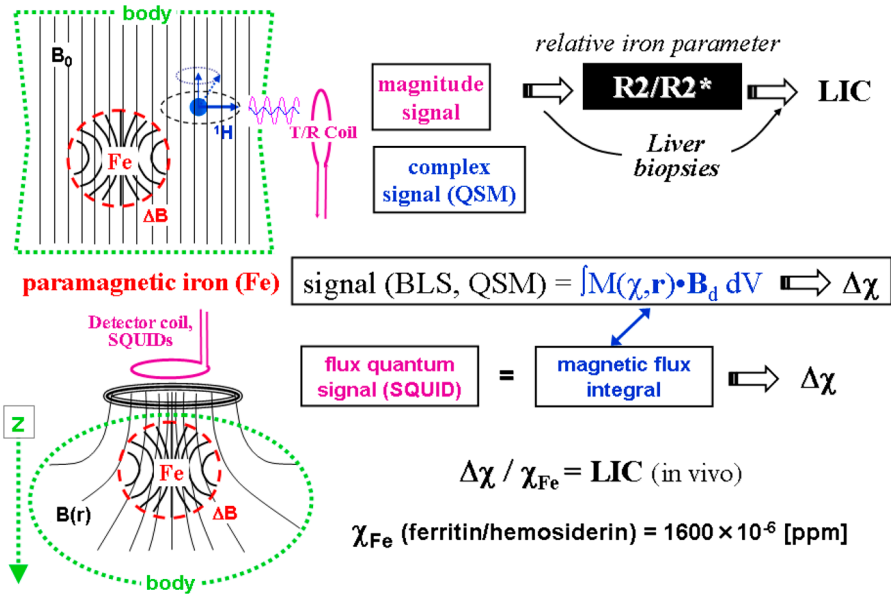


**Figure 7.2** Iron measurements by nuclear (protons,  $^1\text{H}$ ) and electronic (detector coils, SQUIDs) probes: paramagnetic hemosiderin & ferritin iron distorts the static magnetic field ( $B_0$ ,  $B(r)$ ), the field distortion ( $\Delta B$ ) either affects excited protons (after transmission of a resonant RF signal) or induces a current in the electronic detector coil, which is highly sensitive and transformed into magnetic flux quanta by a SQUID. MR picked up by the transmitter/receiver coil (T/R coil) or SQUID signals are generated by the relaxation of the transverse magnetization (blue  $^1\text{H}$  arrow) or by moving the patient inside the magnetic field (green  $z$  arrow), respectively. From the complex, phase or quantum flux signals, the bulk magnetic susceptibility difference  $\Delta\chi$  (relative to a reference medium: air, water, adipose fat) can be analytically derived. From the magnitude of the signal and the resulting relaxation rates ( $R1$ ,  $R2$ ,  $R2^*$ ) LIC can be empirically obtained, after calibration *versus* physico-chemically assessed iron in biopsies or autopsy tissue.

$$\Delta\Phi = \int d/dt(M(\chi, \mathbf{r}) \bullet \mathbf{B}_d) d^3r \quad (7.1)$$

The transverse relaxation rates ( $R2$ ,  $R2^*$ ) can only be transformed from MRI signals (intensities as function of echo time) into iron concentration (LIC) by first establishing a calibration with known tissue iron concentrations, such as in the liver or heart.<sup>15,67</sup> In other tissue, the relaxation rates  $R2$ ,  $R2^*$  ( $1/T2$ ,  $1/T2^*$ ) have to be used as relative (surrogate) iron parameters. The BLS signal (voltage changes *versus* distance or time) can be directly transformed into iron concentration, especially LIC, *via* magnetic flux integrals calculated from first physical principles (eqn (7.10)) and using the known

specific magnetic susceptibility ( $\chi_{\text{Fe}}$ ) for the haemosiderin/ferritin iron compound.<sup>16</sup> In quantitative susceptibility mapping (QSM), the transformation of the MRI signal (phase) into magnetic susceptibility *via* a mathematical operation (convolution) on magnetic dipole and susceptibility functions also relies on known magnetic susceptibilities for haemosiderin and ferritin iron as in BLS.

### 7.2.3.1 Specific Magnetic Volume Susceptibility (Electron Magnetism)

Biosusceptometry (BLS and QSM) exploit the temperature-independent diamagnetic and the temperature-dependent paramagnetic response of biological tissue to an external magnetic field  $H$ . The magnetization vector  $\mathbf{M}$  and its induced field  $B$  in tissue is directly proportional to  $H$  and to the magnetic susceptibility  $\chi$  characterizing the magnetic property of tissue molecules (eqn (7.2)).

$$\mathbf{M} = \chi B \sim (1 + \chi)H \quad (7.2)$$

In tissue, especially in hepatocytes and/or macrophages, the core particles ( $\text{Fe}^{3+}$ -oxyhydroxide) form a ferritin-iron complex inside a water-soluble spherical cavity and exhibit a paramagnetic volume susceptibility due to their electrons in the 3d atomic shell with a maximum of 5 unpaired spins. In iron overload states (Figure 7.1), ferritin will be degraded into water-insoluble *haemosiderin* with a more variable  $\text{Fe}^{3+}$  structure and can be aggregated to  $10^5$ -fold larger clusters inside siderosomes (see also Section 7.3.1).<sup>60</sup> The magnetic volume susceptibility  $\chi$  can be calculated according to the Curie law from the effective magnetic dipole moment  $\mu_{\text{eff}}$  in terms of Bohr magnetons [ $\mu_{\text{B}}$ ] (= magnetic dipole moment of the electron) and temperature  $T$  [K], eqn (7.3).

$$\chi = 1/T \times (\mu_{\text{eff}}/C)^2 \quad (7.3)$$

The constant  $C$  has a value of 5.987 in the MKS-system (2.84 in the cgs-system). The effective magnetic moment for a specific electron spin state  $J$  is calculated as  $\mu_{\text{eff}} = g \times \sqrt{J(J+1)}$  [ $\mu_{\text{B}}$ ] with the Landé factor  $g = 2.0$ . For the free  $\text{Fe}^{3+}$  ion with the maximum spin state  $J = 5/2$ , one would calculate  $\mu_{\text{eff}} = 5.9 \mu_{\text{B}}$ . From chemical structure considerations of coordination bonds with 4 ligands, the existence of 3 unpaired spins was concluded.<sup>68,69</sup> Thus with  $J = 3/2$ , a  $\mu_{\text{eff}}$  of  $3.87 \mu_{\text{B}}$  is obtained, which is close to the experimentally found values for ferritin, haemosiderin, and total iron in Table 7.1. Hilty *et al.* reconstituted apo-ferritin from horse spleen ferritin (HoSF) with 8–24  $\text{Fe}^{3+}$  and with 8  $\text{Fe}^{2+}$  ions. Effective moments between  $3.8 \mu_{\text{B}}$  (intact HoSF) and  $4.9 \mu_{\text{B}}$  ( $\text{HoSF}(8\text{Fe}^{2+})$ ,  $J = 2$ ) were measured by NMR susceptometry.<sup>70</sup>

Different magnetic susceptibilities for ferritin and haemosiderin were measured in various species in the past, see Table 7.1.<sup>69–79</sup> The relatively low

**Table 7.1** Iron specific magnetic susceptibility ( $\chi_{\text{Fe}}$ ) measurements of ferritin and/or haemosiderin in horse spleen ferritin (HoSF), reconstituted HoSF (rHoSF) with  $n\text{Fe}^{3+}$ , rabbit, human (transfusion- and non-transfusion-dependent thalassaemia, TDT and NTDT), and in total liver, spleen, and brain tissue samples ( $J$  = spin state, ( $n$ ) = number of samples).

Species	Preparation	Method	$T$ (K)	Fe (%)	$\chi_{\text{mol}}$ [ $10^6$ ]	$\chi_{\text{Fe}} \pm \text{SD}$ [ $10^6 \text{ cm}^3 \text{ g}^{-1}$ ]	$\mu_{\text{eff}}$ [mB] (310 K)	$\chi_{\text{Fe}}$ [ppm] (310 K)	Reference	Authors	
Fe <sup>3+</sup> -hydroxide	$J = 3/2$	Theory	310		6013	1353	3.877	1353		Physics	
rHoSF(24Fe <sup>3+</sup> )	$J = 3/2$	NMR	310		6083	1369	3.900	1369	70	Hilty <i>et al.</i> , 1994	
<i>ferritin</i> HoSF	Solution	Gouy balance	295		5980	1346	18	3.867	1280	71	Michaelis <i>et al.</i> , 1943
HoSF	Solution	Gouy balance	296		6200	1395		3.937	1332	69	Bayer & Hauser, 1955
HoSF	Commercial	NMR	293		6050	1361		3.889	1287	72	Schoffa, 1965
HoSF	Commercial	Edwards balance	295	7.5	6755	1520	44	4.110	1446	73	Engelhardt, 1992
Rabbit (2)	Iron dextran	Gouy balance	295	14.9	6675	1502	81	4.085	1429	74	Shoden & Sturgeon, 1959
Human (TDT, 3)	Solution	Gouy balance	295	15.9	7273	1637	44	4.264	1557	74	Shoden & Sturgeon, 1960
<i>haemosiderin</i> HoSH	Suspension	Gouy balance	295		4810	1082	65	3.468	1030	71	Michaelis <i>et al.</i> , 1943
Rabbit (2)	iron dextran	Gouy balance	295	25.8	6605	1486	135	4.064	1414	74	Shoden & Sturgeon, 1959
Human (TDT, 3)	Purified	Gouy balance	295	25.9	6987	1572	474	4.180	1496	74	Shoden & Sturgeon, 1960

(continued)

**Table 7.1** (continued)

Species	Preparation	Method	$T$ (K)	Fe (%)	$\chi_{\text{mol}}$ [ $10^6$ ]	$\chi_{\text{Fe}} \pm \text{SD}$ [ $10^6 \text{ cm}^3 \text{ g}^{-1}$ ]	$\mu_{\text{eff}}$ [mB] (310 K)	$\chi_{\text{Fe}}$ [ppm] (310 K)	Reference	Authors
<i>total iron (haemosiderin &amp; ferritin)</i>										
Rabbit livers	iron dextran	Susceptometry	298		6500	1463	4.031	1406	75	Bauman & Harris, 1967
Human livers (5)	Autopsy	Susceptometry	298		7022	1580	60	4.190	76	Messer & Harris, 1967
Liver (NTDT, 4)	Freeze-dried	AC susceptometry	310		5067	1140	110	3.559	78	Hackett <i>et al.</i> , 2007
Spleen (TDT, 15)	Splenectomized	Biosusceptometry	295		7342	1652	145	4.285	77	Zander, 2001
Spleen (NTDT, 11)	Freeze-dried	AC susceptometry	310		6889	1550	230	4.150	78	Hackett <i>et al.</i> , 2007
Spleen (TDT, 7)	Freeze-dried	AC susceptometry	310		5156	1160	250	3.590	78	Hackett <i>et al.</i> , 2007
Human brain (13)	Autopsy (38–81 years)	QSM	310		4311	970	30	3.283	79	Langkammer <i>et al.</i> , 2012

magnetic susceptibility of brain iron, measured in a range from 29 to 239  $\mu\text{g g}_{\text{ww}}^{-1}$  in different brain regions (from white matter to globus pallidus), may also be caused by the QSM measurement technique (see Section 7.3.4.2).<sup>79</sup>

Especially, the susceptibility of the aggregated haemosiderin iron, which dominates iron overload states (Figure 7.1), is not well known. The magnetic volume susceptibility of the water-insoluble haemosiderin iron was found to vary between  $1017 \times 10^{-6}$  and  $2086 \times 10^{-6}$  (dimensionless in SI-units).<sup>71,74</sup> From the chemical similarity of the haemosiderin and ferritin molecular core particles, and from the agreement between magnetic and chemical determinations of iron concentrations in human liver samples with various mixtures of ferritin and haemosiderin iron, one could assume the same magnetic susceptibility value.<sup>80</sup> A reasonable mean value of the susceptibility for human liver haemosiderin/ferritin iron seems to be  $\chi\rho = 1.6 \times 10^{-6} \text{ g}_{\text{liver}} \text{ mg}_{\text{Fe}}^{-1}$  or 1600 ppm at 37 °C ( $\rho = 1.05 \text{ g cm}^{-3}$  for liver tissue) as suggested by Williamson and Kaufman for biomagnetic liver susceptometry.<sup>81</sup> This value is  $10^4$  times higher than from any other competing diamagnetic response ( $\chi < 0$ ) of biologically relevant tissue (water:  $-9.032 \times 10^{-6}$  ppm, fat:  $-(8.2 \pm 0.2) \times 10^{-6}$  ppm, bone:  $-(11.3 \pm 0.3) \times 10^{-6}$  ppm).<sup>82,83</sup>

However, as magnetic measurements on haemosiderin samples are scarce,<sup>60,74</sup> especially at room temperature, differences between the magnetic susceptibility of haemosiderin and ferritin due to size of core particles, iron burden and distribution in different cells (macrophages, hepatocytes, myocytes, acinar and beta cells, brain) are not ruled out up to now.<sup>60,61,74,78,79</sup>

### 7.2.3.2 Iron Concentration and Wet-to-Dry Weight Ratio

Non-invasive iron measurements are *in vivo* measurements and the corresponding native *in vitro* iron measurement (in biopsies or autopsies) would be a wet weight iron concentration. In biopsies with small tissue samples ( $\leq 10$  mg), this may become problematic because of humidity loss in tissue tubes and further processing.<sup>27</sup> In liver biopsies, in contrast to brain autopsy samples, iron concentrations (LIC) have been reported per gram dry weight in recent years.

$$\text{LIC} = \Delta\chi / (\chi_{\text{Fe}}\rho) f_{\text{wdr}} \quad (7.4)$$

In eqn (7.4), LIC is calculated from the relative bulk susceptibility  $\Delta\chi$  (relative to a reference tissue, such as water) and the specific ferritin/haemosiderin iron susceptibility  $\chi_{\text{Fe}}$  including the liver tissue density  $\rho$ , see also Section 7.2.3.1. The widely adopted wet-to-dry weight ratio of  $f_{\text{wdr}}$  (3.46) is based on the water content of 71.1% of normal autopsy liver tissue.<sup>11</sup> In the study of Barry a dry weight of 17% ( $f_{\text{wdr}} = 5.88$ ) of the wet weight was obtained in 61 biopsies (29–47  $\text{mg}_{\text{wet}}$ ), while Zuyderhoudt *et al.* achieved a ratio  $f_{\text{wdr}} = (4.06 \pm 0.61) \text{ g}_{\text{wet weight}} \text{ g}_{\text{dry weight}}^{-1}$  in large liver pieces (5 g post-mortem).<sup>34,63</sup> A critical investigation of the relationship between different liver biopsy preparations

was performed in liver tissue samples resulting in a wet-to-dry weight ratio of  $5.7 \pm 1.4$  to  $6.3 \pm 0.8$  for de-paraffinized, heat-dried liver samples depending on the drying temperature.<sup>84</sup> In a blind direct comparison between LIC [ $\mu\text{g g}_{\text{liver}}^{-1}$ ] by BLS and LIC [ $\mu\text{g g}_{\text{d.w.}}^{-1}$ ] from fresh-tissue heat-dried biopsy excised by cutting needle, a conversion factor of  $6.1 \pm 0.3$  ( $r^2 = 0.92$ ) was obtained.<sup>85</sup> From eqn (7.4) it follows that this conversion factor ( $\approx f_{\text{wdr}}$ ) interacts with the used specific magnetic susceptibility  $\chi_{\text{Fe}}$ .

### 7.2.3.3 Other Magnetic Properties

Another paramagnetic player is heme iron with its deoxyhemoglobin. Although the concentration in blood and tissue is relatively small, its magnetic effect, depending on oxygen saturation fraction ( $[\text{O}_2]$ ) and the hematocrit (Hct) in the blood of the micro-circulation, is exploited by MRI using the blood oxygenation-dependent (BOLD) effect. The magnetic susceptibility difference between deoxyhemoglobin (dox) and oxyhemoglobin (ox),  $\Delta\chi = \text{Hct} (1 - [\text{O}_2]) \Delta\chi_{\text{dox-ox}}$ , can be measured by R2\* in different tissues, with  $\Delta\chi_{\text{dox-ox}} = 3.4$  ppm.<sup>66,86</sup> Similar considerations also apply to the magnetic effect in deoxygenated myoglobin, but this is difficult to differentiate from the preceding BOLD effect.<sup>87</sup>

The superparamagnetism of ferritin (also haemosiderin) is continuously discussed due to its nanometric ferrihydrite core and the anomalous T2 shortening in ferritin solutions similar to that of superparamagnetic nanoparticles (SPIOs).<sup>60</sup> However, the magnetic susceptibility of SPIOs is much larger than that of ferritin. This discrepancy might be explained by a model with paramagnetic iron ions at the ferritin core surface and a smaller number of superparamagnetic particles inside the core.<sup>88</sup>

Ferromagnetic material is found in perturbations from pacemakers, dental clips, tiny metal buttons, some tattoos or inhaled ferromagnetic dust from welding, grinding or smoking.<sup>89</sup>

## 7.3 Iron Measurements: Technique, Analysis, and Calibration

Since the 1980–1990s, different MRI methods such as signal intensity ratio (SIR), spin-echo (SE), or gradient recalled echo (GRE) were introduced for the quantification of iron in the liver and in other organs. A complete survey of different early MRI techniques and other iron measurement methods was made by Jensen.<sup>25</sup> In spite of its complexity, quantitative MRI of iron offers several advantages with respect to 3-dimensional localization (imaging) and detection of small and/or deep-lying tissue regions (brain regions, endocrine glands).

By analogy to electron (atomic) magnetism, characterized by the magnetic moment of a free electron (the Bohr Magneton,  $\mu_{\text{B}} \sim 1/m_e$  see Section 2.1.3.1), nuclear magnetism can be described by the nucleon magneton  $\mu_{\text{N}} \sim 1/m_{\text{n}}$ .

Since the electron mass ( $m_e$ ) is about 2000 times less than the mass of a proton ( $m_p$ ), nuclear magnetism is much weaker than electron magnetism and even weaker for heavier nuclei. However, this weakness is compensated by irradiating a nucleon system with an electromagnetic pulse (RF pulse) of frequency  $\nu$  (also  $2\pi\nu = \omega$ , the Larmor frequency), which is in resonance with its excited energy state,  $\Delta E = h\nu$ , in a magnetic field  $B_0$ , see eqn (7.5), where  $\gamma_n$  is the gyromagnetic ratio for a nuclear isotope possessing a spin.

$$\nu = \gamma_n / (2\pi) B_0 \quad (7.5)$$

At 1 tesla,  $\gamma_n/2\pi$  for protons ( $^1\text{H}$ ) equals 42.6 MHz, while for the iron isotope  $^{57}\text{Fe}$  one only gets 1.4 MHz. However, *in vivo* iron-specific measurement by utilizing the resonance of  $^{57}\text{Fe}$  is confounded by its low relative sensitivity of 0.0034% (100% for protons), which can be partly compensated by isotope enrichment and high magnetic fields (>20 Tesla). For comparison, the gyromagnetic ratio  $\gamma_e$  of electrons is proportional to  $1/m_e$  and thus has a 1000-fold higher frequency (of several GHz) as is used in electron spin resonance.

By analogy to electron magnetism (eqn (7.2) and (7.3)), also the Curie law for nuclei, the “nuclear magnetic susceptibility” ( $\chi_n$ ) can be defined for the magnetization component  $\mathbf{M}_z$  in the direction (z) of the magnetic field  $B_0$  by eqn (7.6):

$$\mathbf{M}_z = \chi_n B_0 = C/T(\mu_N^{\text{eff}})^2 B_0 \quad (7.6)$$

For protons, the analogous definition for the effective nuclear magneton  $\mu_N^{\text{eff}}$  is  $\mu_P^{\text{eff}} = g_P \sqrt{J(J+1)} [\mu_N]$  with the proton  $g$ -factor  $g_P = 5.6$  and spin state  $J = 1/2$ . From eqn (7.6) it follows:

- The magnetization is proportional to the square of  $\mu_P^{\text{eff}}$ , which is also proportional to the square of the gyromagnetic ratio  $\gamma$  (eqn (7.5)).
- Protons have the highest  $\gamma$  value of all isotopes *in vivo* and, together with their high natural abundance, are the most detectable nuclei in MRI.
- Since the magnetization is directly proportional to the magnetic field strength  $B_0$ , higher field strengths (e.g., 3 T vs. 1.5 T) will result in a stronger MR signal.
- Comparison between quantitative *in vivo* measurements and *in vitro* measurements in tissue samples have to take into account a temperature gradient of the nuclear susceptibility of  $+1.5 \text{ s}^{-1} \text{ } ^\circ\text{C}^{-1}$ .<sup>90</sup>

According to eqn (7.1) and (7.6) and Figure 7.2, the resonant radio frequency signal of the protons (64 MHz at 1.5 tesla) received in the detector coil  $B_d$  of an MR imager is determined by the nuclear magnetization of all protons  $\chi_P B_f$  from a selected body volume  $d^3r$ . Currently, there is no satisfactory quantitative theory of the interaction between iron atoms and the nuclear magnetization of the protons in order to calculate the resulting longitudinal and transverse relaxation rates R1 (1/T1), R2 (1/T2), or R2\* (1/T2\*)

from first principles.<sup>91,92</sup> On the other hand, this complex interrelationship may also open up additional information about the haemosiderin and ferritin iron distribution.<sup>93</sup>

In order to measure the magnetic field distortion by paramagnetic iron atoms in the tissue of a subject, one has to generate a magnetic flux alteration in a sensor either by moving the subject or applying an AC field (atomic susceptometry) or by exciting the energy states of protons in a magnetic field (nuclear susceptometry). As with any other magnetometer, such as a conventional induction loop or the superconducting quantum interference device (SQUID) in atomic biosusceptometry, the excited protons serve as a magnetic sensor yielding output signals such as signal intensity (magnitude), phase, and/or frequency shift (see Figure 7.2). In the following sub-sections, quantitative iron measurement methods based on spin-echo (R2), spin-lattice (R1), and gradient recalled echo (R2\*) MRI sequences will be described for the liver (R2, R1) and heart.

In addition, conventional (atomic) and proton biosusceptometry for quantification of liver and brain iron will be presented as well as some X-ray methods.

Acquired MRI raw data are stored as real (Re) and imaginary (Im) data after Fourier transformation of the digitized MR signals in the time space. From these complex data, magnitude (signal intensity,  $\sqrt{\text{Re}^2 + \text{Im}^2}$ ) and phase ( $\{\text{Im}/\text{Re}\}$ ) are calculated for imaging and analysis.

### 7.3.1 Spin-Echo Relaxometry (R2/T2)

In the simplest spin-echo sequence the liver will be exposed to a 90° RF pulse which tilts the proton spins into the transverse *x-y* plane. The whole process of excitation, de-phasing and refocusing of proton spins in a static magnetic field during a spin-echo experiment is schematically illustrated in Figure 7.3. However, spin-spin interaction between protons on the molecular (microscopic) level causes some spins to dephase faster. This irreversible process is described by the transverse or spin-spin relaxation (decay) rate R2 in eqn (7.7). Usually, several 90° pulses, with a repetition time interval TR in between, are applied generating a series of single spin-echoes (SSE). Utilizing several 180° RF pulses after the first 90° excitation pulse leads to a train of multiple spin-echoes (MSE) with equidistant echo spacing.

The resulting signal intensity (magnitude)  $S(t, \text{TR})$  can be described as a function of the echo time  $t = \text{TE}$  and the repetition time TR. Its magnitude and curvature are determined by the longitudinal (spin-lattice) and transverse (spin-spin) relaxation rates R1 ( $=1/\text{T1}$ ) and R2 ( $=1/\text{T2}$ ), respectively. The signal amplitude  $S(0)$  (spin or proton density, intercept) at  $\text{TE} = 0$  and the signal level offset  $S_{\text{LO}}$  are additional unknown parameters in eqn (7.7).<sup>94</sup>

$$S(\text{TE}, \text{TR}) = S(0)(1 - e^{-\text{TR}/\text{T1}})e^{-\text{R2} \times \text{TE}} + S_{\text{LO}}(t \rightarrow \infty) \quad (7.7)$$

In SE measurements, TR is constant and T1 does not change with TE (often  $\text{TR} (1000\text{--}2500 \text{ ms}) > \text{T1}$ , especially as T1 will be shortened in iron-overloaded tissue), thus, eqn (7.7) can be simplified to a mono-exponential function

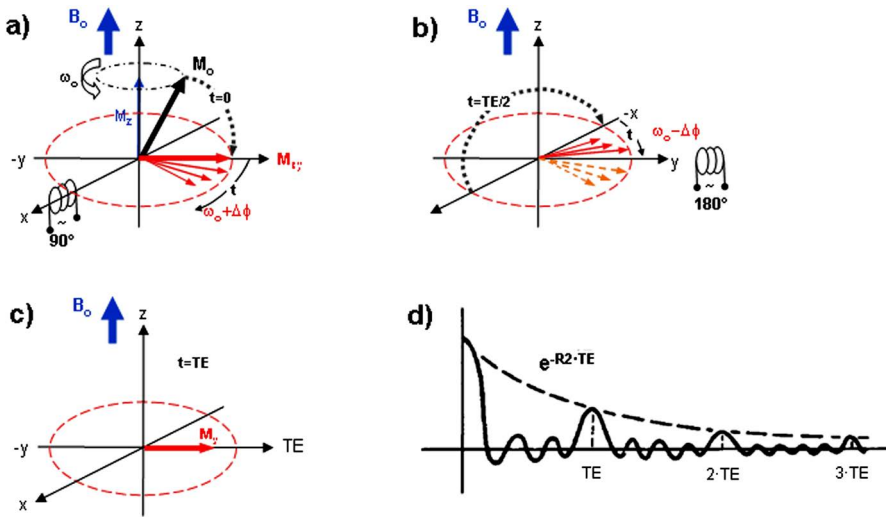


**Figure 7.3** Principle of spin-echo (SE) method: (a) The magnetization  $M_0$ , precessing around the axis  $z$  of the static magnetic field  $B_0$  with the Larmor frequency  $\omega_0$ , is tilted (grey dotted arrow) by a  $90^\circ$  RF pulse into the transverse  $x$ - $y$  plane (thick red arrow  $M_{xy}$ ). The spins contributing to  $M_{xy}$  start to de-phase ( $\omega_0 + \Delta\phi$ ) in the time interval  $TE/2$ . (b) At  $TE/2$  a  $180^\circ$  RF pulse along the  $y$ -axis flips (grey dotted arrow) the de-phased ( $+\Delta\phi$ ) spins to the opposite quadrant of the transverse  $x$ - $y$  plane and the spins start to re-phase ( $-\Delta\phi$ ). (c) At  $TE$  a single SE (SSE) is formed, but meanwhile some spins got lost due to spin-spin interactions and the transverse magnetization  $M_y$  has decayed (shorter red arrow). (d) Applying further  $180^\circ$  RF pulses orthogonally to the decaying magnetization vector at equidistant intervals  $n \times TE/2$  ( $n = 1, 3, 5$ ) will lead to the exponential curve from multiple SE (MSE) amplitudes characterized by the relaxation rate  $R2$ .

with a constant ( $S_{LO}$ ). In the range of low TR additional exponential terms ( $\exp\{TR/T2\}$  and  $\exp\{TE/T1\}$ ) have to be taken into account.<sup>95</sup> There is also a debate about the character of the signal level offset, whether it should characterize a quadratic noise background, tissues with long relaxation times (bi-exponential term or a constant parameter for very long relaxation times), or it should be set to zero.<sup>19,20,96–98</sup> Finally, the model of eqn (7.7) has to be fitted to the signal intensities as a function of TE with the transverse relaxation rate  $R2$  ( $=1/T2$ ), the signal amplitude  $S(0)$ , and the signal level offset  $S_{LO}$  as unknown fit parameters.

The SSE method, as developed by Clarke and St.Pierre (Ferriscan<sup>®</sup>), has now become an acknowledged quantitative procedure for the determination of the liver iron concentration using a standardized measurement protocol, with regular quality control by phantom measurements, and central analysis.<sup>19</sup> This method is often used as reference method for physico-chemical iron quantification in a liver biopsy.<sup>99–101</sup> To overcome the long scan times due to the conventional set of  $90^\circ$ – $180^\circ$  RF pulses with  $TR \geq 1000$  ms, which

gives rise to breathing artefacts, Wood *et al.* applied a SSE sequence with a  $120^\circ$ – $120^\circ$  set of RF pulses and shorter TR/TE (300/3.5 ms) allowing for breath-hold (15 s) data acquisitions per single echo.<sup>20</sup>

In contrast to the SSE method, which uses only the first echo and in which the echo time may vary arbitrarily, the MSE method uses a train of equidistant echoes, which also allows for breath-hold measurements.<sup>102</sup> However, MSE measurements may suffer from imperfections of the refocusing  $180^\circ$  RF pulse or the length of inter-echo spacing.<sup>102,103</sup>

Fat infiltration might become a confounding problem with SE sequences, especially with MSE methods. Papakonstantinou *et al.* found significant differences between R2 without, and R2 with fat suppression in lipid-rich tissue (bone marrow, pancreas) of patients with thalassaemia.<sup>21</sup>

During recent years several calibrations of transverse relaxation rates R2 were performed by iron quantifications in liver biopsies (dry-weight). A selection of representative calibration curves from St. Pierre *et al.* (2005), Wood *et al.* (2005) and Alexopoulou *et al.* (2006) are presented in Figure 7.4.<sup>19,20,102</sup>

The empirical R2 calibration curve of St. Pierre *et al.* (“reference calibration”) shows a curvilinear relationship in its LIC range of 0.3–42.7 mg  $g_{d.w.}^{-1}$ .<sup>19</sup> Beyond liver tissue texture alterations (fibrosis) at high LIC, this may also have been caused by a lower magnetic susceptibility for haemosiderin iron compared to ferritin at high LIC (see Figure 7.1), or by an imperfect estimation of the spin density  $S(0)$  (eqn (7.7)) due to the relatively long 1st TE of 6 ms, especially at high LIC.

From Solomon–Bloembergen equations one should expect a linear relationship of R2 with LIC although the underlying effects from correlation

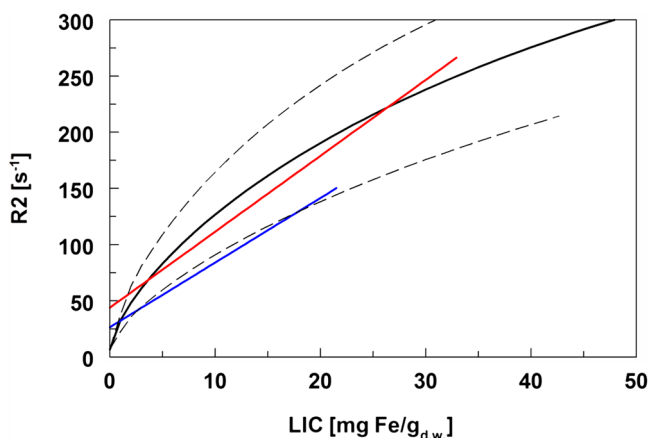


**Figure 7.4** Calibration of transverse relaxation rate R2 by physico-chemical iron quantification in liver biopsies (LIC<sub>dry weight</sub>) using MRI-R2 methods representative for single spin-echo (St. Pierre *et al.*, 2005:  $r^2 = 0.96$ , black line, dashed lines = 95% limits of agreement),<sup>19</sup> breath-hold single spin-echo (Wood *et al.*, 2005:  $r^2 = 0.96$ , red line),<sup>20</sup> and breath-hold multiple spin-echo (Alexopoulou *et al.*, 2006:  $r^2 = 0.76$ , blue line).<sup>102</sup>

time and iron–proton distance may not apply at higher LIC.<sup>91</sup> The R2 linear regression lines of Wood *et al.* (LIC: 1.3–32.9 mg g<sub>d.w.</sub><sup>-1</sup>)<sup>20</sup> and Alexopoulou *et al.* (LIC: 1.4–21.5 mg g<sub>d.w.</sub><sup>-1</sup>)<sup>102</sup> are within the 95% agreement range of the reference calibration.

### 7.3.2 Spin-Lattice Relaxometry (T1/R1)

The rate of recovery of the longitudinal magnetization ( $M_z$ , see Figure 7.3a) after a 90° excitation pulse is described by the longitudinal relaxation rate R1 (1/T1), which can vary from 0.2 s<sup>-1</sup> (cerebrospinal fluid) to 4.1 s<sup>-1</sup> (fat) in normal tissue at 1.5 T. These long recovery times are caused by the transfer of electromagnetic energy from the excited magnetization state ( $M_{xy}$ ) to the thermal equilibrium state ( $M_z$ ) *via* interaction with the phonons of the macroscopic surroundings (the vibrating lattice).

The longitudinal relaxation rate R1 can be measured by performing the SSE method with different TR at constant TE (eqn (7.7)), however, this will require a long scan time. A faster method is the *inversion recovery* pulse sequence (IR), which allows R1 (T1) measurements within a breath-hold. In iron-overload patients with LIC = 1.2–23.9 mg g<sub>d.w.</sub><sup>-1</sup>, R1 rates between 1.6 and 3.4 s<sup>-1</sup> (T1 = 292–634 ms) were determined in the liver by the IR method, which showed a linear relationship with LIC up to 7 mg g<sub>d.w.</sub><sup>-1</sup>.<sup>104</sup>

Although there has been a flood of publications on another fast IR method called *Modified Look-Locker Inversion recovery* (MOLLI) and its fashionable variant, Shortened MOLLI (shMOLLI), mainly used in myocardial T1 mapping, only a few comparative studies with true T1 measurements exist.<sup>105</sup>

Myocardial T1, determined by MOLLI recovery, was compared with T2 and T2\* (range: 4.2–41.7 ms) in TDT patients.<sup>106</sup> A linear relationship ( $r^2 = 0.69$ ) between T1 MOLLI and T2\* was shown for myocardial iron with T2\* < 20 ms (R2\* > 50 s<sup>-1</sup>) and T1 = 500–800 ms, which turned into a quadratic curve in the normal range. A linear relationship ( $r^2 = 0.86$ ) was found for T1 and T2. Similar findings were made for T1 shMOLLI and T2\*.<sup>107</sup> Subjects with normal T1 > 900 ms did not overlap with subjects having cardiac iron levels of T2\* < 20 ms, whilst the clinical significance of low T1 (700–900 ms) in TDT patients with T2\* in the normal range (T2\* > 20 ms, no iron) is debatable with respect to fibrosis or other pathologies.<sup>107</sup>

For simultaneous assessment of fat content and iron concentration in lipid-rich tissue (bone marrow, pancreas, liver) from patients with iron overload, the spin density of water and fat protons have to be separately calculated in eqn (7.9a). Therefore, the knowledge of iron concentration-dependent R1<sub>fat</sub> and R1<sub>water</sub> will be necessary.

### 7.3.3 Gradient-Echo Relaxometry (T2\*/R2\*)

Fast gradient recalled echo (GRE) sequences, for the measurement of liver iron utilize (faster) transverse magnetization with flip angles <90° for the RF pulse and de-phasing (G<sup>-</sup>) plus re-phasing (G<sup>+</sup>) magnetic field gradients instead of

180° RF pulses (Figure 7.3). This allows for shorter scan and echo times, which is always a limitation for the precise determination of transverse relaxation rates. The transverse magnetic relaxation rate  $R2^*$  characterizes the decay of the proton resonance in the vicinity of local magnetic field inhomogeneities caused by susceptibility effects, which are no longer cancelled out by gradient echoes.  $R2^*$  can be described as a sum of decay probabilities from the intrinsic spin–spin relaxation rate  $R2$  plus the extrinsic relaxation rate  $R2'$  (due to field inhomogeneities  $\Delta B$ ;  $\gamma$  is the gyromagnetic ratio) in eqn (7.8).

$$R2^* = R2 + R2' = R2 + \gamma \times \Delta B \quad (7.8)$$

The field inhomogeneity  $\Delta B$  can be transformed into  $\kappa\Delta\chi B_0$  with the constant  $\kappa$  and the bulk magnetic susceptibility  $\Delta\chi$  of iron-containing tissue, see Haacke *et al.*<sup>66</sup> From these relations, one may semi-quantitatively estimate a field-independent iron proportional parameter  $\eta$  by  $R2^* - R2_0 = R2' = \eta B_0$  with  $\eta = \gamma\kappa\Delta\chi$ , which is mainly characterized by the magnetic susceptibility.<sup>26</sup>

In order to measure the relatively small magnetic susceptibility effects from the neighboring iron atoms, a very homogeneous static magnetic field  $B_0 \geq 1.5$  tesla and short echo times (1st TE < 3 ms) are needed. Usually, measures have to be taken to homogenize the main static field  $B_0$  in the target region (active shimming).

### 7.3.3.1 Hepatic $R2^*$

A recent comparison between  $R2$ ,  $R2^*$  and LIC from biopsies has proven that both the reference  $R2$ <sup>19</sup> and  $R2^*$  methods can accurately measure liver iron in a sufficiently wide LIC range.<sup>20,101,108</sup> In addition, MRI- $R2^*$  can be performed within one breath-hold, thus, avoiding breathing artefacts, which have always been a problem with MRI- $R2$  methods with long TRs. Signal intensities measured by GRE- $R2^*$  methods are similarly analyzed as  $R2$  according to eqn (7.9) in the liver as well as in the heart. By variation of the flip angle  $\alpha$ , one could also estimate the spin density (eqn 7.9a).

$$S(\text{TE}) = S^*(0)e^{-R2 \times \text{TE}} + S_{\text{Lo}}(t \rightarrow \infty) \quad (7.9)$$

$$S^*(\text{TR}, \alpha) = S(0)(1 - e^{-\text{TR} \times R1})\sin \alpha / (1 - \cos \alpha e^{-\text{TR} \times R1}) \quad (7.9a)$$

### 7.3.3.2 Cardiac $R2^*$ ( $T2^*$ )

MRI- $R2^*$  celebrated its biggest success in the landmark study of Anderson *et al.* on cardiac iron quantification in patients with  $\beta$ -thalassaemia major.<sup>15</sup> The MRI- $R2^*$  method is more sensitive and better suited to measure the relatively low heart iron concentration than the more classic MRI methods

(R2, SIR). The single breath-hold multi-echo R2\* sequence has emerged as the standard for measuring cardiac iron.<sup>109</sup>

Recently, a calibration of MRI-R2\* by iron quantitation in human heart autopsy samples at 37 °C was successfully performed resulting in a nonlinear relationship (eqn (7.10),  $r^2 = 0.91$ ) with cardiac iron concentration (CIC) in the range of 3.2–25.9 mg g<sub>d.w.</sub><sup>-1</sup> or 500–4050 µg g<sub>w.w.</sub><sup>-1</sup>.<sup>47</sup>

$$\text{CIC} = a \times (\text{R2}^*)^b \quad (7.10)$$

For wet-weight CIC [µg g<sub>w.w.</sub><sup>-1</sup>] from R2\* [s<sup>-1</sup>] and making use of the wet-to-dry weight ratio of 6.4,<sup>43</sup> parameter values of  $a = 1.539 \mu\text{g s g}_{\text{w.w.}}^{-1}$  and  $b = 1.22$  were achieved (see Figure 7.5), which can be transformed into dry-weight CIC [mg g<sub>d.w.</sub><sup>-1</sup>] from T2\* [ms] by  $a = 45.0 \text{ mg (g}_{\text{d.w.}} \text{ ms)}^{-1}$  and  $b = -1.22$ . Worse relationships were obtained for R1 ( $r^2 = 0.52$ ) and R2 ( $r^2 = 0.79$ ).<sup>111</sup>

Cardiac R2\* was also compared with iron concentration calculated from magnetic susceptibility measurements in the apical myocardium by MRI cardio-susceptometry.<sup>110</sup> A linear relationship,  $\text{CIC} [\mu\text{g g}_{\text{w.w.}}^{-1}] = a \text{R2}^* + b$ , from septal R2\* [s<sup>-1</sup>] with  $a = (6.4 \pm 0.4) \mu\text{g s g}_{\text{w.w.}}^{-1}$  and  $b = (-120 \pm 40) \mu\text{g g}_{\text{w.w.}}^{-1}$  was obtained in the range of -100 to 1220 µg g<sub>w.w.</sub><sup>-1</sup>. A similar linear relationship with  $a = 5.5 \mu\text{g s g}_{\text{w.w.}}^{-1}$  and  $b = -196 \mu\text{g g}_{\text{w.w.}}^{-1}$  could be derived from *in vitro* results (25 °C) on a chopped autopsy heart with averaged R2\* adjusted to 37 °C in the range of 960–1325 µg g<sub>w.w.</sub><sup>-1</sup>.<sup>46,90</sup> Agreement between *in vitro* and *in vivo* data was achieved within 95% prediction range although cardiac iron calibration data did not overlap, see Figure 7.5.

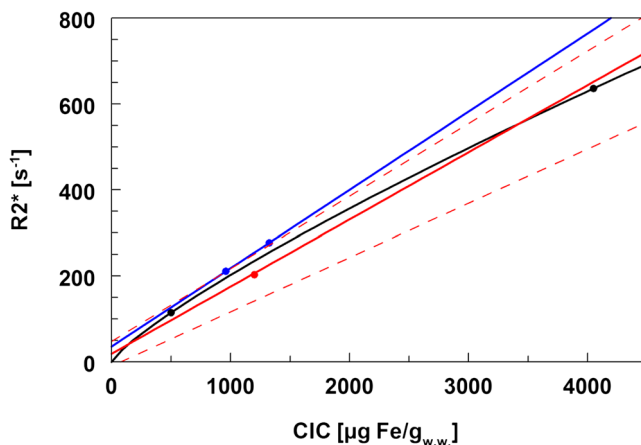


**Figure 7.5** Calibration of gradient-echo transverse relaxation rate R2\* by physico-chemical iron quantification in autopsy hearts (CIC<sub>wet weight</sub>) (Carpenter *et al.*, (2011):  $r^2 = 0.91$ , black line)<sup>47</sup> and by *in vivo* MRI cardio-susceptometry (Wang *et al.*, (2010):  $r^2 = 0.92$ , red line, dashed red lines = 95% prediction range).<sup>110</sup> R2\* calibration derived from chopped autopsy heart is also presented (Ghugre *et al.*, (2006):  $r^2 = 0.46$ , blue line).<sup>46</sup> Circular symbols define the range of cardiac iron calibration data.

### 7.3.3.3 Chemical Shift Relaxometry (CSR)

Another application of  $R2^*$  measurements is based on chemical shift imaging (CSI or Dixon method). Chemical shift effects in lipid-rich tissue from different resonance frequencies (e.g.,  $\Delta\nu = 217$  Hz at 1.5 T of methylene relative to water) are often observed as artifacts in using SE as well as GRE methods.

Applying a fat suppression sequence is one way to resolve these problems in iron overload measurements.<sup>21</sup> Magnetic resonance spectroscopy (MRS) allows quantification of different chemical compounds *in vivo* ( $C^{13}H$ -chains,  $^{31}P$ -ATP) relative to water, and MRS or CSI is heavily used in fat-water quantification in fatty liver diseases, partly with complex algorithms based on real and imaginary MR signal terms.<sup>112</sup> However, chemical shift relaxometry (CSR) in the presence of fat and iron overload, especially in the pancreas and bone marrow, did not find a widespread utilization, probably due to the complexity of the developed algorithms.<sup>112</sup> The fat magnetization,  $M_{xy}^{fat}$ , in the transverse plane behaves differently from water,  $M_{xy}$ , in a fat-water compartment due to resonance shifts (see Figure 7.3 and eqn (7.5)) leading to phase shifts in the de-phasing and re-phasing process. Eqn (7.11) describes the time-signal relaxation function in a fat-water compartment with fat ( $S_f(0)$ ) and water ( $S_w(0)$ ) signal amplitudes in a first approximation.<sup>113</sup> At certain echo times  $t = TE$  [ms], the cosine function in eqn (7.11) will become +1 (in-phase) or -1 (opposed-phase) for a phase shift  $2\pi\nu$  ( $\nu = 0.213$  kHz for fat), which will cause an oscillating signal pattern, see Figure 7.6.<sup>113</sup>

$$S(t) = e^{-R2^*t} \sqrt{S_w(0)^2 + S_f(0)^2 + 2(S_f(0)S_w(0))\cos(2\pi\nu t)} + S_{LO} \quad (7.11)$$

Iron concentration ( $R2^*$ ) and apparent fat content (aFC =  $S_f(0)/[S_f(0) + S_w(0)]$ ) can be simultaneously determined. The *absolute* fat content (FC, proton density

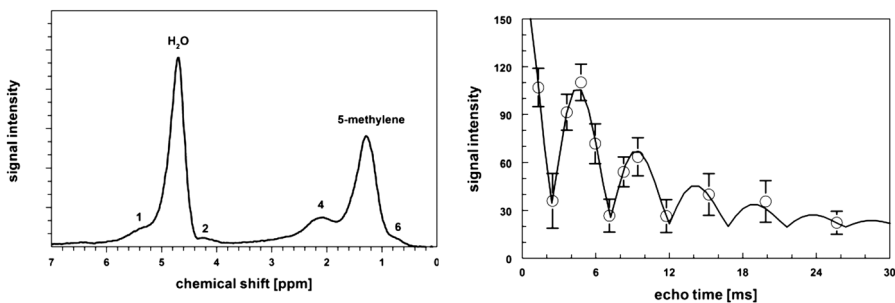


**Figure 7.6** Breath-hold magnetic resonance spectroscopy (MRS, left) and chemical shift relaxometry (CSR, right) in the pancreatic tail of a patient with  $\beta$ -thalassaemia major (age: 23 years, *in vivo* LIC:  $900 \mu g g_{liver}^{-1}$ , HOMA = 2.4). MRS shows the typical fat spectrum also known from the liver.<sup>115</sup> CSR shows the oscillating signal pattern with minima/maxima close to opposed-phase/in-phase echo times. Apparent fat content (aFC = 48%, normal <10%) from CSR ( $R2^* = 126 s^{-1}$ , normal <50  $s^{-1}$ ) and MRS ( $T2$  corrected FC = 52%) agreed within their error limits.<sup>113</sup>

fat fraction, PDFF) can only be obtained with the knowledge of the iron concentration-dependent longitudinal relaxation rates  $R_{1w}$  and  $R_{1f}$  in eqn (7.9a).<sup>113</sup>

Although eqn (7.11) resolves most of the iron measurement problems in lipid-rich tissue,<sup>113,114</sup> there are some shortcomings: only the methylene peak at 217 Hz, accounting for 70% of the lipid spectrum, is considered instead of the whole spectrum,<sup>115</sup> the fat-water dominance above 50% fat content cannot be unambiguously clarified and, especially in iron overload, the assumption  $R_{2^*} = R_{2w}^* = R_{2f}^*$  ("single  $R_{2^*}$  method") will not hold and will need more sophisticated algorithms.<sup>116</sup>

### 7.3.4 Biomagnetic Susceptometry

#### 7.3.4.1 Biomagnetic Liver Susceptometry (Electronic Susceptometry)

Sufficiently sensitive SQUID magnetometers (SQUID = Superconducting Quantum Interference Device), based on the quantum mechanical Josephson effect, became available around 1969. In the case of vertical ( $z$ ) scanning biomagnetic liver susceptometry (BLS), the voltage difference ( $\Delta V(z) = V(z) - V(z \rightarrow \infty)$ ) generated in the SQUID electronics reflects the magnetic flux change ( $\Delta\Phi$ , eqn (7.1)) caused by lowering a patient (with iron overload) below a static inhomogeneous magnetic field. In eqn (7.12) (1st order approximation),  $\Delta V(z)$  is directly proportional to the averaged relative magnetic susceptibility  $\Delta\chi$  of the liver in the sensitivity volume, which is defined by the *magnetic flux integral* calculated from the external magnetic field  $B_f$  and the virtual field from the detector coil  $B_d$  over all volume elements  $dV$  in a distance  $r$  to the lowest coil of the detector coil set (2nd order gradiometer configuration). Eqn (7.12) results in a linear function of the signal voltage *versus* the magnetic flux integral.

$$\Delta V(z) = \Delta\chi C \int B_f(\mathbf{r}) \cdot B_d(\mathbf{r}) dV \quad (7.12)$$

In the practical application of BLS, the difference method is usually employed, which measures the difference in magnetic volume susceptibility  $\Delta\chi$  between the thorax (including the liver with paramagnetic ferritin and haemosiderin iron) and water as reference medium. The precise procedure and the full analysis (2nd order approximation taking also the overlying tissue from the thorax into account) is described elsewhere.<sup>16</sup> This method was validated against the wet-weight iron concentrations of liver biopsies from patients with hereditary haemochromatosis.<sup>65</sup> BLS does not require a calibration by LIC from biopsies, but was rather calibrated (electronic calibration constant  $C$  in eqn (7.12)) by the well-known magnetic susceptibility difference from an air-water interface ( $\Delta\chi = 9.396$  ppm). Other biosusceptometer systems are operating at liquid nitrogen temperatures<sup>17</sup> and even at room temperature without moving the patient,<sup>117</sup> or with air as susceptibility reference medium and scanning patients in the horizontal direction.<sup>18</sup>

### 7.3.4.2 MR-Biosusceptometry and MR-QSM (Nuclear Susceptometry)

Since GRE methods assess local magnetic field inhomogeneities  $\Delta B$  caused by magnetic susceptibility differences  $\Delta\chi$ , one can also generate field and/or phase maps. The basic relationship between the phase  $\Delta\phi$  in an MR image (made up from the real and imaginary term in the complex space) and  $\Delta B$  or  $\Delta v$  is given by eqn (7.13). Thus, the magnetic susceptibility and the resulting iron concentration can be determined from the magnetic field ( $\Delta B$ ), phase ( $\Delta\phi$ ), or frequency maps ( $\Delta v$ ).

$$\Delta\phi = \Delta v \times TE \sim \gamma TE \times \Delta B \sim \Delta\chi \times B_0 \quad (7.13)$$

In certain patient geometries the phase difference  $\Delta\phi$  is related to the magnetic susceptibility difference  $\Delta\chi$  between two adjacent tissue regions by eqn (7.14). The angle  $\theta$  between the main static field  $B_0$  and the target region is  $90^\circ$  for strictly transverse magnitude and phase measurements, while  $S_{\text{hf}}$  is an orientation-independent constant.<sup>112</sup>

$$\Delta\phi = 2\pi TE \times \Delta\chi/3 \times (1 - 3\cos^2\theta + S_{\text{hf}}) \quad (7.14)$$

Using this approach, Wang *et al.* could assess *in vivo* cardiac iron concentrations,<sup>110</sup> while Taylor *et al.* measured the magnetic susceptibility difference from magnetic field maps between thorax and liver tissue in close proximity.<sup>118</sup> A tightly correlated relationship between dry-weight LIC from R2\* and wet-weight LIC from MR-biosusceptometry was obtained ( $r^2 = 0.94$ ).

Quantitative susceptibility mapping (QSM) is an emerging MRI-based technique that measures the magnetic susceptibility of tissue. Unlike MR-biosusceptometry, QSM claims to calculate orientation-independent phase differences and thus iron concentration (angle  $\theta$  in eqn (7.14)). The relationship between magnetic susceptibility and iron concentration is direct and well understood, therefore, QSM offers an attractive alternative to relaxation-based techniques, such as R2\* relaxometry, which rely on empirical calibration curves to establish the relationship to iron concentration. Furthermore, QSM relies on the *phase* of the MR signal whereas R2\* relaxometry relies on the *magnitude* of the acquired signal. Changes to the magnetic susceptibility ( $\Delta\chi$ ) due to the presence of iron overload cause a change in the main (*i.e.*,  $B_0$ ) magnetic field ( $\Delta B(r)$ ). In an MR experiment, as shown in eqn (7.15),<sup>119</sup>  $D(r)$  represents the magnetic dipole response function at location  $r$ ,<sup>120</sup> which is applied to  $\Delta\chi(r)$  *via* a linear convolution operator “ $\cdot$ ”, and  $B_0^{\text{Bkg}}$  represents background contributions to the main magnetic field.

$$\Delta B(r) = (D(r) \cdot \Delta\chi(r)) + B_0^{\text{Bkg}} \quad (7.15)$$

Using a standard gradient-echo MR data acquisition, the magnetic field can be mapped, which yields information about the susceptibility distribution (*i.e.*, iron concentration) using the relationship in eqn (7.15).

MRI-based QSM techniques have recently been developed for the non-invasive measurement of liver iron overload.<sup>121</sup> From the generated susceptibility maps and R2\* maps, significant correlations between ROI based magnetic susceptibility  $\Delta\chi$  (relative to adipose tissue) and R2\* ( $r^2 = 0.94$ ) were obtained, as well as between  $\Delta\chi$  and slice-averaged R2-reference ( $r^2 = 0.76$ ), but  $\Delta\chi$  was systematically biased by a factor of 2, *i.e.*,  $LIC(\Delta\chi) = LIC(R2)/2$ . In a similar study based on field maps, the bulk  $\Delta\chi$  was not biased and a comparable coefficient of determination for predicting LIC(R2) was obtained ( $r^2 = 0.67$ ).<sup>122</sup>

Quantitative susceptibility mapping (QSM) in the brain provides an excellent contrast (magnetic susceptibility), which allows quantitative iron measurements *in vivo*. The origin of this contrast has been attributed to relatively iron-rich paramagnetic structures in the grey matter (*e.g.*, globus pallidus), while CSF and white matter are diamagnetic. Setting the average magnetic susceptibility of white matter to  $-0.03$  ppm, results for CSF (high water content) as a reference medium in  $\Delta\chi = 0.0$  ppm (absolute  $-9.032$  ppm), as in Section 7.3.4.1.<sup>122</sup> From QSM in the brain of 5 healthy males (age: 30–33 years), Lim *et al.*<sup>123</sup> obtained an iron specific susceptibility  $\chi_{Fe}$  of  $738 \times 10^{-6} \text{ cm}^3 \text{ g}_{Fe}^{-1}$  based on the age-adjusted autopsy data of Hallgren and Sourander. Specifically, bulk susceptibilities of  $\Delta\chi = -0.008$  ppm and  $\Delta\chi = (0.103 \pm 0.009)$  ppm were obtained for the thalamus and the globus pallidus, respectively. The iron specific susceptibility  $\chi_{Fe}$  is significantly lower than any value in Table 7.1. In a study with 13 deceased subjects (age: 38–81 years), QSM was performed *in situ*. After temperature adjustment to 37 °C, resulting bulk magnetic susceptibilities were compared with iron concentrations measured by ICP-MS in autopsy specimen. The authors also obtained a relatively small iron specific susceptibility  $\chi_{Fe}$  of  $970 \times 10^{-6} \text{ cm}^3 \text{ g}_{Fe}^{-1}$ .<sup>79</sup>

Different from QSM, the susceptibility weighted imaging (SWI) method does not aim at iron quantification. The contrast enhancement caused by different magnetic susceptibilities between neighbouring tissues will become prominent due to de-phasing spins at sufficiently long echo times ( $TE \approx 40$  ms).<sup>124</sup> Hyperemia due to increased cerebral blood flow is a serious risk of stroke in patients with sickle cell disease (SCD) and is an interesting example for the application of SWI. Quantifying the cerebral venous volume by SWI was accomplished in 21 paediatric SCD patients (HbS  $68 \pm 18\%$ ) in comparison to controls.<sup>125</sup> Significantly smaller volumes were calculated from the SWI contrast images for the SCD patients, especially at 3 T.

### 7.3.5 Other MRI Iron Measurement Techniques

From the very beginning of tissue iron overload assessment in humans, signal intensity ratio (SIR) analysis methods were developed beyond T1 and/or T2 relaxation times. Using a SSE method ( $TE: 35$  ms) at 0.5 T, Johnston *et al.* calculated ratios of liver, spleen, and heart relative to skeletal muscle in patients with hereditary haemochromatosis and in patients receiving

chronic blood transfusions.<sup>126</sup> Patients differed from normal subjects only in liver and spleen but not in the heart. The SIR method of choice for liver iron based on GRE sequences at 1.5 T (TR/TE<sub>1-4</sub>: 120/4–21 ms, FA: 20°, 90°) was developed at the University of Rennes and allows the quantification of LIC within a range of 3.4 to 18 mg g<sub>d.w.</sub><sup>-1</sup> (normal: <2.0).<sup>127</sup> This reference method also allows online analysis by signal intensity data input on the website [www.radio.univ-rennes1.fr](http://www.radio.univ-rennes1.fr).

Proton magnetic resonance spectroscopy (<sup>1</sup>H-MRS), frequently used in patients with fatty liver disease for fat content quantification, may enable reliable measurements of severe hepatic iron overload. Single voxel-sized (3 × 3 × 3 cm<sup>3</sup>) MRS was performed in the liver of 14 biopsied TDT patients with LIC from 0.23 to 37.5 mg g<sub>d.w.</sub><sup>-1</sup> by Wang *et al.*<sup>128</sup> An exponential decay function was fitted to the stimulated echo amplitudes in the voxels. The resulting relaxivity, R2 = 4.9 × LIC + 17.8 (r<sup>2</sup> = 0.90), and the signal-to-noise ratio of 194 at TE = 1.5 ms for the patient with the highest LIC, seem to allow R2 measurements at much higher LIC than 40 mg g<sub>d.w.</sub><sup>-1</sup>. This might be interesting for liver iron assessment at 3 T imagers, where the quantification range is curtailed by a factor of 2 due to the higher sensitivity.

Another MRI method is based on diffusion of molecules due to Brownian motion along a concentration gradient, *e.g.*, transport of molecules through the cell membrane. This molecular movement is de-phasing the spins and thus, irreversibly affecting the relaxation rate R2 (see Section 7.3.3). The signal from both the spin–spin interaction (R2) and the diffusion effect (*D* = diffusion coefficient) can be described by eqn (7.16).<sup>66</sup>

$$S(\text{TE}, b) = S(0)e^{-\text{TE} \times R2} \times e^{-bD} \quad (7.16)$$

The *b*-value,  $b$  [s mm<sup>-2</sup>] =  $\gamma^2 G^2 \text{TE}^3 / 3$ , is determined by the gradient amplitude *G*. For larger TE, the exponential diffusion term dominates (through TE<sup>3</sup>) the signal depending on R2. This concept refers to the well known diffusion weighted imaging (DWI). It was also pointed out by Vymazal *et al.* that the relaxation rate R2 is also dependent on the echo spacing, the diffusion coefficient, and the size of the aggregated ferric oxyhydroxide clusters.<sup>129</sup> Jensen and Chandra (2002) modified the diffusion concept by parameterising the diffusion term *D* into an aggregation index *A* and a diffusion rate R2(*D*).<sup>93</sup> Together with R2, the *reduced relaxation rate* RR2 = R2 – R2(*D*) was defined (this is a simplified definition of RR2). From scanning iron-overload patients with three MSE-trains of different inter-echo spacing (4, 8, 15 ms), the authors were able to successfully demonstrate the separation of total iron into haemosiderin and ferritin iron. Applying this technique later to patients with myocardial iron overload, a fast response to the interruption of regular iron chelation treatment could already be observed within one week by a significant reduction in RR2.<sup>130</sup> The fast response might be explained by the extreme sensitivity of the diffusion rate R2(*D*) in RR2 even to mild iron overload, which is known from the effect of iron deposition in hepatic DWI.<sup>131</sup>

### 7.3.6 Quantitative X-ray Iron Measurement Techniques

Other non-invasive methods, which have exploited the higher electron density of iron atoms ( $Z = 26$ ) relative to water ( $Z = 1$ ), such as X-ray computer tomography (CT), or made use of the X-ray fluorescence (XRF) from excited electrons in the  $K_{\alpha}$ -shell (6.4 keV) of the iron atom, or which used the nuclear resonance scattering (NRS) from  $^{56}\text{Fe}$ , are not used today compared to MRI methods.<sup>132–134</sup> With the exception of NRS, these non-invasive methods, although direct, are not specific for iron or their penetration depth is limited to near surface tissue.

Although tremendous progress has been made in CT technology with respect to speed, resolution, and radiation dose reduction, CT, including dual-energy CT (DECT), is still suffering from the overwhelming non-specific Compton effect (X-ray absorption  $\sim Z$ ) at available higher X-ray energies (80–140 keV). Lower energies, with a preponderance of the photoeffect (X-ray absorption  $\sim Z^3$ ), would not be tolerated due to the higher radiation dose.<sup>135</sup> Dual-energy X-ray absorptiometry (DEXA) is frequently used for bone mineral density (BMD) quantification in the hip and vertebrae in patients with iron overload (TDT, DBA). Moving the target region over the right liver lobe would yield liver-BMD, which was correlated with ferritin in 17 TDT patients and 32 healthy controls ( $r^2 = 0.9$ ).<sup>136</sup> More recently, a study was performed in 37 patients with TDT in order to predict LIC by SQUID biosusceptometry from liver-BMD assessments by DEXA. The prediction of LIC improved from  $r^2 = 0.35$  to  $r^2 = 0.62$  using ferritin alone or a multivariate model of ferritin, body weight, and liver-BMD.<sup>137</sup>

In NRS, the first energy level of  $^{56}\text{Fe}$  with 847 keV can be excited from the radioisotope  $^{56}\text{Mn}$  ( $T_{1/2} = 2.6$  h). Prediction of LIC by NRS was excellent ( $r^2 = 0.96$ ) when compared to LIC from biopsies ( $1\text{--}23 \text{ mg g}_{\text{ww}}^{-1}$ ) in 12 patients with TDT. Iron estimations in the heart by NRS seemed to correlate with LIC only in 2 out of 12 patients with LIC  $> 4 \text{ mg g}_{\text{ww}}^{-1}$ .<sup>134</sup> The method did not become very popular due to the radiation burden (1–2 rem) and the prerequisite of a nuclear reactor.

X-ray fluorescence (XRF) is another quantification method which is specific for iron and other trace elements. XRF uses either a continuous spectrum of X-rays (Bremsstrahlung) or monochromatic X-rays (synchrotron radiation). Although iron levels in the skin were elevated by 200% in a study with TDT patients in comparison to controls, there were concerns about skin contamination, iron input from absorption, and X-ray penetration depth.<sup>133</sup> Non-destructive XRF can supply significant contributions to *in situ* trace element analysis and mapping of autopsy slices, *e.g.*, of the heart and the brain from patients with DBA or Parkinson's disease.<sup>138,139</sup>

## 7.4 Applications of *In vivo* Iron Assessment

Quantitative iron measurements including liver biopsies determine iron concentrations in a certain volume. These volumes can range from the whole organ (MID), to regions of interest (typical ROI: cardiac septum 5 cm,<sup>3</sup> liver

slice 200 cm<sup>3</sup>), to pixel- or voxel-sized (20–260 mm<sup>3</sup>) volumes for an organ slice or down to small pixel volumes as typically in the pituitary gland or brain (3 to <1 mm<sup>3</sup>). *In vivo* iron measurements are always a compromise between resolution (small pixel), quantum statistics (large volumes, thick slices), scan time (breath-hold) and the need for representative clinical information (homogeneity of iron distribution). Measurement of the liver iron concentration is not an exclusive indicator of iron toxicity. In certain other organs and gland tissues, critical organ specific iron concentrations can be reached.<sup>140–142</sup>

### 7.4.1 Liver

Thus far, it has been shown that liver iron concentration (LIC) can be accurately measured by biosusceptometric and MR-relaxation techniques. In the past, it was also shown that liver iron represents 70–90% of total body iron.<sup>1,29</sup>

Since the discovery of the C282Y mutation in the HFE gene and, subsequently, of mutations in at least 4 other genes, the diagnosis of haemochromatosis has been facilitated by the introduction of genetic tests into clinical practice.<sup>10,143</sup> However, for prognostic evaluation of the disease progress and, if indicated, the estimation of the phlebotomy treatment duration, the quantification of liver iron would be recommended. Especially, the usually determined ferritin level as indicator of iron burden may be confounded by several other factors (inflammation, liver fibrosis, life style, iron metabolism) and must be scaled differently relative to LIC in various diseases.<sup>27</sup> Also, in patients suspected for iron overload without informative genotyping, typically in patients with metabolic syndrome, non-invasive quantification of LIC and hepatic fat could be recommended and could be simultaneously performed by MRI-R2\*, see Section 7.3.2.<sup>114</sup>

Total body iron (TBI [mg<sub>Fe</sub>]) was estimated from LIC (1.5–23.8 mg g<sub>d.w.</sub><sup>-1</sup>) in liver biopsies and quantitative phlebotomy treatment in ex-thalassaemia patients 4.3 ± 2.7 years after bone marrow transplantation according to eqn (7.17).<sup>144</sup>

$$\text{TBI} = \text{LIC}_{\text{w.w.}} \times v_{\text{idx}}^{\text{liv}} \times \rho \times \text{BW}/\text{LIF} = 10.6 \times \text{LIC}_{\text{d.w.}} \times \text{BW} \quad (7.17)$$

With the liver volume index ( $v_{\text{idx}}^{\text{liv}}$ ), body weight (BW), liver density ( $\rho$ ), the liver iron fraction (LIF), and the wet-to-dry weight ratio ( $f_{\text{wdr}}$ , Section 7.2.3.2), one could calculate a slope factor of  $v_{\text{idx}}^{\text{liv}} \times \rho / (f_{\text{wdr}} \text{LIF})$ , which was found to be  $(10.6 \pm 2.3) [\text{mg}_{\text{Fe}} \text{kg}^{-1} \text{g}_{\text{d.w.}} \text{mg}_{\text{Fe}}^{-1}] (\pm \text{SD}, r^2 = 0.96)$ .<sup>144</sup> Using reasonable values (liver volume index 25 mL kg<sup>-1</sup>, density 1.05 g<sub>w.w.</sub> mL<sup>-1</sup>, LIF = 0.8,  $f_{\text{wdr}} = 4.0 \text{ g}_{\text{w.w.}} \text{g}_{\text{d.w.}}^{-1}$ ), one would obtain a slope factor of 7.4, which is quite good considering the unknown liver volumes, liver iron fraction, and wet-to-dry-weight ratio. The disease-specific character of the TBI(LIC) relation was demonstrated in hereditary haemochromatosis with a slope factor of  $5.3 \pm 4.2 (r^2 = 0.7)$ .<sup>145</sup> Moreover, one has to bear in mind potential hepatomegaly with increasing LIC.

A more individual TBI can be calculated from liver volumes ( $V_{\text{liv}}$ ), and spleen ( $V_{\text{spl}}$ ) by eqn (7.18) using the liver iron fraction parameter  $\text{LIF} = 0.8 \pm 0.1$  and  $f_{\text{wdrr}}$  in case of dry weight iron concentrations.<sup>146</sup>

$$\text{TBI} = (\text{LIC}_{\text{ww}}V_{\text{liv}} + (\text{SIC}_{\text{ww}}V_{\text{spl}}))/\text{LIF} \quad (7.18)$$

Monitoring iron overload in transfusion dependent patients is usually performed annually or biennially over decades with the aim of achieving a negative or equilibrium iron balance by chelation dose adjustment. However, with the simultaneous influx of iron from blood transfusions and different degrees of patient adherence this may become a challenge. Using the concept of molar efficacy, which is based on the TBI difference per treatment interval, the efficacy of treatment with a single chelator can be calculated for each patient.<sup>146–148</sup> Thus, mean molar efficacies for desferrioxamine, deferiprone, and deferasirox were determined as  $17.6 \pm 4.8\%$ ,  $4.9 \pm 1.4\%$ , and  $27.9 \pm 13.8\%$ , respectively.<sup>146,149</sup> Significantly lower values would indicate poor compliance in a patient, if other reasons could be excluded.

From correlation of LIC with pathological findings, risk thresholds for developing liver fibrosis or cardiac disease have been suggested in the literature for different levels of LIC.<sup>11,150,151</sup> This might be appropriate in iron overload diseases such as hereditary haemochromatosis or MDS.<sup>152,153</sup> However, from the experience with cardiac iron evaluation it should be emphasized that organ iron toxicity can develop even with LIC in an optimum range.<sup>15,154</sup>

## 7.4.2 Spleen

First spleen iron concentration (SIC) measurements revealed 38% lower values ( $1.5\text{--}19.0 \text{ mg g}_{\text{d.w.}}^{-1}$ ) than in the liver and a tight correlation with the total amount of transfused iron.<sup>155,156</sup> In transfused patients, the spleen can accumulate significant iron quantities as a result of increased spleen size. If chelation treatment is monitored by LIC assessment only, high amounts of spleen iron in individual patients can be overlooked. Similar findings were reported by exploring the relationship between spleen size and liver and spleen siderosis by the MRI-SIR method in patients with TDT.<sup>157</sup> Normal spleen iron may reflect the ability of chelators to remove RES iron more easily than parenchymal iron.<sup>29,146</sup> Brewer *et al.* observed different R2–R2\* relationships for liver and spleen in chronically transfused patients with SCD or TDT. Splenic iron did not predict pancreatic, cardiac or renal iron.<sup>158</sup> For NTDT patients, spleen iron accumulation was reduced in comparison with liver iron.<sup>159</sup> Also, in SCD patients with less than 20 blood transfusions, the spleen-to-liver R2 ratio was found to be considerably higher ( $>1$ ) than in controls of NTDT patients. Non-invasive iron measurements in the spleen should take the high amount of blood (about 30% of the spleen volume<sup>156</sup>) into account or in the case of autosplenectomy (SCD), the concentration of iron due to spleen volume shrinkage.

### 7.4.3 Heart

Diagnostic aspects of measuring iron in the heart by MRI address prevention of developing cardiomyopathy and/or arrhythmia at an early stage. Currently, an elevated cardiac iron level of  $R2^* > 50 \text{ s}^{-1}$  ( $T2^* < 20 \text{ ms}$ ) seems to be the earliest indicator of an increased risk of cardiomyopathy as assessed by LVEF or by the ratio of diastolic peak filling rates.<sup>15,160</sup> The early onset of cardiac iron accumulation was investigated in transfused pediatric patients with  $\beta$ -thalassaemia major. Based on these results, a first cardiac MRI- $R2^*$  measurement should be considered at an age of 9 to 10 years.<sup>161</sup> For other iron overload diseases, especially non-transfused patients (NTDT, HH), the incidence of elevated cardiac iron levels is lower, but has still to be verified in larger studies.<sup>152,162</sup> On the other hand, patients with  $R2^* < 100\text{--}200 \text{ s}^{-1}$  ( $T2^* < 10\text{--}5 \text{ ms}$ ) are facing an irreversible heart failure leading to multi-organ failure unless they undergo intensive chelation treatment.<sup>163</sup> Although there is an association between liver and cardiac iron, short-term monitoring of LIC is only of limited use because of a temporal delay of changes in cardiac iron.<sup>163,164</sup>

The question of whether patients diagnosed with cardiac  $T2^* > 20 \text{ ms}$  ( $R2^* < 50 \text{ s}^{-1}$ ) are completely protected from impairment of myocardial function cannot be answered by left ventricular diastolic function parameters such as ejection fraction (LVEF). In a recent study from 63 TDT patients in the normal  $T2^*$  range, 32% still had a  $T1$  lower than normal  $T1 > 900 \text{ ms}$  (see Section 7.3.2).<sup>107</sup> A corresponding answer might have been found by Magri *et al.*, who applied Doppler echocardiography and strain imaging to asymptomatic TDT patients under desferrioxamine (DFO) and deferriprone (DFP) treatment with  $T2^* = 24 \pm 4 \text{ ms}$ .<sup>165</sup> The central finding of significantly reduced strain ( $p < 0.001$ ) in TDT patients compared to age-matched controls was further strengthened by the observation of significantly higher strain values in patients under DFP chelation treatment, which is thought to be more effective in cardiac iron clearance ( $\Delta R2^* = 7.0 \pm 1.7 \text{ s}^{-1}$ ,  $p < 0.001$ ) (see Chapter 4).

### 7.4.4 Pancreas

In iron overload, glucose intolerance and more severely, diabetes mellitus type 2, is a frequently found complication, both in  $\beta$ -thalassaemia major and in hereditary haemochromatosis.<sup>14,166</sup> In microscopy studies, pancreatic iron appeared as haemosiderin in acinar and duct cells, and to a lesser degree in endocrine cells.<sup>167</sup> In advanced states, iron accumulation causes tissue atrophy and fibrosis, but pancreatic exocrine insufficiency is a rare event. In the initial state of iron loading, in carbonyl iron-fed rats, segregation of ferritin particles into the lysosomes of acinar cells was observed, while iron deposits in B cells were only discrete.<sup>168</sup>

Fat infiltration of the pancreas in iron-overloaded patients has been reported by several authors using MRI-SIR and -T2 methods.<sup>169,170</sup> Especially, in 77% of TM patients with overt diabetes, fatty infiltration could be demonstrated with a GRE-T2\* sequence by the relative difference between the in-phase and opposed-phase signals.<sup>171</sup>

Full blown MRI-R2\* was applied to 131 TDT patients over a 4-year period with the following main results: pancreatic R2\* significantly correlated with cardiac R2\* ( $p < 0.001$ ), iron accumulation in the pancreas seemed to occur earlier than in the heart, and a pancreatic R2\*  $> 100 \text{ s}^{-1}$  was a positive predictor for cardiac iron loading (R2\*  $> 50 \text{ s}^{-1}$ ).<sup>172</sup> Similar results were achieved in a few SCD patients accumulating pancreatic iron (R2\* = 114–450  $\text{s}^{-1}$ ) prior to presenting critical cardiac R2\* levels ( $> 50 \text{ s}^{-1}$ ).<sup>173</sup>

Knowing the problematic role of fatty replacement in the pancreas for a precise assessment of iron in this organ, Papakonstantinou *et al.* used fat suppression (FS) for measuring iron by MRI-R2 (R2<sub>FS</sub>) in 21 patients with TDT. In particular, they observed a mean R2<sub>FS</sub> of  $18.1 \pm 6.3 \text{ s}^{-1}$  versus R2 without FS of  $12.9 \pm 6.0 \text{ s}^{-1}$  ( $p < 0.02$ ).<sup>21</sup> As a consequence, chemical shift relaxometry (multi-point Dixon) with simultaneous assessment of iron and fat content was applied in a recent study to patients (TDT, HH, DBA, and other) with iron overload according to LIC. The study revealed pancreatic R2\* above the normal threshold of  $40 \text{ s}^{-1}$  for TDT, DBA, and HH as well as fat contents above 11% (normal), especially for TDT patients with diabetes.<sup>113</sup>

### 7.4.5 Pituitary

The pituitary gland (hypophysis) is outside of the blood brain barrier, which shows up in MR contrast examinations, and is therefore prone to toxic effects from iron overload. Effects from pathological pituitary iron deposition are silent until puberty, but pituitary stimulation testing can only be reliably performed in post pubertal patients. Thus, secondary amenorrhea and hypogonadotropic hypogonadism were reported to be the most common morbidities within 55% of Italian thalassaemia patients born after 1970.<sup>14</sup>

The anterior pituitary gland seems to react most sensitively to early toxic effects from iron overload. Quantitative iron measurements are made by means of MRI-R2 in the relatively small pituitary gland ( $200 \pm 100 \text{ mm}^3$ ). MRI-R2\* measurements are often corrupted by susceptibility artefacts from the air interface of the sphenoid sinus space. In a study with 14 young (8–19 years) and 23 adult (20–44 years) patients with  $\beta$ -thalassaemia major, significantly different R2 rates of  $16.8 \pm 4.2 \text{ s}^{-1}$  and  $22.1 \pm 5.1 \text{ s}^{-1}$  were obtained, respectively.<sup>170</sup> Pituitary R2 showed a significant correlation with pituitary gland height decreasing with progressive siderosis. Age-adjusted pituitary iron (R2) and anterior volume (PV) in transfused patients (4–58 years) gave rise to z-scores, which allowed critical scores of  $z(\text{R2}) > 5$  and  $z(\text{PV}) < -2.5$  to be established for prediction of hypogonadism with significant volume loss in the 2nd decade of life.<sup>22</sup>

Intensive combined chelation treatment by DFO and DFP could restore gonadal function in 50% of males and females as was demonstrated by normalization of hormone parameters (LH, FSH) and replacement therapy (testosterone, estradiol).<sup>13</sup> MRI-R2 measurements may help to identify necessary chelation doses under aggressive treatment regimen to avoid pituitary iron toxicity. Recently, fertility in 7 men with TDT was addressed by pituitary MRI-R2, 3D volume estimations, and sperm quality parameters. R2 seemed to have a better predictive value for sperm concentration than gonadotropin levels.<sup>174</sup>

### 7.4.6 Brain

Measurement of relatively low, but elevated levels of brain iron has gained recent interest because of its relation to neurodegenerative brain iron accumulation (NBIA) disorders and other neurodegenerative diseases such as Parkinson's, Alzheimer's and Huntington's. Iron can enter and/or leave the brain *via* the cerebrospinal fluid or *via* endothelial cells of the blood brain barrier (BBB).<sup>175</sup>

In the landmark work of Hallgren and Sourander, brain iron accumulation with increasing age was well described.<sup>52</sup> Studies transforming *in vivo* MRI parameters (R1, R2, R2\*, magnetic susceptibility) of the basal ganglia into brain iron concentrations still refer to this data.<sup>54</sup> In such a typical study with 26 healthy subjects (age A:  $15.9 \pm 1.6$  years, B:  $32.1 \pm 7.4$  years), MRI-R2 and a magnetic field correlation (MFC) technique were correlated with age-related post-mortem ( $C_{PM}$ ) brain iron reference (Hallgren and Sourander) data.<sup>176</sup> R2 significantly correlated with age adjusted  $C_{PM}$  in the putamen, caudate nucleus, but not in the thalamus or globus pallidus, while MFC correlated with all these nuclei. Brain iron in different nuclei steeply increases in childhood and adolescence (age <20 years) until it levels-out in adulthood (age >40 years) or even decreases in the thalamus.<sup>26,52,177</sup> Testing MRI parameters for significance between these two groups would already be a simple clinical validation test.<sup>176</sup>

Significant positive correlations of magnetic susceptibilities (except for the thalamus) with age were also found with more advanced MRI methods such as quantitative susceptibility mapping (QSM).<sup>178,179</sup> However, a direct comparison of the bulk magnetic susceptibilities (mean  $\Delta\chi \pm SEM$ ) from these two studies shows dramatic differences for the globus pallidus (GP) and the putamen (PT) in elderly subjects (age >55 years):  $\Delta\chi$  (GP) =  $227 \pm 6$  vs.  $74 \pm 1.8$  ppb and  $\Delta\chi$  (PT) =  $153 \pm 10$  vs.  $40 \pm 1.9$  ppb. From these differences one has to conclude that *absolute* magnetic susceptibilities cannot be generated by current QSM methods.

Iron was measured in the basal ganglia by XRF (monochromatic synchrotron X-ray radiation) in post-mortem tissue of elderly (80-year-old) controls and patients with Parkinson's disease (PD).<sup>180</sup> Significantly higher iron concentrations ( $p < 0.01$ ) were found for PD patients in the GP and SN (substantia nigra) of  $295$  and  $280 \mu\text{g g}_{\text{ww}}^{-1}$  versus  $207$  and  $140 \mu\text{g g}_{\text{ww}}^{-1}$  for controls, respectively. In addition, ferritin core particles were counted by electron microscopy resulting in  $6.5 \pm 0.4$  and  $3.0 \pm 0.2$  cores  $\mu\text{m}^{-3}$  for tissue from PD and controls, respectively. This increased loading of ferritin may have implications for magnetic measurements (MRI). The significantly higher iron levels in the SN of patients with PD ( $66 \pm 8$ -years-old) were also confirmed by MRI-R2/R2\* and QSM and demonstrating QSM to be the most sensitive quantitative technique for the detection of iron in PD.<sup>181</sup>

In post-mortem tissue from patients with Alzheimer's disease (AD), the highest iron concentrations (by AAS) were measured in the GP, SN and PT with dry-to-wet weight ratios (DWR) of  $0.34$ ,  $0.24$ , and  $0.25$ , respectively.<sup>182</sup> A

highly significant correlation was achieved between iron concentration from all grey matter samples and DWR adjusted R2 at 4.7 T. Similar findings were presented for AD patients in comparison to young (32-years-old) and elderly (70 years) controls by QSM at 3 T.<sup>183</sup> Especially in the left and right GP and PT, higher magnetic susceptibilities were determined in patients with AD in addition to lower hippocampal volumes (<3500 mm<sup>3</sup>).

NBIA patients including Friedreich's ataxia (FA) are prone to iron accumulation in certain regions of the brain. Iron accumulates in the cerebellar dentate nuclei (DN), but not in the GP of FA patients, especially at an age <20 years in comparison to healthy normals.<sup>184</sup> In other patients with NBIA, such as pantothenate kinase associated neurodegeneration (PKAN), infantile neuroaxonal dystrophy (INAD), neuroferritinopathy (FTL), and aceruloplasminemia (ACP), iron as measured by hyperintense R2\* (= hypointense T2\*) was elevated in the SN.<sup>185</sup> Patients with ACP showed iron accumulation in nearly all basal ganglia including the DN. Patients with PKAN, beyond having elevated iron only in the SN, exclusively showed the "eye-of-the-tiger" sign, which is a hyperintense (iron) ring structure in the globus pallidus.

Proteins in the CNS involved in oxygen transport, nerve fibre (myelin) production, and neurotransmitter metabolism, essentially need iron in balance.<sup>186</sup> However, in some neurodegenerative diseases iron is accumulated in critical brain regions above physiological needs. Iron chelation may offer a new route of neuroprotection and understanding in these diseases. Long-term monitoring of iron chelation treatment in patients with neurodegenerative diseases together with biochemical and neurological indicators associated with motor and cognitive impairment will afford precise, sensitive, and robust methods of *in vivo* iron quantification by MRI. The report of effective chelation of brain iron by deferiprone (DFP, L1) has provided great support for further development of appropriate measurement techniques. During a 6-month trial in 9 Friedreich ataxia patients receiving low dose DFP (20–30 mg kg<sup>-1</sup>d<sup>-1</sup>), slightly elevated R2\* rates (at 1.5 T) of 18.3 ± 1.6 s<sup>-1</sup> (controls: 16.6 ± 1.2 s<sup>-1</sup>) were measured in the dentate nuclei (DN). R2\* in the DN decreased to 15.7 ± 0.7 s<sup>-1</sup> (*p* < 0.002).<sup>187</sup> Improvement of motor symptoms such as gait and balance was reported in 7/9 patients. In a similar trial in NBIA (PKAN) patients, but with a 4-year follow-up, a significant reduction of R2\* with clinical stabilization was reported in the GP in 5/6 patients.<sup>188</sup> An interesting case of a 13-year-old NBIA patient, genetically associated with MPAN, was followed for 0, 8, 16, 24 months on DFP treatment by MRI-R2/-R2\* and QSM at 3 T. At baseline, converted iron concentration (from Langkammer *et al.*<sup>79</sup>) in the GP as well as in the SN was about 850 and 550 μg g<sub>ww</sub><sup>-1</sup> by R2\* and QSM, respectively, which is dramatically higher than in normal subjects. After 24 months of treatment, iron concentrations in the GP fell to 650 and 350 μg g<sub>ww</sub><sup>-1</sup> by R2\* and QSM, respectively, and to a lesser degree in the SN.<sup>189</sup>

In two recent double-blind placebo-controlled randomized clinical DFP trials with early stage PD patients MRI-R2\* (3 T) showed significant reductions of brain iron in the substantia nigra after 12 months<sup>190</sup> with 30 mg kg<sup>-1</sup> day<sup>-1</sup> and in the dentate and caudate nuclei after 3 and 6 months<sup>191</sup> with 20 and

30 mg kg<sup>-1</sup> day<sup>-1</sup>. In the latter study, no significant R2\* reduction was observed on the SN, globus pallidus, putamen and red nucleus. In both studies the PD patients showed an improvement in clinical symptoms (see Chapter 5).

Besides the lipid myelin complex and amyloid plaques in Alzheimer's disease (AD), neuromelanin, which forms stable complexes with Fe<sup>3+</sup>, may interfere with quantitative MRI. Especially in the substantia nigra (SN), melanin increases nearly linearly from <50 µg g<sup>-1</sup> at birth to 3500 µg g<sup>-1</sup> in tissue at an age of 90 years.<sup>192</sup> In PD patients of different disease duration, neuromelanin and iron were determined by a T1-weighted MR sequence and by R2\* at 3 T, respectively.<sup>193</sup> The authors concluded that the neuromelanin signal did not correlate with iron (R2\*) in PD or controls. Since myelin has a high lipid content, it is supposed to be diamagnetic, opposing the paramagnetic effect of iron. Schweser *et al.* reported a method to correct QSM-derived iron concentrations for confounding myelin contributions.<sup>194</sup> Alternatively, the lipid myelin contribution could be assessed together with iron concentration by MRI-R2\* chemical shift relaxometry (see Section 7.3.3.3). In 5 post-mortem samples from AD patients (died at 79 ± 5 years) matched with samples from controls (*n* = 5) with no signs of AD, iron concentration (by ICP-AAS) and plaque density (by silver stained digital histology) as well as R1, R2, and dry-to-wet weight ratio (DWR) by NMR at 1.4 T were assessed.<sup>195</sup> The data did not show any significant correlation between amyloid plaque density and iron, R1, R2, and DWR.

## 7.4.7 Iron in Other Organs, Glands, and Tissue

Iron deposition in other organs and tissue such as the adrenal gland, thyroid, ovary, testis, and lung has not been examined extensively. Recent interest has particularly focussed on kidney and bone marrow.

### 7.4.7.1 Kidney

Renal iron deposition was examined by MRI-R2\* in chronically transfused patients with TDT and SCD.<sup>196</sup> Cortical renal iron (R2\* > 32 s<sup>-1</sup>) was detected in 52% of SCD, but in only 7% of TDT patients. Renal R2\* was positively correlated (*p* < 0.001) with the haemolysis parameter, lactate dehydrogenase (LDH). Previous MRI studies by T2-weighted MRI had also described cortical renal iron deposition in non-transfused SCD and in paroxysmal nocturnal hemoglobinuria.<sup>197,198</sup> A recent trial in young SCD patients (age <16 years) confirmed the findings above with increased kidney R2\* rates in 81% of patients and also confirmed the correlation with intravascular hemolysis markers.<sup>199</sup> Using MRI-R2 in chelation-naïve transfused SCD patients, Vasavda *et al.* found a significant correlation of renal R2 with serum bilirubin in addition to that with LDH and no association with transfusional iron load.<sup>200</sup> As patients age due to improved treatment (chelation), renal disease and tubular dysfunction from cortical iron deposition may become more prevalent.<sup>201</sup>

#### 7.4.7.2 Adrenal Glands

Iron accumulation and/or fatty infiltration in the glands of the hypothalamic-pituitary-adrenal (HPA) axis and/or glucocorticoid therapy, may place patients with TDT, DBA, and other iron overload diseases at risk of acquired endocrine, in particular adrenal, insufficiency (AI). In patients with DBA (age 2–43 years), most of them transfused, 32% had signs of AI, predominantly subclinical.<sup>202</sup> Similarly in TDT, patients were tested positive for AI with normal ACTH levels (61%), but failed the subsequently confirmatory stimulation test for glucocorticoids released from the gland.<sup>203</sup> The authors hypothesized a hypothalamic origin or optimized chelation treatment in their patients having intact HPA function. Although, the adrenal glands play a huge role in the production of essential hormones, the presence of iron deposition in this gland has not been adequately studied so far by MRI. Adrenal hypointensity was qualitatively estimated by T2\*-weighted MRI in TDT patients (age 18–42 years) and was correlated with liver SIR ( $p = 0.003$ ). Hypointensity, in comparison to controls, was noted in 68% of patients and none had enlarged adrenal volume.<sup>204</sup> Iron proportional R2\* of  $118 \text{ s}^{-1}$  (normal  $<50 \text{ s}^{-1}$ ) could be measured in the left adrenal gland of an 18-year-old boy with acquired red cell aplasia on regular blood transfusion and iron chelation treatment.<sup>205</sup>

#### 7.4.7.3 Thyroid

Hypothyroidism in thalassaemia is one of the most frequent endocrinopathies after hypogonadism in TDT and DBA.<sup>14,202</sup> In a trial with TDT patients on intensive combined chelation treatment, hypothyroidism was present in 36% of patients at baseline, and ameliorated after significant decrease of total body iron burden.<sup>13</sup> However, the origin of hypothyroidism, *i.e.*, iron deposition in the thyroid gland or hypothalamic-pituitary dysfunction, is not well known in transfused patients (TDT, DBA). There is no doubt that iron can be found in the thyroid, but quantitative iron measurements by MRI are rare or even absent.<sup>206,207</sup> In a follow-up study, no thyroidal tissue alterations were detected by MRI, while liver iron was markedly reduced.<sup>208</sup> Interestingly, massive amounts of iron (haemosiderin) were observed in thyroid follicular cells from autopsy in neonatal haemochromatosis, similar to haemosiderin laden macrophages in goiter autopsies.<sup>209,210</sup>

#### 7.4.7.4 Testes and Ovaries

Similar to the situation of non-invasive iron measurements in the thyroid is the lack of systematic studies in the gonads, especially in females. In a recent study on fertility in men with TDT, the sperm quality parameters played an important role.<sup>174</sup> However, gonadal function as part of the HPG axis may not be directly involved in systemic iron overload. In hereditary haemochromatosis (HH), haemosiderin deposits were observed in testicular tissue by light

and electron microscopy.<sup>211</sup> Thus, testicular dysfunction may be caused not only by pituitary failure. On the other hand, no significant differences were found in the testes between controls and hypogonadic HH by MRI-R2 at 0.5 T ( $R2 = 12.4 \pm 1.0$  vs.  $11.8 \pm 0.5$  s<sup>-1</sup>), but for the pituitary the difference was significant ( $p < 0.01$ ).<sup>212</sup> Probably, iron overload (mean liver  $R2 = 36$  s<sup>-1</sup>) was no longer severe in these patients due to adequate treatment.

Many women with TDT experience primary or secondary amenorrhea as detected by low levels of gonadotropines (LH/FSH) and estradiol, which did not correlate with liver iron or age.<sup>213</sup> No observations of iron in the ovaries of patients with iron overload diseases are currently known.

#### 7.4.7.5 Bone Marrow

Although bone marrow (BM) is directly involved in erythropoietic activity, iron deposition has not been systematically examined by quantitative MRI. The normal conversion of red (100% at birth, 60% at adulthood) to yellow marrow during lifetime is also subject to a variety of systemic disorders (leukemia, hemoglobinopathy, myelodysplasia, and osteoporosis). Quantitative MRI measurements have to address iron in red BM (40% fat in adulthood) and fat in yellow BM (80% fat in adulthood) but also a trabeculae loss of the spongiosa in osteoporosis. Increased haematopoiesis as in thalassaemia or sickle cell disease can result in a total reconversion of yellow BM depending on blood transfusion and iron chelation treatment.<sup>214</sup> Massive ineffective erythropoiesis (IE) results in intramarrow destruction of 60–80% of erythroid precursors, thereby suppressing hepcidin levels and in turn increasing NTBI generation.<sup>215</sup> This may emphasize the importance of quantitative MRI iron (and fat) assessment in the BM, which can be performed within one abdominal  $R2^*$  scan of liver, spleen, and vertebral BM (VBM).<sup>216</sup> In an early study with leukemia (ALLL, AML, age: 14–57 years) and aplastic anemia (AA) patients and age-matched healthy subjects,  $R1$  and  $R2$  was assessed at 0.6 T in the VBM.<sup>217</sup> Fat fraction could discriminate between the diseases and controls with low  $R1$  for leukemia and high  $R1$  rates for AA.

When applying conventional  $R2$  sequences to the VBM without taking the fat content into account, many studies failed to draw additional information from their relaxometric T2 data in the bone marrow.<sup>218,219</sup> In a follow-up study in patients with TDT, a disagreement between fat-saturated  $R2$  ( $R2$ -FS) and conventional  $R2$  in the bone marrow (as in the pancreas) was found. Correlation between VBM- $R2$  and hepatic  $R2$  only became significant by applying fat suppression in lipid-rich tissue.<sup>21</sup> Recently, significantly elevated  $R2$  rates were reported in the VBM of iron-loading anemias such as SCD ( $n = 40$ , chelation-naïve,  $R2 = 43.2 \pm 21.1$  s<sup>-1</sup>), NTD ( $n = 9$ ,  $R2 = 32.6 \pm 7.0$  s<sup>-1</sup>), and PNH (paroxysmal nocturnal haemoglobinuria:  $n = 15$ , chelation-naïve,  $R2 = 36.1 \pm 19.2$  s<sup>-1</sup>) compared with controls ( $n = 17$ ,  $R2 = 21.8 \pm 4.9$  s<sup>-1</sup>).<sup>159</sup> Bone marrow iron assessment by MRI- $R2^*$  chemical shift relaxometry was presented in 112 iron overload patients (TDT:  $R2^* = 398$  s<sup>-1</sup>, DBA:  $R2^* = 252$  s<sup>-1</sup>, HH:

$R2^* = 95 \text{ s}^{-1}$ , other) and in 14 control subjects ( $R2^* = 95 \text{ s}^{-1}$ ).<sup>215</sup> VBM- $R2^*$  did not correlate with the fat content of the marrow and correlation with chelation dose did not achieve significance.

## 7.5 Conclusion and Prospects

Iron measurements can now routinely be performed in clinical applications either by quantitative magnetic resonance imaging (MRI) using the transverse magnetic relaxation rate  $R2$  or  $R2^*$  ( $1/T2^*$ ) or by electronic biomagnetic liver susceptometry (SQUID). For iron measurements in the heart, the single-breath-hold multi-echo MRI- $R2^*$  method has become a standard modality and is applied in clinical settings beyond research studies. It can now also be transformed into dry-weight/wet-weight cardiac iron concentration (CIC).<sup>47,110</sup> For liver iron concentration (LIC) assessment, calibrated and validated reference methods such as SQUID biosusceptometry and MRI- $R2$ , - $R2^*$  have existed for some time and have proven their therapeutic benefit for patients with systemic iron overload (thalassaemia, haemochromatosis, sickle cell disease, or other anaemias) in *long-term* iron monitoring.<sup>16,19,20</sup> These reference methods are now being used as surrogate methods, since liver biopsies will not be tolerated by patients any longer and autopsy data are often not available. In other tissues such as the pancreas, pituitary, and brain, different MRI methods are employed, but their clinical benefit has yet to be proven, especially in iron chelation trials.

We will see further development in the area of MRI technology, already with the introduction of high field imagers ( $\geq 3$  tesla) into clinical settings. These systems have several advantages beyond a higher sensitivity by using 3D data acquisition (*i.e.*, multi-echo sequences of 20–40 slices within one breath-hold) and software improvements from using complex data for quantitative measurements (real, imaginary, phase). The higher sensitivity will be especially favourable for the assessment of the relatively low iron concentrations in the brain and endocrine glands (pituitary) as well as for magnetic resonance spectroscopy. On the other hand, higher fields are disadvantageous for assessing high iron concentrations in the liver.<sup>220,221</sup> Since the 3 T imagers will probably replace standard 1.5 T imagers in settings dealing with iron overload patients at large, one has to develop methods to overcome the limitation in the high iron range (*e.g.*, single echo, SIR, ultra-fast echo times).

Technologies and analysis methods based on the measurement of magnetic susceptibility in liver and brain will be developed in the near future. Liquid nitrogen cooled or room-temperature based electronic biosusceptometer systems could be calibrated by physical means only and are unlimited in the range of occurring iron concentrations.<sup>17</sup> Quantitative susceptibility mapping (QSM) is a new analysis technique for quantifying iron *in vivo*, especially in the brain, but also in the liver. The relatively high iron concentrations in the liver may be a challenge in the phase mapping. Calibration of QSM using proton magnetometers in magnetised tissue is at least problematic. Validation studies of the accuracy, repeatability, and reproducibility of

QSM will be necessary in order to establish its utility in the research and clinical settings.<sup>222</sup> As long as no standard QSM analysis method has been established, the simultaneous application of routine relaxometry (R2, R2\*) would be recommended in experimental studies.<sup>79</sup>

In systemic iron overload, serum (plasma) ferritin still remains the “work horse” for monitoring the iron burden in the time intervals between measurement appointments. Confounding factors such as inflammation, chelation treatment changes and the specific disease have to be taken into account, however.

## Abbreviations

<b>CIC</b>	cardiac iron concentration
<b>g<sub>d.w.</sub></b>	gram dry weight
<b>g<sub>w.w.</sub></b>	gram wet weight
<b>GRE</b>	gradient recalled echo
<b>HH</b>	hereditary haemochromatosis
<b>LIC</b>	liver iron concentration
<b>MR (MRI)</b>	magnetic resonance (imaging)
<b>MRS</b>	magnetic resonance spectroscopy
<b>NTDT</b>	non-transfusion dependent thalassaemia
<b>QSM</b>	quantitative susceptibility mapping
<b>R1 (T1)</b>	longitudinal relaxation rate (time)
<b>R2 (T2)</b>	transverse relaxation rate (time)
<b>R2* (T2*)</b>	gradient recalled echo relaxation rate (time)
<b>SCD</b>	sickle cell disease
<b>SIR</b>	signal intensity ratio
<b>SQUID</b>	superconducting quantum interference device
<b>TDT</b>	transfusion dependent thalassaemia

## Acknowledgement

The author is gratefully acknowledging the contribution of Samir S. Sharma (Madison) to the QSM chapter and would like to thank Jerry Z. Wang (Dallas) for his training, lasting years, of an amateur into the secrets of MRI.

## References

1. B. Modell and V. Berdoukas, *The Clinical Approach to Thalassaemia*, Grune & Stratton, New York-London, 1984.
2. G. M. Brittenham and D. G. Badman, *Blood*, 2003, **101**, 15.
3. G. M. Addison, M. R. Beamish, C. N. Hales, M. Hodgkins, A. Jacobs and P. Llewellyn, *J. Clin. Pathol.*, 1972, **25**, 326.
4. Y. M. Deugnier, O. Loreal, B. Turlin, D. Guyader, H. Jouanolle, B. Moirand, C. Jacquelinet and P. Brissot, *Gastroenterology*, 1992, **102**, 2050.

5. A. Piga, F. Longo, L. Duca, S. Roggero, T. Vinciguerra, R. Calabrese, C. Hershko and M. D. Cappellini, *Am. J. Hematol.*, 2009, **84**, 29.
6. L. de Swart, J. C. Hendriks, L. N. van der Vorm, Z. I. Cabantchik, P. J. Evans, E. A. Hod, G. M. Brittenham, Y. Furman, B. Wojczyk, M. C. Janssen, J. B. Porter, V. E. Mattijssen, B. J. Biemond, M. A. MacKenzie, R. Origa, R. Galanello, R. C. Hider and D. W. Swinkels, *Haematologica*, 2016, **101**, 38.
7. E. Jones, S. R. Pasricha, A. Allen, P. Evans, C. A. Fisher, K. Wray, A. Premawardhena, D. Bandara, A. Perera, C. Webster, P. Sturges, N. F. Olivieri, T. St Pierre, A. E. Armitage, J. B. Porter, D. J. Weatherall and H. Drakesmith, *Blood*, 2015, **125**, 873.
8. G. O. Walters, F. M. Miller and M. Worwood, *J. Clin. Pathol.*, 1973, **26**, 770.
9. P. Nielsen, R. Fischer, R. Engelhardt and J. Düllmann, *Transfus. Med. Hemother.*, 2003, **30**, 27.
10. J. N. Feder, A. Gnirke, W. Thomas, Z. Tsuchihashi, D. A. Ruddy, A. Basava, F. Dormishian, R. Domingo Jr, M. C. Ellis, A. Fullan, L. M. Hinton, N. L. Jones, B. E. Kimmel, G. S. Kronmal, P. Lauer, V. K. Lee, D. B. Loeb, F. A. Mapa, E. McClelland, N. C. Meyer, G. A. Mintier, N. Moeller, T. Moore, E. Morikang, C. E. Prass, L. Quintana, S. M. Starnes, R. C. Schatzman, K. J. Brunke, D. T. Drayna, N. J. Risch, B. R. Bacon and R. K. Wolff, *Nat. Genet.*, 1996, **13**, 399.
11. N. F. Olivieri and G. M. Brittenham, *Blood*, 1997, **89**, 739.
12. A. R. Cohen, E. Glimm and J. B. Porter, *Blood*, 2008, **111**, 583.
13. K. Farmaki, I. Tzoumari, G. Pappa, G. Chouliaras and V. Berdoukas, *Br. J. Haematol.*, 2010, **148**, 466.
14. C. Borgna-Pignatti, S. Rugolotto, P. De Stefano, H. Zao, M. D. Cappellini, G. C. Del Vecchio, M. A. Romeo, G. L. Forni, M. R. Gamberini, R. Ghilardi, A. Piga and A. Cnaan, *Haematologica*, 2004, **89**, 1187.
15. L. J. Anderson, S. Holden, B. Davis, E. Prescott, C. C. Charrier, N. H. Bunce, D. N. Firmin, B. Wonke, J. Porter, J. M. Walker and D. J. Pennell, *Eur. Heart J.*, 2001, **22**, 2171.
16. R. Fischer and D. Farrell, *Magnetism in Medicine: A Handbook, Completely Revised and Extended Edition*, ed. M. Andrae and H. Nowak, Wiley-VCH, Berlin, 2007, p. 529.
17. D. E. Farrell, C. J. Allen, M. W. Whilden, T. K. Kidane, T. N. Baig, J. H. Tripp, R. W. Brown, S. Sheth and G. M. Brittenham, *IEEE Trans. Magn.*, 2007, **43**(9.1), 3543.
18. M. Marinelli, S. Cuneo, B. Gianesin, A. Lavagetto, M. Lamagna, E. Oliveri, G. Sobrero, L. Terenzani and G. Forni, *IEEE Trans. Appl. Supercond.*, 2006, **16**, 1513.
19. T. G. St Pierre, P. R. Clark, W. Chua-anusorn, A. J. Fleming, G. P. Jeffrey, J. K. Olynyk, P. Pootrakul, E. Robins and R. Lindeman, *Blood*, 2005, **105**, 855.
20. J. C. Wood, C. Enriquez, N. Ghugre, J. M. Tyzka, S. Carson, M. D. Nelson and T. D. Coates, *Blood*, 2005, **106**, 1460.

21. O. Papakonstantinou, K. Foufa, O. Benekos, E. Alexopoulou, M. Mademli, A. Balanika, N. Economopoulos and N. L. Kelekis, *Magn. Reson. Imaging*, 2012, **30**, 926.
22. L. J. Noetzli, A. Panigrahy, S. D. Mittelman, A. Hyderi, A. Dongelyan, T. D. Coates and J. C. Wood, *Am. J. Hematol.*, 2012, **87**, 167.
23. M. J. House, T. G. St Pierre, E. A. Milward, D. G. Bruce and J. K. Olynyk, *Magn. Reson. Med.*, 2010, **63**, 275.
24. G. M. Brittenham, *Ann. N. Y. Acad. Sci.*, 1988, **526**, 199.
25. P. D. Jensen, *Br. J. Haematol.*, 2004, **124**, 697.
26. E. M. Haacke, N. Y. Cheng, M. J. House, Q. Liu, J. Neelavalli, R. J. Ogg, A. Khan, M. Ayaz, W. Kirsch and A. Obenaus, *Magn. Reson. Imaging*, 2005, **23**, 1.
27. R. Fischer and P. R. Harmatz, *Hematol. Am. Soc. Hematol. Educ. Program*, 2009, 215.
28. J. C. Wood, *Br. J. Haematol.*, 2015, **170**, 15.
29. R. Fischer, C. D. Tiemann, R. Engelhardt, P. Nielsen, M. Dürken, E. E. Gabbe and G. E. Janka, *Am. J. Hematol.*, 1999, **60**, 289.
30. A. A. Bravo, S. G. Sheth and S. Chopra, *N. Engl. J. Med.*, 2001, **344**, 495.
31. K. T. Tan, D. K. Rajan, J. R. Kachura, E. Hayeems, M. E. Simons and C. S. Ho, *J. Vasc. Interv. Radiol.*, 2005, **16**, 1215.
32. J. Ludwig, K. P. Batts, T. P. Moyer, W. P. Baldus and V. F. Fairbanks, *Mayo Clin. Proc.*, 1993, **68**, 263.
33. R. Ambu, G. Crisponi, R. Sciote, P. Van Eyken, G. Parodo, S. Iannelli, F. Marongiu, R. Silvagni, V. Nurchi and V. Costa, *et al.*, *J. Hepatol.*, 1995, **23**, 544.
34. M. Barry, *Gut*, 1974, **15**, 411.
35. M. J. Emond, M. P. Bronner, T. H. Carlson, M. Lin, R. F. Labbe and K. V. Kowdley, *Clin. Chem.*, 1999, **45**, 340.
36. E. Butensky, R. Fischer, M. Hudes, L. Schumacher, R. Williams, T. P. Moyer, E. Vichinsky and P. Harmatz, *Am. J. Clin. Pathol.*, 2005, **123**, 146.
37. J. P. Villeneuve, M. Bilodeau, R. Lepage, J. Côté and M. Lefebvre, *J. Hepatol.*, 1996, **25**, 172.
38. N. W. Leung, P. Farrant and T. J. Peters, *J. Hepatol.*, 1986, **2**, 157.
39. G. Faa, M. Terlizzo, C. Gerosa, T. Congiu and E. Angelucci, *Haematologica*, 2002, **87**, 479.
40. N. R. Ghugre, I. Gonzalez-Gomez, H. Shimada, T. D. Coates and J. C. Wood, *J. Microsc.*, 2010, **238**, 265.
41. D. H. Fitchett, D. J. Coltart, W. A. Littler, M. J. Leyland, T. Trueman, D. I. Gozzard and T. J. Peters, *Cardiovasc. Res.*, 1980, **14**, 719.
42. G. Barosi, E. Arbustini, A. Gavazzi, M. Grasso and A. Pucci, *Eur. J. Haematol.*, 1989, **42**, 382.
43. L. M. Buja and W. C. Roberts, *Am. J. Med.*, 1971, **51**, 209.
44. L. J. Olson, W. D. Edwards, J. T. McCall, D. M. Ilstrup and B. J. Gersh, *J. Am. Coll. Cardiol.*, 1987, **10**, 1239.
45. P. D. Jensen, J. P. Bagger, F. T. Jensen, U. Baandrup, U. Christensen and T. Ellegard, *Eur. J. Haematol.*, 1993, **51**, 199.

46. N. R. Ghugre, C. M. Enriquez, I. Gonzalez, M. D. Nelson Jr, T. D. Coates and J. C. Wood, *Magn. Reson. Med.*, 2006, **56**, 681.
47. J. P. Carpenter, T. He, P. Kirk, M. Roughton, L. J. Anderson, S. V. de Noronha, M. N. Sheppard, J. B. Porter, J. M. Walker, J. C. Wood, R. Galanello, G. Forni, G. Catani, G. Matta, S. Fucharoen, A. Fleming, M. J. House, G. Black, D. N. Firmin, T. G. St Pierre and D. J. Pennell, *Circulation*, 2011, **123**, 519.
48. U. Wulfhekel and J. Duellmann, *Folia Haematol. Int. Mag. Klin. Morphol. Blutforsch.*, 1990, **117**, 419.
49. E. Gale, J. Torrance and T. Bothwell, *J. Clin. Invest.*, 1963, **42**, 1076.
50. S. I. Strasser, K. V. Kowdley, G. E. Sale and G. B. McDonald, *Bone Marrow Transplant.*, 1998, **22**, 167.
51. J. R. Connor, P. Ponnuru, X. S. Wang, S. M. Patton, R. P. Allen and C. J. Earley, *Brain*, 2011, **134**, 959.
52. B. Hallgren and P. Sourander, *J. Neurochem.*, 1958, **3**, 41.
53. D. A. Loeffler, J. R. Connor, P. L. Juneau, B. S. Snyder, L. Kanaley, A. J. DeMaggio, H. Nguyen, C. M. Brickman and P. A. LeWitt, *J. Neurochem.*, 1995, **65**, 710.
54. J. Vymazal, A. Righini, R. A. Brooks, M. Canesi, C. Mariani, M. Leonardi and G. Pezzoli, *Radiology*, 1999, **211**, 489.
55. J. Vymazal, R. A. Brooks, C. Baumgarner, V. Tran, D. Katz, J. W. Bulte, R. Bauminger and G. Di Chiro, *Magn. Reson. Med.*, 1996, **35**, 56.
56. K. S. Kaufman, G. C. Papaefthymiou, R. B. Frankel and A. Rosenthal, *Biochim. Biophys. Acta*, 1980, **629**, 522.
57. M. P. Weir, G. A. Sharp and T. J. Peters, *J. Clin. Pathol.*, 1985, **38**, 915.
58. R. J. Ward, M. H. Ramsey, D. P. Dickson, A. Florence, R. R. Crichton, T. J. Peters and S. Mann, *Eur. J. Biochem.*, 1992, **209**, 847.
59. T. C. Iancu, *Electron. Microsc. Rev.*, 1992, **5**, 209.
60. P. D. Allen, T. G. St Pierre, W. Chua-anusorn, V. Ström and K. V. Rao, *Biochim. Biophys. Acta*, 2000, **1500**, 186.
61. S. M. Dubiel, B. Zablotna-Rypien, J. B. Mackey and J. M. Williams, *Eur. Biophys. J.*, 1999, **28**, 263.
62. F. M. Zuyderhoudt, J. W. Sindram, J. J. Marx, G. G. Jörning and J. van Gool, *Hepatology*, 1983, **3**, 232.
63. F. M. Zuyderhoudt, P. Hengeveld, J. van Gool and G. G. Jörning, *Clin. Chim. Acta*, 1978, **86**, 313.
64. P. Nielsen, J. Düllmann, U. Wulfhekel and H. C. Heinrich, *Int. J. Biochem.*, 1993, **25**, 223.
65. R. Fischer, R. Engelhardt, P. Nielsen, E. E. Gabbe, H. C. Heinrich, W. H. Schmiegel and D. Wurbs, *Biomagnetism: Clinical Aspects*, ed. M. Hoke, S. N. Erné, Y. C. Okada and G. L. Romani, Elsevier, Amsterdam, 1992, p. 585.
66. E. M. Haacke, R. W. Brown, M. T. Thompson and R. Venkatesan, *Magnetic Resonance Imaging: Physical Principles and Sequence Design*, Wiley-Liss, New York, 1999.
67. S. I. Mavrogeni, V. Markussis, L. Kaklamanis, D. Tsiapras, I. Paraskevaidis, G. Karavolias, M. Karagiorga, M. Douskou, D. V. Cokkinos and D. T. Kremastinos, *Eur. J. Haematol.*, 2005, **75**, 241.

68. C. D. Coryell, F. Stitt and L. Pauling, *J. Am. Chem. Soc.*, 1937, **59**, 633.
69. E. Bayer and K. H. Hauser, *Experientia*, 1955, **11**, 254.
70. S. Hilty, B. Webb, R. B. Frankel and G. D. Watt, *J. Inorg. Biochem.*, 1994, **56**, 173.
71. L. Michaelis, C. D. Coryell and S. Granick, *J. Biol. Chem.*, 1943, **148**, 463.
72. G. Schoffa, *Z. Naturforsch.*, 1965, **20b**, 167.
73. R. Engelhardt, *Private communication*, 1982.
74. A. Shoden and P. Sturgeon, *Acta Haemat.*, 1960, **23**, 376.
75. J. H. Bauman and J. W. Harris, *J. Lab. Clin. Med.*, 1967, **70**, 246.
76. M. J. Messer and J. W. Harris, *J. Lab. Clin. Med.*, 1967, **70**, 1008.
77. N. Zander, *Thesis*, University Medical Center Hamburg-Eppendorf, 2002.
78. S. Hackett, W. Chua-anusorn, P. Pootrakul and T. G. St Pierre, *Biochim. Biophys. Acta*, 2007, **1772**, 330.
79. C. Langkammer, F. Schweser, N. Krebs, A. Deistung, W. Goessler, E. Scheurer, K. Sommer, G. Reishofer, K. Yen, F. Fazekas, S. Ropele and J. R. Reichenbach, *Neuroimage*, 2012, **62**, 1593.
80. A. Shoden and P. Sturgeon, *Nature*, 1961, **189**, 846.
81. S. J. Williamson and L. Kaufman, *J. Magn. Magn. Mat.*, 1981, **22**, 129.
82. S. M. Sprinkhuizen, C. J. G. Bakker, J. H. Ippel, R. Boelens, M. A. Viergever and L. W. Bartels, *Magn. Reson. Mater. Phys.*, 2012, **25**, 33.
83. J. A. Hopkins and F. W. Wehrli, *Magn. Reson. Med.*, 1997, **37**, 494.
84. M. Ropert-Bouchet, B. Turlin, G. Graham, B. Rabault, A. Le Treut, P. Brissot, O. Loréal, D. Alberti and Y. Deugnier, *BioIron*, 2005, 107.
85. Z. Pakbaz, R. Fischer, J. Butz, D. Foote, E. Hackney-Stephens, E. Fung, B. Fagaly, P. Harmatz and E. Vichinsky, *Blood*, 2006, **108**, 3826.
86. W. M. Spees, D. A. Yablonskiy, M. C. Oswald and J. J. Ackerman, *Magn. Reson. Med.*, 2001, **45**, 533.
87. V. Lebon, C. Brillault-Salvat, G. Bloch, A. Leroy-Willig and P. G. Carlier, *Magn. Reson. Med.*, 1998, **40**, 551.
88. R. A. Brooks, J. Vymazal, R. B. Goldfarb, J. W. Bulte and P. Aisen, *Magn. Reson. Med.*, 1998, **40**, 227.
89. W. Möller, W. Barth, M. Kohlhäufel, K. Häussinger, W. Stahlhofen and J. Heyder, *Exp. Lung. Res.*, 2001, **27**, 547.
90. T. He, G. Smith, J. P. Carpenter, R. Mohiaddin, D. J. Pennell and D. Firmin, *J. Cardiovasc. Magn. Reson.*, 2009, **11**(Suppl 1), P147.
91. R. Engelhardt, J. H. Langkowski, R. Fischer, P. Nielsen, H. Kooijman, H. C. Heinrich and E. Bücheler, *Magn. Reson. Imaging*, 1994, **12**, 999.
92. N. R. Ghugre, T. D. Coates, M. D. Nelson and J. C. Wood, *Magn. Reson. Med.*, 2005, **54**, 1185.
93. S. Sheth, H. Tang, J. H. Jensen, K. Altmann, A. Prakash, B. F. Printz, A. J. Hordof, C. L. Tosti, A. Azabagic, S. Swaminathan, T. R. Brown, N. F. Olivieri and G. M. Brittenham, *Ann. N. Y. Acad. Sci.*, 2005, **1054**, 358.
94. G. L. Wismer, R. B. Buxton, B. R. Rosen, C. R. Fisel, R. F. Oot, T. J. Brady and K. R. Davis, *J. Comput. Assist. Tomogr.*, 1988, **12**, 259.
95. D. A. Ortendahl, N. Hylton, L. Kaufman, J. C. Watts, L. E. Crooks, C. M. Mills and D. D. Stark, *Radiology*, 1984, **153**, 479.

96. P. R. Clark and T. G. St Pierre, *Magn. Reson. Imaging*, 2000, **18**, 431.
97. P. R. Clark, W. Chua-anusorn and T. G. St Pierre, *Magn. Reson. Imaging*, 2003, **21**, 519.
98. T. He, P. D. Gatehouse, G. C. Smith, R. H. Mohiaddin, D. J. Pennell and D. N. Firmin, *Magn. Reson. Med.*, 2008, **60**, 1082.
99. A. A. O. Carneiro, J. P. Fernandes, D. B. de Araujo, J. Elias Jr, A. L. Martinelli, D. T. Covas, M. A. Zago, I. L. Angulo, T. G. St Pierre and O. Baffa, *Magn. Reson. Med.*, 2005, **54**, 122.
100. W. C. Chan, Z. Tejani, F. Budhani, C. Massey and A. Haider, *J. Magn. Reson. Imaging*, 2014, **39**, 1007.
101. M. W. Garbowski, J. P. Carpenter, G. Smith, M. Roughton, M. H. Alam, T. He, D. J. Pennell and J. B. Porter, *J. Cardiovasc. Mag. Reson.*, 2014, **16**, 40.
102. E. Alexopoulou, F. Stripeli, P. Baras, I. Seimenis, A. Kattamis, V. Ladis, E. Efstathopoulos, E. N. Brountzos, A. D. Kelekis and N. L. Kelekis, *J. Magn. Reson. Imaging*, 2006, **23**, 163.
103. S. Majumdar, S. C. Orphanoudakis, A. Gmitro, M. O'Donnell and J. C. Gore, *Magn. Reson. Med.*, 1986, **3**, 397.
104. B. Henninger, C. Kremser, S. Rauch, R. Eder, H. Zoller, A. Finkenstedt, H. J. Michaely and M. Schocke, *Eur. Radiol.*, 2012, **22**, 2478.
105. S. K. Piechnik, V. M. Ferreira, E. Dall'Armellina, L. E. Cochlin, A. Greiser, S. Neubauer and M. D. Robson, *J. Cardiovasc. Magn. Reson.*, 2010, **12**, 69.
106. Y. Feng, T. He, J. P. Carpenter, A. Jabbour, M. H. Alam, P. D. Gatehouse, A. Greiser, D. Messroghli, D. N. Firmin and D. J. Pennell, *J. Magn. Reson. Imaging*, 2013, **38**, 588.
107. D. M. Sado, V. Maestrini, S. K. Piechnik, S. M. Banypersad, S. K. White, A. S. Flett, M. D. Robson, S. Neubauer, C. Ariti, A. Arai, P. Kellman, J. Yamamura, B. P. Schoennagel, F. Shah, B. Davis, S. Trompeter, M. Walker, J. Porter and J. C. Moon, *J. Magn. Reson. Imaging*, 2015, **41**, 1505.
108. J. S. Hankins, M. B. McCarville, R. B. Loeffler, M. P. Smeltzer, M. Onciu, F. A. Hoffer, C. S. Li, W. C. Wang, R. E. Ware and C. M. Hillenbrand, *Blood*, 2009, **113**, 4853.
109. M. Westwood, L. J. Anderson, D. N. Firmin, P. D. Gatehouse, C. C. Charrier, B. Wonke and D. J. Pennell, *J. Magn. Reson. Imaging*, 2003, **18**, 33.
110. Z. J. Wang, R. Fischer, Z. Chu, D. H. Mahoney Jr, B. U. Mueller, R. Muthupillai, E. B. James, R. Krishnamurthy, T. Chung, E. Padua, E. Vichinsky and P. Harmatz, *Magn. Reson. Imaging*, 2010, **28**, 363.
111. J. P. Carpenter, T. He, P. Kirk, M. Roughton, L. J. Anderson, S. V. de Noronha, A. J. Baksi, M. N. Sheppard, J. B. Porter, J. M. Walker, J. C. Wood, G. Forni, G. Catani, G. Matta, S. Fucharoen, A. Fleming, M. House, G. Black, D. N. Firmin, T. G. St Pierre and D. J. Pennell, *J. Cardiovasc. Magn. Reson.*, 2014, **16**, 62.
112. S. B. Reeder and C. Sirlin, *Magn. Reson. Imaging Clin. N. Am.*, 2010, **18**, 337.
113. C. D. Pfeifer, B. P. Schoennagel, R. Grosse, Z. J. Wang, J. Graessner, P. Nielsen, G. Adam, R. Fischer and J. Yamamura, *J. Magn. Reson. Imaging*, 2015, **42**, 196.

114. S. Galimberti, P. Trombini, D. P. Bernasconi, I. Redaelli, S. Pelucchi, G. Bovo, F. Di Gennaro, N. Zucchini, N. Paruccini and A. Piperno, *Scand. J. Gastroenterol.*, 2015, **50**, 429.
115. G. Hamilton, T. Yokoo, M. Bydder, I. Cruite, M. E. Schroeder, C. B. Sirlin and M. S. Middleton, *NMR Biomed.*, 2011, **24**, 784.
116. V. V. Chebrolu, C. D. Hines, H. Yu, A. R. Pineda, A. Shimakawa, C. A. McKenzie, A. Samsonov, J. H. Brittain and S. B. Reeder, *Magn. Reson. Med.*, 2010, **63**, 849.
117. W. F. Avrin and S. Kumar, *Physiol. Meas.*, 2007, **28**, 349.
118. B. A. Taylor, R. B. Loeffler, R. Song, M. B. McCarville, J. S. Hankins and C. M. Hillenbrand, *J. Magn. Reson. Imaging*, 2012, **35**, 1125.
119. L. de Rochefort, T. Liu, B. Kressler, J. Liu, P. Spincemaille, V. Lebon, J. Wu and Y. Wang, *Magn. Reson. Med.*, 2010 Jan, **63**(1), 194–206.
120. M. H. Cohen and F. Keffer, *Phys. Rev.*, 1955, **99**, 1128.
121. S. D. Sharma, D. Hernando, D. E. Horng and S. B. Reeder, *Magn. Reson. Med.*, 2015, **74**, 673.
122. D. Hernando, R. J. Cook, C. Diamond and S. B. Reeder, *Magn. Reson. Med.*, 2013, **70**, 648.
123. I. A. Lim, A. V. Faria, X. Li, J. T. Hsu, R. D. Airan, S. Mori and P. C. van Zijl, *Neuroimage*, 2013, **82**, 449.
124. E. M. Haacke, Y. Xu, Y. C. Cheng and J. R. Reichenbach, *Magn. Reson. Med.*, 2004, **52**, 612.
125. A. M. Winchell, B. A. Taylor, R. Song, R. B. Loeffler, P. Grundlehner, J. S. Hankins, W. C. Wang, R. J. Ogg, C. M. Hillenbrand and K. J. Helton, *AJNR Am. J. Neuroradiol.*, 2014, **35**, 1016.
126. D. L. Johnston, L. Rice, G. W. Vick 3rd, T. D. Hedrick and R. Rokey, *Am. J. Med.*, 1989, **87**, 40.
127. Y. Gandon, D. Olivie, D. Guyader, C. Aubé, F. Oberti, V. Sebillé and Y. Deugnier, *Lancet*, 2004, **363**(9406), 357.
128. Z. J. Wang, J. C. Haselgrove, M. B. Martin, A. M. Hubbard, S. Li, K. Loomes, J. R. Moore, H. Zhao and A. R. Cohen, *J. Magn. Reson. Imaging*, 2002, **15**, 395.
129. J. Vymazal, R. A. Brooks, N. Patronas, M. Hajek, J. W. Bulte and G. Di Chiro, *J. Neurol. Sci.*, 1995, **134**(Suppl), 19.
130. D. Kim, J. H. Jensen, E. X. Wu, L. Feng, W. Y. Au, J. S. Cheung, S. Y. Ha, S. S. Sheth and G. M. Brittenham, *NMR Biomed.*, 2011, **24**, 771.
131. H. Chandarana, R. K. Do, T. C. Mussi, J. H. Jensen, C. H. Hajdu, J. S. Babb and B. Taouli, *AJR Am. J. Roentgenol.*, 2012, **199**, 803.
132. J. C. Wood, A. Mo, A. Gera, M. Koh, T. Coates and V. Gilsanz, *Br. J. Haematol.*, 2011, **53**, 780.
133. R. Gorodetsky, A. Goldfarb, I. Dagan and E. A. Rachmilewitz, *J. Lab. Clin. Med.*, 1985, **105**, 44.
134. L. Wielopolski and E. C. Zaino, *J. Nucl. Med.*, 1992, **33**, 1278.
135. S. Oelckers and W. Graeff, *Phys. Med. Biol.*, 1996, **41**, 1149.
136. B. E. Chatterton, C. M. Thomas and C. G. Schultz, *J. Clin. Densitom.*, 2003, **6**, 283.

137. J. A. Shepherd, B. Fan, Y. Lu, L. Marquez, K. Salama, J. Hwang and E. B. Fung, *J. Clin. Densitom.*, 2010, **13**, 399.
138. M. J. House, A. J. Fleming, M. D. de Jonge, D. Paterson, D. L. Howard, J. P. Carpenter, D. J. Pennell and T. G. St Pierre, *J. Cardiovasc. Magn. Reson.*, 2014, **16**, 80.
139. B. F. Popescu, M. J. George, U. Bergmann, A. V. Garachtchenko, M. E. Kelly, R. P. McCrea, K. Lüning, R. M. Devon, G. N. George, A. D. Hanson, S. M. Harder, L. D. Chapman, I. J. Pickering and H. Nichol, *Phys. Med. Biol.*, 2009, **54**, 651.
140. W. Y. Au, W. W. Lam, W. W. C. Chu, H. L. Yuen, A. S. Ling, R. C. Li, H. M. Chan, H. K. Lee, M. F. Law, H. S. Liu, R. Liang and S. Y. Ha, *Haematologica*, 2008, **93**, 784.
141. W. W. Lam, W. Y. Au, W. C. W. Chu, S. Tam, S. Y. Ha and D. J. Pennell, *J. Magn. Reson. Imaging*, 2008, **28**, 29.
142. O. Papakonstantinou, E. Alexopoulou, N. Economopoulos, O. Benekos, A. Kattamis, S. Kostaridou, V. Ladis, E. Efstathopoulos, A. Gouliamos and N. L. Kelekis, *J. Magn. Reson. Imaging*, 2009, **29**, 853.
143. C. Camaschella, *Blood*, 2005, **106**, 3710.
144. E. Angelucci, G. M. Brittenham, C. E. McLaren, M. Ripalti, D. Baronciani, C. Giardini, M. Galimberti, P. Polchi and G. Lucarelli, *N. Engl. J. Med.*, 2000, **343**, 327.
145. A. L. Francanzani, M. Mattioli, D. Baronciani, G. Brittenham, G. Fiorelli and G. Lucarelli, *Blood*, 1998, **92**(suppl 1), 37b.
146. R. Fischer, F. Longo, P. Nielsen, R. Engelhardt, R. C. Hider and A. Piga, *Br. J. Haematol.*, 2003, **121**, 938.
147. R. J. Bergeron, R. R. Streiff, J. Wiegand, G. Luchetta, E. A. Creary and H. H. Peter, *Blood*, 1992, **79**, 1882.
148. J. C. Wood, P. Zhang, H. Rienhoff, W. Abi-Saab and E. J. Neufeld, *Magn. Reson. Imaging*, 2015, **33**, 761.
149. J. Porter, C. Borgna-Pignatti, M. Baccarani, A. Saviano, S. Abish, R. Malizia, H. Nick, H. Opitz, B. Rabault, I. Gathmann and P. Marks, *Blood*, 2005, **106**, 2690.
150. E. Angelucci, P. Muretto, A. Nicolucci, D. Baronciani, B. Erer, J. Gaziev, M. Ripalti, P. Sodani, S. Tomassoni, G. Visani and G. Lucarelli, *Blood*, 2002, **100**, 17.
151. P. D. Jensen, F. T. Jensen, T. Christensen, J. L. Nielsen and J. Ellegaard, *Blood*, 2003, **101**, 91.
152. J. P. Carpenter, A. E. Grasso, J. B. Porter, F. Shah, J. Dooley and D. J. Pennell, *J. Cardiovasc. Magn. Reson.*, 2013, **15**, 24.
153. J. M. Virtanen, K. J. Remes, M. A. Itälä-Remes, J. P. Saunavaara, M. E. Komu, A. M. Partanen and R. K. Parkkola, *Blood Cancer J.*, 2012, **2**, e49.
154. V. Berdoukas, C. Dakin, A. Freema, I. Fraser, A. Aessopos and T. Bohane, *Haematologica*, 2005, **90**, 685.
155. M. Cazzola, C. Borgna-Pignatti, P. De Stefano, G. Bergamaschi, I. G. Bongo, L. Dezza and F. Avato, *Scand. J. Haematol.*, 1983, **30**, 289.

156. C. Borgna-Pignatti, P. De Stefano, I. G. Bongo, F. Avato and M. Cazzola, *Am. J. Pediatr. Hematol. Oncol.*, 1984, **6**, 340.
157. O. Papakonstantinou, E. E. Drakonaki, T. Maris, A. Vasiliadou, A. Papadakis and N. Gourtsoyiannis, *Abdom. Imaging*, 2015, **40**, 2777.
158. C. J. Brewer, T. D. Coates and J. C. Wood, *J. Magn. Reson. Imaging*, 2009, **29**, 357.
159. L. Gutiérrez, M. J. House, N. Vasavda, E. Drašar, I. Gonzalez-Gascon y Marin, A. G. Kulasekararaj, T. G. St Pierre and S. L. Thein, *PLoS One*, 2015, **10**, e0139220.
160. B. P. Schoennagel, R. Fischer, R. Grosse, C. Berliner, M. Wehbe, G. Kurio, G. Lund, Z. J. Wang, J. Graessner, G. Adam and J. Yamamura, *JACC Cardiovasc. Imaging*, 2016, DOI: 10.1016/j.jcmg.2015.10.017.
161. J. C. Wood, R. Origa, A. Agus, G. Matta, T. D. Coates and R. Galanello, *Haematologica*, 2008, **93**, 917.
162. R. Origa, S. Barella, G. M. Argiolas, P. Bina, A. Agus and R. Galanello, *Haematologica*, 2008, **93**, 1095.
163. L. J. Anderson, M. A. Westwood, S. Holden, B. Davis, E. Prescott, B. Wonke, J. B. Porter, J. M. Walker and D. J. Pennell, *Br. J. Haematol.*, 2004, **127**, 348.
164. L. J. Noetzli, S. M. Carson, A. S. Nord, T. D. Coates and J. C. Wood, *Blood*, 2008, **112**, 2973.
165. D. Magri, S. Sciomer, F. Fedele, G. Gualdi, E. Casciani, P. Pugliese, A. Losardo, G. Ferrazza, E. Pasquazzi, E. Schifano, E. Mussino, R. Quaglione and G. Piccirillo, *Eur. J. Haematol.*, 2008, **80**, 515.
166. G. Strohmeyer, C. Niederau and W. Stremmel, *Ann. N. Y. Acad. Sci.*, 1988, **526**, 245.
167. G. Seifert, *Pancreatic Pathology*, ed. G. Klöppel and P. U. Heitz, Churchill Livingstone, Edinburgh-New York, 1984, p. 39.
168. T. C. Iancu, R. J. Ward and T. J. Peters, *J. Pediatr. Gastroenterol. Nutr.*, 1990, **10**, 95.
169. M. Midiri, A. Lo Casto, G. Sparacia, P. D'Angelo, R. Malizia, M. Finazzo, G. Montalto, L. Solbiati, R. Lagalla and M. De Maria, *Am. J. Roentgenol.*, 1999, **173**, 187.
170. M. I. Argyropoulou, D. N. Kiortsis, L. Astrakas, Z. Metafratzi, N. Chalisos and S. C. Efremidis, *Eur. Radiol.*, 2007, **17**, 3025.
171. O. Papakonstantinou, V. Ladis, S. Kostaridou, T. Maris, H. Berdousi, C. Kattamis and N. Gourtsoyiannis, *Eur. Radiol.*, 2007, **17**, 535.
172. L. J. Noetzli, J. Papudesi, T. D. Coates and J. C. Wood, *Blood*, 2009, **114**, 4021.
173. A. Meloni, M. Puliyl, A. Pepe, V. Berdoukas, T. D. Coates and J. C. Wood, *Am. J. Hematol.*, 2014, **89**, 678.
174. S. T. Singer, D. Killilea, J. H. Suh, Z. J. Wang, Q. Yuan, K. Ivani, P. Evans, E. Vichinsky, R. Fischer and J. F. Smith, *Am. J. Hematol.*, 2015, **90**, E190.
175. R. C. McCarthy and D. J. Kosman, *Cell. Mol. Life Sci.*, 2015, **72**, 709.
176. V. Adisetiyo, J. H. Jensen, A. Ramani, A. Tabesh, A. Di Martino, E. Fieremans, F. X. Castellanos and J. A. Helpert, *J. Magn. Reson. Imaging*, 2012, **36**, 322.

177. S. Aoki, Y. Okada, K. Nishimura, A. J. Barkovich, B. O. Kjos, R. C. Brasch and D. Norman, *Radiology*, 1989, **172**, 381.
178. M. Liu, S. Liu, K. Ghassaban, W. Zheng, D. Diccico, Y. Miao, C. Habib, T. Jazmati and E. M. Haacke, *J. Magn. Reson. Imaging*, 2016, **44**, 59.
179. J. Acosta-Cabronero, M. J. Betts, A. Cardenas-Blanco, S. Yang and P. J. Nestor, *J. Neurosci.*, 2016, **36**, 364.
180. P. D. Griffiths, B. R. Dobson, G. R. Jones and D. T. Clarke, *Brain*, 1999, **122**, 667.
181. J. H. Barbosa, A. C. Santos, V. Tumas, M. Liu, W. Zheng, E. M. Haacke and C. E. Salmon, *Magn. Reson. Imaging*, 2015, **33**, 559.
182. M. J. House, T. G. St Pierre, K. V. Kowdley, T. Montine, J. Connor, J. Beard, J. Berger, N. Siddaiah, E. Shankland and L. W. Jin, *Magn. Reson. Med.*, 2007, **57**, 172.
183. J. Acosta-Cabronero, G. B. Williams, A. Cardenas-Blanco, R. J. Arnold, V. Lupson and P. J. Nestor, *PLoS One*, 2013, **8**, e81093.
184. H. M. Schipper, *Biochim. Biophys. Acta*, 2012, **1822**, 350.
185. A. McNeill, D. Birchall, S. J. Hayflick, A. Gregory, J. F. Schenk, E. A. Zimmerman, H. Shang, H. Miyajima and P. F. Chinnery, *Neurology*, 2008, **70**, 1614.
186. R. J. Ward, F. A. Zucca, J. H. Duyn, R. R. Crichton and L. Zecca, *Lancet Neurol.*, 2014, **13**, 1045.
187. N. Boddaert, K. H. Le Quan Sang, A. Rötig, A. Leroy-Willig, S. Gallet, F. Brunelle, D. Sidi, J. C. Thalabard, A. Munnich and Z. I. Cabantchik, *Blood*, 2007, **110**, 401.
188. G. Cossu, G. Abbruzzese, G. Matta, D. Murgia, M. Melis, V. Ricchi, R. Galanello, S. Barella, R. Origa, M. Balocco, E. Pelosin, R. Marchese, U. Ruffinengo and G. L. Forni, *Parkinsonism Relat. Disord.*, 2014, **20**, 651.
189. U. Löbel, F. Schweser, M. Nickel, A. Deistung, R. Grosse, C. Hagel, J. Fiehler, A. Schulz, M. Hartig, J. R. Reichenbach, A. Kohlschütter and J. Sedlacik, *Ann. Clin. Transl. Neurol.*, 2014, **1**, 1041.
190. D. Devos, S. Moreau, J. C. Devedjian, I. Kluza, M. Petrault, C. Laloux, A. Jonneaux, G. Ryckewaert, G. Garçon, L. Rouaix, A. Duhamel, P. Jissendi, K. Dujardin, F. Auger, L. Ravasi, L. Hopes, G. Grolez, W. Firdaus, B. Sablonnière, I. Strubi-Vuillaume, N. Zahr, A. Destée, J. C. Corvol, D. Pörtl, M. Leist, C. Rose, L. Defebvre, P. Marchetti, Z. I. Cabantchik and R. Bordet, *Antioxid. Redox Signal*, 2014, **21**, 195.
191. A. Martin-Bastida, R. J. Ward, R. Newbould, P. Piccini, D. Sharp, C. Kabba, M. C. Patel, M. Spino, J. Connelly, F. Tricta, R. R. Crichton and D. D. Dexter, *Nat. Commun.*, 2016, in press.
192. L. Zecca, M. Gallorini, V. Schünemann, A. X. Trautwein, M. Gerlach, P. Riederer, P. Vezzoni and D. Tampellini, *J. Neurochem.*, 2001, **76**, 1766.
193. S. Reimão, S. Ferreira, R. G. Nunes, P. Pita Lobo, D. Neutel, D. Abreu, N. Gonçalves, J. Campos and J. J. Ferreira, *Eur. J. Neurol.*, 2016, **23**, 368.
194. F. Schweser, A. Deistung, B. W. Lehr and J. R. Reichenbach, *Neuroimage*, 2011, **54**, 2789.

195. M. J. House, T. G. St Pierre and C. McLean, *Magn. Reson. Med.*, 2008, **60**, 41.
196. A. Schein, C. Enriquez, T. D. Coates and J. C. Wood, *J. Magn. Reson. Imaging*, 2008, **28**, 698.
197. E. S. Siegelman, E. Outwater, C. A. Hanau, S. K. Ballas, R. M. Steiner, V. M. Rao and D. G. Mitchell, *J. Comput. Assist. Tomogr.*, 1994, **18**, 63.
198. J. Rimola, J. Martin, J. Puig, A. Darnell and A. Massuet, *Br. J. Radiol.*, 2004, **77**, 953.
199. J. C. Wood, A. R. Cohen, S. L. Pressel, B. Aygun, H. Imran, L. Luchtman-Jones, A. A. Thompson, B. Fuh, W. H. Schultz, B. R. Davis, R. E. Ware and TWiTCH Investigators, *Br. J. Haematol.*, 2016, **172**, 122.
200. N. Vasavda, L. Gutiérrez, M. J. House, E. Drašar, T. G. St Pierre and S. L. Thein, *Br. J. Haematol.*, 2012, **157**, 599.
201. S. Bhandari and R. Galanello, *Eur. J. Haematol.*, 2012, **89**, 187.
202. A. Lahoti, Y. T. Harris, P. W. Speiser, E. Atsidaftos, J. M. Lipton and A. Vlachos, *Pediatr. Blood Cancer*, 2016, **63**, 306.
203. K. E. Huang, S. D. Mittelman, T. D. Coates, M. E. Geffner and J. C. Wood, *J. Pediatr. Hematol. Oncol.*, 2015, **37**, 54.
204. E. Drakonaki, O. Papakonstantinou, T. Maris, A. Vasiliadou, A. Papadakis and N. Gourtsoyiannis, *Eur. Radiol.*, 2005, **15**, 2462.
205. R. Rakow-Penner, B. Glader, H. Yu and S. Vasanawala, *Pediatr. Radiol.*, 2010, **40**, 1955.
206. S. Noma, J. Konishi, M. Morikawa and Y. Yoshida, *J. Comput. Assist. Tomogr.*, 1988, **12**, 623.
207. T. Shirota, T. Shinoda, T. Aizawa, T. Mizukami, M. Katakura, N. Takasu and T. Yamada, *Clin. Nephrol.*, 1992, **38**, 105.
208. M. Maggiolini, G. De Luca, M. Bria, D. Sisci, S. Aquila, V. Pezzi, M. Lanzino, A. Giorno, O. Tamburrini, M. Della Sala, E. Corcioni, C. Brancati and S. Ando, *Endocrine*, 1995, **3**, 91.
209. Y. L. Suh, S. K. Khang and K. N. Kim, *J. Korean Med. Sci.*, 1991, **6**, 267.
210. R. Jaffar, S. K. Mohanty, A. Khan and A. H. Fischer, *Cytojournal*, 2009, **19**(6), 3.
211. H. J. Vogt, T. Weidenbach, K. H. Marquart and G. E. Vogel, *Andrologica*, 1987, **19**, 532.
212. Y. Miaux, P. Daurelle, A. M. Zagdanski, P. Passa, P. Bourrier and J. Frija, *Eur. Radiol.*, 1995, **5**, 165.
213. S. T. Singer, N. Sweeters, O. Vega, A. Higa, E. Vichinsky and M. Cedars, *Ann. N. Y. Acad. Sci.*, 2010, **1202**, 226.
214. R. P. Guillerman, *Pediatr. Radiol.*, 2013, **43**(suppl), S181.
215. J. B. Porter, P. B. Walter, L. D. Neumayr, P. Evans, S. Bansal, M. Garbowski, M. G. Weyhmiller, P. R. Harmatz, J. C. Wood, J. L. Miller, C. Byrnes, G. Weiss, M. Seifert, R. Grosse, D. Grabowski, A. Schmidt, R. Fischer, P. Nielsen, C. Niemeyer and E. Vichinsky, *Br. J. Haematol.*, 2014, **167**, 692.
216. R. Grosse, B. Schoennagel, R. Fischer, J. Yamamura, S. Acar and P. Nielsen, *Blood*, 2015, **126**, 3358.

217. B. R. Rosen, D. M. Fleming, D. C. Kushner, K. S. Zaner, R. B. Buxton, W. P. Bennet, G. L. Wismer and T. J. Brady, *Radiology*, 1988, **169**, 799.
218. E. E. Drakonaki, T. G. Maris, A. Papadakis and A. H. Karantanas, *Eur. Radiol.*, 2007, **17**, 2079.
219. M. I. Argyropoulou, D. N. Kiortsis, L. Astrakas, Z. Metafratzi, N. Chalissos and S. C. Efremidis, *Eur. Radiol.*, 2007, **17**, 3025.
220. P. Storey, A. A. Thompson, C. L. Carqueville, J. C. Wood, R. A. de Freitas and C. K. Rigsby, *J. Magn. Reson. Imaging*, 2007, **25**, 540.
221. A. Meloni, V. Positano, P. Keilberg, D. De Marchi, P. Pepe, A. Zuccarelli, S. Campisi, M. A. Romeo, T. Casini, P. P. Bitti, C. Gerardi, M. E. Lai, B. Piraino, G. Giuffrida, G. Secchi, M. Midiri, M. Lombardi and A. Pepe, *Magn. Reson. Med.*, 2012, **68**, 543.
222. E. M. Haacke, S. Liu, S. Buch, W. Zheng, D. Wu and Y. Ye, *Magn. Reson. Imaging*, 2015, **33**, 1.

## CHAPTER 8

# *Chelators for Diagnostic Molecular Imaging with Radioisotopes of Copper, Gallium and Zirconium*

MICHELLE T. MA<sup>\*a</sup> AND PHILIP J. BLOWER<sup>a</sup>

<sup>a</sup>King's College London, Division of Imaging Sciences and Biomedical Engineering, 4th Floor Lambeth Wing, St Thomas' Hospital, London SE1 7EH, UK

\*E-mail: [michelle.ma@kcl.ac.uk](mailto:michelle.ma@kcl.ac.uk)

## 8.1 Introduction

Many metallic radionuclides are useful in nuclear medicine for imaging by gamma camera scintigraphy, single photon emission computed tomography (SPECT) and positron emission tomography (PET), and for radionuclide therapy of cancer. Their clinical application depends on deep understanding of their chemistry and in particular the use of chelating ligands.<sup>1,2</sup> This chapter discusses the design of the chelators to match the varying requirements associated with the particular clinical application and the decay properties of the radionuclide, with reference to three illustrative examples chosen for their diversity in chemical and decay properties and their applications: copper-64 (<sup>64</sup>Cu), gallium-68 (<sup>68</sup>Ga) and zirconium-89 (<sup>89</sup>Zr). These

---

RSC Metallobiology Series No. 8

Metal Chelation in Medicine

Edited by Robert Crichton, Roberta J. Ward and Robert C. Hider

© The Royal Society of Chemistry 2017

Published by the Royal Society of Chemistry, [www.rsc.org](http://www.rsc.org)

are all radiometallic isotopes utilised in nuclear medicine for diagnostic PET imaging (although  $^{64}\text{Cu}$  is also considered to have potential applications in targeted radionuclide therapy). The ability of these radiometallic ions to be incorporated into molecular imaging agents that are effective at delivering radioactivity to diseased tissue *in vivo* depends upon the properties of the coordinating ligands. Preparation of radiopharmaceuticals based on these metallic radionuclides at a hospital site is also dependent on highly reproducible and straightforward reactions. As such, the contribution of inorganic chemistry to the field of nuclear medicine has largely concerned chelator design, optimisation of chelator reactivity, and characterisation of their complexes formed with radiometallic ions. Chelating ligands for radioactive metal complexes can dictate the rate at which a metal ion is released *in vivo* or *in vitro*, the biodistribution and pharmacokinetics of a radiotracer *in vivo* and, ultimately, the utility of a radiopharmaceutical for providing clinicians with useful information.

### 8.1.1 Positron Emission Tomography and Molecular Imaging with Peptides and Proteins

Positron emission tomography (PET) is a whole-body diagnostic three-dimensional imaging modality used in nuclear medicine that detects positron emissions arising from the decay of unstable radioisotopes. In a patient, the time and position of decay of a positron-emitting radionuclide can be determined. Thus, if a radionuclide can be selectively transported to diseased tissue in sufficient quantities, it is possible to determine the anatomical location of that tissue. As PET scanners acquire data longitudinally, it is possible, and indeed routine, to map the location of radioactivity in a patient or subject over time.

When a radionuclide decays *via* conversion of a proton to a neutron, a positron is emitted. When this positron collides with an electron, two gamma rays of 511 keV energy are emitted at a trajectory of  $180 \pm 0.5^\circ$  from each other. In a PET scanner, detection of these two gamma rays, both coincident on the same line, occurs *via* a  $360^\circ$  array of scintillation detectors coupled to photomultiplier tubes. Processing and reconstruction of these signals leads to a three-dimensional image mapping the distribution of the radionuclide. The amount of radioactive compound typically used to acquire PET scans is in the picomole to nanomole range and, as such, PET is a highly sensitive technique. However, PET is not a highly resolved technique. Depending on the energy of the emitted positron and the density of tissue, a positron will travel some distance (up to a few mm) whilst losing energy prior to the annihilation event. The higher the energy of the positron, the farther it will travel. Conversely, the distance traversed by a positron decreases with increased density of tissue. Consequently, in combination with other factors,<sup>3</sup> PET is limited to mm–cm resolution. Modern PET scanners include X-ray-computed tomography (CT) scanners so that a PET image of a patient can be co-registered with a CT image. The CT image, with vastly superior resolution of anatomical features, provides an anatomical map and, in the case of solid tumours, can

provide more accurate information on tumour volume. Hence, the essence of PET is imaging the spatial distribution of molecular processes rather than anatomical structure.

Cancer cells, and other diseased cells, can often be characterised by metabolic and molecular peculiarities. These include increased glucose utilisation, hypoxia, antigen production or expression of particular *receptors* on their cell surfaces that are involved in mediating cell proliferation or other events associated with disease progression. Biomolecules that target molecular markers with high affinity and specificity can be utilised to deliver a radionuclide such as a positron emitter to the site of diseased tissue, providing a *molecular imaging agent*. The high sensitivity of PET means that the low quantities of radiopharmaceutical administered to a patient to obtain a PET image are not likely to elicit any adverse physiological effects, or to perturb significantly the process being imaged. From a diagnostic perspective, these pathological or *molecular markers* can provide clinicians with diagnostic and prognostic information that can inform a patient's treatment regime. For instance, the presence of a particular cell-surface protein receptor can indicate that a patient will be more likely to respond to a specific course of therapy. Historically, such pathological information has been obtained using relatively invasive procedures such as biopsies that are limited to providing information at a single site in a patient. The ability to image pathological or molecular markers non-invasively using whole-body scanning techniques circumvents the need for surgical procedures, and provides information at the whole-body level.

*Bifunctional chelators* in PET chemistry incorporate a chelator for coordination of a radiometal, and a functional group that can react with a biomolecule, forming a covalent bond between the chelator and biomolecule. *Peptides* possess no tertiary structure and are, for the most part, obtained synthetically and, as peptide synthesis allows for selective protection and deprotection of specific amino acid residues, site-selective conjugation of a chelator to a peptide is possible. On the other hand, large *proteins* and *antibodies* that possess tertiary and quaternary structure are obtained from biogenic sources and conjugation to bifunctional chelators is often not site-specific unless particular functionality is engineered into the protein or the chelator is conjugated to the protein *via* an enzymatic reaction.<sup>4-8</sup>

### 8.1.2 Reactive Functional Groups for Attachment to Biomolecules

For bifunctional chelators to be useful in the field of radiopharmaceuticals, the conjugation chemistry needs to be relatively straightforward. It is beyond the scope of this chapter to review the latest developments in this ever-expanding field,<sup>9</sup> but it is worth one's while to be familiar with the design principles and the most widely used functionalities with respect to chelator conjugation. The following brief list is far from exhaustive but includes linker chemistry that is pertinent to both commercially available bifunctional chelators and common derivatisations of new chelators.

As peptides and proteins are essentially polymers linked by amide bonds, *amide bond formation* is often employed to covalently attach a bifunctional chelator to a biomolecule. Bifunctional chelators containing carboxylic acids, “activated” carboxylic acids (such as *N*-hydroxysuccinimide esters or tetrafluorophenyl esters) or cyclic anhydrides, can be conjugated to primary amine groups of the N-terminus of peptides and proteins, or of lysine side chains. Similarly, primary amine derivatives of chelators can be reacted with C-termini, or aspartic acid or glutamic acid side chains. The latter requires activation of the carboxylic acid, so conjugation using this strategy is less common and is usually restricted to peptides, where orthogonal synthesis enables site-specific attachment. Amide bonds are generally stable *in vivo* in the absence of enzymatic reactions. As synthetic chelators are not recognised by enzymes that hydrolyse peptide bonds, attachment *via* an amide bond is usually a viable strategy for bioconjugation of a chelator.

*Isothiocyanates* can react with primary amine groups to form thiourea bonds that are stable in the biological milieu. Phenyl or alkyl isothiocyanate derivatives are amongst the most common commercially available bifunctional chelators, and currently there is a prevailing trend in the scientific literature to prepare isothiocyanate derivatives of new chelators intended for bioconjugation.

*Maleimides* allow conjugation of a chelator *via* a reduced cysteine side chain, or other thiol functionality, providing an alternative, and often, site-specific means of attachment.

Reactions of azides and alkynes to form triazoles, and other types of *click chemistry*, have proved useful in decorating biomolecules with chelators. In this instance, the biomolecule has to be first synthesised or engineered to incorporate the azide or alkyne function; unlike thiols, carboxylic acids and primary amines, azide and alkyne groups are not widely prevalent endogenous chemical motifs.

### 8.1.3 Requirements for Chelators that Complex Positron-Emitting Metal Radioisotopes

$^{64}\text{Cu}$ ,  $^{68}\text{Ga}$ , and  $^{89}\text{Zr}$  are positron-emitting metallic isotopes with decay properties suitable for PET imaging, and can be sourced *via* various production routes, the most widely used of which are listed in Table 8.1. Two very important factors must be considered when assessing suitability of chelators for coordination of a radiometal. Firstly, the complexation reaction must be efficient, and secondly, the resulting complex must be sufficiently stable *in vivo*.

The complexation reaction must be efficient for several reasons:

1. The radiometal concentration in solution is very low and falls within the nanomolar range.
2. It is desirable for the chelator–biomolecule conjugate or *bioconjugate* to be present in low amounts. It is difficult to separate out unreacted bioconjugate from radiolabelled bioconjugate, and any unlabelled

**Table 8.1** Decay properties and production routes of  $^{64}\text{Cu}$ ,  $^{68}\text{Ga}$  and  $^{89}\text{Zr}$ .

Isotope	Half-life	Positron ( $\beta^+$ ) decay properties	Production
$^{64}\text{Cu}$	12.7 h	$\beta^+$ 19%, $E_{\text{max}} = 656$ keV (41% electron capture, 40% $\beta^+$ )	Cyclotron, $^{64}\text{Ni}(\text{p},\text{n})$ $^{64}\text{Cu}$
$^{68}\text{Ga}$	68 min	$\beta^+$ 90%, $E_{\text{max}} = 1880$ keV (10% electron capture)	Generator-produced from $^{68}\text{Ge}$ (half-life = 271 days)
$^{89}\text{Zr}$	78 h	$\beta^+$ 23%, $E_{\text{max}} = 897$ keV (77% electron capture)	Cyclotron, $^{89}\text{Y}(\text{p},\text{n})$ $^{89}\text{Zr}$

bioconjugate often remains present in the final formulation that is administered to a patient or subject. Large amounts of unlabelled bioconjugate compete with labelled conjugate for receptor binding *in vivo*. This can effectively block binding of radiolabelled conjugate, and may cause toxicity. The quantitative measure of the amount of radioactivity bound per biologically-active molecule is described as *specific activity* and has units of activity (becquerels, Bq, one decomposition per second) per amount of conjugate (number of moles or mass).

- For short-lived isotopes like  $^{68}\text{Ga}$  (half-life 68 minutes), fast reaction kinetics are essential. In the case of longer-lived isotopes like  $^{64}\text{Cu}$  (12.7 hours) and  $^{89}\text{Zr}$  (78 hours), where there is ample time for reactions that take >1–2 hours, from a practical point of view it is preferable that reactions are fast. Simple, rapid and reproducible complexation chemistry allows for readier acceptance in hospital radiopharmacies.
- Near-quantitative complexation of radiometal at low bioconjugate concentration is also desirable for the same reasons—quantitative or near-quantitative complexation circumvents requirements for additional steps to remove unreacted radiometal, allowing for implementation of simple radiolabelling protocols that are suited to hospital radiopharmacies.

The clinical utility and adaptability of a radiosynthetic protocol for radiopharmaceutical production and formulation depends on the reaction conditions (pH, solvent, temperature), the kinetics of formation of a metal–ligand complex, the radiochemical yield, and whether or not purification procedures are required to remove unwanted by-products, reagents, organic solvents or unreacted radiometal. Ideally the rate should be diffusion-limited, *i.e.* every encounter between the chelator and the radiometal will result in complex formation. This allows for rapid, quantitative reactions that provide a single radiolabelled product at low concentrations of both the chelator and radiometal in aqueous solutions.

It is also critical that the resulting complex is stable *in vivo*, for at least as long as the imaging procedure requires (typically one to six times the half life of the radionuclide) unless instability is a requirement of the targeting mechanism (as in the examples in Sections 8.2.3 and 8.4.3). Dissociation of a radiometal from a chelator will result in the radiometal coordinating to an endogenous

biomolecule or mineral and potential transportation to a non-target organ, causing a decrease in radioactivity accumulation in the target tissue. Ultimately, the quality of the PET image is compromised and radiation doses to non-target organs in the subject may be increased. The overall charge and lipophilicity of the resulting complex is also important—for example, hydrophobic compounds often accumulate in non-target organs such as the liver and gut.

The priority of these requirements—efficient radiolabelling *versus in vivo* stability—differs depending on the half-life of the isotope. For a short half-life isotope, such as  $^{68}\text{Ga}$ , fast radiolabelling kinetics are more important than prolonged *in vivo* stability. In the case of long-lived isotopes, such as  $^{64}\text{Cu}$  and  $^{89}\text{Zr}$ , the opposite is true.

In some cases, instability of a chelate complex can be desirable. Dissociation of a radiometallic ion from a chelator with subsequent trapping of the radiometal in cells can be used to obtain information about the cellular environment, or to track migrating or circulating cells. This instability can arise from a redox event—for example, a hypoxic cellular environment that induces reduction of a metal complex resulting in subsequent dissociation. Alternatively, “metastable” complexes can be designed to dissociate over a specific timeframe.

This chapter is not intended as an exhaustive review of chelators for radiometals in nuclear medicine—the literature in this area has been surveyed in depth in recent years in several excellent reviews and books.<sup>1,2,10–16</sup> Instead, its role is educational, aiming to outline historical developments in chelator chemistry for the PET isotopes  $^{64}\text{Cu}$  (1990's onwards),  $^{68}\text{Ga}$  (2000's onwards) and  $^{89}\text{Zr}$  (2010's onwards). It also aims to highlight the different purposes for which each radiometal is suited. In the light of these different purposes—alongside coordination preferences, decay properties and other practical considerations—the design requirements are altered.

## 8.2 Macrocyclic Chelators for Copper-64: Lessons in Kinetic Stability

Copper-64 is a positron-emitting isotope with a half-life of 12.7 hours and, as such, is suitable for PET imaging using molecular imaging agents based on *both* peptides and proteins. The radionuclide also emits beta particles and Auger electrons, and thus is potentially useful as a radiotherapeutic. For proteins, which are rather more delicate than short peptides because their tertiary structure is important to targeting, it is critical that radiolabelling conditions are mild—near neutral or physiological pH and temperatures at or below 37 °C are required to avoid disruption of tertiary and secondary structure. Additionally, ease of radiolabelling and high radiochemical yields are favourable for clinical translation. Usually  $^{64}\text{Cu}$  is provided as a solution in aqueous hydrochloric acid and, whilst there are some examples of radiotracers based on  $\text{Cu}^+$ ,<sup>17,18</sup> the overwhelming majority of chelator developments have been for  $\text{Cu}^{2+}$ .

Whilst open-chain or acyclic chelators are likely to be important for future innovations in molecular imaging, particularly for  $^{68}\text{Ga}$ , macrocycles have dominated the landscape of bifunctional chelator chemistry for copper

radioisotopes. Non-cyclic chelators of  $\text{Cu}^{2+}$ , even multidentate ones with very high association constants (*e.g.* edta, dtpa) have invariably been found to be too kinetically labile, and hence vulnerable to ligand dissociation and exchange, to be useful as bifunctional chelators for biomolecule labelling.<sup>12,19</sup> Macrocyclic chelators are multidentate ligands where some or all donor atoms are present within a ring. Complexes of macrocycles typically demonstrate both high thermodynamic stability and a high degree of kinetic inertness to substitution in many cases, compared to analogous open-chain or acyclic chelators. This *macrocyclic effect* is a special example of the chelate effect. As the multidentate chelator is pre-organised into a ring structure, the degree of conformational flexibility that is lost upon coordination is significantly lower than that of acyclic or open chain analogues. Additionally, and importantly in the case of  $^{64}\text{Cu}^{2+}$  radiopharmaceuticals, the likelihood of re-coordination of a donor atom following dissociation is high, as the dissociated donor atom remains proximal to the metal centre. Thus, macrocycles can provide kinetically inert complexes with high free energies of activation for dissociation, and relatively rigid geometries enhance this.  $\text{Cu}^{2+}$  ( $d^9$  metal ion) can coordinate up to six ligands in its pseudo-octahedral coordination sphere, although ligand binding along one axis is often significantly weaker (and sometimes absent) as a result of Jahn–Teller electronic effects. In general, chelators that both accommodate Jahn–Teller distortion, and saturate the coordination sphere of  $\text{Cu}^{2+}$  are preferable, as vacant coordination sites can potentially lead to coordination of endogenous protein or peptide ligands, providing a pathway for ligand exchange and thus loss of  $^{64}\text{Cu}^{2+}$  from the radiotracer.

$\text{Cu}^{2+}$  can be reduced to  $\text{Cu}^+$ . Because  $\text{Cu}^+$  ( $d^{10}$  metal ion) has different coordination preferences to  $\text{Cu}^{2+}$ , and is even less inert to ligand exchange, it is important that reduction potentials are sufficiently low to prevent reduction in the potentially reducing intracellular environment, as reduction would lead to faster dissociation and transchelation. For the complexes discussed below, reduction of  $\text{Cu}^{2+}$  to  $\text{Cu}^+$  as a mechanism for loss of  $^{64}\text{Cu}$  is unlikely as reduction potentials are lower than those encountered in the intracellular environment; thus, their redox chemistry is not well-explored.<sup>20</sup>

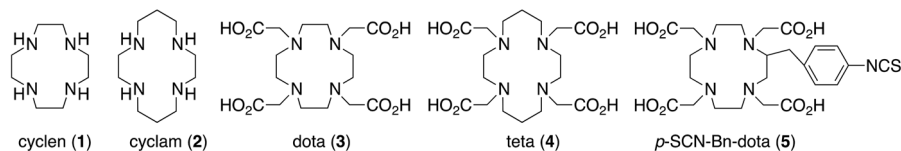
The next section introduces  $\text{Cu}^{2+}$  complexes of the most widely used macrocycles, discusses the most significant advances in macrocyclic chemistry for copper radioisotopes, and finally correlates the *in vivo* behaviour of  $^{64}\text{Cu}^{2+}$ -labelled radiotracers with the kinetic stability and structures of the complexes themselves.

## 8.2.1 Cu Complexes of Macrocycles: Radiolabelling and *In vivo* Stability

### 8.2.1.1 Cyclen, Cyclam, Teta and DOTA – Not All Macrocycles are Equal to the Task!

Very early studies using macrocycles for  $^{64}\text{Cu}^{2+}$  coordination investigated cyclen, cyclam, teta and dota (1–4), firstly for their ability to complex radiopharmaceutical concentrations of  $^{64}\text{Cu}^{2+}$  quantitatively, and secondly for

their ability to retain coordinated  $^{64}\text{Cu}^{2+}$  *in vivo*. Stark differences in both radiolabelling conditions and *in vivo* stability were observed for various complexes and their peptide conjugates, and these differences were attributed to the properties of the  $^{64}\text{Cu}$ -bifunctional chelator complex. Early studies on bifunctional chelators for  $^{64}\text{Cu}^{2+}$  compared the tetraaza macrocycles cyclen (1) and cyclam (2) with their tetracarboxylate derivatives dota (3) and teta (4).<sup>21,22</sup> Radiolabelling yields for peptide conjugates of teta were markedly superior to yields for cyclam<sup>22</sup>—teta derivatives were labelled in 95% radiochemical yield after one hour, whilst after 12 hours only 85% of  $^{64}\text{Cu}^{2+}$  was bound to cyclam derivatives. Furthermore, animal studies demonstrated that  $^{64}\text{Cu}^{2+}$  complexes of the tetraazamacrocycles cyclam, cyclen and their conjugates, exhibited significantly higher liver and kidney activity relative to their tetraacetate derivatives, teta and dota.<sup>21,22</sup> In the case of the unconjugated radiolabelled complexes, this was attributed to the higher positive charges of  $[\text{}^{64}\text{Cu}(\text{cyclam})]^{2+}$  and  $[\text{}^{64}\text{Cu}(\text{cyclen})]^{2+}$  compared to the negative charges of the  $[\text{}^{64}\text{Cu}(\text{dota})]^{2-}$  and  $[\text{}^{64}\text{Cu}(\text{teta})]^{2-}$  complexes.<sup>21</sup> Teta and dota were used almost exclusively as the bifunctional chelators of choice in early studies investigating  $^{64}\text{Cu}$ -labelled peptide conjugates for molecular imaging.



However, despite their advantages over cyclam and cyclen, neither dota nor teta are ideal chelators for  $^{64}\text{Cu}^{2+}$ . Whilst teta conjugates can be radiolabelled quantitatively within an hour at room temperature, both small animal and patient studies of  $\text{Cu}^{2+}$ -radiolabelled teta peptide and antibody conjugates demonstrate significant accumulation of activity in the liver, which is believed to be indicative of dissociation of  $\text{Cu}^{2+}$  radionuclide from the conjugate *in vivo*. Proteins such as superoxide dismutase,<sup>23,24</sup> metallothionein<sup>25</sup> and ceruloplasmin<sup>26</sup> that possess  $\text{Cu}^{2+}$  binding sites can coordinate dissociated  $^{64}\text{Cu}^{2+}$ , and early studies using animals administered a  $^{64}\text{Cu}$ -labelled teta-peptide conjugate demonstrated that  $^{64}\text{Cu}^{2+}$ -bound superoxide dismutase is formed in the liver.

Similarly,  $^{64}\text{Cu}^{2+}$ -dota labelled peptide conjugates also demonstrate significant liver accumulation, which has likewise been attributed to *in vivo* instability,<sup>25,27–29</sup> particularly as the kinetic stability of dota complexes of  $\text{Cu}^{2+}$  is lower than teta complexes (see Section 8.2.2 below). Compounding this problematic instability is the inconsistency in conditions that are required for incorporation of  $^{64}\text{Cu}^{2+}$  into dota derivatives. Many preparations have required temperatures between 60–80 °C and report radiochemical yields less than 80%,<sup>28</sup> whilst other reports suggest that quantitative radiochemical conversion can be achieved at ambient temperature, provided that radionuclide purity is relatively high.<sup>19</sup>

In more recently reported derivatives of dota (3) and teta (4), the functional group at which biomolecules are attached is appended to an alkyl group of the

macrocycle, allowing all four pendant acetate groups to be available for coordination to the metal centre—for example, *p*-SCN-Bn-dota (5).<sup>19,30</sup> This is in contrast to bioconjugates where one of the carboxylate groups has been reacted with a primary amine of a biomolecule, leaving only three acetate ligands and an amide functionality—for example, dota.<sup>28</sup> Compared to carboxylate-linked radiolabelled conjugates of dota, radiotracers based on *p*-SCN-Bn-dota will carry an extra negative charge, potentially altering biodistribution of the resulting radiotracer (see Section 8.2.2 below for further discussion).

The solid phase structures of the Cu<sup>2+</sup> complexes of cyclam,<sup>31</sup> teta<sup>32</sup> and dota<sup>33</sup> as determined by X-ray crystallography are included here for comparative purposes (Figure 8.1). In the [Cu(cyclam)]<sup>2+</sup> complex, the coordination sphere is not saturated by the cyclam ligand—the axial perchlorate counterions coordinate very weakly and would not be expected to remain coordinated in solution. Cu<sup>2+</sup> complexes of either dota or teta adopt distorted octahedral geometry with typical Jahn–Teller effects, although these are not as pronounced as they are for other Cu<sup>2+</sup> complexes, presumably because of the steric constraints of cyclic ligands. When dota is complexed with Cu<sup>2+</sup>, the *N*-donor atoms adopt a *cis* coordination mode, and Cu<sup>2+</sup> is positioned above the plane of the macrocycle. This is a result of the size constraints of the macrocycle. In crystals of [Cu(H<sub>2</sub>dota)], two macrocyclic *N*-donor atoms and the two *O*-donors of the deprotonated carboxylate arms form the equatorial plane, whilst the remaining *N*-donors are positioned axially with longer N–Cu bonds as a result of Jahn–Teller distortion. In contrast, in mononuclear complexes of [Cu(H<sub>2</sub>teta)] and [Cu(teta)]<sup>2-</sup>, the Cu<sup>2+</sup> ion lies in the plane of the larger teta macrocycle, and two deprotonated carboxylate arms are coordinated *trans* to each other, above and below the macrocycle plane. Each six-membered chelate ring is present in the “chair” conformation. Jahn–Teller distortion is also evident in this case, however the axis of elongation differs between the three different sets of crystallographic data reported.<sup>32,34</sup>

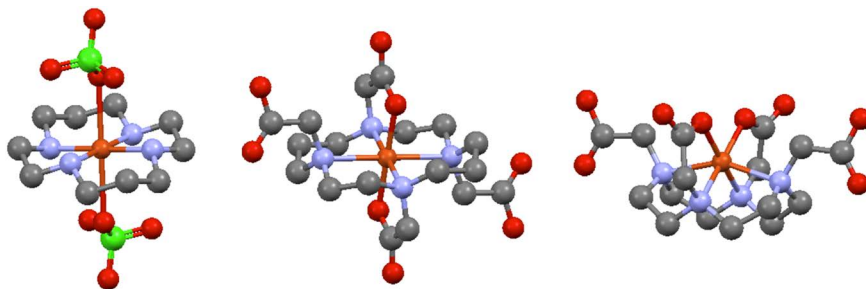


**Figure 8.1** From left to right, representations of the molecular structures of [Cu(cyclam)(ClO<sub>4</sub>)<sub>2</sub>],<sup>31</sup> [Cu(H<sub>2</sub>teta)],<sup>32</sup> and [Cu(dota)]<sup>2-</sup><sup>33</sup> as determined by crystallography. Orange – copper, blue – nitrogen, grey – carbon, red – oxygen, green – chloride. These diagrams and others contained herein (generated in Mercury software courtesy of the Cambridge Crystallographic Data Centre) represent structures determined crystallographically. Hydrogen atoms are omitted for clarity.

### 8.2.1.2 Alternatives to Teta and DOTA – Towards Greater *In vivo* Stability

Innovations in chelators for  $^{64}\text{Cu}^{2+}$  have resulted in  $^{64}\text{Cu}$ -labelled peptide conjugates that do not appreciably release  $^{64}\text{Cu}$  *in vivo*, providing superior PET images with higher target to non-target organ ratios. A  $^{64}\text{Cu}^{2+}$ -labelled conjugate of the ethylene-crossbridged cyclam tetraazamacrocycle bearing two acetate groups, ecb-te2a (**6a**, Figure 8.2), demonstrated decreased liver uptake compared to homologous teta and dota derivatives; unfortunately,  $^{64}\text{Cu}^{2+}$  complexation reactions require high temperatures ( $>90\text{ }^\circ\text{C}$ ) and basic conditions ( $\text{pH} > 8$ ) to achieve quantitative radiochemical yields.<sup>25,28,35</sup> As such, ecb-te2a (**6a**) is not suitable for radiolabelling sensitive biomolecular conjugates such as proteins or antibodies. Substitution of the ethylene bridge for a propylene bridge provides the chelator pcb-te2a (**7a**) that can be radiolabelled in quantitative radiochemical yields after 1 hour at  $70\text{ }^\circ\text{C}$ , or in lower radiochemical yields over longer time periods at lower temperatures.<sup>36</sup> Alternatively, the substitution of carboxylate groups of ecb-te2a (**6a**) by phosphonate groups, to provide chelators ecb-te2p (**6b**) and ecb-te1a1p (**6c**),<sup>37</sup> also leads to higher radiochemical yields under milder conditions. When ecb-te1a1p is conjugated to a protein or peptide *via* its pendant acetate function to form an amide bond, incubation times of up to 1 hour at room temperature are required to achieve radiochemical yields between 60–100% of  $^{64}\text{Cu}$ -labelled bioconjugates.<sup>38</sup> If functionality is engineered into the bifunctional chelator such that the acetate is not utilised as a conjugate attachment point, but remains available to coordinate to a metal centre, radiochemical yields of  $>95\%$  can be achieved in 5 minutes at  $37\text{ }^\circ\text{C}$ .<sup>39,40</sup> In the case of the latter, the stability of the  $^{64}\text{Cu}$ -labelled complex in serum is also increased compared to the former.<sup>39,40</sup> This particular case highlights the importance of conjugation strategy—ensuring that all ligands remain available to coordinate to a metal centre can be critical to optimal radiolabelling and stability in the presence of competing ligands.

In the case of propylene-bridged cyclam-based species, substitution of carboxylate groups of pcb-te2a (**7a**) for phosphonate groups, to furnish pcb-te2p (**7b**) and pcb-te1a1p (**7c**) does not substantially improve radiolabelling.<sup>41,42</sup>

X-ray crystallographic data has been reported for  $\text{Cu}^{2+}$  complexes of the three macrobicyclic chelators, ecb-te2a,<sup>43</sup> ecb-te2p and ecb-te1a1p (Figure 8.2).<sup>37</sup> In these complexes, the ethylene crossbridge significantly constrains

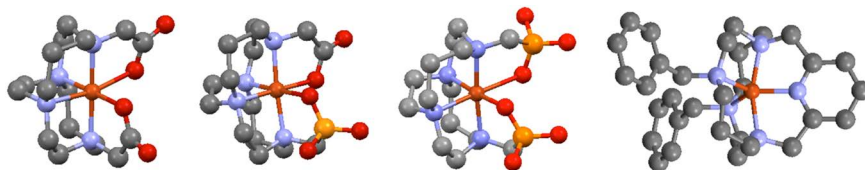
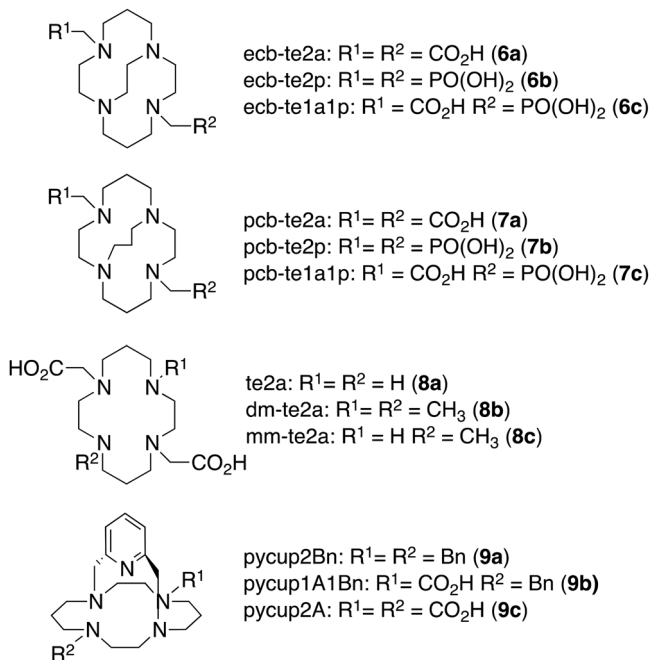


**Figure 8.2** From left to right,  $[\text{Cu}(\text{te2a})]$ ,<sup>43</sup>  $[\text{Cu}(\text{ecb-te1a1p})]$ ,<sup>37</sup> and  $[\text{Cu}(\text{pycup2Bn})]^{2+}$ .<sup>44</sup> Orange – copper, blue – nitrogen, grey – carbon, red – oxygen, yellow – phosphorus.

the geometry of the macrocycle and reduces its flexibility. As a result, the four *N*-donors of the macrocycle bind to  $\text{Cu}^{2+}$  in a *cis* coordination mode and the remaining two carboxylate groups complete the octahedral coordination sphere. In each case, one of the O–Cu–N axes is elongated as a result of Jahn–Teller stabilisation. In the case of the ecb-te1a1p complex, the lengthened Cu–O bond involves the phosphonate ligand group.

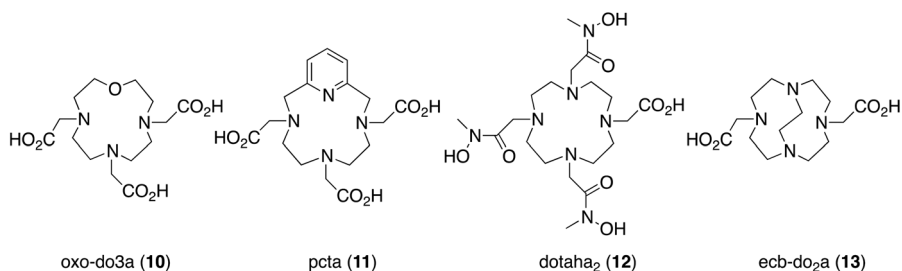


Cyclam derivatives bearing a cross-bridging pyridyl can be substituted at macrocyclic amines to provide pycup2Bn (**9a**), pycup1A1Bn (**9b**) and pycup2A (**9c**).<sup>44</sup> X-ray crystallography of  $[\text{Cu}(\text{pycup2Bn})]^{2+}$  demonstrates that  $\text{Cu}^{2+}$  is coordinated in a trigonal bipyramidal environment (Figure 8.2). DFT studies suggest that the most stable conformation of  $[\text{Cu}(\text{pycup1A1Bn})]^+$  is one in which the acetate ligand is coordinated *trans* to the pyridyl group, providing a hexadentate  $\text{N}_5\text{O}$  coordination environment. The three pycup ligands can all be radiolabelled in quantitative radiochemical yield in 15 minutes at 70 °C at 10  $\mu\text{M}$  concentration of ligand. The complexes are stable in serum and demonstrate high stability in challenge experiments with dota. Pycup2A (**9c**) has been conjugated to a thrombosis-targeting peptide *via* one pendant acetate and the resulting  $^{64}\text{Cu}$ -radiolabelled compound is able to delineate arterial thrombosis in rat models.

The tetraazamacrocycle te2a (**8a**)<sup>45,46</sup> and its methylated derivatives dm-te2a (**8b**) and mm-te2a (**8c**)<sup>47</sup> have been synthesised and  $^{64}\text{Cu}$  complexes of these derivatives demonstrate enhanced *in vivo* stability. For example,  $^{64}\text{Cu}$ -labelled antibody conjugates of te2a exhibit higher tumour uptake, lower liver retention and higher blood activity in mice one and two days after injection

compared to the analogous dota conjugate, suggesting higher resistance of  $[^{64}\text{Cu}(\text{te}2\text{a})]$  to *in vivo* demetallation compared to  $[^{64}\text{Cu}(\text{dota})]^{2-}$ .<sup>46</sup> Interestingly, te2a (**8a**) could be radiolabelled within 20 minutes at 30 °C, whereas dm-te2a (**8b**) and mm-te2a (**8c**) required heating at 50 °C for one hour under the same solution conditions (ammonium acetate, pH 8). The differences in behaviour between teta (**4**), te2a, dm-te2a and mm-te2a highlight how seemingly subtle chemical modifications have significant ramifications, and the particular case of te2a and its derivatives is discussed in more detail later in this section. Like teta, these derivatives can accommodate  $\text{Cu}^{2+}$  at the centre of the macrocyclic ring, with each carboxylate ligand *trans* to the other.<sup>46,48</sup> Jahn–Teller distortion is observed, with lengthening of Cu–O bonds in both cases.

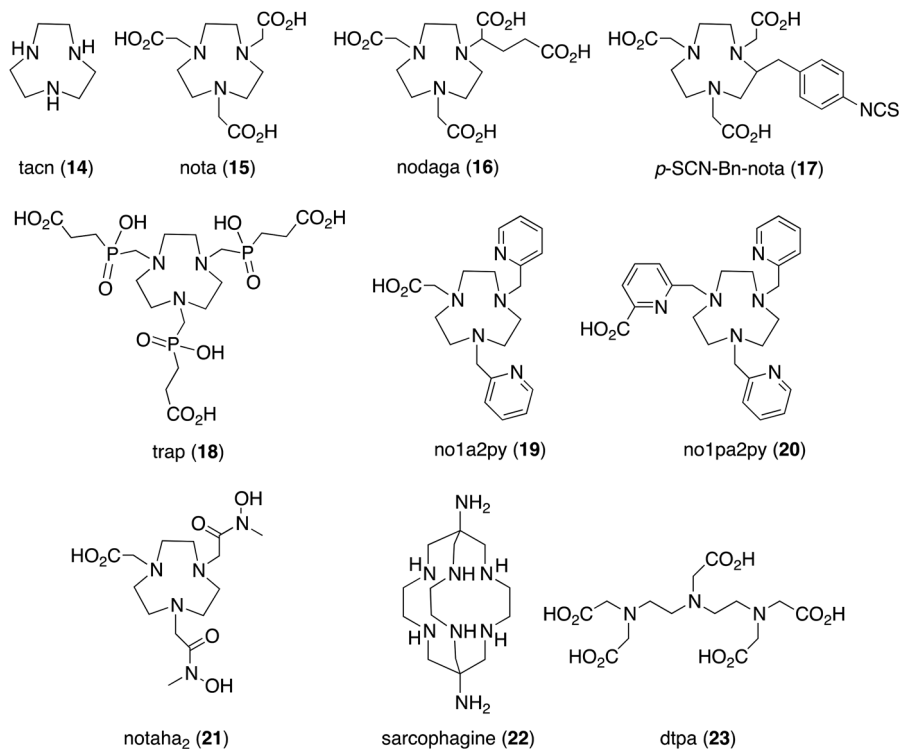
Substitution of the dota macrocycle at a single amine position with an O atom provides the ether-containing chelator, oxo-do3a (**10**). Alternatively, derivatisation with a pyridyl group provides pcta (**11**), containing a “softer” *N*-donor ligand than dota (**3**). Both of these chelators purportedly allow faster radiolabelling of bifunctional chelator conjugates of antibodies at room temperature and improve the stability of the  $^{64}\text{Cu}^{2+}$  chelator,<sup>49</sup> although subsequent studies could not discriminate any meaningful differences in radiolabelling efficiency or *in vivo* stability between dota (**3**), oxo-do3a (**10**) and pcta (**11**).<sup>19</sup> More recently, three of the acetate groups of dota have been replaced with hydroxamate groups, providing the chelator dotaha<sub>2</sub> (**12**) that can be radiolabelled with  $^{64}\text{Cu}^{2+}$  at room temperature at pH 7 in 5 minutes. Initial stability studies suggest that the resulting complex is sufficiently stable to withstand demetallation *in vivo*.<sup>50</sup> To the best of our knowledge, there is no reported information on the coordination environment of the  $\text{Cu}^{2+}$ -dotaha<sub>2</sub> complex. An ethylene-bridged cyclen derivative, ecb-do<sub>2</sub>a (**13**), can be radiolabelled with  $^{64}\text{Cu}^{2+}$  under similar conditions to ecb-te2a (**6a**), however, over the course of several hours,  $[^{64}\text{Cu}(\text{ecb-do}_2\text{a})]$  demonstrates the same *in vivo* instability as  $[^{64}\text{Cu}(\text{dota})]^{2-}$ .<sup>25</sup>



### 8.2.1.3 *Nota and Sarcophagine Derivatives – The State of the Art in Bifunctional Chelators for <sup>64</sup>Cu*

Acetate, phosphinate, pyridyl, picolinate and hydroxamate derivatives of triazacyclononane (tacn) (**14**)—nota (**15**), trap (**18**), no1a2py (**19**), no1pa2py (**20**) and notaha<sub>2</sub> (**21**), respectively—have also been utilised as bifunctional chelators for  $^{64}\text{Cu}^{2+}$ .

Unlike dota and te2a derivatives,  $^{64}\text{Cu}^{2+}$  complexes of nota (15) can be formed at 25 °C in 5 minutes in quantitative radiochemical yields at concentrations of 0.5  $\mu\text{M}$  at neutral pH.<sup>19</sup> Stability studies and *in vitro* experiments indicate that the  $^{64}\text{Cu}^{2+}$  complex of nota is stable *in vivo* with respect to dissociation of  $^{64}\text{Cu}^{2+}$ . Indeed, in comparative studies with dota conjugates, nota derivatives demonstrated higher tumour uptake and decreased liver uptake, attributed to greater complex stability.<sup>29,51</sup> Bifunctional derivatives of nota demonstrate the desirable combination of high radiolabelling efficiencies at very low concentrations of ligand under mild conditions,<sup>19,52</sup> and high *in vivo* stabilities.



Similar to the case of dota, targeting biomolecules can be attached to nota *via* one of its pendant acetate groups, providing a conjugate with two carboxylate and three amine donors (resulting in a neutral complex).<sup>29</sup> Alternatively, functionality can be introduced in a fashion (*e.g. via* a fourth pendant carboxylate group in nodaga (16),<sup>53</sup> or *via* a pendant isothiocyanate in *p*-SCN-Bn-nota (17)<sup>54</sup>) that preserves the coordination sphere of the parent chelator, nota (resulting in a  $\text{Cu}^{2+}$  complex with a single negative charge). The importance of such advances in chelator design should not be overlooked—a recent *in vivo* comparison of  $^{64}\text{Cu}$ -labelled peptide conjugates of dota (3), nota (15) and nodaga (16) reported that animals administered nota- and dota-radio-labelled conjugates exhibited significantly higher liver uptake than those administered the nodaga derivative.<sup>51</sup> Differences in liver accumulation of

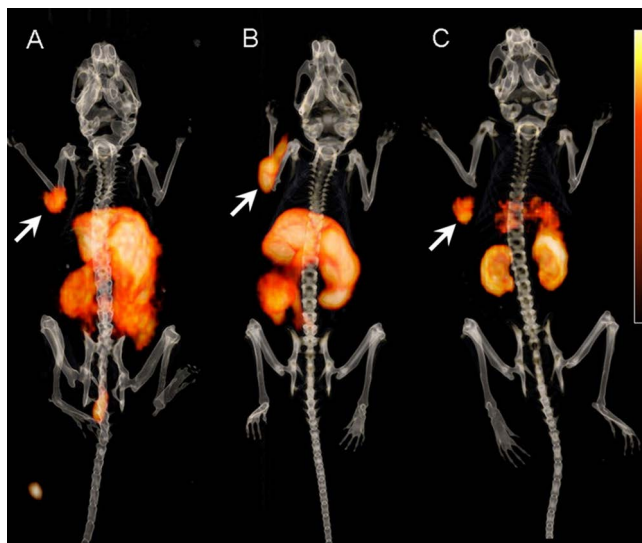


**Figure 8.3** PET/CT images of mice with subcutaneous A431-CCK2R tumours 4 hours after injection of  $^{64}\text{Cu}$ -labelled (A) dota-PP-F11, (B) nota-PP-F11 and (C) nodaga-PP-F11. Radiotracer uptake is clearly visible in the CCK2R tumours (arrow) (scale 1–12% ID  $\text{g}^{-1}$ ). Significantly decreased liver uptake is evident for nodaga-pp-f11 compared to the other tracers. Reprinted with permission from S. Roosenburg *et al.*, *Mol. Pharmaceutics* 11, 3930–3937.<sup>51</sup> Copyright 2014 American Chemical Society.

$^{64}\text{Cu}^{2+}$  were attributed to lower stability of the nota and dota derivatives *in vivo* compared to that of nodaga (Figure 8.3). Nota (**15**) itself, as well as other nota bifunctional chelator derivatives (nodaga (**16**) and *p*-SCN-Bn-nota (**17**)) are commercially available. The differences in complex charge and potential complex stability should be borne in mind when selecting a suitable chelator.

Like dota, nota cannot accommodate  $\text{Cu}^{2+}$  in the centre of its macrocycle. Two representations of nota coordinated to  $\text{Cu}^{2+}$  are presented in Figure 8.4. In the first structure,  $[\text{Cu}(\text{nota})]^-$ , all three of the nota carboxylate arms are deprotonated. The complex adopts a distorted pseudo-trigonal prismatic geometry,<sup>55</sup> presumably a result of the greater rigidity and steric requirements of the ligand compared to teta or dota. In the second structure,  $[\text{Cu}(\text{H}_2\text{nota})\text{Cl}]$ , crystallised under acidic conditions from the trihydrochloride salt of the ligand, only one of the carboxylate groups is deprotonated.<sup>56</sup> One protonated carboxyl oxygen and one deprotonated carboxylate oxygen are coordinated to  $\text{Cu}^{2+}$ , along with a chloride ion. Notably, the Cu–O bond length for the protonated carboxylate is very long (2.56 Å). In  $[\text{Cu}(\text{H}_2\text{nota})\text{Cl}]$ , the presence of only one strongly coordinated acetate group relieves the geometric requirements of the ligand, compared to  $[\text{Cu}(\text{nota})]^-$ , where all three acetate groups are coordinated. In turn this allows  $[\text{Cu}(\text{H}_2\text{nota})\text{Cl}]$  to adopt a distorted octahedral geometry, differing from the pseudo-trigonal prismatic geometry of the deprotonated complex,  $[\text{Cu}(\text{nota})]^-$ . The differences

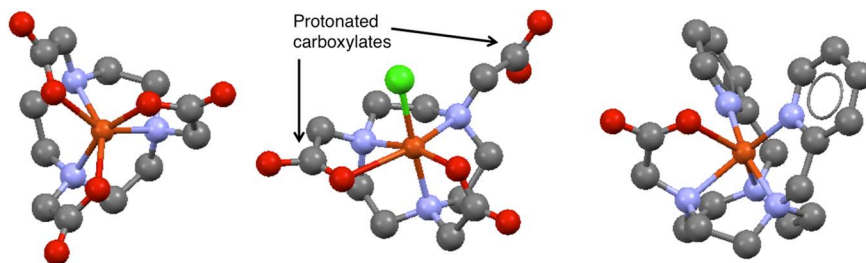


**Figure 8.4** From left to right,  $[\text{Cu}(\text{nota})]^-$ ,<sup>55</sup>  $[\text{Cu}(\text{H}_2\text{nota})\text{Cl}]^-$ <sup>56</sup> (carboxyl protons were not included in the crystallographic information file) and  $[\text{Cu}(\text{no}1\text{a}2\text{py})]^+$ .<sup>57</sup> Orange – copper, blue – nitrogen, grey – carbon, red – oxygen, green – chloride.

in coordination modes observed here could be relevant when considering differences in *in vivo* stability and biodistribution of conjugates of nodaga (hexadentate coordination) and nota (pentadentate coordination).

The ligand, trap (**18**), can be radiolabelled with  $^{64}\text{Cu}^{2+}$  at 25 °C in 5 minutes at pH 3 in quantitative radiochemical yields at 1  $\mu\text{M}$  ligand concentration.<sup>52</sup> However, stability studies have demonstrated that whilst  $^{64}\text{Cu}^{2+}$ -labelled complexes of trap are suitable for short imaging studies (where imaging is undertaken two hours post-injection of radiotracer), they are not sufficiently stable *in vivo* over longer periods of time with respect to dissociation of the metal complex.

Limited studies have demonstrated that no1a2py (**19**) can complex  $^{64}\text{Cu}^{2+}$  at ambient temperatures in 1 minute in quantitative radiochemical yields at 100  $\mu\text{M}$  ligand concentration and near neutral pH.<sup>57</sup> This concentration is rather high compared to concentrations used for ligands such as nota and sarcophagine. Two pyridyl groups, the acetate ligand and the three macrocyclic amines are coordinated to the  $\text{Cu}^{2+}$  centre in a pseudo-octahedral geometry (Figure 8.4). Serum stability studies alongside competition studies with cyclam (**2**) suggest that the resulting complex is stable to *in vivo* demetallation.

The ligand no1pa2py (**20**) has recently been reported to coordinate to  $\text{Cu}^{2+}$  in solution *via* three macrocyclic amines, one pyridyl group and both the N and O atoms of the picolinate group, leaving one uncoordinated pyridyl group.<sup>58</sup> When no1pa2py is reacted with solutions of  $^{64}\text{Cu}^{2+}$  at near neutral pH and ambient temperature over 30 minutes, three distinct complexes are formed, the identities of which are undefined. Whilst this ligand system is certainly very interesting from an inorganic chemist's perspective, the presence of multiple radiolabelled species is undesirable for radiopharmaceutical applications.

Similar to dotha<sub>2</sub> (**12**), preliminary reports of notaha<sub>2</sub> (**21**) indicate that this ligand rapidly coordinates  $^{64}\text{Cu}^{2+}$  to provide a stable complex, but there is no information available at present as to the complex's coordination environment.<sup>50</sup>

Macrobicyclic hexammine derivatives are commonly referred to as “sarcophagines” (**22**). This term was coined by early investigators who noted that

in a hexadentate coordination mode, these ligands (and their relatives, the sepulchrates) encapsulate metal ions almost completely, and thus bear a resemblance to burial vaults such as sarcophagi or sepulchres. The cage-like sarcophagines can be derivatised to provide bifunctional chelator conjugates that can be radiolabelled with  $^{64}\text{Cu}^{2+}$  at very low ligand concentrations (0.5  $\mu\text{M}$ ) at room temperature, and the resulting complexes are highly stable to *in vivo* demetallation pathways.<sup>19,27,59–62</sup> Such *in vivo* stability means that sarcophagine conjugates are suitable for  $^{64}\text{Cu}^{2+}$  protein radiolabelling, where mild temperatures and neutral pH are also required. Furthermore, the complex is sufficiently stable to permit PET image acquisition up to two days after administration of the radiotracer, allowing a radiolabelled protein/antibody sufficient time to clear from the circulation and accumulate at target tissue.<sup>63</sup> Such stability contributes to superior PET image quality, with enhanced contrast between diseased and healthy tissue.

The  $\text{Cu}^{2+}$  complexes of sarcophagines adopt distorted octahedral geometry, with all six of the secondary amines coordinated to the metal ion at neutral pH (Figure 8.5).<sup>27,59,60,64</sup> The  $\text{Cu}^{2+}$  metal ion resides at the centre of the “cavity” of the cage-like ligand structure. Jahn–Teller distortion can be observed in several reported solid-state structures although, again, this is not pronounced as a result of coordination constraints of the macrobicyclic ligand.

### 8.2.2 Kinetic Stability is Critical to *In vivo* Stability – You Can’t Have One Without the Other

Most of the chelators that have been utilised in the design of  $^{64}\text{Cu}$  radiotracers have demonstrated high thermodynamic stability (Table 8.2). Whilst thermodynamic considerations are certainly important in imparting affinity of the chelator for a metal ion, thermodynamic stability constants are not

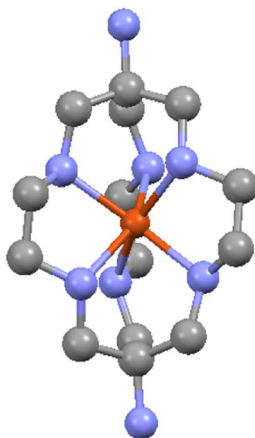


**Figure 8.5**  $[\text{Cu}(\text{sarcophagine})]^{4+}$ .<sup>64</sup> Apical primary amines are protonated. Orange – copper, blue – nitrogen, grey – carbon.

**Table 8.2** Stability constants of Cu<sup>2+</sup> macrocyclic compounds.

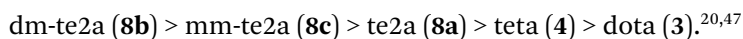
Ligand	Log $K_{[Cu(\text{ligand})]}$
Dtpa	21.4 <sup>65</sup>
Teta	21.87 ± 0.06 <sup>66</sup>
	20.49 ± 0.03 <sup>67</sup>
Dota	22.72 ± 0.04 <sup>66</sup>
	22.25 ± 0.03 <sup>67</sup>
Nota	21.63 ± 0.03 <sup>68</sup>

reliable predictors for *in vivo* stability. For example, the stability constant of [Cu(dtpa)]<sup>3-</sup> is higher than that of teta, dota and nota (Table 8.2), but dtpa is of little use for <sup>64</sup>Cu radiotracers. After 24 hours incubating in serum, >80% of <sup>64</sup>Cu<sup>2+</sup> originally bound to a dtpa-antibody conjugate dissociated to serum proteins, indicative of very low stability in the presence of competing endogenous molecules.<sup>19</sup>

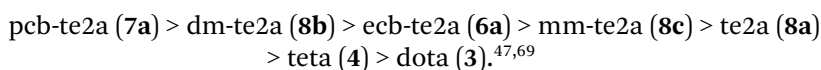
When a nanomolar amount of a radiopharmaceutical is injected intravenously, the radiopharmaceutical is diluted at least 1000-fold in the human blood stream and is exposed to relatively high concentrations of proteins and other molecules that can compete for metal binding. Several endogenous proteins bind Cu<sup>2+</sup>, including albumin in blood, and superoxide dismutase, ceruloplasmin and metallothionein in the liver. Dissociation of a ligand or chelator will likely result in radiometal coordination to an endogenous protein and, correspondingly, high non-target organ or background activity, compromising image quality. It is thus imperative that the radiometal forms a highly inert complex, one in which the kinetics of dissociation and transchelation are very slow. Without possessing sufficient kinetic stability, even the most thermodynamically stable complexes known will not survive, because of the very high concentration of competing ligands and metals compared to the radiotracer, and because of endogenous metabolic pathways that tightly regulate distribution of metals *in vivo*. *Kinetic stability* has been implicated as the critical factor in determining whether or not a <sup>64</sup>Cu-chelate complex is stable *in vivo*. As stated earlier, macrocyclic ligands generally display higher kinetic stability than non-macrocyclic ones. Within the macrocycle itself, a ligand donor atom that dissociates remains anchored within the proximity of the metal by at least two other coordinated donor atoms. Clearly, however, not all macrocycles are optimal for application in radiopharmaceuticals. Certainly, rigid structures lend themselves to high kinetic stability. Both the cross-bridged macrobicyclic ligands, ecb-te2a (**6a**) and sarcophagine (**22**), are highly kinetically stable. The bicyclic nature of the species decreases conformational flexibility, resulting in high kinetic inertness. Similarly, it has been proposed that the smaller macrocycle of nota (**15**) compared to that of dota (**3**) and teta (**4**) also results in a more rigid complex—a smaller ring size correlates with a lower degree of conformational flexibility, and thus nota complexes of Cu<sup>2+</sup> are more kinetically stable than those of dota or teta.

There are several ways to experimentally determine whether or not the kinetic stability of a complex is likely to be sufficient to render it stable *in vivo*. These include acid dissociation studies, challenge experiments with other chelators, copper exchange studies, serum stability studies, stability in the presence of superoxide dismutase, and *in vivo* studies.

Acid dissociation studies have compared the half-lives of  $\text{Cu}^{2+}$  complexes under highly acidic conditions (typically, 5 M to 12 M HCl, at 50 to 90 °C). Although such studies self-evidently do not mimic physiological conditions, they can be useful predictors of kinetic stability, and thus the likelihood that a complex will remain intact *in vivo*. Under such acidic conditions, where potentially coordinating amines and carboxylates are normally protonated, the complexes themselves, if governed by thermodynamic stability alone, should dissociate immediately. If, however, the complexes are kinetically inert, ligand dissociation is slow, and persistent coordination of the chelate to the metal centre protects coordinating atoms from immediate protonation. The rate of dissociation in acidic solution is an indicator of comparative kinetic stability. For example, the order of stability with respect to acid dissociation for the series of tetraazamacrocycle complexes follows the order:



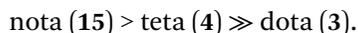
As alluded to above, this interesting series demonstrates that subtle modifications to tetraazamacrocycle derivatives influence the kinetic stability of the complex—overall, alkylation of te2a increases kinetic stability, whereas substitution with acetate groups to give the parent compound, tetra, decreases kinetic stability. Intriguingly, when the cross-bridged species are introduced to this series, one observes that the  $\text{Cu}^{2+}$  complex of dm-te2a (**8b**) is more kinetically stable than that of ecb-te2a (**6a**), but less kinetically stable than that of pcb-te2a (**7a**):



The fact that the  $\text{Cu}^{2+}$  complex of pcb-te2a is more stable than ecb-te2a suggests that for complexes that adopt the same coordination geometry, the size of a macrocyclic ring or cross-bridge effects relative stability. Additionally, the higher stability of dm-te2a to acid-mediated dissociation compared to that of ecb-te2a, but not mm-te2a, suggests that there are electronic effects at play in the stabilisation of the  $\text{Cu}^{2+}$  complexes. The kinetic stability imparted by incorporation of an ethylene cross-bridge is not just a factor of the complex's increased rigidity.

Copper exchange studies involve incubating labelled  $^{64}\text{Cu}^{2+}$  complexes in a solution containing non-radioactive  $\text{Cu}^{2+}$  ions.<sup>70</sup> There are only a couple of examples of assessing kinetic stability using this approach for  $\text{Cu}^{2+}$ , despite the fact that such a method provides a true measure of kinetic stability independent of thermodynamic factors (*e.g.* metal–protein association constants) under mild conditions (ambient temperatures, pH 4–8) that are more representative of the physiological environment than acid dissociation studies. In the presence of excess non-radioactive  $^{\text{nat}}\text{Cu}^{2+}$ , a thermodynamically stable

but kinetically labile  $^{64}\text{Cu}^{2+}$  complex will exchange  $\text{Cu}^{2+}$  ions. In contrast, a kinetically inert  $^{64}\text{Cu}^{2+}$  complex will not substitute its  $^{64}\text{Cu}^{2+}$  ion for a non-radioactive  $^{\text{nat}}\text{Cu}^{2+}$  present in the environment. This method has demonstrated that the kinetic inertness or stability of  $\text{Cu}^{2+}$  complexes of the acetate-substituted azamacrocycles at pH 6–7.5 follows the order:



This order is in general agreement with the superior *in vivo* stability of  $^{64}\text{Cu}$ -labelled nota (15) or nodaga (16) conjugates compared to homologous dota (3) derivatives.

Stability studies with known  $\text{Cu}^{2+}$  binding proteins, such as albumin or macroglobulin found in serum, or superoxide dismutase 1 (SOD) abundant in the liver and kidneys, are also useful in predicting *in vivo* stability. In such experiments, radiolabelled complexes are incubated in serum, or in solutions containing SOD, and dissociation of  $^{64}\text{Cu}^{2+}$  to protein is monitored over time. If a complex does not withstand competition from proteins *ex vivo*, this can be taken as a reliable indicator that the complex will not withstand competition from the same proteins *in vivo*. However, caution is advised in concluding that a complex is sufficiently stable if it does not lose its radiometal in a serum stability or protein competition experiment. These experiments do not dilute the radiolabelled compound to the same degree as *in vivo*, and particularly in the case of serum stability studies, the ratio of ligand to endogenous protein is likely higher in such experiments than *in vivo*. They also do not take into account transport pathways and delivery of radiometal to organs, such as the liver and kidneys, that metabolise complexes. However, such studies have demonstrated that sarcophagine (22) complexes of  $^{64}\text{Cu}^{2+}$  are more stable to transchelation by serum proteins and SOD, than dota (3), tetra (4), nota (15) and cyclam (2).<sup>71</sup>

Comparative *in vivo* experiments using small animals (for the most part mice) can be useful to assess not only *in vivo* stability, but also the timescale of dissociation of  $^{64}\text{Cu}$  from a chelator *in vivo*, the fate of any dissociated  $^{64}\text{Cu}^{2+}$ , and whether kinetic stability is associated with *in vivo* stability. As discussed above, numerous studies have demonstrated that *in vivo* dissociated  $^{64}\text{Cu}^{2+}$  accumulates in the liver,<sup>23–26</sup> and thus high liver activity can, with caution, be indicative of complex instability.<sup>28,29,35,46,51</sup> Comparative biodistribution studies have demonstrated stark differences between using conjugates of the open chain diethylenetriamine pentaacetic acid (dtpa) (23) chelator with those of macrocycles—PET images of animals administered the former exhibit large amounts of activity in the liver, consistent with serum stability studies that demonstrate high transchelation of  $^{64}\text{Cu}^{2+}$  to serum proteins. In contrast, the use of a macrocyclic chelator such as sarcophagine results in the radiotracer retaining  $^{64}\text{Cu}^{2+}$ , and the majority of radioactivity remains associated with the blood pool (Figure 8.6).<sup>19</sup> In another comparative study, animals administered a  $^{64}\text{Cu}$ -labelled sarcophagine peptide demonstrated higher tumour accumulation one day after administration than animals administered the analogous  $^{64}\text{Cu}$ -labelled dota peptide conjugate. It was suggested that the higher

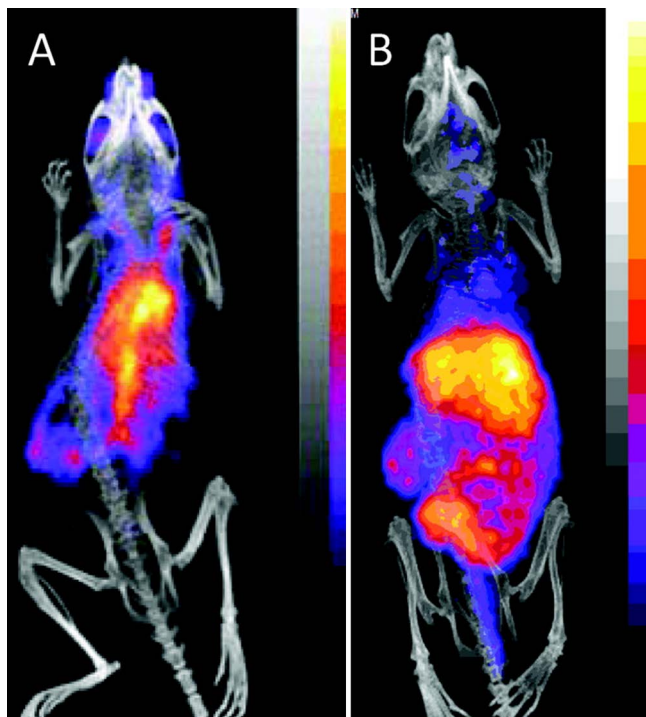


**Figure 8.6** PET/CT images of Balb/C mice 24 hours after injection with  $^{64}\text{Cu}$ -rituximab-immunoconjugates. (A)  $^{64}\text{Cu}$ -sarcophagine-CO-rituximab and (B)  $^{64}\text{Cu}$ -dtpa-rituximab are given as examples of a macrocycle containing immunoconjugates (A, showing predominantly blood pool activity, indicative of kinetic stability of the Cu-sarcophagine complex) and an immunoconjugate containing dtpa derivatives (B, showing predominantly liver and gut activity, indicative of dissociation of the Cu-dtpa complex). Reprinted with permission from M. S. Cooper *et al.*, *Bioconjugate Chem.* 23, 1029–1039.<sup>19</sup> Copyright 2012 American Chemical Society.

accumulation of activity for the sarcophagine derivative could be attributed to its lack of dissociation of  $^{64}\text{Cu}^{2+}$ .<sup>27</sup>

The pharmacokinetics of a radiotracer is not simply dependant on complex stability, but on overall charge and lipophilicity as well, and thus seemingly small differences in a series of chelators can result in substantial contrasts in their respective biodistributions. Take, for example, the case of the highly stable  $^{64}\text{Cu}^{2+}$  complexes of sarcophagine ligands. Sarcophagine bifunctional chelator derivatives can be modified in the apical position, and investigators have exploited this functionality to study the effect of charge on the biodistribution of chimeric antibody conjugates in non-tumour-bearing mice. Substitution of the apical primary amine (SarAr) to a neutral methyl group ( $(\text{CH}_3)(\text{CO}_2\text{H})\text{sar}$ ) and a sulfonate group ( $(\text{SO}_3\text{H})(\text{CO}_2\text{H})\text{sar}$ ) resulted overall in a progressive decrease in the positive charge localised at the  $^{64}\text{Cu}^{2+}$  sarcophagine complex and a concomitant net decrease in positive charge of the antibody (Figure 8.7).

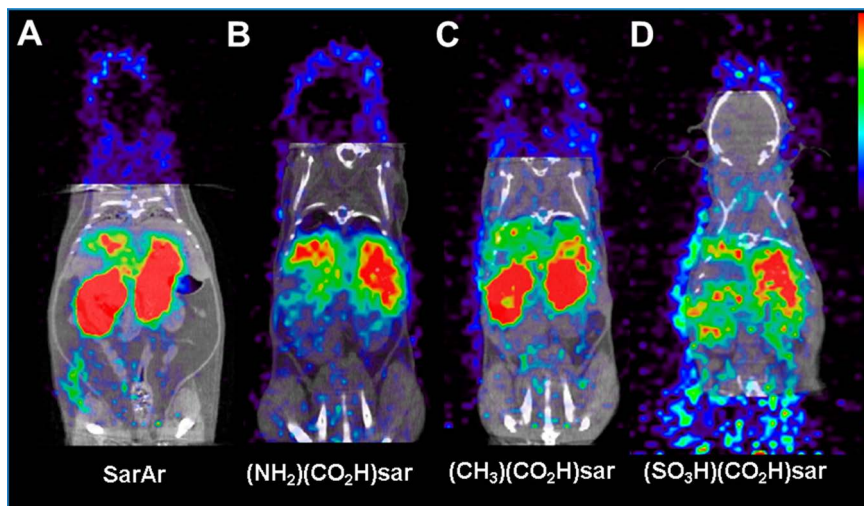


**Figure 8.7** PET/CT images of mice injected with fragment antibody ch14.18- $\Delta C_{H2}$  labelled with  $^{64}\text{Cu}$  via SarAr (A),  $(\text{NH}_2)(\text{CO}_2\text{H})\text{sar}$  (B),  $(\text{CH}_3)(\text{CO}_2\text{H})\text{sar}$  (C), and  $(\text{SO}_3\text{H})(\text{CO}_2\text{H})\text{sar}$  (D) 48 hours after injection. PET image is in colour scale; CT image is in grey scale. Reprinted with permission from J. L. J. Dearling *et al.*, *Bioconjugate Chem.* 26, 707–717.<sup>30</sup> Copyright 2015 American Chemical Society.

Correspondingly, a 6-fold decrease in kidney retention was observed that was attributed to a decrease in retention by the kidneys' negatively charged glomerulus basal cells.<sup>30</sup> At the same time, investigators also compared the biodistribution of  $^{64}\text{Cu}^{2+}$ -labelled nota, dota and teta chimeric antibody conjugates with all of the sarcophagine derivatives. The liver and kidney retention of the teta and nota radiotracers was lower in all cases than their sarcophagine counterparts. The substantially lower kidney retention was attributed to the anionic charge of the resulting  $^{64}\text{Cu}$  complexes of teta and nota.

Whilst cross-bridged and substituted teta structures are sufficiently stable, all require a degree of heating to incorporate  $^{64}\text{Cu}$  quantitatively. Teta itself does not require heating, but there is evidence of *in vivo* instability, whilst dota requires heating and its complex also is not stable to *in vivo* demetalation. There is also little correlation between the degree of cross-linking of the macrocycle and the conditions under which high radiochemical yields are obtained. Certainly the cross-bridged ecb-te2a requires prolonged heating to achieve sufficient  $^{64}\text{Cu}^{2+}$  incorporation compared to teta, but macrobicyclic sarcophagine species do not. It is likely that kinetic barriers to  $^{64}\text{Cu}^{2+}$  coordination and dissociation are related to ligand strain within transition states. Sarcophagine chelators and nota derivatives with three pendant acetate groups meet the requirements for molecular imaging based on proteins and antibodies: high radiolabelling yields at room temperature and *in vivo* stability of the  $^{64}\text{Cu}^{2+}$  complex over prolonged periods of time.

### 8.2.3 Targeting Based on Chelate Reactivity: Bioreduction and Dissociation

In the previous section the emphasis was on design of chelators that impose kinetic inertness on complexes in order to retain the link between the radio-metal and the targeting vehicle for as long as possible *in vivo*. An alternative strategy for radiotracer design is to build reactivity into the chelate complexes in order to achieve tissue selectivity. This approach is illustrated by the bis(thiosemicarbazone) (btsc) class of ligands (**24**) which form  $\text{Cu}^{2+}$  complexes with applications based on their lipophilicity, control of their  $\text{Cu}^{2+/1+}$  reduction potential and the balance between rate of dissociation and re-oxidation following the reduction. The  $\text{Cu}^{2+}$  complexes are four-coordinate, square-planar complexes (*e.g.* Figure 8.8) and undergo one-electron reduction under physiological conditions. A remarkable feature of this process is the exquisite control of the reduction potential that can be exercised by alkylation of the diimine backbone of the ligand ( $\text{R}^1$ ,  $\text{R}^2$ , **24**, Table 8.3).<sup>72-74</sup> Compared to the non-alkylated complexes ( $\text{R}^1 = \text{R}^2 = \text{H}$ ), replacement of one hydrogen with an alkyl group ( $\text{R}^1 = \text{H}$ ,  $\text{R}^2 = \text{CH}_3$ ,  $\text{C}_2\text{H}_5$  *etc.*) shifts the reduction potential negatively by *ca.* 80 mV, while the second alkylation ( $\text{R}^1 = \text{alkyl}$ ,  $\text{R}^2 = \text{alkyl}$ ) shifts it more negative still by a further 80 mV. Alkylation at  $\text{R}^1$  and  $\text{R}^2$  also has the (probably related) effects of rendering the reduced  $\text{Cu}^+$  complex more resistant to dissociation and compressing the Cu-S bond distances.<sup>75</sup> This control allows selection of different tissue-targeting applications. These complexes readily cross plasma membranes and enter cells by virtue of their lipophilicity and planar structure, whereupon they are exposed to intracellular reducing agents. The non-backbone-alkylated complexes ( $\text{R}^1 = \text{R}^2 = \text{H}$ ) are rapidly reduced and immediately dissociate (rapid acid-catalysed



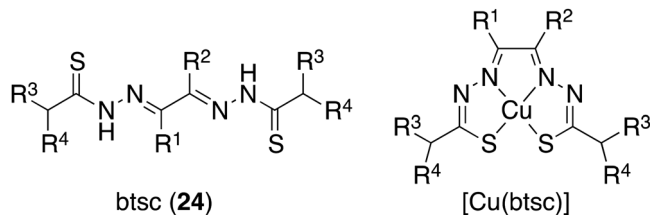
**Figure 8.8** Structure of  $[\text{Cu}(\text{atsm})]$ .<sup>75</sup> Orange – copper, blue – nitrogen, grey – carbon, red – oxygen, green – chloride.

**Table 8.3** Structure of selected bis(thiosemicarbazone) ligands (**24**).

Ligand	$\text{R}^1$	$\text{R}^2$	$\text{R}^3$	$\text{R}^4$
atsm	$\text{CH}_3$	$\text{CH}_3$	$\text{CH}_3$	H
gtsm	H	H	$\text{CH}_3$	H
ptsm	$\text{CH}_3$	H	$\text{CH}_3$	H
ats	$\text{CH}_3$	$\text{CH}_3$	H	H
cts	$\text{C}_2\text{H}_5$	$\text{CH}_3$	H	H

dissociation following reduction has been confirmed by cyclic voltammetry),<sup>76</sup> allowing the copper to become trapped as part of the intracellular copper pool. Thus, these complexes deliver radiocopper indiscriminately to cells and tissues in proportion to blood flow, and can be used as blood flow tracers or cell labelling agents (although efflux of the radiocopper from cells over the ensuing few hours precludes long term cell tracking with these tracers<sup>77</sup>). The bis-backbone-alkylated complexes ( $R^1$  and  $R^2$  = alkyl) are reduced within cells more slowly and resist dissociation for longer (again, as demonstrated by cyclic voltammetry),<sup>72,76</sup> allowing the opportunity to become re-oxidised to the  $Cu^{2+}$  complex which can diffuse back out of the cell if molecular oxygen is present. These complexes thus release their radiocopper only in the absence of oxygen, leading to intracellular trapping of copper only in hypoxic cells. The prototypical complex in this class, [Cu(atsm)] (Table 8.3), is in clinical use as a hypoxia imaging agent,<sup>78–80</sup> for example to identify tumours that may be resistant to radiotherapy because of hypoxia. Complexes with a single backbone alkyl group show intermediate reduction potentials and are rapidly trapped by a bioreductive/dissociative mechanism with only a slight hypoxia-induced increase in intracellular trapping. The prototype [Cu(ptsm)] (Table 8.3) has found clinical acceptance as a blood-flow imaging agent<sup>81</sup> and cell labelling agent for short-term cell tracking by PET.<sup>82</sup> Lipophilic complexes such as [Cu(gtsm)] that bypass biological transport mechanisms and deliver  $^{64}Cu^{2+}$  intracellularly are proving useful tools for studying copper metabolism and trafficking, and the ways in which this is altered by disease pathology.<sup>83</sup>

Alkylation of the terminal nitrogen atoms ( $R^3$  and  $R^4$ ), on the other hand, scarcely affects the reduction potential and can be used to control lipophilicity and hence allow useful variations in pharmacokinetics. For example, while [Cu(atsm)] and [Cu(gtsm)]<sup>83</sup> ( $R^3 = CH_3$ ,  $R^4 = H$ ) are able to cross the blood–brain barrier,<sup>84</sup> the less lipophilic [Cu(ats)] ( $R^3 = R^4 = H$ ) does not; and [Cu(cts)] and [Cu(ats)] are both hypoxia-selective tracers but with less uptake in, and faster clearance from, normoxic cells than [Cu(atsm)] because of their lower lipophilicity, offering promise of improved hypoxia imaging.<sup>85,86</sup>



### 8.2.4 Outlook for Clinical Applications of Copper-64

Clinical molecular PET imaging applications using  $^{64}Cu$  were expected to be based on (a) its relatively long half-life, allowing imaging with antibody conjugates, and radiolabelled cells; and (b) its ability to be simply incorporated

into chelator-peptide conjugates for imaging peptide receptor expression. However,  $^{89}\text{Zr}$  and  $^{68}\text{Ga}$ , respectively, are likely to supersede  $^{64}\text{Cu}$  for these purposes, and so the future of  $^{64}\text{Cu}$  remains unclear.  $^{89}\text{Zr}$  possesses an even longer half-life than  $^{64}\text{Cu}$ , allowing for antibody and cell tracking using PET up to two weeks post-administration of radiopharmaceutical, and the advent of the commercially available  $^{68}\text{Ga}$  generator has provided an economical and accessible source of a metallic PET isotope for peptide receptor expression imaging. On the other hand,  $^{64}\text{Cu}$  emits beta particles and Auger electrons, and thus is potentially useful as a clinical radiotherapeutic. Despite strong preclinical evidence,<sup>87–89</sup> this radiotherapeutic utility is yet to be explored clinically.

Copper complexes of btsc ligands, particularly  $[\text{Cu}(\text{atms})]$ , have been clinically tested for hypoxia imaging in oncology (including lung, brain, colorectal and cervical cancers)<sup>79,80,90–92</sup> and neurological degenerative disorders.<sup>93,94</sup> These studies have employed  $^{64}\text{Cu}$  as well as the shorter-lived Cu PET isotopes,  $^{60}\text{Cu}$  (half-life 24 min, positron emission 93%, electron capture 7%),  $^{61}\text{Cu}$  (half-life 3.3 h, positron emission 62%, electron capture 38%) and  $^{62}\text{Cu}$  (half-life 9.7 min, positron emission 98%, electron capture 2%). Whilst these radiotracers have demonstrated that Cu uptake can predict poor patient prognosis associated with hypoxia, the complexity of interpretation of  $[\text{Cu}(\text{atms})]$  imaging—dependant not only on hypoxia but on image acquisition time, perfusion and likely copper transport mechanisms—makes  $[\text{Cu}(\text{atms})]$  less attractive for this application.<sup>79</sup>

## 8.3 Acyclic and Macrocyclic Chelators for Gallium-68: A Short Half-Life Necessitates Efficient Radiolabelling

### 8.3.1 Gallium-68 in the Clinic: Its Current Utility and Future Potential

The short half-life (68 minutes) and positron emission properties of  $^{68}\text{Ga}$  make it ideal for molecular imaging of peptide receptor expression, as peptide-based molecular imaging agents can clear circulation rapidly and accumulate at target tissue within 1–2 hours. The short half-life means that prolonged stability *in vivo* is less important than it is for  $^{64}\text{Cu}$ , while rapid labelling is more important.  $^{68}\text{Ga}$  is available from the  $^{68}\text{Ge}/^{68}\text{Ga}$  generator, and is usually eluted from the generator in aqueous 0.1–0.4 M HCl solution. All relevant chemistry involves the  $\text{Ga}^{3+}$  oxidation state. After elution, it can be processed to preconcentrate  $^{68}\text{Ga}$  and remove any contaminating adventitious metal ions (such as  $^{68}\text{Ge}^{4+}$ ,  $\text{Ti}^{4+}$ ,  $\text{Zn}^{2+}$ ),<sup>95,96</sup> or it can be used directly. In almost all cases, a buffering or neutralising agent is added to increase pH, enabling reaction to occur. The parent isotope, germanium-68, has a half-life of 271 days and, as such, the  $^{68}\text{Ge}/^{68}\text{Ga}$  generator provides a stable source of  $^{68}\text{Ga}$  in hospitals, with generators typically possessing a useable lifetime of

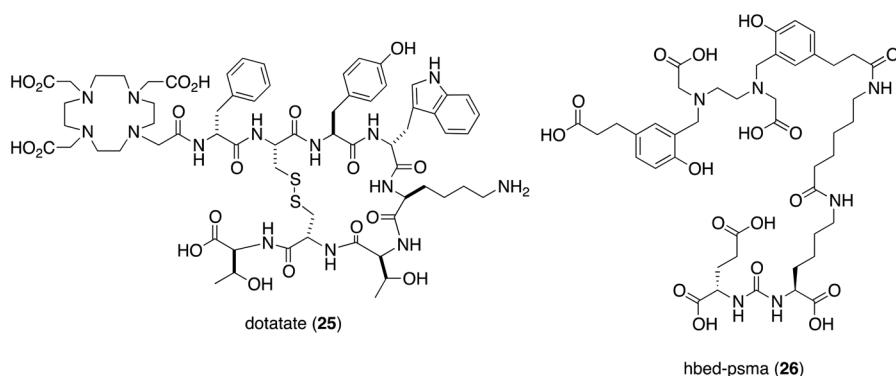
six to twelve months. This accessibility has led to rapid adoption of  $^{68}\text{Ga}$  in clinical PET centres, with the radiopharmaceuticals  $^{68}\text{Ga}$ -dotatate<sup>97</sup> (for neuroendocrine tumour imaging, Figure 8.9) and  $^{68}\text{Ga}$ -hbed-psma<sup>98</sup> (for prostate cancer imaging) used on a daily basis (ligands 25 and 26). The diagnostic information provided by such scans informs therapeutic regimes, particularly in the case of peptide receptor radionuclide therapy.

Molecular imaging agents based on short peptides are not subject to the same temperature and pH constraints as proteins. They do not possess tertiary structure, while any important secondary structure motifs are enforced by covalent bonds and will rapidly attain physiological equilibrium conformations once in the biological milieu. To date, high temperature synthesis has been the norm for  $^{68}\text{Ga}$ -labelled peptide imaging agents. Additionally, as  $^{68}\text{Ga}$  is a PET isotope, its radiopharmaceutical use has so far been confined to pre-existing hospital PET centres that are typically well-equipped to undertake complex radiochemical syntheses (such as those based on  $^{18}\text{F}$ ). Thus, multistep chemistry and post-synthetic purification



**Figure 8.9**  $^{68}\text{Ga}$ -dotatate PET scan of middle aged woman with widespread metastases expressing somatostatin-2 receptors that bind dotatate peptide. The patient subsequently underwent peptide receptor radionuclide therapy. Reprinted with permission from M. S. Hofman *et al.*, *J. Med. Imaging Radiat. Oncol.* 56, 40–47.<sup>97</sup> Copyright 2012 John Wiley and Sons.

protocols that have typified  $^{68}\text{Ga}$  radiochemical syntheses have not limited its expansion over the past decade. However, as PET scanning facilities increase, simple kit-based preparations of  $^{68}\text{Ga}$  radiopharmaceuticals that proceed rapidly at room temperature and require nothing more complex than a shielded syringe, will be critical to its widespread adoption. If kit-based syntheses can be realised, the  $^{68}\text{Ge}/^{68}\text{Ga}$  generator has the potential to become the PET equivalent of the  $^{99}\text{Mo}/^{99\text{m}}\text{Tc}$  generator (85% of radiodiagnostic imaging procedures currently utilise SPECT  $^{99\text{m}}\text{Tc}$  radiopharmaceuticals that are synthesised from simple, ready-to-use kits). Importantly, if  $^{68}\text{Ga}$  radiolabelling can proceed under near-neutral pH conditions at ambient temperature, PET imaging with  $^{68}\text{Ga}$ -labelled proteins such as scFv antibodies, affibodies and other small proteins with short clearance and localisation times will be feasible.



The following section introduces molecular imaging agents based on  $^{68}\text{Ga}$  that have become clinically important in the past decade and follows on with a discussion of how novel chelators have the potential to increase the utility of  $^{68}\text{Ga}$  from a clinical perspective. Although there are some parallels with the development of  $^{64}\text{Cu}$  chelators—namely the initial use of “classical” macrocyclic ligands such as dota (3), saturation of the hexadentate coordination sphere of  $\text{Ga}^{3+}$  and the pursuit of radiolabelling at room temperature—other factors have dictated novel ligand design:

1. The shorter half-life of  $^{68}\text{Ga}$  requires rapid radiolabelling, whether at elevated temperature or not, and so acyclic chelators have played a prominent role in the most recent chelator developments. Acyclic chelators are more flexible than macrocyclic ligands, and so activation energies for complex formation can be significantly lower and complex formation is faster.
2. The short half-life of  $^{68}\text{Ga}$  has also meant that long term *in vivo* stability of the  $^{68}\text{Ga}$  complex is less likely to be a confounding issue in selection of chelators—most images will be acquired within two hours after administration of the radiopharmaceutical. Thus, kinetic stability is less paramount, allowing for selection of an acyclic chelator.

3. Finally, the higher charge and smaller ionic radius of  $\text{Ga}^{3+}$  means that “harder” ligands than those typically employed for  $\text{Cu}^{2+}$  have potential (see below), and so hexadentate  $\text{O}_6$  chelators have been employed for coordination of  $^{68}\text{Ga}^{3+}$ .

It would be remiss to discuss chelators for  $^{68}\text{Ga}$  without mention of the gamma-emitting isotope,  $^{67}\text{Ga}$  (half-life 78 hours). Indeed, formulations of  $^{67}\text{Ga}$  salts and weak complexes have been clinically used to image lymphoma (widely assumed to be related to it binding to transferrin in serum), alongside preclinical studies of protein biodistribution.<sup>99</sup> Many of the chelators described here have also been labelled with  $^{67}\text{Ga}$ , enabling the kinetic stability of the resulting complexes to be assessed over a period of several days. It is likely that  $^{67}\text{Ga}$  will remain of interest to chemists working in the field of bifunctional chelators, particularly in relation the therapeutic potential of its Auger electron emissions,<sup>100,101</sup> however the relatively recent surge in development of bifunctional chelators for  $\text{Ga}^{3+}$  has been driven by the advent of the  $^{68}\text{Ge}/^{68}\text{Ga}$  generator.

### 8.3.2 Macrocycles for Gallium-68

The macrocycle dota (3) has been widely employed as a bifunctional chelator for  $^{68}\text{Ga}^{3+}$ , and its peptide conjugate with the somatostatin-2 targeting peptide, Tyr<sup>3</sup>-octreotate (dotatate, 25), is used daily in many PET imaging centres as a molecular imaging radiopharmaceutical for neuroendocrine tumours.<sup>97</sup> This is despite the fact that high temperatures (in excess of 80 °C), acidic conditions (pH 2–5), reaction times of 5–20 minutes and post-synthetic purification procedures are required for radiopharmaceutical synthesis. Diagnostic PET images using  $^{68}\text{Ga}$ -dotatate demonstrate high contrast and resolution (Figure 8.9). Additionally, the dota chelator can also be used to coordinate other radiometals, including the  $\beta^-$  emitters  $^{90}\text{Y}^{3+}$  and  $^{177}\text{Lu}^{3+}$  that are used in peptide receptor radionuclide therapy (PRRT). Thus the conjugate dotatate can act as a precursor for both diagnostic and therapeutic radiopharmaceuticals, with diagnostic PET information influencing whether or not to pursue a course of PRRT and helping to determine the amount of therapeutic radioactivity that ought to be administered to a patient. X-ray crystallographic analysis reveals that, like copper in  $[\text{Cu}(\text{dota})]^{2-}$ ,  $\text{Ga}^{3+}$  in  $[\text{Ga}(\text{dota})]^-$  and its functionalised derivatives is coordinated to four tertiary amines and two pendant acetate groups on either side of the ring in a distorted octahedral geometry<sup>102</sup> with the two acetate ligands *cis* to each other (Figure 8.10).

$\text{Ga}^{3+}$  possesses a similar ionic radius, and the same charge, as  $\text{Fe}^{3+}$  and, like  $\text{Fe}^{3+}$ , it can bind to the endogenous  $\text{Fe}^{3+}$  transporter protein transferrin *in vivo*.<sup>103</sup> Many stability studies utilise transferrin competition experiments as a predictor of *in vivo* stability (analogous to the case of using albumin or superoxide dismutase in competition experiments to assess stability of  $^{64}\text{Cu}$  radiopharmaceuticals).<sup>104–106</sup> There is little evidence that  $^{68}\text{Ga}^{3+}$  complexes of dota dissociate *in vivo* and so, in this respect, dota is a suitable chelating ligand for  $^{68}\text{Ga}^{3+}$  radiopharmaceuticals.

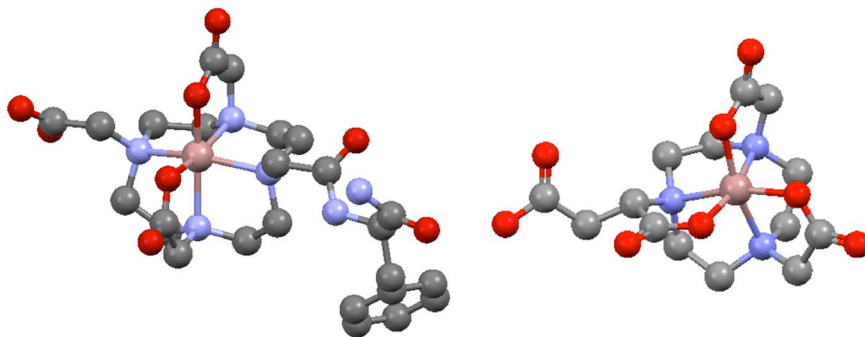


**Figure 8.10** Structures of the neutral bifunctional chelator complexes of  $\text{Ga}^{3+}$ : [Ga(dota)] conjugated to the amino acid phenylalanine (left);<sup>102</sup> [Ga(nodaga)] coordinated in a  $\text{N}_3\text{O}_3$  mode, with a pendant carboxylic acid available for conjugation (right).<sup>107</sup> Pink – gallium, blue – nitrogen, grey – carbon, red – oxygen.

Derivatives of the smaller macrocycle, nota (15), have also been extensively used to coordinate  $^{68}\text{Ga}^{3+}$ . These include nodaga (16) and *p*-SCN-Bn-nota (17). X-ray crystallographic studies of [Ga(nodaga)] and [Ga(nota)] reveal that in both cases, the complex is in a distorted octahedral environment with the three N ligands in a *fac* geometry with respect to one another (Figure 8.10).<sup>107,108</sup> Unlike dota and its conjugates, nota/nodaga conjugates can be radiolabelled at room temperature in radiochemical yields in excess of 95% at pH 3.5–4 within 10 minutes,<sup>109,110</sup> although many workers have continued to heat reaction mixtures at temperatures in excess of 80 °C. The resulting complexes are resistant to *in vivo* demetallation. It has been reported that there are no appreciable differences in *in vivo* stability or biodistribution between conjugates of nota ( $\text{N}_3\text{O}_2$  pentadentate coordination) and nodaga ( $\text{N}_3\text{O}_3$  hexadentate coordination) over the relevant time periods for imaging with  $^{68}\text{Ga}^{3+}$  (<4 hours).<sup>51</sup> However, most studies have employed nodaga derivatives or compounds that preserve an  $\text{N}_3\text{O}_3$  coordination sphere allowing coordinative saturation of  $\text{Ga}^{3+}$  by the macrocycle.

The macrocycle pcta (11) also coordinates  $^{68}\text{Ga}^{3+}$  in over 95% radiochemical yield under milder conditions than those used for dota labelling, although it requires slightly elevated temperatures compared to nota (40 °C, 5 minutes, pH 4.5).<sup>110</sup> The stability of a pcta–peptide conjugate in the presence of transferrin is comparable to the homologous nota derivative—the pcta conjugate retained 93% of  $^{68}\text{Ga}^{3+}$ , whereas the nota conjugate retained 98% of  $^{68}\text{Ga}^{3+}$ .<sup>104</sup> Oxo-do3a (10) has also been evaluated—radiolabelling is highly efficient at room temperature at pH 4–5, but the complex is unstable *in vivo*, with significant accumulation of activity observed in bone.<sup>104</sup>

Sarcophagine derivatives coordinate  $^{68}\text{Ga}^{3+}$  in an octahedral,  $\text{N}_6$  environment and are stable *in vivo* but, in contrast to the rapid reaction kinetics and favourable conditions for  $^{64}\text{Cu}^{2+}$  labelling, incorporation of  $^{68}\text{Ga}^{3+}$  into a sarcophagine ligand (22) requires non-aqueous reaction solutions and high temperatures (85 °C) for prolonged periods of time (30 min) (Figure 8.11).<sup>106</sup>

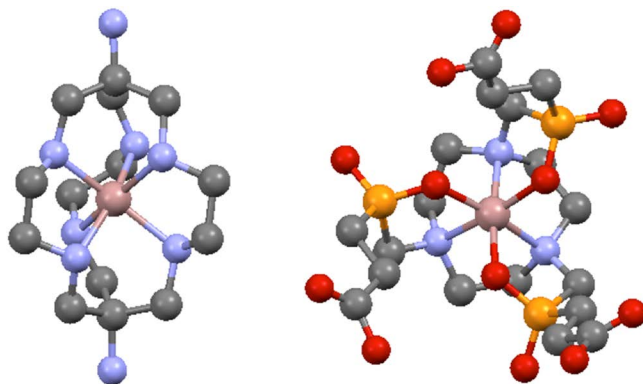


**Figure 8.11** Left:  $[\text{Ga}(\text{sarcophagine})]^{4+}$ .<sup>106</sup> One apical primary amine is protonated ( $-\text{NH}_3^+$ ) and one is in its neutral form ( $-\text{NH}_2$ ). Right:  $[\text{Ga}(\text{trap})]$ .<sup>114</sup> Pendant, non-coordinating carboxylate groups are protonated. Pink – gallium, blue – nitrogen, grey – carbon, red – oxygen, yellow – phosphorus.

Whilst *nota* and *pcta* represent an improvement on *dota* with respect to room temperature labelling, acidic pH conditions ( $\text{pH} < 5$ ) are still required. This is because at neutral or near-neutral pH, aqueous  $\text{Ga}^{3+}$  forms insoluble hydroxides, and unless radiolabelling is extremely rapid, or “solubilising” weakly chelating ligands such as citrate are present in solution,  $^{68}\text{Ga}^{3+}$  will form unreactive colloidal material. Thus, one of the challenges for chemists in the synthesis of bifunctional chelators has included the design of new chelators that react extremely rapidly with  $^{68}\text{Ga}^{3+}$  (where the rate of reaction is diffusion-controlled) such that the  $^{68}\text{Ga}^{3+}$  chelation reaction outcompetes  $^{68}\text{Ga}^{3+}$  colloid formation in the reaction mixture.

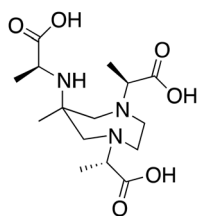
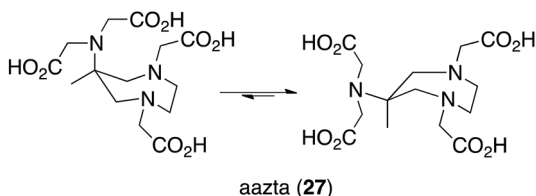
The “trap” series of ligands (**18**), which consist of phosphinic acid derivatives of *tacn* (**14**), have proved more suitable for use with  $\text{Ga}^{3+}$ -based radiopharmaceuticals than  $\text{Cu}^{2+}$  analogues.  $\text{Ga}^{3+}$  coordinates to three phosphinate O atoms and three *tacn* N atoms in an octahedral environment, with N atoms in a *fac* array, similar to the case of  $[\text{Ga}(\text{nota})]$  (Figure 8.11).<sup>111</sup> The trap ligand (**18**) also contains three pendant carboxylate groups, enabling attachment of up to three targeting biomolecules. This can be advantageous, as incorporation of multiple copies of a targeting motif or peptide into a radiotracer can result in enhanced uptake at target tissue *in vivo*.<sup>112</sup> The  $^{68}\text{Ga}$ -radiolabelled compounds are stable to demetallation under *in vivo* conditions. The advantages of trap conjugates over those of *nota* and *dota* lie in the very high specific activities that can be achieved in 5 minutes reaction time at pH 2 with heating at 95 °C—of the order of terabequerels  $\mu\text{mol}^{-1}$ —20-fold and 40-fold higher than typically achieved for *nota* and *dota*, respectively. Conjugates of trap are therefore highly appealing chelators for situations where very high specific activity is essential, for example, when receptor expression is very low but specific, or when biological targeting vectors demonstrate high pharmacological activity, thus requiring an absolute minimum amount of conjugate to be administered.<sup>112</sup> On the other hand, at room temperature, near

quantitative radiochemical yields of radiotracer (90–95%) are only achieved at concentrations corresponding to 100  $\mu\text{M}$  (or 10 nmol) of chelator after 15 minutes reaction time and, although this is superior to what is achieved with nota and dota in a side-by-side comparison,<sup>113</sup> it is inferior to what is observed with acyclic derivatives discussed below.

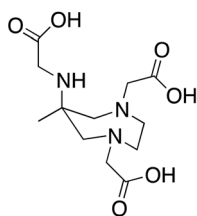
### 8.3.3 Halfway Between Macrocycles and Open-Chain Chelators: Data Derivatives

The “data” series of compounds (27–31), comprising carboxylate-substituted 6-amino-perhydro-1,4-diazepine (aazta) derivatives, can coordinate  $^{68}\text{Ga}^{3+}$  in an  $\text{N}_3\text{O}_3$  coordination mode. The “parent” triamine compound is a constitutional isomer of tacn (14), the macrocyclic triamine from which nota is derived, with two amines in a seven-membered ring, and the third appended to the ring. Functionalisation of the primary amine with an additional carboxylate group results in the aazta compound (27). The aazta and its data derivatives represent a “class” of ligands intermediate between macrocycles and acyclic ligands. The speciation and reactivity of the chelators with  $\text{Ga}^{3+}$  is also subject to conformations adopted by the data ligand in the unbound state.<sup>115</sup>

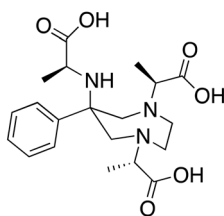
When the aazta ligand adopts a conformation in which the 6-amino group (the amine group external to the ring) is equatorial (27), the ligand cannot coordinate to  $\text{Ga}^{3+}$  in a  $\text{N}_3\text{O}_3$  binding mode, however this conformation is preferred for steric reasons. Thus, coordination of aazta to  $\text{Ga}^{3+}$  can lead to kinetically trapped complexes in which the coordination sphere of  $\text{Ga}^{3+}$  is only partially occupied by donor atoms of the aazta ligand. Indeed, when aazta is labelled with  $^{68}\text{Ga}^{3+}$ , three different species, of unknown structure, are formed.



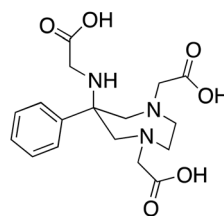
data-p (28)



data-m (29)



data-p-ph (30)



data-ph (31)

“Preorganisation” of a conformer *via* such chemical modification can assist reactivity of such chelators with  $^{68}\text{Ga}^{3+}$ . Incorporation of a 6-phenyl substituent in data-p-ph (30) and data-ph (31) favours a conformation in which the 6-amino group is axial, because now the 6-phenyl group is the bulkiest

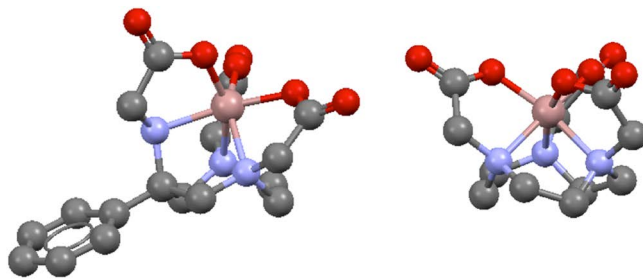


**Figure 8.12** Structures of  $[\text{Ga}(\text{data-ph})]^{116}$  (left) and  $[\text{Ga}(\text{nota})]^{108}$  (right) for comparison. Pink – gallium, blue – nitrogen, grey – carbon, red – oxygen.

substituent on the ring and, for steric reasons, prefers being in the equatorial position (see Figure 8.12 for the structure of the  $\text{Ga}^{3+}$  complex). Ligands data-p (**28**), data-pph (**30**) and data-ph (**31**) all react with  $^{68}\text{Ga}^{3+}$  to form single species at pH 4–7.<sup>116</sup> Out of this series of data chelators, data-ph (**31**) provides the highest radiochemical yield when reacted with  $^{68}\text{Ga}^{3+}$  at pH 4–5.<sup>117</sup> It is notable that  $^{68}\text{Ga}^{3+}$  preferentially coordinates to all of the data derivatives in preference to nota (**15**), and stability experiments indicated excellent stability in the presence of serum, transferrin, dtpa (**23**) and  $\text{Fe}^{3+}$ . Additionally, each data chelator is labelled with  $^{68}\text{Ga}^{3+}$  at concentrations of  $5\ \mu\text{M}$  in >95% radiochemical yield after 5 minutes reaction time at ambient temperature at pH 5, and the chelator data-pph (**30**) can be radiolabelled in >95% radiochemical yield at  $5\ \mu\text{M}$  and pH 7 in 10 minutes at ambient temperature.<sup>117</sup> To the best of our knowledge, bifunctional data derivatives are not currently available, however such compounds are likely to be of interest.

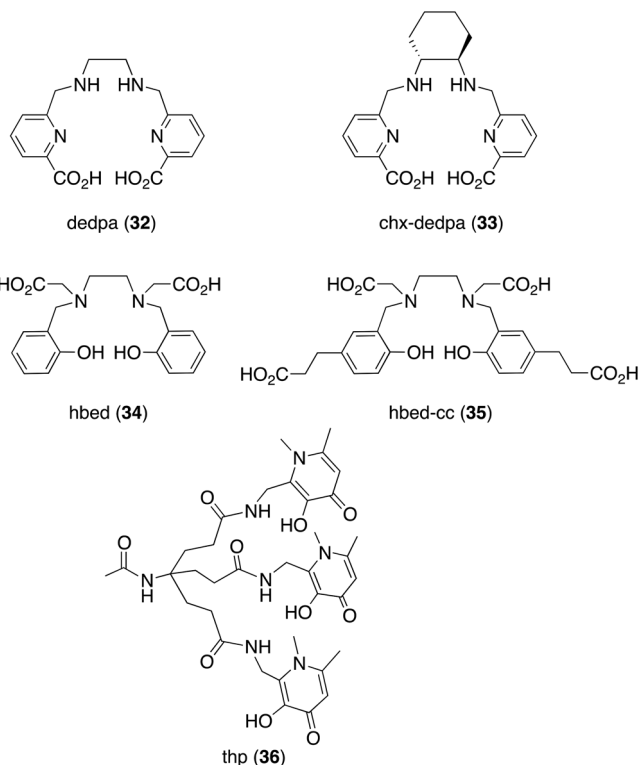
### 8.3.4 Acyclic Chelators for Gallium-68 Provide Rapid Radiolabelling at Room Temperature

Acyclic chelators designed for  $^{68}\text{Ga}^{3+}$  have generally demonstrated favourable, fast complexation reactions and quantitative radiochemical incorporation at ambient temperatures. Competition studies have indicated that the labelled complexes are sufficiently stable for *in vivo* imaging with  $^{68}\text{Ga}^{3+}$ . The most well-developed examples of such chelators include derivatives of dedpa (**32**), hbed (**34**), and thp (**36**).

The acyclic chelator dedpa (**32**) possesses two secondary amines and two pyridine carboxylate functions that coordinate to  $\text{Ga}^{3+}$  in an octahedral  $\text{N}_4\text{O}_2$  binding mode, where the two pyridyl groups are *trans* with respect to one another (Figure 8.13).<sup>105,118</sup> There is no evidence of other *cis/trans* isomers forming. All bond lengths from donor ligand atoms to the  $\text{Ga}^{3+}$  metal centre are similar in  $[\text{Ga}(\text{dedpa})]^+$ , contrasting to those in the  $\text{Ga}^{3+}$  complexes of nota and dota (where a range of bond lengths can be observed), demonstrating the excellent fit of the  $\text{Ga}^{3+}$  ionic radius to the ligand “cavity” in the ligand-bound conformation.

Peptide conjugates of dedpa (**32**) can be radiolabelled with  $^{68}\text{Ga}^{3+}$  and  $^{67}\text{Ga}^{3+}$  in over 97% radiochemical yield in 10 minutes at room temperature at pH 4.5 using 1 nmol of conjugate (at a concentration of approximately  $1\ \mu\text{M}$ ).<sup>119</sup> Whilst radiolabelled peptide conjugates demonstrated specific target uptake, persistent radioactivity in the blood pool was observed. Stability studies in the presence of transferrin demonstrated that over two hours, some  $^{67}\text{Ga}^{3+}$  transchelated to transferrin—between 5–30% depending on the specific radiotracer.

Incorporation of a *1R,2R-trans*-cyclohexane group in place of the central ethylene group in the backbone of dedpa provides a chelator that gives rise to only a single stereoisomer.<sup>118</sup> The  $^{67/68}\text{Ga}$  radiolabelling efficiency of this new ligand chx-dedpa (**33**) is not as high as that of the parent complex dedpa (**32**). For chx-dedpa, a concentration of  $10\ \mu\text{M}$  is required for quantitative radiolabelling at room temperature. This is possibly a result of the increased strain imparted on the ligand backbone by the *1R,2R-trans*-cyclohexane group—the lower flexibility of the ligand backbone results in lower radiolabelling efficiencies. On the other hand, in a side-by-side comparison,  $[\text{}^{67}\text{Ga}(\text{chx-dedpa})]^+$  was more stable in the presence of transferrin ( $90.5 \pm 4.4\%$ ) than  $[\text{}^{67}\text{Ga}(\text{dedpa})]^+$  ( $74.7 \pm 3.5\%$ ) after 2 hours incubation.



The chelator hbed (**34**) contains two phenol groups and two acetate groups tethered to an ethylenediamine group, providing a tetraanionic  $\text{N}_2\text{O}_4$  donor system. The phenol rings can be substituted, enabling tuning of both

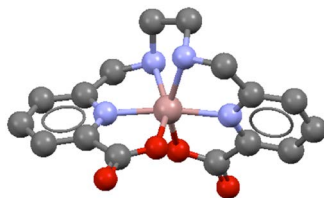


**Figure 8.13**  $[\text{Ga}(\text{dedpa})]^+$ .<sup>105</sup> Pink – gallium, blue – nitrogen, grey – carbon, red – oxygen.

hydrophilicity and the acidity of phenolic protons—an electron withdrawing sulfonate group in the *para* position can lower the  $\text{p}K_{\text{a}}$  of phenolic protons, potentially enabling the ligand to coordinate metal ions at lower pH than the parent complex. At the same time, the sulfonate group imparts hydrophilicity to the chelator and increases the negative charge of the complex.<sup>120</sup> Various other derivatives include propionate, ethyl amine and ethyl isothiocyanate substituents.<sup>121,122</sup> The propionate *para*-substituted chelator, commonly referred to as hbed-cc (35) has become clinically important. The peptide motif Glu-NH-CO-NH-Lys, containing a urea group, is a pharmacophore for the prostate-specific membrane antigen (PSMA) expressed in prostate cancer. The hbed-cc conjugate of this peptide (26) is the precursor to a  $^{68}\text{Ga}$ -labelled PET radiopharmaceutical that is used clinically to diagnose and monitor metastatic or recurrent prostate cancer.<sup>98,123</sup> Although the first clinical trial data have only been published recently,  $^{68}\text{Ga}$ -hbed-psma has had significant clinical impact globally in several centres in terms of management of patients with recurrent prostate cancer.

The hbed-cc conjugates,<sup>124,125</sup> including the “hbed-psma” conjugate,<sup>126</sup> can be labelled at room temperature, at  $\mu\text{M}$  concentrations (and in this case, amounts as low as 0.1 nmol) in >99% radiochemical yield in less than one minute, and the resulting radiotracer is stable in serum and in the presence of excess amounts of transferrin. However, in clinical preparations, this conjugate is usually labelled at elevated temperatures of at least 80 °C. This is because coordination of hbed and its derivatives to  $\text{Ga}^{3+}$  results in formation of geometric isomers (that can be separated by reverse phase HPLC and can be distinguished in  $^1\text{H}$  NMR spectra) and the ratio of these isomers differs depending on the temperature at which the reaction is performed.<sup>121,126</sup> Presumably, the predominating isomer at elevated temperatures is the thermodynamically preferred product. From a regulatory perspective, the presence of different geometric isomers is undesirable, as it is possible that the different isomers have different pharmacological profiles. There is little evidence available enabling unambiguous assignment of the geometric isomers (Figure 8.14) formed and detailed NMR and X-ray crystallographic studies are needed to elucidate the geometry of  $[\text{Ga}(\text{hbed})]^-$  and its derivatives definitively. However, X-ray crystallographic data for  $[\text{Ti}^{\text{IV}}(\text{hbed})]^{127}$  and high spin  $[\text{Fe}^{\text{III}}(\text{hbed})]^{128}$  (Figure 8.15) are available. Both of these complexes are octahedral, contain a metal ion with a similar ionic radius to that of  $\text{Ga}^{3+}$

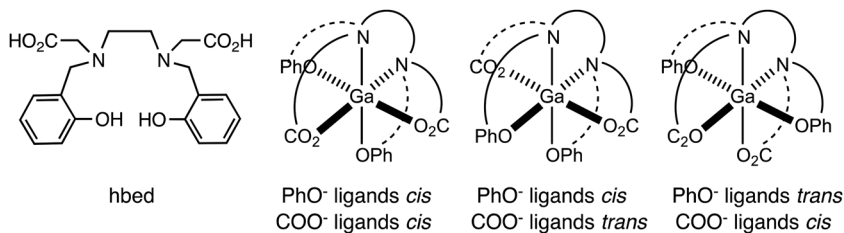


**Figure 8.14** Possible geometric isomers for  $[\text{Ga}(\text{hbed})]^-$ . Note that for each possible isomer depicted here, a stereoisomer will also be possible.

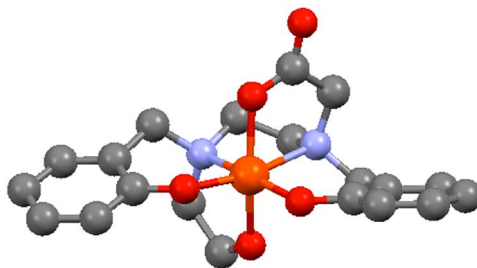


**Figure 8.15** Structure of  $[\text{Fe}^{\text{III}}(\text{hbed})]^-$ .<sup>128</sup> Orange – iron, blue – nitrogen, grey – carbon, red – oxygen.

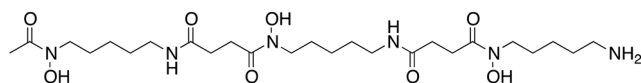
( $\text{Ga}^{3+}$ : 76.0 pm,  $\text{Fe}^{3+}$ : 78.5 pm (high spin),  $\text{Ti}^{4+}$ : 74.5 pm in octahedral environments), have a crystal field stabilisation energy of 0, and were prepared with a degree of heating (50 °C for  $[\text{Ti}^{\text{IV}}(\text{hbed})]$  and refluxing in aqueous solution for  $[\text{Fe}^{\text{III}}(\text{hbed})]^-$ ). In both the  $[\text{Ti}^{\text{IV}}(\text{hbed})]$  and  $[\text{Fe}^{\text{III}}(\text{hbed})]^-$  structures, the phenol ligands are *cis* to each other and occupy the equatorial plane with the amine donors, with the carboxylate ligands *trans* to each other.

Hydroxypyridinone derivatives, particularly those based on the 1,6-dimethyl-3-hydroxypyridin-4-one motif, were originally designed for coordination of  $\text{Fe}^{3+}$ , but with the similar ionic radii, charge and ligand preferences of high spin  $\text{Fe}^{3+}$  and  $\text{Ga}^{3+}$ , these thp chelators have immense utility in the field of coordination of  $\text{Ga}^{3+}$  radioisotopes. Bifunctional tripodal tris(hydroxypyridinone) (thp) chelators (based on three 1,6-dimethyl-3-hydroxypyridin-4-one groups) can coordinate  $^{68}\text{Ga}^{3+}$  at near quantitative radiochemical yields (>95%) at room temperature, near-neutral pH and concentrations of 5  $\mu\text{M}$  (nmol of conjugate) in under 2 min, providing a neutral complex, where the ligand is bound to  $\text{Ga}^{3+}$  in an  $\text{O}_6$  binding mode.<sup>129</sup> Conjugates radiolabelled with  $^{68}\text{Ga}^{3+}$  are stable in serum and *in vivo* with respect to demetalation, accumulate at target receptors *in vivo* and clear predominantly *via* a renal pathway.<sup>130,131</sup> The rapid radiolabelling kinetics at neutral pH at room temperature also allow for radiolabelling of proteins and antibodies that are more sensitive to elevated temperatures and large deviations from neutral

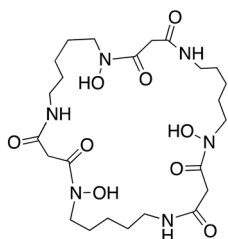
pH than peptides. The thp chelators are favourable candidates for simple kit-based preparations of  $^{68}\text{Ga}$ -labelled radiopharmaceuticals, providing a chelator platform for expanded use of the  $^{68}\text{Ga}/^{68}\text{Ge}$  generator to radiopharmacies equipped only for simple kit-based radiosyntheses, similar to those used for  $^{99\text{m}}\text{Tc}$  radiopharmaceuticals.

### 8.3.5 Siderophores for Coordination of Gallium-68

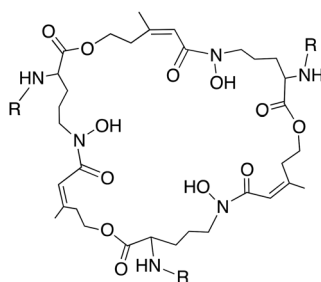
Siderophores are biosynthesised and secreted by bacteria, fungi and some plants to sequester  $\text{Fe}^{3+}$ —the resulting  $\text{Fe}^{3+}$  complexes are selectively taken up from the environment by bacteria to obtain  $\text{Fe}^{3+}$ . Siderophore complexes of  $\text{Fe}^{3+}$  have extraordinarily high stability constants and there has been interest in using them for coordination of  $^{67}\text{Ga}^{3+}$  and  $^{68}\text{Ga}^{3+}$ . The acyclic siderophore, desferrioxamine-B (dfo) (37), possesses three hydroxamate groups and complexes  $\text{Ga}^{3+}$  in an  $\text{O}_6$  environment. Antibody conjugates radiolabelled with  $^{67}\text{Ga}^{3+}$  via a dfo bifunctional chelator do not demonstrate good stability of the chelate complex, either *in vitro* or *in vivo*.<sup>132,133</sup> However, alternative macrocyclic siderophores containing three hydroxamate groups have been used to complex  $^{68}\text{Ga}^{3+}$ , notably ferrioxamine E (foxe) (38) and triacetylfusarinine C (tafc) (39), and the resulting radiotracers can be used as PET tracers for fungal *Aspergillus fumigatus* *in vivo* infections, a significant cause of death in immunocompromised patients that often goes undetected. In both cases, the  $^{68}\text{Ga}$ -labelled complex, as an analogue of the  $\text{Fe}^{3+}$  complex, is recognised by fungal cell siderophore uptake receptors.<sup>134,135</sup>



dfo (37)



foxe (38)

tafc: R = COCH<sub>3</sub> (39)

fsc: R = H, targeting peptide (40)

Modification of tafc to remove acetyl groups provides the (36-membered) macrocyclic chelator, fsc (40), containing three hydroxamates for metal coordination alongside three primary amines available for conjugation to three targeting biomolecules.<sup>136</sup> Bioconjugates containing multiple copies of a targeting motif or peptide often exhibit enhanced uptake at target

tissue *in vivo*. Radiotracers based on fsc can be prepared under favourable mild radiolabelling conditions—an fsc conjugate bearing three targeting peptides targeting angiogenesis markers in tumours can be radiolabelled with  $^{68}\text{Ga}^{3+}$  at room temperature in >95% RCY at pH 4–5 using less than 1 nmol of conjugate.

### 8.3.6 Chelator Design and Clinical Impact

The enormous impact of  $^{68}\text{Ga}$ -dotatate and  $^{68}\text{Ga}$ -hbed-psma on patient management combined with available generator technology portends that  $^{68}\text{Ga}$  will have a significantly greater role in clinical nuclear medicine than  $^{64}\text{Cu}$ , and indeed may enter routine use on a similar footing as  $^{99\text{m}}\text{Tc}$ . The development of clinical  $^{68}\text{Ga}$  radiolabelling methodologies over the next few years will be greatly facilitated by kit-based radiosyntheses. For inorganic chemists, the ligand design challenges for  $^{68}\text{Ga}$  differ from those for  $^{64}\text{Cu}$ —chelators capable of rapid, quantitative coordination of  $^{68}\text{Ga}^{3+}$  at low ligand concentration will be key to ensuring that radiosyntheses are simple to undertake in a hospital environment, thus providing clinical benefits of the  $^{68}\text{Ga}$  generator technology to the widest patient base.

## 8.4 Development of Chelators for Zirconium-89: Work in Progress

$^{89}\text{Zr}$  (zirconium-89) has a half-life of 78 hours—six times longer than that of  $^{64}\text{Cu}$ —and decay properties (Table 8.1) that render it suitable for PET imaging. Antibodies typically require at least 24 hours to clear circulation and accumulate at target receptors *in vivo* sufficiently for useful images to be obtained. For example, in the case of oncological targets, optimal tumour-to-background activity in PET images is often achieved three days after administration of the radiolabelled antibody conjugate, or *immunoconjugate*, and the half-life of  $^{89}\text{Zr}$  matches these requirements.

Clinical interest in long-lived PET isotopes is relatively recent. This is largely due to the expansion of PET facilities, the increased clinical utility of antibodies for immunotherapy and the wider commercial availability of  $^{89}\text{Zr}$ . The gamma-emitting isotope  $^{111}\text{In}$ , with a half-life of 67 hours, has been of clinical importance over the past few decades for whole-body diagnostic molecular imaging of biodistribution of biomolecules, including antibodies, using either two-dimensional planar scintigraphy or three-dimensional SPECT scans. However, as clinical PET provides higher resolution and more reliable quantification than SPECT, there is a clinical demand for  $^{89}\text{Zr}$ -labelled antibodies.

For example, trastuzumab is an antibody targeting HER2 receptors and is used clinically for treatment of metastatic breast cancers. However, not all patients respond to (the rather costly) trastuzumab therapy due to the

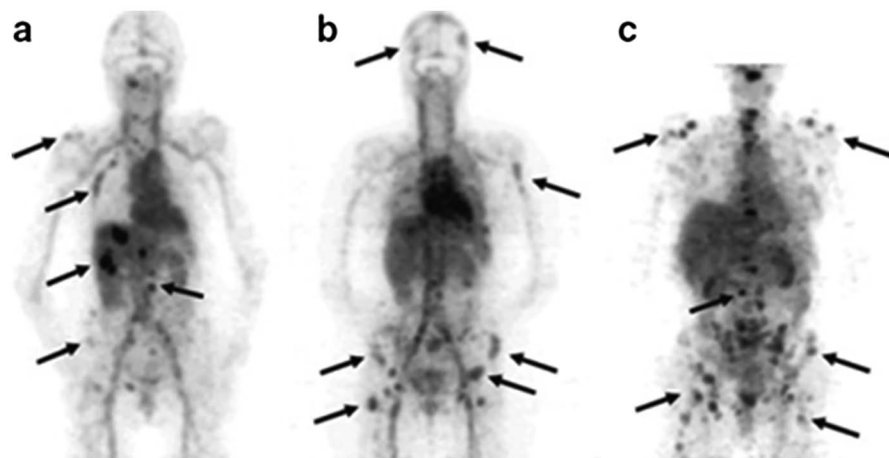


**Figure 8.16** PET scans of  $^{89}\text{Zr}$ -dfo-trastuzumab uptake 5 days after injection. (a) A patient with liver and bone metastases, and (b and c) two patients with multiple bone metastases. A number of lesions have been specifically indicated by arrows. Note that even five days post-injection, radioactivity in the major blood vessels remains significant. Reprinted with permission from E. C. Dijkers *et al.*, *Clin. Pharmacol. Ther.* 87, 586–592.<sup>137</sup> Copyright 2010 John Wiley and Sons.

absence of HER2 expression, and so whole-body imaging to assess HER2 status is of interest prior to administration of immunotherapy. Immunoconjugates of dfo-trastuzumab radiolabelled with  $^{89}\text{Zr}$  have been utilised clinically, with the best tumour-to-background contrast achieved three days post-injection of the radiotracer (Figure 8.16).<sup>137</sup>

#### 8.4.1 Hexadentate Chelators for Zirconium-89: Sufficient, But Suboptimal

Radiochemical solutions of  $^{89}\text{Zr}$  are usually provided in aqueous oxalic acid solution, where  $^{89}\text{Zr}$  is complexed by oxalate anions to give the eight-coordinate complex  $[\text{}^{89}\text{Zr}(\text{ox})_4]^{4-}$  (ox = oxalate). All radiochemistry to date has utilised Zr in oxidation state 4+; the relatively high charge density means that  $\text{Zr}^{4+}$  is a relatively hard metal ion with preferences for negatively charged oxygen ligands. Up until 2014, chelator chemistry for  $^{89}\text{Zr}$  was confined to the siderophore, dfo (37), which was fortuitously found to be an efficacious bifunctional chelator for zirconium and can be functionalised *via* its terminal primary amine to provide a variety of attachment groups for bioconjugation. Attempts to use conventional ligands such as dtpa (23),<sup>138</sup> or apply novel ligand systems based on phosphonate derivatives of dedpa,<sup>139</sup> proved unsuccessful, with either negligible  $^{89}\text{Zr}^{4+}$  binding or radiochemical yields <15%,

respectively. Radiolabelling of dfo-antibody conjugates generally involves incubating the immunoconjugate with solutions of  $[\text{}^{89}\text{Zr}(\text{ox})_4]^{4-}$  at pH 6–7 for 20–60 minutes. Depending on radiochemical yield, the radiolabelled conjugate can be used without purification, or unreacted  $^{89}\text{Zr}^{4+}$  is removed using disposable size-exclusion columns.<sup>140</sup>

Ligand dfo (37) coordinates to  $\text{Zr}^{4+}$  *via* its hydroxamate groups; DFT studies have predicted that when coordinated to dfo,  $\text{Zr}^{4+}$  has a coordination number of eight, with water molecules occupying two coordination sites located *cis* to each other, and dfo coordinated *via* six hydroxamate O atoms.<sup>141</sup> Studies by NMR confirm hydroxamate coordination, and that coordination of the terminal primary amine is unlikely.<sup>142</sup> Proton NMR signals are broad, and broaden as temperature is decreased. The variation in NMR line shape with temperature suggests exchange of proton environments in solution, however neither the nature of this exchange, nor mechanisms of exchange could be elucidated.

There are currently no available reports on the solid state structure of dfo coordinated to  $\text{Zr}^{4+}$ , however crystallographic, NMR and potentiometric studies have demonstrated that four *N*-methyl acetohydroxamate (Me-aha) ligands (42), each coordinating in a bidentate fashion, can occupy the coordination sphere of  $\text{Zr}^{4+}$  (Figure 8.17), and that there is a thermodynamic preference for the 1 : 4 complex.<sup>143</sup>

When  $^{89}\text{Zr}$  is administered as  $[\text{}^{89}\text{Zr}(\text{ox})_4]^{4-}$ , radioactivity rapidly accumulates in the skeleton, and four hours post-injection, the vertebrae and major joints of the animal can be easily visualised.<sup>142</sup> Whilst dfo has proved useful to date, some experiments have demonstrated bone uptake of  $^{89}\text{Zr}$  at late imaging times, suggesting that after prolonged exposure to the *in vivo* milieu,

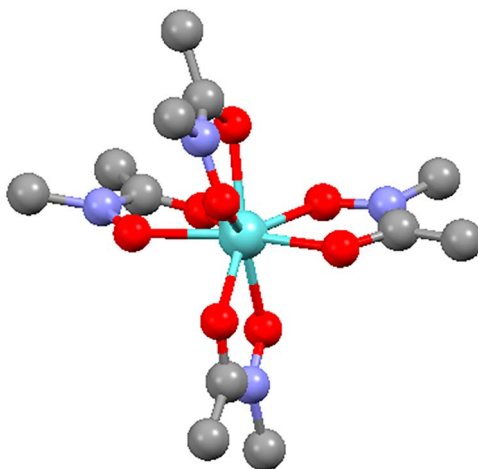


**Figure 8.17** Structure of  $[\text{Zr}(\text{Me-aha})_4]$ .<sup>143</sup> Light blue – zirconium, blue – nitrogen, grey – carbon, red – oxygen.

$^{89}\text{Zr}$  dissociates from dfo and subsequently accumulates in bone.<sup>6,141,144</sup> Thus, there has been a recent effort to develop alternative chelators for  $^{89}\text{Zr}^{4+}$  that provide complexes of higher kinetic stability.

Other hexadentate chelators that have been studied for  $^{89}\text{Zr}$  coordination include fsc (40) and thp (36) chelators—derivatives discussed above for  $^{68}\text{Ga}$  coordination. The thp chelators are demonstrably not suitable for *in vivo* imaging with  $^{89}\text{Zr}$ , even though competition experiments indicate a thermodynamic preference for  $\text{Zr}^{4+}$  coordination to thp over dfo.<sup>142</sup> A  $^{89}\text{Zr}$ -labelled thp-immunoconjugate administered to normal animals indicated high bone uptake 24 hours post-injection, that increased over the course of a week. In contrast, the dfo derivative largely remained in the blood pool, although some bone uptake was observed (Figure 8.18). Just as for  $^{64}\text{Cu}$ , high kinetic

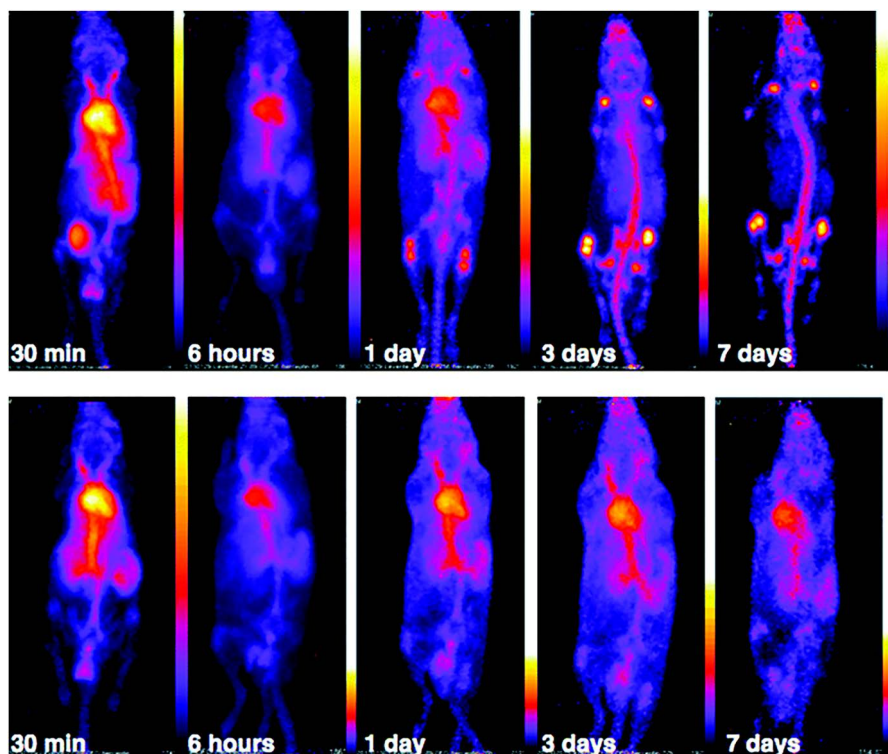


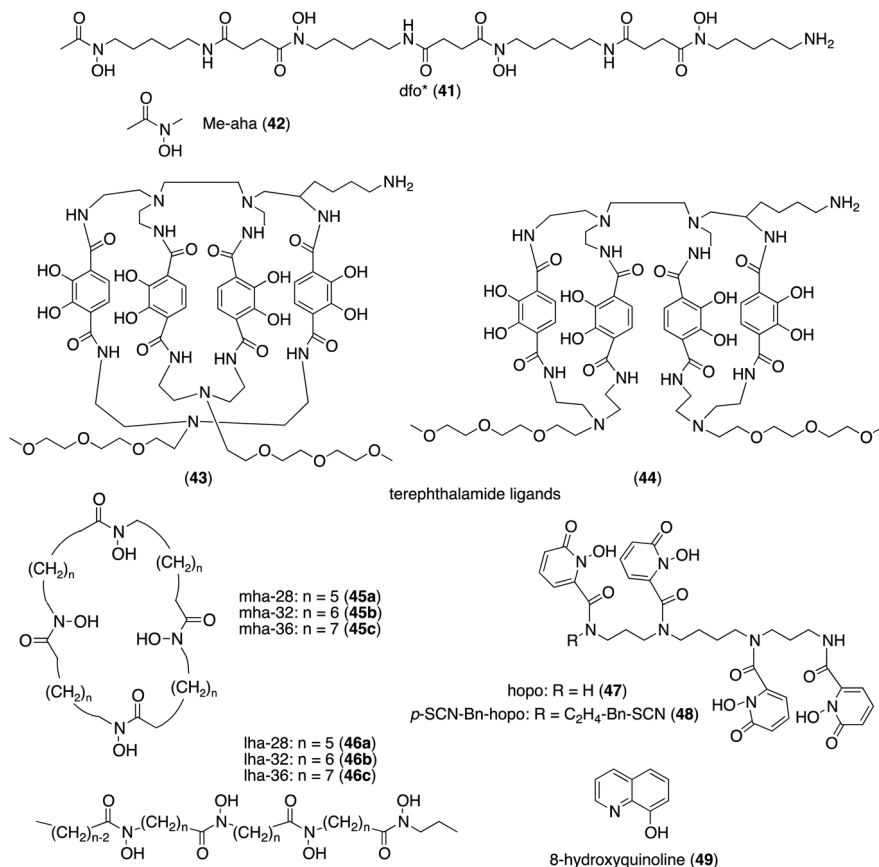
**Figure 8.18** PET scans of mice administered  $^{89}\text{Zr}$ -thp-trastuzumab (top) and  $^{89}\text{Zr}$ -dfo-trastuzumab (bottom). PET images indicate that  $^{89}\text{Zr}^{4+}$  dissociates from thp-trastuzumab, with the skeleton of the animal administered  $^{89}\text{Zr}$ -thp-trastuzumab clearly visible before 3 days after injection. This is in marked contrast to the animal administered  $^{89}\text{Zr}$ -dfo-trastuzumab, where the blood pool remains visible out to 7 days after injection. Reprinted with permission from M. T. Ma *et al.*, Dalton Trans. 44, 4884–4900.<sup>142</sup> Copyright 2015 Royal Society of Chemistry.

stability is paramount and “trumps” thermodynamic stability in applications of  $^{89}\text{Zr}$  bioconjugates *in vivo*.

The same fsc trimeric peptide conjugate described above for  $^{68}\text{Ga}$ —three hydroxamates incorporated into a 36-membered macrocycle (**40**)—has also been assessed for  $^{89}\text{Zr}$ .<sup>145</sup> The radiotracer is cleared rapidly from circulation and accumulates at receptor sites at sufficiently high concentration to allow excellent delineation of the tumour at one hour post-injection. One day post-injection, the tumour retains accumulated radioactivity, and there is no evidence that  $^{89}\text{Zr}^{4+}$  has dissociated from the radiotracer—*i.e.* there is negligible bone uptake. Competition studies demonstrate both the  $^{89}\text{Zr}^{4+}$  complexes of the fsc conjugate and the parent bifunctional chelator tafc (**38**) are stable to incubation at pH 7 with 1000-fold excess of edta chelator over the course of one week (<10% transchelation of  $^{89}\text{Zr}$  to edta). In contrast, over half of  $^{89}\text{Zr}$  transchelates from dfo to edta under the same conditions. Given that the distance between adjacent hydroxamate groups in dfo (9 atoms) and fsc/tafc (10 atoms) differs by only a single atom, these results suggest that among hexadentate ligands, macrocyclic topologies can significantly improve kinetic stability and thus *in vivo* stability for  $^{89}\text{Zr}^{4+}$  complexes when compared to open chain topologies.

#### 8.4.2 Octadentate Chelators for $^{89}\text{Zr}^{4+}$ : Will Saturation of the Coordination Sphere Provide Enhanced Stability *In vivo*?

As discussed above,  $\text{Zr}^{4+}$  can bind up to eight ligands in its coordination sphere. Several ligand systems have been developed for  $^{89}\text{Zr}^{4+}$  that saturate this coordination sphere, and in the case of hydroxamate chelators, accommodate a thermodynamic preference for four bidentate ligands. Ligand dfo\* (**41**) is an octadentate synthetic derivative of dfo containing four hydroxamate groups.<sup>146</sup> NMR studies of the non-radioactive  $[\text{Zr}(\text{dfo}^*)]$  complex indicate that multiple isomers are formed—in light of the combinations of geometric isomers that could feasibly form from a highly flexible, acyclic chelator, this is unsurprising. In the presence of a 300-fold excess of dfo, a dfo\* peptide conjugate coordinated to  $^{89}\text{Zr}^{4+}$  quantitatively and retained radiometal over the course of 24 hours, whereas under the same conditions, the homologous dfo conjugate retained less than 10%. The increased stability of the  $[\text{Zr}(\text{dfo}^*)]$  derivative compared to the analogous  $[\text{Zr}(\text{dfo})]^+$  species is possibly a result of a full  $\text{Zr}^{4+}$  coordination sphere in the case of the dfo\* (**41**). If transmetallation of  $\text{Zr}^{4+}$  to competing ligands is facilitated by a reaction pathway with an intermediate in which both the bifunctional chelator and the competitor are coordinated to the metal centre, employing an octadentate chelator in place of a hexadentate chelator can render this pathway less feasible. To the best of our knowledge, *in vivo* experiments utilising dfo\*-conjugates have not yet been reported.



Dimacrobicyclic catechol-functionalised terephthalamide derivatives (**43** and **44**) that coordinate  $^{89}\text{Zr}^{4+}$  in an  $\text{O}_8$  octadentate coordination environment *via* the four catechol groups have also been synthesised.<sup>147</sup> Both terephthalamide derivatives were  $^{89}\text{Zr}$ -labelled in quantitative radiochemical yield achieved after 15 minutes incubation, with specific activities of  $\approx 1 \text{ GBq } \mu\text{mol}^{-1}$ , and both  $^{89}\text{Zr}$ -labelled complexes were resistant to transchelation to either serum proteins or to dtpa over the course of one week. In the latter experiment,  $[\text{}^{89}\text{Zr}(\text{dfo})]^+$  was not resistant to transchelation to dtpa, with over 50% of  $^{89}\text{Zr}^{4+}$  transchelated to dtpa after four days.

One of the most elegant chemical developments in the field of  $^{89}\text{Zr}$  coordination chemistry incorporates four hydroxamate groups into macrocyclic rings of three varying sizes—28-, 32- and 36-membered rings, referred to here as mha-28, mha-32 and mha-36, respectively (**45**).<sup>148</sup> Homologous acyclic derivatives were also synthesised (referred to here as lha-28, lha-32 and lha-36) (**46**). The study demonstrated that whilst the mha-28 (**45a**) and mha-32 (**45b**) ligands could not quantitatively label  $^{89}\text{Zr}^{4+}$  under the radiolabelling conditions employed, mha-36 (**45c**) and lha-36 (**46c**) could quantitatively coordinate  $^{89}\text{Zr}^{4+}$  at ambient temperature at pH 7 over two

hours. Furthermore, [ $^{89}\text{Zr}(\text{mha-36})$ ] was more stable to edta competition (>90% intact after 24 hours incubation) than both its acyclic derivative [ $^{89}\text{Zr}(\text{lha-36})$ ] and dfo (both <80%). On the other hand, the 28- and 32-membered macrocyclic complexes, [ $^{89}\text{Zr}(\text{mha-28})$ ] and [ $^{89}\text{Zr}(\text{mha-32})$ ] were not stable to edta competition (0% and <40% intact respectively after 24 hours incubation). The lower stability and lower radiochemical yields of [ $^{89}\text{Zr}(\text{mha-28})$ ] and [ $^{89}\text{Zr}(\text{mha-32})$ ] were attributed to ring strain. The larger 36-membered ring is of sufficient size to alleviate this strain, whilst providing structural rigidity and increased stability. Thus, the macrocyclic effect results in increased stability of [ $^{89}\text{Zr}(\text{mha-36})$ ] compared to its acyclic homologue [ $^{89}\text{Zr}(\text{lha-36})$ ].

An octadentate hydroxypyridinone ligand (hopo) has also been developed, with each of the four 1-hydroxypyridin-2-one groups appended to an acyclic chain (47).<sup>149</sup> In contrast to the 3-hydroxypyridin-4-one group in thp, 1-hydroxypyridin-2-ones are known to have lower affinity for metal ions. For a single 1-hydroxypyridin-2-one group, this is four to five orders of magnitude lower than the corresponding 3-hydroxypyridin-4-one group.<sup>150</sup> Nonetheless, the hopo ligand (47) has demonstrated potential utility in molecular PET imaging with  $^{89}\text{Zr}^{4+}$ . Crystallographic analysis indicates that the four hydroxypyridinone ligands are coordinated to the  $\text{Zr}^{4+}$  centre in a distorted dodecahedral environment (Figure 8.19). A bifunctional chelator derivative, *p*-SCN-Bn-hopo (48), has been conjugated to the trastuzumab antibody, and can be radiolabelled at room temperature with  $^{89}\text{Zr}^{4+}$ , although radiochemical yields have not been specified in the report.<sup>144</sup> This  $^{89}\text{Zr}$ -hopo-trastuzumab is stable *in vivo*: in a direct comparison with  $^{89}\text{Zr}$ -dfo-trastuzumab, the hopo derivative demonstrated comparable tumour uptake and comparable persistence in the blood pool, but significantly lower bone uptake (Figure 8.20). The hopo bifunctional chelator (48) is the first ligand to demonstrate

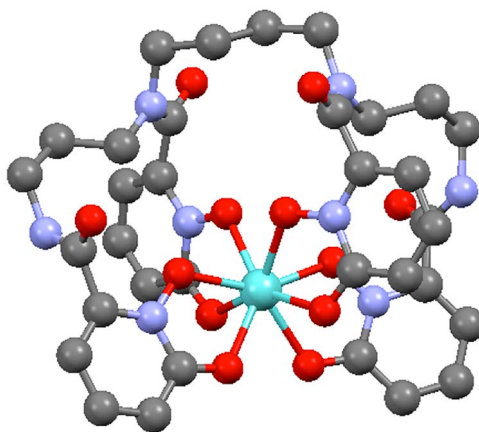


**Figure 8.19** Structure of [ $\text{Zr}(\text{hopo})$ ].<sup>144</sup> Light blue – zirconium, blue – nitrogen, grey – carbon, red – oxygen.

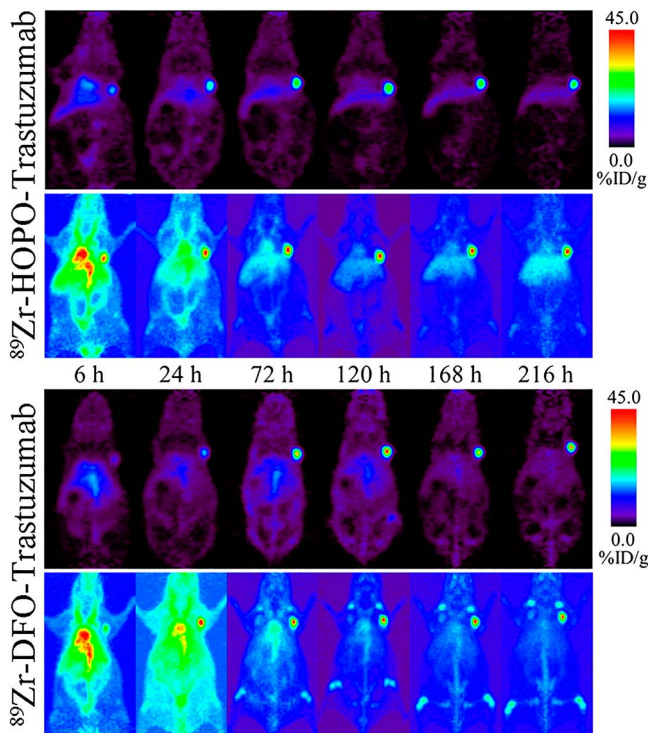


**Figure 8.20** PET images of  $^{89}\text{Zr}$ -hopo-trastuzumab (top) and  $^{89}\text{Zr}$ -dfo-trastuzumab (bottom) in mice with HER2-positive tumours on their right shoulders. Representative PET images are shown for each compound following a single mouse over 9 days. Both compounds show good tumour-to-background contrast, but the  $^{89}\text{Zr}$ -dfo-trastuzumab shows evidence of bone uptake suggesting *in vivo* release of  $^{89}\text{Zr}^{4+}$ . Reprinted with permission from M. A. Deri *et al.*, *Bioconjugate Chem.* 26, 2579–2591.<sup>144</sup> Copyright 2015 American Chemical Society.

prolonged *in vivo* stability (at least one week) with respect to the  $^{89}\text{Zr}^{4+}$  complex. It will be of significant interest to the radiochemical and nuclear medicine community to compare the performance of hopo (47) and dfo\* (41), as well as other new  $^{89}\text{Zr}^{4+}$  ligand platforms that are as yet, unfunctionalised for attachment to biomolecules.

### 8.4.3 Metastable Lipophilic Zirconium Chelates

Designing kinetic lability rather than inertness into Zr complexes has important applications, similar to the case of  $^{64}\text{Cu}$ -labelled btsc complexes discussed above. Incorporation of radioactivity into cells is important for tracking cell migration *in vivo*, and has been part of routine nuclear medicine activity since the early 1980s. The early methods relied on lipophilic complexes of  $^{111}\text{In}$  (gamma emitter with a half-life of 68 hours), most commonly

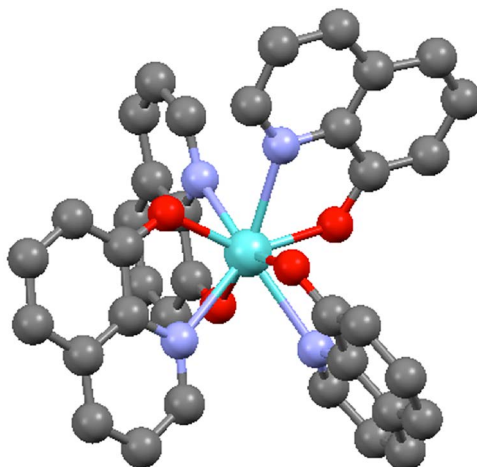


**Figure 8.21** Structure of  $[\text{Zr}(\text{oxinate})_4]$ .<sup>154</sup> Light blue – zirconium, blue – nitrogen, grey – carbon, red – oxygen.

the complex of 8-hydroxyquinoline (49),  $[\text{In}(\text{oxinate})_3]$ ,<sup>151</sup> which are able to deliver  $^{111}\text{In}^{3+}$  across the plasma membrane of leukocytes taken from patients with suspected inflammatory or infectious disease, allowing subsequent trapping of the radionuclide more or less irreversibly in the cells. It is generally assumed that once inside the cell, dissociation of the complexes leads to binding of  $\text{In}^{3+}$  to intracellular macromolecules. Re-injection of the labelled cells into the patient allowed the migration of cells to be tracked by gamma camera imaging. Modern applications of cell tracking associated with new developments in immunology and cell-based therapies place more exacting demands on cell tracking, creating a demand for PET imaging. This has led to a similar approach using  $^{89}\text{Zr}$  and, again, 8-hydroxyquinoline provides a suitable chelating ligand forming uncharged lipophilic  $[\text{Zr}(\text{oxinate})_4]$ <sup>152</sup> (Figure 8.21) which is able to transport  $^{89}\text{Zr}^{4+}$  into cells. Presumably because there are no native transport mechanisms specific for  $\text{Zr}^{4+}$ , the radionuclide is retained very effectively within the cells allowing imaging of its location and migration for at least 2 weeks (Figure 8.22).<sup>153</sup>

## 8.5 Conclusions

The radiometallic PET isotopes  $^{64}\text{Cu}$ ,  $^{68}\text{Ga}$  and  $^{89}\text{Zr}$  enable access to a suite of molecular imaging applications provided that the radiochemistry that underpins preparation of these radiotracers is efficient and simple to undertake in a hospital radiopharmacy. This efficiency is largely dependent on the ability of ligands to quantitatively and rapidly complex these radiometallic ions, and to provide complexes of sufficient *in vivo* stability over the time period from injection to image acquisition. The ongoing contribution of inorganic chemists in providing new ligands that meet these requirements,

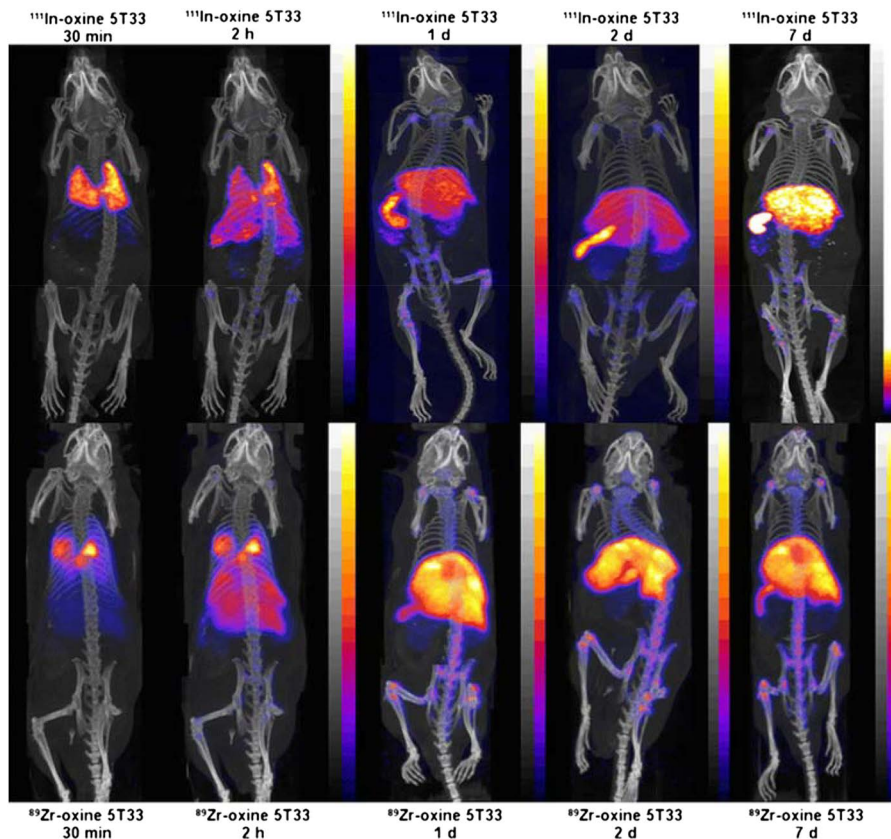


**Figure 8.22** PET/CT and SPECT/CT images of mice administered with [ $^{111}\text{In}(\text{oxinate})_3$ ]- or [ $^{89}\text{Zr}(\text{oxinate})_4$ ]-labelled cells. Scans of  $^{111}\text{In}$  (top) and  $^{89}\text{Zr}$  (bottom) are reported from 30 minutes to 7 days after administration of mice with labelled cells.  $^{111}\text{In}$  SPECT and  $^{89}\text{Zr}$  PET showed qualitatively similar migration patterns in the first few hours after inoculation with accumulation of cells in lungs at 30 minutes followed by migration to liver, spleen and bone marrow by 24 hours. Reprinted with permission from P. Charoenphun *et al.*, *Eur. J. Nucl. Med. Mol. Imaging*, 2015, 42, 278,<sup>153</sup> under the terms of the Creative Commons Attribution License.

particularly in the case of  $^{89}\text{Zr}$  and  $^{68}\text{Ga}$ , will be critical to widespread clinical adoption of these isotopes.

## Abbreviations

- CT** X-ray computed tomography  
**PET** Positron emission tomography  
**SPECT** Single proton emission computed tomography

## Acknowledgements

We thank the Centre of Excellence in Medical Engineering Centre funded by the Wellcome Trust and EPSRC (WT088641/Z/09/Z), the King's College London and UCL Comprehensive Cancer Imaging Centre funded by the CRUK and EPSRC in association with the MRC and DoH (England), and by the NIHR Biomedical Research Centre at Guy's and St Thomas' NHS Foundation Trust and King's College London. The views expressed are those of the author(s) and not necessarily those of the NHS, the NIHR or the DoH.

## References

1. P. J. Blower, *Dalton Trans.*, 2015, **44**, 4819.
2. E. W. Price and C. Orvig, *Chem. Soc. Rev.*, 2014, **43**, 260.
3. W. W. Moses, *Nucl. Instrum. Methods Phys. Res., Sect. A*, 2011, **648**, S236.
4. A. J. de Graaf, M. Kooijman, W. E. Hennink and E. Mastrobattista, *Bioconjugate Chem.*, 2009, **20**, 1281.
5. T. S. Young and P. G. Schultz, *J. Biol. Chem.*, 2010, **285**, 11039.
6. J. N. Tinianow, H. S. Gill, A. Ogasawara, J. E. Flores, A. N. Vanderbilt, E. Luis, R. Vandlen, M. Darwish, J. R. Junutula, S.-P. Williams and J. Marik, *Nucl. Med. Biol.*, 2010, **37**, 289.
7. B. M. Paterson, K. Alt, C. M. Jeffery, R. I. Price, S. Jagdale, S. Rigby, C. C. Williams, K. Peter, C. E. Hagemeyer and P. S. Donnelly, *Angew. Chem., Int. Ed.*, 2014, **53**, 6115.
8. B. M. Zeglis, C. B. Davis, R. Aggeler, H. C. Kang, A. Chen, B. J. Agnew and J. S. Lewis, *Bioconjugate Chem.*, 2013, **24**, 1057.
9. G. Hermanson, *Bioconjugate Techniques*, Academic Press, Elsevier, London, 3rd edn, 2013.
10. T. J. Wadas, E. H. Wong, G. R. Weisman and C. J. Anderson, *Chem. Rev.*, 2010, **110**, 2858.
11. *The Chemistry of Molecular Imaging*, ed. N. Long and W.-T. Wong, John Wiley and Sons, New Jersey, 2015.
12. P. J. Blower, J. S. Lewis and J. Zweit, *Nucl. Med. Biol.*, 1996, **23**, 957.
13. M. T. Ma and P. S. Donnelly, *Curr. Top. Med. Chem.*, 2011, **11**, 500.
14. D. J. Berry, R. T. Martin de Rosales, P. Charoenphun and P. J. Blower, *Mini-Rev. Med. Chem.*, 2012, **12**, 1174.
15. L. K. Meszaros, A. Dose, S. C. G. Biagini and P. J. Blower, *Inorg. Chim. Acta*, 2010, **363**, 1059.
16. R. Torres Martin de Rosales, E. Arstad and J. Blower Philip, *Targeted Oncol.*, 2009, **4**, 183.
17. J. S. Lewis, J. Zweit, J. L. J. Dearling, B. C. Rooney and P. J. Blower, *Chem. Commun.*, 1996, 1093.
18. J. S. Lewis, S. L. Heath, A. K. Powell, J. Zweit and P. J. Blower, *J. Chem. Soc., Dalton Trans.*, 1997, 855.
19. M. S. Cooper, M. T. Ma, K. Sunassee, K. P. Shaw, J. D. Williams, R. L. Paul, P. S. Donnelly and P. J. Blower, *Bioconjugate Chem.*, 2012, **23**, 1029.

20. M. Shokeen and C. J. Anderson, *Acc. Chem. Res.*, 2009, **42**, 832.
21. T. M. Jones-Wilson, K. A. Deal, C. J. Anderson, D. W. McCarthy, Z. Kovacs, R. J. Motekaitis, A. D. Sherry, A. E. Martell and M. J. Welch, *Nucl. Med. Biol.*, 1998, **25**, 523.
22. C. J. Anderson, T. S. Pajeau, W. B. Edwards, E. L. C. Sherman, B. E. Rogers and M. J. Welch, *J. Nucl. Med.*, 1995, **36**, 2315.
23. L. A. Bass, M. Wang, M. J. Welch and C. J. Anderson, *Bioconjugate Chem.*, 2000, **11**, 527.
24. B. E. Rogers, C. J. Anderson, J. M. Connett, L. W. Guo, W. B. Edwards, E. L. C. Sherman, K. R. Zinn and M. J. Welch, *Bioconjugate Chem.*, 1996, **7**, 511.
25. C. A. Boswell, X. Sun, W. Niu, G. R. Weisman, E. H. Wong, A. L. Rheingold and C. J. Anderson, *J. Med. Chem.*, 2004, **47**, 1465.
26. G. R. Mirick, R. T. O'Donnell, S. J. DeNardo, S. Shen, C. F. Meares and G. L. DeNardo, *Nucl. Med. Biol.*, 1999, **26**, 841.
27. B. M. Paterson, P. Roselt, D. Denoyer, C. Cullinane, D. Binns, W. Noonan, C. M. Jeffery, R. I. Price, J. M. White, R. J. Hicks and P. S. Donnelly, *Dalton Trans.*, 2014, **43**, 1386.
28. J. C. Garrison, T. L. Rold, G. L. Sieckman, S. D. Figueroa, W. A. Volkert, S. S. Jurisson and T. J. Hoffman, *J. Nucl. Med.*, 2007, **48**, 1327.
29. A. F. Prasanphanich, P. K. Nanda, T. L. Rold, L. Ma, M. R. Lewis, J. C. Garrison, T. J. Hoffman, G. L. Sieckman, S. D. Figueroa and C. J. Smith, *Proc. Natl. Acad. Sci. U. S. A.*, 2007, **104**, 12462.
30. J. L. J. Dearling, B. M. Paterson, V. Akurathi, S. Betanzos-Lara, S. T. Treves, S. D. Voss, J. M. White, J. S. Huston, S. V. Smith, P. S. Donnelly and A. B. Packard, *Bioconjugate Chem.*, 2015, **26**, 707.
31. P. A. Tasker and L. Sklar, *J. Cryst. Mol. Struct.*, 1975, **5**, 329.
32. J. D. Silversides, C. C. Allan and S. J. Archibald, *Dalton Trans.*, 2007, 971.
33. A. Riesen, M. Zehnder and T. A. Kaden, *Helv. Chim. Acta*, 1986, **69**, 2067.
34. A. Riesen, M. Zehnder and T. A. Kaden, *Acta Crystallogr., Sect. C: Cryst. Struct. Commun.*, 1988, **44**, 1740.
35. J. E. Sprague, Y. Peng, X. Sun, G. R. Weisman, E. H. Wong, S. Achilefu and C. J. Anderson, *Clin. Cancer Res.*, 2004, **10**, 8674.
36. D. N. Pandya, N. Bhatt, G. I. An, Y. S. Ha, N. Soni, H. Lee, Y. J. Lee, J. Y. Kim, W. Lee, H. Ahn and J. Yoo, *J. Med. Chem.*, 2014, **57**, 7234.
37. R. Ferdani, D. J. Stigers, A. L. Fiamengo, L. Wei, B. T. Y. Li, J. A. Golen, A. L. Rheingold, G. R. Weisman, E. H. Wong and C. J. Anderson, *Dalton Trans.*, 2012, **41**, 1938.
38. Y. Guo, R. Ferdani and C. J. Anderson, *Bioconjugate Chem.*, 2012, **23**, 1470.
39. Z. Cai, Q. Ouyang, D. Zeng, K. N. Nguyen, J. Modi, L. Wang, A. G. White, B. E. Rogers, X.-Q. Xie and C. J. Anderson, *J. Med. Chem.*, 2014, **57**, 6019.
40. D. Zeng, Q. Ouyang, Z. Cai, X.-Q. Xie and C. J. Anderson, *Chem. Commun.*, 2014, **50**, 43.
41. N. Bhatt, N. Soni, Y. S. Ha, W. Lee, D. N. Pandya, S. Sarkar, J. Y. Kim, H. Lee, S. H. Kim, G. I. An and J. Yoo, *ACS Med. Chem. Lett.*, 2015, **6**, 1162.

42. A. V. Dale, G. I. An, D. N. Pandya, Y. S. Ha, N. Bhatt, N. Soni, H. Lee, H. Ahn, S. Sarkar, W. Lee, P. T. Huynh, J. Y. Kim, M.-R. Gwon, S. H. Kim, J. G. Park, Y.-R. Yoon and J. Yoo, *Inorg. Chem.*, 2015, **54**, 8177.
43. E. H. Wong, G. R. Weisman, D. C. Hill, D. P. Reed, M. E. Rogers, J. S. Condon, M. A. Fagan, J. C. Calabrese, K.-C. Lam, I. A. Guzei and A. L. Rheingold, *J. Am. Chem. Soc.*, 2000, **122**, 10561.
44. E. Boros, E. Rybak-Akimova, J. P. Holland, T. Rietz, N. Rotile, F. Blasi, H. Day, R. Latifi and P. Caravan, *Mol. Pharmaceutics*, 2014, **11**, 617.
45. D. N. Pandya, J. Y. Kim, J. C. Park, H. Lee, P. B. Phapale, W. Kwak, T. H. Choi, G. J. Cheon, Y.-R. Yoon and J. Yoo, *Chem. Commun.*, 2010, **46**, 3517.
46. D. N. Pandya, N. Bhatt, A. V. Dale, J. Y. Kim, H. Lee, Y. S. Ha, J.-E. Lee, G. I. An and J. Yoo, *Bioconjugate Chem.*, 2013, **24**, 1356.
47. A. V. Dale, D. N. Pandya, J. Y. Kim, H. Lee, Y. S. Ha, N. Bhatt, J. Kim, J. J. Seo, W. Lee, S. H. Kim, Y.-R. Yoon, G. I. An and J. Yoo, *ACS Med. Chem. Lett.*, 2013, **4**, 927.
48. J. Chapman, G. Ferguson, J. F. Gallagher, M. C. Jennings and D. Parker, *J. Chem. Soc., Dalton Trans.*, 1992, 345.
49. C. L. Ferreira, D. T. Yapp, E. Lamsa, M. Gleave, C. Bensimon, P. Jurek and G. E. Kiefer, *Nucl. Med. Biol.*, 2008, **35**, 875.
50. S. Ait-Mohand, C. Denis, G. Tremblay, M. Paquette and B. Guerin, *Org. Lett.*, 2014, **16**, 4512.
51. S. Roosenburg, P. Laverman, L. Joosten, M. S. Cooper, P. K. Kolenc-Peitl, J. M. Foster, C. Hudson, J. Leyton, J. Burnet, W. J. G. Oyen, P. J. Blower, S. J. Mather, O. C. Boerman and J. K. Sosabowski, *Mol. Pharmaceutics*, 2014, **11**, 3930.
52. J. Simecek, H.-J. Wester and J. Notni, *Dalton Trans.*, 2012, **41**, 13803.
53. K.-P. Eisenwiener, M. I. M. Prata, I. Buschmann, H.-W. Zhang, A. C. Santos, S. Wenger, J. C. Reubi and H. R. Maecke, *Bioconjugate Chem.*, 2002, **13**, 530.
54. T. J. McMurry, M. Brechbiel, C. Wu and O. A. Gansow, *Bioconjugate Chem.*, 1993, **4**, 236.
55. K. Wieghardt, U. Bossek, P. Chaudhuri, W. Herrmann, B. C. Menke and J. Weiss, *Inorg. Chem.*, 1982, **21**, 4308.
56. M. J. Van der Merwe, J. C. A. Boeyens and R. D. Hancock, *Inorg. Chem.*, 1985, **24**, 1208.
57. G. Gasser, L. Tjioe, B. Graham, M. J. Belousoff, S. Juran, M. Walther, J.-U. Kuenstler, R. Bergmann, H. Stephan and L. Spiccia, *Bioconjugate Chem.*, 2008, **19**, 719.
58. M. Roger, L. M. P. Lima, M. Frindel, C. Platas-Iglesias, J.-F. Gestin, R. Delgado, V. Patinec and R. Tripier, *Inorg. Chem.*, 2013, **52**, 5246.
59. M. T. Ma, M. S. Cooper, R. L. Paul, K. P. Shaw, J. A. Karas, D. Scanlon, J. M. White, P. J. Blower and P. S. Donnelly, *Inorg. Chem.*, 2011, **50**, 6701.
60. M. T. Ma, J. A. Karas, J. M. White, D. Scanlon and P. S. Donnelly, *Chem. Commun.*, 2009, 3237.
61. S. D. Voss, S. V. Smith, N. DiBartolo, L. J. McIntosh, E. M. Cyr, A. A. Bonab, J. L. J. Dearling, E. A. Carter, A. J. Fischman, S. T. Treves, S. D.

- Gillies, A. M. Sargeson, J. S. Huston and A. B. Packard, *Proc. Natl. Acad. Sci. U. S. A.*, 2007, **104**, 17489.
62. H. Cai, J. Fissekis and P. S. Conti, *Dalton Trans.*, 2009, 5395.
63. B. M. Paterson, G. Buncic, L. E. McInnes, P. Roselt, C. Cullinane, D. S. Binns, C. M. Jeffery, R. I. Price, R. J. Hicks and P. S. Donnelly, *Dalton Trans.*, 2015, **44**, 4901.
64. P. V. Bernhardt, R. Bramley, L. M. Engelhardt, J. M. Harrowfield, D. C. R. Hockless, B. R. Korybut-Daszkiewicz, E. R. Krausz, T. Morgan, A. M. Sargeson, B. W. Skelton and A. H. White, *Inorg. Chem.*, 1995, **34**, 3589.
65. *Critical Stability Constants, Vol. 1: Amino Acids*, ed. A. E. Martell and R. M. Smith, Plenum Press, New York, 1974.
66. S. Chaves, R. Delgado and J. J. R. Frausto da Silva, *Talanta*, 1992, **39**, 249.
67. E. T. Clarke and A. E. Martell, *Inorg. Chim. Acta*, 1991, **190**, 27.
68. A. Bevilacqua, R. I. Gelb, W. B. Hebard and L. J. Zompa, *Inorg. Chem.*, 1987, **26**, 2699.
69. D. N. Pandya, A. V. Dale, J. Y. Kim, H. Lee, Y. S. Ha, G. I. An and J. Yoo, *Bioconjugate Chem.*, 2012, **23**, 330.
70. V. Maheshwari, J. L. J. Dearling, S. T. Treves and A. B. Packard, *Inorg. Chim. Acta*, 2012, **393**, 318.
71. K. Zarschler, M. Kubeil and H. Stephan, *RSC Adv.*, 2014, **4**, 10157.
72. T. C. Castle, R. I. Maurer, F. E. Sowrey, M. J. Went, C. A. Reynolds, E. J. L. McInnes and P. J. Blower, *J. Am. Chem. Soc.*, 2003, **125**, 10040.
73. J. L. J. Dearling, J. S. Lewis, G. E. D. Mullen, M. J. Welch and P. J. Blower, *J. Biol. Inorg. Chem.*, 2002, **7**, 249.
74. J. L. J. Dearling and P. J. Blower, *Chem. Commun.*, 1998, 2531.
75. P. J. Blower, T. C. Castle, A. R. Cowley, J. R. Dilworth, P. S. Donnelly, E. Labisbal, F. E. Sowrey, S. J. Teat and M. J. Went, *Dalton Trans.*, 2003, 4416.
76. R. I. Maurer, P. J. Blower, J. R. Dilworth, C. A. Reynolds, Y. Zheng and G. E. D. Mullen, *J. Med. Chem.*, 2002, **45**, 1420.
77. P. Charoenphun, R. Paul, A. Weeks, D. Berry, K. Shaw, G. Mullen, J. Ballinger and P. Blower, *Eur. J. Nucl. Med. Mol. Imaging*, 2011, **38**, S294.
78. Y. Fujibayashi, H. Taniuchi, Y. Yonekura, H. Ohtani, J. Konishi and A. Yokoyama, *J. Nucl. Med.*, 1997, **38**, 1155.
79. C. Yip, P. J. Blower, V. Goh, D. B. Landau and G. J. R. Cook, *Eur. J. Nucl. Med. Mol. Imaging*, 2015, **42**, 956.
80. F. Dehdashti, M. A. Mintun, J. S. Lewis, J. Bradley, R. Govindan, R. Laforest, M. J. Welch and B. A. Siegel, *Eur. J. Nucl. Med. Mol. Imaging*, 2003, **30**, 844.
81. T. R. Wallhaus, J. Lacy, R. Stewart, J. Bianco, M. A. Green, N. Nayak and C. K. Stone, *J. Nucl. Cardiol.*, 2001, **8**, 67.
82. J. Huang, C. C. I. Lee, J. L. Sutcliffe, S. R. Cherry and A. F. Tarantal, *Mol. Imaging*, 2008, **7**, 1.
83. J. Baguna Torres, E. Andreozzi, J. Dunn, M. Siddique, I. Szanda, D. Howlett, K. Sunassee and P. Blower, *J. Nucl. Med.*, 2016, **57**, 109.
84. J. L. J. Dearling, E. D. G. Mullen, J. S. Lewis, M. J. Welch and P. J. Blower, *J. Labelled Compd. Radiopharm.*, 1999, **42**, S276.

85. M. G. Handley, R. A. Medina, E. Mariotti, G. D. Kenny, K. P. Shaw, R. Yan, T. R. Eykyn, P. J. Blower and R. Southworth, *J. Nucl. Med.*, 2014, **55**, 488.
86. R. A. Medina, E. Mariotti, D. Pavlovic, K. P. Shaw, T. R. Eykyn, P. J. Blower and R. Southworth, *J. Nucl. Med.*, 2015, **56**, 921.
87. J. S. Lewis, R. Laforest, T. L. Buettner, S.-K. Song, Y. Fujibayashi, J. M. Connett and M. J. Welch, *Proc. Natl. Acad. Sci. U. S. A.*, 2001, **98**, 1206.
88. C. J. Anderson, L. A. Jones, L. A. Bass, E. L. C. Sherman, D. W. McCarthy, P. D. Cutler, M. V. Lanahan, M. E. Cristel, J. S. Lewis and S. W. Schwarz, *J. Nucl. Med.*, 1998, **39**, 1944.
89. J. M. Connett, C. J. Anderson, L.-W. Guo, S. W. Schwarz, K. R. Zinn, B. E. Rogers, B. A. Siegel, G. Philpott and M. J. Welch, *Proc. Natl. Acad. Sci. U. S. A.*, 1996, **93**, 6814.
90. A. Hino-Shishikura, U. Tateishi, H. Shibata, T. Yoneyama, T. Nishii, I. Torii, K. Tateishi, M. Ohtake, N. Kawahara and T. Inoue, *Eur. J. Nucl. Med. Mol. Imaging*, 2014, **41**, 1419.
91. F. Dehdashti, P. W. Grigsby, J. S. Lewis, R. Laforest, B. A. Siegel and M. Welch, *J. Nucl. Med.*, 2008, **49**, 201.
92. D. W. Dietz, F. Dehdashti, P. W. Grigsby, R. S. Malyapa, R. J. Myerson, J. Picus, J. Ritter, J. S. Lewis, M. J. Welch and B. A. Siegel, *Dis. Colon Rectum*, 2008, **51**, 1641.
93. M. Ikawa, H. Okazawa, T. Tsujikawa, A. Matsunaga, O. Yamamura, T. Mori, T. Hamano, Y. Kiyono, Y. Nakamoto and M. Yoneda, *Neurology*, 2015, **84**, 2033.
94. M. Ikawa, H. Okazawa, T. Kudo, M. Kuriyama, Y. Fujibayashi and M. Yoneda, *Nucl. Med. Biol.*, 2011, **38**, 945.
95. K. P. Zhernosekov, D. V. Filosofov, R. P. Baum, P. Aschoff, H. Bihl, A. A. Razbash, M. Jahn, M. Jennewein and F. Roesch, *J. Nucl. Med.*, 2007, **48**, 1741.
96. E. Eppard, M. Wuttke, P. L. Nicodemus and F. Roesch, *J. Nucl. Med.*, 2014, **55**, 1023.
97. M. S. Hofman, G. Kong, O. C. Neels, P. Eu, E. Hong and R. J. Hicks, *J. Med. Imaging Radiat. Oncol.*, 2012, **56**, 40.
98. A. Afshar-Oromieh, C. M. Zechmann, A. Malcher, M. Eder, M. Eisenhut, H. G. Linhart, T. Holland-Letz, B. A. Hadaschik, F. L. Giesel, J. Debus and U. Haberkorn, *Eur. J. Nucl. Med. Mol. Imaging*, 2014, **41**, 11.
99. R. J. Hicks, *Leuk. Lymphoma*, 2006, **47**, 2440.
100. S. V. Govindan, D. M. Goldenberg, S. E. Elsamra, G. L. Griffiths, G. L. Ong, M. W. Brechbiel, J. Burton, G. Sgouros and M. J. Mattes, *J. Nucl. Med.*, 2000, **41**, 2089.
101. R. B. Michel, M. W. Brechbiel and M. J. Mattes, *J. Nucl. Med.*, 2003, **44**, 632.
102. A. Heppeler, S. Froidevaux, H. R. Macke, E. Jermann, M. Behe, P. Powell and M. Hennig, *Chem.-Eur. J.*, 1999, **5**, 1974.
103. W. R. Harris and V. L. Pecoraro, *Biochemistry*, 1983, **22**, 292.
104. C. L. Ferreira, E. Lamsa, M. Woods, Y. Duan, P. Fernando, C. Bensimon, M. Kordos, K. Guenther, P. Jurek and G. E. Kiefer, *Bioconjugate Chem.*, 2010, **21**, 531.

105. E. Boros, C. L. Ferreira, J. F. Cawthray, E. W. Price, B. O. Patrick, D. W. Wester, M. J. Adam and C. Orvig, *J. Am. Chem. Soc.*, 2010, **132**, 15726.
106. M. T. Ma, O. C. Neels, D. Denoyer, P. Roselt, J. A. Karas, D. B. Scanlon, J. M. White, R. J. Hicks and P. S. Donnelly, *Bioconjugate Chem.*, 2011, **22**, 2093.
107. J. P. Andre, H. R. Maecke, M. Zehnder, L. Macko and K. G. Akyel, *Chem. Commun.*, 1998, 1301.
108. A. S. Craig, D. Parker, H. Adams and N. A. Bailey, *J. Chem. Soc., Chem. Commun.*, 1989, 1793.
109. I. Velikyan, H. Maecke and B. Langstrom, *Bioconjugate Chem.*, 2008, **19**, 569.
110. C. L. Ferreira, D. T. T. Yapp, D. Mandel, R. K. Gill, E. Boros, M. Q. Wong, P. Jurek and G. E. Kiefer, *Bioconjugate Chem.*, 2012, **23**, 2239.
111. J. Notni, P. Hermann, J. Havlickova, J. Kotek, V. Kubicek, J. Plutnar, N. Loktionova, J. Riss Patrick, F. Rosch and I. Lukes, *Chem.-Eur. J.*, 2010, **16**, 7174.
112. J. Notni, K. Pohle and H.-J. Wester, *Nucl. Med. Biol.*, 2013, **40**, 33.
113. J. Notni, J. Simecek, P. Hermann and H.-J. Wester, *Chem.-Eur. J.*, 2011, **17**, 14718.
114. J. Notni, P. Hermann, J. Havlickova, J. Kotek, V. Kubicek, J. Plutnar, N. Loktionova, P. J. Riss, F. Roesch and I. Lukes, *Chem.-Eur. J.*, 2010, **16**, 7174.
115. B. P. Waldron, D. Parker, C. Burchardt, D. S. Yufit, M. Zimny and F. Roesch, *Chem. Commun.*, 2013, **49**, 579.
116. D. Parker, B. P. Waldron and D. S. Yufit, *Dalton Trans.*, 2013, **42**, 8001.
117. J. Seemann, B. P. Waldron, F. Roesch and D. Parker, *ChemMedChem*, 2015, **10**, 1019.
118. C. F. Ramogida, J. F. Cawthray, E. Boros, C. L. Ferreira, B. O. Patrick, M. J. Adam and C. Orvig, *Inorg. Chem.*, 2015, **54**, 2017.
119. E. Boros, C. L. Ferreira, D. T. T. Yapp, R. K. Gill, E. W. Price, M. J. Adam and C. Orvig, *Nucl. Med. Biol.*, 2012, **39**, 785.
120. R. J. Motekaitis, Y. Sun and A. E. Martell, *Inorg. Chim. Acta*, 1989, **159**, 29.
121. J. Schuhmacher, G. Klivenyi, W. E. Hull, R. Matys, H. Hauser, H. Kalthoff, W. H. Schmiegel, W. Maier-Borst and S. Matzku, *Nucl. Med. Biol.*, 1992, **19**, 809.
122. C. J. Mathias, Y. Sun, M. J. Welch, M. A. Green, J. A. Thomas, K. R. Wade and A. E. Martell, *Nucl. Med. Biol.*, 1988, **15**, 69.
123. M. Eder, M. Schaefer, U. Bauder-Wuest, W.-E. Hull, C. Waengler, W. Mier, U. Haberkorn and M. Eisenhut, *Bioconjugate Chem.*, 2012, **23**, 688.
124. M. Eder, B. Waengler, S. Knackmuss, F. LeGall, M. Little, U. Haberkorn, W. Mier and M. Eisenhut, *Eur. J. Nucl. Med. Mol. Imaging*, 2008, **35**, 1878.
125. M. Eder, A. V. Krivoshein, M. Backer, J. M. Backer, U. Haberkorn and M. Eisenhut, *Nucl. Med. Biol.*, 2010, **37**, 405.
126. M. Eder, O. Neels, M. Mueller, U. Bauder-Wuest, Y. Remde, M. Schaefer, U. Hennrich, M. Eisenhut, A. Afshar-Oromieh, U. Haberkorn and K. Kopka, *Pharmaceuticals*, 2014, **7**, 779.
127. A. D. Tinoco, C. D. Incarvito and A. M. Valentine, *J. Am. Chem. Soc.*, 2007, **129**, 3444.

128. S. K. Larsen, B. G. Jenkins, N. G. Memon and R. B. Lauffer, *Inorg. Chem.*, 1990, **29**, 1147.
129. D. J. Berry, Y. Ma, J. R. Ballinger, R. Tavaré, A. Koers, K. Sunassee, T. Zhou, S. Nawaz, G. E. D. Mullen, R. C. Hider and P. J. Blower, *Chem. Commun.*, 2011, **47**, 7068.
130. M. T. Ma, C. Cullinane, C. Imberti, J. Baguna Torres, S. Y. A. Terry, P. Roselt, R. J. Hicks and P. J. Blower, *Bioconjugate Chem.*, 2016, **27**, 309.
131. M. T. Ma, C. Cullinane, K. Waldeck, P. Roselt, R. J. Hicks and P. J. Blower, *EJNMMI Res.*, 2015, **5**, 52.
132. S. V. Govindan, R. B. Michel, G. L. Griffiths, D. M. Goldenberg and M. J. Mattes, *Nucl. Med. Biol.*, 2005, **32**, 513.
133. J. E. Ryser, K. Rose, R. Jones, A. Pelegrin, A. Donath, R. Egeli, A. Smith and R. E. Offord, *Nucl. Med. Biol.*, 1998, **25**, 261.
134. M. Petrik, G. M. Franssen, H. Haas, P. Laverman, C. Hoertnagl, M. Schrettl, A. Helbok, C. Lass-Floerl and C. Decristoforo, *Eur. J. Nucl. Med. Mol. Imaging*, 2012, **39**, 1175.
135. M. Petrik, H. Haas, M. Schrettl, A. Helbok, M. Blatzer and C. Decristoforo, *Nucl. Med. Biol.*, 2012, **39**, 361.
136. P. A. Knetsch, C. Zhai, C. Rangger, M. Blatzer, H. Haas, P. Kaeopookum, R. Haubner and C. Decristoforo, *Nucl. Med. Biol.*, 2015, **42**, 115.
137. E. C. Dijkers, T. H. Oude Munnink, J. G. Kosterink, A. H. Brouwers, P. L. Jager, J. R. de Jong, G. A. van Dongen, C. P. Schroeder, M. N. Lub-de Hooge and E. G. de Vries, *Clin. Pharmacol. Ther.*, 2010, **87**, 586.
138. L. R. Perk, O. J. Visser, M. Stigter-Van Walsum, M. J. W. D. Vosjan, G. W. M. Visser, J. M. Zijlstra, P. C. Huijgens and G. A. M. S. van Dongen, *Eur. J. Nucl. Med. Mol. Imaging*, 2006, **33**, 1337.
139. E. W. Price, B. M. Zeglis, J. S. Lewis, M. J. Adam and C. Orvig, *Dalton Trans.*, 2014, **43**, 119.
140. M. J. W. D. Vosjan, L. R. Perk, G. W. M. Visser, M. Budde, P. Jurek, G. E. Kiefer and G. A. M. S. van Dongen, *Nat. Protoc.*, 2010, **5**, 739.
141. J. P. Holland, V. Divilov, N. H. Bander, P. M. Smith-Jones, S. M. Larson and J. S. Lewis, *J. Nucl. Med.*, 2010, **51**, 1293.
142. M. T. Ma, L. K. Meszaros, B. M. Paterson, D. J. Berry, M. S. Cooper, Y. Ma, R. C. Hider and P. J. Blower, *Dalton Trans.*, 2015, **44**, 4884.
143. F. Guerard, Y.-S. Lee, R. Tripier, L. P. Szajek, J. R. Deschamps and M. W. Brechbiel, *Chem. Commun.*, 2013, **49**, 1002.
144. M. A. Deri, S. Ponnala, P. Kozlowski, B. P. Burton-Pye, H. T. Cicek, C. Hu, J. S. Lewis and L. C. Francesconi, *Bioconjugate Chem.*, 2015, **26**, 2579.
145. C. Zhai, D. Summer, C. Rangger, G. M. Franssen, P. Laverman, H. Haas, M. Petrik, R. Haubner and C. Decristoforo, *Mol. Pharmaceutics*, 2015, **12**, 2142.
146. M. Patra, A. Bauman, C. Mari, C. A. Fischer, O. Blacque, D. Haussinger, G. Gasser and T. L. Mindt, *Chem. Commun.*, 2014, **50**, 11523.
147. D. N. Pandya, S. Pailloux, D. Tatum, D. Magda and T. J. Wadas, *Chem. Commun.*, 2015, **51**, 2301.

148. F. Guerard, Y.-S. Lee and M. W. Brechbiel, *Chem.–Eur. J.*, 2014, **20**, 5584.
149. M. A. Deri, S. Ponnala, B. M. Zeglis, G. Pohl, J. J. Dannenberg, J. S. Lewis and L. C. Francesconi, *J. Med. Chem.*, 2014, **57**, 4849.
150. M. Amelia Santos, *Coord. Chem. Rev.*, 2002, **228**, 187.
151. A. M. Peters, *Q. J. Nucl. Med. Mol. Imaging*, 2005, **49**, 304.
152. T. J. Ferris, P. Charoenphun, L. K. Meszaros, G. E. D. Mullen, P. J. Blower and M. J. Went, *Dalton Trans.*, 2014, **43**, 14851.
153. P. Charoenphun, L. K. Meszaros, K. Chuamsaamarkkee, E. Sharif-Paghaleh, J. R. Ballinger, T. J. Ferris, M. J. Went, G. E. D. Mullen and P. J. Blower, *Eur. J. Nucl. Med. Mol. Imaging*, 2015, **42**, 278.
154. P. Kathirgamanathan, S. Surendrakumar, J. Antipan-Lara, S. Ravichandran, V. R. Reddy, S. Ganeshamurugan, M. Kumaraverl, V. Arkley, A. J. Blake and D. Bailey, *J. Mater. Chem.*, 2011, **21**, 1762.

# Subject Index

- absorption
  - of arsenic/arsenicals, 63–64
  - of cadmium intoxication, 86–87
  - lead intoxication, 78–80
  - of mercury/mercurials, 70–73
- aceruloplasminaemia, 169–172
- actinide chelation
  - chemical structures for, 187–192
    - coordination chemistry criteria, 188
    - and new actinide-selective agents, 188–192
  - medical and public health relevance of, 183–187
  - limitations of, 187
  - metabolism and clinical course, 184–185
  - treatment recommendations for, 186–187
- viable treatments
  - animal rule, 203–205
  - current status of, 205–206
  - formulation development, 199–202
  - pharmaceutical approaches, 201–202
  - safety determination and regulatory approval, 202–206
  - structural modifications of DTPA, 200–201
  - in vitro* evaluation techniques and *ex vivo* binding, 195
  - high-throughput screening methods, 194–195
  - solution thermodynamics, 193–194
  - in vivo* efficacy determination and animal model selection, 196–197
  - decorporation studies, 197–199
- acute copper poisoning, 95
- acute iron poisoning, 94–95
- acute mercury intoxication, 76–78
- acyclic chelators, for gallium-68, 290–294
- AD. *see* Alzheimer's disease (AD)
- adrenal glands, and non-invasive iron measurements, 245
- aging
  - brain
    - and copper homeostasis, 156
    - and iron homeostasis, 154–155
    - and zinc homeostasis, 156–157
    - inflammation and, 157
  - aliphatic diamines, 35
  - aluminium toxicity, 15–17
  - Alzheimer's disease (AD), 163–166
  - amide bond formation, 263
  - aminocarboxylates, 36–37
  - animal model selection, 196–197

- arsenic/arsenicals intoxication, 63–68  
 absorption and metabolism of, 63–64  
 chelation therapy for, 66–68  
 chronic arsenic poisoning, 68  
 diagnostic measures and interventional levels, 66  
 toxicity of, 64–66  
 clinical, 65–66  
 mechanism of, 64–65
- BBB. *see* blood–brain barrier (BBB)
- bidentate ligands  
 aliphatic diamines, 35  
 aminocarboxylates, 36–37  
 catechols, 31–33  
 heterocyclic amines, 35  
 hydroxamates, 33  
 hydroxycarboxylates, 37  
 hydroxypyranones, 35  
 hydroxypyridinones, 33–35  
 hydroxyquinolines, 36
- bifunctional chelators, 262
- blood–brain barrier (BBB), 81, 158
- blood oxygenation-dependent (BOLD) effect, 224
- blood transfusion  
 and inherited anaemias effects, 107–109  
 and iron distribution, 109–113  
 and iron homeostasis, 106–107
- BOLD. *see* blood oxygenation-dependent (BOLD) effect
- bone marrow, and non-invasive iron measurements, 246–247
- brain, aging  
 and copper homeostasis, 156  
 and iron homeostasis, 154–155  
 and zinc homeostasis, 156–157
- cadmium intoxication, 85–92  
 absorption and metabolism of, 86–87  
 chelation treatment for, 90–92  
 diagnostic markers and intervention level, 90  
 toxicity of, 87–89  
 clinical, 88–89  
 mechanism of, 88
- cadmium toxicity, 14
- cardiac iron level, 240
- catechols, 31–33
- chelate effect, of ligands, 37–39
- chelation therapy  
 for arsenic, 66–68  
 for cadmium intoxication, 90–92  
 for mercury/mercurials intoxication, 76–78
- chelators. *see also specific types*  
 bifunctional, 262  
 conventional, 61  
 drawbacks and misuse of, 62–63  
 iron (*see* iron chelators)  
 macrocyclic (*see* macrocyclic chelators)  
 and nutrition, 52  
 pharmacokinetics, 47–49  
 toxicity of, 49–52  
 genotoxicity, 52  
 immunotoxicity, 51–52  
 and metal-dependent enzymes, 49–51  
 nephrotoxicity, 51  
 neurotoxicity, 51  
 for zirconium-89, 295–303  
 hexadentate, 296–299  
 metastable lipophilic, 302–303  
 octadentate, 299–302  
 overview, 295–296
- chemical shift relaxometry (CSR), 232–233
- chemical structures, for actinide chelation, 187–192  
 coordination chemistry criteria, 188

- and new actinide-selective agents, 188–192
  - polyamino-carboxylic acid derivatives, 189–190
  - poly-phosphonic acid chelators and macrocyclic structures, 192
  - siderophore mimics, 190–191
- chronic arsenic poisoning, 68
- cobalt toxicity, 9
- complex lability, of ligands, 39–41
- coordination chemistry criteria, 188
- copper-64
  - macrocyclic chelators for overview, 265–266
  - radiolabelling and *in vivo* stability, 266–275
- copper toxicity, 10–12
- CSR. *see* chemical shift relaxometry (CSR)
- deferasirox (DFX)
  - effects on heart, 132
  - iron excretion and iron balance, 131–132
  - pharmacokinetics and metabolism, 130–131
  - tolerability, 134–135
- deferiprone (DFP)
  - effects on heart, 129–130
  - effects on iron balance, 129
  - pharmacokinetics, 128–129
  - physicochemical properties and iron binding, 127–128
  - tolerability, 134
- denticity, of ligands, 37–39
- desferrioxamine (DFO)
  - effects on heart, 126–127
  - iron balance and ferritin, 125–126
  - long-term effects, 126
  - and morbidity, 127
  - pharmacokinetics of free ligand and iron complexes, 125
  - physicochemical properties and iron binding, 124–125
  - and tolerability, 133–134
- DFO. *see* desferrioxamine (DFO)
- DFP. *see* deferiprone (DFP)
- Environmental Protection Agency (EPA), 63
- EPA. *see* Environmental Protection Agency (EPA)
- essential metals
  - toxicity due to, 4–12
    - calcium and magnesium, 7–8
    - cobalt, 9
    - iron and copper, 10–12
    - manganese, 9–10
    - molybdenum, 12
    - sodium and potassium, 4–7
    - zinc, 8–9
- Freiderich's ataxia, 168–169
- gallium-68
  - acyclic chelators for, 290–294
  - design and clinical impact, 295
  - macrocyclic chelators for, 286–289
    - utility and potential, 283–286
  - siderophores for coordination of, 294–295
- genotoxicity, 52
- gold poisoning, 93–94
- gradient-echo relaxometry, 229–233
  - cardiac, 230–231
  - chemical shift relaxometry (CSR), 232–233
  - hepatic, 230
- “hard/soft” acids and bases (HSAB), 57
- HD. *see* Huntington's disease (HD)

- heavy metal intoxication
- acute copper poisoning, 95
  - acute iron poisoning, 94–95
  - arsenic/arsenicals, 63–68
    - absorption and metabolism of, 63–64
    - chelation therapy for, 66–68
    - chronic arsenic poisoning, 68
    - clinical toxicity of, 65–66
    - diagnostic measures and interventional levels, 66
    - mechanism of, 64–65
    - toxicity of, 64–66
  - cadmium, 85–92
    - absorption and metabolism of, 86–87
    - chelation treatment for, 90–92
    - diagnostic markers and intervention level, 90
    - toxicity of, 87–89
  - drawbacks and misuse of chelators, 62–63
  - lead, 78–85
    - absorption and metabolism, 78–80
    - diagnostic measures and intervention levels, 82
    - toxicity of, 80–82
    - treatment of, 82–85
  - mercury/mercurials, 68–78
    - absorption and metabolism of, 70–73
    - chelation treatment for, 76–78
    - diagnostics and intervention levels, 75–76
    - Hg<sup>0</sup>, 70–71
    - inorganic, 71–72
    - organic, 72–73
    - toxicology of, 73–75
    - and noble metals
      - gold poisoning, 93–94
      - silver poisoning, 92–93
    - overview, 56–57
    - thallium poisoning, 95–96
    - toxicology of, 58–59
    - treatment for, 59–62
      - conventional chelators, 61
      - new chelators, 61–62
  - heterocyclic amines, 35
  - hexadentate chelators, for zirconium-89, 296–299
  - high-throughput screening methods, 194–195
  - homeostasis
    - brain copper, 156
    - brain iron, 154–155
    - brain zinc, 156–157
  - HSAB. *see* “hard/soft” acids and bases (HSAB)
  - Huntington’s disease (HD), 174–175
  - hydroxamates, 33
  - hydroxycarboxylates, 37
  - hydroxypyranones, 35
  - hydroxypyridinones, 33–35
  - hydroxyquinolines, 36
  - hypothyroidism, and non-invasive iron measurements, 245
  - IARC. *see* International Agency for Research on Cancer (IARC)
  - ICH. *see* Intracerebral haemorrhage (ICH)
  - immunotoxicity, 51–52
  - inflammation, and aging, 157
  - inherited anaemias effects, 107–109
  - inorganic mercury, 71–72
  - International Agency for Research on Cancer (IARC), 58
  - Intracerebral haemorrhage (ICH), 166–167
  - in vitro* evaluation techniques

- actinide chelation
  - and *ex vivo* binding, 195
  - high-throughput screening methods, 194–195
  - solution thermodynamics, 193–194
- in vivo* efficacy determination
  - actinide chelation
    - and animal model selection, 196–197
    - decorporation studies, 197–199
- iron chelators
  - deferasirox (DFX)
    - effects on heart, 132
    - iron excretion and iron balance, 131–132
    - pharmacokinetics and metabolism, 130–131
  - deferiprone (DFP)
    - effects on heart, 129–130
    - effects on iron balance, 129
    - pharmacokinetics, 128–129
    - physicochemical properties and iron binding, 127–128
  - desferrioxamine (DFO)
    - effects on heart, 126–127
    - iron balance and ferritin, 125–126
    - long-term effects, 126
    - and morbidity, 127
    - pharmacokinetics of free ligand and iron complexes, 125
    - physicochemical properties and iron binding, 124–125
  - high binding constant and selectivity, 113–114
  - and inhibition of key metabolic pools, 114–117
  - practical use of, 135–140
    - combination of DFP plus DFX, 140
    - combinations of DFO plus DFX, 140
    - combinations of DFP with DFO, 139–140
    - and myocardial iron, 136–137
    - patients in heart failure, 137–138
    - patients not responding to monotherapy regimens, 139
    - patients with acceptable levels, 135–136
    - patients with rapidly falling serum ferritin, 138–139
    - patients with unacceptable levels, 136
  - properties and clinical beneficial effects of, 124–132
  - unwanted effects of, 132–135
    - deferasirox tolerability, 134–135
    - deferiprone tolerability, 134
    - and desferrioxamine tolerability, 133–134
    - iron deprivation role, 132–133
- iron distribution, and blood transfusion, 109–113
- iron homeostasis
  - and blood transfusion, 106–107
  - and inherited anaemias effects, 107–109
- iron-mediated damage, 122–123

- iron overload
- monitoring and treatment
    - iron-mediated damage, 122–123
  - labile plasma iron (LPI), 123–124
  - liver iron concentration (LIC), 120–121
  - myocardial iron
    - estimation, 122
  - plasma non-transferrin iron (NTBI), 123–124
  - serum ferritin (SF), 117–120
  - urinary 24 h iron
    - estimation, 123
- iron storage molecules
- biochemical properties of, 217–218
  - magnetic properties of, 218–224
  - magnetic volume susceptibility, 220–223
  - wet-to-dry weight ratio, 223–224
- iron toxicity, 10–12
- isothiocyanates, 263
- kidney, and non-invasive iron measurements, 244
- labile plasma iron (LPI), 123–124
- lead intoxication, 78–85
- absorption and metabolism, 78–80
  - diagnostic measures and intervention levels, 82
  - toxicity of, 80–82
  - treatment of, 82–85
- lead toxicity, 13–14
- LIC. *see* liver iron concentration (LIC)
- ligands
- bidentate
    - aliphatic diamines, 35
    - aminocarboxylates, 36–37
    - catechols, 31–33
    - heterocyclic amines, 35
    - hydroxamates, 33
    - hydroxycarboxylates, 37
    - hydroxypyranones, 35
    - hydroxypyridinones, 33–35
    - hydroxyquinolines, 36
  - binding to serum albumin, 45–47
  - biological properties, 43
  - chelate effect, 37–39
  - chemistry, 26–29
  - complex lability, 39–41
  - denticity, 37–39
  - lipophilicity and molecular weight, 43–44
  - metabolism, 44–45
  - redox activity, 41–43
  - selectivity, 29–31
  - lipophilicity and molecular weight, 43–44
- liver iron concentration (LIC), 238–239
- monitoring and treatment, 120–121
- LPI. *see* labile plasma iron (LPI)
- MAC. *see* maximum allowable concentration (MAC)
- macrocyclic chelators
- for copper-64
    - overview, 265–266
    - radiolabelling and *in vivo* stability, 266–275
  - for gallium-68, 286–289
    - design and clinical impact, 295
    - siderophores for coordination of, 294–295
    - utility and potential, 283–286
  - and open-chain chelators, 289–290

- macular degeneration, and neurodegenerative diseases, 176
- maleimides, 263
- manganese toxicity, 9–10
- maximum allowable concentration (MAC), 69
- maximum permissible limit (MPL), 63
- mercury/mercurials intoxication, 68–78
  - absorption and metabolism of, 70–73
  - chelation treatment for, 76–78
  - diagnostics and intervention levels, 75–76
  - Hg<sup>0</sup>, 70–71
  - inorganic, 71–72
  - organic, 72–73
  - toxicology of, 73–75
    - clinical, 74–75
    - mechanism of, 73
- mercury toxicity, 15
- metabolism
  - of arsenic/arsenicals, 63–64
  - of cadmium intoxication, 86–87
  - lead intoxication, 78–80
  - of mercury/mercurials, 70–73
- metal-dependent enzymes, 49–51
- metal ions, and neurodegenerative diseases
  - Alzheimer's disease (AD), 163–166
  - Freiderich's ataxia, 168–169
  - Intracerebral haemorrhage (ICH), 166–167
  - multiple sclerosis (MS), 168
  - Parkinson's disease (PD), 160–163
- metal toxicity
  - essential metals
    - magnesium and calcium, 2–3
    - sodium and potassium, 2
    - toxicity due to, 4–12
    - zinc, 3
  - non-essential metals, 12–13
    - toxicity due to, 13–17
  - overview, 1–2
- metastable lipophilic chelators, 302–303
- Modified Look-Locker Inversion recovery (MOLLI), 229
- molecular weight, and lipophilicity, 43–44
- MOLLI. *see* Modified Look-Locker Inversion recovery (MOLLI)
- molybdenum toxicity, 12
- MPL. *see* maximum permissible limit (MPL)
- MS. *see* multiple sclerosis (MS)
- multiple sclerosis (MS), 168
- myocardial iron estimation, 122
- NBIA. *see* neurodegenerative brain iron accumulation (NBIA)
- nephrotoxicity, 51
- neurodegenerative brain iron accumulation (NBIA), 169–176, 242–243
  - aceruloplasminaemia, 169–172
  - Huntington's disease (HD), 174–175
  - neuroferritinopathy, 172
  - pantothenate kinase-associated neurodegeneration, 172–174
  - Wilson's disease, 175–176
- neurodegenerative diseases
  - aging brain
    - and brain copper homeostasis, 156
    - and brain iron homeostasis, 154–155
    - and brain zinc homeostasis, 156–157
  - blood-brain barrier (BBB), 158
  - description, 157–158
  - inflammation and, 157
  - and macular degeneration, 176
  - metal ions and

- neurodegenerative diseases  
(*continued*)
- Alzheimer's disease (AD), 163–166
  - Freiderich's ataxia, 168–169
  - Intracerebral haemorrhage (ICH), 166–167
  - multiple sclerosis (MS), 168
  - Parkinson's disease (PD), 160–163
  - overview, 153
- neuroferritinopathy, 172
- neurotoxicity, 51
- new actinide-selective agents, 188–192
- polyamino-carboxylic acid derivatives, 189–190
  - poly-phosphonic acid chelators and macrocyclic structures, 192
  - siderophore mimics, 190–191
- noble metals, and heavy metal intoxication
- gold poisoning, 93–94
  - silver poisoning, 92–93
- non-essential metals, 12–13
- sources and routes of exposure, 18–19
  - toxicity due to, 13–17
  - aluminium, 15–17
  - cadmium, 14
  - lead, 13–14
  - mercury, 15
- non-invasive iron measurements
- applications
    - and adrenal glands, 245
    - bone marrow, 246–247
    - cardiac iron level, 240
    - and hypothyroidism, 245
    - and kidney, 244
    - liver iron concentration (LIC), 238–239
  - neurodegenerative brain iron accumulation (NBIA), 242–243
  - and pancreas, 240–241
  - and pituitary gland, 241
  - spleen iron concentration (SIC), 239
  - testes and ovaries, 245–246
  - biomagnetic susceptometry
    - liver, 233
    - MR-biosusceptometry and MR-QSM, 234–235
  - gradient-echo relaxometry, 229–233
    - cardiac, 230–231
    - chemical shift relaxometry (CSR), 232–233
    - hepatic, 230
  - iron storage molecules
    - biochemical properties of, 217–218
    - magnetic properties of, 218–224
    - magnetic volume susceptibility, 220–223
    - wet-to-dry weight ratio, 223–224
  - other MRI techniques, 235–236
  - overview, 213–215
  - quantitative X-ray techniques, 237
  - reference standards for, 215–217
    - bone marrow, 216
    - liver biopsy, 215
    - post-mortem brain, 216–217
    - quantitative heart biopsy and autopsy, 216
  - spin-echo relaxometry, 226–229
  - spin-lattice relaxometry, 229

- NTBI. *see* plasma non-transferrin iron (NTBI)
- nuclear magnetic susceptibility, 225
- nutrition, and chelators, 52
- octadentate chelators, for zirconium-89, 299–302
- open-chain chelators, 289–290
- organic mercury, 72–73
- ovaries, and non-invasive iron measurements, 245–246
- pancreas, and non-invasive iron measurements, 240–241
- pantothenate kinase-associated neurodegeneration, 172–174
- Parkinson's disease (PD), 160–163
- PD. *see* Parkinson's disease (PD)
- PET. *see* positron emission tomography (PET)
- pituitary gland, and non-invasive iron measurements, 241
- plasma non-transferrin iron (NTBI), 123–124
- polyamino-carboxylic acid derivatives, 189–190
- poly-phosphonic acid chelators and macrocyclic structures, 192
- positron emission tomography (PET), 261–262
- QSM. *see* quantitative susceptibility mapping (QSM)
- quantitative susceptibility mapping (QSM), 220
- quantitative X-ray techniques, 237
- radiolabelling and *in vivo* stability, macrocyclic chelators, 266–275  
 alternatives to teta and dota, 269–271  
 bioreduction and dissociation, 281–282  
 clinical applications of, 282–283  
 cyclen, cyclam, teta and dota, 266–268  
 kinetic stability, 275–280  
 nota and sarcophagine derivatives, 271–275  
 redox activity, of ligands, 41–43  
 selectivity, of ligands, 29–31  
 serum albumin, and ligands, 45–47  
 serum ferritin (SF), 117–120  
 shMOLLI. *see* Shortened MOLLI (shMOLLI)
- Shortened MOLLI (shMOLLI), 229
- SIC. *see* spleen iron concentration (SIC)
- siderophore mimics, 190–191
- silver poisoning, 92–93
- solution thermodynamics, 193–194
- spin-echo relaxometry, 226–229
- spin-lattice relaxometry, 229
- SPIONs. *see* superparamagnetic nanoparticles (SPIONs)
- spleen iron concentration (SIC), 239
- SQUID. *see* superconducting quantum interference device (SQUID)
- superconducting quantum interference device (SQUID), 226
- superparamagnetic nanoparticles (SPIONs), 224
- testes, and non-invasive iron measurements, 245–246
- thallium poisoning, 95–96
- toxicity  
 of arsenic/arsenicals, 64–66  
 clinical, 65–66  
 mechanism of, 64–65  
 of cadmium, 87–89  
 clinical, 88–89  
 mechanism of, 88  
 of chelators, 49–52  
 genotoxicity, 52  
 immunotoxicity, 51–52  
 and metal-dependent enzymes, 49–51

- toxicity (*continued*)  
  nephrotoxicity, 51  
  neurotoxicity, 51  
  due to essential metals, 4–12  
    calcium and magnesium, 7–8  
    cobalt, 9  
    iron and copper, 10–12  
    manganese, 9–10  
    molybdenum, 12  
    sodium and potassium, 4–7  
    zinc, 8–9  
  due to non-essential metals, 13–17  
    aluminium, 15–17  
    cadmium, 14  
    lead, 13–14  
    mercury, 15  
  of lead, 80–82
- toxicology  
  of heavy metals, 58–59  
  of mercury/mercurials  
    intoxication, 73–75  
    clinical, 74–75  
    mechanism of, 73
- urinary 24 h iron  
  estimation, 123
- viable treatments, of actinide  
  chelation  
    animal rule, 203–205  
    current status of, 205–206  
    formulation development, 199–202  
    pharmaceutical approaches, 201–202  
    safety determination and regulatory approval, 202–206  
    structural modifications of DTPA, 200–201
- Wilson's disease, 175–176
- zirconium-89, chelators for, 295–303  
  hexadentate, 296–299  
  metastable lipophilic, 302–303  
  octadentate, 299–302  
  overview, 295–296